Cryptotephra deposition and preservation in four sub-Arctic lakes in Yukon, Canada

by

Jordan Russell Harvey

A thesis submitted in partial fulfillment of the requirements for the degree of

Master of Science

Department of Earth and Atmospheric Sciences

University of Alberta

Abstract

Cryptotephra research is one of the fastest growing subfields of tephrochronology. Here the extraction, processing, and analytical techniques required for cryptotephra studies are reviewed and assessed in detail. A workflow is suggested depending on the site's characteristics to improve the quality of data. The debate surrounding acid digestion procedures and their potential to alter glass geochemistry is specifically addressed, eliminating the concern for glass alteration if methods are correctly followed. Guidelines for tephra identification, shard profile interpretation, and analytical procedures such as the use of secondary standards and time-dependent intensity corrections are presented. The result is a detailed protocol that acts as a guide through the methods of cryptotephra research in lake and peat cores for new researchers to the field while simultaneously improving interlaboratory comparability. Further, four Yukon lakes were processed for cryptotephra to refine their chronologies and support the paleoenvironmental studies at each site. The full Holocene record at Hanging Lake was examined, the Holocene to late Pleistocene at Gravel Lake, and the Pleistocene to Holocene transition at Barlow Lake. Surface cores of Chapman Lake and Gravel Lake were also fully assessed. Multiple limiting factors were found at these lakes, obstructing the preservation and identification of primary cryptotephra deposits. Reworking, secondary deposition, and presence of nearby loess deposits all complicated shard profiles. However, evidence of multiple Holocene eruptions from Mt. Churchill, Augustine, and Aniakchak, and the identification of Redoubt 1989/90, Katmai 1912, Ruppert tephra, Ksudach KS_2, and eight unknown glass shard populations reinforce the potential of cryptotephra research on Yukon Lakes.

Acknowledgements

In March of 2017, I attended an ATLAS talk titled 'Volcanoes and Volcanic Ash in the Quaternary Sciences' by Dr. Britta Jensen, discussing the applicability of tephra research in Quaternary science and the correlation of ultra-distal tephra deposits across oceans. The passion and excitement for research shown in this presentation inspired me to pursue grad school and enter the world of tephrochronology. Through the highs and lows of this journey, I still share this same excitement for tephra research given to me during that ATLAS talk.

First and foremost, I would like to thank Dr. Britta Jensen for her continued support, patience, and invaluable advice throughout the past few years. Britta's refined balance between guidance and hands-off management has empowered me to think critically and navigate my own research. Her passion for tephrochronology has inspired and motivated me through every conversation we have, and I am eternally grateful for receiving this opportunity.

I would also like to thank the many mentors and professors at the University of Alberta: Dr. Duane Froese and Dr. Alberto Reyes, who have provided guidance since my first years as an undergrad student, Dr. Lauren Davies for teaching me the art of cryptotephra processing, Dr. Andrew Locock for his assistance and advice on the electron microprobe, Dr. Alistair Monteath for providing support and advice in the lab, and many others in the Earth & Atmospheric Science department. Thanks to Joel Pumple, Shaun Woudstra, and Scott Cocker for assisting with core subsampling and processing. A special thanks to Dr. Takehiko Suzuki, MITACS, and the Japan Society for the Promotion of Science for the opportunity to extend my research to the Tokyo Metropolitan Area, and to Rupertsland Institute for their support to help me achieve my goals.

Last but definitely not least, I would like to thank my parents, Chuck and Sharon, and my incredible partner Chanel for their patience and understanding throughout my academic career. Through the many late nights writing or counting slides on a microscope, my family, colleagues, and friends have been there to support me every step of the way.

Table of Contents

List of Tables

List of Figures

Chapter 1. Introduction

Tephrochronology, or the study of volcanic ash (tephra), plays a significant role in a number of fields including volcanology, archeology, paleoclimatology, hazard assessment, and Quaternary stratigraphy and chronology (e.g., Beaudoin et al., 1996; Beierle and Smith, 1998; Connor et al., 2001; Lowe, 2011; Lowe et al., 2012; Narcisi et al., 2019; Plunkett et al., 2020). Traditionally, tephrochronology refers largely to the use of tephra beds as chronostratigraphic markers to date and correlate sedimentary sequences between sites. Each tephra is deposited across hundreds to thousands of kilometres in a period of days to weeks, representing a near-instantaneous event on the geologic time scale. In addition, each tephra is uniquely identifiable by its geochemical composition through the use of Fe-Ti oxides in ilmenites (e.g., Lerbekmo, 1975; Preece et al., 2014) or analyses of glass shards through major, minor, or trace elements (e.g., Westgate and Gorton, 1981; Lowe et al., 2017). These qualities, along with stratigraphy, morphological characteristics of glass shards (e.g., McLean et al., 2018; Jensen et al., 2019), mineralogy, and other methods of characterization can be collectively used to identify the ash layer, correlate it to its specific eruption, and apply the correlated tephra's relative age as an isochron. When done correctly, precise chronologies of paleoenvironmental records or sedimentary sequences are produced using this reliable and effective method (e.g., Lowe, 2011; Lowe and Alloway, 2015).

In North America, tephra research has been widely used to develop both eruption histories and Quaternary stratigraphy for over 60 years (e.g., Stuiver et al., 1964; Westgate and Dreimanis, 1967; Sarna-Wojcicki et al., 1987; Mullineaux, 1996; Lakeman et al., 2008; Jensen et al., 2013). Early mapping of Quaternary deposits in interior Yukon and Alaska recognized numerous significant visible tephra from Wrangell and Aleutian Arc- Alaska Peninsula volcanoes that were stratigraphically significant (e.g., Péwé, 1952, 1975). Developments in the ability to geochemically characterize tephra, such as individual glass shard geochemistry through electron microprobe analyses (Smith and Westgate, 1968), led to an explosion of research in the region, led by John Westgate in the early 1980's and continuing to today (e.g., Westgate et al., 1983, 1990; Preece et al., 1999, 2000, 2011, 2014; Froese et al., 2002; Jensen et al., 2008, 2011, 2013). This resulted in a well-established tephrostratigraphy in the Yukon and Alaska, although largely for the early to late Pleistocene. In contrast, the last ~30,000 years features fewer visible and less characterized tephra beds in the interior of Alaska and Yukon (e.g., Davies et al., 2016); in the Yukon this is limited to the bilobate White River Ash (e.g., Lerbekmo et al., 1975). However, the Aleutian-Arc Alaska Peninsula volcanoes have been active throughout this time, and recent studies have suggested that numerous Holocene eruptions may be preserved in the area as non-visible deposits – i.e., cryptotephra (e.g., Monteath et al., 2017; Davies, 2018, in review).

The emergence of cryptotephra research in the 1990s (e.g., Dugmore, 1989; Pilcher and Hall, 1992) once again expanded the geographic extent of tephrochronology, allowing identification of cryptotephra deposits thousands of kilometres from their source volcano and enabling the correlation of sites across continents (e.g., Pyne-O'Donnell et al., 2012; Jensen et al., 2014; van der Bilt et al., 2017; Plunkett and Pilcher, 2018). However, at these distances, the low concentrations of glass shards (as low as a few shards per gram of sediment) require a time-consuming and careful sample preparation to accurately identify shard peaks within stratigraphic sections. Cryptotephra methodologies involve multiple phases, including extracting glass shards from surrounding sediment through sieving and heavy liquid separation, mounting the glass shards for counting to locate the deposits, and preparing the higher peaks of shard concentrations for geochemical analyses (Davies, 2015). Each phase increases the potential to lose glass shards or damage the glass through geochemical alteration if the inappropriate techniques have been applied or are incorrectly followed. Therefore, it is essential to establish a consistent methodological procedure for cryptotephra analysis to produce high quality and reliable data that allow for a confident inter-laboratory comparison of geochemical results. Although discussed broadly through the literature (e.g., Turney et al., 1997; Dugmore et al., 1992; Blockley et al., 2005: Swindles et al., 2010; Davies 2015; Lane et al., 2017), there is no one source that provides a thorough assessment and description of all the steps involved in the identification and analyses of cryptotephra, and there is still significant debate about the inclusion of some procedures (e.g., Blockley et al., 2005; Roland et al., 2015; Monteath et al., 2019; Cooper et al., 2019).

This thesis aims to review and describe the various methods required for cryptotephra research, combine them into a single comprehensive protocol, and apply these techniques to four lakes to determine the effectiveness and limitations of cryptotephra work in sub-Arctic lacustrine sites in the Yukon. The following two sections provide context for the main chapters within this thesis. The first section consists of a brief overview of cryptotephra methodology and the necessity for a detailed cryptotephra protocol, followed by a section reviewing historical research on visible and non-visible tephra deposits in the Yukon and Alaska area.

1.1. Cryptotephra Methodology

The field of cryptotephra has seen rapid advancements in processing and analytical techniques over the last few decades, improving the detection of glass shards and pushing the geographic boundaries of tephrochronology (Davies, 2015). Cryptotephra methods involve the initial processing and extraction of glass shards from their surrounding sediment through the following techniques: acid digestion of peats (e.g., Dugmore et al., 1992), ashing of sediments (e.g., Heiri et al., 2001; Payne and Blackford, 2008), sieving, and density separation to isolate glass (e.g., Turney et al., 1997; Blockley et al., 2005). Once glass shards are isolated, samples are mounted to slides and counted on a microscope to create a shard concentration profile. Depths containing higher concentrations of glass shards can then be re-processed and mounted for geochemical identification where a potential tephra correlation can be made. Although technological advancements have improved the efficiency of data interpretation in tephrochronology (e.g., Bolton et al., 2020), the initial processing and extraction techniques of cryptotephra require large amounts of lab work and are not easily avoided. While alternative techniques of tephra detection, such as computed tomography scanning (e.g., van der bilt et al., 2020), magnetic susceptibility (e.g., Peters et al., 2010; McCanta et al., 2015; Di Roberto et al., 2018), or X-ray fluorescence (e.g., Kylander et al., 2011; Balascio et al., 2015) have successfully identified visible tephra deposits, low concentration cryptotephra deposits are too small to be consistently detected. Ultimately, the conventional methods of cryptotephra extraction and detection by microscope examination remain the most reliable approach for low concentration cryptotephra work.

Modifications and adaptations of conventional cryptotephra methods have taken place since the emergence of the methods by Dugmore et al. (1989). This has resulted in inconsistent methodologies and conflicting opinions on the proper applications of each method. For example, the standard practice of acid digestion to break down organic material in peats or organic-rich sediments (Dugmore et al., 1992) has been argued to cause geochemical alteration of glass shards, resulting in inaccurate geochemical compositions when analyzed (Blockley et al., 2005; Roland et al., 2015; Monteath et al., 2019; Cooper et al., 2019). Incorrect use of methods can lead to the loss or alteration of glass shards and potentially waste valuable material. In addition, the characteristics of each site are important to consider prior to processing, as peat sites will require different methods than sediment-rich lakes. A detailed examination and protocol of cryptotephra methodology would be a valuable addition to the field of tephrochronology, as it would provide a consistent guide through the processing, mounting, and analysis stages of cryptotephra research, and suggest appropriate methods depending on a site's characteristics. There is no current protocol in cryptotephra that combines all these qualities, but I have developed one here that is presented in Chapter two.

1.2. Yukon Holocene Tephra

As previously mentioned, most research in the interior of Yukon and Alaska has been on early to late Pleistocene visible tephra deposits (e.g., Péwé, 1975; Naeser et al., 1982; Westgate et al. 1990; Preece et al., 1999, 2011; Jensen et al., 2008, 2013). Early to late Holocene records have been studied, but these records are typically examinations of proximal deposits directly surrounding the volcanoes (e.g., Begét and Nye, 1994; Waitt and Begét, 2009; Schiff et al., 2010), or the immediate surrounding region (e.g., Begét et al., 1994, de Fontaine et al., 2007; Fierstein and Hildreth, 2008). Unfortunately, many of these studies do not report any glass geochemical data, and those that do often only report averages and standard deviations or a limited amount of data points, which are of limited use for comparison (e.g., Begét et al., 1994; Riehle et al., 1990; Waitt and Begét, 2009). In the Yukon, the only visible tephra deposits are the White River Ash from Mount Churchill, comprised of the ~1097 cal BP eastern lobe and ~1625 cal BP northern lobe (Lerbekmo et al., 1975; Jensen et al., 2014; Toohey and Sigl, 2017; Reuther et al., 2020). However, the volcanoes of the Aleutian-Arc Alaska Peninsula were active throughout the Holocene and would have deposited many tephras as non-visible deposits in the Yukon region. Specifically, there are well-documented tephra such as Fisher-Funk from the early Holocene (e.g., Carson et al., 2002), the Jarvis Ash and Aniakchak CFE II from the middle Holocene (e.g., Kaufman et al. 2012; Beget et al., 1991), multiple Augustine volcano eruptions (e.g., G, C, I; Waitt and Begét, 2009) through late Holocene, and historic eruptions like Novarupta-Katmai 1912 (e.g., Hildreth, 1983; Hildreth and Fierstein, 2000) that may be present beyond their visible mapped limits. The development of cryptotephra research has created an opportunity to further explore the late to early Pleistocene tephra records of Yukon and interior Alaska, where additional tephra deposits would be of great benefit. However, cryptotephra research in the Yukon and Alaska is sparse (e.g., Payne et al., 2008; Monteath et al., 2017), with only one record from the central Yukon from a peatland by Davies (2018). The results of this study show numerous cryptotephra deposits in Yukon – reinforcing the potential in the region – but the sheer number of deposits in parts of the record also reveal some challenges in interpretation.

Lake sediments in the Yukon are the source of many valuable paleoenvironmental reconstructions of the Pleistocene and Holocene (e.g., Cwynar, 1982; Kaufman et al., 2004; Kurek et al., 2009; Schweger et al., 2011). However, they often suffer from inaccurate radiocarbon chronologies caused by preserved old carbon reintroduced into younger sediment, and a lack of terrestrial organic material (e.g., Cwynar, 1982; Nelson et al., 1988; Kaufman et al., 2004; Oswald et al., 2005). Additional chronologic tools are necessary and cryptotephra are one of the few alternative options to refine their chronologies. However, to date, no Yukon lakes have been examined to explore the applicability of cryptotephra to dating these lacustrine deposits. In Chapter three I address this research problem by examining four lake records in the Yukon.

1.3. Objectives and Chapter Summaries

The previous sections have summarized the evolution of cryptotephra methodology and reviewed the past research on visible and non-visible tephra research in Yukon. Through this examination, I have highlighted areas where contributions can be made to the field of tephrochronology, and those contributions were used to develop my thesis. Chapter two provides a detailed review and assessment of the various processing methods used in cryptotephra research and provides a detailed workflow to guide researchers on best practices to ensure quality data. Chapter three examines four Yukon lakes to refine their chronologies and explore the potential for using cryptotephra to develop their age models. Chapter four summarizes the results of the thesis and describes future research opportunities related to the thesis topic.

The following is a more detailed summary of the specific objectives I achieve in the following thesis:

1. Review, critically assess and summarize the processing and extraction techniques in cryptotephra research, focusing on peat and lake cores.

2. Highlight the factors that will influence which techniques should be applied to a sample and provide an easy to follow workflow for a given sample.

3. Integrate and modify literature and internal laboratory protocols to outline best practices in tephra identification, mounting for tephra counts and analyses, and interpretation of shard concentration profiles.

4. Report in detail, for the first time, the use of time-dependent intensity corrections, secondary standards, and 5µm beam diameters for EPMA analysis on cryptotephra.

5. Use this systematic approach to examine cryptotephra deposits in sediments from four Yukon lakes to refine/built their age models and help develop the limited late Pleistocene to Holocene tephrostratigraphic framework for the region.

6. Report and suggest approaches to minimize the limitations and challenges associated with cryptotephra research on lakes in this region.

1.4. References

Balascio, N.L., Francus, P., Bradley, R.S., Schupack, B.B., Miller, G.H., Kvisvik, B.C., Bakke, J., Thordarson, T., 2015. Investigating the use of scanning x-ray fluorescence to locate cryptotephra in minerogenic lacustrine sediment: experimental results, in Micro-XRF Studies of Sediment Cores. Springer 17, 305-324.

Beaudoin, A.B., Wright, M., Ronaghan, B., 1996. Late quaternary landscape history and archaeology in the 'Ice-Free Corridor': Some recent results from Alberta. Quaternary International 32, 113-126.

Begét, J.E., Reger, R.D., Pinney, D., Gillispie, T., Campbell, K., 1991. Correlation of the Holocene Jarvis Creek, Tangle Lakes, Cantwell, and Hayes Tephras in South-Central and Central Alaska. Quatern. Res. 35, 174-189.

Begét, J.E., Nye, C.J., 1994. Postglacial eruption history of Redoubt Volcano, Alaska. J. Volcanol. Geotherm. Res. 62, 31-54.

Begét, J.E., Stihler, S.D., Stone, D.B., 1994. A 500-year-long record of tephra falls from Redoubt Volcano and other volcanoes in upper Cook Inlet, Alaska. J. Volcanol. Geotherm. Res. 62, 55-67.

Beierle, B., Smith, D.G., 1998. Severe drought in the early Holocene (10,000–6800 BP) interpreted from lake sediment cores, southwestern Alberta, Canada. Palaeogeogr. , Palaeoclimatol. , Palaeoecol. 140, 75-83.

Blockley, S.P.E., Pyne-O'Donnell, S.D.F., Lowe, J.J., Matthews, I.P., Stone, A., Pollard, A.M., Turney, C.S.M., Molyneux, E.G., 2005. A new and less destructive laboratory procedure for the physical separation of distal glass tephra shards from sediments. Quaternary Science Reviews 24, 1952-1960.

Bolton, M.S., Jensen, B.J., Wallace, K., Praet, N., Fortin, D., Kaufman, D., De Batist, M., 2020. Machine learning classifiers for attributing tephra to source volcanoes: an evaluation of methods for Alaska tephras. Journal of Quaternary Science 35, 81-92.

Carson, E.C., Fournelle, J.H., Miller, T.P. and Mickelson, D.M., 2002. Holocene tephrochronology of the Cold Bay area, southwest Alaska Peninsula. Quaternary Science Reviews, 21, 2213-2228.

Connor, C.B., Hill, B.E., Brandi, W., Franklin, N.M., Femina, P.C., 2001. Estimation of Volcanic Hazards from Tephra Fallout. Nat. Hazards Rev. 2, 33-42.

Cooper, C.L., Savov, I.P., Swindles, G.T., 2019. Standard chemical-based tephra extraction methods significantly alter the geochemistry of volcanic glass shards. J. Quaternary Sci 34, 697-707.

Cwynar, L.C., 1982. A Late-Quaternary Vegetation History from Hanging Lake, Northern Yukon. Ecol. Monogr. 52, 1-24.

Davies, L.J., 2018. The development of a Holocene cryptotephra framework in northwestern North America (Doctoral dissertation). University of Alberta, Edmonton, AB. https://doi.org/10.7939/R3HX1660C

Davies, L.J., Appleby, P., Jensen, B.J.L., Magnan, G., Mullan-Boudreau, G., Noernberg, T., Shannon, B., Shotyk, W., van Bellen, S., Zaccone, C., Froese, D.G., 2018. High-resolution age modelling of peat bogs from northern Alberta, Canada, using pre- and post-bomb 14C, 210Pb and historical cryptotephra. Quaternary Geochronology 47, 138-162.

Davies, L. J., Jensen, B. J. L., Kaufman, D. S. Late Holocene cryptotephra from Cascade Lake, Alaska: supporting data for a 21,000-year multi-chronometer Bayesian age model, Geochronology Discussions [preprint], https://doi.org/10.5194/gchron-2021-18, in review, 2021.

Davies, S.M., 2015. Cryptotephras: the revolution in correlation and precision dating. J. Quaternary Sci. 30, 114-130.

Davies, L.J., Jensen, B.J., Froese, D.G., Wallace, K.L., 2016. Late Pleistocene and Holocene tephrostratigraphy of interior Alaska and Yukon: Key beds and chronologies over the past 30,000 years. Quaternary Science Reviews 146, 28-53.

de Fontaine, C.S., Kaufman, D.S., Scott Anderson, R., Werner, A., Waythomas, C.F., Brown, T.A., 2007. Late Quaternary distal tephra-fall deposits in lacustrine sediments, Kenai Peninsula, Alaska. Quatern. Res. 68, 64-78.

Di Roberto, A., Smedile, A., Del Carlo, P., De Martini, P.M., Iorio, M., Petrelli, M., Pantosti, D., Pinzi, S., Todrani, A., 2018. Tephra and cryptotephra in a ~60,000-year-old lacustrine sequence from the Fucino Basin: new insights into the major explosive events in Italy. Bulletin of Volcanology 80, 20.

Dugmore, A., 1989. Icelandic volcanic ash in Scotland. Scottish Geographical Magazine, 105:3, 168-172.

Dugmore, A.J., Newton, A.J., Sugden, D.E., Larsen, G., 1992. Geochemical stability of fine-grained silicic Holocene tephra in Iceland and Scotland. J. Quaternary Sci. 7, 173-183.

Fierstein, J., Hildreth, W., 2008. Kaguyak dome field and its Holocene caldera, Alaska Peninsula. J. Volcanol. Geotherm. Res. 177, 340-366.

Froese, D., Westgate, J., Preece, S., Storer, J., 2002. Age and significance of the Late Pleistocene Dawson tephra in eastern Beringia. Quaternary Science Reviews 21, 2137-2142.

Heiri, O., Lotter, A.F., Lemcke, G., 2001. Loss on ignition as a method for estimating organic and carbonate content in sediments: reproducibility and comparability of results. J. Paleolimnol. 25, 101-110.

Hildreth, W., 1983. The compositionally zoned eruption of 1912 in the valley of ten thousand smokes, Katmai National Park, Alaska. J. Volcanol. Geotherm. Res. 18, 1-56.

Hildreth, W., Fierstein, J., 2000. Katmai volcanic cluster and the great eruption of 1912. Geological Society of America Bulletin 112, 1594-1620.

Jensen, B.J.L., Froese, D.G., Preece, S.J., Westgate, J.A., Stachel, T., 2008. An extensive middle to late Pleistocene tephrochronologic record from east-central Alaska. Quaternary Science Reviews 27, 411-427.

Jensen, B.J.L., Preece, S.J., Lamothe, M., Pearce, N.J.G., Froese, D.G., Westgate, J.A., Schaefer, J., Begét, J., 2011. The variegated (VT) tephra: A new regional marker for middle to late marine isotope stage 5 across Yukon and Alaska. Quaternary International 246, 312-323.

Jensen, B.J.L., Reyes, A.V., Froese, D.G., Stone, D.B., 2013. The Palisades is a key reference site for the middle Pleistocene of eastern Beringia: new evidence from paleomagnetics and regional tephrostratigraphy. Quaternary Science Reviews 63, 91-108.

Jensen, B.J.L., Pyne-O'Donnell, S., Plunkett, G., Froese, D.G., Hughes, P.D.M., Sigl, M., McConnell, J.R., Amesbury, M.J., Blackwell, P.G., van den Bogaard, C., Buck, C.E., Charman, D.J., Clague, J.J., Hall, V.A., Koch, J., Mackay, H., Mallon, G., McColl, L., Pilcher, J.R., 2014. Transatlantic distribution of the Alaskan White River Ash. Geology 42, 875-878.

Jensen, B.J.L., Beaudoin, A.B., Clynne, M.A., Harvey, J., Vallance, J.W., 2019. A re-examination of the three most prominent Holocene tephra deposits in western Canada: Bridge River, Mount St. Helens Yn and Mazama. Quaternary International 500, 83-95.

Kaufman, D.S., Ager, T.A., Anderson, N.J., Anderson, P.M., Andrews, J.T., Bartlein, P.J., Brubaker, L.B., Coats, L.L., Cwynar, L.C., Duvall, M.L., Dyke, A.S., Edwards, M.E., Eisner, W.R., Gajewski, K., Geirsdóttir, A., Hu, F.S., Jennings, A.E., Kaplan, M.R., Kerwin, M.W., Lozhkin, A.V., MacDonald, G.M., Miller, G.H., Mock, C.J., Oswald, W.W., Otto-Bliesner, B.L., Porinchu, D.F., Rühland, K., Smol, J.P., Steig, E.J., Wolfe, B.B., 2004. Holocene thermal maximum in the western Arctic (0–180°W). Quaternary Science Reviews 23, 529-560.

Kaufman, D.S., Jensen, B.J.L., Reyes, A.V., Schiff, C.J., Froese, D.G., Pearce, N.J.G., 2012. Late Quaternary tephrostratigraphy, Ahklun Mountains, SW Alaska. J. Quaternary Sci. 27, 344-359.

Kurek, J., Cwynar, L.C., Vermaire, J.C., 2009. A late Quaternary paleotemperature record from Hanging Lake, northern Yukon Territory, eastern Beringia. Quatern. Res. 72, 246-257.

Kylander, M.E., Lind, E.M., Wastegård, S., Löwemark, L., 2012. Recommendations for using XRF core scanning as a tool in tephrochronology. The Holocene 22, 371-375.

Lakeman, T.R., Clague, J.J., Menounos, B., Osborn, G.D., Jensen, B.J.L., Froese, D.G., 2008. Holocene tephras in lake cores from northern British Columbia, Canada. Can. J. Earth Sci. 45, 935–947.

Lane, C.S., Lowe, D.J., Blockley, S.P.E., Suzuki, T., Smith, V.C., 2017. Advancing tephrochronology as a global dating tool: Applications in volcanology, archaeology, and palaeoclimatic research. Quaternary Geochronology 40, 1-7.

Lerbekmo, J.F., Westgate, J.A., Smith, D.G.W., Denton, G.H., 1975. New data on the character and history of the White River volcanic eruption, Alaska, in: Suggate, R.P., Cresswell, M.M., (Eds.), Quaternary studies. Wellington, Royal Society of New Zealand, 203–209.

Lowe, D.J., 2011. Tephrochronology and its application: A review. Quaternary Geochronology 6, 107-153.

Lowe, D.J., Alloway, B., 2015. Tephrochronology. Encyclopedia of Scientific Dating Methods, 783-799.

Lowe, J., Barton, N., Blockley, S., Ramsey, C.B., Cullen, V.L., Davies, W., Gamble, C., Grant, K., Hardiman, M., Housley, R., Lane, C.S., Lee, S., Lewis, M., MacLeod, A., Menzies, M., Müller, W., Pollard, M., Price, C., Roberts, A.P., Rohling, E.J., Satow, C., Smith, V.C., Stringer, C.B., Tomlinson, E.L., White, D., Albert, P., Arienzo, I., Barker, G., Borić, D., Carandente, A., Civetta, L., Ferrier, C., Guadelli, J., Karkanas, P., Koumouzelis, M., Müller, U.C., Orsi, G., Pross, J., Rosi, M., Shalamanov-Korobar, L., Sirakov, N., Tzedakis, P.C., 2012. Volcanic ash layers illuminate the resilience of Neanderthals and early modern humans to natural hazards. Proc. Natl. Acad. Sci. USA 109, 13532-13537.

Lowe, D.J., Pearce, N.J.G., Jorgensen, M.A., Kuehn, S.C., Tryon, C.A., Hayward, C.L., 2017. Correlating tephras and cryptotephras using glass compositional analyses and numerical and statistical methods: Review and evaluation. Quaternary Science Reviews 175, 1-44.

McCanta, M.C., Hatfield, R.G., Thomson, B.J., Hook, S.J., Fisher, E., 2015. Identifying cryptotephra units using correlated rapid, nondestructive methods: VSWIR spectroscopy, X-ray fluorescence, and magnetic susceptibility. Geochem. Geophys. Geosyst. 16, 4029-4056.

McLean, D., Albert, P.G., Nakagawa, T., Suzuki, T., Staff, R.A., Yamada, K., Kitaba, I., Haraguchi, T., Kitagawa, J., Smith, V.C., 2018. Integrating the Holocene tephrostratigraphy for East Asia using a high-resolution cryptotephra study from Lake Suigetsu (SG14 core), central Japan. Quaternary Science Reviews 183, 36-58.

Monteath, A.J., van Hardenbroek, M., Davies, L.J., Froese, D.G., Langdon, P.G., Xu, X., Edwards, M.E., 2017. Chronology and glass chemistry of tephra and cryptotephra horizons from lake sediments in northern Alaska, USA. Quatern. Res. 88, 169-178.

Monteath, A.J., Teuten, A.E., Hughes, P.D.M., Wastegård, S., 2019. Effects of the peat acid digestion protocol on geochemically and morphologically diverse tephra deposits. J. Quaternary Sci. 34, 269-274.

Mullineaux, D.R., 1996. Pre-1980 tephra-fall deposits erupted from Mount St. Helens, Washington. Professional Paper, U.S. Geological Survey.

Naeser, N.D., Westgate, J.A., Hughes, O.L., Péwé, T.L., 1982. Fission-track ages of late Cenozoic distal tephra beds in the Yukon Territory and Alaska. Canadian Journal of Earth Sciences 19, 2167-2178.

Narcisi, B., Petit, J.R., Delmonte, B., Batanova, V. and Savarino, J., 2019. Multiple sources for tephra from AD 1259 volcanic signal in Antarctic ice cores. Quaternary Science Reviews, 210, 164-174.

Nelson, R.E., Carter, L.D., Robinson, S.W., 1988. Anomalous radiocarbon ages from a Holocene detrital organic lens in Alaska and their implications for radiocarbon dating and paleoenvironmental reconstructions in the Arctic. Quatern. Res. 29, 66-71.

Oswald, W.W., Anderson, P.M., Brown, T.A., Brubaker, L.B., Hu, F.S., Lozhkin, A.V., Tinner, W., Kaltenrieder, P., 2005. Effects of sample mass and macrofossil type on radiocarbon dating of arctic and boreal lake sediments. The Holocene 15, 758-767.

Payne, R.J., Blackford, J.J., 2008. Extending the Late Holocene Tephrochronology of the Central Kenai Peninsula, Alaska. Arctic 61, 243-254.

Payne, R., Blackford, J., van der Plicht, J., 2008. Using cryptotephras to extend regional tephrochronologies: An example from southeast Alaska and implications for hazard assessment. Quatern. Res. 69, 42-55.

Peters, C., Austin, W.E.N., Walden, J., Hibbert, F.D., 2010. Magnetic characterisation and correlation of a Younger Dryas tephra in North Atlantic marine sediments. J. Quaternary Sci. 25, 339-347.

Péwé, T.L., 1953. Geomorphology of the Fairbanks area, Alaska. ProQuest Dissertations and Theses.

Péwé, T.L., 1975. Quaternary Geology of Alaska. US Government Printing Office.

Pilcher, J.R., Hall, V.A., 1992. Towards a tephrochronology for the Holocene of the north of Ireland. The Holocene 2, 255-259.

Plunkett, G., Pilcher, J.R., 2018. Defining the potential source region of volcanic ash in northwest Europe during the Mid-to Late Holocene. Earth-Sci. Rev. 179, 20-37.

Plunkett, G., Sigl, M., Pilcher, J.R., McConnell, J.R., Chellman, N., Steffensen, J.P. and Büntgen, U., 2020. Smoking guns and volcanic ash: the importance of sparse tephras in Greenland ice cores. Polar research, 39.

Preece, S.J., Westgate, J.A., Stemper, B.A., Péwé, T.L., 1999. Tephrochronology of late Cenozoic loess at Fairbanks, central Alaska. gsabulletin 111, 71-90.

Preece, S.J., Westgate, J.A., Alloway, B.V., Milner, M.W., 2000. Characterization, identity, distribution, and source of late Cenozoic tephra beds in the Klondike district of the Yukon, Canada. Can. J. Earth Sci. 37, 983-996.

Preece, S.J., Pearce, N.J.G., Westgate, J.A., Froese, D.G., Jensen, B.J.L., Perkins, W.T., 2011. Old Crow tephra across eastern Beringia: a single cataclysmic eruption at the close of Marine Isotope Stage 6. Quaternary Science Reviews 30, 2069-2090.

Preece, S.J., McGimsey, R.G., Westgate, J.A., Pearce, N.J.G., Hart, W.K., Perkins, W.T., 2014. Chemical complexity and source of the White River Ash, Alaska and Yukon. geosphere 10, 1020-1042.

Pyne-O'Donnell, S.D.F., Hughes, P.D.M., Froese, D.G., Jensen, B.J.L., Kuehn, S.C., Mallon, G., Amesbury, M.J., Charman, D.J., Daley, T.J., Loader, N.J., Mauquoy, D., Street-Perrott, F.A., Woodman-Ralph, J., 2012. High-precision ultra-distal Holocene tephrochronology in North America. Quaternary Science Reviews 52, 6-11.

Reuther, J., Potter, B., Coffman, S., Smith, H., Bigelow, N., 2020. Revisiting the timing of the Northern lobe of the white river ash volcanic event in Eastern Alaska and Western Yukon. Radiocarbon 62, 169-188.

Riehle, J.R., Bowers, P.M., Ager, T.A., 1990. The Hayes tephra deposits, and upper Holocene marker horizon in south-central Alaska. Quatern. Res. 33, 276-290.

Roland, T.P., Mackay, H., Hughes, P.D.M., 2015. Tephra analysis in ombrotrophic peatlands: A geochemical comparison of acid digestion and density separation techniques. J. Quaternary Sci. 30, 3-8.

Sarna-Wojcicki, A.M., Morrison, S.D., Meyer, C.E., Hillhouse, J.W., 1987. Correlation of upper Cenozoic tephra layers between sediments of the western United States and eastern Pacific Ocean and comparison with biostratigraphic and magnetostratigraphic age data. Geological Society of America Bulletin 98, 207–223.

Schiff, C.J., Kaufman, D.S., Wallace, K.L., Ketterer, M.E., 2010. An improved proximal tephrochronology for Redoubt Volcano, Alaska. Journal of Volcanology and Geothermal Research 193, 203–214.

Schweger, C., Froese, D., White, J.M., Westgate, J.A., 2011. Pre-glacial and interglacial pollen records over the last 3 Ma from northwest Canada: Why do Holocene forests differ from those of previous interglaciations? Quaternary Science Reviews 30, 2124-2133.

Smith, D.G.W., Westgate, J.A., 1968. Electron probe technique for characterising pyroclastic deposits. Earth Planet. Sci. Lett. 5, 313-319.

Stuiver, M., Borns, H.W., Denton, G.H., 1964. Age of a widespread layer of volcanic ash in the southwestern Yukon Territory. Arctic 17, 259-261.

Swindles, G.T., De Vleeschouwer, F., Plunkett, G., 2010. Dating peat profiles using tephra: stratigraphy, geochemistry and chronology. Mires and Peat 7.

Toohey, M., Sigl, M., 2017. Volcanic stratospheric sulfur injections and aerosol optical depth from 500 BCE to 1900 CE. Earth System Science Data 9, 809-831.

Turney, C.S.M., Harkness, D.D., Lowe, J.J., 1997. The use of microtephra horizons to correlate Late-glacial lake sediment successions in Scotland. J. Quaternary Sci. 12, 525-531.

van der Bilt, Willem GM, Lane, C.S., Bakke, J., 2017. Ultra-distal Kamchatkan ash on Arctic Svalbard: towards hemispheric cryptotephra correlation. Quaternary Science Reviews 164, 230-235.

van der Bilt, Willem GM, Cederstrøm, J.M., Støren, E.W., Berben, S.M., Rutledal, S., 2020. Rapid tephra identification in geological archives with Computed Tomography (CT): experimental results and natural applications. Frontiers in Earth Science 8, 710.

Waitt, R.B., Begét, J.E., 2009. Volcanic Processes and Geology of Augustine Volcano, Alaska. US Geological Survey.

Westgate J.A., Dreimanis A. 1967. Volcanic ash layers of recent age at Banff National Park, Alberta, Canada. Canadian Journal of Earth Sciences 4,155-61.

Westgate, J.A., Gorton, M.P., 1981. Correlation Techniques in Tephra Studies, 73-94. In: Self S., Sparks R.S.J. (eds) Tephra Studies. NATO Advanced Study Institutes Series (Series C — Mathematical and Physical Sciences), vol 75. Springer, Dordrecht. https://doi.org/10.1007/978-94-009-8537-7_5

Westgate, J.A., Hamilton, T.D., Gorton, M.P., 1983. Old Crow tephra: A new late Pleistocene stratigraphic marker across north-central Alaska and western Yukon Territory. Quatern. Res. 19, 38-54.

Westgate, J.A., Stemper, B.A., Péwé, T.L., 1990. A 3 my record of Pliocene-Pleistocene loess in interior Alaska. Geology 18(9), 858-861.

Chapter 2. Evaluation of processing techniques applied to cryptotephra deposits in sedimentary and peat environments

2.1. Introduction

There has been an increasing emphasis on the development and refinement of tephra processing and analytical methods in the past few decades. The main goal of this work is to expand the geographic applicability of the field, making it increasingly possible to recover reliable and reproducible data from the most difficult to analyze distal visible and non-visible volcanic ash deposits. The history, development and theory behind tephrochronology is well documented with several authors offering broad general syntheses of processing and analytical approaches that are common practice in tephra research (e.g., Lowe, 2011; Davies, 2015; Lane et al., 2014, 2017; Pearce et al., 2014; Lowe et al., 2017; Abbott et al., 2020). In particular, the study of tephra deposits not visible to the naked eye (cryptotephra) has seen explosive growth with the development and/or modification of methods such as heavy liquid density separation to isolate glass (e.g., Turney et al., 1997; Blockley et al., 2005), acid digestion to remove organic material (e.g., Dugmore et al., 1992), ashing of sediments (e.g., Heiri et al., 2001; Payne and Blackford, 2008), and general mounting and analytical procedures for glass shards (e.g., Froggart, 1992; Pearce et al., 1999; Pearce et al., 2007; Jensen et al., 2008; Kuehn and Froese, 2010; Kuehn et al., 2011; Hayward, 2012; Hall and Hayward, 2014; Iverson et al., 2017). Improved processing and analytical techniques have made it possible to increase the detection and recovery of glass shards and produce consistent geochemical data for low-concentration and very fine-grained tephra deposits. In turn, tephrostratigraphic frameworks are now covering much greater geographic regions as progressively more distal study sites are explored for cryptotephra, while older regions are re-examined using new methods.

Although several methodological focused publications exist (e.g., Blockley et al., 2005; Swindles et al., 2010), including a broad summary on various cryptotephra methods (Davies, 2015), there is no existing overview that compiles them into a comprehensive protocol. As cryptotephra research has expanded, questions have been raised about some approaches, while others have been modified or changed to make them more applicable to different settings. For example, the potential to cause geochemical alteration of glass through acid digestion has led to disagreements in the inclusion of this process during while extracting cryptotephra for geochemical analyses (Dugmore et al., 1992; Blockley et al., 2005; Roland et al., 2015; Monteath et al., 2019a; Cooper et al., 2019). Environmental and geochemical characteristics of the sample site and tephra themselves are also crucial when determining how to approach a study, as some techniques are only suitable for a specific environment or specific type of tephra sample. Application of unsuitable methodological steps while conducting cryptotephra can be very disadvantageous for a project, as it may result in the loss of valuable material or the inability to extract the tephra shards from the sample (e.g., Stanton et al., 2010).

Here we present a comprehensive examination and overview of the various methods used in processing of cryptotephra. The paper will focus on samples in lake sediment and peat, provide a detailed synthesis of each step, examine some of the main challenges and problems, and offer solutions that are most suitable for a deposit to obtain the best results. The goal of the paper is to provide a consistent framework for cryptotephra processes to minimize the risk of geochemical alterations and inter-laboratory inconsistencies in data, and act as a guide for new cryptotephra researchers who may not have a full understanding of the various techniques.

2.2. Site and Sample Considerations

The physical and ecological characteristics of a site will influence how a lake/bog should be selected and processed for cryptotephra analyses. Careful selection of methods based on site and sample characteristics can increase the recovery of glass shards and optimize processing times. The delicate nature and low concentrations of glass shards in many cryptotephra samples requires an initial assessment to map out the processing steps. Each additional step applied to the sample will increase the handling time and probability of losing tephra grains. For cryptotephra specific studies, the assessment should start with the initial site selection. The complexity of cryptotephra deposition and effects on shard profiles by site and sample characteristics have been widely examined (e.g., Payne et al., 2005; Davies et al., 2007, Pyne-O'Donnell, 2011; Davies, 2015; Watson et al., 2015, 2016: McLean et al., 2018). Here we briefly summarize some of the considerations of these authors and how they can affect the workflow of cryptotephra research.

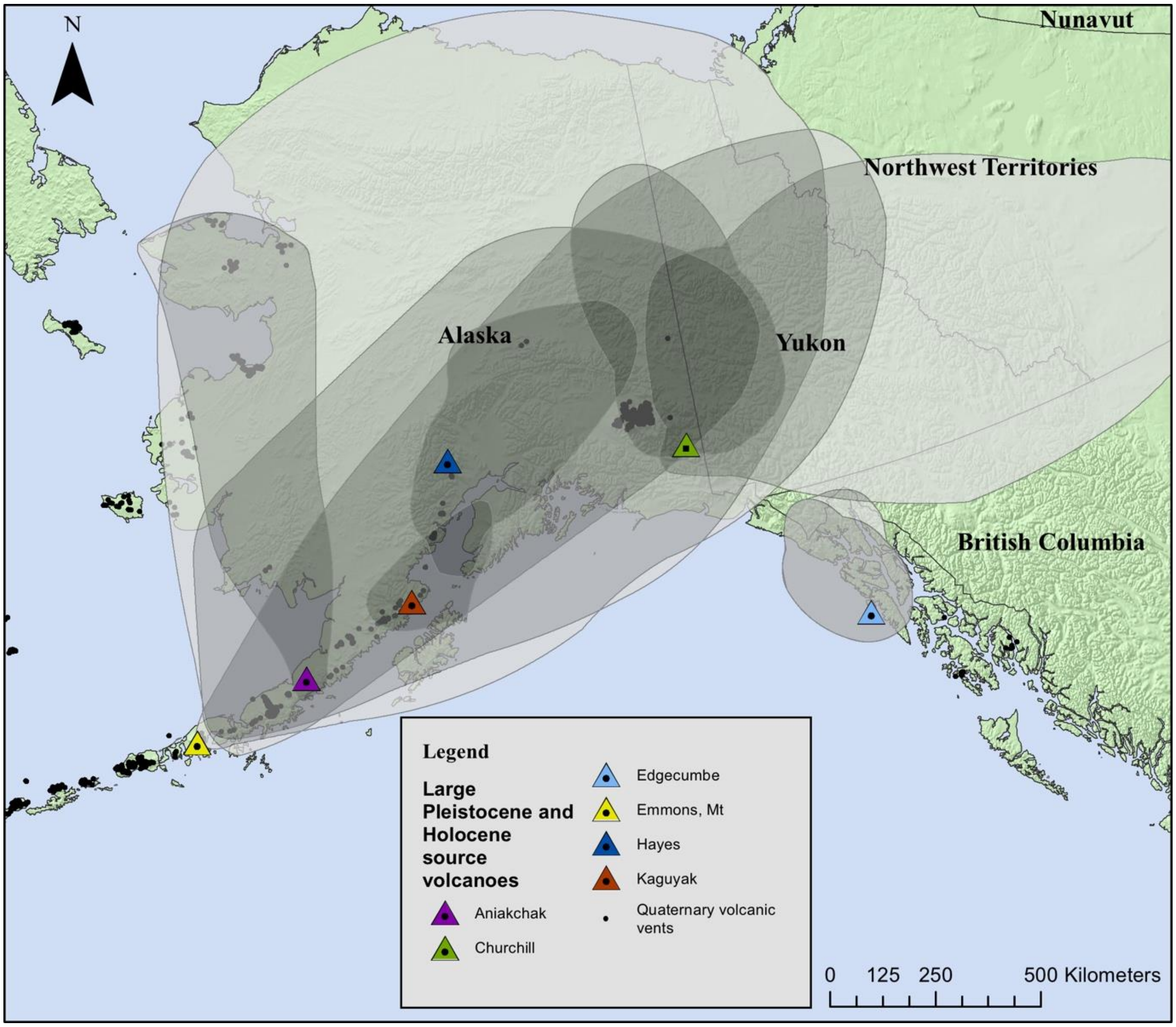

Figure 2.1: A map of Alaska, USA and northern Canada, showing the distribution and considerable overlap of visible tephra footprints from several widely dispersed late Pleistocene and Holocene eruptions. These are just a number of potential units that could be reworked in regional cryptotephra studies that may overwhelm and mask the detection of the cryptotephra. Data for tephra depositional areas were adapted from Mulliken et al. (2018).

The study site's proximity to active volcanoes should first be considered prior to processing. In general, sites that are ~1000 km or less from source have the potential for a much higher flux of glass throughout the sequence due to proximity, reworked visible tephra, and presence of tephra from smaller eruptions (e.g., Davies, 2018; McLean et al., 2018). A general understanding of the eruption history of the 'local' volcanic fields/arcs will help determine how samples from the site are processed and interpreted. This knowledge could anticipate the use of a pollen spike to allow for the counting of high concentration deposits or could aid in the interpretation of multiple geochemical populations within a peak as reworking versus multiple eruptive events. Regional tephra frameworks for source regions (e.g., Froggatt & Lowe, 1990; Machida, 1999: Machida and Arai, 2003; Jensen et al., 2008; Kaufman et al., 2012; Lowe et al., 2015), or other cryptotephra studies published for the area (e.g., Payne et al., 2008; Davies et al., 2016; Mackay et al., 2016; Lane et al., 2012, 2017; McLean et al., 2018) can be referred to in order to gather an estimation of the presence and characteristics of tephra layers. This includes studies of volcanism that may have occurred prior to the time of interest because older units may be reworked into the site's sediments (Fig. 2.1; e.g., Zawalna-Geer et al., 2016; McLean et al., 2018; Bolton et al., 2020). However, it should be emphasized that one individual site or core will not accurately represent the entire regional tephrostratigraphy, as the presence and concentration of tephra deposits can be variable both within a single site and between sites <10 km from each other (Pyne-O'Donnell, 2011; Watson et al., 2016; Fortin et al., 2019; Jensen et al, in review).

Site assessments should consider how tephra may be deposited into a particular site, taking into account the surrounding geology, geomorphology and drainage characteristics. Ombrotrophic bogs are ideal for preserving primary tephra because they are hydrologically isolated, i.e., do not have through-flowing water and are atmospherically-fed. In comparison, lakes and fens can collect tephra through secondary deposition as sediment enters the catchment through streams/inlets and erosion. For lacustrine sites the number of inflowing streams, water depth, sediment composition, size of the watershed, and any major environmental changes that may have been experienced through time should be considered. Inflowing streams can deposit reworked tephra to the lake, as erosion of the catchment area remobilizes tephra long after the initial eruption (Thompson et al., 1986; Sarna-Wojcicki, et al., 1997; Boygle, 1999). This is particularly problematic in regions close to active volcanoes (e.g., McLean et al., 2018), or where visible ash beds are present in the landscape, as demonstrated by the inclusion of the ~30,000 cal BP Dawson tephra (Demuro et al., 2008) and White River Ash (~1.7 ka) in all three analyzed depths of a 23 cm surface core taken at Chapman Lake, Yukon (Fig. 2.2; Chapter 3). Sediment accumulation rates have also been shown to influence the distribution of tephra deposits on lake beds (Pyne O'Donnell, 2011), while water depth can alter the preservation of tephra through animals (e.g., moose) trampling sediment in shallow lakes or wave-induced mixing of sediment (Håkanson and Jansson, 1983; Boygle, 1999;

Mackay et al., 2012). Rapid changes in grain size, sediment flux or organic content through a core profile may be caused by a shift in environmental conditions and indicate destabilization of the landscape. High-energy events like storms, fires, or earthquakes can remobilize tephra and other material from the catchment area and increase sediment input into the lake (Lowe, 2011; McLean et al., 2018). In addition, low-density sediments and gyttjas in lakes can allow vertical movement of tephra through the stratigraphic column (e.g., Beierle and Bond, 2002). Watershed characteristics such as size, vegetation type and elevation have been shown to affect the presence and concentrations of tephra, as perennial snow or vegetation can retain tephra and gradually release it into the lake over hundreds of years (Davies et al., 2007).

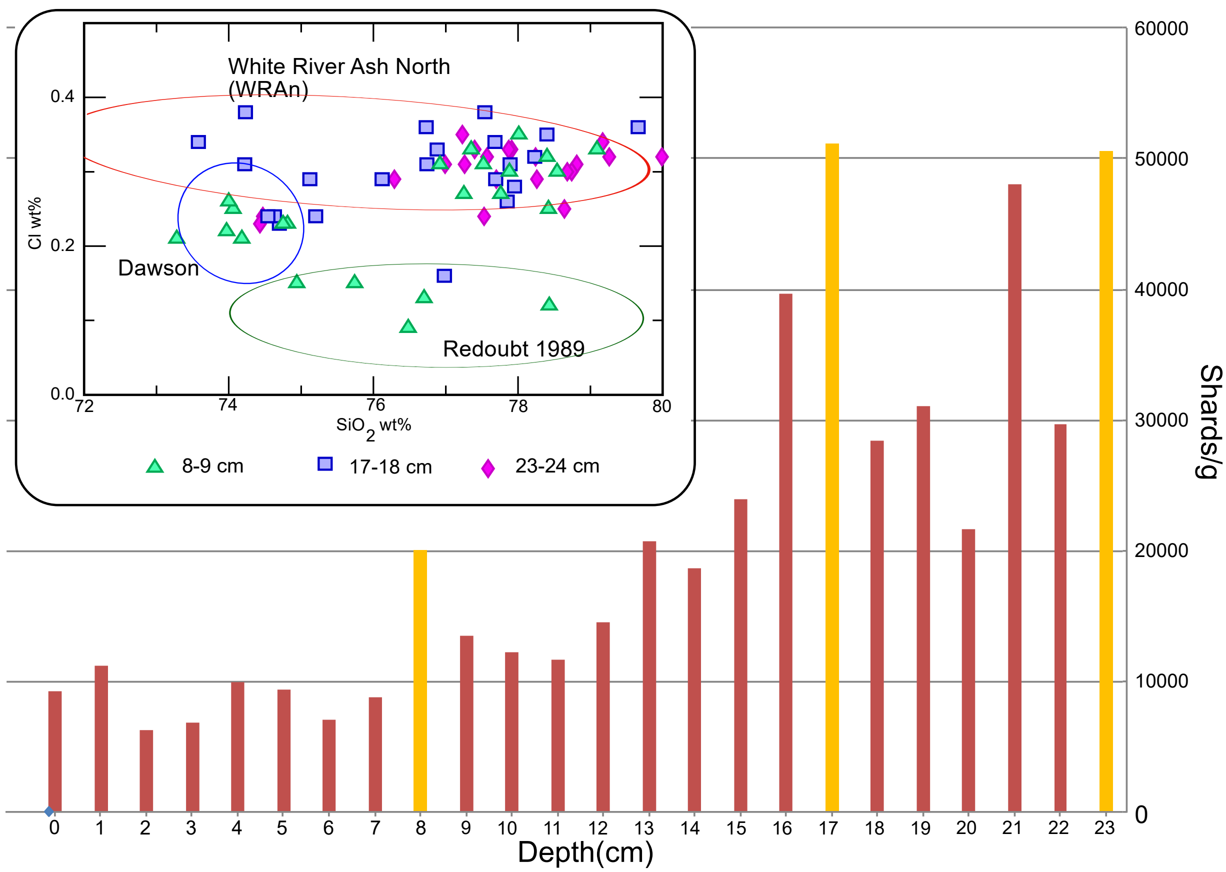

Figure 2.2: Glass shard counts and analyses from the Chapman Lake surface core, showing reworked Dawson tephra (~30 ka) in all three samples analyzed, and abundant White River Ash north (~1.7 ka). Redoubt 1989-90 at 8-9 cm peak is the only potential primary air-fall unit. Yellow bars in profile indicate the three depths analyzed for geochemistry.

Although ombrotrophic peat bogs are generally ideal sites for cryptotephra studies, many of the above characteristics of lakes should be considered for some bog sites as well, such as fens, where flowing water and vegetation type are problematic for preserving cryptotephra. Also, while peat bogs are less susceptible to vertical movement of tephra (Payne et al., 2005), vegetation dynamics (e.g., root channels or changes in peat accumulation rates), percolation, changes in water-table depth, and settling processes can cause vertical movement of tephra in peats (Watson et al., 2015; Mackay et al., 2016). For example, peats with a *Sphagnum*-dominated composition tend to trap and hold tephra shards in place (Watson et al., 2015), while Mackay et al. (2016) encountered multiple horizons of reworked White River Ash east (WRAe) during a time of variable Ericaceae growth. These shrub's roots could have created vertical channels for the tephra to move through, allowing vertical mixing to occur.

For all sites, long-term snow or ice cover, when combined with strong winds or fluvial processes, can cause local redistribution and patchiness of tephra horizons (e.g., Boygle, 1999; Bergman et al., 2004). Microtopography and slope of stratigraphy in the core can alter the presence and location of tephra peaks; cores collected on a sloped area of a peat or lakebed can contain angled tephra layers resulting in diffused peaks on a shard profile (Davies, 2015). Any site with an aeolian input is susceptible to detrital tephra deposition because, for example, air-born silt in much of western North America and the mid-west USA contains tephra. These detrital grains can completely mask any primary depositional signal (e.g., Irwin Smith Bog, Michigan, Jensen et al., in review). For lakes, redeposition of sediment may also occur due to slumping, sliding, or turbidity currents (Mackay et al., 2012), whereas microtopography in peats can affect the collection of tephra towards hollows (Dugmore and Newton, 1992; Payne and Gehrels, 2010). The resulting effects on shard profile interpretation due to these processes will be discussed in further detail in section 2.5 below. In addition to those mentioned above, many other environmental factors such as bioturbation (e.g., Stanton et al., 2010; Griggs et al., 2014) or anthropogenic activity (e.g., Swindles et al., 2013; Davies et al., 2018) can affect the mechanics of cryptotephra deposition and preservation in lakes and peats. In the end, it is likely that one or more of these factors will be present in any given site.

The dynamics of tephra depositional processes of lakes versus peats tend to favour preservation in peats, a supposition confirmed by Watson et al. (2016) who found that the number of identified eruptions was higher at peat sites than similarly located lakes. However, incomplete records were found in both environments, resulting in the recommendation of using peat and lake sites to achieve the most comprehensive results for an area. Additionally, given the small area sampled by a single core, ideally, more than one core should be collected at any one site to develop a more complete tephra record (e.g., Sydney Bog, Maine, Jensen et al., in review).

To summarize, problems will arise when conducting cryptotephra research on sites with the following conditions: relatively proximal to an active volcanic region, has/had through-flowing water, has aeolian sedimentary input, visible tephra layers are present in the drainage basin, long-term snow/ice cover, or sloped surfaces/microtopography. Not all these conditions can be avoided, but if identified should be taken into account during sample collection, processing and data analysis. Lake sites should be sampled from the flattest central area of a lake that is deep and large enough to avoid any inflowing/outflowing streams (or, ideally, a lake without inflowing streams), trampling of sediment, wind-induced mixing and slumping/sliding of banks (Fig. 2.3). For peats, a hydrologically isolated ombrotrophic bog with a consistent accumulation rate would be ideal to produce a high-resolution cryptotephra record with distinct primary-deposition tephra horizons.

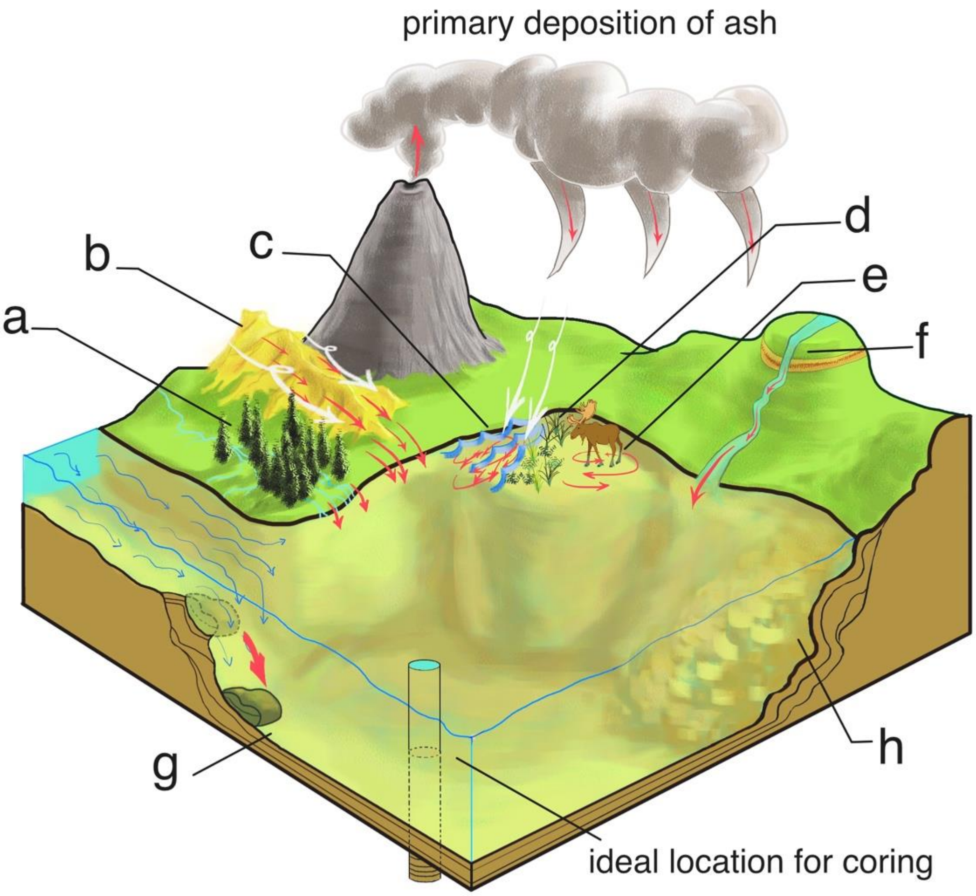

Figure 2.3: Examples of site characteristics that may affect cryptotephra preservation in lake sediments. As opposed to primary deposition directly from ash clouds, secondary deposition of ash occurs through gradual input from the watershed (a) or through aeolian transport (b). Wave-induced mixing (c), vegetation changes (d), and trampling by animals (e) will cause reworking of sediments, and inflowing streams can collect tephra from visible ash layers (f). Sloped lake beds will redistribute older ash layers onto younger sediment through slumping and sliding (g) and will alter the presence and location of tephra (h).

2.3. Cryptotephra Processing and Extraction

Processing steps for shard counting and geochemical analyses largely overlap, but there are some key divergences. The ideal workflow will be dependent on site characteristics mentioned above, the nature of the resulting samples, and their volume. In this section, we summarize methods for processing cryptotephra for shard counting and geochemical analysis, discuss modifications for certain samples, and review situations to be considered before samples are subjected to irreversible steps.

2.3.1. Sampling strategy and loss on ignition

A peat or lake core is sampled contiguously into set intervals to develop a glass shard concentration profile (Fig. 2.4). This profile is used to identify potential tephra that are then re-sampled for geochemical analysis. Sampling can be done in the field during initial core extraction, or in the lab. The sampling interval, availability of material (e.g., is the core designated for other research or already sampled), and the coring methods should all be considered prior to sampling.

Before sub-sampling, it is helpful to know what coring techniques were used and if the cores have been previously sampled. The type of corer will impact the compaction of sediment, sediment mixing in un-packed material or the necessity for multiple overlapping sub-cores to produce a continuous record (e.g., surface core, vibracore, gravity core, or Russian core; Chapter 3, Davies et al., 2007). To avoid cross-contamination between depths, during the splitting, extraction of the core and sampling the outer surface should be scraped off to avoid collection of smeared or mixed material.

The core's total length, accumulation rate, and desired resolution will determine the sampling interval. If the core is shorter and/or the site has a lower accumulation rate, a contiguous sampling interval of every ~1 cm is recommended. However, this is labour-intensive for longer cores (e.g., >2 m) and those with high accumulation rates. Here, it is standard to sample 5 to 10 cm contiguous sections, with finer-resolution sampling carried out in sections with notable shard peaks (Fig. 2.4; e.g., Bergman et al., 2004; Pyne O'Donnell, 2007; Lane et al., 2014). The lower resolution may miss multiple peaks or low concentration tephra masked by higher concentration tephra (e.g., Timms et al., 2017; Pyne O'Donnell and Jensen, 2020, Jensen et al., in review).

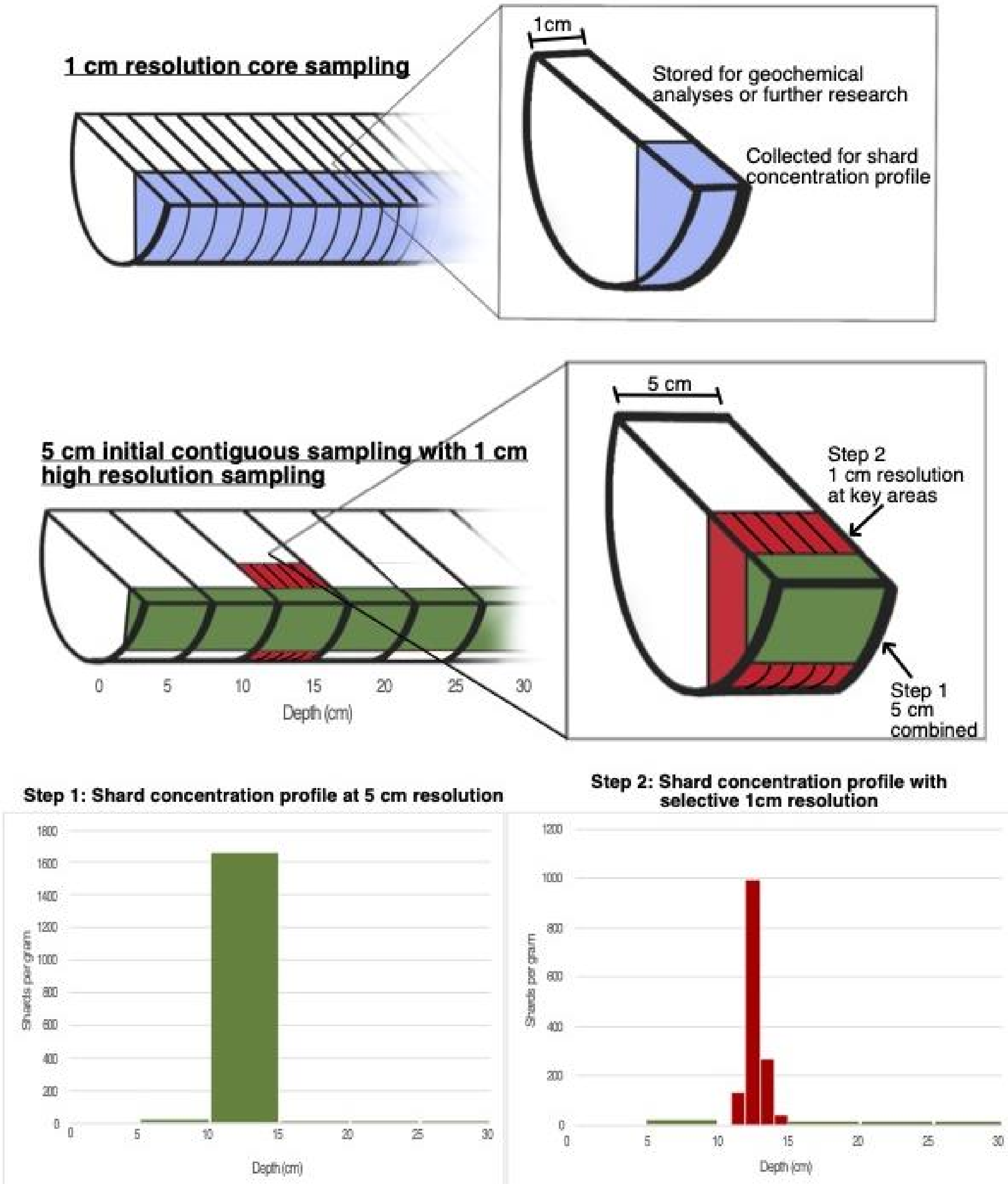

Figure 2.4: Cryptotephra sampling is contiguous; the entire length is sampled with no gaps. In many cases the first step is ‘range-finder’ sampling and counting at 5 to 10 cm intervals (step one), where peaks are recounted at a high-resolution (step two).

The volume of available material and potential shard concentration also determines the workflow. Not much material is required for cryptotephra work, however, for a region with low concentrations of tephra (e.g., northeastern Europe and North America) sampled at 1-cm resolution, there should be at least 3-4 cm^3 available for counting (1 cm^3) and geochemical analyses (2-3 cm^3). This is important because ashing samples for loss on ignition (LOI), often the first step in processing for counting, alters glass geochemistry (Fig. 2.5; e.g., Dugmore et al., 1992; Pilcher & Hall, 1992; Rose et al., 1996; Gehrels et al., 2008). Having enough material for geochemical analyses is critical – studies with limited material should avoid LOI and process one sample for both counting and geochemical analyses.

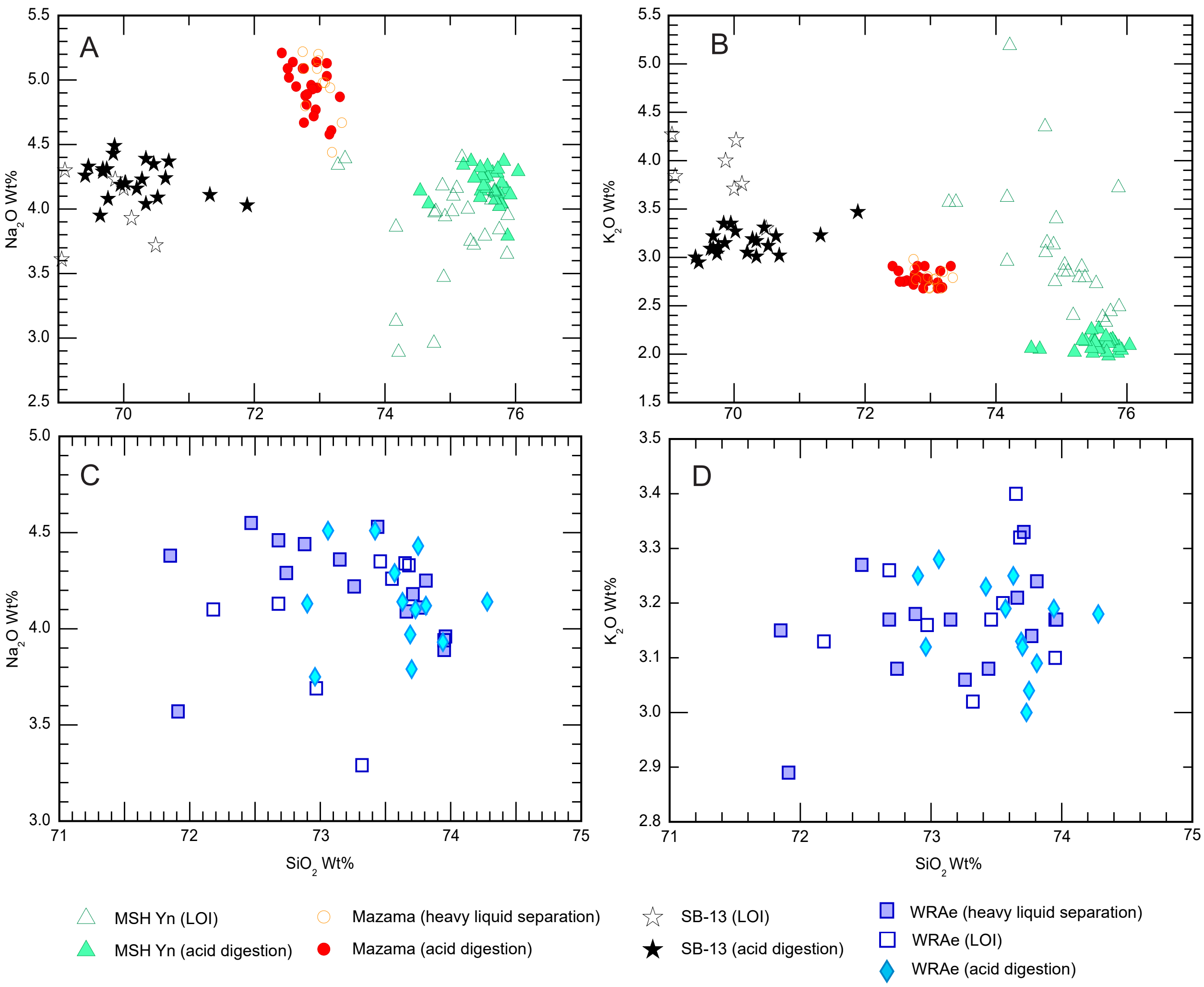

Figure 2.5: (A-B) Bivariate plots of Mount. St. Helens Yn, Mazama and SB-13 (Sydney Bog, Maine). Samples underwent LOI (section 2.3.1), heavy liquid separation (section 2.3.3), or acid digestion (section 2.4.2). LOI-exposed samples show significant alteration in K_2O, and to a lesser degree, in Na_2O. Acid digestion did not alter samples as shown by the lack of offset from density separated splits. (C-D) LOI exposure did not impact the White River Ash, eastern lobe (WRAe), indicating some samples are less prone to alteration. All samples are from Bloomingdale Bog (NY State) and Sydney Bog and analysed at the University of Alberta (Jensen et al., in review).

When sufficient material is available, the first processing step for preparing samples for shard counts involves ashing the sample in a muffle furnace to remove the organic content. LOI measurements can then be calculated to determine the percentage of organic content at each depth, which can be used to interpret shifts in vegetation type, climate, or depositional processes. LOI methods were adopted from paleoecological studies (e.g., Heiri et al., 2001) by Pilcher and Hall (1992) and Hall et al. (1994) to locate cryptotephra in peat. It has since been accepted as a standard procedure for cryptotephra processing (e.g., Blockley et al., 2005; Payne et al., 2005; Payne and Gehrels, 2010), although there are differences in combustion temperature, exposure time, and sample sizes between laboratories. Ashed samples are faster to sieve, the lack of organics results in cleaner slides for counting, and the glass shards have no organic material to cling to during density separation. In regions with very high concentrations, an abrupt drop in organic content may be indicative of a visible or near-visible tephra isochron at that depth. This has been found in both peats (e.g., Dempster Highway peat record, Davies, 2018) and lakes (e.g., Lake Pupuke, Zawalna-Geer et al., 2016).

Maintaining a consistent methodology for the ashing of lake sediments has been advised by Heiri et al. (2001) to avoid inaccurate inter-laboratory measurements, which can occur when different temperatures and combustion times are used. We have developed a standard procedure for ashing both peat and lake sediments for tephra extraction. We recommend working with no more than 20-30 samples in a batch; that batch size can fit inside most smaller muffle furnaces and is a manageable number to avoid any sample mix-ups. First, weigh each empty crucible with a high precision scale. Assuming a 1 cm sample interval, place approximately 1 cm^3 of material into each crucible and dry in an oven at 90˚C for 24 hours, or until completely dry. Weigh each crucible again immediately after drying to obtain the dry sample weight – used to determine shard concentrations. Once dry and weighed, place the crucibles into a muffle furnace to be combusted at 550˚C for 4 hours, with an increase of 40˚C/min. Crucibles should be evenly distributed to ensure complete combustion. Afterwards weigh each crucible for a third time and calculate LOI by using the ratio between the post-combustion weight and dry weight. After LOI, each sample is placed into a 15 mL conical bottom centrifuge tube using a stainless-steel spatula or similar tool. A 10% HCl solution is used to rinse any remaining material into the tube. Samples should remain in 10% HCl for at least 4 hours until all reactions have finished. Dilute acid dissolves any carbonate and helps disaggregate clumps formed during ashing, assisting in the next step of sieving.

If the same sample is to be counted and analysed, alternative methods are used to remove organics. Samples with low amounts of fine organic material (e.g., lake sediments) are placed in 30% H_2O_2 for ~12-24 hours to break apart the organic material prior to sieving and density separation (section 2.3.3). Organic-rich samples like peat will require stronger chemical treatment such as acid digestion (see section 2.4.2). Floatation (Blockley et al. 2005) is not always sufficient to extract glass from peat, especially in low concentration samples, as the glass catches on the peat.

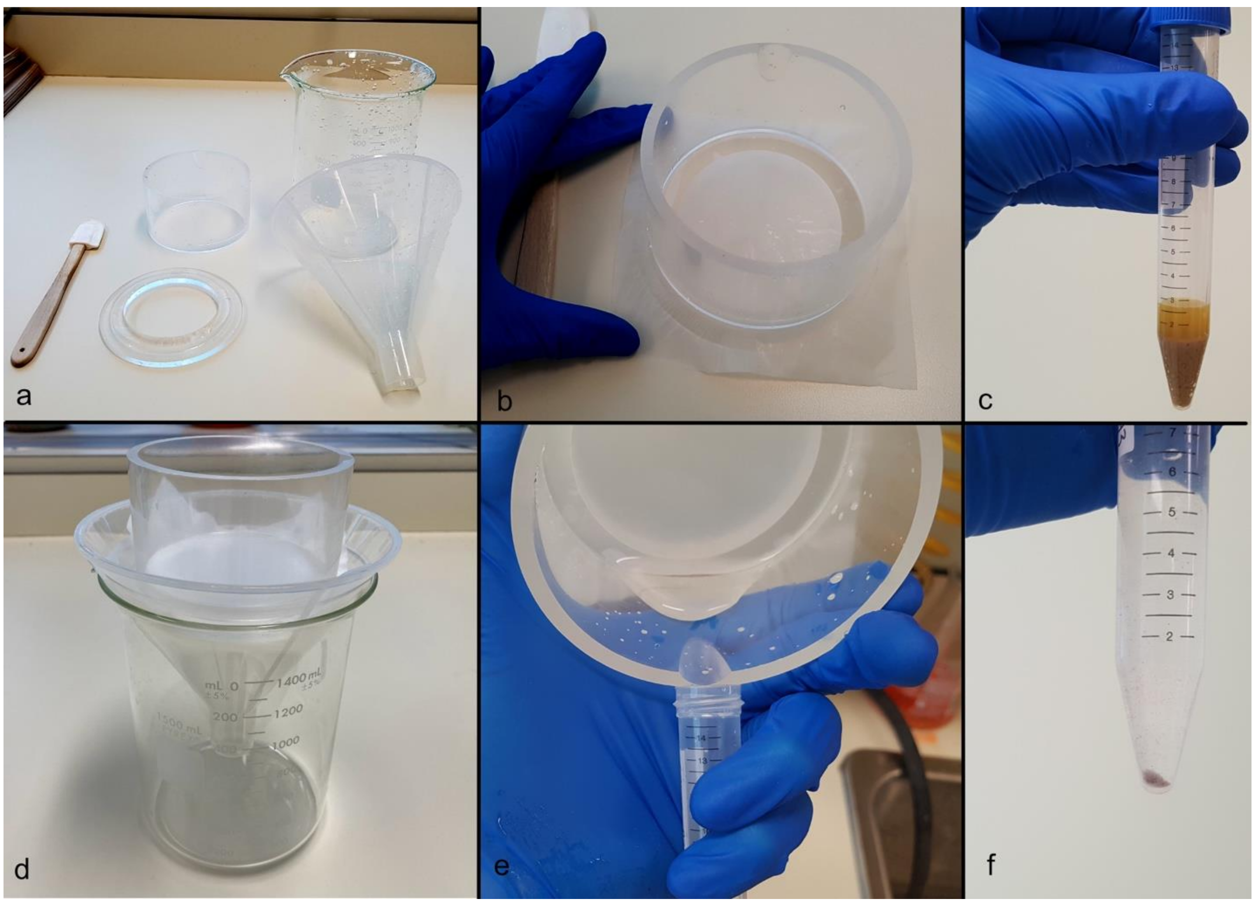

Figure 2.6: (a) Sieving instruments: spatula, sieve frame, 1000mL beaker, plastic funnel. (b) Reusable nylon mesh is placed in the frame and pulled tight to reduce wrinkles. (c) 15mL centrifuge tube with sample and 10% HCl will be filled with de-ionized water before sieving. (d) The complete sieve set up. (e) Once sieved, the remaining material is rinsed back into the clean centrifuge tube. Rinse the frame with water multiple times to ensure all material has been poured back into the tube. (f) Remaining material, post sieving.

2.3.2. Sieving

In processing for counting or geochemical analyses, all samples require sieving to remove clay, fine silt, coarse sediments, and organics, including LOI or acid-digested residue. Sieving can save a significant amount of time when counting or picking points for analyses. All samples are sieved through a fine nylon mesh, usually between 15-25 µm, to remove fine silt, clay, and dissolved organics. Samples with coarser material can also be sieved through a coarser nylon mesh (120 µm or 80 µm) stacked over the finer mesh sieve.

Sieve frames and disposable nylon mesh (Fig. 2.6b) are used because the mesh is pressed upon, which would destroy more expensive metal mesh sieves. A small, flexible, silicone spatula is used to lightly smear the sample across the mesh to help move material through these fine mesh sizes. When sieving multiple samples for shard counting, the same sieve mesh may be used for more than one sample if the mesh and tools are thoroughly washed between samples and the samples are systematically sieved by depth. This minimizes cross-contamination between samples while reducing consumption of nylon mesh. It is not uncommon to re-use mesh up to 5 times, but the frequency of mesh changes depends on the resilience of the mesh, type of sample (sediment-rich or not), and potential concentration of tephra populations. For example, lake samples containing large amounts of clays and silts require longer sieving times, wear down the sieve mesh faster, and the fine silt and clay will eventually clog the mesh. The mesh should be inspected (typically held up to a light) between each sample and discarded when it appears stretched, damaged, dirty, or otherwise worn down. Mesh is replaced between samples that are being processed for geochemical analysis.

The typical sieving process involves placing sieve frame with mesh in a plastic funnel over a 1000 mL beaker (Fig. 2.6d). The sample should be sitting in HCl/H_2O_2 in a 15mL centrifuge tube; fill the tube with de-ionized water, pour into the middle of the sieve mesh, and rinse the tube into the sieve frame. Using a wash bottle, lightly spray de-ionized water around the sieve frame to collect the sample into the centre. Then gently break apart the sample and spread it around the centre of the mesh using a small silicone spatula, making sure there is always some water in the frame with the sample. Apply enough pressure so the material breaks apart, but not so much that the mesh is stretched. Continue to periodically rinse the sample with water between passes with the spatula until the bulk of finer material has passed through. At this point, the sieve frame is filled with higher volumes of deionized water to continue to flush any remaining fine particles. Repeat these steps as many times as necessary, typically two to three more iterations for sediment-rich samples or one more for samples with little to no silt. Samples containing larger grain sizes are first sieved through a 80-120 µm mesh in a separate sieve frame stacked on top of the finer mesh using the same techniques described above. When fully sieved, rinse the spatula into the sieve, wash all the material into one side of the frame and decant into a 15mL centrifuge tube (Fig. 2.6f). Disassemble the sieve and wash all the parts (including funnel and beaker) between samples. Pay careful attention to the sieve mesh, which can withstand vigorous washing under running water involving rubbing the mesh against itself.

After sieving, samples are ready for density separation, but first, examine the sample under a microscope by placing a few drops onto a well slide. Re-sieve the sample if it still contains observable clay/silt particles (Fig. 2.7). Samples that are visible at this point or contain low concentrations of minerals, organics and biogenic silica may not require density separation if the glass shards are easily identifiable. In this case the sample is ready to mount for shard counting and/or geochemical analyses. Otherwise, density separation(s) is required and each 15 mL tube is centrifuged ~2500-3000 rpm for 5 minutes and the water is decanted. Conical bottom 15 ml centrifuge tubes are recommended because the surface tension of the water will allow you to (almost) fully decant without sample loss. Once the water is removed the sample is ready for density separation.

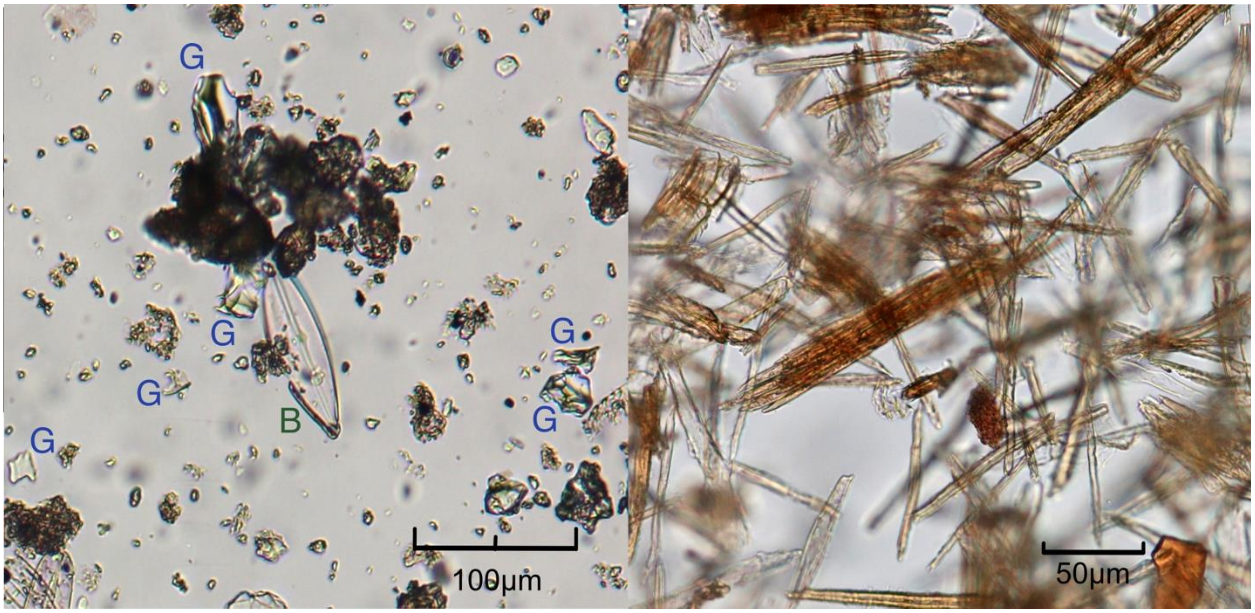

Figure 2.7: Images of samples in a well-slide (Left) A sieved lake sample requiring further sieving before density separation; B = biogenic silica, G = glass shards. (Right) A lake sample containing large amounts of plant fibres after an initial density separation to remove minerals. Glass shards are not visible without an additional separation to remove the organic material. This sample was treated with 30% H_2O_2 (not ashed) as it was being processed for geochemical analyses.

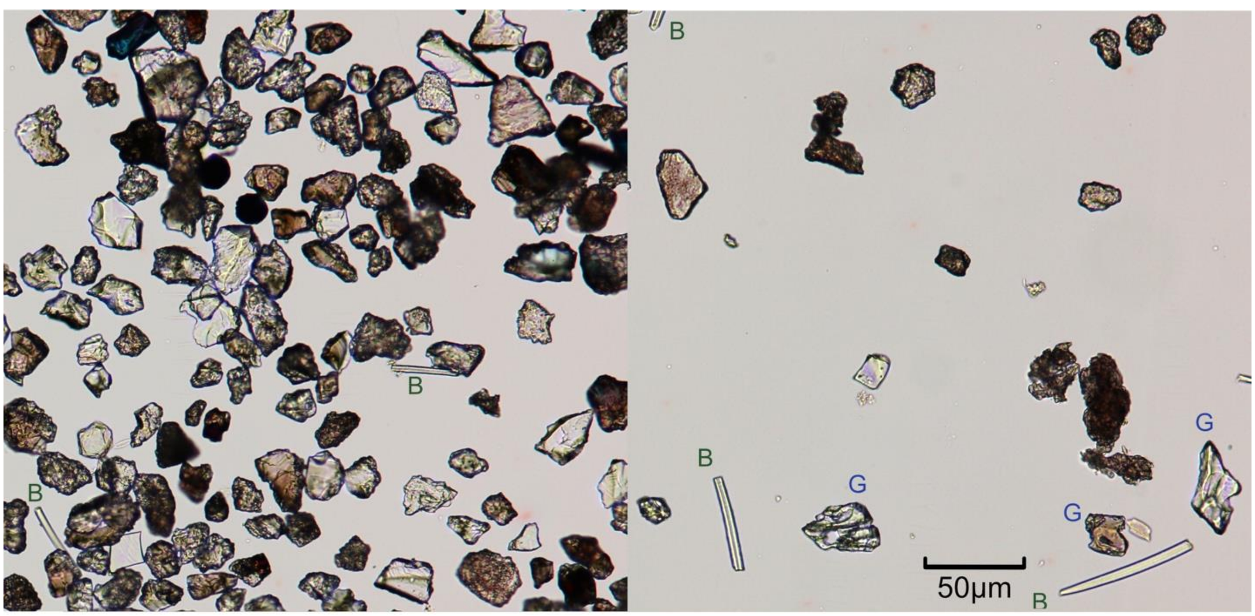

Figure 2.8: Well slide images of a sample before (left) and after (right) density separation at 2.45 g/cm^3 to float glass and remove minerals. Biogenic silica (B) and other organic material still remain but are not abundant enough to prevent the identification of glass shards (G).

2.3.3. Density Separation for counting and glass analysis

Cryptotephra studies were not widely carried out on lake sediments until Turney et al. (1998) applied density separation to cryptotephra deposits. Glass shards were concentrated by performing two density floats at 2.4 and 2.5 g/cm^3, where the concentrated glass at a density of 2.4-2.5 g/cm^3 would be kept for analysis. Blockley et al. (2005) refined this process for more organic-rich samples (e.g., peat) as an alternative method to acid or alkali treatments (discussed in section 2.4.2 below). Blockley et al. (2005) used a heavy liquid at ~2.45 g/cm^3 to float the glass, with an additional float at ~2.0 g/cm^3 to remove organics (Fig. 2.7). The density of 2.45 g/cm^3 is an ideal density to float glass in most samples, but should be raised to ~2.5 g/cm^3 if working with denser basaltic glass. To effectively remove biogenic silica (e.g., diatoms, phytoliths), and/or plant fibres we recommend using a slightly higher density of ~2.1-2.2 g/cm^3 (Fig. 2.8). Another approach involves dissolving the biogenic silica with heated dilute alkalis, leaving the glass and minerals (Rose et al., 1996). This process is not recommended as it may also geochemically alter the glass shards, while the floatation method is safe and effective. The effect of higher pH on glass is not as well documented as lower pH, although experiments suggest glasses of all composition are more sensitive to higher alkalinity solutions (e.g., Wolff-Boenisch et al., 2004).

Several different heavy liquids are available for density separation, but many are toxic and unnecessary for cryptotephra processing. Heavy liquids such as Tetrabromoethane (TBE) or Methylene Iodide (MI) are toxic and require the use of a fume hood. These heavy liquids have higher densities more suitable for separation of heavy minerals. Inorganic heavy liquids such as sodium poly(meta)tungstate (SPT) and Lithium heteropolytungstate (LST) are more suitable for cryptotephra work (Table 2.1) and are commonly used for tephra extraction (e.g., Turney, 1998; Katoh et al., 1999; Wastegård et al., 2001; Blockley et al., 2005; Davies et al., 2016; Foo et al., 2020). Both LST and SPT are non-toxic, able to be used outside of a fume hood, and are reusable. SPT and LMT (lithium metatungstate) have a higher viscosity at higher densities, less of a concern with glass, but can affect mineral separations. LST can reach a higher density (up to 2.95 g/mL) at room temperature while maintaining a lower viscosity. Additionally, LST is more stable at higher temperatures and reconstitutes more faithfully if accidently left to dry to crystal form. The density of these non-toxic heavy liquids is lowered to the desired density by adding deionized water, measured using a hydrometer or sink-floats in a beaker. The water must be well mixed with the heavy liquid prior to measuring, as the water will float on the heavy liquid.

Table 2.1: Comparison of the two main inorganic heavy liquids used in cryptotephra research

Heavy Liquid	Viscosity (cP)	Max density (g/mL)	Advantages	Disadvantages
sodium polytungstate (SPT)	4 @ 2.4 g/mL 19 @ 2.8 g/mL 60 @ 3.1g/mL	3.08 (at 25˙C)	-Non-toxic -Reusable	-Viscosity can interfere with heavy density separation
lithium heteropolytungstates (LST)	4 @ 2.4 g/mL 10 @ 2.8 g/mL	2.95 (at 25˙C) or up to 3.6 at higher temperatures	-Non-toxic -Reusable -Lowest viscosity -Infinite shelf life -High thermal stability	-Most expensive

For the process of density separation, about 4 mL of a heavy liquid of ideal density (depending on whether floating glass or organics/biogenic silica) is pipetted into each centrifuge tube (more can be used but less is not recommended). The sample is thoroughly mixed by a vortex mixer (or a gentle swirling by hand) to suspend all the glass shards. Once mixed, samples are centrifuged at ~2500-3000 rpm for 15 minutes. If floating glass, carefully decant the float and ~¾ of the LST into a clean centrifuge tube. A gentle pouring motion is used to avoid disturbing the heavy minerals – the surface tension is less due to the heavy liquid. Add up to 10 ml of de-ionized water to the glass float, and up to 6 ml to the heavies. Agitate both tubes, centrifuge for 5 minutes, and carefully decant the dilute LST into a beaker to be filtered for reuse. Caution is necessary to avoid decanting the entire sample. Samples must be rinsed several times, although less water is required for subsequent rinses; up to 5 times for the glass float, and 2-3 times for the heavies. The glass float can be inspected again in a well-slide to determine if an additional float is necessary to remove any organics or biogenic silica. If a lighter float is needed, repeat these steps using a density of ~2.1-2.2 g/cm^3. The glass is now the heavier fraction, which should be rinsed ~5 times, whereas the floated organics/biogenic silica can be rinsed 1-2 times. If the LST isn't completely removed, it will recrystalize during mounting, potentially ruining the sample for counting and/or analyses.

The heavy liquid is recycled by filtering the dilute LST/SPT through a low porosity filter paper at least twice. Filtering the dilute solution increases the filtering speed, which can be slow with a lower porosity (≤10-5 μm) filter. The cleaned dilute solution is placed on a hot plate (< 75 °C) or in an oven (< 90 °C) to evaporate the water to return the heavy liquid to its original density.

2.4. Mounting Procedures

Mounting procedures depend on whether the sample was prepared for counting and/or geochemical analysis. Additional processing steps may be required depending on the relative concentration of glass shards in the sample. As discussed above, the processed sample should be examined under a well slide before mounting. Low shard concentrations with high mineral or biogenic content can make shard counting or analysis difficult. In contrast, high concentrations of glass may require the addition of a pollen spike to accurately quantify the glass shards. This section will discuss what steps should be taken to ensure reliable counts and geochemical data.

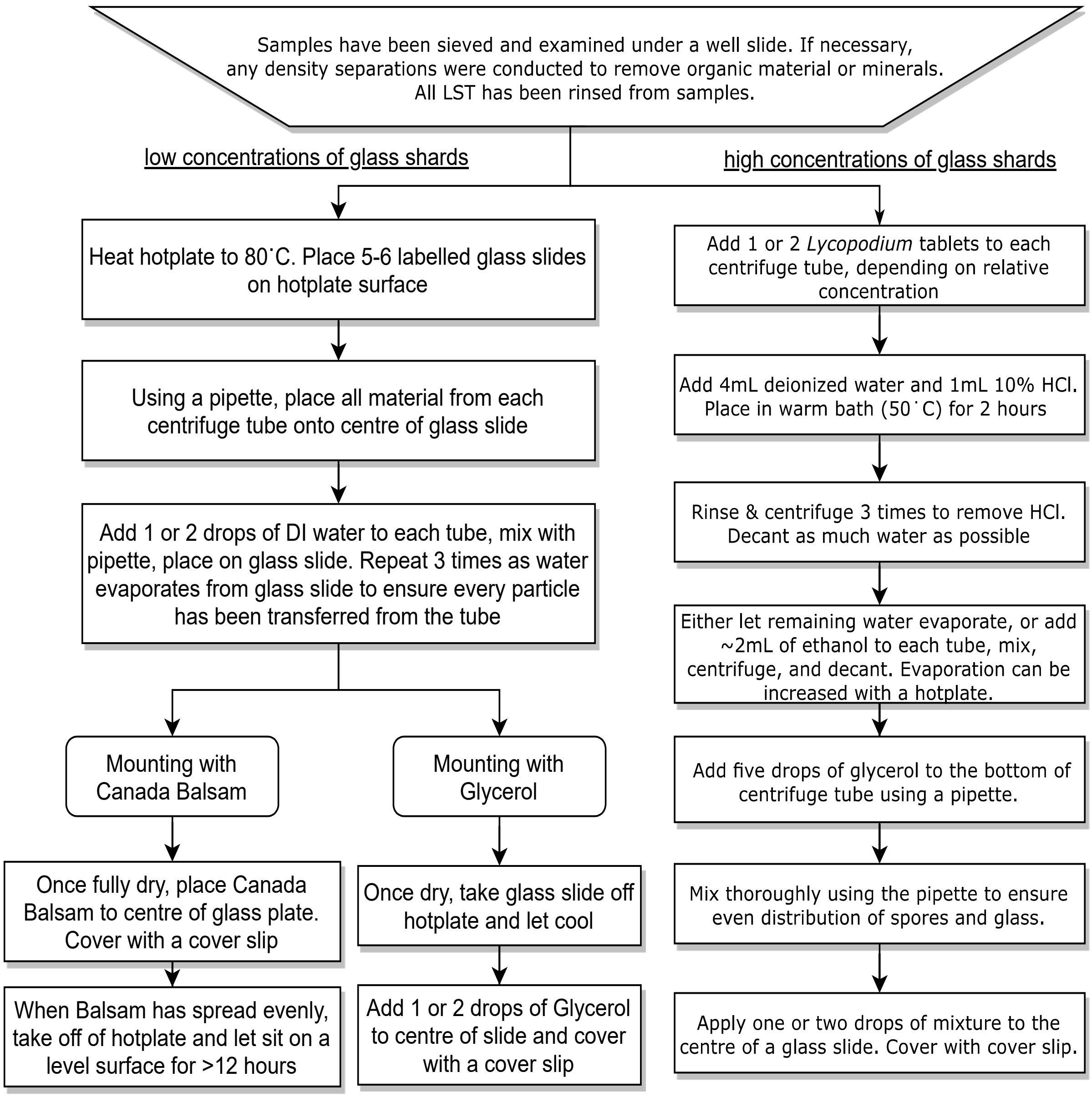

Figure 2.9: Flow chart of typical mounting procedures for the counting of glass shards. It is imperative to mount all processed material onto the slide for non-spiked samples. The definition of "low" and "high" concentrations are relative; counting up to 500 or even 1000 shards/cm^3 may be exhausting to some but bearable to others. In general, if concentrations are in the range of thousands of shards per gram, it is preferable to spike the sample.

2.4.1. Mounting on glass slides for quantification

Following density separation (if necessary), the concentrated glass from each sample is mounted onto a glass slide to estimate glass shard concentrations (e.g., Dugmore et al., 1995; Rose et al., 1996; Hall and Pilcher, 2002; Gehrels et al. 2006). Mounting procedures vary depending on nature of the sample, and a suggested workflow is outlined in Figure 2.9. The way the samples are mounted will depend on whether the same sample is being used for counting and analyses, if glass concentrations are high enough to merit pollen spiking, and if the mounts are meant to be permanent. If there is a possibility, due to sample limitations, that the material on the quantified slide may have to be recovered for analyses, a non-permanent mounting medium is recommended. Non-permanent mounts allow for the recovery of the material on the slide for geochemical analysis after counting, although the sample must not have undergone LOI. Alternatively, samples for both counting and analyses can be mounted on glass slides with epoxy, and although slides can be somewhat more difficult to polish, this ensures all shards counted can also be analyzed (e.g., Swindles et al., 2010). Samples being mounted only for counting can also be mounted in a permanent medium to facilitate long-term storage. Common mounting mediums are summarized in Table 2.2, and personal preference will be factor as glass will appear differently in each type of medium. For example, Blockley et al. (2005) suggests the use of glycerol or Euparol over Canada balsam in samples containing large quantities of biogenic silica because their refractive indices allow better differentiation of biogenic silica from volcanic glass. Canada balsam is the recommended medium for permanent mounts, although storage of glycerol slides is possible by placing clear nail polish or latex/acrylic paint on the corners of the cover slip to hold it in place. Glycerol, which is water-soluble, is used if the same sample for counting is intended for geochemical analyses (if not making a permanent epoxy mounted slide).

Table 2.2: Comparison of mounting mediums used for cryptotephra shard counts

Mounting Medium	Refractive index	Density	Characteristics	Recommended application
Canada Balsam	1.52 (20˚C)	0.99 g/cm^3	-Yellow colour -Very viscous -Dries hard -Requires heat for mounting -Pink hue of glass under microscope	Permanent mounts or long-term storage of slides.
Glycerol	1.47	1.26 g/cm^3	-Colourless -Low viscosity -Yellow/green hue of glass under microscope -Spreads evenly across slide	Temporary mounts, low availability of material, and pollen-spiked samples.
Histomount	1.58	0.95 g/cm^3	-Colourless -Dries fast -Stable -Hard when dry	Used in Gehrels et al (2006) and Payne and Gehrels (2010). Permanent mount
Euparal	1.48 (as a liquid) 1.54 (as a solid)	0.99 g/cm^3	-Alternative to Canada Balsam -Natural resin -Not sensitive to water -Solidification time is dependent on temperature and mount contents -Can be dissolved to recover sample	Temporary mounts, samples containing large quantities of biogenic silica (used in Blockley et al., 2005)

Pollen spiking might be necessary to accurately quantify samples with high concentrations of glass shards. In this case a known concentration of marker grains (e.g., *Lycopodium* spores) are added to the sample and counted alongside the tephra shards to accurately estimate the shard concentration. *Lycopodium* spore tablets purchased from Lund University (https://www.geology.lu.se/services/pollen-tablets) are the most commonly used marker grain, but an alternative are black ceramic microspheres discussed in Kitaba and Nakagawa (2017) that have shown greater resistance to chemical and physical stresses compared to conventional methods, though their use with cryptotephra processing has not yet been tested. Gehrels et al. (2006) first applied pollen spikes to assist in counting cryptotephra, and the method has been successfully applied in several other cryptotephra studies (e.g., Bourne, 2012; Griggs et al., 2014; Zawalna-Geer et al., 2016). Tablets containing a known concentration of spores are added and dissolved to each processed sample prior to mounting. Spores are mounted along with the glass shards, and both glass and spores are simultaneously counted until a predetermined number of spores have been found. Once tallied up, the formula $\boldsymbol{c} = \boldsymbol{l} \times (\boldsymbol{a}/\boldsymbol{bd})$ is applied, where *c* is the relative concentration of glass per gram, *l* is the total number of spores added to the sample, *a* is the number of shards counted, *b* is the number of spores counted, and *d* is the dry weight of the sample (Gehrels et al., 2006). Repeated trials have shown that pollen spiking can reliably estimate the true concentration of a sample. Procedures in Gehrels et al. (2006) used one tablet of *Lycopodium* spores to 1g of peat and extracted 500 µL of suspended material to be mounted in histomount. Spores and glass shards were both counted until 100 spores had been found.

We have modified the methods of Gehrels et al. (2006) by using glycerol, rather than water, as the mounting medium and for transferring the spiked sample to the slide. Glycerol has a higher viscosity than water and will ensure the glass shards and pollen spike remain suspended together once mixed, preventing differential settling to the bottom of the centrifuge tube during the mounting, retaining an accurate ratio of glass to spike (Fig. 2.10). The processes are as follows: prior to pollen spiking, following the previous processing steps, the sample will be in water in a 15 ml tube. The water is decanted after centrifuging at ~2500 rpm for 5 minutes, then the pollen tablet can be added and dissolved with dilute HCl. Once dissolved and rinsed multiple times to remove any acid, the remaining water is removed by adding 1-2 mL of ethanol, which is then centrifuged and decanted. This step is repeated once more until only the spiked sample and a small bit of ethanol is remaining. The tube is left open for the ethanol to evaporate, or a hotplate can be used to accelerate the evaporation. Once dry, the glycerol is added and thoroughly mixed with the sample to ensure even distribution. Mixing (and application of material to slides) can be done using any small tool such as a glass stir rod, wooden stick, micropipette, or disposable pipette, with the latter two the easiest and most consistent method for application. Approximately one to two drops of the sample are added to each slide, using a disposable pipette or micropipette.

In Zawalna-Geer et al. (2016), all shards mounted to the glass slide were counted in order to avoid counting bias due to the potential of grain migration to the edges of the cover slip (Brookes and Thomas, 1967, as cited in Zawalna-Geer et al., 2016). However, because our method does not use water or dry the sample onto the glass slide before applying a mounting medium, it is less likely that the glass and pollen will be unevenly distributed across the slide.

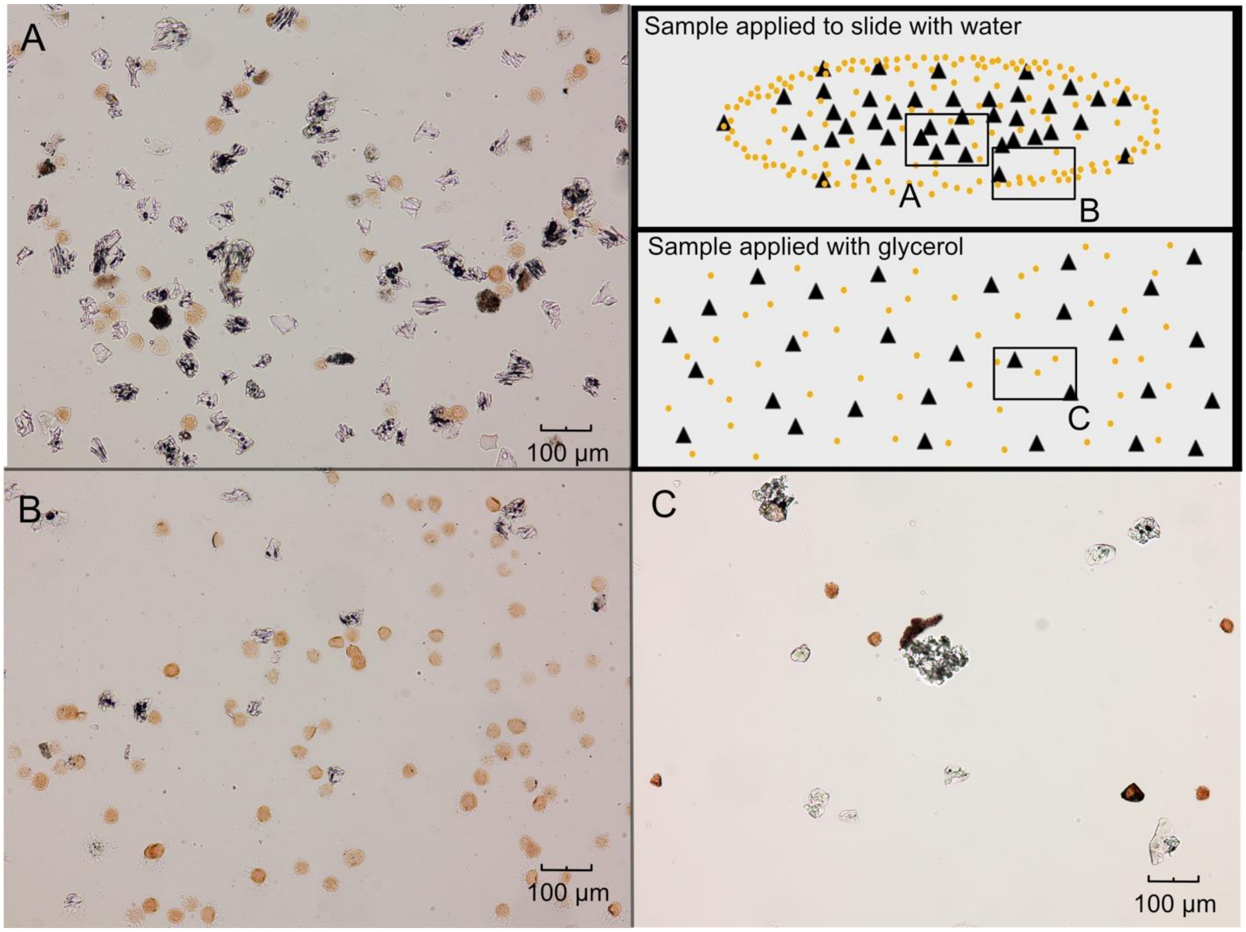

Figure 2.10: Comparison of pollen spiked mounts using the standard pollen spiking method (A and B) and the new modified method (C). Uneven distributions of glass shards (black triangles) and pollen (green circles) are found when using standard methods, with a higher percentage of lycopodium found near the outer rim of the material and a higher percentage of glass in the centre. Samples applied with glycerol were more evenly distributed across the entire slide.

Studies have suggested using at least 100 spike counts per slide is sufficient for reliable estimations of tephra concentrations (Gehrels et al., 2006; Payne and Gehrels, 2010). However, established research protocols in studies counting other objects using pollen spikes suggest this is likely a minimum value. For example, 300-350 exogenous spore counts per slide were recommended when working with Sporormiella (Etienne and Jouffroy-Bapicot, 2014). Finsinger and Willy (2005), in establishing protocols for charcoal studies, recommended 200-300 total counts of 'objects of interest' and marker grains when the ratio of objects of interest to marker grains stays between 0.1 and 0.9 per slide. This raises the important point of a minimum amount of 'objects of interest' that should be counted regardless of the pollen spike - concentration of shards can be highly variable between samples, thus the ratio of objects of interest to marker grains can vary widely.

A minimum shard count of 30 per slide with a minimum spore count of 300 forms a baseline where experiments show that counts below this led to unreliable concentrations (Fig. 2.11; discussed below). On the other hand, very high shard concentrations may only require a count of 100 pollen spores (i.e., the ratio of objects of interest to spores is well over 1). Overall, the number of counts required depends on the concentration of tephra and the amount of material processed. Low amounts of processed material can cause large variations in shard concentration when converting to shards per gram. This issue was encountered when preparing samples from a lake surface core. Pollen spikes were added based on the high glass concentrations in samples deeper in the main core. However, concentrations were lower because the dry weight of the samples was very low, 0.1 g on average, due to the higher organic and water content of the surface core samples. This made it difficult to count a minimum of 30 shards per slide, although all were counted to ~300-350 spores in two different areas of the slide to compare their concentration estimates (Fig. 2.11). The final concentration profiles showed similar trends and peaks despite the low shard to pollen ratios. However, differences between the two concentration estimates on some samples were quite large, generally the greatest in samples where less than 20 shards were counted (Fig. 2.11). Increasing the minimum shard counts to ~30 should improve the shard estimations, but this problem could have been avoided by adding more material to the low weight samples at the start of the process. In another experiment, five spiked sample slides with very low shard to pollen ratios were counted to at least 100 shards and pollen counts were recorded every 5 shards counted. Despite the low shard to pollen ratio (0.02-0.07) and pollen counts reaching up to 3500, shard concentration estimates did not appear to be more inaccurate at any region of the slide. However, samples containing lower dry weights saw larger fluctuations in concentration throughout the counting process. These experiments clearly show that a minimum amount of dry sample should also be a considered when attempting to determine accurate concentration estimates.

	Counted From upper third of slide			Counted from lower third of slide		
Depth (cm)	Shard to Pollen ratio	Equivalent shards	Shards per gram	Shard to Pollen ratio	Equivalent shards	Shards per gram
7	39 : 353	2053	14257	41 : 376	2026	14072
8	23 : 422	1013	9646	24 : 364	1225	11669
9	10 : 307	605	6439	16 : 334	890	9470
10	17 : 312	1013	9927	22 : 357	1145	11227
11	27 : 322	1558	15276	27 : 322	1558	15276
12	23 : 310	1379	10942	24 : 353	1263	10027
13	23 : 344	1242	12550	23 : 323	1323	13366
14	20 : 335	1109	11929	17 : 330	957	10294
15	21 : 311	1255	13942	24 : 318	1402	15583
16	15 : 353	790	10967	10 : 321	579	8040
17	32 : 305	1950	18221	33 : 302	2031	18978
18	23 : 308	1388	22027	17 : 314	1006	15970
19	12 : 302	738	13186	9 : 302	554	9889
20	9 : 306	547	5306	10 : 309	601	5839
21	18 : 310	1079	13321	7 : 368	353	4364
22	19 : 321	1100	8661	20 : 314	1184	9320
23	34 : 303	2085	26065	32 : 316	1882	23523
24	27 : 334	1502	23472	29 : 317	1700	26563
25	19 : 305	1158	15644	26 : 302	1600	21620
26	15 : 305	914	9723	17 : 300	1053	11203

A

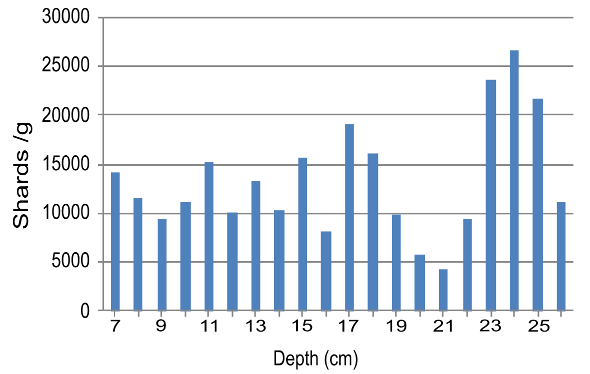

B

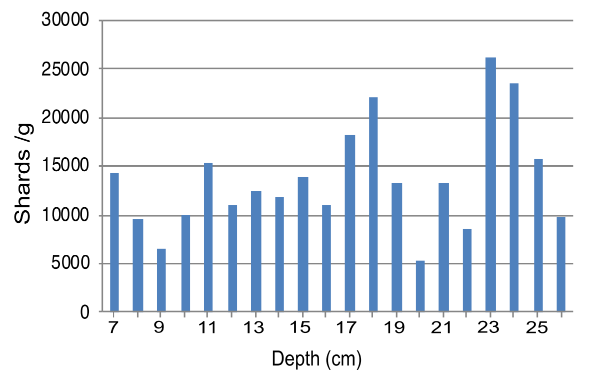

Figure 2.11: A comparison of two separate concentration profiles from the same set of pollen-spiked slides. Both counts start from the slide's right side (closest to the label), with the first counts halfway up the slide (A) and the second from the lower third (B). Three horizontal passes across each slide were enough to reach a total of ~300-350 counted pollen spores. Although the counts are not identical, both sets identify similar trends and concentration peaks in the profile.

2.4.2. Processing and Mounting for Microprobe analysis

Processing shards for microprobe analyses overlaps with the sample preparation, sieving and density separation procedures required for quantification of shards, however additional considerations are required. Because samples subjected to LOI cannot be used for geochemical analyses, and while the floatation methods previously discussed work well for concentrating glass in most lake sediments without ashing, peat samples are more challenging. This section will review methods used to extract glass from peat specifically for microprobe analyses, reviewing the floatation vs. acid digestion debate. Hand-picking of shards is also reviewed for samples that have a low abundance of shards mixed with other grains, as well as the steps taken to mount a sample in pucks for geochemical analysis.

2.4.2.1. Acid digestion

The use of acid digestion (Persson, 1971; Dugmore et al., 1992; Pilcher and Hall, 1996) to remove organic material has been a long-debated method due to the potential alteration of glass, affecting its geochemistry (Blockley et al., 2005; Lane et al., 2014; Roland et al., 2015; Cooper et al., 2019; Monteath et al., 2019a). Acid digestion is used to dissolve the organic component of samples from peat bogs or other organic-rich samples where H_2O_2 is not sufficient to break down the highly fibrous material (e.g., Dugmore et al., 1992; Watson et al., 2016). The method involves placing the sample in a beaker with enough concentrated sulphuric acid to cover the sample. It is then placed on a hot plate, treated with concentrated nitric acid, and subjected to moderate heat to start the reaction, but not brought to a boil. Additional drops of nitric acid are added judiciously to the sample until the organic material is dissolved. As mentioned in the density separation section above (2.3.3), the stepped floatation methods of Blockley et al. (2005) work as an effective alternative to acid digestion in many sediments. However, highly fibrous peat samples can trap glass shards during density separation, resulting in lower recovery of glass shards than acid digestion (Roland et al., 2015; Monteath et al., 2019). In peat samples containing only tens of shards per gram, this is a significant drawback and emphasizes the need for acid digestion. Here we review the current state of the debate in the literature and provide an assessment of how the method can be safely used in cryptotephra processing.

Experimental work on natural glass alternation and dissolution, driven by research into nuclear waste glasses, has shown that outside of the intermediate pH range of 5-8, natural volcanic glasses are subject to dissolution, with mafic glass being more prone to these effects (e.g., Crovisier et al., 2003; Pollard et al., 2003; Wolff-Boenishch et al., 2004; Declercq et al., 2013). This led to concern that acid-digestion could similarly alter glass shards. Blockley et al. (2005) explored this and recommended against the use of aggressive chemical treatments for tephra extraction. In their experiments, ICP-MS analyses showed an increased concentration of major and minor cations in leachate from glass shards sitting for two weeks in beakers of dilute nitric acid, demineralized water, and lithium hydroxide. Results confirm that tephra dissolution and geochemical alteration occurs in all tested solvents to varying degrees, with time being a significant factor in the dissolution process. These results confirm the conclusions of previous studies, but do not rule out the use of acid digestion on peats if the process is done in a shorter time frame than the described experiments. To confirm this, Roland et al. (2015) applied a principal component analysis (PCA) to major and minor oxide Electron microprobe (EPMA) data to determine alteration of Hekla-4, a rhyolitic tephra widely distributed across Europe, when processed through either density separation or acid digestion. Results found no statistical difference between the two methods, confirming initial geochemical tests by Dugmore et al. (1992). In contrast, Cooper et al. (2019) used a permutational multivariate analysis of variance (PERMANOVA) on EPMA data from a range of tephra samples with various compositions, each treated to four different extraction treatments (no treatment, LOI + HCl acid, acid digestion, and base digestion). Basaltic and andesitic glass samples showed more variability in geochemistry, whereas rhyolitic samples, such as those tested by Roland et al. (2015), were more resistant to alteration. However, a contemporary study by Monteath et al. (2019a) reported no observable geochemical or visual differences between acid digestion treated or density separated tephra, even with a variety of geochemical compositions and morphologies. Bivariate and PCA plots of EPMA data found no statistical differences in treatment methods, and SEM analyses showed no physical degradation on the outer surfaces of individual glass shards.

A careful examination of methodologies in these papers shows that they aren't directly comparable, with differences in the temperature and exposure time. Cooper et al. (2019) follow the methods of Persson (1971), where the hotplate was turned on to its maximum level (~300˚C) in order to boil the sulfuric acid. Tephra is then exposed to this temperature for the entirety of the experiment (approximately two and a half hours) until the reaction has ended. However, this is not the standard method used for cryptotephra; Roland et al. (2015), Monteath et al. (2019a) and others (e.g., Davies et al., 2003, 2005; Pilcher and Hall, 1996; Hall and Pilcher, 2002; Pilcher et al., 2005; Wohlfarth et al., 2006; Davies, 2015; Davies et al., 2018) use the acid digestion method as described by Dugmore et al. (1995). Here heat is only applied to the solution once all acids have been added, and heat is turned off once the sample has been fully digested, often after approximately one hour. In practice, the heat applied is relatively low and the solution not brought to a boil, but there have been no reported measurements of temperature using this methodology. To test the temperature difference between the two methods, we measured the temperatures of the solution using the Dugmore et al. (1995) methodology. In six separate samples over two batches, the maximum temperature reached was 125˚C, with the samples reaching an average maximum temperature of 100-120˚C when the hotplate is turned on (Fig. 2.12). Hotplates were only on for 15 minutes in all cases, with temperatures set to 4.5/10 on a Corning PC-400 Hot Plate. Prior to turning the hotplate on, temperatures remained around ambient room temperature with brief increases of a few degrees when first adding HNO_3 to the solution. This significant difference in temperatures and exposure time is the likely cause for the very different conclusions of Monteath et al. (2019a) and Cooper et al. (2019). This is supported by experimental evidence that shows dissolution is enhanced at higher temperatures and longer exposure times (e.g., Blockley et al., 2005; Strachan, 2017). Four of the acid digested samples were mounted and analyzed for major and minor oxide geochemistry alongside an untreated split of each sample, with no observable differences in composition (Fig. 2.13) and no signs of physical or chemical degradation (Fig. 2.14). None of this challenges that fact that acidic (or alkaline) solutions alter natural glasses, however, it does suggest that the application of acid-digestion under moderate temperatures and shorter times does not notably alter glass shards. However, we should note that these results are only applicable to glass >25 μm.

To further this conclusion, apart from Cooper et al. (2019) there are no published data that indicate that acid-digestion impacts geochemical analyses. Many researchers have utilized this method for decades (e.g., Pilcher and Hall, 1996; Hall and Pilcher, 2002; Pilcher et al., 1996, 2005; Plunkett et al., 2004; Davies et al., 2007, Mackay et al., 2016; Watson et al., 2016; Monteath et al., 2019b), and there has been no evidence that the data produced by these labs has differed from those avoiding acid digestion. Much of these data are available in Tephrabase, available at https://www.tephrabase.org/, or in supplementary datasets released with the publications themselves. These observations emphasize the importance of creating a standard methodology for cryptotephra processing and extraction to avoid unnecessary damage to samples and to ensure reliable inter-laboratory comparison of data.

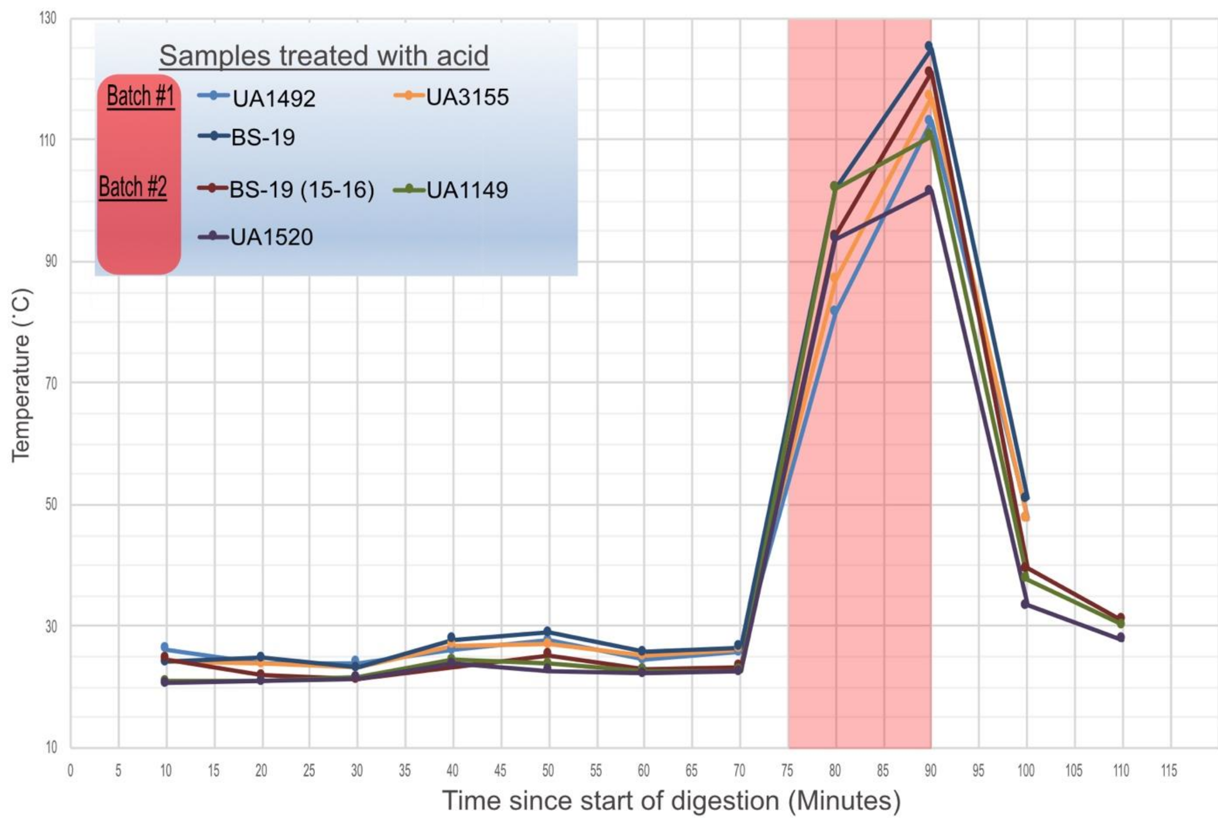

Figure 2.12: Temperatures recorded during the acid digestion procedure, following the methods of Dugmore et al. (1995). Red rectangle highlights the time periods where hotplate was set to 4.5/10. Heat was applied until the peat samples (BS) were fully dissolved.

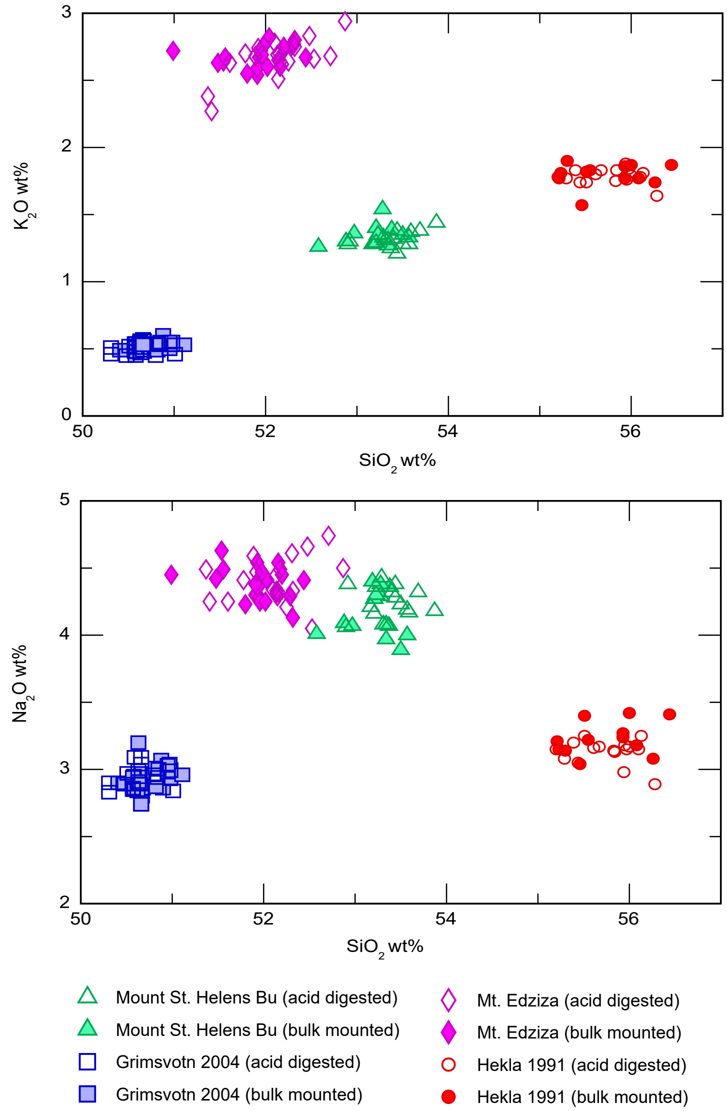

Figure 2.13: Bivariate plots of Na_2O and K_2O vs. SiO_2 (wt%) of four different basaltic tephra consecutively analyzed on a JEOL8900R superprobe. Glass shards are 45-75 microns in size and were either untreated (bulk mounted) or acid-digested using the standard procedures of Dugmore et al. (1995). No observable differences are found in any of the sample's geochemistry. Samples were selected for comparison to earlier studies and to represent different compositions and include: Mount St. Helens tephra Bu, Washington state, USA (UA3155; collected by Jordan Harvey, 2018), Grimsvotn Nov. 2004 eruption, Iceland (UA1492; collected by Thor Thordarson, 2008), Mt. Edziza complex, west flank Williams cone, BC, Canada (UA1149; collected by Gerald Osborn, 2007), and Hekla 1991 eruption, east slopes, Iceland (collected by Thor Thordarson, 1991). ID3506 (Lipari obsidian), BHVO-2G, and Laki secondary standards were run through the experiment.

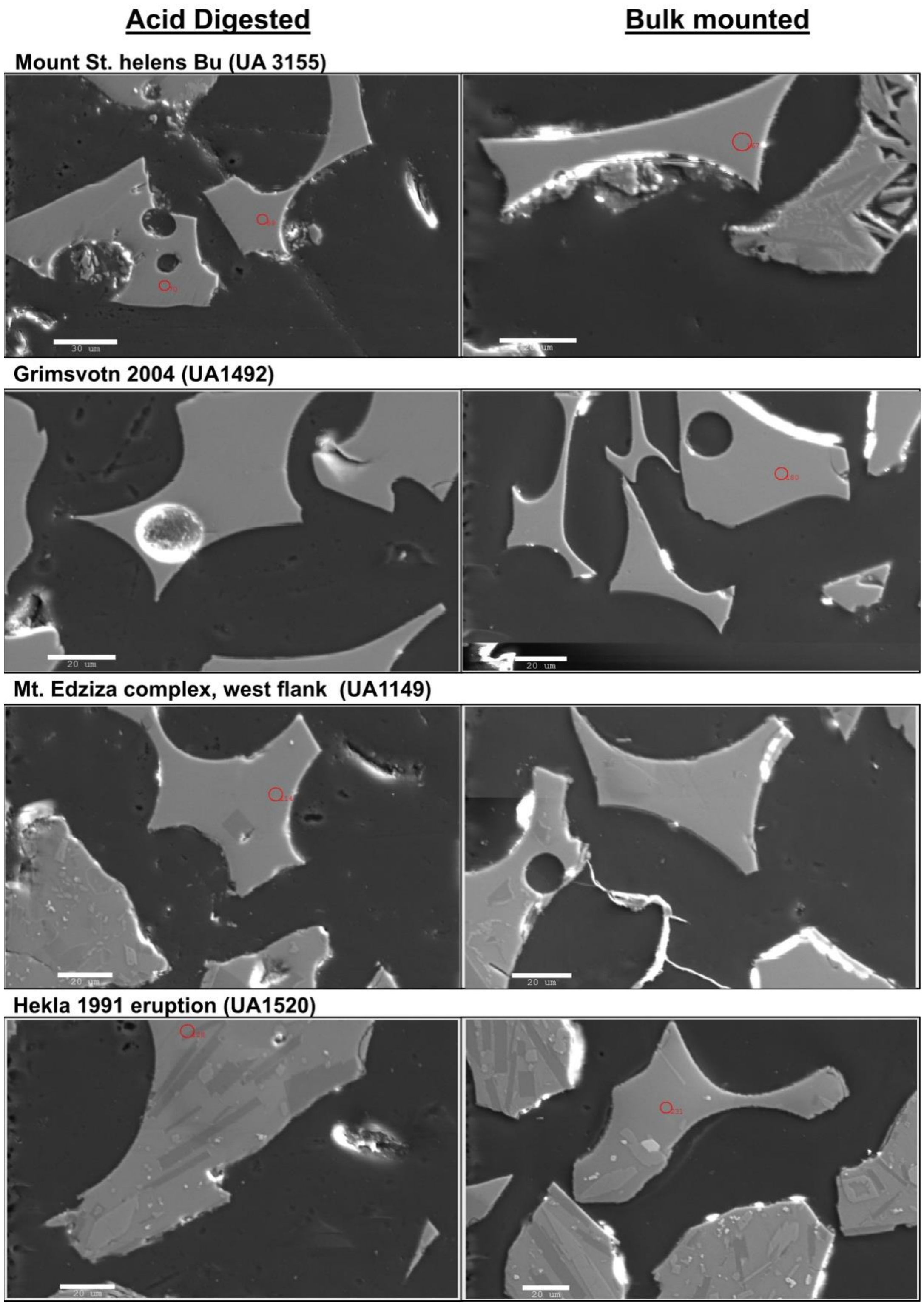

Figure 2.14: SE images of four duplicate basalt samples, processed either with the acid digestion methods of Dugmore et al. (1995) (left) or bulk mounted (right). Red circles indicate analysed points. Alteration is most obvious on the outer rims of samples resulting in jagged edges.

2.4.2.2. Hand-picking glass shards

Hand-picking shards may be necessary with low glass concentrations and/or when the glass concentrate contains abundant non-glass material. It is time-consuming but saves analytical time and guarantees exposure of shards at the surface of the puck. Picking shards has been described by Lane et al. (2014), where gas chromatography syringes attached to a micromanipulator were used to pick shards in de-ionized water. However, it can be done with more common instruments (Fig. 2.15). The concentrate (sitting in de-ionized water) is transferred by pipette to a well slide or petri dish sitting under a microscope. Fine tweezers or a pick are used to separate glass shards from other minerals and a 100 µL micropipette with a fine tip is used to transfer the shards into the hole of a pre-drilled acrylic puck. Shards should be placed directly in the centre of the puck's hole. Regularly check the puck under a microscope to ensure the shards were successfully transferred, and the micropipette tips to make sure none remain. De-ionized water will fill each hole as shards are transferred, and the puck can be placed on a hotplate at 50-80˚C to increase evaporation rates.

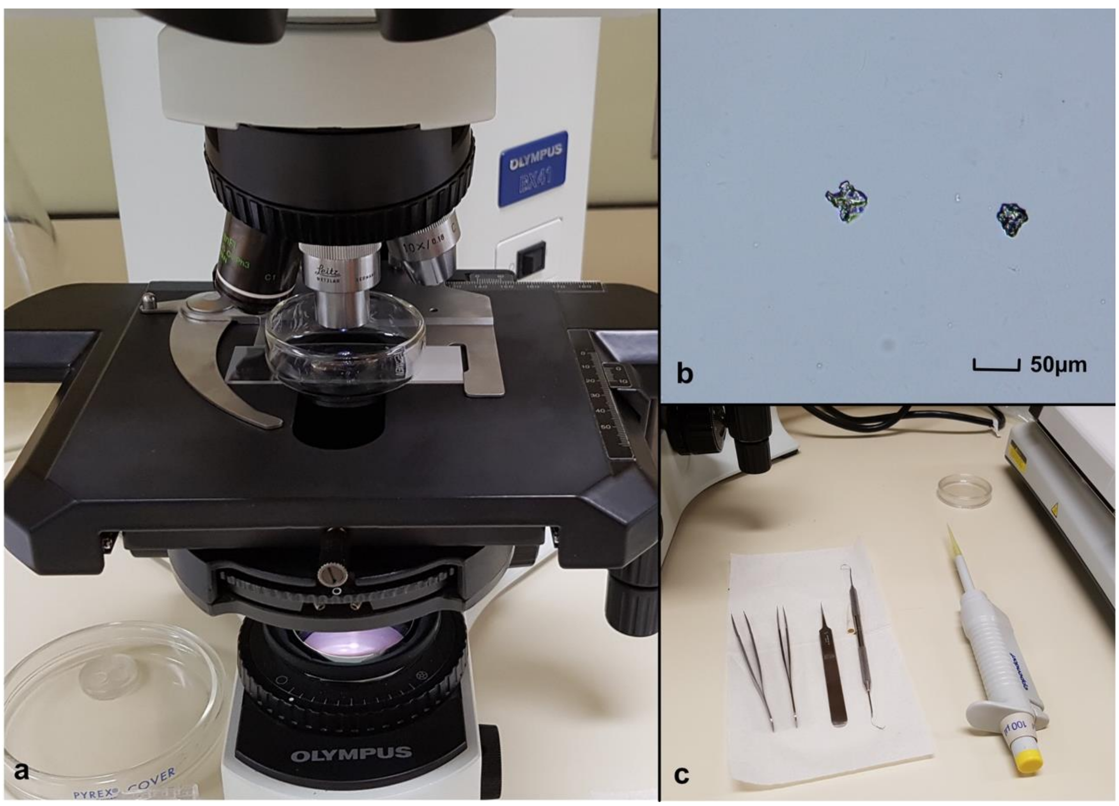

Figure 2.15: Set up for hand-picking, concentrate is placed in a well slide or petri dish with de-ionized water or ethanol (a). When a shard is located (b), it is isolated using fine tweezers or a pick and extracted with a micropipette (c).

2.4.2.3. Mounting samples for geochemical analysis

Samples can be mounted in several ways including glass slides covered in epoxy (e.g., Hall and Pilcher, 2002; Swindles et al., 2010; Watson et al., 2016), circular epoxy moulds mounted on silicon rubber (Hall and Hayward, 2014; Watson et al., 2016), and multi-sample mounts made from epoxy (e.g., Dunbar et al., 2003) or acrylic (e.g., Jensen et al., 2008; Davies et al., 2016) pucks. We find ~1” diameter (2.54 cm) acrylic pucks with 3 to 9 pre-drilled holes are an effective way to mount cryptotephra. They are produced from clear acrylic rods sliced into shorter sections and placed in a drill press to drill holes – the hole diameter (0.2-0.5 cm) depends on the number of holes per puck. These lengths are then sliced into individual pucks. They can also be made from acrylic sheets cut to spec in a computer numerical control (CNC) machine. The pucks are less than 0.47 cm thick to be compatible with all CAMECA and JEOL stages. Pucks can also be produced using a mold to create an epoxy puck that is then drilled. The disadvantage of this method is it is time consuming for higher volume labs and requires the use of more expensive epoxy to make the puck itself.

For mounting, pucks are placed on double-sided tape adhered to a strong flat solid surface and placed on a hot plate (Fig. 2.16). Samples are added by pipetting suspended material into each hole, allowing multiple samples to be mounted simultaneously to the same puck. Each sample is placed into its hole using its own designated pipette. Once water has evaporated, the sample is covered in epoxy and left to cure. This method places the sample at the surface being polished, and ensures that surface is flat, minimizing the polishing required and exposing the samples at the same time. It also avoids the issues often encountered in glass slides where the random distribution of the sample in the epoxy and uneven surface can lead to loss of grains during polishing and some grains not being exposed. Having multiple samples in one puck is also advantageous when working on analytical instruments with limited sample capacity.

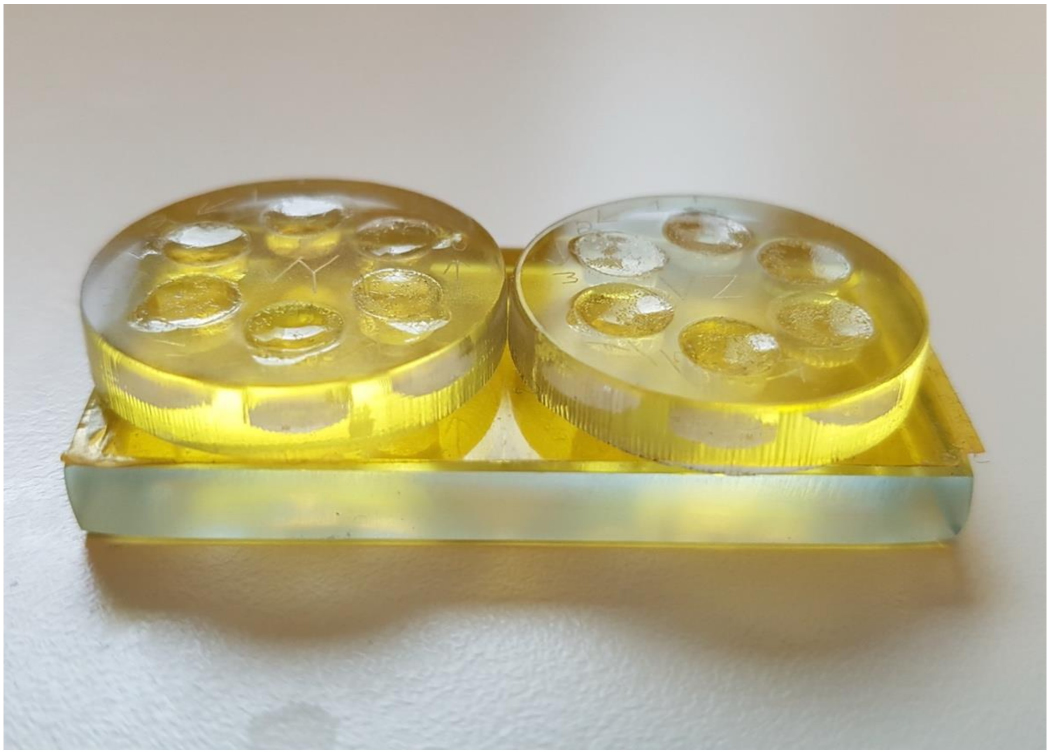

Figure 2.16: Two six-hole acrylic pucks placed on double-sided Kapton tape attached to a glass plate. Samples were individually placed into each hole, evaporated, covered in Specifix-20 epoxy, and labeled in a counter-clockwise orientation. Pucks are left at room temperature until fully cured (2-3 days for Specifix-20) before removing from tape.

The type of double-sided tape is important because some have surface textures and may react with the epoxy and/or being heated. We have experimented with multiple double-sided tapes and use two types, Kapton tape and ASLAN DK 4. Kapton tape is recommended for cryptotephra applications where the sample and puck may be exposed to higher temperatures over longer periods on a hotplate. Kapton uses a strong silicone adhesive that has little surface texture, can withstand temperatures up to 260°C, and is stable when exposed to reactive epoxies (e.g., SpeciFix-20 by Struers). We use the LINQTAPE™ PIT1SD Series 1-mil Polyimide (Kapton) double-sided tape from Caplinq (https://www.caplinq.com). The tape does absorb moisture that can cause bubbles to form beneath the tape after it is adhered to a flat surface and heated – potentially forming an uneven surface on a mounted sample. To avoid this, it should be placed in an oven (~75°C) and degassed for about 1 hour before use. For mounting dry samples, or those requiring less heating, we use the MountFilm Remove ASLAN DK 4 tape produced by Aslan (https://www.aslanfolien.de/en/index.html). This tape has a removable and a permanent adhesive on each side, is relatively non-reactive, adheres well to the acrylic pucks, has virtually no surface texture and is resistant to moderate temperatures (< 80 °C). This tape will react to SpeciFix-20 thus cannot be used with this epoxy.

Several epoxies are suitable for mounting tephra for geochemical analysis, although their varying properties make some more appropriate than others for different samples (Table 2.3). We have experimented with several epoxies (e.g., Struers SpeciFix 20/40, Buehler EpoThin, Epoxy Technology Epo-Tek 301), and use different ones for different applications. Important properties of epoxy include hardness (shore value), shrinkage, viscosity, adherence to grains, and chemical composition (i.e., if hit during analysis how may it alter the data). All the epoxies noted here have relatively low viscosity, which ensures proper penetration through the sample and fewer air bubbles, and pot lives are generally an hour or more, giving time for mounting samples. They also have high hardness, generally low shrinkage and good adherence, although cure times vary from hours to days. When mounting visible tephras, or samples with abundant glass, all are suitable. However, cryptotephra samples with low abundances are more suited to epoxies with the highest hardness, adherence to grains and no (or minimal) shrinkage. Shrinkage in epoxies can be a major challenge because it can result in a concave shape in the mount that will polish unevenly, causing sample loss. Struers SpeciFix-20 epoxy is our preferred epoxy for cryptotephra work due to its nearly absent shrinkage, high hardness, and high adherence to particles, preventing plucking while polishing. Disadvantages are that it must be used in a fume hood, is reactive to some double-sided tapes, and has a slow curing time. Epoxy resin-hardener reactions are exothermic, so epoxies will cure more quickly at larger volumes and slower at smaller volumes, and this is strikingly notable in SpeciFix-20. This epoxy has an official cure time of 8 hours at room temperature, but we recommend, in particular when mounting in small holes (< 8 mm), a minimum of 24-48 hours to ensure maximum hardness when polishing. SpeciFix-40 epoxy is a suitable alternative with a faster curing time of 3.5 hours at 50˚C, or 24 hours at room temperature. It also has an acceptable shore value, is much less reactive and does not require a fume hood. However, it can experience minor shrinkage that worsens as the epoxy ages. This is less of a concern with high concentration samples, and this epoxy is used almost exclusively for visible tephra work. Table 2.3 compares the epoxies used, along with the recommended epoxies tested by the Department of Geosciences ion-microprobe facility at the University of Edinburgh (https://www.ed.ac.uk/geosciences/facilities/ionprobe/technical/epoxyresins). The latter includes the chemical composition of the epoxies they tested, pertinent information to understand what elements may be impacted if the epoxy is hit with the electron beam.

Table 2.3: Comparison of epoxies commonly used in the geosciences as a mounting medium

						Tests by University of Edinburgh*		
Epoxy	**Viscosity** (measured in centipoise. Water and olive oil equal 1 and 84 cP, respectively, at 20˚C)	**Cure time**	**Pot life**	**Shrinkage**	**Hardness (shore value)**, provided by supplier	**Hardness** (shore D hardness avg +/- Stdev)	**Bonding to 1.5-2.5mm glass balls**** (3 measurements of gaps between resin and glass balls)	**Engwell score** (/50)***
Struers SpeciFix 20	No value supplied but very low	8 hours (recommend 24-48 hours)	60 min	none	84	82.8 +/- 0.45	2.92um 2.40um 3.20um	36.5
Struers SpeciFix 40	No value supplied but low	3.5 hours at 40-60˚C, 24 hours at room temp	>60 min	low	82	N/A	N/A	N/A
Buehler EpoThin	Low (200-350 cP at 25˚C)	9 hours at room temp	60 min	Not supplied	~78	79.1 +/- 0.71	1.96um 6.66um 4.49um	32
Epoxy Technology Epo-Tek 301	Very low (100-200 cP at 23˚C)	2 hours at 65˚C	1-2 hours	Not supplied	85	87.5 +/- 0.14	N/A	N/A
Struers Epofix	No value supplied but very low	~12 hours	30 min	none	78	80.1 +/- 1.10	<1.00um	36
Epoxicure	Moderate (400-600 cP)	6 hours at room temperature	30 min	low	82	85.3 +/-0.46 at room temp, 84.9 +/-0.18 at 65˚C	1.02 um, 0.96 um, 0.72 um @ room temp 7.32um,8.54um , 6.16um (65˚C)	40 when cured at room temp, 33 at 65˚C

*https://www.ed.ac.uk/geosciences/facilities/ionprobe/technical/epoxyresins
** Three measurements were taken for each epoxy, measuring the distance of the gap between a glass ball and the epoxy, indicating the epoxy's ability to bond. Lower gaps equal stronger bonding.
***Engwell score calculated as a summation of individual property scores, from 1 to 5, with 5 being the most ideal performance of the epoxy in each category. The tested properties were viscosity, vacuum test, hardness, cure time, composition, bonding, gap, relief, luminescence, and e-beam damage, with a maximum score of 50.

2.4.2.4. Polishing mounted samples

A properly polished tephra mount ensures shards are visible during analytical sessions and helps produce quality geochemical data. If glass shards are not properly exposed and polished to a flat surface, EPMA analysis can inaccurately measure the composition (Hall and Hayward, 2014; Lowe et al., 2017). Too much relief around each shard can cause the electron beam to hit the sample at an angle, reducing the intensity of X-rays reaching the spectrometers. Although different mount types are used in cryptotephra analysis, the polishing methods are largely the same. Increasingly fine grit polishing papers (or polishing powders) are used to expose, section and polish the glass shards, and throughout this process, mounts are periodically checked under a reflective-light microscope to assess the exposure of shards and quality of polish. (Fig. 2.17).

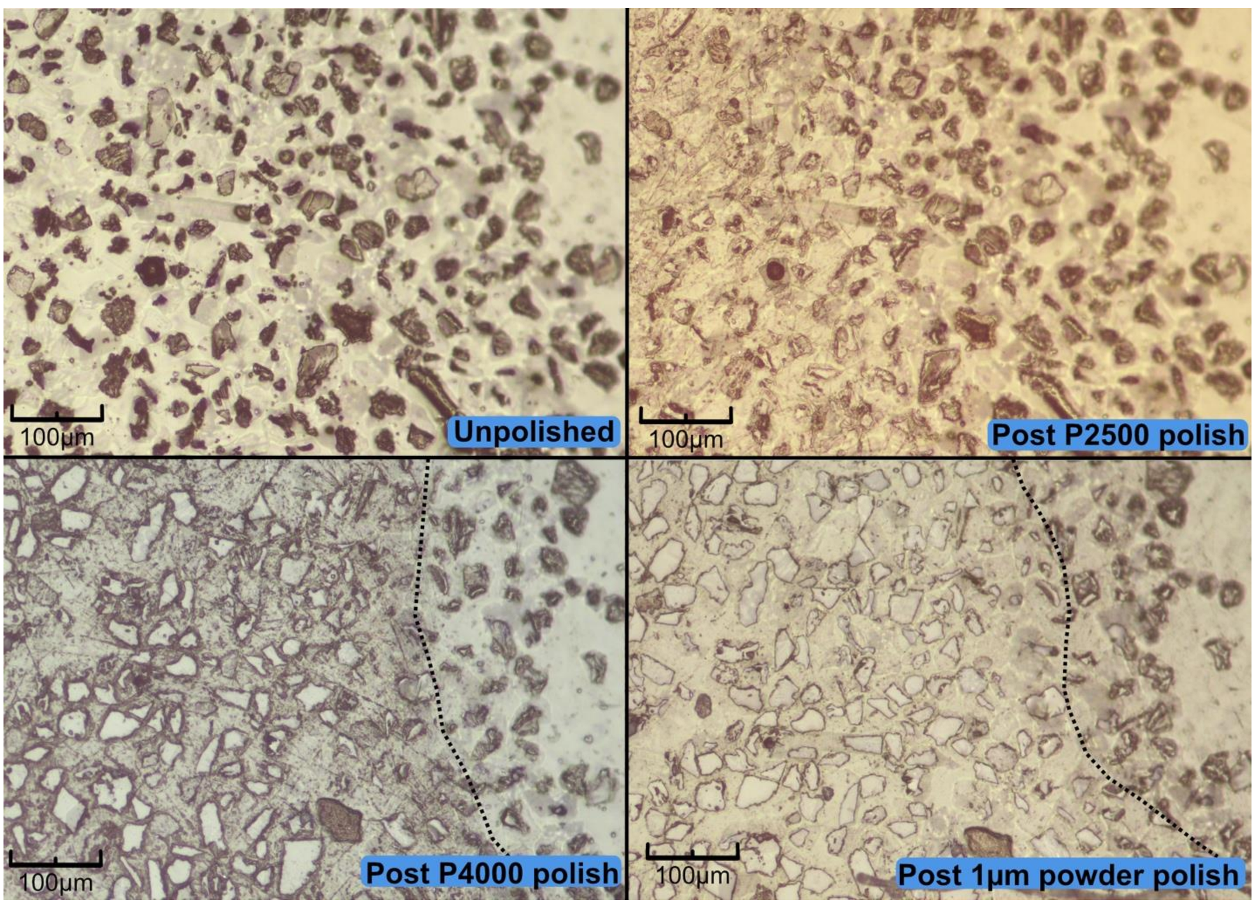

Figure 2.17: Reflected-light microscopy images of the various stages of polishing. This sample had an uneven surface, where a divot on the right side of the image (right of the dashed line) was not being polished as well as the main surface.

Polishing can be done on a motorized polishing wheel, or by hand lapping with polishing powder on a glass plate or waterproof silicon carbide (SiC) polishing paper. For any method of polishing the sample puck should be frequently rotated to avoid streaking lines in one direction. Cryptotephra samples with low concentrations should avoid or minimally use coarser grits of SiC paper or powder (e.g., ≥P1500 or 13 micron grit sizes) (Swindles et al., 2010). In our experience SiC papers result in a better and more consistent polish than powders on a glass plate. A typical polish will start with P1500 (13 microns) and/or P2500 (8 microns) papers to initially expose and section the shards. Care must be taken because shards will be at or near the surface, but they should be clearly sectioned to expose enough surface area for analyses and remove the outer layer of glass that may be affected by chemical and physical alteration (Blockley et al., 2005). If the epoxy shrunk during the mounting procedure, uneven polishing may also occur (Fig. 2.17). An irregular surface cannot be fixed, but to avoid sample loss do not cut the sample until the face is flat, just polish the section that is at the surface. If more analyses are required the puck can be polished down further at a later date. After the coarser grits have exposed the glass and evened the surface, a P4000 (5 micron) polishing paper is used to remove any rough textures, scratches and optimizing the maximum surface area for each shard. The final polishing stage uses 1µm alumina polishing powder wetted with deionized water on a hard surface polishing pad with little relief (e.g., Struers MD-Pan 8" Polishing cloth). On a wheel, this step can take as little as a minute, and achieves a significant improvement in smoothness on the surface of the shards. It is easy to over-polish at any of these stages, therefore samples should be constantly monitored.

Mounts are cleaned after polishing, ideally in an ultrasonic bath, to rid the surface of any residue. They also need to be thoroughly dried prior to carbon-coating because any trapped moisture will cause the coating to bubble and potentially rupture during analyses. The mount can be placed in a warm oven for several hours, but the temperature must be kept below the epoxy's thermal stability. The mount should be made several days prior to analyses to allow the epoxy to off gas and thoroughly dry. Figure 2.18 presents a flow chart outlining the typical procedure for mounting cryptotephra at the University of Alberta. Note that polishing times will vary depending on the type of mount you are working with, the shore value of epoxy used, and the condition of the polishing pad, among many other factors. Thus, modifications to the process will need to be made for each lab.

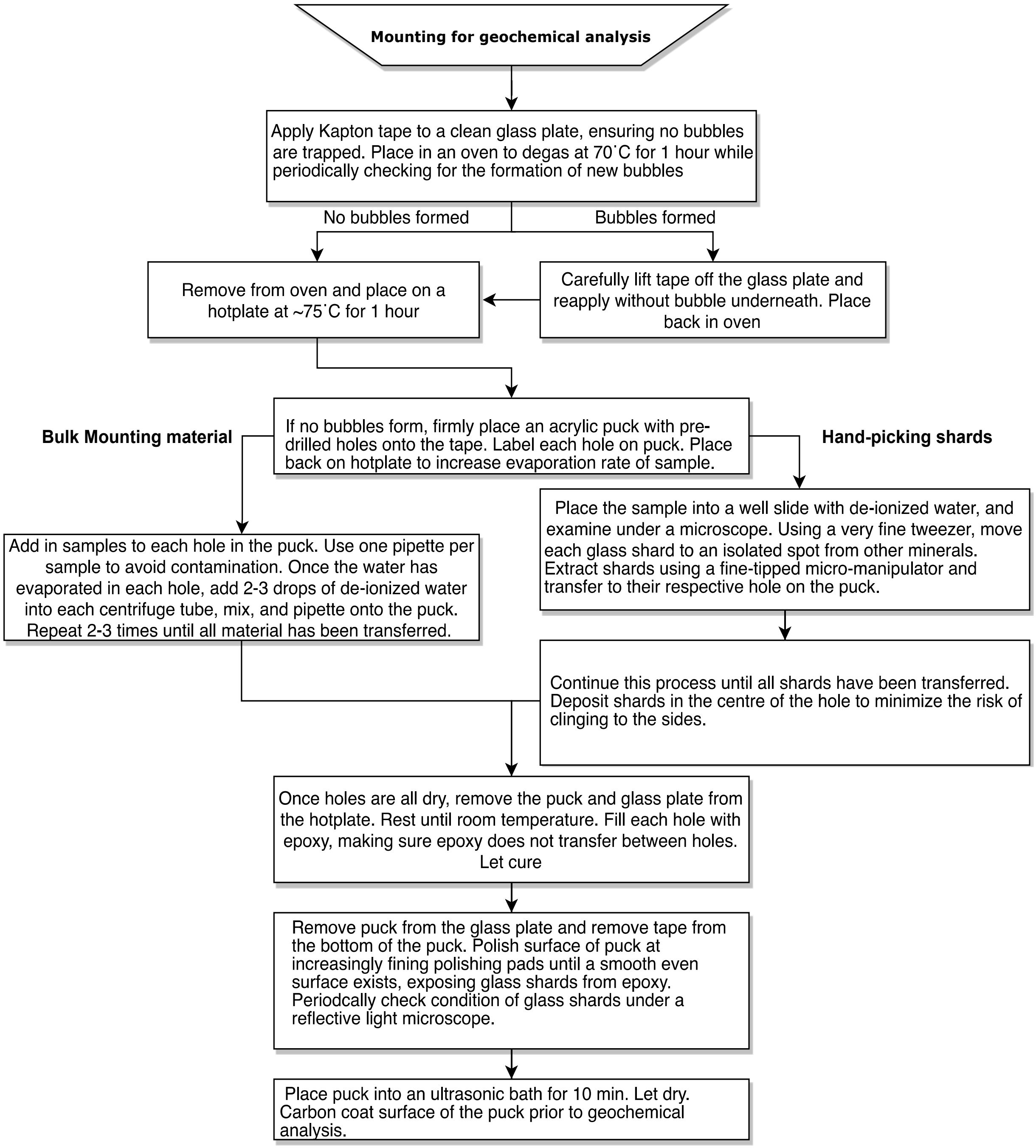

Figure 2.18: Flow chart of typical mounting procedures for geochemical analysis of cryptotephra samples.

2.5. Data Collection and Analysis

2.5.1. Tephra Identification and Quantification

Glass shards are counted using an optical microscope, the type (e.g., petrographic, biologic) is flexible, but ideally the microscope will have objective lenses of 5x, 10x, 20x, a polarizing lens and counting stage. Inexperienced researchers should examine slides that have been previously counted for training purposes. Concentrations may be overestimated by misidentifying similar-looking minerals (e.g., quartz) and biologic fragments (e.g., phytoliths, diatom fragments), or by counting detrital glass shards with primary shards resulting in inaccurate peaks.

Becoming familiar with different glass shard morphologies is a key factor for accurate identification (Fig. 2.19). The most distinct morphology is that of inflated pumices, characterized by their high vesicularity. Vesicles are present in various morphological types – such as blocky pumice and fluted pumice – while platy shards are flat and typically contain few or no vesicles. Platy and cuspate-type glass shards will have sharp edges and may display conchoidal fracturing. Due to the amorphous nature of glass, it is isotropic and will be fully extinct in all orientations when under cross-polarized light. This is a key characteristic that will help distinguish glass shards from similar looking minerals, such as quartz, which also forms conchoidal fractures. Quartz, and other minerals like feldspar, are not isotropic, displaying interference colours under cross-polarized light. Biogenic silica is also isotropic, but often can be distinguished from volcanic glass by morphology. If present, small minerals (i.e., microlites or phenocrysts) within a glass shard can be a helpful distinguishing feature. Additional assistance in identifying glass shards includes a searchable database of common lacustrine components provided by the Tool for Microscopic Identification (TMI), National Lacustrine Core Facility (LacCore), University of Minnesota (Myrbo et al., 2001). McLean et al. (2018) also present some very helpful figures on shard morphology and determination of reworked/detrital tephra. When counting samples mounted using Canada balsam or glycerol, the glass shards will exhibit different colours due to the mounting medium's different refractive indices. Glass shards in Canada balsam have a pink/purple hue compared to the surrounding material, while shards in glycerol will have a light green hue. Lastly, shards have a glassy surface texture, except when shards have been physically or chemically altered as highly acidic or alkaline environments may cause corrosion, leaching, or other damage to the surface (Blockley et al., 2005).

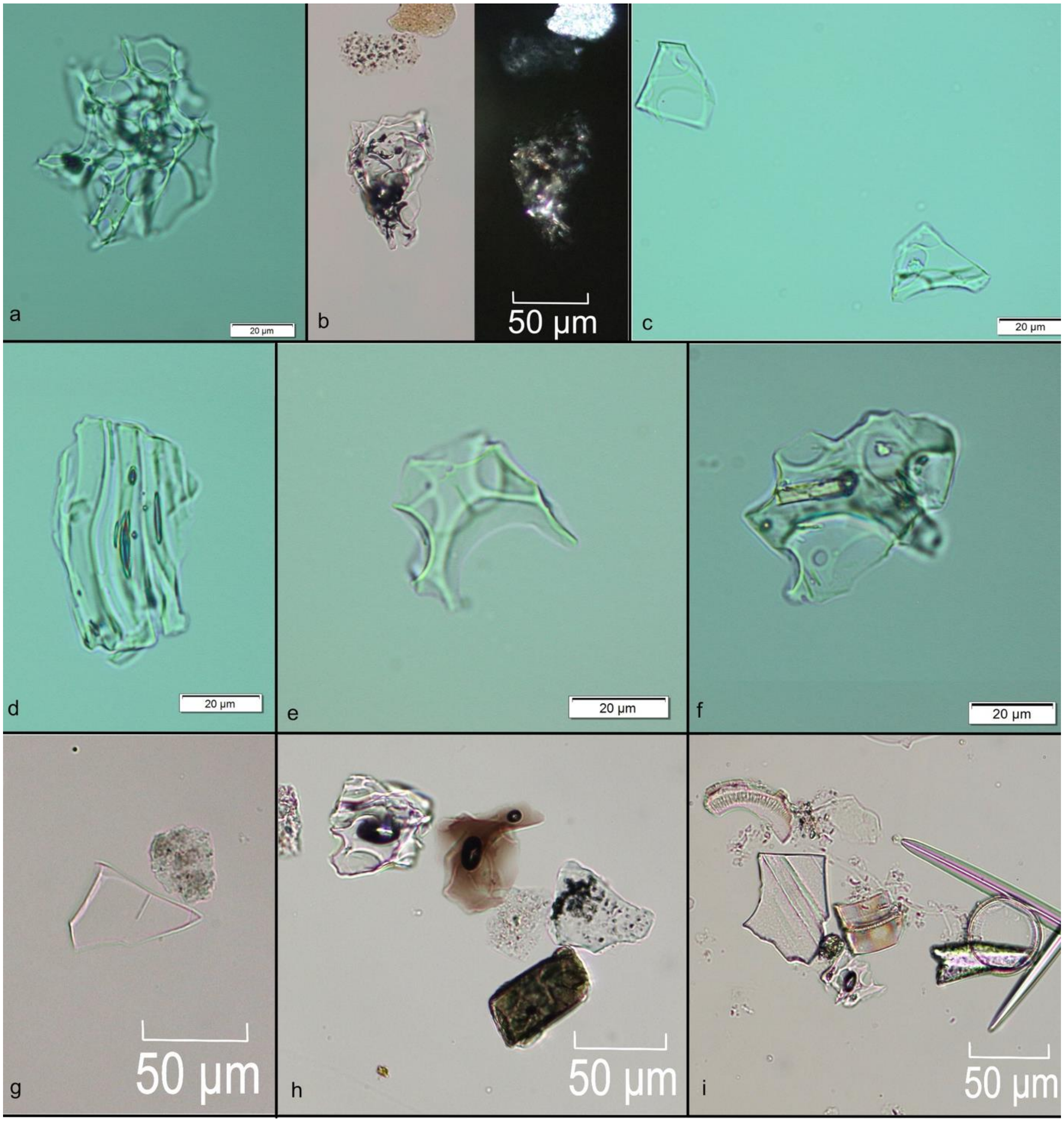

Figure 2.19: Various morphologies and identifying features of glass shards. (a) Highly-vesicular pumice. (b) Pumice shard with microlites or precipitate caught in vesicles, visible under pross-polarized light on right. (c) Platy shard. (d) Stretched pumice with elongated vesicles. (e) Cuspate shard with sharp edges. (f) Blocky pumice with phenocryst. (g) Platy shard. (h) Brown shard in centre, clear vesicular pumice to the left. (i) Assorted biogenic silica fragments next to a pumice shard in the lower middle and a large weathered platy shard to its upper left.

If possible, weathered detrital glass shards should be identified and counted separately from unweathered glass shards. Reworking and redeposition can physically weather glass, where, for example, sharp edges and conchoidal fractures may be rounded or broken off. Detrital shards may also show more signs of chemical weathering, such as pitting and a hazy surface texture (Fig. 2.20). Some of these features may also occur to primary glass, particularly if the sample site is particularly alkaline or acidic. However, it can be possible to differentiate detrital tephra, especially when taking site characteristics in mind (Chapter 3), allowing some peaks to be identified that would otherwise have been missed if counting all glass shards together.

Typical cryptotephra detection methods are very time consuming and often destructive (e.g., LOI). This has led to the search for more efficient and non-destructive alternatives (also discussed in Gehrels et al., 2008; Davies et al., 2015). Techniques such as magnetic susceptibility (e.g., Peters et al., 2010), spectroscopy (e.g., Caseldine et al., 1999), continuously-imaging flow cytometer (e.g., D'Anjou et al., 2014), or X-ray fluorescence (e.g., Kylander et al., 2011; Balascio et al., 2015) have identified tephra deposits in peats and mineral-rich sediments with varying success. Each technique has been largely successful in identifying visible tephra deposits; however, few have been able to detect cryptotephra. Some exceptions include developments in magnetic susceptibility instruments that assisted in the detection of six non-visible tephra layers in alluvial and lacustrine deposits from Fucino Basin, Italy (Di Roberto et al., 2018). A combination of multiple techniques, including visible to shortwave infrared spectroscopy, magnetic susceptibility, and X-ray fluorescence, collectively enhanced cryptotephra detection in marine cores (McCanta et al., 2015). Most recently, van der Bilt et al. (2020) applied Computed Tomography (CT) scanning to synthetic cores, detecting cryptotephra deposits at a µm level thickness and concentrations as low as ~300 shards/cm^3. Despite this work, the most reliable and consistent cryptotephra detection method remains the conventional procedure of ashing and shard counting.

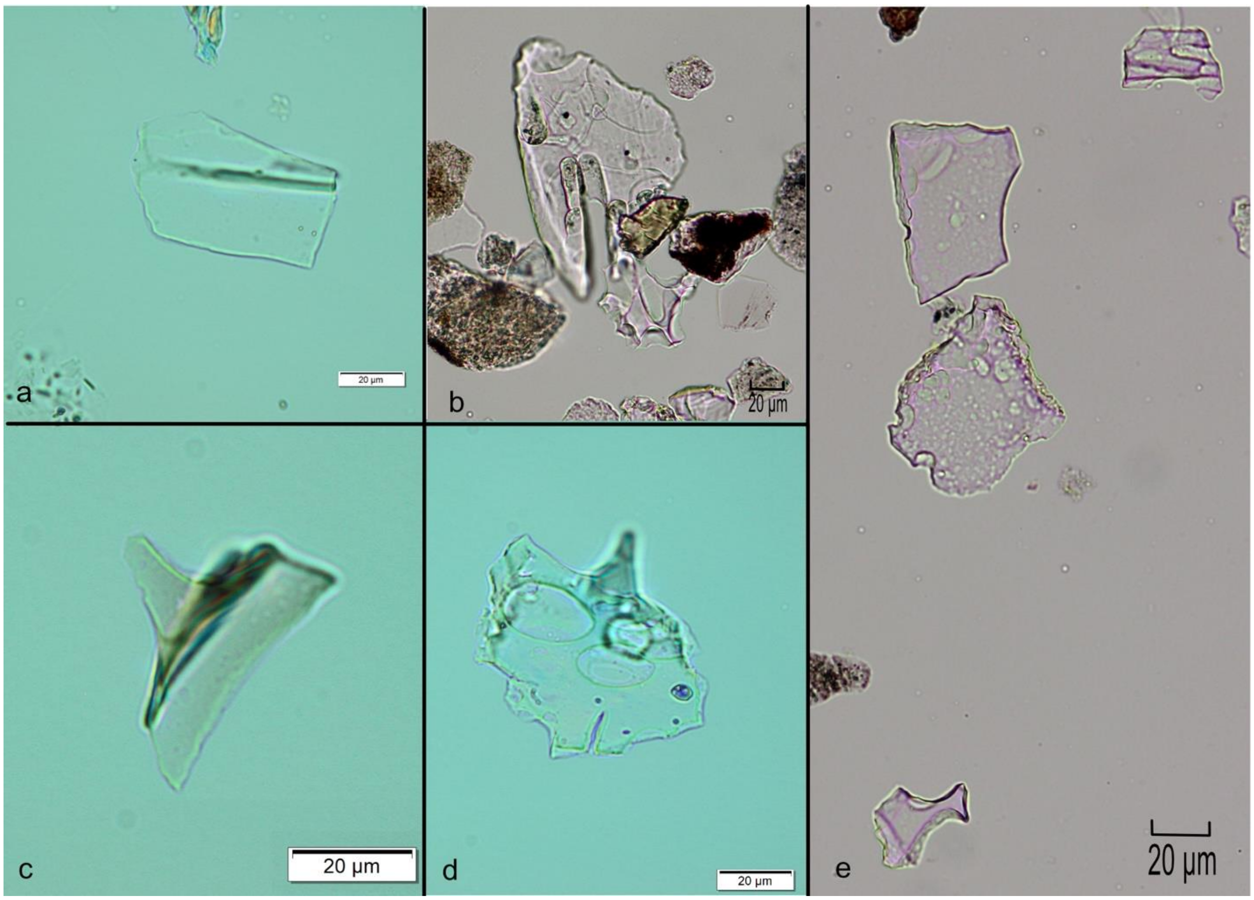

Figure 2.20: Examples of weathering on glass shards. (a) Platy shard with roughened edges and visible pitting of surface. (b) Two heavily weathered shards surrounded by minerals. (c) Brown shard with pitted surface and roughened edges. (d) Larger pumice with surface weathering. (e) Severely weathered shards with hazy surface texture and pitting. Non-detrital shards can have weathered textures, and there is often a gradation between obviously detrital and primary deposits that complicate shard counting. The level of surface weathering seen in a, c, and d can occur in primary shards in acidic environments, while the significant rounding seen in b and c, and hazy whitish hue in e are classic features of older reworked and weathered detrital grains.

2.5.2. Shard Profiles

Once the samples have been counted, a shard concentration profile is made to identify tephra layers within the core. However, it is not always clear where the primary tephra are within a profile. Site-specific characteristics such as detrital and/or reworked/remobilized glass (e.g., Maclean et al., 2018; Monteath et al., 2019b), sediment density (e.g., Beierle and Bond, 2002), sediment accumulation rates (e.g., Davies et al., 2018), or vegetation changes (e.g., Saco Heath bog in Mackay et al., 2016), can all alter the distribution and concentrations of glass peaks in the core.

Four different shard concentration profiles in Figure 2.21 are examples of how shard profiles can vary, although any one profile could feature a mix of profile types. An ideal tephra profile (Fig. 2.21 Type A) will contain discrete narrow peaks concentrated into a few centimetres or less. The peak in shards corresponds to the primary deposition of a tephra, with no evidence of reworking up or down core. Ombrotrophic bogs are common places to find these types of profiles, but peaks like this can be found in any site where there is little background glass, bioturbation, or reworking. If a higher concentration tephra has been deposited in a basin, it is susceptible to secondary deposition and the profile may contain broader tephra peaks with long tails or multiple pulses (Fig. 2.21 Type B). Gradual release of tephra into a lake or fen will produce wide peaks that can make it difficult or impossible to identify a specific depth for an isochron (e.g., Davies et al., 2007; Zawalna-Geer et al., 2016; McLean et al., 2018). However, if there is little or no downward movement of the tephra, 'time of first appearance' could be used in this case to provide a maximum age for the sediment in which it is first found (e.g., Jensen et al., 2016). Settling of tephra through less dense sediments can smooth peaks and extend them below the true deposit (Beierle and Bond, 2002; Davies et al., 2007), although this is generally more prominent in higher concentration tephras (Fig. 2.21 Type C). Other types of reworking may also cause redeposition of tephra, resulting in messy peaks and mixed signals. For example, turbidites and partial collapsing of a sloped lakebed will redeposit older tephra layers into younger sediments (e.g., Zawalna-Geer et al., 2016), and bioturbation can cause mixing of sediments and widened peaks. Another complexity is introduced if the sediment that is transported to a site contains detrital glass, such as loess in Alaska or the Midwest USA, or wind-blown dust in the Falkland Islands (Monteath et al., 2019b). In these cases, concentration profiles will show no clear peaks because tephra input may be more controlled by climate and vegetation changes at the site. Fortunately, if the detrital glass is distinguishable from the primary glass, they can be counted separately and presented as different series on the profile (Fig. 2.21 Type D). If the detrital signal is not too strong, primary tephra deposits may be detected and extracted for geochemical analysis. On the contrary, other sites may contain a detrital signal that can overwhelm the primary tephra layers. In summary, the profiles in Fig 2.21 represent some of the main patterns that may be seen in tephra concentration profiles of lakes and peat cores, and many sites will likely contain some combination of several.

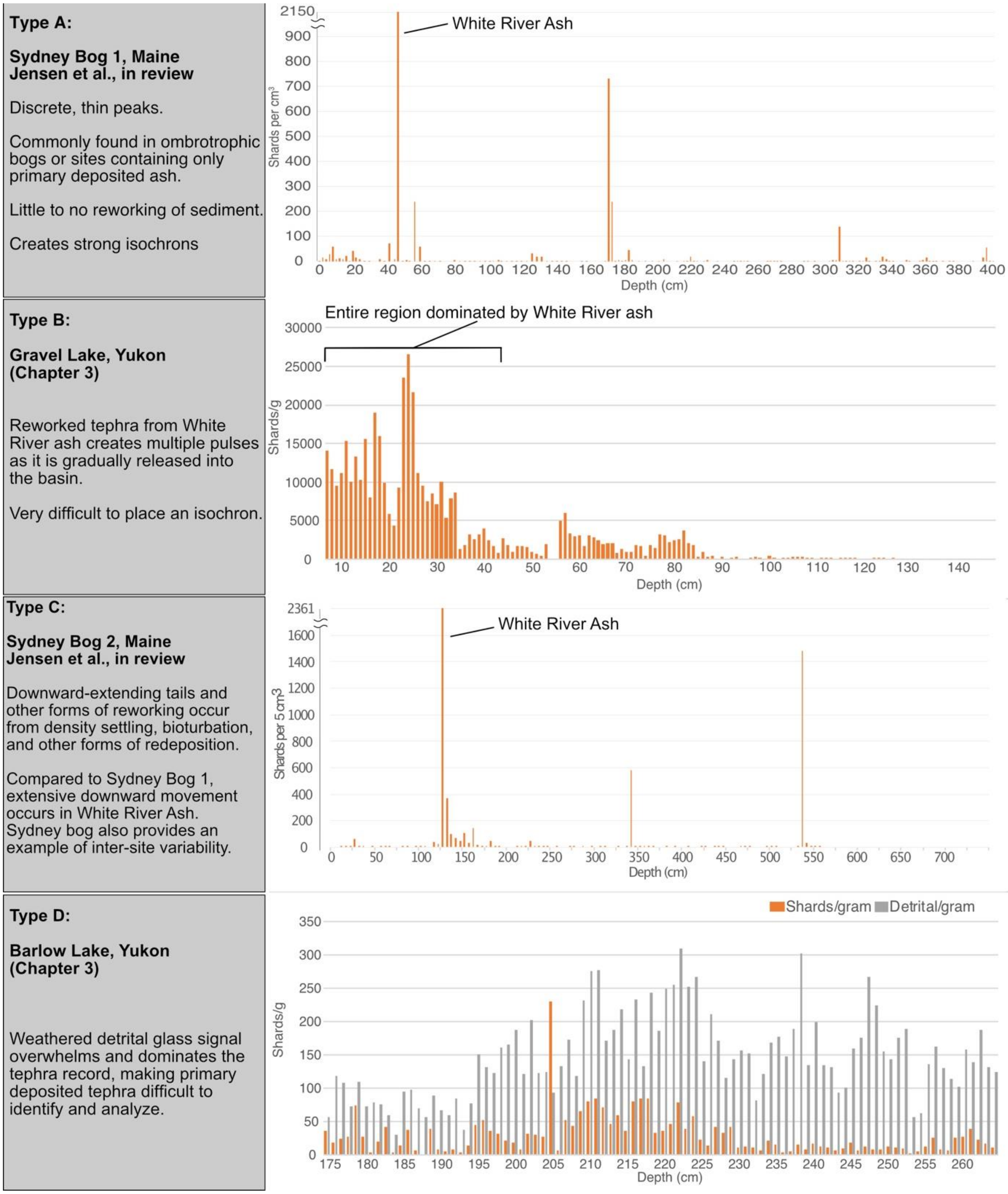

Figure 2.21: Four shard profiles, each representing a different main pattern found in lake or peat deposits.

2.5.3. Analytical Results

There are numerous papers that detail geochemical and statistical analyses in tephrochronology that are also pertinent for cryptotephra research (e.g., Smith and Westgate, 1968; Hunt and Hill 1993; Jensen et al., 2008; Kuehn et al., 2011; Hayward, 2012; Pearce et al., 2014; Lowe et al., 2017; Bolton et al., 2020). Particularly, the problem of sodium migration (or sodium-loss) is well understood in electron microprobe (EMP) glass analyses and is largely avoidable through the application of a de-focussed beam (~10 μm) and lower currents (6 nA) (e.g., Lineweaver, 1963; Nielsen and Sigurdsson, 1981; Smith and Westgate, 1968; Hunt and Hill, 1993, 1996; Morgan and London, 1996, 2005; Spray and Rae, 1995; Jensen et al., 2008). Cryptotephra, due to their small size, present a challenge because they often require a smaller beam size for analysis. Here we will not delve into the details of EMP and trace element analyses in regard to cryptotephra as they are specifically addressed in detail the literature (e.g., Pearce et al., 2007; Tomlinson et al., 2010; Hayward, 2012; Iverson et al., 2017). However, we will briefly outline several unique procedures used at the University of Alberta, specifically the selection of secondary standards and application of time-dependent intensity (TDI) corrections (e.g., Davies et al., 2018; Jensen et al., 2019; Bolton et al., 2020; Foo et al., 2020).

The geochemical analysis of tephra requires the use of secondary standards. Regularly collecting secondary standard data over the course of an analytic run checks the quality of the calibration, monitors for drift, and shows any beam induced modification (e.g., sodium-loss). When choosing secondary standards, it is important to have some sense of the general composition of the sample(s), and how sensitive they may be to an electron beam.

There are a suite of glass secondary standards, ranging from doped synthetic to natural glass that are commonly used in labs for tephra research. However, synthetic glass (e.g., NIST) and homogenized natural glasses (e.g., ATHO-G, StHs6/80-G) are not hydrated and more robust in terms of resisting sodium-loss (Morgan and London, 1996, 2005), thus are not recommended for use – although they are the only available certified standards. The lack of certified natural secondary standards was a long-standing concern that was addressed by Kuehn et al. (2011) for EMP in a large interlaboratory comparison project. Four natural glasses were used – Lipari obsidian (rhyolite; ID3506), Old Crow tephra (rhyolite; UA1099), Sheep Track tephra (phonolite;

UA 1554) and Laki AD 1783 (basalt; AD 1783) – and consensus major and minor element geochemical values were reported. These four standards tend to behave more similarly to the tephras under analyses, thus are more appropriate to use. Lipari obsidian samples like ID 3506 have already been in use as a secondary standard at a number of tephra labs (Hunt and Hill, 1995; Kuehn et al. 2011), and it has been widely adopted across many new laboratories since this time. A similar intercomparison is currently in progress for trace element analyses (Pearce, pers comm).

The composition of secondary standards should also be similar to the unknowns. For example, rhyolitic tephra will not be as effective at monitoring oxides more prevalent in basalts (e.g., Ti, Mg, Ca). If a range of compositions are being analysed, secondary standards reflecting that range should also be analysed. This also extends to calibration standards – if basalts are to be analyzed, it is more appropriate to use a basalt in the calibration of some elements (Si, Al) than more felsic glasses. The Probe for EPMA software (Donovan et al., 2015) is a powerful tool that can ensure that even on days where rhyolites and basalts are analysed together, the calibration standards used for the run can be changed. For example, when analyzing the calibration standards both a rhyolite and basalt are run. After the data are collected on the unknowns two different data output files can be produced, one that uses the rhyolite to calibrate, and another where the basalt was used.

Similarly, Si-rich hydrous and alkali-rich glasses are more susceptible to sodium-loss than others (e.g., Morgan and London, 1996; Kuehn et al., 2011). Sodium-loss is a major consideration when working on cryptotephra, as the glass is often rhyolitic and smaller beam diameters are generally required for analyses. The Lipari obsidian is less sensitive to the electron beam than some tephra because it is young and minimally hydrated (e.g., Kuehn et al., 2011). For this reason, we use at least two secondary standards, the Lipari obsidian and Old Crow tephra. Old Crow tephra is secondarily hydrated, older (~140 ka), and more sensitive to the electron beam, making it more likely to be affected by analytical problems than other standards such as ID3506.

Cryptotephra analyses often requires the use of a 3 or 5 micron beam, but a beam this focused will create sodium migration if no measures are taken to prevent this process. The most widely used approach to solving this challenge is to dramatically lower the beam current as well as alter count times and the order of analyses (e.g., Hayward, 2012). Unfortunately, the very low currents impact the count rates for the analyses, decreasing the precision of the data. An alternative is to simply reduce the beam size, maintain the current, induce sodium-loss, but track the sodium-loss as it occurs and correct for it. This is known as time-dependent intensity (TDI) correction.

TDI corrections have been attempted manually but can now be done using the Probe for EPMA software (Donovan et al., 2015). During EPMA, as the x-ray intensity (measured as counts per second, cps) of more volatile elements such as Na and K decrease, intensities of Si and Al can correspondingly increase. When the TDI software is enabled, it takes periodic measurements at pre-determined intervals to track the change in cps over time. The most sensitive elements (Na, K, Al, Si) should be measured first because TDI can only be applied to the first set of elements measured (i.e., the first five elements for a five spectrometer EMP). The intensity measurements are then plotted against time, where a best-fit log-linear or log-quadratic formula is added. The y-intercept (where time equals 0) can be extrapolated from this data and gives an estimate of the true intensity of the element before sodium migration takes place (Fig. 2.22). If there are no significant changes in intensity over time for some elements, TDI corrections can be turned off for them, while maintained on those that required corrections. TDI can also be turned on or off for different samples. For example, if a rhyolite was measured in the same run as a basalt, and that basalt did not experience sodium-loss while the rhyolite did, two separate files can be produced, one with TDI on for the rhyolite, the other with it completely off for the basalt (see Fig. 2.23). In practice, we typically find that only corrections for Na and Si, or just Na, are required utilizing the typical TDI analytical settings used.

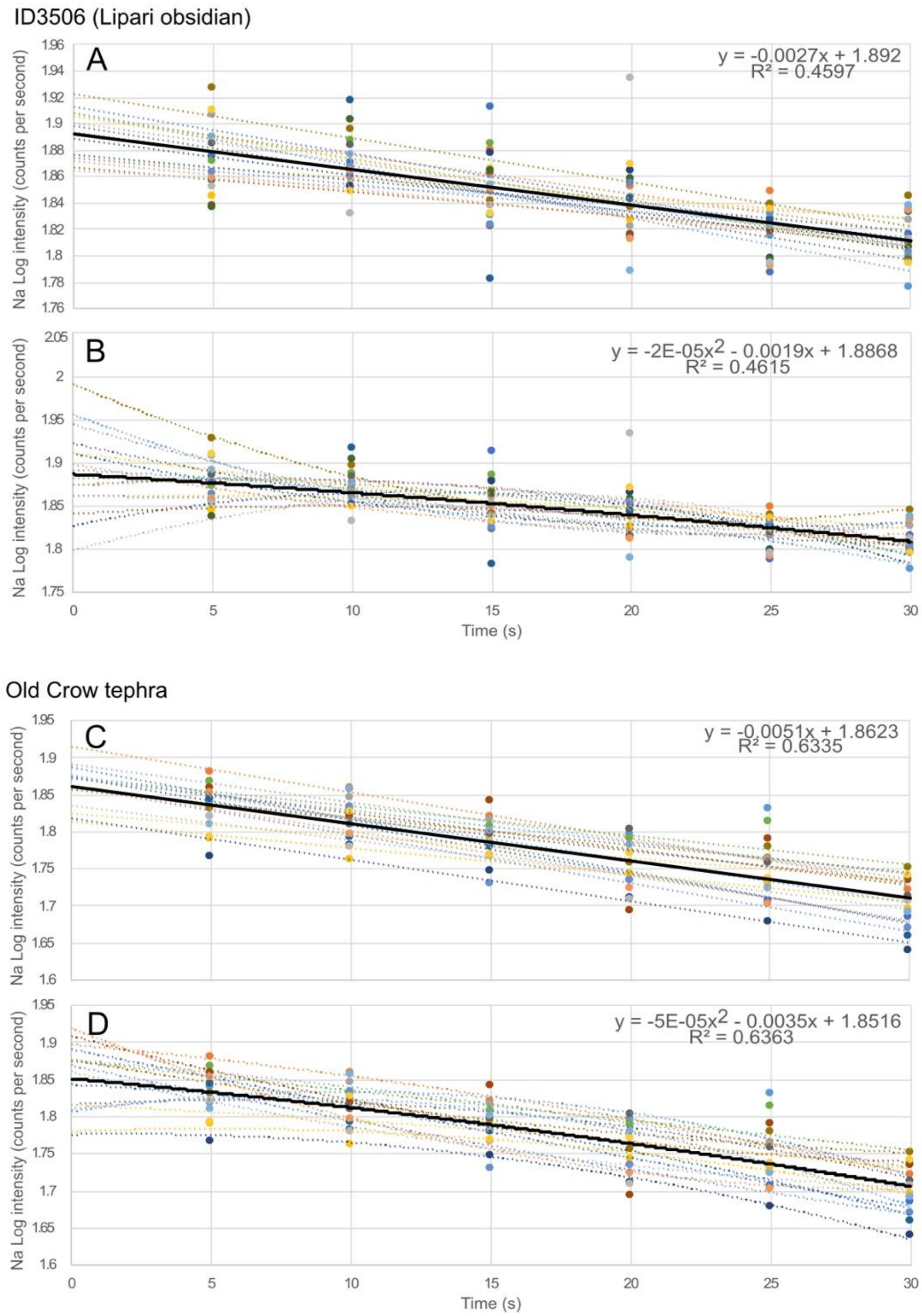

Figure 2.22: Na Log intensity vs. time plot of 17 ID3506 (A and B) and 16 Old-Crow tephra (C and D) measurements during TDI corrections. Log-linear corrections estimate the true Na intensity when extrapolated to the y-intercept, shown by the dotted lines above. Dark black line and included equation represent the best fit line for all measured values. Although log-quadratic functions (B and D) are suitable for more beam-sensitive material, log-linear functions (A and C) are a better fit for TDI analysis of tephra. Samples were run under the following conditions: 15keV, 6nA, 5 µm beam diameter, and a peak acquisition time of 30 seconds divided into 6 TDI intervals.

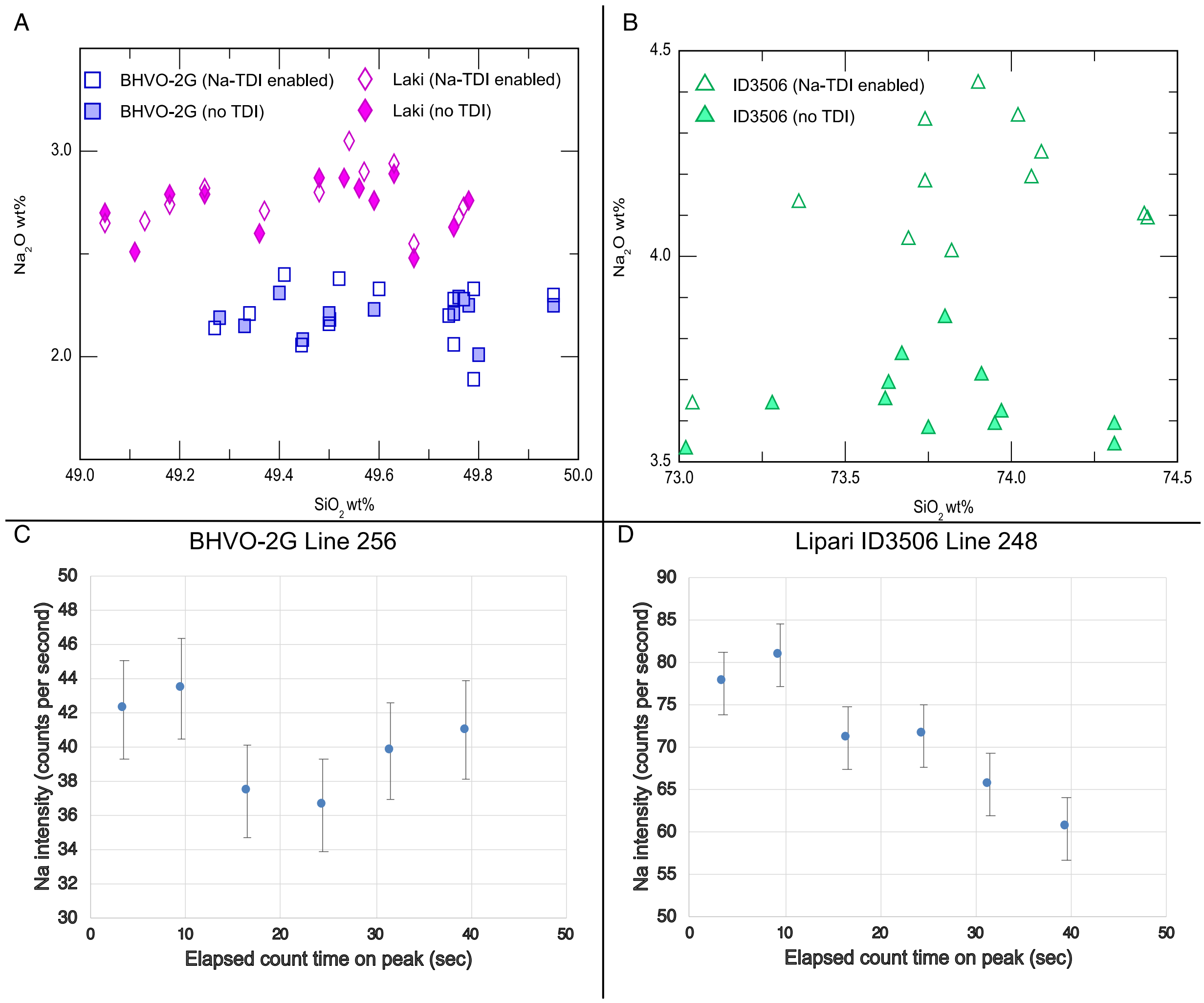

Figure 2.23: Rhyolites like Lipari ID3506 (b and d) are more prone to alkali migration, resulting in lowered Na intensity over time during the analyses (d). Basaltic tephra such as the BHVO-2G and Laki secondary standards (a and c) are less sensitive to beam exposure (c).

The standard conditions for cryptotephra analyses at the University of Alberta microprobe lab are an accelerating voltage of 15keV, 6nA beam current, 5 µm beam diameter, with a peak acquisition time of 20 to 30 seconds. Changes in the intensity of counts are monitored at six intervals over the acquisition time, with Na and/or Si then corrected using a log-linear TDI correction. Initial experiments with a 3 µm beam diameter and a 4nA beam current found the best results when TDI was on for Na_2O, SiO_2 and K_2O. This resulted in reasonable analyses on ID 3506, Walcott tuff, and the Sheep Track tephra (Fig. 2.24). Offsets on Al_2O_3 for Lipari and Walcott were minor enough that they could be corrected offline, but this is not ideal. Because Al_2O_3 is measured in the second set of oxides (with five crystals only five oxides can be measured simultaneously), it is not correctable by TDI. We have also been unable to successfully analyse the more sensitive Old Crow at this smaller diameter beam (Fig. 2.24). Further experimentation will examine rearranging measurement order to ensure Si, Na, Al and K are run in the first set of measurements, thus correctable by TDI, although this will notably lengthen analytical times. To address the issues with Old Crow, the most likely solution will require modifying the beam current; either lowering it, which will impact count rates and precision, or potentially increasing it and/or the count interval, which may produce a more easily correctable curve.

Overall, using the appropriate secondary standards and using the aforementioned 5µm beam and TDI setup, our lab has been able to produce reliable and consistent results in both visible and cryptotephra projects (e.g., Davies et al., 2018; Jensen et al., 2019; Monteath et al., 2019b; Foo et al., 2020; Otiniano et al., 2020; Pyne-O'Donnell and Jensen, 2020; Bolton et al., 2020). These data also show, in particular the 3 µm experiments, how different tephras have different sensitivities to the electron beam, reinforcing the practice of using secondary standards that are most similar (both compositionally and in terms of hydration) to the samples being analysed.

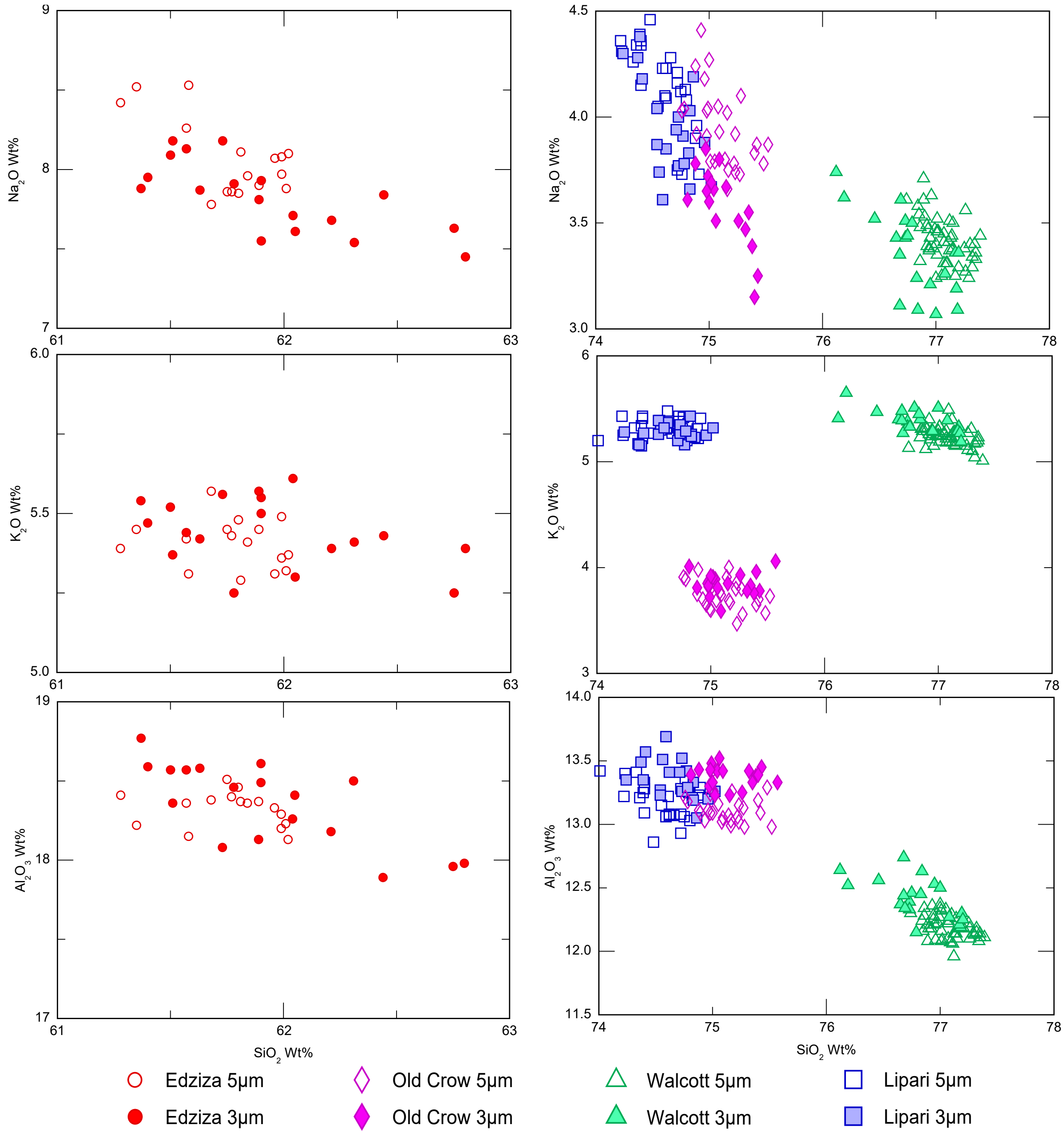

Figure 2.24: Comparison of EPMA analysis between 5 µm beam diameter at 6nA (open symbols) and 3 µm beam diameter at 4nA (closed symbols) conditions. Careful adjustments to the peak acquisition time and use of TDI corrections on Na, Si, and K have produced similar results between both analyses, but Old Crow tephra is still too sensitive to the smaller beam diameter to produce reliable results. Increased Al_2O_3 values in the rhyolitic 3-micron analyses display the heightened effects of alkali migration from more focused beams, whereas the Sheep Track tephra (Edziza) is more resistant. Further experiments are taking place to make 3-micron beam analyses a reliable and viable option for tephra research.

2.6. Conclusions

Cryptotephra research is challenging and requires a consistent methodology to produce reliable results. The processing and analyses of cryptotephra, if done incorrectly, can lead to the loss of valuable shards and may result in inaccurate or inconclusive results. As each peat and lake site is unique, processing and extraction techniques will need to be adjusted to fit the characteristics of the sample. Here we have outlined a comprehensive protocol from the initial sub-sampling and processing of a core, to extraction and mounting of tephra for shard counting and geochemical analysis, to the characterization and interpretation of results in the form of tephra concentration profiles and geochemical analyses. Our main conclusions are:

1. It is important to understand the individual site's characteristics prior to processing the sample, as some steps will need to be altered or avoided depending on a variety of factors including (but not limited to): location, proximity to volcanoes, primary/secondary tephra depositional processes, surrounding geologic features (e.g. loess deposits or perennial snow beds), vegetation presence/types, approximate accumulation rates, or general lake features (e.g. inflowing streams, water depth, sediment type, watershed size, etc.).
2. Processing steps such as LOI, sieving, and density separations are required to effectively recover and isolate glass shards from the rest of the material. These techniques are crucial to build reliable tephra concentration profiles and recover enough material to collected geochemical data. However, in some cases steps may have to be modified or avoided, such as LOI when the same sample is to be used for both counting and analyses.
3. Mounting processes are adjusted depending on the tephra concentration and amount of available material. Additional steps such as pollen spiking (for shard counting) or acid digestion (for geochemical analysis) may be required. Processed material is mounted to a glass slide for initial counts, whereas the material is mounted in acrylic pucks and covered in epoxy for microprobe or ICP-MS analysis.
4. To identify potential isochrons or key areas of interest in a core, proper interpretation of tephra concentration profiles is essential, but can be complicated by factors such as: reworked/detrital tephra, gradual release of tephra from watershed/perennial snow beds, density-induced settling of tephra, or bioturbation.

5. Careful consideration of secondary standards and the use of TDI correction software (or analytical modifications such as those presented by Hayward, 2012) can ensure reliable analyses of cryptotephra samples on an electron microprobe. These tools will minimize the likelihood of analytical errors caused by geochemical drift/offset during analysis or alkali migration.

2.7. References

Abbott, P.M., Jensen, B.J., Lowe, D.J., Suzuki, T., Veres, D., 2020. Crossing new frontiers: extending tephrochronology as a global geoscientific research tool. Journal of Quaternary Science 35, 1-8.

Balascio, N.L., Francus, P., Bradley, R.S., Schupack, B.B., Miller, G.H., Kvisvik, B.C., Bakke, J., Thordarson, T., 2015. Investigating the use of scanning x-ray fluorescence to locate cryptotephra in minerogenic lacustrine sediment: experimental results, in Anonymous Micro-XRF Studies of Sediment Cores. Springer, 305-324.

Beierle, B., Bond, J., 2002. Density-induced settling of tephra through organic lakesediments. J. Paleolimnol. 28, 433-440.

Bergman, J., Wastegård, S., Hammarlund, D., Wohlfarth, B., Roberts, S.J., 2004. Holocene tephra horizons at Klocka Bog, west-central Sweden: aspects of reproducibility in subarctic peat deposits. J. Quaternary Sci. 19, 241-249.

Blockley, S.P.E., Pyne-O'Donnell, S.D.F., Lowe, J.J., Matthews, I.P., Stone, A., Pollard, A.M., Turney, C.S.M., Molyneux, E.G., 2005. A new and less destructive laboratory procedure for the physical separation of distal glass tephra shards from sediments. Quaternary Science Reviews 24, 1952-1960.

Bolton, M.S., Jensen, B.J., Wallace, K., Praet, N., Fortin, D., Kaufman, D., De Batist, M., 2020. Machine learning classifiers for attributing tephra to source volcanoes: an evaluation of methods for Alaska tephras. Journal of Quaternary Science 35, 81-92.

Boygle, J., 1999. Variability of tephra in lake and catchment sediments, Svínavatn, Iceland. Global and Planetary Change 21, 129-149.

Bourne, A.J., 2012. The late Quaternary tephrochronology of the Adriatic region: implications for the synchronisation of marine records. Doctoral dissertation, University of London

Brookes, D., Thomas, K.W., 1967. The distribution of pollen grains on microscope slides part I. The non-randomness of the distribution. pollen et spores 9, 921-629.

Caseldine, C., Baker, A., Barnes, W.L., 1999. A rapid, non-destructive scanning method for detecting distal tephra layers in peats. The Holocene 9, 635-638.

Cooper, C.L., Savov, I.P., Swindles, G.T., 2019. Standard chemical-based tephra extraction methods significantly alter the geochemistry of volcanic glass shards. J. Quaternary Sci 34, 697-707.

Crovisier, J., Advocat, T., Dussossoy, J., 2003. Nature and role of natural alteration gels formed on the surface of ancient volcanic glasses (Natural analogs of waste containment glasses). J. Nucl. Mater. 321, 91-109.

D'Anjou, R.M., Balascio, N.L., Bradley, R.S., 2014. Locating cryptotephra in lake sediments using fluid imaging technology. J. Paleolimnol. 52, 257-264.

Davies, L.J., 2018. The development of a Holocene cryptotephra framework in northwestern North America (Doctoral dissertation). University of Alberta, Edmonton, AB. https://doi.org/10.7939/R3HX1660C

Davies, L.J., Jensen, B.J.L., Froese, D.G., Wallace, K.L., 2016. Late Pleistocene and Holocene tephrostratigraphy of interior Alaska and Yukon: Key beds and chronologies over the past 30,000 years. Quaternary Science Reviews 146, 28-53.

Davies, L.J., Appleby, P., Jensen, B.J.L., Magnan, G., Mullan-Boudreau, G., Noernberg, T., Shannon, B., Shotyk, W., van Bellen, S., Zaccone, C., Froese, D.G., 2018. High-resolution age modelling of peat bogs from northern Alberta, Canada, using pre- and post-bomb 14C, 210Pb and historical cryptotephra. Quaternary Geochronology 47, 138-162.

Davies, S.M., 2015. Cryptotephras: the revolution in correlation and precision dating. J. Quaternary Sci. 30, 114-130.

Davies, S.M., Wastegård, S., Wohlfarth, B., 2003. Extending the limits of the Borrobol Tephra to Scandinavia and detection of new early Holocene tephras. Quatern. Res. 59, 345-352.

Davies, S.M., Hoek, W.Z., Bohncke, S.J., Lowe, J.J., O'Donnell, S.P., Turney, C.S., 2005. Detection of Lateglacial distal tephra layers in the Netherlands. Boreas 34, 123-135.

Davies, S.M., Elmquist, M., Bergman, J., Wohlfarth, B., Hammarlund, D., 2007. Cryptotephra sedimentation processes within two lacustrine sequences from west central Sweden. The Holocene 17, 319-330.

Declercq, J., Diedrich, T., Perrot, M., Gislason, S.R., Oelkers, E.H., 2013. Experimental determination of rhyolitic glass dissolution rates at 40–200 C and 2< pH< 10.1. Geochim. Cosmochim. Acta 100, 251-263.

Demuro, M., Roberts, R.G., Froese, D.G., Arnold, L.J., Brock, F., Ramsey, C.B., 2008. Optically stimulated luminescence dating of single and multiple grains of quartz from perennially frozen loess in western Yukon Territory, Canada: Comparison with radiocarbon chronologies for the late Pleistocene Dawson tephra. Quaternary Geochronology 3, 346-364.

Di Roberto, A., Smedile, A., Del Carlo, P., De Martini, P.M., Iorio, M., Petrelli, M., Pantosti, D., Pinzi, S., Todrani, A., 2018. Tephra and cryptotephra in a ~60,000-year-old lacustrine sequence from the Fucino Basin: new insights into the major explosive events in Italy. Bulletin of Volcanology 80, 20.

Donovan, J.J., Kremser, D., Fournelle, J.H., Goemann, K., 2015. Probe for EPMA: Acquisition, automation and analysis, version 11: Eugene, Oregon, Probe Software. Inc., http://www.probesoftware.com .

Dugmore, A.J., Newton, A.J., 1992. Thin tephra layers in peat revealed by X-radiography. Journal of Archaeological Science 19, 163-170.

Dugmore, A.J., Newton, A.J., Sugden, D.E., Larsen, G., 1992. Geochemical stability of fine-grained silicic Holocene tephra in Iceland and Scotland. J. Quaternary Sci. 7, 173-183.

Dugmore, A.J., Larsen, G.r., Newton, A.J., 1995. Seven tephra isochrones in Scotland. The Holocene 5, 257-266.

Dunbar, N.W., Zielinski, G.A., Voisins, D.T., 2003. Tephra layers in the Siple Dome and Taylor Dome ice cores, Antarctica: Sources and correlations. Journal of Geophysical Research: Solid Earth 108, 2374.

Etienne, D., Jouffroy-Bapicot, I., 2014. Optimal counting limit for fungal spore abundance estimation using Sporormiella as a case study. Vegetation history and archaeobotany 23, 743-749.

Finsinger, W., Tinner, W., 2005. Minimum count sums for charcoal-concentration estimates in pollen slides: Accuracy and potential errors. The Holocene 15, 293-297.

Foo, Z.H., Jensen, B.J.L., Bolton, M.S.M., 2020. Glass geochemical compositions from widespread tephras erupted over the last 200 years from Mount St. Helens. J. Quaternary Sci. 35, 102-113.

Fortin, D., Praet, N., McKay, N.P., Kaufman, D.S., Jensen, B.J.L., Haeussler, P.J., Buchanan, C., De Batist, M., 2019. New approach to assessing age uncertainties – The 2300-year varve chronology from Eklutna Lake, Alaska (USA). Quaternary Science Reviews 203, 90-101.

Froggatt, P.C., Lowe, D.J., 1990. A review of late Quaternary silicic and some other tephra formations from New Zealand: Their stratigraphy, nomenclature, distribution, volume, and age. N. Z. J. Geol. Geophys. 33, 89-109.

Froggatt, P.C., 1992. Standardization of the chemical analysis of tephra deposits. Report of the ICCT Working Group. Quaternary International 13-14, 93-96.

Gehrels, M.J., Lowe, D.J., Hazell, Z.J., Newnham, R.M., 2006. A continuous 5300-yr Holocene cryptotephrostratigraphic record from northern New Zealand and implications for tephrochronology and volcanic hazard assessment. The Holocene 16, 173-187.

Gehrels, M.J., Newnham, R.M., Lowe, D.J., Wynne, S., Hazell, Z.J., Caseldine, C., 2008. Towards rapid assay of cryptotephra in peat cores: Review and evaluation of various methods. Quaternary International 178, 68-84.

Griggs, A.J., Davies, S.M., Abbott, P.M., Rasmussen, T.L., Palmer, A.P., 2014. Optimising the use of marine tephrochronology in the North Atlantic: a detailed investigation of the Faroe Marine Ash Zones II, III and IV. Quaternary Science Reviews 106, 122-139.

Håkanson, L., Jansson, M., 1983. Principles of Lake Sedimentology. Springer-verlag Berlin.

Hall, V.A., McVicker, S.J., Pilcher, J.R., 1994. Tephra-linked landscape history around 2310 BC of some sites in counties Antrim and Down, 245-253.

Hall, V.A., Pilcher, J.R., 2002. Late-Quaternary Icelandic tephras in Ireland and Great Britain: detection, characterization and usefulness. The Holocene 12, 223-230.

Hall, M., Hayward, C., 2014. Preparation of micro- and crypto-tephras for quantitative microbeam analysis. Geological Society, London, Special Publications 398, 21-28.

Hayward, C., 2012. High spatial resolution electron probe microanalysis of tephras and melt inclusions without beam-induced chemical modification. The Holocene 22, 119-125.

Heiri, O., Lotter, A.F., Lemcke, G., 2001. Loss on ignition as a method for estimating organic and carbonate content in sediments: reproducibility and comparability of results. J. Paleolimnol. 25, 101-110.

Hunt, J.B., Hill, P.G., 1993. Tephra geochemistry: a discussion of some persistent analytical problems. The Holocene 3, 271-278.

Hunt, J.B., Hill, P.G., 1996. An inter-laboratory comparison of the electron probe microanalysis of glass geochemistry. Quaternary International 34-36, 229-241.

Iverson, N.A., Kalteyer, D., Dunbar, N.W., Kurbatov, A., Yates, M., 2017. Advancements and best practices for analysis and correlation of tephra and cryptotephra in ice. Quaternary Geochronology 40, 45-55.

Jensen, B.J.L., Froese, D.G., Preece, S.J., Westgate, J.A., Stachel, T., 2008. An extensive middle to late Pleistocene tephrochronologic record from east-central Alaska. Quaternary Science Reviews 27, 411-427.

Jensen, B.J., Beaudoin, A.B., 2016. Geochemical characterization of tephra deposits at archaeological and palaeoenvironmental sites across south-central Alberta and southwest Saskatchewan, in Anonymous Back on the Horse: Recent Developments in Archaeological and Palaeontological Research in Alberta. Archaeological Survey of Alberta Occasional Paper no. 36, 154-160.

Jensen, B.J.L., Beaudoin, A.B., Clynne, M.A., Harvey, J., Vallance, J.W., 2019. A re-examination of the three most prominent Holocene tephra deposits in western Canada: Bridge River, Mount St. Helens Yn and Mazama. Quaternary International 500, 83-95.

Jensen, B.J.L., Davies, L., Nolan, C., Pyne-O'Donnell, S., Monteath, A.J., Ponomareva, V., Portnyagin, M., Booth, R., Hughes, P., Bursik, M., Cook, E., Plunkett, G., Luo, Y., Vallance, J.W., Cwynar, L.C., Pearson, D.G. A latest Pleistocene and Holocene composite tephrostratigraphic framework for northeastern North America. Submitted to Quaternary Science Reviews, 2021.

Katoh, S., Danhara, T., Hart, W.K., WoldeGabriel, G., 1999. Use of sodium polytungstate solution in the purification of volcanic glass shards for bulk chemical analysis. Nature and Human Activities 4, 45-54.

Kaufman, D.S., Jensen, B.J.L., Reyes, A.V., Schiff, C.J., Froese, D.G., Pearce, N.J.G., 2012. Late Quaternary tephrostratigraphy, Ahklun Mountains, SW Alaska. J. Quaternary Sci. 27, 344-359.

Kitaba, I., Nakagawa, T., 2017. Black ceramic spheres as marker grains for microfossil analyses, with improved chemical, physical, and optical properties. Quaternary International 455, 166-169.

Kuehn, S.C., Froese, D.G., 2010. Tephra from Ice—A Simple Method to Routinely Mount, Polish, and Quantitatively Analyze Sparse Fine Particles. Microscopy and Microanalysis 16, 218-225.

Kuehn, S.C., Froese, D.G., Shane, P.A., Participants, I.I., 2011. The INTAV intercomparison of electron-beam microanalysis of glass by tephrochronology laboratories: results and recommendations. Quaternary International 246, 19-47.

Kylander, M.E., Lind, E.M., Wastegård, S., Löwemark, L., 2012. Recommendations for using XRF core scanning as a tool in tephrochronology. The Holocene 22, 371-375.

Lane, C.S., Blockley, S.P.E., Lotter, A.F., Finsinger, W., Filippi, M.L., Matthews, I.P., 2012. A regional tephrostratigraphic framework for central and southern European climate archives during the Last Glacial to Interglacial transition: comparisons north and south of the Alps. Quaternary Science Reviews 36, 50-58.

Lane, C.S., Cullen, V.L., White, D., Bramham-Law, C.W.F., Smith, V.C., 2014. Cryptotephra as a dating and correlation tool in archaeology. Journal of Archaeological Science 42, 42-50.

Lane, C.S., Lowe, D.J., Blockley, S.P.E., Suzuki, T., Smith, V.C., 2017. Advancing tephrochronology as a global dating tool: Applications in volcanology, archaeology, and palaeoclimatic research. Quaternary Geochronology 40, 1-7.

Lineweaver, J.L., 1963. Oxygen outgassing caused by electron bombardment of glass. J. Appl. Phys. 34, 1786-1791.

Lowe, D.J., 2011. Tephrochronology and its application: A review. Quaternary Geochronology 6, 107-153.

Lowe, D.J., Ramsey, C.B., Housley, R.A., Lane, C.S., Tomlinson, E.L., 2015. The RESET project: constructing a European tephra lattice for refined synchronisation of environmental and archaeological events during the last c. 100 ka. Quaternary Science Reviews 118, 1-17.

Lowe, D.J., Pearce, N.J.G., Jorgensen, M.A., Kuehn, S.C., Tryon, C.A., Hayward, C.L., 2017. Correlating tephras and cryptotephras using glass compositional analyses and numerical and statistical methods: Review and evaluation. Quaternary Science Reviews 175, 1-44.

Machida, H., 1999. The stratigraphy, chronology and distribution of distal marker-tephras in and around Japan. Global Planet. Change 21, 71-94.

Machida, H., Arai, F., 2003. Atlas of Tephra in and around Japan. University of Tokyo Presse, 120.

Mackay, E.B., Jones, I.D., Folkard, A.M., Barker, P., 2012. Contribution of sediment focussing to heterogeneity of organic carbon and phosphorus burial in small lakes. Freshwat. Biol. 57, 290-304.

Mackay, H., Hughes, P.D.M., Jensen, B.J.L., Langdon, P.G., Pyne-O'Donnell, S.D.F., Plunkett, G., Froese, D.G., Coulter, S., Gardner, J.E., 2016. A mid to late Holocene cryptotephra framework from eastern North America. Quaternary Science Reviews 132, 101-113.

McCanta, M.C., Hatfield, R.G., Thomson, B.J., Hook, S.J., Fisher, E., 2015. Identifying cryptotephra units using correlated rapid, nondestructive methods: VSWIR spectroscopy, X-ray fluorescence, and magnetic susceptibility. Geochem. Geophys. Geosyst. 16, 4029-4056.

McLean, D., Albert, P.G., Nakagawa, T., Suzuki, T., Staff, R.A., Yamada, K., Kitaba, I., Haraguchi, T., Kitagawa, J., Smith, V.C., 2018. Integrating the Holocene tephrostratigraphy for East Asia using a high-resolution cryptotephra study from Lake Suigetsu (SG14 core), central Japan. Quaternary Science Reviews 183, 36-58.

Monteath, A.J., Teuten, A.E., Hughes, P.D.M., Wastegård, S., 2019a. Effects of the peat acid digestion protocol on geochemically and morphologically diverse tephra deposits. J. Quaternary Sci. 34, 269-274.

Monteath, A.J., Hughes, P.D.M., Wastegård, S., 2019b. Evidence for distal transport of reworked Andean tephra: Extending the cryptotephra framework from the Austral volcanic zone. Quaternary Geochronology 51, 64-71.

Morgan, G.B., London, D., 1996. Optimizing the electron microprobe analysis of hydrous alkali aluminosilicate glasses. Am. Mineral. 81, 1176-1185.

Morgan, G.B., VI, London, D., 2005. Effect of current density on the electron microprobe analysis of alkali aluminosilicate glasses. American Mineralogist 90, 1131-1138.

Mulliken, K.M., Schaefer, J.R., Cameron, C.E., 2018. Geospatial distribution of tephra fall in Alaska: a geodatabase compilation of published tephra fall occurrences from the Pleistocene to the present. Miscellaneous Publication MP 164, Alaska Division of Geological & Geophysical Surveys, Fairbanks, Alaska, United States. https://doi.org/10.14509/29847

Myrbo, A., Morrison, A., and McEwan, R., 2011. Tool for Microscopic Identification (TMI). http://tmi.laccore.umn.edu. Accessed on 27 July 2020

Nielsen, C.H., Sigurdsson, H., 1981. Quantitative methods for electron microprobe analysis of sodium in natural and synthetic glasses. Am. Mineral. 66, 547-552.

Otiniano, G.A., Porter, T.J., Benowitz, J.A., Bindeman, I.N., Froese, D.G., Jensen, B.J.L., Davies, L.J., Phillips, M.A., 2020. A Late Miocene to Late Pleistocene Reconstruction of Precipitation Isotopes and Climate From Hydrated Volcanic Glass Shards and Biomarkers in Central Alaska and Yukon. Paleoceanography and Paleoclimatology 35, e2019PA003791.

Payne, R.J., Blackford, J.J., 2008. Extending the Late Holocene Tephrochronology of the Central Kenai Peninsula, Alaska. Arctic 61, 243-254.

Payne, R.J., Kilfeather, A.A., van der Meer, Jaap JM, Blackford, J.J., 2005. Experiments on the taphonomy of tephra in peat. Suo , 147-156

Payne, R., Blackford, J., van der Plicht, J., 2008. Using cryptotephras to extend regional tephrochronologies: An example from southeast Alaska and implications for hazard assessment. Quatern. Res. 69, 42-55.

Payne, R., Gehrels, M., 2010. The formation of tephra layers in peatlands: an experimental approach. Catena 81, 12-23.

Pearce, N.J.G., Westgate, J.A., Perkins, W.T., Eastwood, W.J., Shane, P., 1999. The application of laser ablation ICP-MS to the analysis of volcanic glass shards from tephra deposits: bulk glass and single shard analysis. Global and Planetary Change 21, 151-171.

Pearce, N.J.G., Denton, J.S., Perkins, W.T., Westgate, J.A., Alloway, B.V., 2007. Correlation and characterisation of individual glass shards from tephra deposits using trace element laser ablation ICP-MS analyses: current status and future potential. J. Quaternary Sci. 22, 721-736.

Pearce, N.J.G, Abbott, P.M., Martin-Jones, C., 2014. Microbeam methods for the analysis of glass in fine-grained tephra deposits: a SMART perspective on current and future trends. Geological Society, London, Special Publications 398, 29-46.

Persson, C., 1971. Tephrochronological Investigation of Peat Deposits in Scandinavia and on the Faroe Islands. Sveriges reproduktions AB (distr.).

Peters, C., Austin, W.E.N., Walden, J., Hibbert, F.D., 2010. Magnetic characterisation and correlation of a Younger Dryas tephra in North Atlantic marine sediments. J. Quaternary Sci. 25, 339-347.

Pilcher, J.R., Hall, V.A., 1992. Towards a tephrochronology for the Holocene of the north of Ireland. The Holocene 2, 255-259.

Pilcher, J.R., Hall, V.A., McCormac, F.G., 1996. An outline tephrochronology for the Holocene of the north of Ireland. Journal of Quaternary Science: Published for the Quaternary Research Association 11, 485-494.

Pilcher, J., Hall, V., 1996. Tephrochronological studies in Northern England. Holocene 6, 100-105.

Pilcher, J., Bradley, R.S., Francus, P., Anderson, L., 2005. A Holocene tephra record from the Lofoten Islands, arctic Norway. Boreas 34, 136-156.

Plunkett, G.M., Pilcher, J.R., McCormac, F.G., Hall, V.A., 2004. New dates for first millennium BC tephra isochrones in Ireland. The Holocene 14, 780-786.

Pollard, A.M., Blockley, S., Ward, K.R., 2003. Chemical alteration of tephra in the depositional environment: theoretical stability modelling. Journal of Quaternary Science 18, 385-394.

Prince, T.J., Pisaric, M.F.J., Turner, K.W., 2018. Postglacial Reconstruction of Fire History Using Sedimentary Charcoal and Pollen From a Small Lake in Southwest Yukon Territory, Canada. Frontiers in Ecology and Evolution 6, 209.

Pyne-O'Donnell, S.D., 2007. Three new distal tephras in sediments spanning the Last Glacial–Interglacial Transition in Scotland. Journal of Quaternary Science: Published for the Quaternary Research Association 22, 559-570.

Pyne-O'Donnell, S., 2011. The taphonomy of Last Glacial–Interglacial Transition (LGIT) distal volcanic ash in small Scottish lakes. Boreas 40, 131-145.

Pyne-O'Donnell, S.D.F., Jensen, B.J.L., 2020. Glacier Peak and mid-Lateglacial Katla cryptotephras in Scotland: potential new intercontinental and marine-terrestrial correlations. J. Quaternary Sci. 35, 155-162.

Roland, T.P., Mackay, H., Hughes, P.D.M., 2015. Tephra analysis in ombrotrophic peatlands: A geochemical comparison of acid digestion and density separation techniques. J. Quaternary Sci. 30, 3-8.

Rose, N.L., Golding, P.N.E., Battarbee, R.W., 1996. Selective concentration and enumeration of tephra shards from lake sediment cores. The Holocene 6, 243-246.

Sarna-Wojcicki, A.M., Meyer, C.E., Wan, E., 1997. Age and correlation of tephra layers, position of the Matuyama-Brunhes chron boundary, and effects of Bishop ash eruption on Owens Lake, as determined from drill hole OL-92, southeast California. Geological Society of America Special Papers 317, 79-90.

Smith, D.G.W., Westgate, J.A., 1968. Electron probe technique for characterising pyroclastic deposits. Earth Planet. Sci. Lett. 5, 313-319.

Spray, J.G., Rae, D.A., 1995. Quantitative electron-microprobe analysis of alkali silicate glasses; a review and user guide. The Canadian Mineralogist 33, 323-332.

Stanton, T., Snowball, I., Zillén, L., Wastegård, S., 2010. Validating a Swedish varve chronology using radiocarbon, palaeomagnetic secular variation, lead pollution history and statistical correlation. Quaternary Geochronology 5, 611-624.

Strachan, D., 2017. Glass dissolution as a function of pH and its implications for understanding mechanisms and future experiments. Geochim. Cosmochim. Acta 219, 111-123.

Swindles, G.T., De Vleeschouwer, F., Plunkett, G., 2010. Dating peat profiles using tephra: stratigraphy, geochemistry and chronology. Mires and Peat 7.

Swindles, G.T., Galloway, J., Outram, Z., Turner, K., Schofield, J.E., Newton, A.J., Dugmore, A.J., Church, M.J., Watson, E.J., Batt, C., 2013. Re-deposited cryptotephra layers in Holocene peats linked to anthropogenic activity. The Holocene 23, 1493-1501.

Thompson, R., Bradshaw, R.H.W., Whitley, J.E., 1986. The distribution of ash in Icelandic lake sediments and the relative importance of mixing and erosion processes. J. Quaternary Sci. 1, 3-11.

Timms, R.G.O., Matthews, I.P., Palmer, A.P., Candy, I., Abel, L., 2017. A high-resolution tephrostratigraphy from Quoyloo Meadow, Orkney, Scotland: Implications for the tephrostratigraphy of NW Europe during the Last Glacial-Interglacial Transition. Quaternary Geochronology 40, 67-81.

Tomlinson, E.L., Thordarson, T., Müller, W., Thirlwall, M., Menzies, M.A., 2010. Microanalysis of tephra by LA-ICP-MS — Strategies, advantages and limitations assessed using the Thorsmörk ignimbrite (Southern Iceland). Chemical Geology 279, 73-89.

Turney, C.S.M., Harkness, D.D., Lowe, J.J., 1997. The use of microtephra horizons to correlate Late-glacial lake sediment successions in Scotland. J. Quaternary Sci. 12, 525-531.

Turney, C.S.M., 1998. Extraction of rhyolitic component of Vedde microtephra from minerogenic lake sediments. J. Paleolimnol. 19, 199-206.

van der Bilt, Willem GM, Cederstrøm, J.M., Støren, E.W., Berben, S.M., Rutledal, S., 2020. Rapid tephra identification in geological archives with Computed Tomography (CT): experimental results and natural applications. Frontiers in Earth Science 8, 710.

Wastegård, S., Björck, S., Grauert, M., Hannon, G.E., 2001. The Mjáuvøtn tephra and other Holocene tephra horizons from the Faroe Islands: a link between the Icelandic source region, the Nordic Seas, and the European continent. The Holocene 11, 101-109.

Watson, E.J., Swindles, G.T., Lawson, I.T., Savov, I.P., 2015. Spatial variability of tephra and carbon accumulation in a Holocene peatland. Quaternary Science Reviews 124, 248-264.

Watson, E.J., Swindles, G.T., Lawson, I.T., Savov, I.P., 2016. Do peatlands or lakes provide the most comprehensive distal tephra records? Quaternary Science Reviews 139, 110-128.

Westgate, J.A., Hamilton, T.D., Gorton, M.P., 1983. Old Crow tephra: a new late Pleistocene stratigraphic marker across north-central Alaska and western Yukon Territory. Quatern. Res. 19, 38-54.

Wohlfarth, B., Blaauw, M., Davies, S.M., Andersson, M., Wastegård, S., Hormes, A., Possnert, G., 2006. Constraining the age of Lateglacial and early Holocene pollen zones and tephra horizons in southern Sweden with Bayesian probability methods. Journal of Quaternary Science: Published for the Quaternary Research Association 21, 321-334.

Wolff-Boenisch, D., Gislason, S.R., Oelkers, E.H., Putnis, C.V., 2004. The dissolution rates of natural glasses as a function of their composition at pH 4 and 10.6, and temperatures from 25 to 74 C. Geochim. Cosmochim. Acta 68, 4843-4858.

Zawalna-Geer, A., Lindsay, J.M., Davies, S., Augustinus, P., Davies, S., 2016. Extracting a primary Holocene crytoptephra record from Pupuke maar sediments, Auckland, New Zealand. J. Quaternary Sci. 31, 442-457.

Chapter 3. Cryptotephra deposition in four sub-Arctic lakes, Yukon, Canada

3.1. Introduction

Tephrochronology uses volcanic ash deposits as stratigraphic markers to date and correlate sedimentary records (Lowe, 2011). The emergence of cryptotephra research (Dugmore, 1989; Pilcher and Hall, 1992), which uses non-visible tephra deposits (e.g., Davies, 2015), has dramatically enhanced the geographic extent of tephrochronology applications. Cryptotephra deposits are now regularly identified thousands of kilometres away from source volcanoes (e.g., Jensen et al., 2014; van der Bilt et al., 2017; Plunkett and Pilcher, 2018). At the same time, more studies are exploring the applicability of cryptotephra research in areas more proximal to volcanic regions that also contain visible beds (e.g., McLean et al., 2018). Motivating this work are factors such as large gaps between visible units and the possibility of identifying smaller, less explosive, eruptions that occur more frequently. However, the presence of visible tephra and large quantities of reworked tephra in the sediment require a much more careful assessment of the cryptotephra records in these regions (e.g., Zawalna-Geer et al., 2016; Martin-Jones et al., 2017; Maclean et al., 2018; Davies, 2018).

Lake sediments are a primary source for late Pleistocene to Holocene paleoenvironmental change in the Yukon and Alaska (e.g., Anderson et al., 2001; Levy et al., 2004; Kaufman et al., 2004; Schweger et al., 2011; Graham et al., 2016). Radiocarbon (^{14}C) dating is the primary method used to develop age models for these lake sediments (e.g., Abbott and Stafford, 1996; Kaufman et al., 2004). However, ^{14}C dates can be unreliable from Arctic and sub-Arctic lakes due to slow decomposition rates in the surrounding watershed, resulting in old carbon being reworked into younger sediments (e.g., Shuur et al., 2008), and a general paucity of organic material that can lead to a reliance on bulk sediments or aquatic macrofossils potentially contaminated by carbon from surrounding sediments or bedrock (e.g., Nelson et al., 1988; Kaufman et al., 2004; Oswald et al., 2005; Kennedy et al., 2010; Schreiner et al., 2014; Davies et al., 2018). Tephrochronology can be an alternative way to improve the chronology of these difficult to date sites.

Tephra research in Yukon and Alaska has mainly focused on visible beds, particularly early to late Pleistocene deposits (e.g., Péwé, 1975; Naeser et al., 1982; Westgate et al., 1990; Preece et al., 1999, 2011; Jensen et al., 2008, 2013). The distribution and age of Holocene tephra deposits in the interior of Alaska and Yukon is generally less well understood (e.g., Davies et al., 2016), and visible tephra in Yukon are limited to the White River Ash eruptions at ~1625 cal BP and ~1097 cal BP (e.g., Jensen et al., 2014; Toohey and Sigl, 2017; Reuther et al., 2020). While major eruptions such as the White River ash eastern lobe (Jensen et al., 2014) and Aniakchak CFE II (Riehle et al., 1987; Davies et al., 2016) are also found in Greenland, allowing for precise age estimations, they are only present as visible deposits over limited regions. However, with over 80 major volcanic centres actively erupting over the Holocene from the Alaska Peninsula-Aleutian Arc and Wrangell volcanic field of Alaska (e.g., Miller et al., 1998), Yukon sediment records likely contain numerous cryptotephra deposits. To date, there is only one cryptotephra record from the Yukon – an examination of a peat deposit from central Yukon (Davies, 2018). Results found multiple eruptions of Mt. Churchill, correlations to several known Holocene eruptions (e.g., Redoubt 1989/90; Augustine C), and many previously unknown tephra deposits. The first cryptotephra studies in Alaska were peat records from the Kenai Peninsula and Alaska Panhandle (Payne and Blackford, 2008; Payne et al., 2008). Since then, several lake records have been reported from the interior of Alaska, from the southern Brooks Range, Alaska Highway corridor (Monteath et al., 2017), and the northern Brooks Range (Davies et al., in review) (Fig. 3.1). Collectively, these studies show that cryptotephra are present and identifiable in this region although no lake records have been examined in the Yukon.

In this study, we report cryptotephra records from four lakes located in interior Yukon; Hanging Lake near the Barn Mountains of northern Yukon (Cwynar, 1982; Kurek et al., 2009), Chapman Lake in the Ogilvie Mountains of north-central Yukon (Terasmae and Hughes, 1966; Beierle, 2001), and Gravel and Barlow Lakes in central Yukon (Beierle, 2001) (Fig. 3.1). These represent the first cryptotephra records in the Yukon derived from lake deposits. The main objective is to assess how suitable these lakes are for cryptotephra studies and use the cryptotephra records between the lakes and previous studies to refine the lake's age models. Results show many challenges with cryptotephra deposition in Yukon lakes (e.g., secondary deposition, reworking, recurring geochemically identical tephra populations), but also refine the chronologies of Hanging and Gravel Lakes, contribute at least eight new previously unknown tephras to the regional tephrostratigraphy, and provide new evidence for multiple Mt. Churchill and Aniakchak eruptions over the Holocene.

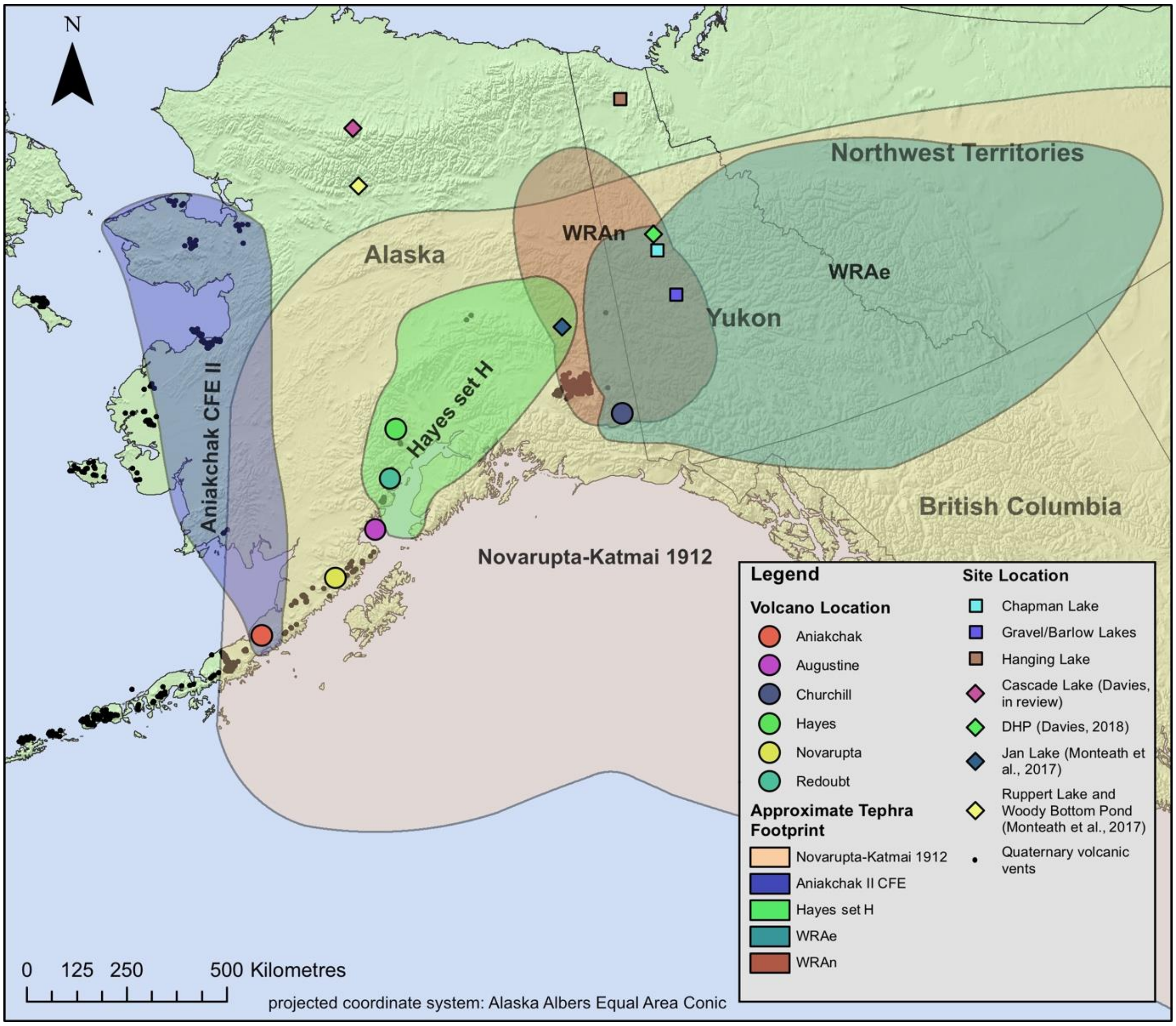

Figure 3.1: Location of the four Yukon lakes in this study and other interior Yukon and Alaska cryptotephra sites. Tephra distributions from Holocene eruptions of Mt. Churchill (White River Ash eastern and northern lobes; WRAe/WRAn), Novarupta-Katmai 1912, Hayes set H, and Aniakchak CFE II are examples of key deposits that are expected as cryptotephra in these lake sediments (adapted from Mulliken et al., 2018). It should be noted that the distribution of Novarupta-Katmai 1912 is likely partially based on historical observations as it is much larger than the distribution of the visible and reported cryptotephra deposits. Tephra from the Hayes set H eruption, specifically layer F2, also known as the Jarvis Ash or unit G (Riehle 1994: Wallace et al., 2014; Davies et al., 2016) was not located in this study, although it is present in the Dempster Highway peatland (DHP; Davies, 2018).

3.2. Site descriptions and sampling

Hanging Lake is the most northern site, located ~80 km south of the Beaufort Sea (68° 21′ N, 138° 21′ W; Fig. 3.1). This lake is approximately 60 ha in size and sits ~500 m asl within the foothills of the Barn Mountains. It has no inflowing streams, an outlet on the northeast end, and has a maximum water depth of 9.5 m on its southern end. Shale, siltstones and sandstones underlie the lake, which sits in a raised basin (Kurek et al., 2009). Based on the smaller size of the drainage basin and its far northern location in the Barn mountains, we expect lower concentrations of tephra at this site. Tussock tundra, wet sedge meadows, heath tundra, and fellfields are some of the modern vegetation surrounding the lake (Cwynar, 1982), which lies in a region of continuous permafrost. Holocene temperatures were fairly stable at the lake, with a mean July air temperature ranging from ~10 to 12 ºC (Kurek et al., 2009).

Hanging Lake is considered an important paleoclimate record as it is in eastern Beringia (non-glaciated Yukon and Alaska), is one of the few paleoenvironmental records in the northern Yukon and has a sediment record that is believed to extend into the last glacial maximum (e.g., Cwynar, 1982; Kurek et al., 2009). Two Hanging Lake cores were collected from the southern end of the lake and age-depth models were made for each core; the first using bulk sediments (Cwynar, 1982) and the second using eight AMS ^{14}C dates from plant macrofossils and chironomid chitin (Kurek et al., 2009). However, the age models contain conflicting ages and significant errors. We re-examine the chronology of Hanging Lake by building a new Bayesian age-model based on the radiocarbon ages of Kurek et al. (2009) and attempt to provide additional chronologic control by using cryptotephra deposits.

Barlow Lake (63°45' N, 137°43' W) is located in central Yukon off the Dempster Highway and was selected, alongside Chapman and Gravel Lakes, as part of a multidisciplinary project to determine the changing vegetation structure and environmental conditions of sub-Arctic lakes at the end of the last glacial maximum. Because of the focus on the late glacial, Barlow was only sampled from 174 to 264 cm depth for tephra counts – focussed around the visible transition from coarser sediment to silty gytjja, interpreted to be the Pleistocene to Holocene transition. Gravel and Chapman Lakes have been previously studied (discussed below), but Barlow Lake has not been previous cored. However, proxy records from the lake sediments may be similar to

Gravel Lake as they are only ~11km from each other. Barlow Lake sits at ~600 m asl, is 80 ha in size and has a water depth of ~5 m. No material for radiocarbon dating was found in the basal portion of the lake sediments, limiting the age estimation to the gradual rise in LOI used as a rough indicator for the transition from the late Pleistocene to Holocene (Fig. 3.4).

Chapman Lake (64° 51' N, 138° 20' W) is one of many kettle lakes in the Ogilvie Mountains, located just off the Dempster Highway and ~40 km south of the Dempster Highway peat (DHP) site (Davies, 2018). Local vegetation at the lake includes alpine shrub tundra, including Salix sp. and Betula glandulosa, and Picea mariana in isolated depressions (Beierle, 2001). At an elevation of ~1000 m asl, the shallow, closed basin lake sits on top of a terminal moraine complex thought to be of Reid age (>200,000 BP), with underlying sediments of glacial till and some glaciolacustrine silts and sands found in nearby exposures (Beierle, 2001). Previous studies describe a maximum water depth of 3 m with an area of ~140 ha.

Gravel Lake (63° 48' N, 137° 53' W) is ~11 km northwest of Barlow Lake in central Yukon off the Klondike Highway. Gravel Lake has an elevation of ~650 m, is roughly 40 ha, and had a water depth of ~1.5 m at the coring locations in April 2017. Gravel Lake is a closed basin lake with a few ephemeral streams, the surrounding vegetation comprises of black spruce and birch boreal forest (Beierle, 2001). X-ray diffraction analysis of Gravel Lake sediments confirmed that it is derived mainly from nearby loess deposits, consisting of quartz and clinochlore (Beierle, 2001). Considering their proximity, it seems likely that the loess deposits are a sediment source for the neighbouring Barlow Lake. Previous research on Gravel Lake derived an age model using radiocarbon dates from four terrestrial macrofossils collected from Chapman Lake (discussed below), tied to the Gravel Lake using eight prominent sedimentary changes, and wiggle-matching the Gravel Lake late Holocene-Pleistocene LOI profile to the Greenland GISP2 δ^{18}O record (Beierle, 2001; Fig. 3.9). The new Gravel Lake core has been sampled for radiocarbon, and the LOI profile closely matches that of the original core. Table 3.1 summarizes all lake core descriptions and extraction methods for these sites.

Table 3.1: Core descriptions for the five cores analyzed for cryptotephra.

Core location	Coordinates	Coring method	Total core length	Section examined for cryptotephra
Gravel Lake, central Yukon	63° 48' N, 137° 53' W	Vibracore	2.23 m	7 cm to 220 cm below top of core
Barlow Lake, central Yukon	63°45' N, 137°43' W	Vibracore	4.20 m	1.74 m to 2.64 m below top of core
Hanging Lake, northern Yukon	68° 21′ N, 138° 21′ W	Livingstone piston sampler	3.69 m	15 cm – 183 cm below top of core
Chapman Lake, central Yukon	64° 51' N, 138° 20' W	Glu Core	24 cm	0 to 24 cm
Gravel Lake, central Yukon	63° 48' N, 137° 53' W	Glu Core	22 cm	0 to 22 cm

3.3. Methods

3.3.1. Subsampling

Gravel, Barlow and Chapman Lakes were cored in April 2017 using a vibracorer. The cores were split into top and bottom halves for ease of transportation, frozen and transported to the University of Alberta for subsampling. The sediment-water interface and the upper ~25 cm of the lake sediments were collected using a Glu corer, each surface core was subsampled in 1 cm intervals in the field. These surface cores were measured from the top of the mud-water interface to the base of the core.

The bottom half of the Gravel Lake core was cut into three ~50 cm sub-sections (B1, B2, and B3) and were split, along with the top core, using a circular saw. The core was initially sub-sampled for DNA, where sections were partially thawed for easier sampling and the top 0.1-0.3 mm of material was skimmed off the core's exposed interior surface to eliminate any chance of contamination. To sample for cryptotephra, the sub-cores were refrozen, removed from their tubing, scraped to remove outer surface, and cut into 1 cm sections. The entire working half of the lower sub-cores (B2 and B3) were cut into 1cm slices, where half of each 1cm slice was collected for counting and analyses. The upper sections (B1 and top core) had 1/3 of the core cut lengthwise, which was then sliced into 1 cm sections. The archive half of the top core was used as the working half was deformed due to melting and refreezing. Barlow Lake was not sub-sampled for DNA and cut and sampled as the B2/B3 sub-cores of Gravel Lake. Because the Pleistocene to Holocene transition was targeted, only the lower ~200 cm of the core was split and partially subsampled (Table 3.1).

Hanging Lake was separately cored by Kurek et al. (2009) using a Livingstone piston corer and crank drill-driver. Sediments were provided as contiguous 0.5 cm samples individually stored in vials filled with water. Due to the limited volume of material available for each sample, we combined two 0.5 cm samples, lowering the resolution to 1 cm (Table 3.1).

3.3.2. Cryptotephra extraction and counting

Each sample comprised approximately of one cubic centimetre of bulk sediment. Batches of 20-25 samples were dried overnight in a 90˚C oven, then combusted in a 550 ˚C furnace for 4 hours at a temperature increase of 40˚C/min. Samples were weighed before and after combustion to determine loss on ignition (LOI) values. Due to sample availability, combustion was avoided in the Chapman Lake surface core and at 143-183 cm in Hanging Lake and were instead treated to 30% hydrogen peroxide (H_2O_2) for 24 hours, diluted, and decanted. Once ashed or treated with H_2O_2, each sample was placed in 10% HCl for ~12 hours to remove any carbonate minerals and then sieved through a 20 µm nylon mesh to remove clays, fine silts, and dissolved organics. Samples containing larger grain sizes were first sieved through an 80 µm mesh. All samples were density separated to isolate the glass shards from the remaining minerogenic sediments. Lithium heteropolytungstate (LST) was diluted to a density of 2.45-2.47 g/cm^3, with an additional separation at 2.1-2.15 g/cm^3 if the sample contained more significant quantities of biogenic silica or residual organics if LOI was avoided.

Samples with higher tephra concentrations were spiked with a known concentration of Lycopodium spores before mounting on a glass slide. In this case, a Lycopodium tablet was dissolved in dilute HCl with the sample, then centrifuged, rinsed with water, and decanted three times to remove all acid and as much liquid as possible. Glycerol was directly added to the centrifuge tube and thoroughly mixed with the sample-pollen mixture to ensure even distribution. Once mixed, the glycerol is placed directly onto a glass slide; glass shards and lycopodium were counted separately.

Non-spiked samples were mounted using Canada Balsam, but glycerol was used if the sample had not been subjected to LOI and was potentially needed for geochemical analyses. This was the case for a section of Hanging Lake (143-183 cm below TOC), where extremely low concentrations made it difficult to extract enough glass for analyses. In cores containing a noticeable weathered glass input, weathered shards were counted separately when possible. Weathered shards were identified by pitting or hazy surface textures, rounded or broken off edges, and signs of abrasion.

Depths containing potential isochrons or higher concentrations of glass shards were re-sampled for geochemical analyses. Samples with fine organic material were treated to 30% H_2O_2 for 12-24 hours, sieved, and density separated to float the glass. A lighter density separate was used to float remaining organic material and/or biogenic silica if necessary. Samples were transferred by pipette into pre-drilled acrylic pucks mounted on double-sided tape and placed on a hotplate. Hanging Lake samples containing concentrations of <~20 shards per gram were hand-picked and shards were transferred to the mount using a petri dish, micro-pipette and a microscope. Once dried, holes were filled with epoxy, cured, polished and carbon-coated for geochemical analyses.

3.3.3. Geochemical analyses

Major and minor oxide composition was obtained by Electron Probe Micro-analyses (EPMA) on a JEOL-8900R superprobe at the University of Alberta. Standard analytical conditions for cryptotephra analysis were used, including an accelerating voltage of 15keV, 6nA beam current, and a 5 µm beam diameter (e.g., Jensen et al., 2019; Foo et al., 2020). To avoid the effects of alkali migration (Hunt and Hill, 1993, 1996; Morgan and London, 1996, 2005; Spray and Rae, 1995), we applied Time-dependent Intensity (TDI) corrections using the Probe for Windows software (Donovan et al., 2015). Either Na or both Na and Si oxides were treated to log-linear corrections as needed. Lipari obsidian (ID3506) and Old Crow tephra (Kuehn et al., 2011) were analyzed as secondary standards throughout EPMA analyses to monitor for drift or calibration issues. Offline corrections were made per oxide if the secondary standards showed signs of a consistent offset within ~1% - 5% of accepted values (Kuehn et al. 2011); samples were reanalyzed if the offset is greater.

3.3.4. Core characterization and radiocarbon sampling

Eight radiocarbon dates from Kurek et al. (2009) were rerun through the OxCal P_sequence model (IntCal20; Reimer et al., 2020) to update the Hanging Lake chronology using a Bayesian model. Calibrated ages for each depth can be found in the Appendix. Core scans were conducted on the Gravel Lake main core using a GeoTek Multi-Sensor Core Logger (MSCL). Core thickness, gamma density, and magnetic susceptibility were measured for each sub-section of the core and combined into one profile. Ultra high-resolution imagery of the Gravel Lake core was made using a Geotek Core Imaging System (MSCL-CIS). Fe-Ti oxide minerals were extracted and analyzed in Gravel and Hanging Lake cores to assist in the differentiation of White River Ash north and east. Three terrestrial Picea needle fragments and three aquatic seeds were picked from Gravel Lake for radiocarbon dating, in addition to a sample of unidentified organic fragments collected from the base of the core in the field. All ^{14}C ages are reported in Table 3.2 alongside their composite depths, sample size (where available), sample descriptions, fractions of the modern standard, δ14C, and calibrated ages. ^{14}C samples were calibrated using IntCal 20 on OxCal 4.4 software (Reimer et al., 2020; Bronk Ramsey, 2009).

Table 3.2: Radiocarbon dates for Gravel Lake, Yukon

Composite depth (cm)	Sample size (mg C)	Sample material dated	fraction modern	±	$\delta^{14}C$ (‰)	±	^{14}C age (BP)	±	cal BP (two-sigma)
31-32	>1mg	Seed (Nuphar sp.)	0.7346	0.0013	-265.4	1.3	2480	15	2710-2489
32-33	0.038	Needle fragment (Picea)	0.8524	0.0032	-147.6	3.2	1280	35	1291-1124
37-38	0.077	Needle tip (Picea)	0.8264	0.0018	-173.6	1.8	1530	20	1510-1351
90-91	0.06	Seed fragment (unconfirmed, but likely Potamogeton sp.)	0.5421	0.0025	-457.9	2.5	4920	40	5730-5587
98-99	0.052	Carbonized needle fragment (Picea)	0.5782	0.0027	-421.8	2.7	4400	40	5270-4858
156-157	>1mg	Seed (Potamogeton sp.)	0.4562	0.0008	-543.8	0.8	6305	15	7267-7165
core catch material (~223)	0.019	Unidentified organic fragments	0.2202	0.0143	-779.8	14.3	12160	530	15924-13103

Calibrated using IntCal20 on OxCal 4.4 (Reimer et al., 2020; Bronk Ramsey, 2009).

Macrofossil ID by Dr. Alwynne Beaudoin and Diana Tirlea of the Royal Alberta Museum, Edmonton, Alberta

3.4. Results

The following sections describe the glass shard concentration profiles for each lake and the geochemistry of the shard peaks selected for analysis. Results are presented by lake, with subsections organized by geochemical populations that are either correlated to known tephra/sources or are previously unreported. Major-element geochemistry is summarized in Table 3.3 for Hanging Lake, Table 3.4 for Chapman Lake, Table 3.5 for Gravel Lake surface core, and Tables 3.6 and 3.7 for the Gravel Lake main core. The depths analyzed are noted on each shard profile with details in Appendix Tables S1 (Hanging Lake), S4 (Barlow Lake), S7 (Chapman Lake) and S10 (Gravel Lake). All individual analyses are in supplementary Tables S2, S5, S8, and S11.

Machine learning classifiers of Bolton et al. (2020) are used on all analyzed samples to help parse the data and determine the source volcano if possible. Ten source volcanoes are used for predictions, including: Aniakchak, Augustine, Churchill, Dawson, Fischer, Hayes, Kaguyak, Katmai, Redoubt, and Spurr. Each analysis is given ten prediction values (i.e., one for each volcano) as percentages, shown in Table S13 and S14, indicating the likelihood that the glass shard came from each volcano. Note that the total percentage of the ten volcanoes has to add to 100%, so if the glass shard is sourced from a volcano not included in the training data, it will still be given a prediction towards the ten included. In general, predictions less than ~65% suggest either sourcing from another volcano, an eruption not included in the training data, or a composition that falls within a region where compositional fields of sources overlap. Final determinations are confirmed through plotting of data.

Table 3.3: Geochemical populations of Hanging Lake, Yukon

Depth (ccd)	UA #	Shard s/g	Pop'n		SiO_2	TiO_2	Al_2O_3	FeOt	MnO	MgO	CaO	Na_2O	K_2O	Cl	Total	H_2Od	*n*	Potential Volcanic source/eruption
HL 26-27	3360	31	a	Mean	75.11	0.19	13.86	1.32	0.06	0.31	1.54	4.20	3.17	0.30	100	1.67		
				St.Dev	0.86	0.08	0.35	0.32	0.05	0.10	0.34	0.38	0.48	0.05	0	1.31	8	WRAe?
HL 29-30	3361	42	a	Mean	76.83	0.15	13.05	1.15	0.06	0.18	1.04	3.83	3.49	0.31	100	1.78		
				St.Dev	0.91	0.06	0.65	0.12	0.03	0.07	0.38	0.31	0.37	0.03	0	1.64	20	WRA-like
HL 34-35	3362	108	a	Mean	76.53	0.18	13.08	1.22	0.05	0.24	1.19	3.83	3.43	0.32	100	2.24		
				St.Dev	1.90	0.06	0.99	0.22	0.01	0.11	0.46	0.31	0.21	0.03	0	1.39	18	WRAn
HL 38-39	3363	27	a	Mean	76.05	0.15	13.43	1.21	0.06	0.25	1.35	3.95	3.31	0.30	100	1.56		
				St.Dev	2.42	0.06	1.15	0.39	0.03	0.16	0.61	0.36	0.26	0.06	0	0.85	6	WRA-like
HL 43-44	3364	48	a	Mean	76.49	0.14	13.24	1.11	0.05	0.21	1.24	3.90	3.38	0.29	100	2.04		
				St.Dev	1.58	0.04	0.91	0.19	0.02	0.09	0.38	0.36	0.27	0.04	0	1.17	20	WRA-like
HL 80-81	3452	26			77.77	0.08	12.71	0.75	0.04	0.14	0.95	3.83	3.66	0.09	100	2.06	1	Unknown
HL 90-92	3450	4+51	a	Mean	72.92	0.39	14.71	1.90	0.05	0.44	1.59	5.11	2.74	0.19	100	1.36		
				St.Dev	0.40	0.04	0.13	0.01	0.01	0.01	0.01	0.53	0.00	0.03	0	0.32	2	Unknown
			b	Mean	76.66	0.04	13.29	0.39	0.07	0.07	0.80	3.85	4.77	0.08	100	4.38		
				St.Dev	0.12	0.02	0.09	0.12	0.01	0.01	0.01	0.20	0.12	0.02	0	1.43	3	Unknown
HL 91-92	3385	51			72.74	0.61	15.22	4.23	0.16	0.82	2.89	1.04	2.15	0.17	100	7.192	1	Unknown
HL 156-157	3432	7	a	Mean	71.88	0.37	14.85	2.12	0.03	0.55	2.33	5.12	2.58	0.22	100	3.68		
				St.Dev	0.43	0.01	0.04	0.03	0.00	0.00	0.04	0.40	0.03	0.03	0	0.20	2	Unknown

3.4.1. Hanging Lake

The glass shard concentration profile for the upper 183 centimetres of Hanging Lake is shown in Figure 3.2, along with LOI measurements collected during cryptotephra processing and a reference LOI profile from previous studies of the core by Kurek et al. (2009). According to the Kurek et al. (2009) age model, this sampled section of the core represents the full extent of the Holocene. LOI was not measured between 142-183 cm to allow tephra from counting slides to be recovered for geochemical analyses. Tephra concentrations in Hanging Lake were low, ranging from 0-50 shards/g with one exception of 108 shards/g at 34-35 cm. Sixteen depths were resampled for geochemical analyses, but despite multiple extraction attempts, only five resulted in >5 points analyzed (discussed below). No glass could be analyzed for depths 18-19 cm, 49-50 cm, 64-65 cm, 80-81 cm, 81-82 cm, and 86-87 cm, with only one point analyzed for 91-92 cm. A second attempt to recover shards using the remainder of sample material was unsuccessful for 18-19 cm, 25-27 cm, 86-87 cm, and 91-92 cm. Therefore, the material was later hand-picked to isolate glass shards to be mounted and analyzed separately, with varying success. Although a few shards were able to be isolated and mounted, no consistent populations were detected as there were too few analyses. More sample material is required to geochemically identify the smaller peaks found below 44 cm. See Appendix Table S1 for additional information of depths processed.

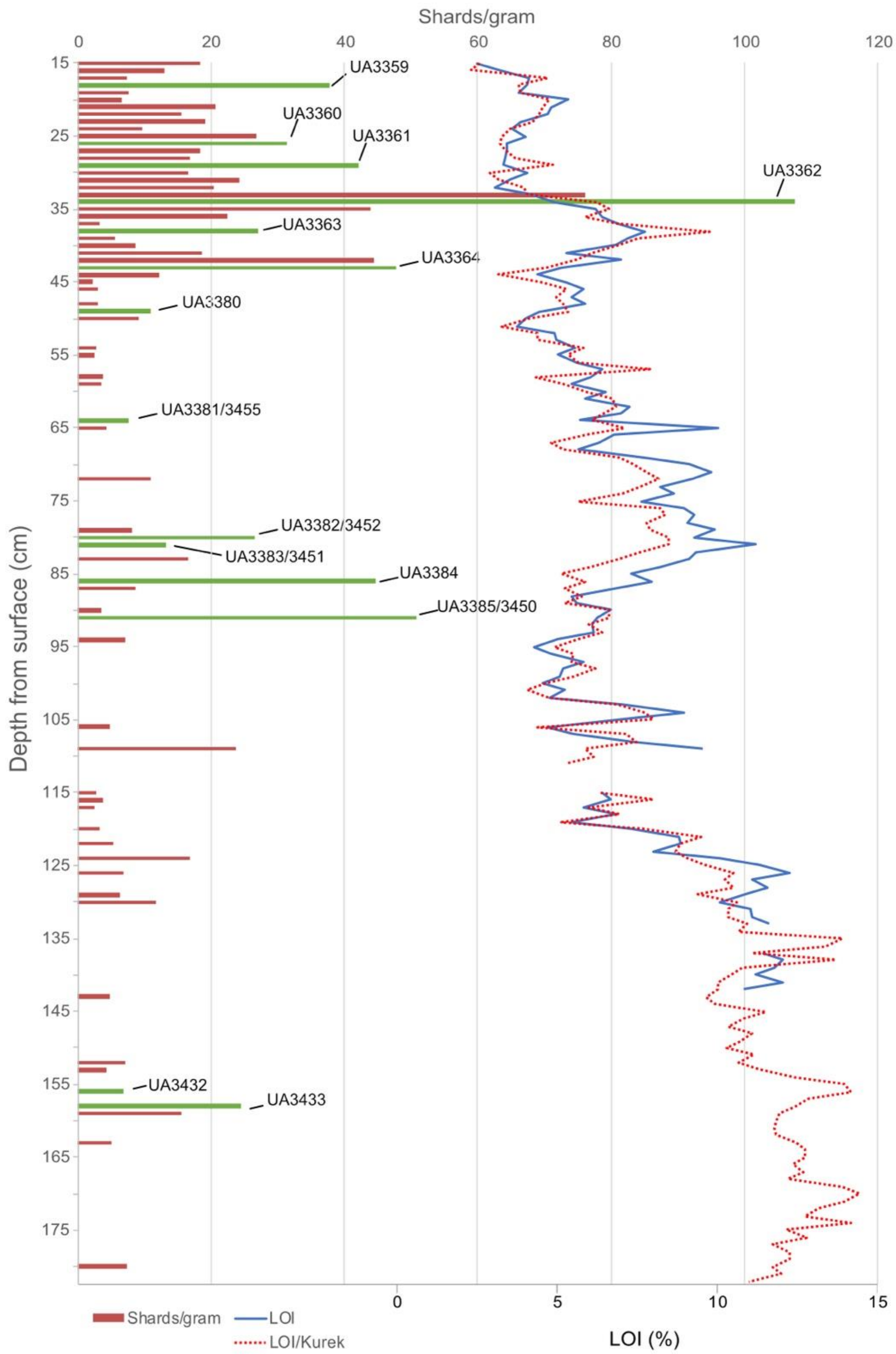

Figure 3.2: Tephra profile and LOI measurements of Hanging Lake, Yukon. Depths shown in green were processed for geochemistry, but not all were successfully analysed. LOI was not recorded in the lower sections of the core, but the LOI closely follows that of Kurek et al. (2009) in the upper regions and would likely follow the same pattern. Shard peaks at 109 cm, 124 cm, and 130 cm have not been processed for geochemistry at this time.

White River Ash

Shards with White River Ash (WRA) like geochemistry are found throughout the top ~45 cm of the Hanging Lake core, with one pronounced main peak at 34-35 cm (UA3362; 108 shards/g), a secondary peak at 43-44 cm (UA3364; 48 shards/g), and several sharp rises in concentration at 26-27 cm (UA3360; 31 shards/g), 29-30 cm (UA3361; 42 shards/g), and 38-39 cm (UA3363; 27 shards/g) surrounding the main peak (Fig. 3.2). WRA, sourced from Mount Churchill of the Wrangell volcanic field, is a formal stratigraphic name for what was originally thought to be one widely spread visible tephra deposit in the Yukon and Alaska, but is now known to comprise of two (e.g., Péwé, 1975; Lerbekmo et al., 1975; Fig. 3.1). The two units are the eastern lobe (WRAe; ~1097 cal BP) and the northern lobe (WRAn; ~1625 cal BP) (Fig. 3.1; Jensen et al., 2014; Toohey and Sigl, 2017; Reuther et al., 2020).

The machine learning classifiers of Bolton et al. (2020) were initially used to determine the potential source(s) of these samples (Table S13). All SiO_2 analyses below ~76.5 wt% have higher prediction coefficients (>~0.8) to Mt. Churchill WRA reference material, whereas the higher-Si analyses have predictions split between Churchill and Redoubt volcano, near Cook Inlet, Alaska. Redoubt can be discounted as a source due to its distinctly lower Cl concentration. In addition, proximal (sample 11c) and distal (Sixtymile) WRAn data from Preece et al. (2014), not included in the training dataset, support a correlation to WRAn (or WRAn-like tephra) as they also contain the distinct higher SiO_2 population dominant at Hanging Lake. Two variations of WRAn are recorded in the Sixtymile area, WRA-Na with a wide SiO_2 range of ~71-79 wt% and WRA-Nb with a relatively limited range of ~75-78 wt%. Although they haven't been found at the same location, WRA-Nb is found ~20-30 cm above the typical depth of WRA-Na samples and was interpreted by Preece et al. (2014) to be either a younger eruption or the final most silicic deposits of the WRAn eruption. It is not clear which of the two variations the Hanging Lake samples fall under, as they overlap with both, but the majority of WRA glass in Hanging Lake falls within the higher-SiO_2 range of WRA-Nb. WRAn cryptotephra from other northern distal sites such as Cascade Lake (Davies et al., in review) and the DHP site (Davies, 2018) also resemble the WRAn samples of Hanging Lake (Fig. 3.3), with higher proportions of high-SiO_2 glass than WRA samples in Gravel Lake (discussed below).

Overall, the geochemistry is similar between most WRA peaks at Hanging Lake, following the same trends in oxides and SiO_2 ranging from 72 to 80 wt% (Fig. 3.3). However, the sample at 26-27 cm has a SiO_2 range from 73.71-75.95 wt% and is missing the higher-Si shards found in all other WRA-like samples. WRAe has this more limited SiO_2 range, helping differentiate it from WRAn (Fig. 3.3.; Preece et al., 2014). Although there are too few shards analyzed here to determine if this peak is indeed WRAe, its presence ~7 cm above the main WRAn peak is stratigraphically sound. Fe-Ti oxide compositions are more diagnostic in differentiating between the two lobes (e.g., Lerbekmo 1975; Preece et al., 2014), but we were unsuccessful in extracting magnetite and ilmenite originating from the tephra to further test this correlation.

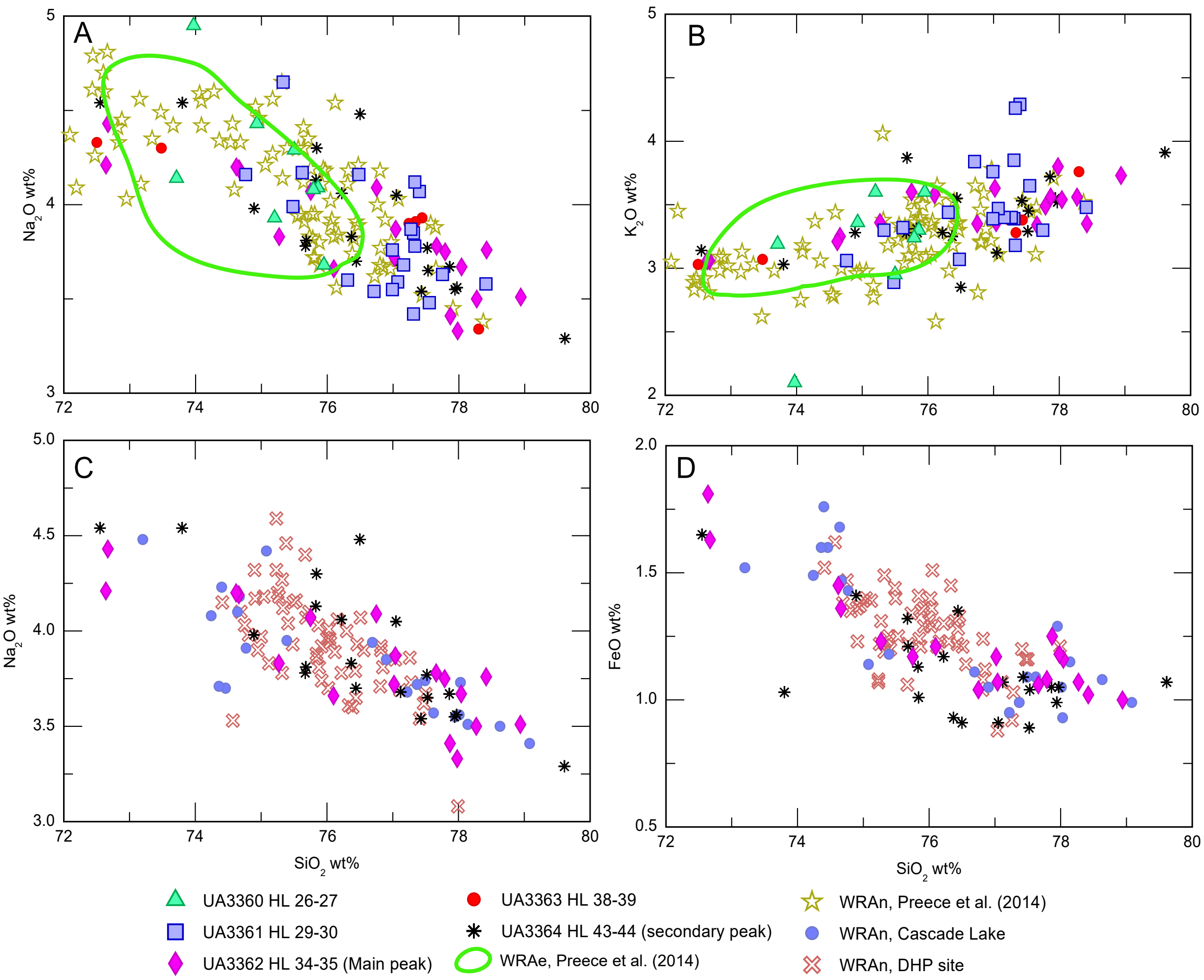

Figure 3.3: (A,B) Hanging Lake major element geochemistry compared to proximal and distal samples of WRAn and WRAe (Preece et al., 2014). Comparison between all Hanging Lake WRA samples and WRAn samples ~50 km north of Mt. Churchill on the north side of the White River and Sixtymile site at the border between Yukon and Alaska (Preece et al., 2014). The relatively limited SiO_2 range of UA3360 overlaps with WRAe, but more points are required for a proper comparison. (C,D) Hanging Lake main and secondary peaks show the same high SiO_2 range (74-79 wt%) and geochemistry as WRAn samples from Cascade Lake, Yukon (Davies et al., in review) and DHP site, Yukon (Davies, 2018).

3.4.2. Barlow Lake

The shard concentration profile, LOI, and samples analysed from the targeted 90 cm sub-section (composite depth 174- 264 cm) of the Barlow Lake core are summarized in Figure 3.4. This section was chosen as the sharp change in organic content from 55.7% at 174 cm to 1.1% at 264 cm indicates the Pleistocene to Holocene transition (Fig. 3.4). The non-weathered glass profile shows relatively minor fluctuations with one sharp peak at 231 cm and concentrations ranging from ~0-100 shards/gram. However, this profile is overwhelmed by weathered shards concentrations of ~100-300 shards/gram. An increase in LOI towards the Holocene is accompanied by a decrease in weathered glass concentrations, suggesting shallower depths of the core may be less affected by weathered glass signal.

Six depths were selected for geochemical analyses: 178-179 cm (UA3190), 195-196 (UA3191), 204-205 cm (UA3192), 216-217 cm (UA3193), 190-191 cm (UA3194), and 260-261 cm (UA3195), although only the first five samples were successfully analyzed. Depths were selected based on peaks in non-weathered tephra, except for 190-191 cm that represented a peak in weathered shards with little non-weathered glass. Geochemical data of all samples show no discernable tephra populations (Fig. 3.5). The majority of shards analyzed have scattered CaO and FeO, variable amounts of high K_2O, and low Na_2O. The most extreme examples show Na_2O of ~1.5 wt% and K_2O of ~7 wt%, with H_2O contents of 5-10%. This geochemistry is representative of weathered glass that has been geochemically altered and hydrated over time, resulting in low totals and heterogeneity (e.g., Jensen et al., 2016; Monteath et al., 2019). All the samples do have a few shards that are not weathered, but the number of analyses are too low to determine any populations. Machine learning classifiers also show no consistency, with predictions of Dawson, Redoubt, Aniakchak, and Kaguyak source volcanoes.

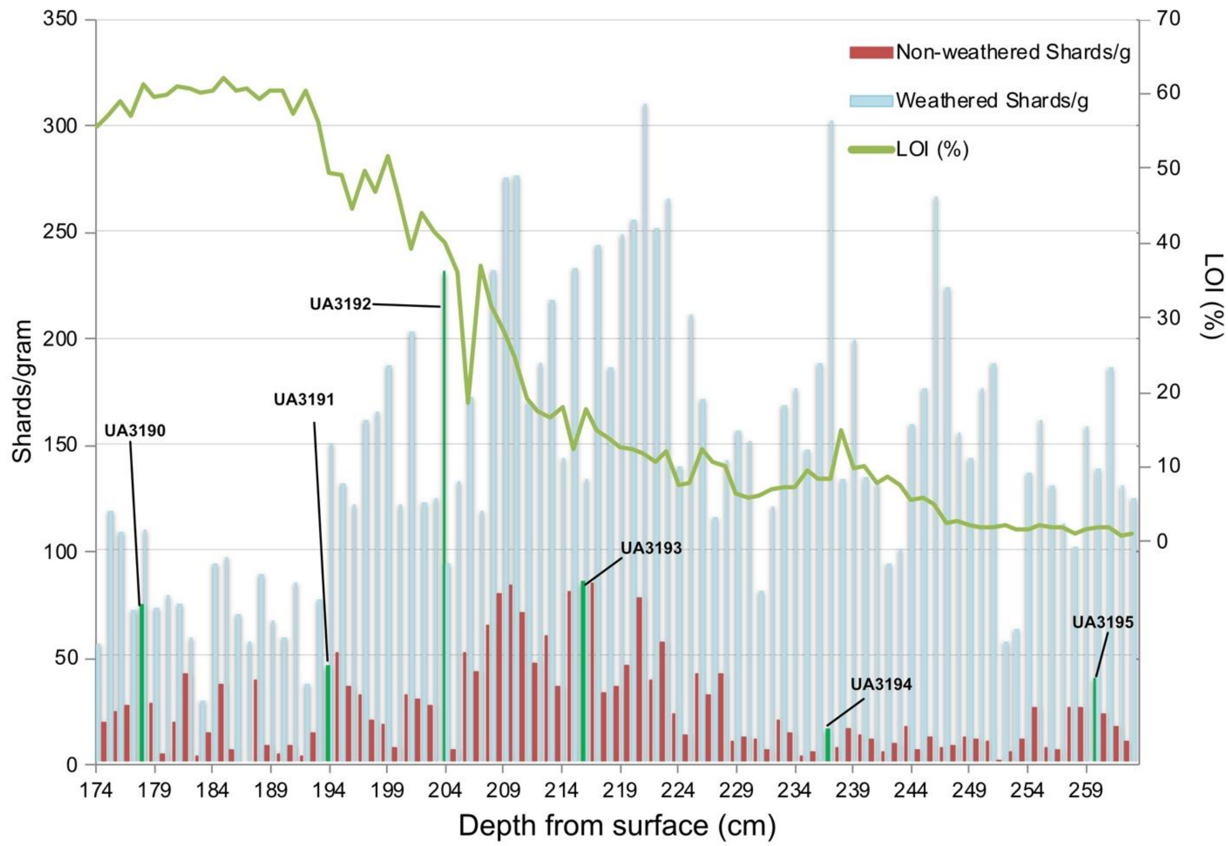

Figure 3.4: Tephra profile of Barlow Lake. Weathered tephra (blue) was counted separately from non-weathered shards (red) to identify any potential primary eruptions. LOI values rise from 0% to 60%, which is interpreted to be the Pleistocene to Holocene transition.

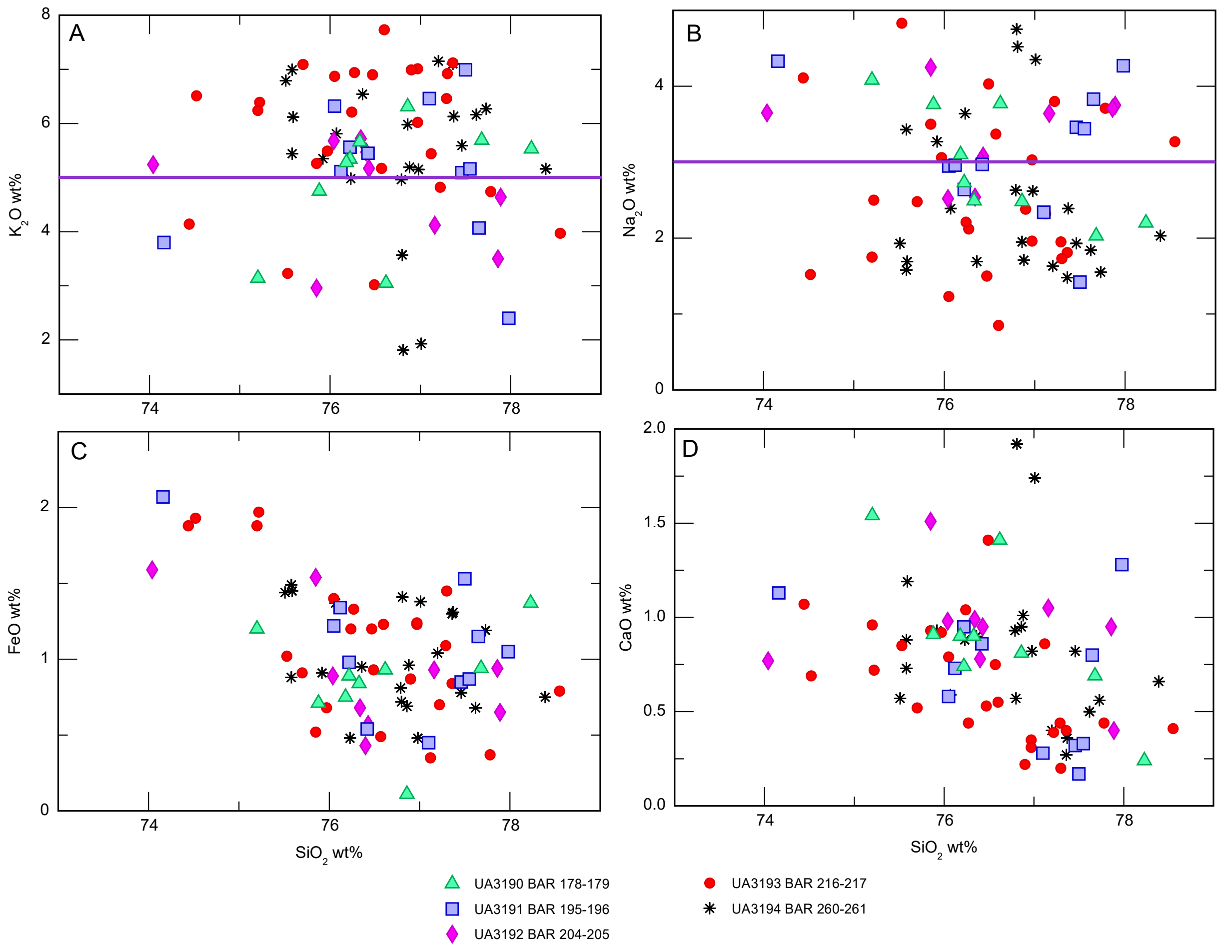

Figure 3.5: (A,B) Barlow Lake glass shards contain large amounts of weathered glass, characterized by low Na_2O, high K_2O, and high SiO_2. Alaskan tephra generally rarely have K_2O much above 5 wt% and Na_2O much below 3 wt % (purple lines in A and B). (C,D) Scattering is also likely to occur in FeO and CaO oxides when shards have been geochemically altered. There are shards in each sample that are not noticeably weathered but the data do not form any coherent trends or populations.

Table 3.4: Geochemical populations of Chapman Lake, Yukon

Depth (ccd)	UA #	Shards /g	Pop'n		SiO_2	TiO_2	Al_2O_3	FeOt	MnO	MgO	CaO	Na_2O	K_2O	Cl	Total	H_2Od	*n*	Potential Volcanic source/eruption
CHP-Sfc 8-9 cm	3499	20053	a	Mean	74.15	0.28	13.67	2.01	0.06	0.22	1.25	4.57	3.61	0.23	100	2.01		
				StDev	0.52	0.06	0.26	0.15	0.03	0.02	0.06	0.25	0.06	0.02	0	0.58	7	Dawson
			b	Mean	77.92	0.17	12.34	1.05	0.05	0.14	0.87	3.68	3.54	0.31	100	3.75		
				StDev	0.65	0.04	0.34	0.08	0.01	0.03	0.17	0.27	0.29	0.03	0	1.57	11	WRA-like
			c	Mean	76.46	0.30	13.00	1.28	0.05	0.25	1.15	3.66	3.75	0.13	100	3.25		
				StDev	1.30	0.06	0.63	0.27	0.03	0.06	0.26	0.38	0.49	0.02	0	1.90	5	Redoubt 1989-1990
CHP-Sfc 17-18 cm	3500	51098	a	Mean	74.52	0.28	13.73	2.04	0.06	0.23	1.24	4.14	3.56	0.26	100	4.29		
				StDev	0.21	0.04	0.10	0.05	0.02	0.01	0.01	0.11	0.13	0.04	0	0.75	4	Dawson
			b	Mean	76.91	0.13	13.09	1.13	0.06	0.20	1.20	3.79	3.25	0.32	100	3.55		
				StDev	1.60	0.04	0.81	0.17	0.02	0.09	0.35	0.42	0.26	0.04	0	1.45	17	WRA-like
CHP-Sfc 23-24 cm	2501	50582	a	Mean	74.45	0.26	13.60	2.02	0.08	0.25	1.24	4.30	3.62	0.23	100	3.06		
				StDev	0.03	0.00	0.01	0.05	0.02	0.01	0.00	0.01	0.03	0.00	0	1.32	2	Dawson
			b	Mean	78.08	0.14	12.42	1.09	0.05	0.16	0.92	3.59	3.32	0.31	100	3.84		
				StDev	0.91	0.04	0.54	0.06	0.02	0.04	0.21	0.34	0.19	0.03	0	1.43	19	WRA-like

3.4.3. Chapman surface core

The Chapman Lake surface core, 24 cm in length, contains high concentrations of glass and three geochemical populations that correlate to WRA, Dawson tephra, and Redoubt 1989-1990 (Table 3.4). The Chapman Lake profile has concentrations ranging from 6194-51098 shards/gram, lessening towards the top, with peaks at 8-9 (UA3499), 17-18 (UA3500), 21-22, and 23-24 (UA3501) cm (Fig. 3.6).

Three depths (8-9 cm/UA3499, 17-18 cm/UA3500, and 23-24 cm/UA3501) were selected for geochemical analysis, and all contain multiple populations of WRA-like and Dawson tephra (Fig. 3.7; Scott and McGimsey, 1994; Preece et al., 2011a: Preece et al., 2011b). The WRA-like population is found in all three depths and contains the similar high-SiO_2 population linked to WRAn found in Hanging Lake. UA3499 and UA3501 only contain higher-SiO_2 shards (~77-80 wt%), but UA3500 has the typical broad range of SiO_2 (73.6-79.7 wt%). The ~30,000 cal BP Dawson tephra (Demuro et al., 2008) is also present in all three samples, showing how secondary deposition is a major contributor to the concentration profile in Chapman Lake. However, the smaller peak at 8-9 cm also contains glass shards correlated to the 1989-1990 eruption of Redoubt volcano in the Cook Inlet, Alaska (e.g., Scott and McGimsey, 1994; Davies et al., 2016; Bolton et al., 2020).

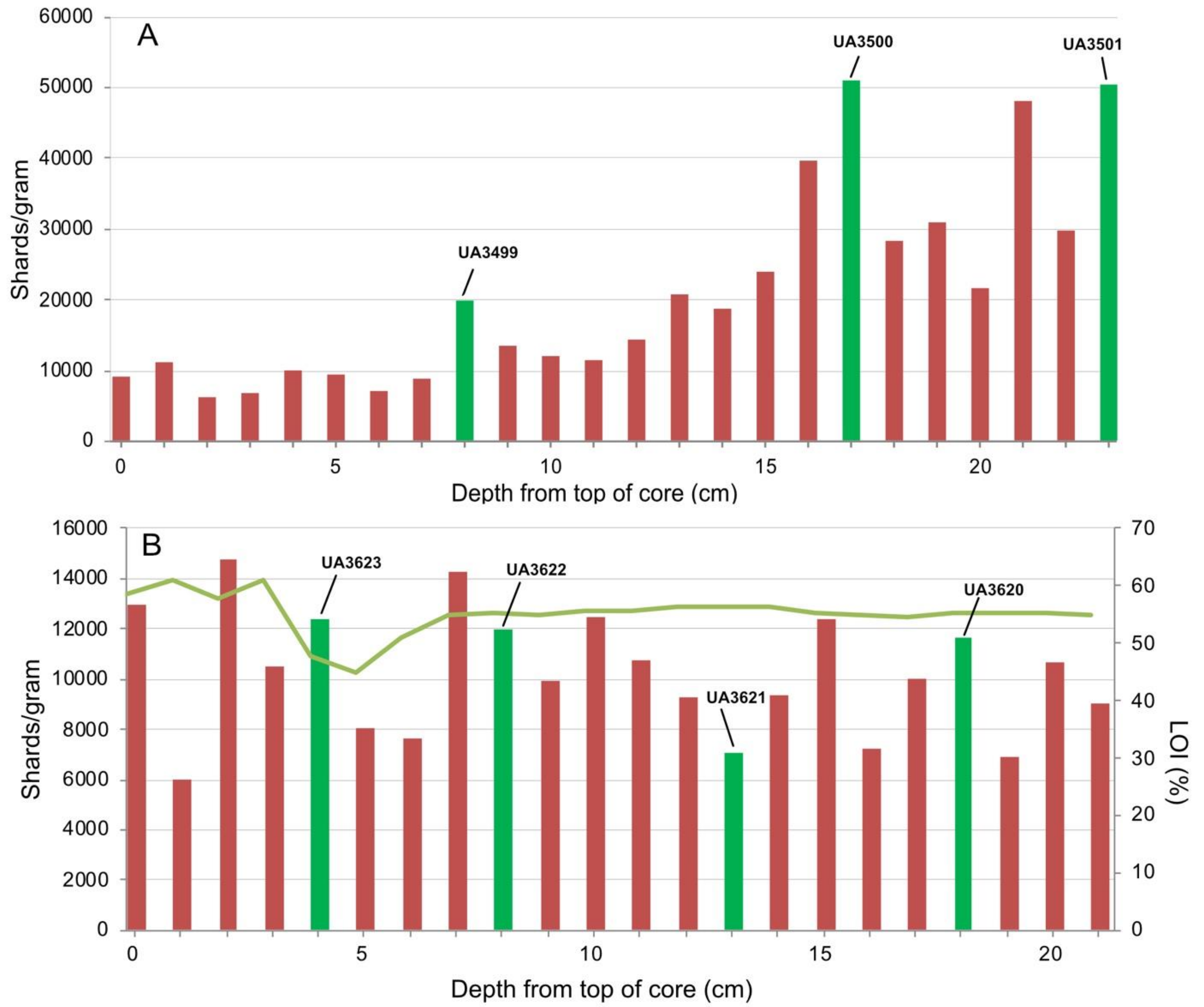

Figure 3.6: Chapman Lake (A) and Gravel Lake (B) surface core glass shard concentration profiles. The Chapman Lake profile contains distinct peaks and gradual changes in concentration between samples, whereas Gravel Lake has no real discernable peaks and trends. Analyzed depths for Gravel Lake were initially selected after counting up to 200 spiked pollen per sample, however it was later determined that the low shard to pollen ratios made these initial counts unreliable. The core was later recounted up to 50 glass shards per sample, altering the location of depths of interest. Depths 2, 7, 10, and 15 cm will be reprocessed for future geochemical analyses.

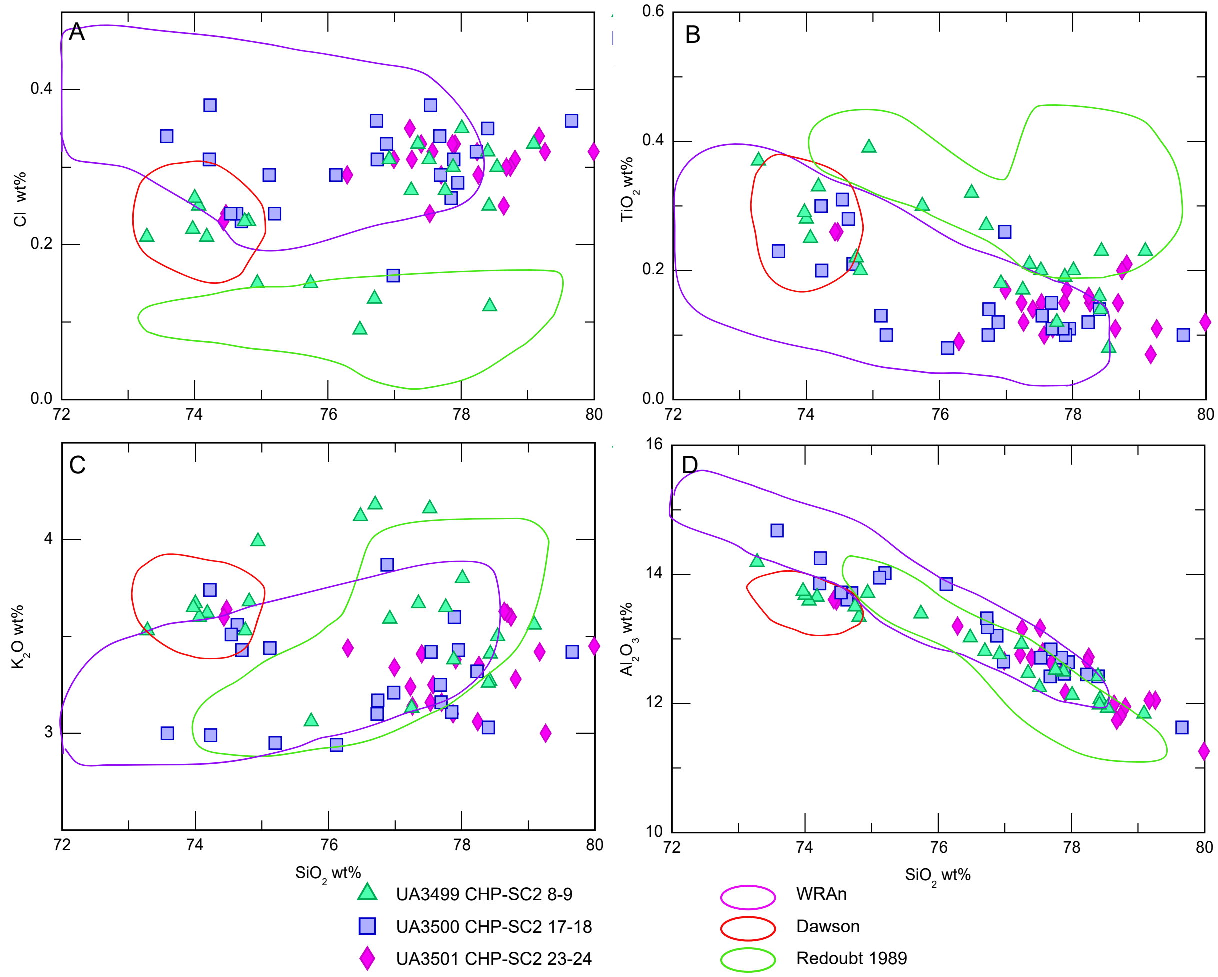

Figure 3.7: The Chapman Lake surface core contains three geochemical populations; WRAn, compared here to reference data encompassing the entire range of WRAn (Jensen, 2007; Preece et al., 2014), Dawson tephra (UA1000; Scott and McGimsey, 1994;), and Redoubt 1989-90 (UA2754; Preece et al., 2011a: Preece et al., 2011b). Redoubt and WRA are similar geochemically (e.g., C and D), but can differentiated with Cl and TiO_2 (A and B).

Table 3.5: Geochemical populations of Gravel Lake surface core

Depth (ccd)	UA #	Shards/g	Pop'n		SiO_2	TiO_2	Al_2O_3	FeOt	MnO	MgO	CaO	Na_2O	K_2O	Cl	Total	H_2Od	*n*	Potential Volcanic source/eruptio n
GRV Sfc 4-5 cm	3623	12689	a	Mean	75.85	0.32	12.99	1.67	0.05	0.30	1.43	4.27	2.95	0.21	100	1.57		
				StDev	2.48	0.16	1.35	0.53	0.03	0.22	0.69	0.30	0.24	0.04	0	2.01	13	Novarupta-Katmai 1912
			b	Mean	74.89	0.16	13.87	1.22	0.05	0.27	1.51	4.33	3.43	0.36	100	3.34		
				StDev	0.72	0.05	0.34	0.21	0.01	0.08	0.16	0.23	0.17	0.06	0	3.34	15	WRA-like
GRV Sfc 8-9 cm	3622	18028	a	Mean	74.34	0.20	14.15	1.38	0.06	0.32	1.64	4.34	3.32	0.32	100	2.21		
				StDev	1.14	0.06	0.62	0.21	0.03	0.08	0.26	0.24	0.25	0.05	0	1.23	19	WRA-like
			b	Mean	71.65	0.07	16.64	0.91	0.02	0.14	2.75	5.40	2.28	0.18	100	2.21		
				StDev	0.50	0.04	0.31	0.09	0.02	0.04	0.09	0.33	0.04	0.01	0	0.40	3	unknown
GRV Sfc 13-14 cm	3621	9291	a	Mean	75.07	0.18	13.77	1.30	0.04	0.28	1.48	4.23	3.40	0.32	100	2.59		
				StDev	1.63	0.05	0.88	0.17	0.02	0.09	0.36	0.40	0.27	0.07	0	2.09	16	WRA-like
			b	Mean	68.58	0.78	15.24	3.80	0.16	0.97	2.70	4.84	2.80	0.18	100	1.48		
				StDev	1.08	0.01	0.34	0.49	0.02	0.22	0.56	0.44	0.15	0.01	0	0.32	3	unknown
			c	Mean	77.66	0.17	12.31	1.17	0.04	0.18	0.96	3.92	3.40	0.23	100	2.67		
				StDev	1.00	0.05	0.39	0.14	0.04	0.09	0.27	0.58	0.32	0.10	0	3.01	4	unknown
GRV Sfc 18-19 cm	3620	13515	a	Mean	74.57	0.19	14.05	1.34	0.05	0.31	1.58	4.16	3.47	0.34	100	2.23		
				StDev	1.09	0.05	0.52	0.20	0.02	0.09	0.27	0.21	0.24	0.05	0	1.87	23	WRAe?

3.4.4. Gravel Lake

Surface core

The Gravel Lake surface core does not have distinct peaks, but higher concentrations at 4-5 cm (UA3623), 8-9 cm (UA3622), 13-14 cm (UA3621), and 18-19 cm (UA3620) were selected for geochemical analyses (Fig. 3.6). High concentrations of tephra are present from 6000-15000 shards per gram. The lack of distinct peaks is typical of upper Gravel Lake sediments in the main core, discussed below. Geochemistry of these samples overlaps with populations in the main core, with Katmai 1912 and WRA found within surface core samples (Fig. 3.8). These populations are discussed alongside the results from the main core below.

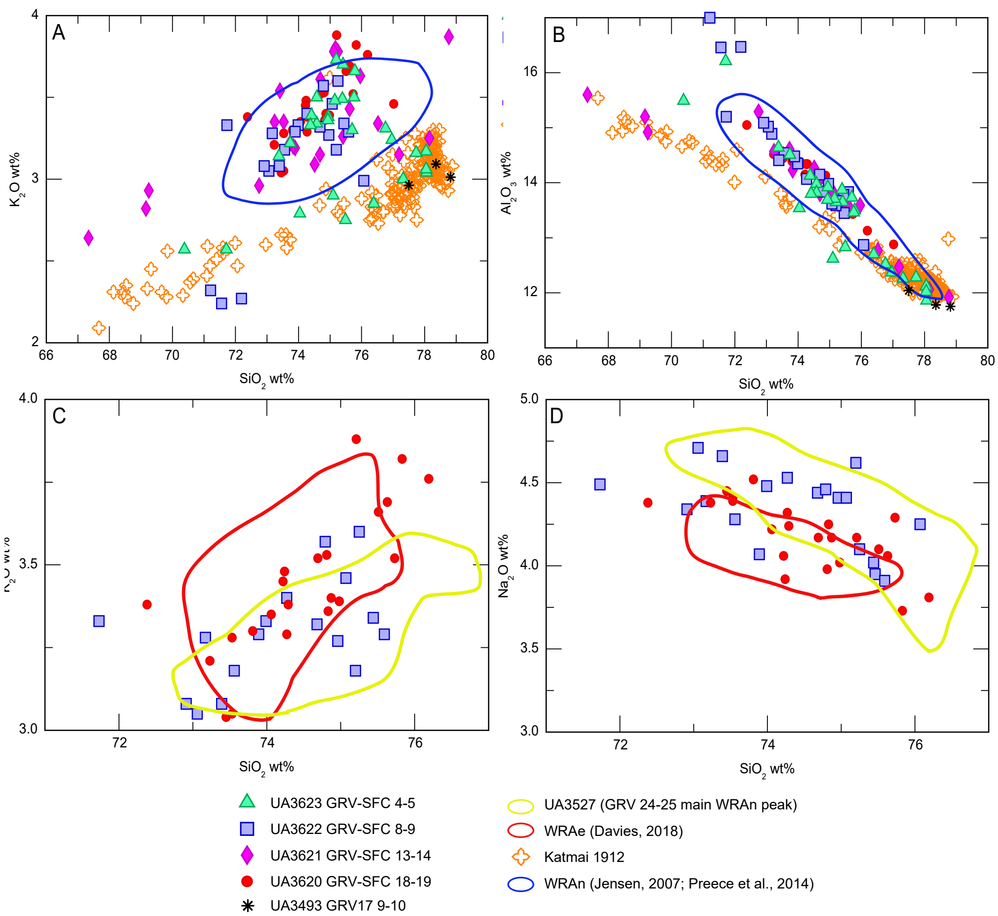

Figure 3.8: Gravel Lake surface core sample geochemistry. (A,B) Katmai 1912 and WRA populations compared to reference WRAn (Jensen, 2007; Preece et al., 2014), shown as a field for clarity. (C,D) UA3620 (18-19 cm) is similar to WRAe from DHP (Davies, 2018); other surface core samples (e.g. UA3622) are more like Gravel Lake's main WRAn peak (UA3527). However these samples will need to be analyzed together to confirm these observations.

Table 3.6: Geochemical populations of Gravel Lake main core, depths 7-87 cm

Depth (ccd)	UA #	Shards/g	Pop'n		SiO_2	TiO_2	Al_2O_3	FeOt	MnO	MgO	CaO	Na_2O	K_2O	Cl	Total	H_2Od	*n*	Potential Volcanic source/eruption
GRV17 7-8 cm	3526	14072	a	Mean	74.55	0.20	14.09	1.39	0.05	0.33	1.60	4.25	3.31	0.30	100	2.22		
				StDev	0.93	0.09	0.33	0.25	0.02	0.09	0.19	0.31	0.23	0.04	0	1.15	14	WRA-like
			b	Mean	67.06	1.14	14.68	4.31	0.07	1.53	3.60	3.86	3.69	0.08	100	1.66		
				StDev	1.53	0.08	0.31	0.12	0.01	0.26	0.38	0.08	0.62	0.01	0	0.46	3	unknown
GRV17 9-10 cm	3493	9470	a	Mean	75.27	0.15	13.89	1.30	0.05	0.28	1.56	4.00	3.24	0.35	100	2.80		
				StDev	0.82	0.05	0.32	0.21	0.02	0.07	0.18	0.20	0.18	0.05	0	1.44	18	WRA-like
			b	Mean	78.19	0.28	11.88	1.37	0.01	0.16	0.98	3.96	3.02	0.19	100	1.56		
				StDev	0.67	0.11	0.16	0.23	0.00	0.04	0.21	0.26	0.07	0.02	0	0.54	3	Novarupta-Katmai 1912
GRV17 17-18 cm	3494	18978	a	Mean	75.29	0.17	13.88	1.28	0.05	0.26	1.51	4.13	3.18	0.31	100	2.43		
				StDev	0.73	0.04	0.37	0.15	0.02	0.07	0.17	0.20	0.18	0.03	0	1.18	25	WRA-like
GRV17 24-25 cm	3527	26563	a	Mean	75.09	0.21	13.77	1.39	0.05	0.32	1.46	4.15	3.33	0.31	100	2.96		
				StDev	1.10	0.06	0.52	0.16	0.02	0.07	0.24	0.35	0.17	0.06	0	1.76	19	WRAn
GRV17 25-26 cm	3495	21620	a	Mean	75.17	0.17	13.97	1.31	0.05	0.28	1.53	4.10	3.17	0.31	100	2.57		
				StDev	0.77	0.04	0.47	0.14	0.02	0.05	0.21	0.31	0.16	0.03	0	0.93	25	WRAn
GRV17 31-32 cm	3496	10060	a	Mean	75.03	0.21	13.96	1.39	0.06	0.32	1.53	4.08	3.19	0.30	100	2.37		
				StDev	1.14	0.09	0.56	0.25	0.03	0.07	0.23	0.31	0.13	0.06	0	0.67	18	WRA-like
			b	Mean	74.75	0.35	13.88	2.03	0.13	0.44	2.34	4.08	1.83	0.24	100	1.84		
				StDev	0.01	0.02	0.04	0.14	0.02	0.06	0.08	0.28	0.03	0.01	0	0.12	2	Hayes?
GRV17 32-33 cm	3497	5369	a	Mean	74.83	0.18	14.13	1.35	0.05	0.30	1.62	4.09	3.21	0.30	100	2.78		
				StDev	0.86	0.03	0.43	0.13	0.02	0.05	0.24	0.17	0.11	0.03	0	0.67	21	WRA-like

			b	Mean	74.22	0.33	13.79	2.03	0.15	0.49	2.37	4.49	1.93	0.24	100	1.44		
				StDev	0.17	0.02	0.07	0.07	0.04	0.07	0.01	0.06	0.06	0.02	0	0.57	2	Hayes?
GRV17 34-35 cm	3491	8685	a	Mean	75.28	0.16	13.77	1.24	0.05	0.26	1.48	4.23	3.27	0.33	100	1.58		
				StDev	0.50	0.03	0.33	0.11	0.02	0.05	0.12	0.22	0.17	0.05	0	0.70	13	WRA-like
			b	Mean	71.20	0.52	14.82	2.45	0.16	0.52	1.75	5.49	2.92	0.23	100	0.19		
				StDev	0.64	0.05	0.02	0.00	0.04	0.03	0.05	0.49	0.03	0.01	0	0.08	2	Aniakchak
GRV17 40-41 cm	3498	4032	a	Mean	74.78	0.19	14.04	1.40	0.05	0.32	1.63	4.08	3.24	0.34	100	3.23		
				StDev	0.82	0.04	0.44	0.19	0.02	0.07	0.21	0.30	0.15	0.05	0	1.79	22	WRA-like
			b	Mean	71.17	0.49	15.04	2.49	0.15	0.54	1.80	5.11	3.03	0.23	100	1.61		
				StDev	0.38	0.02	0.10	0.05	0.01	0.07	0.04	0.15	0.00	0.05	0	0.13	2	Aniakchak
GRV17 42-43	3490	1740	a	Mean	75.07	0.21	13.82	1.38	0.05	0.31	1.57	4.09	3.25	0.33	100	1.56		
				StDev	1.01	0.06	0.48	0.18	0.02	0.07	0.22	0.17	0.18	0.10	0	0.91	14	WRA-like
			b	Mean	77.34	0.23	12.63	1.55	0.05	0.39	2.17	3.86	1.61	0.24	100	0.47		
				StDev	0.26	0.03	0.19	0.07	0.03	0.04	0.08	0.11	0.11	0.06	0	1.55	3	Augustine
			c	Mean	74.91	0.28	13.60	1.86	0.10	0.44	2.22	4.46	1.94	0.25	100	0.16		
				StDev	0.06	0.01	0.21	0.05	0.02	0.03	0.05	0.04	0.08	0.01	0	0.56	2	unknown
GRV17 43-44 cm	3489	873	a	Mean	75.11	0.19	13.99	1.39	0.05	0.31	1.58	3.89	3.23	0.33	100	2.16		
				StDev	0.85	0.04	0.45	0.22	0.03	0.08	0.20	0.20	0.15	0.04	0	0.79	21	WRA-like
GRV17 44-45cm	3524	2718	a	Mean	75.86	0.20	13.54	1.27	0.05	0.27	1.44	3.98	3.18	0.29	100	3.31		
				StDev	1.47	0.04	0.63	0.15	0.02	0.06	0.20	0.39	0.43	0.07	0	1.67	16	WRA-like
GRV17 49-50 cm	3488	1631	a	Mean	70.99	0.52	14.98	2.52	0.14	0.57	1.80	5.24	3.07	0.21	100	2.27		
				StDev	0.41	0.05	0.21	0.24	0.03	0.11	0.23	0.38	0.16	0.03	0	2.82	9	Aniakchak
			b	Mean	77.19	0.27	12.59	1.55	0.07	0.39	2.11	3.98	1.67	0.23	100	2.71		
				StDev	0.59	0.04	0.27	0.06	0.03	0.04	0.05	0.56	0.04	0.03	0	1.68	5	Augustine
			c	Mean	75.40	0.18	13.73	1.29	0.06	0.26	1.41	4.11	3.30	0.33	100	2.92		
				StDev	0.71	0.05	0.29	0.12	0.03	0.04	0.15	0.34	0.19	0.03	0	1.63	13	WRA-like

GRV17 57-58 cm	3487	5938	a	Mean	74.80	0.20	14.11	1.38	0.05	0.33	1.57	4.09	3.24	0.31	100	2.60		
				StDev	0.54	0.04	0.22	0.12	0.02	0.04	0.09	0.28	0.07	0.03	0	1.51	13	WRA-like
			b	Mean	77.50	0.24	12.59	1.51	0.06	0.37	2.06	3.82	1.68	0.22	100	2.09		
				StDev	0.44	0.05	0.20	0.07	0.03	0.03	0.10	0.27	0.08	0.03	0	1.36	18	Augustine
GRV17 65-66 cm	3486	1899	a	Mean	75.21	0.30	13.52	1.84	0.09	0.41	2.11	4.33	1.97	0.27	100	1.24		
				StDev	0.06	0.01	0.21	0.06	0.03	0.05	0.09	0.35	0.01	0.05	0	0.40	2	Unknown
			b	Mean	77.87	0.26	12.53	1.49	0.08	0.35	2.02	3.53	1.71	0.19	100	1.58		
				StDev	0.30	0.04	0.09	0.09	0.01	0.02	0.12	0.22	0.10	0.01	0	2.66	4	Augustine
			c	Mean	75.00	0.18	14.03	1.34	0.05	0.32	1.66	3.99	3.15	0.36	100	2.53		
				StDev	0.53	0.01	0.27	0.08	0.02	0.04	0.14	0.31	0.11	0.14	0	1.35	5	WRA-like
			d	Mean	78.46	0.20	12.59	1.08	0.04	0.24	1.36	3.53	2.36	0.19	100	4.39		
				StDev	0.44	0.05	0.06	0.01	0.02	0.05	0.19	0.06	0.05	0.07	0	0.14	2	Unknown
			e	Mean	71.46	0.52	14.87	2.40	0.15	0.50	1.72	5.21	3.01	0.21	100	0.73		
				StDev	0.17	0.05	0.18	0.06	0.03	0.03	0.03	0.31	0.08	0.02	0	1.19	7	Aniakchak
GRV17 67-68 cm	3523	2085	a	Mean	71.24	0.50	15.10	2.40	0.14	0.50	1.67	5.21	3.07	0.21	100	1.63		
				StDev	0.46	0.05	0.21	0.05	0.03	0.04	0.07	0.30	0.15	0.03	0	1.45	27	Aniakchak
			b	Mean	75.13	0.19	14.00	1.26	0.04	0.27	1.53	4.12	3.22	0.31	100	2.30		
				StDev	0.73	0.04	0.60	0.17	0.02	0.07	0.30	0.32	0.31	0.06	0	0.84	11	WRA-like
			c	Mean	77.23	0.24	12.72	1.54	0.07	0.38	2.05	3.89	1.71	0.21	100	3.33		
				StDev	0.33	0.05	0.09	0.11	0.03	0.01	0.14	0.11	0.13	0.03	0	1.91	5	Augustine
			d	Mean	65.82	1.04	13.81	5.69	0.07	3.58	3.89	3.23	2.81	0.09	100	2.03		
				StDev	2.42	0.05	1.75	1.44	0.04	2.72	0.07	0.43	0.46	0.03	0	0.94	2	Unknown
GRV17 69-70 cm	3542	1315	a	Mean	74.84	0.19	13.96	1.32	0.05	0.27	1.56	4.33	3.26	0.30	100	2.23		
				StDev	0.80	0.06	0.44	0.18	0.02	0.06	0.19	0.19	0.15	0.04	0	0.78	16	WRA-like
			b	Mean	76.93	0.29	12.65	1.48	0.06	0.35	2.10	4.38	1.60	0.20	100	1.71		
				StDev	0.39	0.05	0.20	0.05	0.04	0.03	0.03	0.66	0.01	0.04	0	0.94	3	Augustine

GRV17 72-73 cm	3541	1825	a	Mean	74.30	0.27	13.81	1.90	0.10	0.45	2.13	4.82	2.02	0.25	100	1.80		
				StDev	0.48	0.02	0.33	0.13	0.05	0.05	0.17	0.20	0.17	0.04	0	1.71	6	Ruppert
GRV17 73-74 cm	3540	1683	a	Mean	73.73	0.31	14.34	2.00	0.07	0.49	2.37	4.65	1.85	0.24	100	1.48		
				St. Dev	74.12	0.30	14.70	1.98	0.12	0.52	2.67	3.41	1.96	0.28	100	1.70	2	Ruppert
			b	Mean	73.49	0.29	14.59	1.74	0.09	0.40	1.73	4.27	3.16	0.33	100	3.50		
				StDev	1.91	0.13	0.43	0.47	0.08	0.11	0.24	1.18	0.11	0.07	0	1.66	4	WRA-like
			c	Mean	77.25	0.25	12.99	1.61	0.08	0.37	1.98	3.52	1.78	0.23	100	2.35		
				StDev	1.07	0.03	0.71	0.24	0.03	0.04	0.12	0.91	0.13	0.01	0	0.65	4	Augustine
GRV17 75-76 cm	3539	2338	a	Mean	76.56	0.29	12.89	1.57	0.08	0.39	2.20	4.19	1.66	0.21	100	3.22		
				StDev	0.95	0.04	0.35	0.26	0.02	0.10	0.27	0.25	0.12	0.04	0	1.22	13	Augustine
			b	Mean	70.88	0.47	15.14	2.37	0.15	0.49	1.70	5.64	3.00	0.20	100	1.61		
				StDev	0.23	0.05	0.13	0.07	0.03	0.03	0.04	0.23	0.05	0.02	0	0.77	8	Aniakchak
			c	Mean	74.82	0.16	13.92	1.28	0.03	0.25	1.48	4.54	3.29	0.30	100	2.90		
				StDev	0.32	0.04	0.24	0.03	0.03	0.03	0.02	0.34	0.06	0.02	0	0.86	3	WRA-like
GRV17 77-78 cm	3534	3491	a	Mean	77.31	0.26	12.67	1.55	0.08	0.38	2.09	3.80	1.70	0.21	100	3.10		
				StDev	0.46	0.04	0.19	0.08	0.02	0.04	0.12	0.28	0.11	0.02	0	1.38	19	Augustine
			b	Mean	70.92	0.52	15.20	2.43	0.14	0.51	1.70	5.30	3.11	0.21	100	2.05		
				StDev	0.18	0.05	0.26	0.03	0.03	0.02	0.05	0.31	0.05	0.02	0	1.13	4	Aniakchak
			c	Mean	75.38	0.19	13.74	1.33	0.07	0.29	1.37	4.05	3.34	0.32	100	3.19		
				StDev	0.71	0.02	0.53	0.07	0.03	0.01	0.20	0.25	0.21	0.01	0	1.58	6	WRA-like
GRV17 82-83 cm	3533	3686	a	Mean	77.16	0.29	12.63	1.55	0.07	0.35	2.05	4.09	1.66	0.21	100	3.87		
				StDev	0.40	0.04	0.22	0.05	0.02	0.07	0.17	0.21	0.12	0.02	0	0.79	6	Augustine
			b	Mean	75.50	0.20	13.66	1.26	0.06	0.27	1.37	4.13	3.30	0.32	100	3.26		
				StDev	0.77	0.08	0.42	0.09	0.01	0.02	0.18	0.56	0.17	0.03	0	1.11	4	WRA-like
GRV17 86-87 cm	3619	993	a	Mean	76.76	0.27	12.92	1.50	0.07	0.38	2.12	4.14	1.67	0.21	100	2.73		

	StDev	0.41	0.03	0.39	0.07	0.02	0.04	0.11	0.26	0.10	0.04	0	1.85	18	Augustine
b	Mean	73.36	0.36	14.00	2.20	0.08	0.45	1.99	4.63	2.73	0.25	100	0.77		
	StDev	0.18	0.06	0.21	0.37	0.02	0.14	0.36	0.23	0.13	0.02	0	0.73	3	unknown
c	Mean	75.22	0.26	14.03	1.36	0.08	0.30	1.64	4.24	2.68	0.24	100	6.37		
	StDev	2.84	0.11	1.26	0.50	0.05	0.14	0.45	0.69	0.55	0.10	0	5.02	6	unknown

Table 3.7: Geochemical populations of Gravel Lake main core, depths 93-202 cm

Depth (ccd)	UA #	Shards/g	Pop'n		SiO_2	TiO_2	Al_2O_3	FeOt	MnO	MgO	CaO	Na_2O	K_2O	Cl	Total	H_2Od	*n*	Potential Volcanic source/eruption
GRV17 93-94 cm	3532	282	a	Mean	77.41	0.23	12.76	1.46	0.07	0.36	2.15	3.84	1.58	0.19	100	1.93		
				StDev	0.24	0.05	0.14	0.10	0.01	0.05	0.06	0.15	0.09	0.02	0	0.40	4	Augustine
			b	Mean	75.72	0.29	13.18	1.80	0.06	0.49	1.90	3.64	2.74	0.23	100	2.68		
				StDev	0.04	0.10	0.60	0.52	0.04	0.20	0.43	0.51	0.66	0.05	0	1.00	3	unknown
GRV17 97-98 cm	3531	372	a	Mean	77.26	0.28	12.67	1.53	0.07	0.38	2.03	3.93	1.70	0.20	100	3.20		
				StDev	0.49	0.03	0.43	0.11	0.02	0.04	0.18	0.34	0.05	0.01	0	1.49	8	Augustine
			b	Mean	75.00	0.23	13.84	1.30	0.04	0.28	1.45	4.33	3.29	0.31	100	2.78		
				StDev	0.06	0.03	0.14	0.08	0.02	0.04	0.01	0.03	0.05	0.02	0	0.32	3	WRA-like
GRV17 100-101 cm	3530	408	a	Mean	77.34	0.26	12.81	1.60	0.07	0.41	2.18	3.49	1.68	0.20	100	2.95		
				StDev	0.40	0.06	0.14	0.05	0.03	0.03	0.06	0.35	0.06	0.02	0	0.37	8	Augustine
GRV17 113-114 cm	3528	244	a	Mean	75.31	0.16	14.01	1.27	0.06	0.26	1.51	3.98	3.22	0.29	100	2.60		
				StDev	0.49	0.03	0.24	0.06	0.02	0.04	0.08	0.35	0.03	0.02	0	0.92	7	WRA-like
GRV17 123-124 cm	3538	155	a	Mean	73.08	0.36	14.04	2.49	0.08	0.31	1.57	5.03	2.91	0.16	100	3.20		
				StDev	0.31	0.05	0.39	0.25	0.02	0.05	0.11	0.64	0.71	0.07	0	1.67	5	unknown
			b	Mean	76.61	0.18	13.18	1.13	0.06	0.25	1.27	4.40	2.80	0.16	100	5.56		
				StDev	1.42	0.03	0.87	0.19	0.01	0.05	0.14	0.33	0.39	0.08	0	2.18	7	unknown
GRV17 133-134 cm	3535	110	a	Mean	73.59	0.31	14.08	2.58	0.09	0.37	1.67	4.45	2.69	0.22	100	3.36		
				StDev	0.09	0.03	0.26	0.09	0.01	0.02	0.01	0.23	0.07	0.02	0	3.05	3	unknown
			b	Mean	78.89	0.20	12.47	1.03	0.07	0.21	1.16	3.52	2.36	0.14	100	5.75		
				StDev	0.24	0.02	0.12	0.04	0.01	0.03	0.03	0.12	0.02	0.01	0	0.31	3	unknown
			c	Mean	77.81	0.31	12.42	1.40	0.06	0.33	1.61	3.75	2.15	0.18	100	4.37		
				StDev	0.58	0.02	0.09	0.12	0.03	0.05	0.25	0.24	0.16	0.02	0	1.79	3	unknown

GRV17 135-136 cm	3536	93	a	Mean	74.34	0.45	12.88	2.11	0.08	0.36	1.55	4.01	3.91	0.40	100	3.13		
				StDev	2.49	0.07	0.98	0.38	0.03	0.16	0.60	0.38	0.16	0.06	0	2.21	3	unknown
			b	Mean	77.47	0.27	12.73	1.43	0.05	0.30	1.96	3.86	1.81	0.16	100	3.12		
				StDev	0.71	0.06	0.45	0.18	0.02	0.06	0.38	0.23	0.24	0.02	0	1.77	10	Augustine
GRV17 140-141 cm	3537	55	a	Mean	75.07	0.39	12.64	1.84	0.05	0.32	1.40	4.05	3.93	0.42	100	4.05		
				StDev	1.82	0.09	0.73	0.37	0.03	0.14	0.46	0.38	0.31	0.05	0	1.36	21	
GRV17 156-157 cm	3618	26	a	Mean	70.22	0.50	14.73	3.81	0.16	0.71	2.82	5.58	1.29	0.24	100	4.83		
				StDev	0.92	0.13	0.07	0.44	0.04	0.17	0.26	0.37	0.06	0.11	0	4.36	7	KS2
			b	Mean	75.57	0.41	12.33	1.78	0.05	0.33	1.31	4.55	3.40	0.35	100	4.31		
				StDev	1.48	0.03	0.45	0.23	0.05	0.02	0.06	0.40	1.05	0.11	0	0.93	2	unknown
			c	Mean	77.81	0.23	12.50	1.04	0.10	0.22	1.17	4.25	2.57	0.14	100	5.20		
				StDev	0.03	0.04	0.07	0.05	0.00	0.05	0.05	0.18	0.02	0.02	0	0.50	2	Augustine
GRV17 162-163 cm	3617	18	a	Mean	76.58	0.37	12.65	1.56	0.05	0.35	1.45	4.15	2.72	0.16	100	3.27		
				StDev	1.68	0.21	0.53	0.74	0.02	0.19	0.34	0.25	0.28	0.08	0	2.29	11	unknown
			b	Mean	74.05	0.25	13.77	1.91	0.03	0.25	1.21	4.69	3.66	0.23	100	3.54		
				StDev	0.30	0.01	0.13	0.01	0.04	0.05	0.00	0.23	0.24	0.01	0	1.14	2	Dawson?
			c	Mean	75.75	0.49	12.47	1.85	0.06	0.37	1.51	3.77	3.63	0.11	100	2.80		
				StDev	2.76	0.39	0.26	1.05	0.04	0.19	0.31	0.75	0.90	0.08	0	2.81	3	unknown
			d	Mean	76.73	0.26	13.05	1.43	0.06	0.37	1.94	4.23	1.76	0.21	100	5.81		
				StDev	0.27	0.04	0.18	0.13	0.04	0.05	0.28	0.31	0.19	0.09	0	2.97	5	Augustine
GRV17 188-189 cm	3615	10	a	Mean	78.26	0.24	12.24	1.10	0.06	0.20	1.09	3.87	2.76	0.21	100	5.78		
				StDev	0.51	0.06	0.12	0.10	0.02	0.03	0.05	0.26	0.12	0.06	0	2.81	8	unknown
			b	Mean	77.99	0.31	12.41	0.93	0.03	0.12	0.75	2.70	4.72	0.05	100	5.14		
				StDev	1.21	0.17	0.83	0.26	0.02	0.08	0.27	0.84	0.73	0.02	0	2.18	6	unknown
GRV17 201-202 cm	3614	21	a	Mean	75.22	0.38	13.33	1.75	0.04	0.34	1.49	4.35	2.94	0.21	100	3.94		
				StDev	0.33	0.04	0.20	0.06	0.02	0.03	0.11	0.27	0.10	0.05	0	2.89	12	Redoubt?

Main core

Gravel Lake contains the most geochemical populations and highest concentrations of all four study sites. LOI, magnetic susceptibility, core thickness, and gamma-ray density measurements are presented in Figure 3.9, and non-weathered shard profiles are presented in Figure 3.10. The top six centimetres of the main core was not processed for cryptotephra, as it was lost during coring. Large variations in glass shard concentration are found in the Gravel Lake main core (Tables 3.6 and 3.7), with the highest concentrations of non-weathered glass from 7-88 cm at an average concentration of 5476 shards/g (Table 3.6). A steep drop in concentration occurs at ~90 cm, followed by a steady decrease until ~140 cm where primary concentrations remain below 30 shards/g to the base of the core. Weathered glass shard concentrations show less dramatic variance throughout the core, with concentrations in the order of hundreds of shards per gram (Fig. 3.11). There is no obvious pattern to the variability of weathered glass concentrations, although a correlation may exist between LOI where steep drops in LOI, such as ~175 and ~198 cm, are associated with decreases in weathered glass concentration. A total of 37 depths were selected for geochemical analyses based on non-weathered glass shard profiles and geochemical results, summarized in Table 3.6 for depths 7-87 cm and Table 3.7 for depths 87-222 cm.

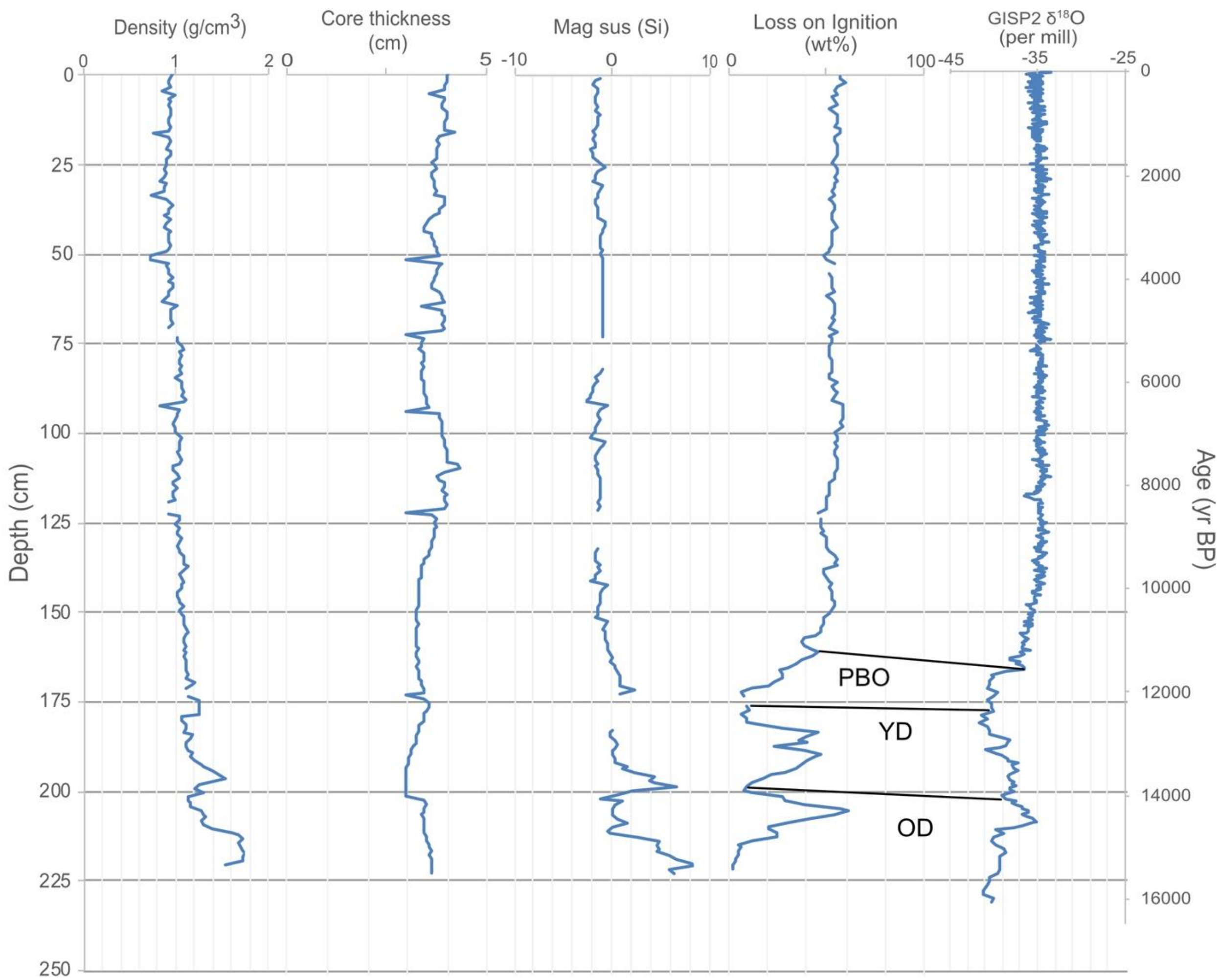

Figure 3.9: Gravel Lake core scan data collected on a GeoTek Multi-Sensor Core Logger (MSCL), including density, core thickness, and magnetic susceptibility. LOI values were collected while processing cryptotephra and are compared to the GISP2 $\delta^{18}O$ isotope record from Greenland ice cores. LOI and $\delta^{18}O$ signals show similar trends, indicating temperature changes in Greenland are reflected in organic content within Gravel Lake, such as the Younger Dryas (YD), Older Dryas (OD), and Pre-boreal Oscillation (PBO) events. GISP2 $\delta^{18}O$ record adapted from Grootes and Stuiver (1997).

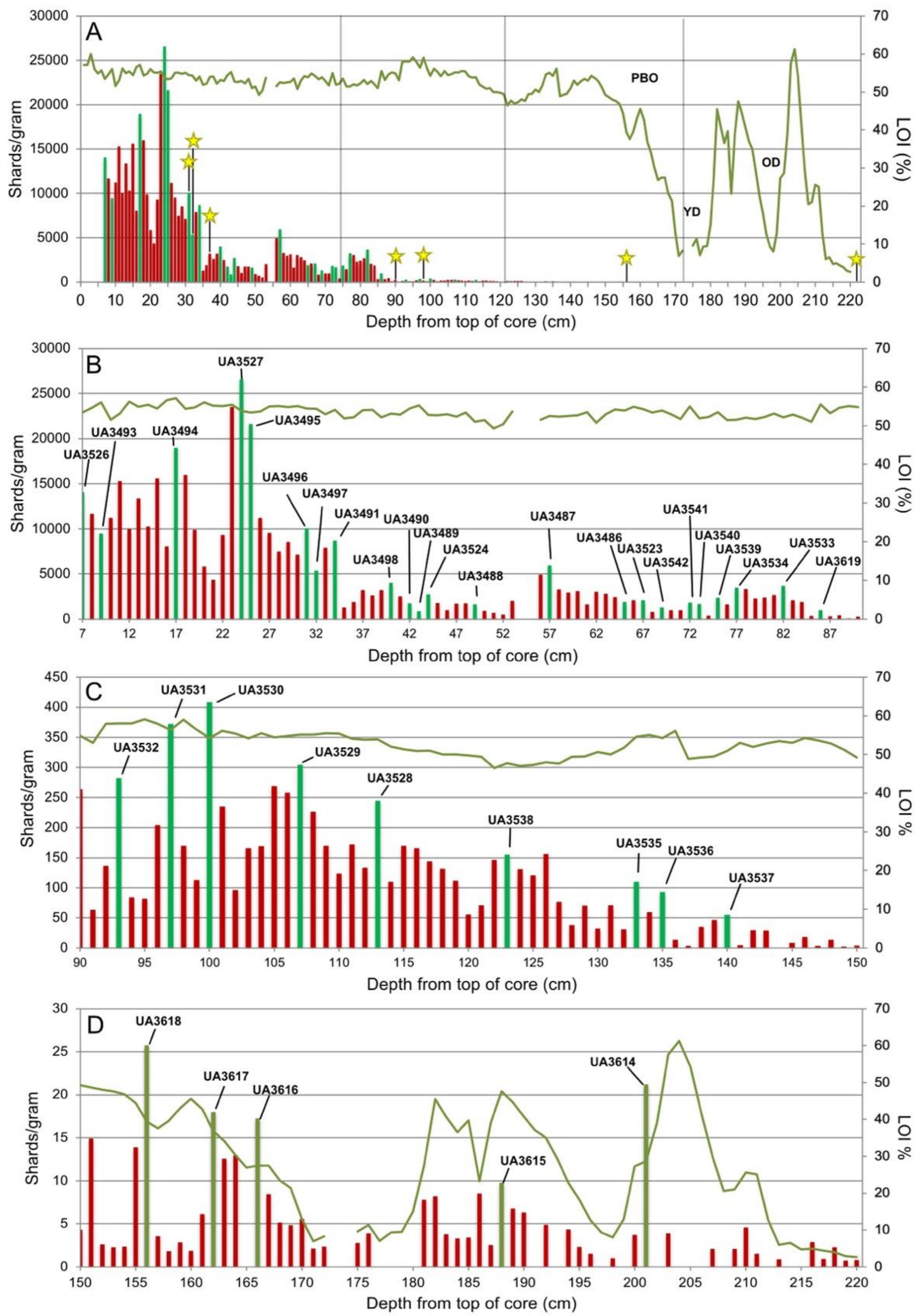

Figure 3.10: Gravel Lake shard concentration profile with LOI values shown on secondary axis. Full core and depths of ^{14}C dates (yellow stars; Table 3.2) are shown in (A), with vertical lines showing splits in the full core. (B) 7 to 90 cm. (C) 90 to 50 cm. (D) 150 to 220 cm. Green bars indicate depths processed for geochemistry.

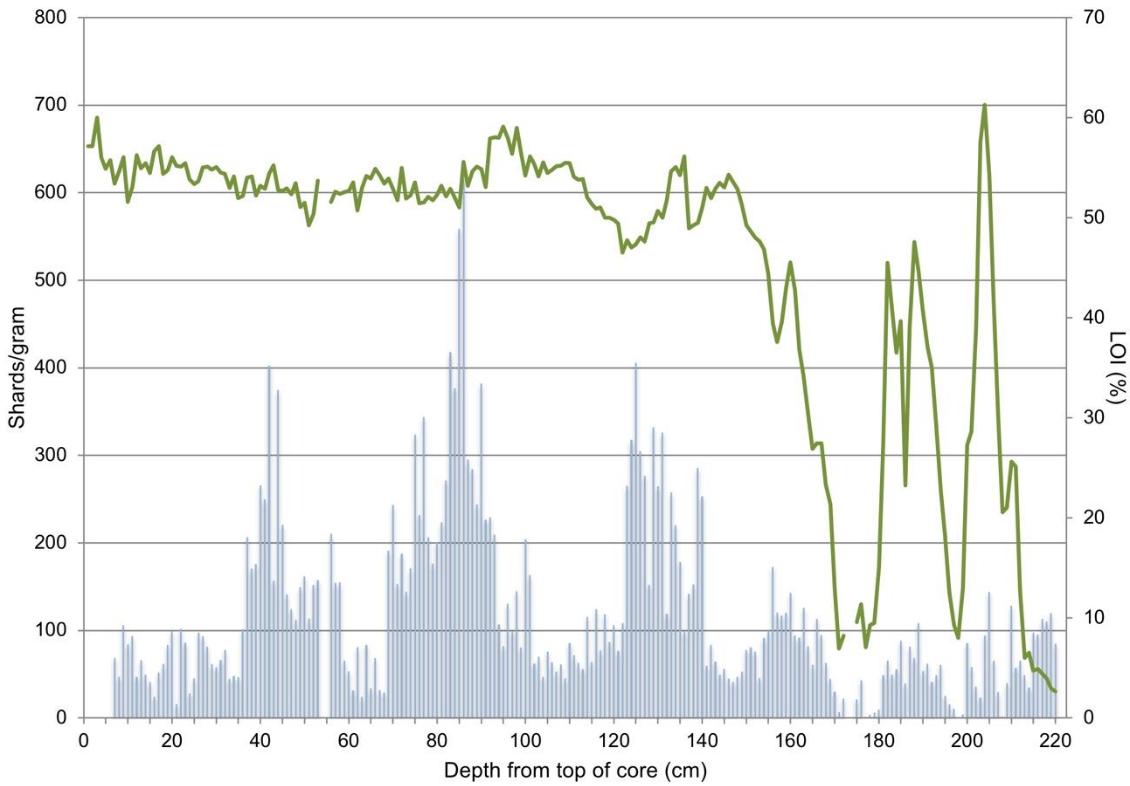

Figure 3.11: Weathered glass profile of Gravel Lake main core. Drops in weathered shard concentrations are seen when LOI decreases in the lower depths of the core.

3.4.4.1. Correlated Tephra Populations

Katmai 1912

Samples UA3493 (Gravel Lake main core, 9-10 cm below top of core) and UA3623 (Gravel Lake surface core, 4-5 cm) contain a geochemical population that correlates to the Novarupta/Katmai 1912 eruption from the Alaska Peninsula (Hildreth, 1983; Hildreth and Fierstein, 2000) (Fig. 3.8). This was the largest eruption of the 20th and 21st centuries but does not form a widely distributed visible bed in the Yukon and Alaska as the plume went largely to the southeast (Hildreth and Fierstein, 2000). It is present in Greenland however, as well as the Dempster Highway peat record (Coulter et al., 2012; Davies, 2018). Katmai 1912 is only found at these two depths and consists of half of the analyzed shards in the surface core sample and only three shards of 26 in the main core, both accompanied by WRA tephra. The top of the main core is compressed, which suggests that the depth it is found in the surface core is more accurate, but the lack of a clear peak makes isochron placement difficult.

Mount Churchill

The highest concentrations of Gravel Lake consist of relatively large frothy and phenocryst-rich pumice that is predicted by machine learning classifiers to be Mt. Churchill tephra – namely WRA. These WRA-like populations are found in all samples from the surface core, as well as between 7-82 cm, 97-98 cm, and 113-114 cm in the main core (Tables 3.5, 3.6, and 3.7). The highest concentrations are within the top ~45 cm of the main core (Fig. 3.12). The most significant peak at 24-25 cm in the main Gravel Lake core (UA3527; ~26,500 shards/g) is most likely WRAn; however, this peak has a different geochemistry than the main Hanging Lake WRAn peak (Fig. 3.13). Unlike UA3362 in Hanging Lake, the main peak of Gravel Lake has a SiO_2 range of 72.8 to 77.2 wt% that includes some high SiO_2 shards but also has the lower SiO_2 range seen in sites such as the Duke River fan site, south-west Yukon (Jensen, 2007). Within the highest concentrations of WRA glass are three radiocarbon dates at 31-32 cm, 32-33 cm, and 37-38 cm, derived from one aquatic seed and two picea needle fragments. All three samples are found below the main WRAn peak, and have ages of 2710-2489, 1291-1124, and 1510-1351 cal BP, respectively. The implications of these ages are discussed in section 3.6 below.

All analyzed depths from the surface core to 69-70 cm in the main core contain a WRA-like population that may be the dominant population, or a minor sub-population. Although most are difficult to distinguish from one another, some variation exists in the SiO_2 ranges (Fig. 3.12). Some samples have more condensed clusters of points (e.g., 44-45cm/UA3524, with the majority of points plotting 74.5-75.5 SiO_2 wt%), while others have much broader ranges (e.g., 43-44 cm/UA3489 at 73.5-76.5 SiO_2 wt%), even when the samples are within 1 cm of each other. Additionally, a smaller secondary peak is present sixteen centimetres below the main peak. Gravel Lake's secondary peak occurs at 40-41 cm (UA3498; 4032 shards/g) and has no notable differences from the main peak. The heterogeneous nature of WRA makes it difficult to differentiate these samples without additional data (e.g., Fe-Ti oxides, trace elements); Fe-Ti oxides were separated from several depths, but only detrital mineral grains were found. The potential implications of the multiple WRA peaks, and how they compare to other regional studies are discussed later.

One sample from the Gravel surface core displays slight geochemical differences suggesting both WRAn and WRAe are present (Fig. 3.8). UA3620 (18-19 cm depth) more closely resembles WRAe and is the only surface core sample that contains a single geochemical population. K_2O is one of the best oxides to differentiate between WRAe and WRAn, where WRAe has higher on average K_2O than WRAn. UA3620 shows this relationship and plots with WRAe (Fig. 3.8). The geochemistry of the WRA-like populations in the other three peaks in the Gravel Lake surface core do not show any particular affinity to either WRAe or WRAn.

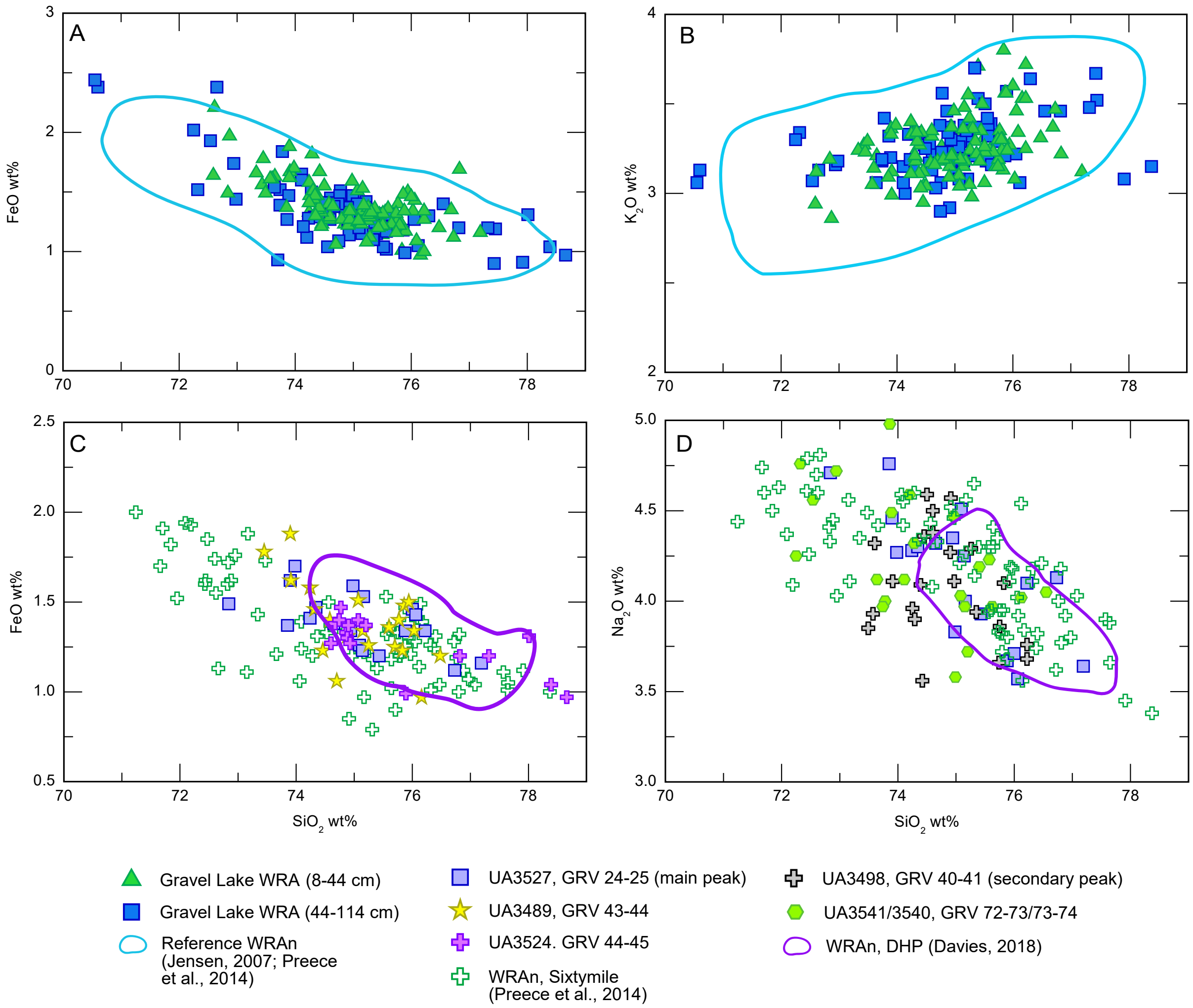

Figure 3.12: (A,B) WRA-like tephra in the Gravel Lake main core are compared to reference WRAn tephra (blue outline; Jensen, 2007; Preece et al., 2014). Shards are separated as 8-44 cm depth (green triangles) which represents the main peak of WRAn and its tails, and 44-114 cm (blue squares) which represents the other WRA-like samples scattered in the upper part of the core. Shards are difficult to differentiate and nearly all points fall within the expected values of WRAn, making it difficult to tell reworked tephra from primary deposits. (C) The main peak of WRAn (UA3527) is compared to WRAn samples from Sixtymile site (Preece et al., 2014) and DHP site (purple outline; Davies, 2018). UA3489 and UA3524 are examples of subtle differences that do exist between some WRA-like samples. (D) The main peak, secondary peak, and UA3541/UA3540 samples show an SiO_2 range slightly greater than the tephra found at DHP site, more similar to the Sixtymile area (Preece et al., 2014).

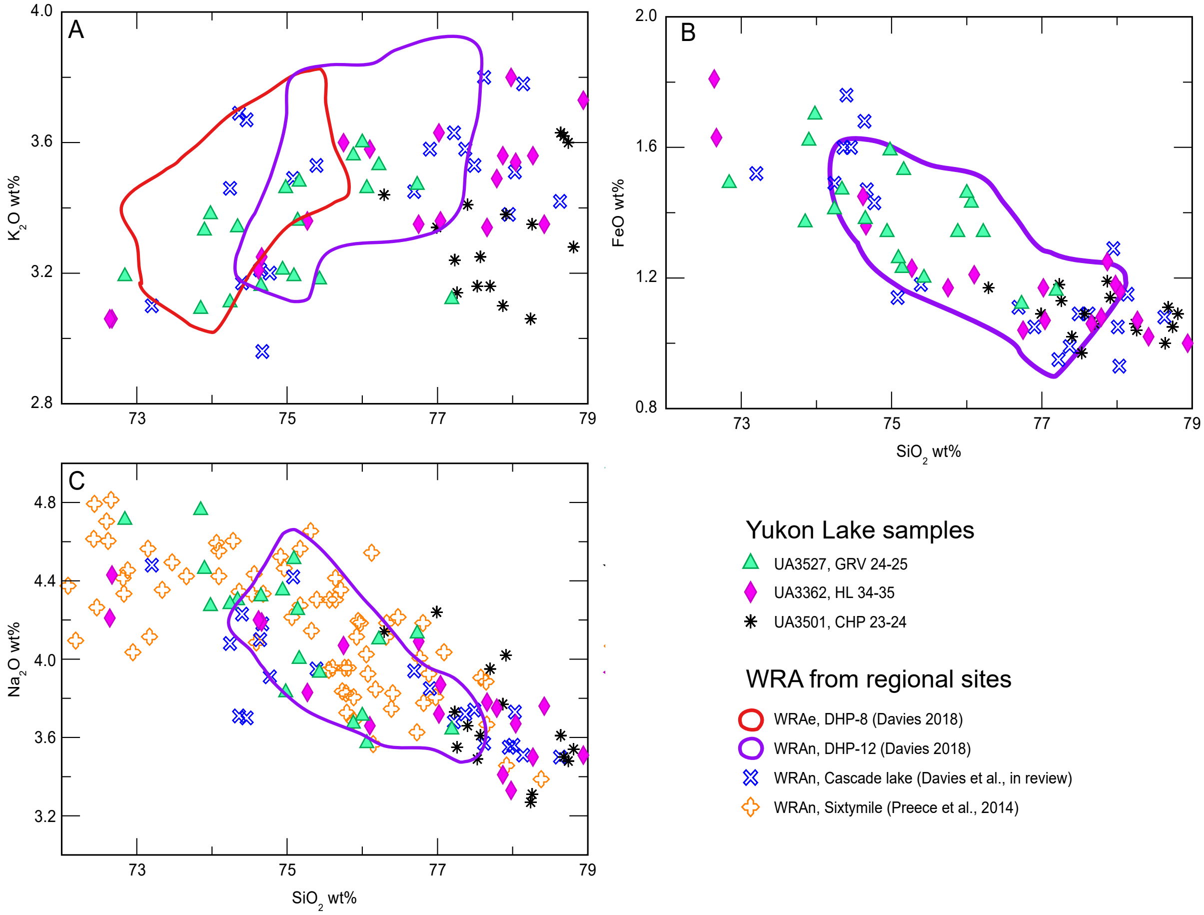

Figure 3.13: (A,B) Geochemical comparison between the three largest peaks of WRA shards at Gravel, Hanging, and Chapman Lakes to WRA tephra from regional sites. (C) Gravel Lake's UA3527 has an SiO_2 range more similar to Sixtymile (Preece et al., 2014), whereas Hanging Lake's UA3362 and Chapman Lake's UA3501 contain the higher-SiO_2 tephra found in northern sites such as Cascade Lake (Davies et al., in review).

Aniakchak

A distinct geochemical population in the Gravel Lake main core is present in multiple samples between the depths of ~30-80 cm. The morphology of these grains differ from the vesicle-rich WRA tephra, comprising of largely platy or blocky, clear, and fluted shards. Aniakchak-like shards were found in low concentrations (1-5 shards) at 7-8 cm (UA3526), 31-32 cm (UA3496), 34-35 cm (UA3491), 40-41 cm (UA3498), 57-58 cm (UA3487), and 69-70 cm (UA3542), in addition to Churchill and Augustine-like populations (discussed below) (Tables 3.6 and 3.7). Three zones – 49-50 cm (UA3488), 65-68 cm (UA3486 and UA3523), and 75-78 cm (UA3539 and 3534) – contain larger shard concentrations. Sample UA3523 at 67-68 cm contains the highest proportion of Aniakchak-like shards, where they form the dominant geochemical population (n=31/64).

Geochemically these data suggest a correlation to Aniakchak, a volcano in the Alaska Peninsula that has had two caldera forming eruptions over the Holocene (CFE I, between ~ 9,500–7,000 cal BP; CFE II, 3510-3290 cal BP) in additional to several other large eruptions that have distributed visible tephra largely to the north of the vent (e.g., Kaufman et al., 2012; Bacon et al., 2014; Davies et al., 2016). The Aniakchak-like geochemical population in Gravel Lake correlates to the higher-SiO_2 population of CFE II, which has SiO_2 values between 70-72 wt% (Fig. 3.14). Potential evidence of other Holocene Aniakchak eruptions, such as the 3.1 ka and 5.8 ka Lone Spruce Pond samples of Kaufman et al. (2012) are also compared to the samples in Gravel Lake, with identical major-element geochemistry (Fig. 3.14).

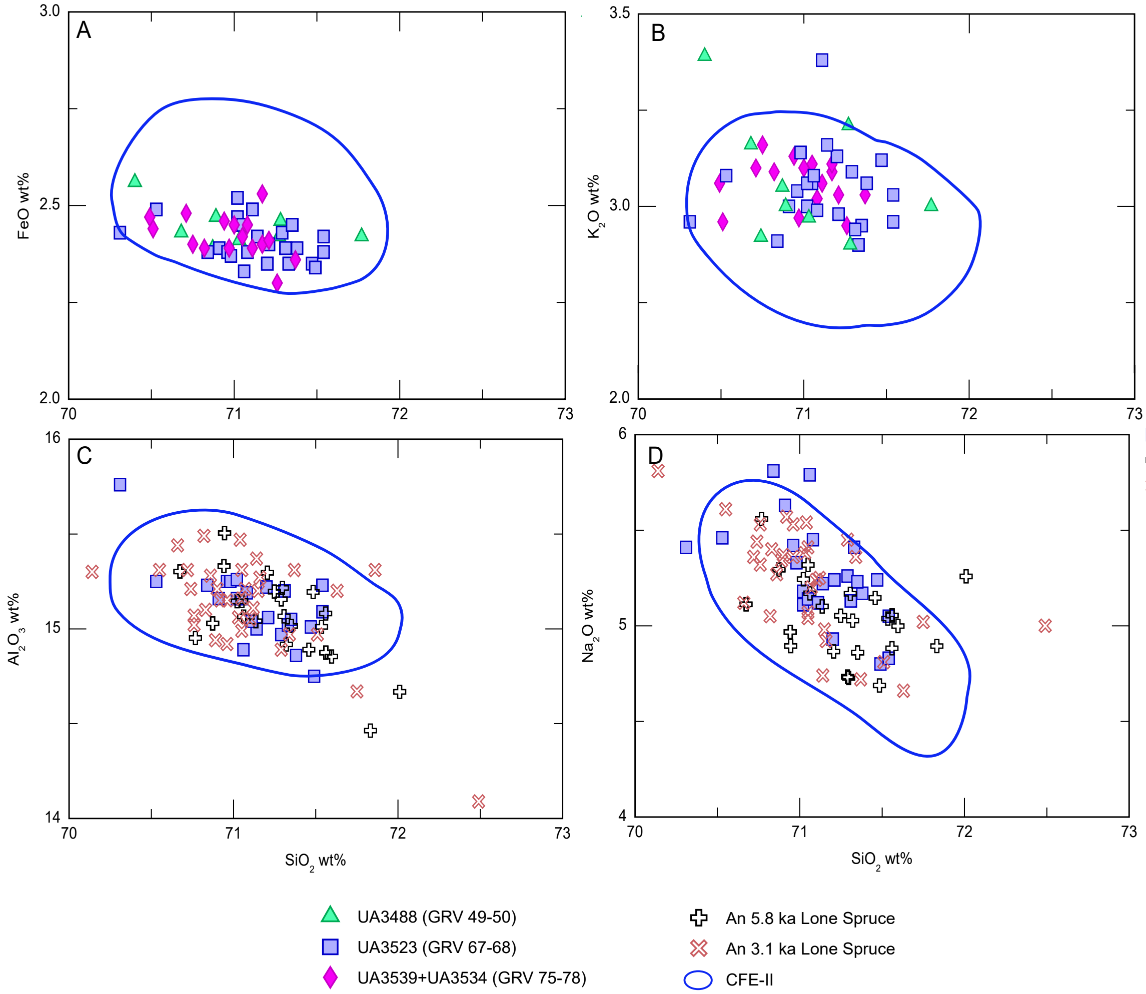

Figure 3.14: (A,B) Comparison of the three main Aniakchak peaks in Gravel Lake to reference CFE II tephra (blue circles; Davies et al., 2016). (C,D) All three Aniakchak peaks are geochemically similar to the 5.8ka and 3.1ka Lone Spruce samples from Kaufman et al. (2012).

Augustine

A high-SiO_2 (77-78 wt%) low-K_2O (~1.5-1.8 wt%) geochemical population associated with large clear pumice shards with small occasional vesicles is widely dispersed across the Gravel Lake main core. This geochemical grouping is found between 42 to 163 cm, with minor populations found at 42-43 cm (UA3490), 49-50 cm (UA3488), 65-66 cm (UA3486), 67-68 cm (UA3523), 73-74 cm (UA3540), 82-83 cm (UA3533), 93-94 cm (UA3532), 156-157 cm (UA3618), and 162-163 cm (UA3617) (Tables 3.6 and 3.7). It is often a minor population in samples from peaks that have other more dominant geochemical populations (e.g., in all three zones of high Aniakchak-like concentrations). These multiple inputs complicate the concentration profiles, resulting in less obvious "peaks" for each potential event. Four regions contain higher concentrations of the tephra – 57-58 cm (UA3487), 75-78 cm (UA3539 and UA3534), 86-87 cm (UA3619), and 97-101 cm (UA3531 and UA3530) – where this tephra has the highest proportion of analyzed shards compared to other populations (Tables 3.6 and 3.7).

The geochemistry of these samples is largely homogenous and are predicted by machine learning to be sourced from either Augustine or Kaguyak volcanoes of Alaska, although higher prediction values are given to Augustine in most analyses. Augustine volcano is an island in southwestern Cook Inlet, Alaska, and has repeatedly erupted throughout the Holocene, with at least fifteen tephra-forming eruptions recorded in proximal deposits over the last 2,200 years (Waitt and Begét, 2009). Evidence of older eruptions on the island is limited because of the recent activity, but do exist (Waitt and Begét, 2009). Lemke (2000) used glass geochemistry to link tephra from early to mid-Holocene eruptions on the south flank of the island to nine visible tephra layers from Homer and Anchor Point peat sites on the Kenai Peninsula (Riehle et al., 1998; Waitt and Begét, 2009). These data were compared to our results and show complete overlap in their compositions (Fig. 3.15).

The three high concentration samples of these Augustine-like tephra at 57-58 cm (UA3487), 75-78 cm (UA3539 and UA3534), and 93-100 cm (UA3532, UA3531, and UA3530) have largely indistinguishable geochemistry (Fig. 3.15). UA3619 (86-87 cm) is more homogenous with a lower SiO_2 average (76.76 wt%; Table 3.6), but the other samples largely overlap with a slightly greater clustering in UA 3487 around ~77.5 wt%. Two older Augustine-like samples at depths 135-136 cm (U3536) and 162-163 cm (UA3617) are similar to the main peaks in most oxides but contain shards that have notably lower CaO and higher Na_2O that may represent another population (Fig. 3.15C).

Several other cryptotephra studies have reported Augustine-like deposits in their Holocene records, but individual eruptions are hard to identify due to the lack of data from individual eruptions and the homogenous geochemistry of many Augustine tephra (e.g., Payne et al., 2008; Pyne-O'Donnell et al., 2012; Blockley et al., 2015; Monteath et al., 2017; Davies et al., 2018). This includes J127 from Jan Lake, eastern Alaska; a <1 mm thick ash bed with an age of 4240-4820 cal yr BP (Monteath et al., 2017), and multiple Augustine-like samples at the DHP section of Davies et al. (2018). One of the largest defined peaks, UA 3619 (86-87 cm), may also potentially be of similar age to this mid-Holocene tephra based on a terrestrial macrofossil date of 5270-4858 cal BP at 98-99 cm (Table 3.2). DHP-38 (4820±480 cal yr BP) was correlated to tephra J127 (Davies, 2018), and both are compared to the Gravel Lake samples here. Geochemical data of DHP-38 and J127 from 2015 were initially used for comparison, both showing slightly higher CaO (~2.35 vs. 2.15 wt%), but generally overlapping with Gravel Lake samples. DHP-38 was re-run alongside UA3539 in 2021, and now overlaps fully with Gravel Lake geochemistry (Fig. 3.15C). The CaO wt% offset seen in J127 is likely a result of analytical differences, as it was run on the same day as the initial DHP-38 sample in 2015. Further analyses of J127 are required for a better comparison.

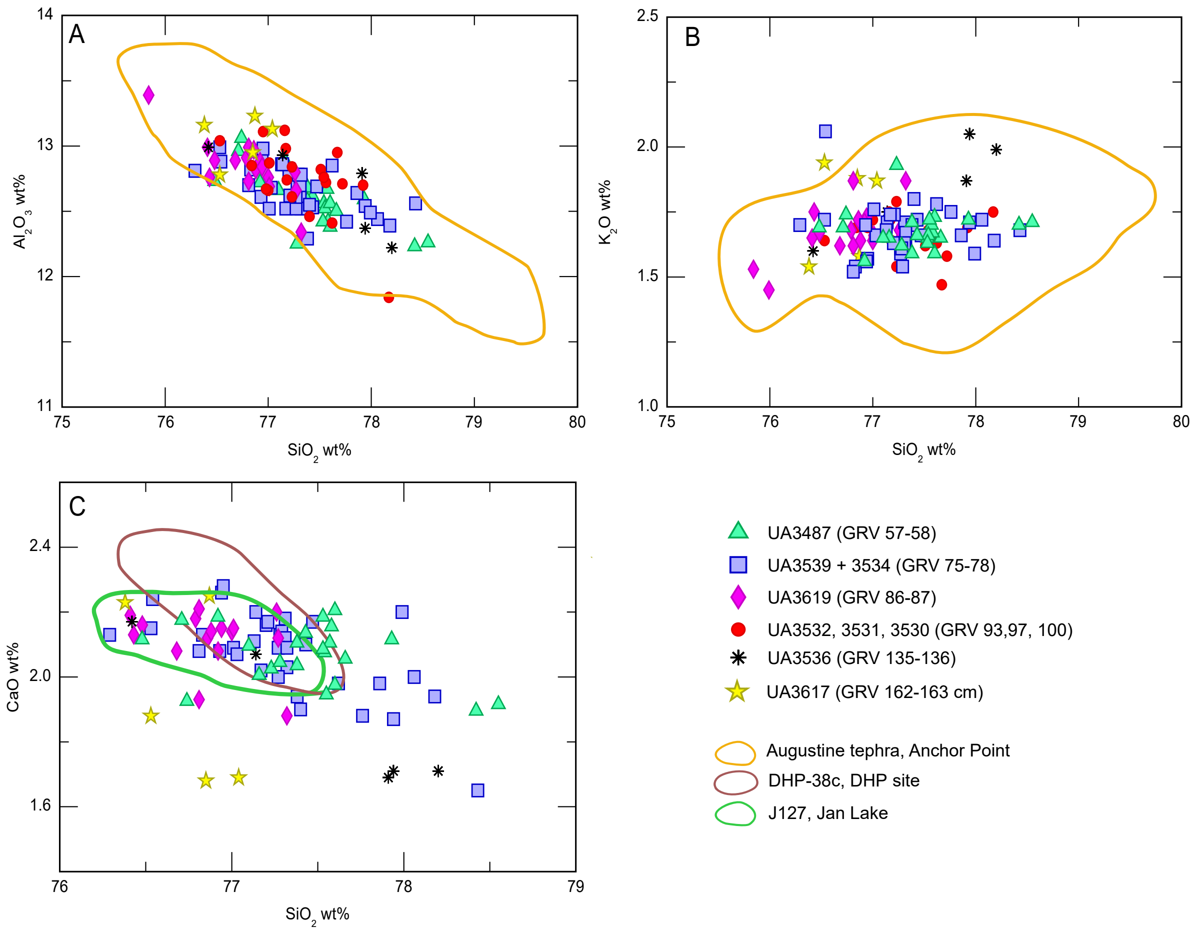

Figure 3.15: Comparison of Augustine-like peaks to proximal and distal Augustine-like samples. (A,B) The compositional field defined by ten Augustine-correlated samples from Anchor Point (orange circle) encompasses the Augustine-like samples in Gravel Lake (Lemke, 2000). (C) Tephra J127 from Jan Lake, eastern Alaska (Monteath et al., 2017) and DHP-38c from DHP, central Yukon (Davies, 2018) are geochemically similar to the Augustine-like samples of Gravel Lake but J127 has slightly higher CaO. Variability in CaO and K_2O show older Augustine-like samples UA3536 and 3617 may be composed of more than one tephra

3.4.4.2. Discrete populations of Gravel Lake

Ten unique geochemical populations were identified in Gravel Lake; most have no known correlations (Fig. 3.16). These populations are found as relatively small peaks with lower concentrations than the weathered glass at the same depth. Below ~90 cm, shard concentrations start to drop significantly (Fig. 3.10A), allowing the identification of smaller peaks. The drop in concentration is roughly around 4500 to 5000 cal BP, based on the terrestrial macrofossil date of 5270-4858 cal BP at 98-99 cm. With only one other ^{14}C date between 98 cm and the core catch material, it is difficult to predict the ages of these discrete populations and therefore difficult to make confident correlations to specific tephra. We briefly describe these populations in stratigraphic order and suggest potential correlations where possible.

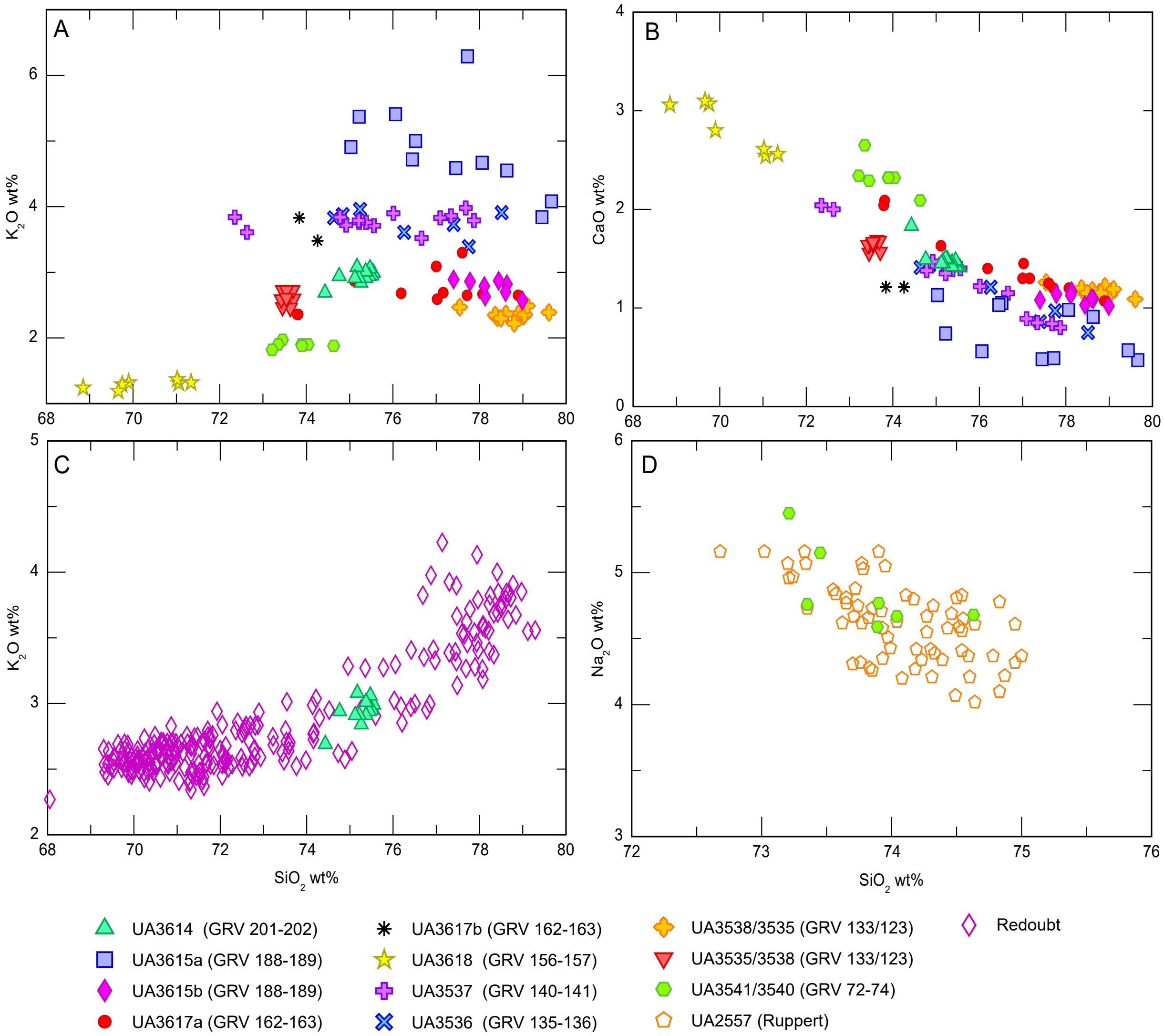

Figure 3.16: Unique geochemical populations found in Gravel Lake. (A,B) Biplots of all the populations found below 90 cm when background glass concentrations drop. Lower CaO and Na_2O (not shown; see Appendix) indicate potential weathering in some points of UA3615a. (C) UA3614 (GRV 201-202 cm) plots with Redoubt tephra (Bolton et al., 2020). (D) UA3541 and UA3540 (GRV 72-74 cm) are geochemically identical to the Ruppert tephra from Ruppert Lake, Alaska (Monteath et al., 2017).

UA 3540 and UA 3541 (Gravel Lake, 72-74 cm)

A unique low-K_2O (~2 wt%; Table 3.7) rhyolitic population occurs six centimetres below the primary Aniakchak CFE II peak and has low (50-70%) machine-learning predictions to Augustine volcano. This minor population is found with an assortment of mixed glass shards, most WRA-like glass compositions. The glass composition of this population is similar to two nearby sites (Fig. 3.16). At DHP, Davies (2018) reports a tephra (DHP-35), also with multiple populations and located slightly below the CFE II, with an age of ~4255 cal BP. However, DHP-35 is slightly higher in Al_2O_3 and is notably lower in Cl (0.12 vs. 0.27 wt%). In addition, Ruppert tephra from Ruppert Lake in the Brooks Range, Alaska (Monteath et al., 2017) is geochemically identical to UA3540/3541. Ruppert tephra was located in both sediment cores of Ruppert Lake, yielding two estimated ages of 3230-2930 cal yr BP and 2920-2520 cal yr BP; a new modelled age of 2800-2130 cal yr BP incorporates all sites the tephra is present (Jensen et al., in review). However, the estimated age of Ruppert tephra does not fit with the stratigraphic position of UA 3540/3541. Ruppert is younger than Aniakchak CFE II (~3.6 ka) – with the main population of that tephra found above UA 3540/3541 at 67-68 cm. This conflict in geochemistry and stratigraphy is discussed in section 3.5.2.

UA 3536/3537 (Gravel Lake, 135 and 140 cm)

A high-Cl (~0.4 wt%; Table 3.7) rhyolitic population is the only population at a small peak at 140-141 cm and is one of two populations at 135-136 cm, and has low predictions to Katmai, Churchill, and Redoubt volcanoes. Glass shards found at 140-141 cm were microlitic blocky and bubble-wall shards. Multiple morphologies existed in 135-136 cm, with the same microlitic blocky shards, as well as minor vesicular pumice and clean cuspate shards. The cuspate shards are similar in morphology to those of the Augustine-like samples, which is the secondary population of 135-136 cm (Table 3.7). The high Cl and a SiO_2 range (72.35-78.5 wt%) make this unknown sample unique from other populations in this study. There is some scatter in the geochemistry of UA 3536 and 3537 that may be caused by partial analysis of microlites (Fig. 3.16). No similar tephras were found in the literature.

UA 3618 (Gravel Lake, 156-157 cm)

UA3618 contains multiple populations, including a rhyodacite (68.85–71.34 wt%) with relatively high Na_2O and FeO_t, and low K_2O (Table 3.7; Fig. 3.16). This population produced 40-60% predictions to the Fisher volcano. A review of the literature and University of Alberta tephra geochemical database shows that these data are unique and there are no known tephra from the Yukon or Alaska with this distinctive geochemistry. Instead, the high-Fe low-K characteristics are more similar to tephra from Ksudach caldera, Kurile Islands, Russia (e.g., Braitseva and Ponomareva, 1997). UA3618 is geochemically similar to the Ksudach KS_2 tephra and overlaps with reference KS_2 data (Ponomareva et al., 2017; Portnyagin et al., 2020) and a distal KS_2 correlative from Thin-Ice Pond, Nova Scotia (TI-323; Fig. 3.17; Jensen et al., in review). Two KS_2 correlatives from Pechora Lake and Olive-backed Lake are also compared to UA 3618, although they have slightly lower Na_2O values (Plunkett et al., 2015). The higher Na_2O values in both UA3618 and TI-323 may be attributed to analytical conditions between studies, for example TI-323 was analyzed at Kiel and Edinburgh, and only the Edinburgh data shows the higher Na_2O wt% (Jensen et al., in review).

The age of the caldera-forming KS_2 eruption is estimated to be 6877-6693 cal yr BP based on proximal data (Ponomareva et al., 2017), although other ages have been suggested as well. Plunkett et al. (2015) have age estimates of 7350–7180 and 7300–7160 cal yr BP for their lake samples, more consistent with the age of TI-323 (7185-6970 cal yr BP; Jensen et al., in review). The ^{14}C sample collected at this depth has an age of 7267-7165 cal yr BP and supports this correlation rather than to the other possible Ksudach correlative – KS_4 (10,150-9700 cal yr BP; Bazanova et al., 2016) – especially because this date is on an aquatic seed that would bias it to an older age. However, the age of KS_4 does agree better with the extrapolated age at this depth based on the wiggle-matched LOI-GISP2 record of Beierle (2001). Glass analyses of reference materials are necessary to resolve this correlation, although bulk geochemistry of KS_4 suggests it will have a notably different composition from KS_2 (Bazanova et al., 2016). The correlation to a Kamchatkan source is not unusual, as tephras from this region (including KS_2) have been found across a large portion of the northern Hemisphere (e.g., van der Bilt, 2017; Cook, 2018; Davies, 2018; Mackay et al., 2016; Jensen et al., in review; Davies et al., in review).

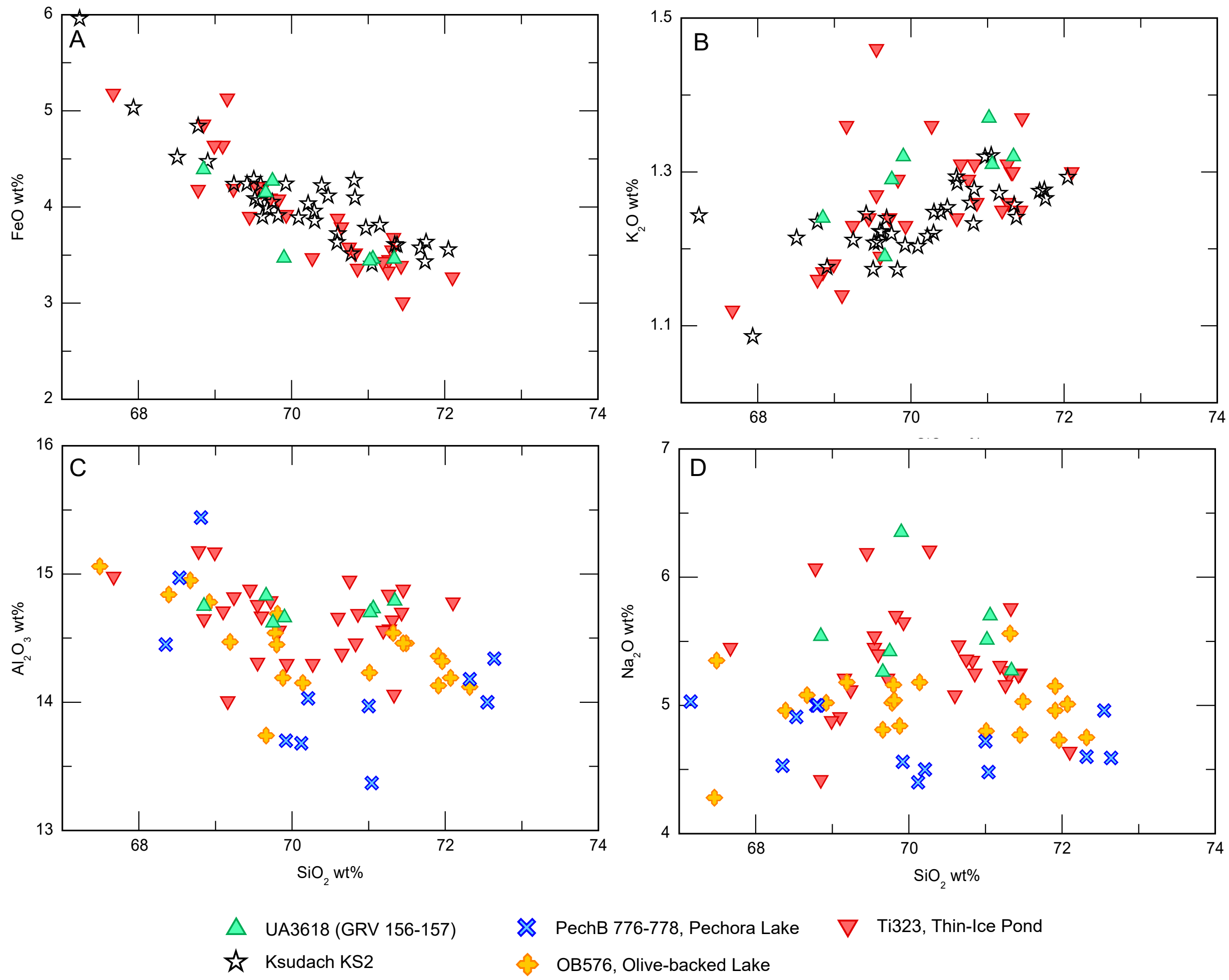

Figure 3.17: (A,B) KS_2 data from TephraKam (Portnyagin et al., 2020), Ponomareva et al. (2017) and TI-323 (Jensen et al., in review) are geochemically similar to UA3618. (C,D) Distal KS_2 from Pechora Lake (PechB 776-778) and Olive-backed Lake (OB576), northern Kamchatka (Plunkett et al., 2015), are similar to UA3618 but have slightly lower Al_2O_3 and Na_2O.

UA3614 (Gravel Lake, 201-202 cm)

The oldest discrete shard population is at 201-202 cm, at the transition into the Older Dryas (~14000 years BP) based on the wiggle-matching of Beierle (2001) (Fig. 3.10). This population is represented by a small peak (21 shards/g) of clean platy and blocky shards that reside among a comparably larger quantity (58 shards/g) of weathered shards with hazy surfaces and rounded down edges. Despite the lower concentration of glass and weathered shards, we were able to successfully analyse this sample, which is a relatively homogenous rhyolite (SiO_2 ~75.22 wt%; Table 3.7) that has moderate (70-80%) predictions to the Redoubt volcano.

UA3614 is compared to geochemical data from Holocene Redoubt tephra and overlaps in all major and minor oxides (Fig. 3.16C; Bolton et al., 2020). Begét and Nye (1994) report the first eruptive post-glacial episode of Redoubt in the form of the Harriet Point debris avalanche. No geochemical data exists for comparison, but with an estimated age of 10,500 to 13,000 yr BP this eruptive event may be related to UA3614, which has a similar geochemistry to Redoubt volcano and was deposited roughly around this time.

Newly described tephra

Six additional tephra with rhyolitic glass compositions are found in the lower depths of Gravel Lake that do not have any potential correlations. One population, located at 123-124 cm (UA3538a) and 133-134 cm (UA3535a), is relatively homogenous, with SiO_2 ~73 wt%, relatively high FeOt (~2.6 wt%) and moderately low K_2O (~2.6 wt%). This population is unique to these two samples and is not found anywhere else in the core. UA3617b (162-163 cm) contains a very small population, with SiO_2 ~74 wt%, low CaO (1.21 wt%) and low MgO (~0.25 wt%). UA3615b is found at 188-189 cm and contains higher K_2O (~4.9 wt%) and lower Na_2O (~2.8wt%), with low Cl (~0.06wt%). Scattering in CaO and FeOt occurs in some of these points, indicating potential weathering of the sample. In addition to the above populations, each of these depths contains secondary populations; UA3535b/3538b (123-124 and 133-134 cm), UA3617a (162-163 cm), and UA3615a (188-189 cm). These populations contain similarly high SiO_2 (76-80 wt%), Na_2O of 3-4.5 wt%, and low TiO_2 (0.1-0.3 wt%), but differences in K_2O (Fig. 3.16) and Al_2O_3 (Table 3.7) differentiate the populations.

3.5. Discussion

3.5.1. White River Ash: Interpretation of results

The White River Ash is one of few visible Holocene tephra deposits in the Yukon and its use as a regional marker bed has resulted in a series of studies defining the distribution and geochemical variations between WRAn and WRAe lobes (e.g., Lerbekmo and Campbell, 1968; Péwé, 1975; Lerbekmo et al., 1975; Lerbekmo, 2008). The exceptional distribution of WRAe across North American and into Europe has resulted in a geochemically well-characterized tephra (e.g., Pyne-O'Donnell et al., 2012; Jensen et al., 2014; Mackay et al., 2016). However, considerable overlap in glass geochemistry and limited published geochemical data for WRAn has made it challenging to confidently differentiate the two lobes where their distributions overlap. While Fe-Ti oxide geochemistry has been shown to be an effective way to differentiate the lobes (Lerbekmo et al., 1975; Richter et al., 1995; Preece et al., 2014), these heavy minerals can be challenging to extract from cryptotephra deposits as we found in this study.

In proximal deposits surrounding Mt. Churchill and distal deposits in the Sixtymile area, Preece et al. (2014) differentiated the eastern and northern lobes of WRA using ilmenites and major element geochemistry, and further characterized each lobe with two additional geochemical sub-units (WRA-Na, WRA-Nb, WRA-Ea, and WRA-Eb). Proximal WRA-Na samples such as location 11 contained heterogeneity within the same site, showing increasing glass SiO_2 content from the bottom to the top of the bed and suggesting a layered magma chamber during the eruption of WRAn. In comparison, WRA-Nb was found at one distal Sixtymile location and only contains the higher-SiO_2 range seen at the top of the location 11 bed. This data suggests either a layered magma chamber during the eruption of WRAn where partial preservation is occurring at a given location, or there are potentially multiple eruptions taking place over a short period of time. WRA-Ea and WRA-Eb are found within the same site and are separated by 10 cm of peat, suggesting the upper WRA-Eb is a younger event (e.g., Lena tephra; Payne et al. 2008). These data from Preece et al. (2014) corroborate the geochemical variation seen here and in other studies (e.g., Davies, 2018; Davies et al., 2019; Davies et al., in review) between WRA samples. It is important to note that despite the geochemical variation seen in the WRAn samples, there is no evidence for varying ages between the main distal visible deposits (e.g., Reuther et al., 2020). Regardless, various studies (e.g., Payne et al., 2008; Preece et al., 2014; Davies, 2018; Davies et al., 2019) are building a growing body of evidence of multiple Churchill eruptions over the Holocene beyond the established pair of WRAn and WRAe. Here we take a closer look at the WRA-like geochemical populations in three of the four Yukon Lakes in this study, compare these results to others records in the region (e.g., Preece et al., 2014; Davies, 2018; Davies et al., in review), and determine if the records here provide any further insight in additional activity from Mount Churchill.

Comparison between Yukon Lake sites

The highest glass concentration peaks in Hanging Lake (UA3362; 29-30 cm) and Gravel Lake (UA3527; 24-25 cm) cores are correlated to WRAn. Relative to the location of Mt. Churchill, it makes sense that the highest concentration peaks found in the Yukon lakes are associated with the WRAn lobe. These lakes fall either within or near the limit of visible distribution of the northern lobe, while the northern limit of visible distribution of the eastern lobe is to the south of all sites (Lerbekmo et al., 1975; Robinson, 2001; Preece et al., 2014). We should note that WRAn has been reported as a visible deposit in western Yukon (e.g., Lerbekmo and Campbell, 1969; Péwé, 1975), and a visible ash bed has been previously reported when coring Gravel Lake, found in the expected location of WRA (C. Schweger 2021, pers. comm). However, the younger radiocarbon dates (Table 3.2) present below the WRAn peak in Gravel Lake are highly problematic. There are two ways of interpreting these dates; (1) the main peak is WRAe and the secondary peak at 40-41 cm (UA3498) is WRAn, or; (2) there are severe problems with reworking in the upper portion of the Gravel Lake core. Currently we prefer the latter hypothesis based on the extensive tails of WRA glass shards both above and below the main peak and the repetitive mixed populations throughout the upper 45 cm of the core.

This correlation to WRAn rather than WRAe is also supported by the major and minor element geochemistry of the main and secondary peaks. They show geochemical characteristics more comparable to visible WRAn deposits (Jensen, 2007; Preece et al., 2014) and WRAn from other cryptotephra research sites (Davies, 2018; Davies et al., in review) – namely the greater range of SiO_2. Gravel Lake's main WRA peak almost fully encompasses the proximal sample variability, while further north samples from Hanging Lakes are dominated by the highest SiO_2 population that is unique to WRAn (Fig. 3.13). Geochemical comparisons to WRAn from DHP, which is ~150 km north of Gravel Lake on the northern side of the Ogilvie Mountains, are intermediate. In DHP-1, the WRAn main peak's SiO_2 values do not have quite as great of a range (74.5-76.5 wt%) than at Gravel Lake and not as dominated by the highest SiO_2 shards as in Hanging Lake (75-79 wt%). WRAn material from Cascade Lake (Davies et al., in review), another high-latitude lake north of the Brooks Range, Alaska, contains the same higher-SiO_2 range population of WRAn as Hanging Lake. This higher SiO_2 population has only been previously reported in upper proximal WRAn deposits (e.g., sample 11c) and in one Sixtymile location (Location 16, WRA-Nb) which was labeled as a sub-unit of WRAn (Preece et al., 2014). This study adds to a growing body of evidence that there are differences in WRAn glass geochemistry that are reflective of geographical location; the SiO_2 range of WRAn decreases towards the north, with the highest SiO_2 population dominant in the furthest northern sites of Hanging and Cascade Lakes. This may be the result of winnowing in the eruption plume that could be aggravated by major orographic barriers like the Ogilvie and Richardson Mountains, and Brooks Range.

Despite the reports of visible ash at both Gravel Lake and DHP sites, with DHP visible ash collected and confirmed as WRAn, the main Gravel Lake WRAn peak has a lower concentration (26563 shards/g) than the DHP main WRAn peak (2149678 shards/5cm^3; Davies, 2018). Both Gravel Lake and DHP fall in what is currently mapped the WRAn tephra footprint, so we would potentially expect smaller concentrations at DHP as it is further north. Reasons for the lower concentration in Gravel Lake may be the result of smearing of the peak up and down the core (as indicated by problematic radiocarbon dates and mixed populations), and variable preservation across the lake sediments. As noted earlier, a core retrieved from the lake in 1977 contained a visible unit, indicting some parts of the lake may have better preserved portions of the upper sediments.

WRAe

The Gravel Lake surface core contains one depth at 18-19 cm (UA3620) with glass geochemistry more similar to WRAe (AD 853±1; 1097 cal yr BP; Toohey and Sigl, 2017). UA3620 contains a higher K_2O trend than all other Gravel Lake WRA samples and a more limited SiO_2 range (73-76 wt%) more typical for WRAe (Fig. 3.8). This limited SiO_2 range is also documented in the shallowest Hanging Lake WRA sample UA3360 (depth 26-27 cm). However, the considerable overlap between WRAn and WRAe is problematic, and any differences may be due to the relatively fewer number of shards analysed, in particular for the Hanging Lake sample. Re-analyses of these samples to increase data points and with reference material for direct comparison will be necessary but may not be conclusive. Attempts to obtain

Fe-Ti oxide geochemistry have been stymied by our inability to extract any magnetite or ilmenite associated with the tephra (i.e., glass rimmed).

Refinement of Chronology

The main WRAn peak of Hanging Lake helps refine the lake's current chronology, which is based on eight ^{14}C dates of twig fragments, moss fragments, and chironomid chitin (Kurek et al., 2009 Table 1). The WRAn peak at 34-35 cm, with estimated mean age of WRAn (1625 cal BP; Reuther et al., 2020), is located between twig fragments at 14-15 cm (1172-1067 cal yr BP) and 91-92 cm (6848-6738 cal yr BP). Our Bayesian age model gives an estimated mean age of ~2590 cal BP and a 2σ range of 4475-1090 cal BP for the depth of the WRAn peak. The WRAn isochron shows that the Hanging Lake age model likely trends old. Unfortunately, the inability to successfully extract glass from lower intervals limits the application of tephrochronology at this lake.

The Gravel Lake chronology has previously relied on wiggle-matching the LOI to the GISP $\delta^{18}O$ record (Beierle, 2001). New ^{14}C dates and potential tephra correlations do provide some new age control to the core, some of which varies from the earlier model. At the base of the core, unidentified organic fragments produced a two sigma age of 15920-13100 cal BP and aligns with the expected age of this depth based on fluctuating LOI signals representing Older and Younger Dryas events. However, the very small sample size gives large uncertainty in the estimated age, and the unidentified organic material could contain old carbon. Dated aquatic seeds do show older calibrated dates than the nearby terrestrial needle fragments although it is hard to determine if there is a consistent offset due to potential issues of reworking and unknown sedimentation rates. Despite this the dates below ~50 cm they still support independent tephra observations. At 156-157 cm, an aquatic seed (Potamogeton sp.) has an estimated age of 7267-7165 cal BP. This agrees with the potential correlation of UA3618 to KS_2 despite the potential bias of the radiocarbon age given the large uncertainty in age of KS_2 (~7300-6880 cal yr BP; Plunkett et al., 2015; Ponomareva et al., 2017; Jensen et al., in review). Radiocarbon dates at 98-99 cm (5270-4858 cal BP; Picea fragment) and 90-91 cm (5730-5587 cal BP; aquatic seed) are found at the sharp increase in shard concentrations seen ~90 cm in Gravel Lake. A similar trend is observed in the DHP peat core, with the rise in glass shard concentration beginning around

4500 cal BP (Davies, 2018), providing some confidence in at least the terrestrial ^{14}C date at 98-99 cm. In the shallower regions of Gravel Lake where severe reworking has taken place, ^{14}C dates do not align with our tephra observations. The largest peak of WRAn at 24-25 cm (UA3527) is found above two terrestrial Picea fragments found at 37-38 cm (1510-1351 cal BP) and 32-33 cm (1291-1124 cal BP), both dated younger than WRAn (1625 cal BP; Reuther et al., 2020). This interferes with an isochron placement at this highest concentration peak. However, the geochemistry of this peak is much more consistent with WRAn than WRAe, although the latter would agree better with the radiocarbon dates. These upper regions are full of mixed geochemical populations, smearing of WRA across the upper 45 cm of the core, and high concentrations of glass. In this case, we cannot be fully confident in the placement of a WRAn isochron at 24-25 cm, as it is clear that large amounts of sediment mixing is occurring in this region, and the presence of younger ^{14}C dates below the WRA peak cannot be ignored. The alternative placement of WRAn on the secondary peak at 40-41cm would address the conflicting ^{14}C ages, but it would be difficult to produce a higher concentration peak secondary peak ~16 cm above the main peak and nothing like this has been previously observed in the literature. Therefore, we suggest 24-25 cm as the isochron, but given the mixed populations, peak smearing, and conflicting results, the upper ~45 cm, and potentially upper 90 cm of this Gravel Lake core is not reliable for further paleoenvironmental studies. However, below these depths the radiocarbon dates are more coherent with tephra results, peaks are more defined, and unique tephra arise – collectively suggesting a more reliable record.

3.5.2. Gravel Lake: Reworking or multiple eruptions?

Gravel Lake has three recurring geochemical populations throughout the Holocene, originating from Mt. Churchill, Aniakchak, and most likely Augustine, but the specific number of eruptions is challenging to determine. Notably, the top ~100 cm of the core contains widened peaks and higher concentrations, with all sampled depths between 50-100 cm containing multiple geochemical populations of the three. Much of this complexity is likely related to redeposition and reworking. Secondary deposition occurs after a larger event deposits tephra into the surrounding watershed and that deposit is washed into the lake for some time after the initial event. This would explain an increase in general shard concentrations following the deposition of the main peak of WRAn at 24-25 cm. However, Gravel Lake also suffers from down core movement of tephra, caused by bioturbation or density-induced settling. At an average lake depth of ~1.5 m, mixing may have occurred from trampling by moose or other wildlife in the area (Håkanson and Jansson, 1983; Boygle, 1999; Mackay et al., 2012). Bioturbation will also cause mixing of sediments as roots of aquatic plants can push younger sediment down into lower depths. Presence of Potamogeton and Nuphar polysepala in Holocene depths of Gravel Lake suggest the potential for such processes, and the presence of younger macrofossils >10cm below the peak of WRAn could be potentially explained by bioturbation. Low-density gytjja has also been shown to allow downward movements of tephra (Beierle and Bond, 2002) and is another potential contributing factor to the Gravel Lake shard profile, which has an average density of 0.94 g/cc in the top 100 cm of the core (Fig. 3.9). This type of mixing is more common with visible tephra deposits, but the high concentrations of WRAn in Gravel Lake could be affected. Ultimately, smearing of shard peaks, high concentrations of WRAn and problematic ^{14}C dates make the upper 90 cm of the Gravel Lake unusable for environmental studies as it is apparent there is substantial vertical movement of both minerogenic and biologic material.

Despite these challenges, we cannot dismiss that some of these repetitive geochemical populations represent multiple eruptions from the same source. At the DHP site in central Yukon, Davies (2018) observed 35 analyses with WRA-like tephra during the Holocene. Five periods of activity were determined, with >10 WRA-like shards found per sample, although many of these depths are likely due to reworking. However, high confidence was placed on seven depths which were identified as "primary eruptions" from Mt. Churchill, with calibrated ages of 155±65, 1175±130 (WRAe), 1505±200 (WRAn), 2540±235, 4875±480, 5925±430, and the oldest eruption sometime between 9135-8180 cal BP (Davies 2018). Although the chronology at Gravel Lake is much poorer, a similar pattern is seen in the lake with the first trace of Churchill-like tephra deposited at 113-114 cm. We expect this depth to be sometime after 7000 yr BP due to the presence of KS_2 and the ^{14}C date of 7267-7165 cal BP at 156-157 cm.

Aniakchak is one of the most active volcanoes in the Alaskan Peninsula with at least forty explosive eruptions recorded in the Holocene and at least two caldera-forming eruptions (CFE I, between ~ 9500-7000 cal BP; CFE II, 3510-3290 cal BP) (Miller and Smith, 1987; Riehle et al., 1999; Neal et al., 2001; Bacon et al., 2014). Most of these eruptions have only been identified in proximal deposits and are poorly dated (e.g., Bacon et al., 2014), making it difficult to correlate distal Aniakchak-like tephra to proximal deposits (e.g., Kaufman et al., 2012). This is further complicated by distal tephras with identical major and minor element geochemistry to the higher SiO_2 population of Aniakchak's CFE II. Populations with identical geochemistry to CFE II were found in the Ahklun Mountains of SW Alaska with ages of ~400, 3100, and 5800 BP (Kaufman et al., 2012) (Fig. 3.14). Only the older event was distinguishable from CFE II by trace element geochemistry and it is still unclear if the 3.1 ka and 400 cal yr BP events are reworked CFE II or primary; although there is significant proximal evidence of a large eruption around 400 cal yr BP (e.g., Bacon et al. 2014). In one of two cores from Ruppert Lake, eastern Alaska, samples RS151 (4070-3760 cal yr BP) and RS126 (3650-3180 cal yr BP) are also identical in major and minor element geochemistry to the higher-Si population of CFE II, but are separated by 25 cm of sediment (Monteath et al., 2017). The lower layer is argued to belong to an earlier pre-caldera eruption rather than a reworked layer because of the well-preserved laminations showing no evidence of bioturbation or reworking between the two peaks. Depending on the veracity of their age model an alternative interpretation may be that they represent CFE II and the 3.1 ka event. Additionally, a cryptotephra (ECR162) from a peat core collected from Eaglecrest Bog, southeast Alaska was correlated to Aniakchak, with an age of 5300-5030 cal yr BP (Payne et al., 2008).

Gravel Lake contains three higher concentrations of an Aniakchak CFE II like tephra at 49-50 cm (UA3488), 67-68 (UA3523) and 75-78 cm (UA3539 and UA3534), in addition to six other depths with 1-5 shards of this population, all of which are found mixed with WRA or Augustine-like tephra populations. Lower concentrations are likely to be reworked shards from primary deposits, however all three of the higher concentration samples have the potential to be primary deposits. Like the deposits described above, these samples are also geochemically indistinguishable to each other and CFE II (Fig. 3.14). In UA3523 (67-68 cm) over half of the analyzed shards belong to this CFE II population, the only sample where it is the predominant population. This would make it the most likely isochron for the Aniakchak CFE II eruption, however the presence of a geochemical population identical to Ruppert tephra at 72-74 cm (UA3541 and UA 3540) complicates this interpretation. Ruppert tephra has an age of 2800-2130 cal yr BP (Jensen et al., in review) and is found above the CFE II tephra in Ruppert Lake

(Monteath et al., 2017), Nordan's Pond Bog (Pyne-O'Donnell et al, 2012), and Cascade Lake (Davies et al., in review). With this complication, the first sign of CFE II in the core at 75-78 cm (UA3539 and UA3534) may be the most likely location for an isochron placement of CFE II. While this does work with the ^{14}C age of 5270-4858 cal BP at 98-99 cm, the amount of mixing occurring in the upper 90 cm gives us low confidence in our ability to place an isochron.

3.5.3. Tephra taphonomy and preservation

Cryptotephra limitations in sub-Arctic lakes

All of the lakes in this study contain different problems with tephra preservation and extraction, each hindering the use of cryptotephra as a chronological tool in this region. Hanging Lake's high silt content combined with relatively low shard concentrations (typically between 0-60 shards/g) caused difficulty in extracting glass for analyses. Only the greater concentration samples at 26-27 cm, 29-30 cm, 34-35 cm, 38-39 cm, and 43-44 cm, containing WRAn and other WRA-like populations were successfully analyzed. Below 44 cm, shards were hand-picked but too few analyses were obtained to allow for any interpretations or correlations.

The top ~90 cm of the Gravel Lake main core contains high concentrations of glass and mixed geochemical populations that are difficult to interpret. This complexity is partially the result of reworking and secondary deposition but is also related to an increase in tephra deposition into the basin. The close proximity of Gravel Lake to Mt. Churchill and the resulting deposition of WRAn as a visible (or near visible) deposit to this region is likely one of the main factors for the complicated profile. Density-induced settling and vertical reworking may explain why the upper 44 cm of Gravel Lake is dominated by WRA shards. Concentrations drop between 34-90 cm (although still relatively high, up to ~5000 shards/g), and other geochemical populations likely related to Aniakchak and Augustine emerge, However, wide, ill-defined peaks cause difficulty in identifying individual eruptions. Below 90 cm, discrete tephra populations are able to be found as defined peaks when counted separately from weathered glass. In addition, radiocarbon dates are consistent with each other, and geochemistry of glass shards becomes more coherent. Higher confidence is able to be placed in these lower depths, and the decrease in reworking effects produces a more reliable cryptotephra record for Gravel Lake.

Regional increase in glass shard concentrations

Concentrations of glass shards in Gravel Lake notably increase above 90 cm, below this increase peaks are more defined and contain unique non-repeating geochemical populations. Radiocarbon dates at 90-91 cm and 98-99 cm suggest this happens around 5000 cal yr BP. This increase in glass shard concentrations around 5000 cal yr BP, and another just prior to the deposition of WRAn are reflected in other regional cryptotephra sites. The DHP site of Davies et al. (2018) shares a similar rise in concentration around the mid-Holocene, estimated at ~4500 cal yr BP. Both cores also show another increase in concentrations starting around 2500 cal yr BP, although, like Gravel Lake, the high concentrations of the overlying WRAn make it difficult to ascertain if that is simply related to downward movement. Hanging Lake and Cascade Lake both see roughly similar patterns when the records go far enough back. Although with much lower concentrations and a problematic age-model, concentrations of glass in Hanging Lake clearly decrease ~15 cm below WRAn (~50 cm), and potentially again at ~95 cm. Although only the last ~5000 years was counted in Cascade Lake, there is a similar decrease in concentrations about 10 cm below WRAn (~ 2000 cal yr BP) (Davies et al., in review). Problems inherent in many of the sites (e.g., bad age models for Hanging Lake and Gravel Lake), the shorter length of the Cascade Lake record, and burden of WRAn on the landscape, make it hard to determine if these patterns are robust. However, the marked change at ~5000 cal yr BP seen in Gravel Lake and DHP is particularly notable.

The increase in glass shard concentrations after the mid-Holocene could be related to a number of causes, including changes in eruption frequency, atmospheric circulation, vegetation structure at the site, and/or depositional processes. Records of eruptions from the Alaska volcanoes do not suggest there is a marked increase in frequency after 5000 cal yr BP (e.g., Miller and Smith, 1987; deFontaine et al., 2007). It also seems unlikely that there would be a large enough change in vegetation or depositional processes at Gravel Lake and DHP that could explain this change – particularly with no other variation at this time in other proxies (e.g., LOI). Another plausible mechanism is a shift in atmospheric circulation patterns. An examination of cryptotephra study sites in eastern North America concluded that changes in atmospheric circulation led to an increase in the frequency of tephra populations starting around the deposition of Mazama Ash (ca. 7,600 cal yr BP), as the Laurentide ice sheet collapsed (Monteath, 2020). It is possible that a similar atmospheric shift in the mid-Holocene may have occurred in this region causing winds to shift into a pattern more likely to deliver higher quantities of ash from the southwest. However, more cryptotephra sites in the Yukon and Alaska are necessary to determine if this is a real pattern and what the causes may be.

Potential of other lake sites and input of weathered glass shards

The decrease in mixing and shard concentrations below below ~90 cm in Gravel Lake introduces a new challenge where weathered shard concentrations become equal to or greater than the non-weathered shard concentrations. Separate counting of non-weathered shards led to the identification of several small peaks that would have otherwise been missed. In Barlow Lake the weathered glass concentrations overwhelmed any primary tephra deposits – although counted separately, analyses were dominated by scattered points with low Na_2O and high K_2O, indicative of weathered glass. While the lower depths of Barlow Lake are not suitable for cryptotephra, the decrease in weathered shards going into the Holocene suggest the upper depths have potential for a suitable cryptotephra record. The proximity to Gravel Lake means it is likely to have preserved a similar tephra record, but Barlow Lake is deeper, eliminating reworking caused by wave-induced mixing or trampling. The main core of Chapman Lake also has the potential for a interpretable tephra record. Detrital glass such as the Dawson tephra is found in the surface core, but the sediment record still preserved the Redoubt 1989/90 eruption. This suggests older more prominent eruptions (e.g., WRAn, Aniakchak, Jarvis; all present in nearby DHP) may be identifiable despite the secondary tephra deposition in the basin.

Weathered glass concentrations, likely related to loess input, were also examined to determine if any patterns were recognizable. The Barlow Lake record shows a steady decrease in weathered glass from 206 cm to the shallowest counted sample at 174 cm, with a commensurate increase in organic content (Fig. 3.4). The lowest depths of Gravel Lake show an opposite relationship in concentration and LOI; assuming the correlation of the LOI record to the GISP2 $\delta^{18}O$ record is relatively sound, the drop in LOI associated with the Younger and Older Dryas also sees a decrease in weathered shard concentrations. This seems counter intuitive as a decrease in organic content should be associated with an increase in weathered shards if the glass is coming from nearby loess deposits, the suggested source of Gravel Lake sediment (Beierle 2001). However, Beierle (2001) also reports an increase in clastic sediment flux but a decrease in modal grain size in these stadial events. An increase in sediment flux may be explained by a decrease in surrounding vegetation and commensurate increase in re-mobilization of loess deposits during these drier and colder events. An increased clastic flux would also suggest a rise in weathered shard concentrations, but with a maximum grain size of 10 µm recorded during these events, we hypothesize that by sieving our samples at 20 µm, the decrease in weathered glass shard concentration is in fact more reflective of a change in grain-size. The lower modal grain size seen at the Younger and Older Dryas events are not found in upper Holocene deposits, so this relationship is not reflective of other Holocene rises in weathered glass shard concentrations. Lower depths of the 4.2 m Barlow Lake core will need to be processed in order to determine if a similar trend is occurring at that age.

3.6. Conclusions

This paper presents the first attempt at using cryptotephra to date and correlate lake sediments in the Yukon and reveals many challenges. Reworking of sediments through wave-induced mixing and/or bioturbation can disturb the preservation of tephra, as seen in the upper depths of Gravel Lake. Direct deposition of a visible or near-visible tephra into a lake can cause reworking through density-induced mixing or other factors that overwhelm the record and mask lower concentration primary tephras, as seen in Gravel, Chapman and Hanging Lakes. Visible deposits of tephra in the catchment basins, such as WRAn and older exposed Pleistocene tephras, causes redeposition of these units through time. Sites with loess like Gravel and Barlow Lakes have primary glass populations masked by detrital glass. However, the successful identification of several isochrons does show that a careful selection of study sites can avoid some of these issues. This includes avoiding lakes with loess as a major sediment source to limit weathered glass input and focusing on closed basin lakes to minimize redeposition from older visible tephra layers. It is difficult to avoid issues associated with near-visible ash deposition (WRAn), but ways to minimize this problem include collecting multiple cores (some may have less reworking than others) and counting different morphologies separately (e.g., McLean et al., 2018).

Multiple recurring geochemical populations similar to the WRA, Aniakchak CFE II, and Augustine-like tephra occur through Gravel Lake. Reworking and secondary deposition may cause some of this repetition but these three sources are known to produce geochemically indistinct tephra. A comparison to other sites in Yukon and Alaska suggests that some of these populations may represent multiple eruptive episodes (e.g., Lemke, 2000; Waitt and Begét, 2009; Kaufman et al., 2012; Bacon et al., 2014; Preece et al., 2014; Monteath et al., 2017; Davies et al., 2016; Davies, 2018; Davies et al., in review). These results will also benefit future studies on the Holocene eruption frequency and tephra distribution of Alaskan volcanoes.

Despite these complications, primary tephra deposits were identified in these records. Distinct peaks of WRAn in Gravel (UA3527) and Hanging Lakes (UA3362) refine the chronologies of the sites, where current age model at Hanging Lake greatly overestimates the age of the sediment at the WRAn peak. A tephra correlated to the Redoubt 1989-1990 eruption (UA3499) is found in Chapman Lake, among reworked WRA and Dawson tephras, showing the potential for other identifiable primary tephras in lower depths of the lake despite the secondary input. Primary tephra was found in the shallow depths of Gravel Lake, including Novarupta-Katmai 1912 (UA3493/UA3623), and WRAe (UA3620). Gravel Lake contains ten discrete tephras, including a population in UA3540/UA3541 that is identical to Ruppert tephra (Monteath et al., 2017; Jensen et al., in review), and UA2618 that likely correlates to KS_2 (Ponomareva et al., 2017). The remaining are uncorrelated, but collectively these tephras contribute to the late Pleistocene to Holocene regional tephrostratigraphy of Alaska and Yukon.

3.7. References

Abbott, M.B., Stafford, T.W., 1996. Radiocarbon Geochemistry of Modern and Ancient Arctic Lake Systems, Baffin Island, Canada. Quatern. Res. 45, 300-311.

Anderson, L., Abbott, M.B., Finney, B.P., 2001. Holocene Climate Inferred from Oxygen Isotope Ratios in Lake Sediments, Central Brooks Range, Alaska. Quatern. Res. 55, 313-321.

Bacon, C.R., Neal, C.A., Miller, T.P., McGimsey, R.G., Nye, C.J., 2014. Postglacial eruptive history, geochemistry, and recent seismicity of Aniakchak volcano, Alaska Peninsula. Professional Paper, U.S. Geological Survey.

Bazanova, L.I., Melekestsev, I.V., Ponomareva, V.V., Dirksen, O.V. and Dirksen, V.G., 2016. Late Pleistocene and Holocene volcanic catastrophes in Kamchatka and in the Kuril Islands. Part 1. Types and classes of catastrophic eruptions as the leading components of volcanic catastrophism. Journal of volcanology and seismology 10, 151-169.

Begét, J.E., Nye, C.J., 1994. Postglacial eruption history of Redoubt Volcano, Alaska. J. Volcanol. Geotherm. Res. 62, 31-54.

Beierle, B.D., 2001. Late Quaternary climatic and glacial history of the west-central Yukon Territory, Canada (Doctoral dissertation). Queen's University, Kingston, Ontario, Canada.

Beierle, B., Bond, J., 2002. Density-induced settling of tephra through organic lakesediments. J. Paleolimnol. 28, 433-440.

Bolton, M.S., Jensen, B.J., Wallace, K., Praet, N., Fortin, D., Kaufman, D., De Batist, M., 2020. Machine learning classifiers for attributing tephra to source volcanoes: an evaluation of methods for Alaska tephras. Journal of Quaternary Science 35, 81-92.

Boygle, J., 1999. Variability of tephra in lake and catchment sediments, Svínavatn, Iceland. Global and Planetary Change 21, 129-149.

Blockley, S.P.E., Pyne-O'Donnell, S.D.F., Lowe, J.J., Matthews, I.P., Stone, A., Pollard, A.M., Turney, C.S.M., Molyneux, E.G., 2005. A new and less destructive laboratory procedure for the physical separation of distal glass tephra shards from sediments. Quaternary Science Reviews 24, 1952-1960.

Blockley, S.P.E., Edwards, K.J., Schofield, J.E., Pyne-O'Donnell, S.D.F., Jensen, B.J.L., Matthews, I.P., Cook, G.T., Wallace, K.L., Froese, D., 2015. First evidence of cryptotephra in palaeoenvironmental records associated with Norse occupation sites in Greenland. Quaternary Geochronology 27, 145–157.

Braitseva, O.A., Ponomareva, V.V., Sulerzhitsky, L.D., Melekestsev, I.V., Bailey, J., 1997. Holocene key-marker tephra layers in Kamchatka, Russia. Quatern. Res. 47, 125-139.

Bronk Ramsey, C., 2009. Bayesian Analysis of Radiocarbon Dates. Radiocarbon 51, 337-360.

Cook, E., Portnyagin, M., Ponomareva, V., Bazanova, L., Svensson, A., Garbe-Schönberg, D., 2018. First identification of cryptotephra from the Kamchatka Peninsula in a Greenland ice core: Implications of a widespread marker deposit that links Greenland to the Pacific northwest. Quaternary Science Reviews 181, 200-206.

Coulter, S.E., Pilcher, J.R., Plunkett, G., Baillie, M., Hall, V.A., Steffensen, J.P., Vinther, B.M., Clausen, H.B., Johnsen, S.J., 2012. Holocene tephras highlight complexity of volcanic signals in Greenland ice cores. J. Geophys. Res. 117.

Cwynar, L.C., 1982. A Late-Quaternary Vegetation History from Hanging Lake, Northern Yukon. Ecol. Monogr. 52, 1-24.

Davies, L.J., Jensen, B.J., Froese, D.G., Wallace, K.L., 2016. Late Pleistocene and Holocene tephrostratigraphy of interior Alaska and Yukon: Key beds and chronologies over the past 30,000 years. Quaternary Science Reviews 146, 28-53.

Davies, L.J., 2018. The development of a Holocene cryptotephra framework in northwestern North America (Doctoral dissertation). University of Alberta, Edmonton, AB. https://doi.org/10.7939/R3HX1660C

Davies, L.J., Jensen, B.J.L., Harvey, J.R., Froese, D.G., (Jul. 2019) Evidence for multiple large Holocene eruptions of Mt. Churchill, Alaska. Oral presentation, XX INQUA Congress, Dublin, Ireland.

Davies, L. J., Jensen, B. J. L., Kaufman, D. S. Late Holocene cryptotephra from Cascade Lake, Alaska: supporting data for a 21,000-year multi-chronometer Bayesian age model, Geochronology Discussions [preprint], https://doi.org/10.5194/gchron-2021-18, in review, 2021.

Davies, S.M., 2015. Cryptotephras: the revolution in correlation and precision dating. J. Quaternary Sci. 30, 114-130.

de Fontaine, C.S., Kaufman, D.S., Scott Anderson, R., Werner, A., Waythomas, C.F., Brown, T.A., 2007. Late Quaternary distal tephra-fall deposits in lacustrine sediments, Kenai Peninsula, Alaska. Quatern. Res. 68, 64-78.

Demuro, M., Roberts, R.G., Froese, D.G., Arnold, L.J., Brock, F., Ramsey, C.B., 2008. Optically stimulated luminescence dating of single and multiple grains of quartz from perennially frozen loess in western Yukon Territory, Canada: comparison with radiocarbon chronologies for the late Pleistocene Dawson tephra. Quaternary Geochronology 3, 346-364.

Donovan, J.J., Kremser, D., Fournelle, J.H., Goemann, K., 2015. Probe for EPMA: Acquisition, automation and analysis, version 11: Eugene, Oregon, Probe Software. Inc., http://www.probesoftware.com .

Dugmore, A.J., 1989. Icelandic volcanic ash in Scotland. Scottish Geographical Magazine 105, 168–172.

Dugmore, A.J., Newton, A.J., 1992. Thin tephra layers in peat revealed by X-radiography. Journal of Archaeological Science 19, 163-170.

Fierstein, J., Hildreth, W., 2008. Kaguyak dome field and its Holocene caldera, Alaska Peninsula. J. Volcanol. Geotherm. Res. 177, 340-366.

Foo, Z.H., Jensen, B.J.L., Bolton, M.S.M., 2020. Glass geochemical compositions from widespread tephras erupted over the last 200 years from Mount St. Helens. J. Quaternary Sci. 35, 102-113.

Graham, R.W., Belmecheri, S., Choy, K., Culleton, B.J., Davies, L.J., Froese, D., Heintzman, P.D., Hritz, C., Kapp, J.D., Newsom, L.A., Rawcliffe, R., Saulnier-Talbot, É, Shapiro, B., Wang, Y., Williams, J.W., Wooller, M.J., 2016. Timing and causes of mid-Holocene mammoth extinction on St. Paul Island, Alaska. Proc. Natl. Acad. Sci. USA 113, 9310.

Grootes, P.M., M. Stuiver. 1997. Oxygen 18/16 variability in Greenland snow and ice with 10^3 to 10^5-year time resolution. Journal of Geophysical Research 102, 26455-26470.

Håkanson, L., Jansson, M., 1983. Principles of Lake Sedimentology. Springer-verlag Berlin.

Hildreth, W., 1983. The compositionally zoned eruption of 1912 in the valley of ten thousand smokes, Katmai National Park, Alaska. J. Volcanol. Geotherm. Res. 18, 1-56.

Hildreth, W., Fierstein, J., 2000. Katmai volcanic cluster and the great eruption of 1912. Geological Society of America Bulletin 112, 1594-1620.

Hunt, J.B., Hill, P.G., 1993. Tephra geochemistry: a discussion of some persistent analytical problems. The Holocene 3, 271-278.

Hunt, J.B., Hill, P.G., 1996. An inter-laboratory comparison of the electron probe microanalysis of glass geochemistry. Quaternary International 34-36, 229-241.

Jensen, B.J.L. 2007. Tephrochronology of Middle to Late Pleistocene Loess in East-central Alaska (MSc thesis). University of Alberta, Edmonton, Alberta.

Jensen, B.J.L., Froese, D.G., Preece, S.J., Westgate, J.A., Stachel, T., 2008. An extensive middle to late Pleistocene tephrochronologic record from east-central Alaska. Quaternary Science Reviews 27, 411-427.

Jensen, B.J.L., Reyes, A.V., Froese, D.G., Stone, D.B., 2013. The Palisades is a key reference site for the middle Pleistocene of eastern Beringia: new evidence from paleomagnetics and regional tephrostratigraphy. Quaternary Science Reviews 63, 91-108.

Jensen, B.J., Pyne-O'Donnell, S., Plunkett, G., Froese, D.G., Hughes, P.D., Sigl, M., McConnell, J.R., Amesbury, M.J., Blackwell, P.G., van den Bogaard, C., Buck, C.E., 2014. Transatlantic distribution of the Alaskan white river ash. Geology 42(10), 875-878.

Jensen, B.J.L., Evans, M.E., Froese, D.G., Kravchinsky, V.A., 2016. 150,000 years of loess accumulation in central Alaska. Quaternary Science Reviews 135, 1-23.

Jensen, B.J.L., Beaudoin, A.B., Clynne, M.A., Harvey, J., Vallance, J.W., 2019. A re-examination of the three most prominent Holocene tephra deposits in western Canada: Bridge River, Mount St. Helens Yn and Mazama. Quaternary International 500, 83-95.

Kaufman, D.S., Ager, T.A., Anderson, N.J., Anderson, P.M., Andrews, J.T., Bartlein, P.J., Brubaker, L.B., Coats, L.L., Cwynar, L.C., Duvall, M.L., Dyke, A.S., Edwards, M.E., Eisner, W.R., Gajewski, K., Geirsdóttir, A., Hu, F.S., Jennings, A.E., Kaplan, M.R., Kerwin, M.W., Lozhkin, A.V., MacDonald, G.M., Miller, G.H., Mock, C.J., Oswald, W.W., Otto-Bliesner, B.L., Porinchu, D.F., Rühland, K., Smol, J.P., Steig, E.J., Wolfe, B.B., 2004. Holocene thermal maximum in the western Arctic (0–180°W). Quaternary Science Reviews 23, 529-560.

Kaufman, D.S., Jensen, B.J.L., Reyes, A.V., Schiff, C.J., Froese, D.G., Pearce, N.J.G., 2012. Late Quaternary tephrostratigraphy, Ahklun Mountains, SW Alaska. J. Quaternary Sci. 27, 344-359.

Kennedy, K.E., Froese, D.G., Zazula, G.D., Lauriol, B., 2010. Last Glacial Maximum age for the northwest Laurentide maximum from the Eagle River spillway and delta complex, northern Yukon. Quaternary Science Reviews 29, 1288-1300.

Kuehn, S.C., Froese, D.G., Shane, P.A., Participants, I.I., 2011. The INTAV intercomparison of electron-beam microanalysis of glass by tephrochronology laboratories: results and recommendations. Quaternary International 246, 19-47.

Kurek, J., Cwynar, L.C., Vermaire, J.C., 2009. A late Quaternary paleotemperature record from Hanging Lake, northern Yukon Territory, eastern Beringia. Quatern. Res. 72, 246-257.

Lemke, K.J., 2000. Holocene Tephrostratigraphy, Southern Kenai Peninsula, Lower Cook Inlet, Alaska. Utah State University.

Lerbekmo, J.F., Campbell, F.A., 1969. Distribution, composition, and source of the White River Ash, Yukon Territory. Can. J. Earth Sci. 6, 109-116.

Lerbekmo, J.F., Westgate, J.A., Smith, D.G.W., Denton, G.H., 1975. New data on the character and history of the White River volcanic eruption, Alaska. Suggate, R.P., Cresswell, M.M., (Eds.), Quaternary studies. Wellington, Royal Society of New Zealand, 203–209.

Lerbekmo, J.F., 2008. The White river ash: largest Holocene Plinian tephra. Canadian Journal of Earth Sciences 45, 693-700.

Levy, L.B., Kaufman, D.S., Werner, A., 2004. Holocene glacier fluctuations, Waskey Lake, northeastern Ahklun Mountains, southwestern Alaska. The Holocene 14, 185-193.

Loewen, M., Wallace, K., Coombs, M.L., 2018. Geochemistry of Augustine Volcano's Holocene Tephra Record. AGU Fall Meeting Abstracts 2018, V33D-0278.

Lowe, D.J., 2011. Tephrochronology and its application: A review. Quaternary Geochronology 6, 107-153.

Mackay, E.B., Jones, I.D., Folkard, A.M., Barker, P., 2012. Contribution of sediment focussing to heterogeneity of organic carbon and phosphorus burial in small lakes. Freshwat. Biol. 57, 290-304.

Martin-Jones, C.M., Lane, C.S., Pearce, N., Smith, V.C., Lamb, H.F., Oppenheimer, C., Asrat, A., Schaebitz, F., 2017. Glass compositions and tempo of post-17 ka eruptions from the Afar Triangle recorded in sediments from lakes Ashenge and Hayk, Ethiopia. Quaternary Geochronology 37, 15-31.

McLean, D., Albert, P.G., Nakagawa, T., Suzuki, T., Staff, R.A., Yamada, K., Kitaba, I., Haraguchi, T., Kitagawa, J., Smith, V.C., 2018. Integrating the Holocene tephrostratigraphy for East Asia using a high-resolution cryptotephra study from Lake Suigetsu (SG14 core), central Japan. Quaternary Science Reviews 183, 36-58.

Miller, T.P., Smith, R.L., 1987. Late Quaternary caldera-forming eruptions in the eastern Aleutian arc, Alaska. Geology 15, 434-438.

Miller, T.P., McGimsey, R.G., Richter, D.H., Riehle, J.R., Nye, C.J., Yount, M.E., Dumoulin, J.A., 1998. Catalog of the Historically Active Volcanoes of Alaska. United States Department of the Interior, United States Geological Survey.

Monteath, A.J., van Hardenbroek, M., Davies, L.J., Froese, D.G., Langdon, P.G., Xu, X., Edwards, M.E., 2017. Chronology and glass chemistry of tephra and cryptotephra horizons from lake sediments in northern Alaska, USA. Quatern. Res. 88, 169-178.

Monteath, A.J., Hughes, P.D.M., Wastegård, S., 2019. Evidence for distal transport of reworked Andean tephra: Extending the cryptotephra framework from the Austral volcanic zone. Quaternary Geochronology 51, 64-71.

Monteath, A.J., 2020. Examining patterns of past ash dispersal in distal cryptotephra deposits (Doctoral dissertation). University of Southampton, England.

Morgan, G.B., London, D., 1996. Optimizing the electron microprobe analysis of hydrous alkali aluminosilicate glasses. Am. Mineral. 81, 1176-1185.

Morgan, G.B., VI, London, D., 2005. Effect of current density on the electron microprobe analysis of alkali aluminosilicate glasses. American Mineralogist 90, 1131-1138.

Mulliken, K.M., Schaefer, J.R., Cameron, C.E., 2018. Geospatial distribution of tephra fall in Alaska: a geodatabase compilation of published tephra fall occurrences from the Pleistocene to the present. Miscellaneous Publication MP 164, Alaska Division of Geological & Geophysical Surveys, Fairbanks, Alaska, United States. https://doi.org/10.14509/29847

Naeser, N.D., Westgate, J.A., Hughes, O.L., Péwé, T.L., 1982. Fission-track ages of late Cenozoic distal tephra beds in the Yukon Territory and Alaska. Canadian Journal of Earth Sciences 19, 2167-2178.

Nelson, R.E., Carter, L.D., Robinson, S.W., 1988. Anomalous radiocarbon ages from a Holocene detrital organic lens in Alaska and their implications for radiocarbon dating and paleoenvironmental reconstructions in the Arctic. Quatern. Res. 29, 66-71.

Oswald, W.W., Anderson, P.M., Brown, T.A., Brubaker, L.B., Hu, F.S., Lozhkin, A.V., Tinner, W., Kaltenrieder, P., 2005. Effects of sample mass and macrofossil type on radiocarbon dating of arctic and boreal lake sediments. The Holocene 15, 758-767.

Payne, R.J., Blackford, J.J., 2008. Extending the Late Holocene Tephrochronology of the Central Kenai Peninsula, Alaska. Arctic 61, 243-254.

Payne, R., Blackford, J., van der Plicht, J., 2008. Using cryptotephras to extend regional tephrochronologies: An example from southeast Alaska and implications for hazard assessment. Quatern. Res. 69, 42-55.

Péwé, T.L., 1975. Quaternary Geology of Alaska. US Government Printing Office.

Pilcher, J.R., Hall, V.A., 1992. Towards a tephrochronology for the Holocene of the north of Ireland. The Holocene 2, 255–259.

Plunkett, G., Coulter, S.E., Ponomareva, V.V., Blaauw, M., Klimaschewski, A., Hammarlund, D., 2015. Distal tephrochronology in volcanic regions: Challenges and insights from Kamchatkan lake sediments. Global Planet. Change 134, 26-40.

Plunkett, G., Pilcher, J.R., 2018. Defining the potential source region of volcanic ash in northwest Europe during the Mid-to Late Holocene. Earth-Sci. Rev. 179, 20-37.

Ponomareva, V., Portnyagin, M., Pendea, I.F., Zelenin, E., Bourgeois, J., Pinegina, T., Kozhurin, A., 2017. A full holocene tephrochronology for the Kamchatsky Peninsula region: Applications from Kamchatka to North America. Quaternary Science Reviews 168, 101-122.

Portnyagin, M. V., Ponomareva, V. V., Zelenin, E. A., Bazanova, L. I., Pevzner, M. M., Plechova, A. A., Rogozin, A. N., and Garbe-Schönberg, D.: TephraKam: geochemical database of glass compositions in tephra and welded tuffs from the Kamchatka volcanic arc (northwestern Pacific), Earth Syst. Sci. Data, 12, 469–486.

Preece, S.J., Westgate, J.A., Stemper, B.A., Péwé, T.L., 1999. Tephrochronology of late Cenozoic loess at Fairbanks, central Alaska. Gsa bulletin 111, 71-90.

Preece, S.J., Pearce, N.J.G., Westgate, J.A., Froese, D.G., Jensen, B.J.L., Perkins, W.T., 2011. Old Crow tephra across eastern Beringia: a single cataclysmic eruption at the close of Marine Isotope Stage 6. Quaternary Science Reviews 30, 2069-2090.

Preece, S.J., Westgate, J.A., Froese, D.G., Pearce, N.J.G., Perkins, W.T., 2011. A catalogue of late Cenozoic tephra beds in the Klondike goldfields and adjacent areas, Yukon Territory. Can. J. Earth Sci. 48, 1386-1418.

Preece, S.J., McGimsey, R.G., Westgate, J.A., Pearce, N.J.G., Hart, W.K., Perkins, W.T., 2014. Chemical complexity and source of the White River Ash, Alaska and Yukon. geosphere 10, 1020-1042.

Pyne-O'Donnell, S.D.F., Hughes, P.D.M., Froese, D.G., Jensen, B.J.L., Kuehn, S.C., Mallon, G., Amesbury, M.J., Charman, D.J., Daley, T.J., Loader, N.J., Mauquoy, D., Street-Perrott, F.A., Woodman-Ralph, J., 2012. High-precision ultra-distal Holocene tephrochronology in North America. Quaternary Science Reviews 52, 6-11.

Reimer, P.J., Austin, W.E.N., Bard, E., Bayliss, A., Blackwell, P.G., Bronk Ramsey, C., Butzin, M., Cheng, H., Edwards, R.L., Friedrich, M., Grootes, P.M., Guilderson, T.P., Hajdas, I., Heaton, T.J., Hogg, A.G., Hughen, K.A., Kromer, B., Manning, S.W., Muscheler, R., Palmer, J.G., Pearson, C., van der Plicht, J., Reimer, R.W., Richards, D.A., Scott, E.M., Southon, J.R., Turney, C.S.M., Wacker, L., Adolphi, F., Büntgen, U., Capano, M., Fahrni, S.M., Fogtmann-Schulz, A., Friedrich, R., Köhler, P., Kudsk, S., Miyake, F., Olsen, J., Reinig, F., Sakamoto, M., Sookdeo, A., Talamo, S., 2020. The IntCal20 Northern Hemisphere Radiocarbon Age Calibration Curve (0–55 cal kBP). Radiocarbon 62, 725-757.

Reuther, J., Potter, B., Coffman, S., Smith, H., Bigelow, N., 2020. Revisiting the timing of the Northern lobe of the white river ash volcanic event in Eastern Alaska and Western Yukon. Radiorarbon 62, 169-188.

Richter, D.H., Preece, S.J., Mcgimsey, R.G., Westgate, J.A., 1995. Mount Churchill, Alaska: source of the late Holocene White River Ash. Can. J. Earth Sci. 32, 741-748.

Riehle, J.R., Meyer, C.E., Ager, T.A., Kaufman, D.S., Ackerman, R.E., 1987. The Aniakchak tephra deposit, a late Holocene marker horizon in western Alaska. U.S. Geological Survey Circular 990, 19-22.

Riehle, J.R., 1994. Heterogeneity, Correlatives, and Proposed Stratigraphic Nomenclature of Hayes Tephra Set H, Alaska. Quatern. Res. 41, 285-288.

Riehle, J.R., Waitt, R.B., Meyer, C.E., and Calk, L.C., 1998, Age of formation of Kaguyak Caldera, eastern Aleutian arc, Alaska, estimated by tephrochronology: U.S. Geological Survey Professional Paper 1595, 161–168

Riehle, J.R., Meyer, C.E., Miyaoka, R.T., 1999. Data on Holocene Tephra (Volcanic Ash) Deposits in the Alaska Peninsula and Lower Cook Inlet Region of the Aleutian Volcanic Arc, Alaska. US Geological Survey, Open-File Report.

Schreiner, K.M., Bianchi, T.S., Rosenheim, B.E., 2014. Evidence for permafrost thaw and transport from an Alaskan North Slope watershed. Geophysical Research Letters 41, 3117-3126.

Schuur, E.A., Bockheim, J., Canadell, J.G., Euskirchen, E., Field, C.B., Goryachkin, S.V., Hagemann, S., Kuhry, P., Lafleur, P.M., Lee, H., 2008. Vulnerability of permafrost carbon to climate change: Implications for the global carbon cycle. Bioscience 58, 701-714.

Schweger, C., Froese, D., White, J.M., Westgate, J.A., 2011. Pre-glacial and interglacial pollen records over the last 3 Ma from northwest Canada: Why do Holocene forests differ from those of previous interglaciations? Quaternary Science Reviews 30, 2124-2133.

Scott, W.E., McGimsey, R.G., 1994. Character, mass, distribution, and origin of tephra-fall deposits of the 1989–1990 eruption of Redoubt Volcano, south-central Alaska. J. Volcanol. Geotherm. Res. 62, 251-272.

Spray, J.G., Rae, D.A., 1995. Quantitative electron-microprobe analysis of alkali silicate glasses; a review and user guide. The Canadian Mineralogist 33, 323-332.

Terasmae, J., Hughes, O.L., 1966. Late-Wisconsinan chronology and history of vegetation in the Olgivie Mountains, Yukon Territory, Canada. The Paleobotanist 15, 235-242.

Toohey, M., Sigl, M., 2017. Volcanic stratospheric sulfur injections and aerosol optical depth from 500 BCE to 1900 CE. Earth System Science Data 9, 809-831.

van der Bilt, Willem GM, Lane, C.S., Bakke, J., 2017. Ultra-distal Kamchatkan ash on Arctic Svalbard: towards hemispheric cryptotephra correlation. Quaternary Science Reviews 164, 230-235.

Waitt, R.B., Begét, J.E., 2009. Volcanic Processes and Geology of Augustine Volcano, Alaska. US Geological Survey.

Wallace, K., Coombs, M.L., Hayden, L.A., Waythomas, C.F., 2014. Significance of a near-source tephra-stratigraphic sequence to the eruptive history of Hayes Volcano, south-central Alaska. US Geological Survey Scientific Investigations Report 5133.

Westgate, J.A., Stemper, B.A., Péwé, T.L., 1990. A 3 my record of Pliocene-Pleistocene loess in interior Alaska. Geology 18, 858-861.

Zawalna-Geer, A., Lindsay, J.M., Davies, S., Augustinus, P., Davies, S., 2016. Extracting a primary Holocene crytoptephra record from Pupuke maar sediments, Auckland, New Zealand. J. Quaternary Sci. 31, 442-457.

Chapter 4. Conclusion

4.1. Summary of Outcomes

The field of cryptotephra has rapidly advanced over the last few decades. Techniques were steadily developed and refined to detect and extract lower concentrations of glass shards and geochemically analyse smaller grains. This has progressively expanded the applicability of tephrochronology to further geographic extents. However, as the methods have advanced, there have been few attempts to meaningfully collate and critically examine them, making it difficult for those unfamiliar with this research to enter the field. In Chapter 2 of this thesis, I review and assess the progression of techniques and present a detailed workflow of cryptotephra methods. Initial processing steps, including LOI, sieving, and density separation, have been described with modifications for different situations. Mounting of glass shards for counting and geochemical analyses are also summarized, including a modified method of spiking slides when counting higher-concentration samples. Conflicting opinions on the effects of acid digestion on glass shards are tested and dismissed as disparities between methods in different studies are shown to be the cause of the conflicting results. Data analysis and interpretation are also discussed, including the use of secondary standards, time-dependent intensity corrections to avoid Na-loss when using smaller beam sizes, and ongoing tests to produce 3 μm EPMA. Lastly, I provide examples of glass shard identification and several shard profiles to aid the interpretation of results by helping resolve the potential complications at each site (e.g., reworking of sediments, secondary deposition, detrital glass). The result is the first thorough overview of the methodological approach for cryptotephrochronology and a comprehensive protocol that will be a valuable resource for inexperienced researchers and those new to the field.

Chapter three presents the first cryptotephra records produced from lake sites within Yukon, revealing the limitations of cryptotephra work in these sub-Arctic lakes. Hanging Lake in northern Yukon contains very low concentrations of glass shards, and the combination of mineral-rich sediments makes it challenging to extract glass shards for analyses. Secondary deposition is another significant complication, as shown by the identification of Dawson tephra within the surface core of Chapman Lake. The presence of nearby loess deposits containing detrital glass at Gravel and Barlow Lakes can interfere with identifying primary ash deposits, requiring the separate counting of weathered glass shards. One of the most severe complications is the reworking of sediments, as seen in the upper 90 cm of Gravel Lake. The upper depths of Gravel Lake show significant mixing of glass shards from Mt. Churchill, Aniakchak, and Augustine, as well as problematic radiocarbon dates. However, while a portion of these populations may be reworked, some may be primary as proximal and distal tephra records suggest multiple Holocene eruptive episodes from these volcanoes (e.g., Lemke, 2000; Waitt and Begét, 2009; Kaufman et al., 2012; Bacon et al., 2014; Preece et al., 2014; Monteath et al., 2017; Davies et al., 2016; Davies, 2018; Davies et al., in review).

Despite these complications, shard peaks were successfully correlated to tephra in three of the four lakes. Tephra related to the White River Ash was found in Hanging, Chapman, and Gravel Lakes, and distinct peaks of WRAn at Hanging and Gravel Lakes have aided in refining their chronologies. In addition, correlations were made to Ruppert tephra (Monteath et al., 2017; Jensen et al., in review) and the KS_2 tephra from Kamchatka, Russia (Braitseva and Ponomareva, 1997). Finally, eight other unique populations were found in Gravel Lake's lower depths, which have no known correlations in the region. These populations, along with geochemical populations related to Redoubt, Novarupta-Katmai, Aniakchak, Augustine, and WRA, are reported and contribute to the tephrostratigraphic framework of northwestern North America.

4.2. Future Research

This work illustrates the potential for future cryptotephra research within the Yukon. Regardless of the complications found here, successful identification of several isochrons and new tephra show that given the right circumstances these lake sediments can be dated and correlated using cryptotephra, including the sites studied here. Weathered glass concentrations in Barlow Lake start to decrease near the top of the sampled section as organic content increased to 56%, which should improve the ability to identify and extract primary deposits. The upper depths of the core have the potential to contain a similar tephra record to nearby Gravel Lake but with minor reworking, since the lake is 3m deeper. The lower depths of Chapman Lake also have potential and the main core has already been subsampled and partially processed for shard counts. At Hanging Lake, low availability of material made it difficult to extract enough glass shards and entire samples were consumed. A new core of Hanging Lake could provide enough sediment to identify the smaller shard peaks. With this new knowledge of cryptotephra deposition and preservation in Yukon lakes, we can make a more educated decision in what sites would be most suited to this work and move towards the development of a refined tephrostratigraphy for the late Pleistocene and Holocene in this region. In addition, these distal sites present one of the better opportunities to determine the complex eruption histories of the more active volcanoes in Alaska, such as Augustine and Aniakchak, and those that were not believed to be as active, such as Mount Churchill.

4.3. References

Bacon, C.R., Neal, C.A., Miller, T.P., McGimsey, R.G., Nye, C.J., 2014. Postglacial eruptive history, geochemistry, and recent seismicity of Aniakchak volcano, Alaska Peninsula. Professional paper, U.S. Geological Survey.

Braitseva, O.A., Ponomareva, V.V., Sulerzhitsky, L.D., Melekestsev, I.V., Bailey, J., 1997. Holocene key-marker tephra layers in Kamchatka, Russia. Quatern. Res. 47, 125-139.

Davies, L.J., Jensen, B.J., Froese, D.G., Wallace, K.L., 2016. Late Pleistocene and Holocene tephrostratigraphy of interior Alaska and Yukon: Key beds and chronologies over the past 30,000 years. Quaternary Science Reviews 146, 28-53.

Davies, L.J., 2018. The development of a Holocene cryptotephra framework in northwestern North America (Doctoral dissertation). University of Alberta, Edmonton, AB. https://doi.org/10.7939/R3HX1660C

Davies, L. J., Jensen, B. J. L., Kaufman, D. S. Late Holocene cryptotephra from Cascade Lake, Alaska: supporting data for a 21,000-year multi-chronometer Bayesian age model, Geochronology Discussions [preprint], https://doi.org/10.5194/gchron-2021-18, in review, 2021.

Jensen, B.J.L., Davies, L., Nolan, C., Pyne-O'Donnell, S., Monteath, A.J., Ponomareva, V., Portnyagin, M., Booth, R., Hughes, P., Bursik, M., Cook, E., Plunkett, G., Luo, Y., Vallance, J.W., Cwynar, L.C., Pearson, D.G. A latest Pleistocene and Holocene composite tephrostratigraphic framework for northeastern North America. Submitted to Quaternary Science Reviews, 2021.

Kaufman, D.S., Jensen, B.J.L., Reyes, A.V., Schiff, C.J., Froese, D.G., Pearce, N.J.G., 2012. Late Quaternary tephrostratigraphy, Ahklun Mountains, SW Alaska. J. Quaternary Sci. 27, 344-359.

Lemke, K.J., 2000. Holocene Tephrostratigraphy, Southern Kenai Peninsula, Lower Cook Inlet, Alaska (MSc thesis). Utah State University.

Monteath, A.J., van Hardenbroek, M., Davies, L.J., Froese, D.G., Langdon, P.G., Xu, X., Edwards, M.E., 2017. Chronology and glass chemistry of tephra and cryptotephra horizons from lake sediments in northern Alaska, USA. Quatern. Res. 88, 169-178.

Preece, S.J., McGimsey, R.G., Westgate, J.A., Pearce, N.J.G., Hart, W.K., Perkins, W.T., 2014. Chemical complexity and source of the White River Ash, Alaska and Yukon. geosphere 10, 1020-1042.

Waitt, R.B., Begét, J.E., 2009. Volcanic Processes and Geology of Augustine Volcano, Alaska. Professional paper, U.S. Geological Survey.

Bibliography

Abbott, M.B., Stafford, T.W., 1996. Radiocarbon Geochemistry of Modern and Ancient Arctic Lake Systems, Baffin Island, Canada. Quatern. Res. 45, 300-311.

Abbott, P.M., Jensen, B.J., Lowe, D.J., Suzuki, T., Veres, D., 2020. Crossing new frontiers: extending tephrochronology as a global geoscientific research tool. Journal of Quaternary Science 35, 1-8.

Anderson, L., Abbott, M.B., Finney, B.P., 2001. Holocene Climate Inferred from Oxygen Isotope Ratios in Lake Sediments, Central Brooks Range, Alaska. Quatern. Res. 55, 313-321.

Bacon, C.R., Neal, C.A., Miller, T.P., McGimsey, R.G., Nye, C.J., 2014. Postglacial eruptive history, geochemistry, and recent seismicity of Aniakchak volcano, Alaska Peninsula. Professional Paper, U.S. Geological Survey.

Balascio, N.L., Francus, P., Bradley, R.S., Schupack, B.B., Miller, G.H., Kvisvik, B.C., Bakke, J., Thordarson, T., 2015. Investigating the use of scanning x-ray fluorescence to locate cryptotephra in minerogenic lacustrine sediment: experimental results, in Anonymous Micro-XRF Studies of Sediment Cores. Springer, 305-324.

Bazanova, L.I., Melekestsev, I.V., Ponomareva, V.V., Dirksen, O.V. and Dirksen, V.G., 2016. Late Pleistocene and Holocene volcanic catastrophes in Kamchatka and in the Kuril Islands. Part 1. Types and classes of catastrophic eruptions as the leading components of volcanic catastrophism. Journal of volcanology and seismology 10, 151-169.

Beaudoin, A.B., Wright, M., Ronaghan, B., 1996. Late quaternary landscape history and archaeology in the 'Ice-Free Corridor': Some recent results from Alberta. Quaternary International 32, 113-126.

Begét, J.E., Reger, R.D., Pinney, D., Gillispie, T., Campbell, K., 1991. Correlation of the Holocene Jarvis Creek, Tangle Lakes, Cantwell, and Hayes Tephras in South-Central and Central Alaska. Quatern. Res. 35, 174-189.

Begét, J.E., Stihler, S.D., Stone, D.B., 1994. A 500-year-long record of tephra falls from Redoubt Volcano and other volcanoes in upper Cook Inlet, Alaska. J. Volcanol. Geotherm. Res. 62, 55-67.

Begét, J.E., Nye, C.J., 1994. Postglacial eruption history of Redoubt Volcano, Alaska. J. Volcanol. Geotherm. Res. 62, 31-54.

Beierle, B., Smith, D.G., 1998. Severe drought in the early Holocene (10,000–6800 BP) interpreted from lake sediment cores, southwestern Alberta, Canada. Palaeogeogr. , Palaeoclimatol. , Palaeoecol. 140, 75-83.

Beierle, B.D., 2001. Late Quaternary climatic and glacial history of the west-central Yukon Territory, Canada (Doctoral dissertation). Queen's University, Kingston, Ontario, Canada.

Beierle, B., Bond, J., 2002. Density-induced settling of tephra through organic lakesediments. J. Paleolimnol. 28, 433-440.

Bergman, J., Wastegård, S., Hammarlund, D., Wohlfarth, B., Roberts, S.J., 2004. Holocene tephra horizons at Klocka Bog, west-central Sweden: aspects of reproducibility in subarctic peat deposits. J. Quaternary Sci. 19, 241-249.

Boygle, J., 1999. Variability of tephra in lake and catchment sediments, Svínavatn, Iceland. Global and Planetary Change 21, 129-149.

Blockley, S.P.E., Pyne-O'Donnell, S.D.F., Lowe, J.J., Matthews, I.P., Stone, A., Pollard, A.M., Turney, C.S.M., Molyneux, E.G., 2005. A new and less destructive laboratory procedure for the physical separation of distal glass tephra shards from sediments. Quaternary Science Reviews 24, 1952-1960.

Blockley, S.P.E., Edwards, K.J., Schofield, J.E., Pyne-O'Donnell, S.D.F., Jensen, B.J.L., Matthews, I.P., Cook, G.T., Wallace, K.L., Froese, D., 2015. First evidence of cryptotephra in palaeoenvironmental records associated with Norse occupation sites in Greenland. Quaternary Geochronology 27, 145–157.

Bolton, M.S., Jensen, B.J., Wallace, K., Praet, N., Fortin, D., Kaufman, D., De Batist, M., 2020. Machine learning classifiers for attributing tephra to source volcanoes: an evaluation of methods for Alaska tephras. Journal of Quaternary Science 35, 81-92.

Boygle, J., 1999. Variability of tephra in lake and catchment sediments, Svínavatn, Iceland. Global and Planetary Change 21, 129-149.

Bourne, A.J., 2012. The late Quaternary tephrochronology of the Adriatic region: implications for the synchronisation of marine records. Doctoral dissertation, University of London

Braitseva, O.A., Ponomareva, V.V., Sulerzhitsky, L.D., Melekestsev, I.V., Bailey, J., 1997. Holocene key-marker tephra layers in Kamchatka, Russia. Quatern. Res. 47, 125-139.

Bronk Ramsey, C., 2009. Bayesian Analysis of Radiocarbon Dates. Radiocarbon 51, 337-360.

Brookes, D., Thomas, K.W., 1967. The distribution of pollen grains on microscope slides part I. The non-randomness of the distribution. pollen et spores 9, 921-629.

Carson, E.C., Fournelle, J.H., Miller, T.P. and Mickelson, D.M., 2002. Holocene tephrochronology of the Cold Bay area, southwest Alaska Peninsula. Quaternary Science Reviews, 21, 2213-2228.

Caseldine, C., Baker, A., Barnes, W.L., 1999. A rapid, non-destructive scanning method for detecting distal tephra layers in peats. The Holocene 9, 635-638.

Connor, C.B., Hill, B.E., Brandi, W., Franklin, N.M., Femina, P.C., 2001. Estimation of Volcanic Hazards from Tephra Fallout. Nat. Hazards Rev. 2, 33-42.

Cook, E., Portnyagin, M., Ponomareva, V., Bazanova, L., Svensson, A., Garbe-Schönberg, D., 2018. First identification of cryptotephra from the Kamchatka Peninsula in a Greenland ice core: Implications of a widespread marker deposit that links Greenland to the Pacific northwest. Quaternary Science Reviews 181, 200-206.

Cooper, C.L., Savov, I.P., Swindles, G.T., 2019. Standard chemical-based tephra extraction methods significantly alter the geochemistry of volcanic glass shards. J. Quaternary Sci 34, 697-707.

Coulter, S.E., Pilcher, J.R., Plunkett, G., Baillie, M., Hall, V.A., Steffensen, J.P., Vinther, B.M., Clausen, H.B., Johnsen, S.J., 2012. Holocene tephras highlight complexity of volcanic signals in Greenland ice cores. J. Geophys. Res. 117.

Crovisier, J., Advocat, T., Dussossoy, J., 2003. Nature and role of natural alteration gels formed on the surface of ancient volcanic glasses (Natural analogs of waste containment glasses). J. Nucl. Mater. 321, 91-109.

Cwynar, L.C., 1982. A Late-Quaternary Vegetation History from Hanging Lake, Northern Yukon. Ecol. Monogr. 52, 1-24.

D'Anjou, R.M., Balascio, N.L., Bradley, R.S., 2014. Locating cryptotephra in lake sediments using fluid imaging technology. J. Paleolimnol. 52, 257-264.

Davies, L.J., 2018. The development of a Holocene cryptotephra framework in northwestern North America (Doctoral dissertation). University of Alberta, Edmonton, AB. https://doi.org/10.7939/R3HX1660C

Davies, L.J., Jensen, B.J.L., Froese, D.G., Wallace, K.L., 2016. Late Pleistocene and Holocene tephrostratigraphy of interior Alaska and Yukon: Key beds and chronologies over the past 30,000 years. Quaternary Science Reviews 146, 28-53.

Davies, L.J., Appleby, P., Jensen, B.J.L., Magnan, G., Mullan-Boudreau, G., Noernberg, T., Shannon, B., Shotyk, W., van Bellen, S., Zaccone, C., Froese, D.G., 2018. High-resolution age modelling of peat bogs from northern Alberta, Canada, using pre- and post-bomb 14C, 210Pb and historical cryptotephra. Quaternary Geochronology 47, 138-162.

Davies, L.J., Jensen, B.J.L., Harvey, J.R., Froese, D.G., (Jul. 2019) Evidence for multiple large Holocene eruptions of Mt. Churchill, Alaska. Oral presentation, XX INQUA Congress, Dublin, Ireland.

Davies, L. J., Jensen, B. J. L., Kaufman, D. S. Late Holocene cryptotephra from Cascade Lake, Alaska: supporting data for a 21,000-year multi-chronometer Bayesian age model, Geochronology Discussions [preprint], https://doi.org/10.5194/gchron-2021-18, in review, 2021.

Davies, S.M., 2015. Cryptotephras: the revolution in correlation and precision dating. J. Quaternary Sci. 30, 114-130.

Davies, S.M., Wastegård, S., Wohlfarth, B., 2003. Extending the limits of the Borrobol Tephra to Scandinavia and detection of new early Holocene tephras. Quatern. Res. 59, 345-352.

Davies, S.M., Hoek, W.Z., Bohncke, S.J., Lowe, J.J., O'Donnell, S.P., Turney, C.S., 2005. Detection of Lateglacial distal tephra layers in the Netherlands. Boreas 34, 123-135.

Davies, S.M., Elmquist, M., Bergman, J., Wohlfarth, B., Hammarlund, D., 2007. Cryptotephra sedimentation processes within two lacustrine sequences from west central Sweden. The Holocene 17, 319-330.

Declercq, J., Diedrich, T., Perrot, M., Gislason, S.R., Oelkers, E.H., 2013. Experimental determination of rhyolitic glass dissolution rates at 40–200 C and 2< pH< 10.1. Geochim. Cosmochim. Acta 100, 251-263.

de Fontaine, C.S., Kaufman, D.S., Scott Anderson, R., Werner, A., Waythomas, C.F., Brown, T.A., 2007. Late Quaternary distal tephra-fall deposits in lacustrine sediments, Kenai Peninsula, Alaska. Quatern. Res. 68, 64-78.

Demuro, M., Roberts, R.G., Froese, D.G., Arnold, L.J., Brock, F., Ramsey, C.B., 2008. Optically stimulated luminescence dating of single and multiple grains of quartz from perennially frozen loess in western Yukon Territory, Canada: Comparison with radiocarbon chronologies for the late Pleistocene Dawson tephra. Quaternary Geochronology 3, 346-364.

Di Roberto, A., Smedile, A., Del Carlo, P., De Martini, P.M., Iorio, M., Petrelli, M., Pantosti, D., Pinzi, S., Todrani, A., 2018. Tephra and cryptotephra in a ~60,000-year-old lacustrine sequence from the Fucino Basin: new insights into the major explosive events in Italy. Bulletin of Volcanology 80, 20.

Donovan, J.J., Kremser, D., Fournelle, J.H., Goemann, K., 2015. Probe for EPMA: Acquisition, automation and analysis, version 11: Eugene, Oregon, Probe Software. Inc., http://www.probesoftware.com .

Dugmore, A.J., 1989. Icelandic volcanic ash in Scotland. Scottish Geographical Magazine 105, 168–172.

Dugmore, A.J., Newton, A.J., 1992. Thin tephra layers in peat revealed by X-radiography. Journal of Archaeological Science 19, 163-170.

Dugmore, A.J., Newton, A.J., Sugden, D.E., Larsen, G., 1992. Geochemical stability of fine-grained silicic Holocene tephra in Iceland and Scotland. J. Quaternary Sci. 7, 173-183.

Dugmore, A.J., Larsen, G.r., Newton, A.J., 1995. Seven tephra isochrones in Scotland. The Holocene 5, 257-266.

Dunbar, N.W., Zielinski, G.A., Voisins, D.T., 2003. Tephra layers in the Siple Dome and Taylor Dome ice cores, Antarctica: Sources and correlations. Journal of Geophysical Research: Solid Earth 108, 2374.

Etienne, D., Jouffroy-Bapicot, I., 2014. Optimal counting limit for fungal spore abundance estimation using Sporormiella as a case study. Vegetation history and archaeobotany 23, 743-749.

Fierstein, J., Hildreth, W., 2008. Kaguyak dome field and its Holocene caldera, Alaska Peninsula. J. Volcanol. Geotherm. Res. 177, 340-366.

Finsinger, W., Tinner, W., 2005. Minimum count sums for charcoal-concentration estimates in pollen slides: Accuracy and potential errors. The Holocene 15, 293-297.

Foo, Z.H., Jensen, B.J.L., Bolton, M.S.M., 2020. Glass geochemical compositions from widespread tephras erupted over the last 200 years from Mount St. Helens. J. Quaternary Sci. 35, 102-113.

Fortin, D., Praet, N., McKay, N.P., Kaufman, D.S., Jensen, B.J.L., Haeussler, P.J., Buchanan, C., De Batist, M., 2019. New approach to assessing age uncertainties – The 2300-year varve chronology from Eklutna Lake, Alaska (USA). Quaternary Science Reviews 203, 90-101.

Froese, D., Westgate, J., Preece, S., Storer, J., 2002. Age and significance of the Late Pleistocene Dawson tephra in eastern Beringia. Quaternary Science Reviews 21, 2137-2142.

Froggatt, P.C., Lowe, D.J., 1990. A review of late Quaternary silicic and some other tephra formations from New Zealand: Their stratigraphy, nomenclature, distribution, volume, and age. N. Z. J. Geol. Geophys. 33, 89-109.

Froggatt, P.C., 1992. Standardization of the chemical analysis of tephra deposits. Report of the ICCT Working Group. Quaternary International 13-14, 93-96.

Gehrels, M.J., Lowe, D.J., Hazell, Z.J., Newnham, R.M., 2006. A continuous 5300-yr Holocene cryptotephrostratigraphic record from northern New Zealand and implications for tephrochronology and volcanic hazard assessment. The Holocene 16, 173-187.

Gehrels, M.J., Newnham, R.M., Lowe, D.J., Wynne, S., Hazell, Z.J., Caseldine, C., 2008. Towards rapid assay of cryptotephra in peat cores: Review and evaluation of various methods. Quaternary International 178, 68-84.

Graham, R.W., Belmecheri, S., Choy, K., Culleton, B.J., Davies, L.J., Froese, D., Heintzman, P.D., Hritz, C., Kapp, J.D., Newsom, L.A., Rawcliffe, R., Saulnier-Talbot, É, Shapiro, B., Wang, Y., Williams, J.W., Wooller, M.J., 2016. Timing and causes of mid-Holocene mammoth extinction on St. Paul Island, Alaska. Proc. Natl. Acad. Sci. USA 113, 9310.

Griggs, A.J., Davies, S.M., Abbott, P.M., Rasmussen, T.L., Palmer, A.P., 2014. Optimising the use of marine tephrochronology in the North Atlantic: a detailed investigation of the Faroe Marine Ash Zones II, III and IV. Quaternary Science Reviews 106, 122-139.

Grootes, P.M., M. Stuiver. 1997. Oxygen 18/16 variability in Greenland snow and ice with 10^3 to 10^5-year time resolution. Journal of Geophysical Research 102, 26455-26470.

Håkanson, L., Jansson, M., 1983. Principles of Lake Sedimentology. Springer-verlag Berlin.

Hall, V.A., McVicker, S.J., Pilcher, J.R., 1994. Tephra-linked landscape history around 2310 BC of some sites in counties Antrim and Down, 245-253.

Hall, V.A., Pilcher, J.R., 2002. Late-Quaternary Icelandic tephras in Ireland and Great Britain: detection, characterization and usefulness. The Holocene 12, 223-230.

Hall, M., Hayward, C., 2014. Preparation of micro- and crypto-tephras for quantitative microbeam analysis. Geological Society, London, Special Publications 398, 21-28.

Hayward, C., 2012. High spatial resolution electron probe microanalysis of tephras and melt inclusions without beam-induced chemical modification. The Holocene 22, 119-125.

Heiri, O., Lotter, A.F., Lemcke, G., 2001. Loss on ignition as a method for estimating organic and carbonate content in sediments: reproducibility and comparability of results. J. Paleolimnol. 25, 101-110.

Hildreth, W., 1983. The compositionally zoned eruption of 1912 in the valley of ten thousand smokes, Katmai National Park, Alaska. J. Volcanol. Geotherm. Res. 18, 1-56.

Hildreth, W., Fierstein, J., 2000. Katmai volcanic cluster and the great eruption of 1912. Geological Society of America Bulletin 112, 1594-1620.

Hunt, J.B., Hill, P.G., 1993. Tephra geochemistry: a discussion of some persistent analytical problems. The Holocene 3, 271-278.

Hunt, J.B., Hill, P.G., 1996. An inter-laboratory comparison of the electron probe microanalysis of glass geochemistry. Quaternary International 34-36, 229-241.

Iverson, N.A., Kalteyer, D., Dunbar, N.W., Kurbatov, A., Yates, M., 2017. Advancements and best practices for analysis and correlation of tephra and cryptotephra in ice. Quaternary Geochronology 40, 45-55.

Jensen, B.J.L. 2007. Tephrochronology of Middle to Late Pleistocene Loess in East-central Alaska (MSc thesis). University of Alberta, Edmonton, Alberta.

Jensen, B.J.L., Froese, D.G., Preece, S.J., Westgate, J.A., Stachel, T., 2008. An extensive middle to late Pleistocene tephrochronologic record from east-central Alaska. Quaternary Science Reviews 27, 411-427.

Jensen, B.J.L., Preece, S.J., Lamothe, M., Pearce, N.J.G., Froese, D.G., Westgate, J.A., Schaefer, J., Begét, J., 2011. The variegated (VT) tephra: A new regional marker for middle to late marine isotope stage 5 across Yukon and Alaska. Quaternary International 246, 312-323.

Jensen, B.J.L., Reyes, A.V., Froese, D.G., Stone, D.B., 2013. The Palisades is a key reference site for the middle Pleistocene of eastern Beringia: new evidence from paleomagnetics and regional tephrostratigraphy. Quaternary Science Reviews 63, 91-108.

Jensen, B.J., Pyne-O'Donnell, S., Plunkett, G., Froese, D.G., Hughes, P.D., Sigl, M., McConnell, J.R., Amesbury, M.J., Blackwell, P.G., van den Bogaard, C., Buck, C.E., 2014. Transatlantic distribution of the Alaskan white river ash. Geology 42(10), 875-878.

Jensen, B.J.L., Evans, M.E., Froese, D.G., Kravchinsky, V.A., 2016. 150,000 years of loess accumulation in central Alaska. Quaternary Science Reviews 135, 1-23.

Jensen, B.J., Beaudoin, A.B., 2016. Geochemical characterization of tephra deposits at archaeological and palaeoenvironmental sites across south-central Alberta and southwest Saskatchewan, in Anonymous Back on the Horse: Recent Developments in Archaeological and Palaeontological Research in Alberta. Archaeological Survey of Alberta Occasional Paper no. 36, 154-160.

Jensen, B.J.L., Beaudoin, A.B., Clynne, M.A., Harvey, J., Vallance, J.W., 2019. A re-examination of the three most prominent Holocene tephra deposits in western Canada: Bridge River, Mount St. Helens Yn and Mazama. Quaternary International 500, 83-95.

Jensen, B.J.L., Davies, L., Nolan, C., Pyne-O'Donnell, S., Monteath, A.J., Ponomareva, V., Portnyagin, M., Booth, R., Hughes, P., Bursik, M., Cook, E., Plunkett, G., Luo, Y., Vallance, J.W., Cwynar, L.C., Pearson, D.G. A latest Pleistocene and Holocene composite tephrostratigraphic framework for northeastern North America. Submitted to Quaternary Science Reviews, 2021.

Katoh, S., Danhara, T., Hart, W.K., WoldeGabriel, G., 1999. Use of sodium polytungstate solution in the purification of volcanic glass shards for bulk chemical analysis. Nature and Human Activities 4, 45-54.

Kaufman, D.S., Ager, T.A., Anderson, N.J., Anderson, P.M., Andrews, J.T., Bartlein, P.J., Brubaker, L.B., Coats, L.L., Cwynar, L.C., Duvall, M.L., Dyke, A.S., Edwards, M.E., Eisner, W.R., Gajewski, K., Geirsdóttir, A., Hu, F.S., Jennings, A.E., Kaplan, M.R., Kerwin, M.W., Lozhkin, A.V., MacDonald, G.M., Miller, G.H., Mock, C.J., Oswald, W.W., Otto-Bliesner, B.L., Porinchu, D.F., Rühland, K., Smol, J.P., Steig, E.J., Wolfe, B.B., 2004. Holocene thermal maximum in the western Arctic (0–180°W). Quaternary Science Reviews 23, 529-560.

Kaufman, D.S., Jensen, B.J.L., Reyes, A.V., Schiff, C.J., Froese, D.G., Pearce, N.J.G., 2012. Late Quaternary tephrostratigraphy, Ahklun Mountains, SW Alaska. J. Quaternary Sci. 27, 344-359.

Kennedy, K.E., Froese, D.G., Zazula, G.D., Lauriol, B., 2010. Last Glacial Maximum age for the northwest Laurentide maximum from the Eagle River spillway and delta complex, northern Yukon. Quaternary Science Reviews 29, 1288-1300.

Kitaba, I., Nakagawa, T., 2017. Black ceramic spheres as marker grains for microfossil analyses, with improved chemical, physical, and optical properties. Quaternary International 455, 166-169.

Kuehn, S.C., Froese, D.G., 2010. Tephra from Ice—A Simple Method to Routinely Mount, Polish, and Quantitatively Analyze Sparse Fine Particles. Microscopy and Microanalysis 16, 218-225.

Kuehn, S.C., Froese, D.G., Shane, P.A., Participants, I.I., 2011. The INTAV intercomparison of electron-beam microanalysis of glass by tephrochronology laboratories: results and recommendations. Quaternary International 246, 19-47.

Kurek, J., Cwynar, L.C., Vermaire, J.C., 2009. A late Quaternary paleotemperature record from Hanging Lake, northern Yukon Territory, eastern Beringia. Quatern. Res. 72, 246-257.

Kylander, M.E., Lind, E.M., Wastegård, S., Löwemark, L., 2012. Recommendations for using XRF core scanning as a tool in tephrochronology. The Holocene 22, 371-375.

Lakeman, T.R., Clague, J.J., Menounos, B., Osborn, G.D., Jensen, B.J.L., Froese, D.G., 2008. Holocene tephras in lake cores from northern British Columbia, Canada. Can. J. Earth Sci. 45, 935–947.

Lane, C.S., Blockley, S.P.E., Lotter, A.F., Finsinger, W., Filippi, M.L., Matthews, I.P., 2012. A regional tephrostratigraphic framework for central and southern European climate archives during the Last Glacial to Interglacial transition: comparisons north and south of the Alps. Quaternary Science Reviews 36, 50-58.

Lane, C.S., Cullen, V.L., White, D., Bramham-Law, C.W.F., Smith, V.C., 2014. Cryptotephra as a dating and correlation tool in archaeology. Journal of Archaeological Science 42, 42-50.

Lane, C.S., Lowe, D.J., Blockley, S.P.E., Suzuki, T., Smith, V.C., 2017. Advancing tephrochronology as a global dating tool: Applications in volcanology, archaeology, and palaeoclimatic research. Quaternary Geochronology 40, 1-7.

Lemke, K.J., 2000. Holocene Tephrostratigraphy, Southern Kenai Peninsula, Lower Cook Inlet, Alaska. Utah State University.

Lerbekmo, J.F., Campbell, F.A., 1969. Distribution, composition, and source of the White River Ash, Yukon Territory. Can. J. Earth Sci. 6, 109-116.

Lerbekmo, J.F., Westgate, J.A., Smith, D.G.W., Denton, G.H., 1975. New data on the character and history of the White River volcanic eruption, Alaska. Suggate, R.P., Cresswell, M.M., (Eds.), Quaternary studies. Wellington, Royal Society of New Zealand, 203–209.

Lerbekmo, J.F., 2008. The White river ash: largest Holocene Plinian tephra. Canadian Journal of Earth Sciences 45, 693-700.

Levy, L.B., Kaufman, D.S., Werner, A., 2004. Holocene glacier fluctuations, Waskey Lake, northeastern Ahklun Mountains, southwestern Alaska. The Holocene 14, 185-193.

Lineweaver, J.L., 1963. Oxygen outgassing caused by electron bombardment of glass. J. Appl. Phys. 34, 1786-1791.

Loewen, M., Wallace, K., Coombs, M.L., 2018. Geochemistry of Augustine Volcano's Holocene Tephra Record. AGU Fall Meeting Abstracts 2018, V33D-0278.

Lowe, D.J., 2011. Tephrochronology and its application: A review. Quaternary Geochronology 6, 107-153.

Lowe, J., Barton, N., Blockley, S., Ramsey, C.B., Cullen, V.L., Davies, W., Gamble, C., Grant, K., Hardiman, M., Housley, R., Lane, C.S., Lee, S., Lewis, M., MacLeod, A., Menzies, M., Müller, W., Pollard, M., Price, C., Roberts, A.P., Rohling, E.J., Satow, C., Smith, V.C., Stringer, C.B., Tomlinson, E.L., White, D., Albert, P., Arienzo, I., Barker, G., Borić, D., Carandente, A., Civetta, L., Ferrier, C., Guadelli, J., Karkanas, P., Koumouzelis, M., Müller, U.C., Orsi, G., Pross, J., Rosi, M., Shalamanov-Korobar, L., Sirakov, N., Tzedakis, P.C., 2012. Volcanic ash layers illuminate the resilience of Neanderthals and early modern humans to natural hazards. Proc. Natl. Acad. Sci. USA 109, 13532-13537.

Lowe, D.J., Alloway, B., 2015. Tephrochronology. Encyclopedia of Scientific Dating Methods, 783-799.

Lowe, D.J., Ramsey, C.B., Housley, R.A., Lane, C.S., Tomlinson, E.L., 2015. The RESET project: constructing a European tephra lattice for refined synchronisation of environmental and archaeological events during the last c. 100 ka. Quaternary Science Reviews 118, 1-17.

Lowe, D.J., Pearce, N.J.G., Jorgensen, M.A., Kuehn, S.C., Tryon, C.A., Hayward, C.L., 2017. Correlating tephras and cryptotephras using glass compositional analyses and numerical and statistical methods: Review and evaluation. Quaternary Science Reviews 175, 1-44.

Machida, H., 1999. The stratigraphy, chronology and distribution of distal marker-tephras in and around Japan. Global Planet. Change 21, 71-94.

Machida, H., Arai, F., 2003. Atlas of Tephra in and around Japan. University of Tokyo Presse, 120.

Mackay, E.B., Jones, I.D., Folkard, A.M., Barker, P., 2012. Contribution of sediment focussing to heterogeneity of organic carbon and phosphorus burial in small lakes. Freshwat. Biol. 57, 290-304.

Mackay, H., Hughes, P.D.M., Jensen, B.J.L., Langdon, P.G., Pyne-O'Donnell, S.D.F., Plunkett, G., Froese, D.G., Coulter, S., Gardner, J.E., 2016. A mid to late Holocene cryptotephra framework from eastern North America. Quaternary Science Reviews 132, 101-113.

Martin-Jones, C.M., Lane, C.S., Pearce, N., Smith, V.C., Lamb, H.F., Oppenheimer, C., Asrat, A., Schaebitz, F., 2017. Glass compositions and tempo of post-17 ka eruptions from the Afar Triangle recorded in sediments from lakes Ashenge and Hayk, Ethiopia. Quaternary Geochronology 37, 15-31.

McCanta, M.C., Hatfield, R.G., Thomson, B.J., Hook, S.J., Fisher, E., 2015. Identifying cryptotephra units using correlated rapid, nondestructive methods: VSWIR spectroscopy, X-ray fluorescence, and magnetic susceptibility. Geochem. Geophys. Geosyst. 16, 4029-4056.

McLean, D., Albert, P.G., Nakagawa, T., Suzuki, T., Staff, R.A., Yamada, K., Kitaba, I., Haraguchi, T., Kitagawa, J., Smith, V.C., 2018. Integrating the Holocene tephrostratigraphy for East Asia using a high-resolution cryptotephra study from Lake Suigetsu (SG14 core), central Japan. Quaternary Science Reviews 183, 36-58.

Miller, T.P., Smith, R.L., 1987. Late Quaternary caldera-forming eruptions in the eastern Aleutian arc, Alaska. Geology 15, 434-438.

Miller, T.P., McGimsey, R.G., Richter, D.H., Riehle, J.R., Nye, C.J., Yount, M.E., Dumoulin, J.A., 1998. Catalog of the Historically Active Volcanoes of Alaska. United States Department of the Interior, United States Geological Survey.

Monteath, A.J., van Hardenbroek, M., Davies, L.J., Froese, D.G., Langdon, P.G., Xu, X., Edwards, M.E., 2017. Chronology and glass chemistry of tephra and cryptotephra horizons from lake sediments in northern Alaska, USA. Quatern. Res. 88, 169-178.

Monteath, A.J., Teuten, A.E., Hughes, P.D.M., Wastegård, S., 2019a. Effects of the peat acid digestion protocol on geochemically and morphologically diverse tephra deposits. J. Quaternary Sci. 34, 269-274.

Monteath, A.J., Hughes, P.D.M., Wastegård, S., 2019b. Evidence for distal transport of reworked Andean tephra: Extending the cryptotephra framework from the Austral volcanic zone. Quaternary Geochronology 51, 64-71.

Monteath, A.J., 2020. Examining patterns of past ash dispersal in distal cryptotephra deposits (Doctoral dissertation). University of Southampton, England.

Morgan, G.B., London, D., 1996. Optimizing the electron microprobe analysis of hydrous alkali aluminosilicate glasses. Am. Mineral. 81, 1176-1185.

Morgan, G.B., VI, London, D., 2005. Effect of current density on the electron microprobe analysis of alkali aluminosilicate glasses. American Mineralogist 90, 1131-1138.

Mulliken, K.M., Schaefer, J.R., Cameron, C.E., 2018. Geospatial distribution of tephra fall in Alaska: a geodatabase compilation of published tephra fall occurrences from the Pleistocene to the present. Miscellaneous Publication MP 164, Alaska Division of Geological & Geophysical Surveys, Fairbanks, Alaska, United States. https://doi.org/10.14509/29847

Mullineaux, D.R., 1996. Pre-1980 tephra-fall deposits erupted from Mount St. Helens, Washington. Professional Paper, U.S. Geological Survey.

Myrbo, A., Morrison, A., and McEwan, R., 2011. Tool for Microscopic Identification (TMI). http://tmi.laccore.umn.edu. Accessed on 27 July 2020

Naeser, N.D., Westgate, J.A., Hughes, O.L., Péwé, T.L., 1982. Fission-track ages of late Cenozoic distal tephra beds in the Yukon Territory and Alaska. Canadian Journal of Earth Sciences 19, 2167-2178.

Narcisi, B., Petit, J.R., Delmonte, B., Batanova, V. and Savarino, J., 2019. Multiple sources for tephra from AD 1259 volcanic signal in Antarctic ice cores. Quaternary Science Reviews, 210, 164-174.

Nelson, R.E., Carter, L.D., Robinson, S.W., 1988. Anomalous radiocarbon ages from a Holocene detrital organic lens in Alaska and their implications for radiocarbon dating and paleoenvironmental reconstructions in the Arctic. Quatern. Res. 29, 66-71.

Nielsen, C.H., Sigurdsson, H., 1981. Quantitative methods for electron microprobe analysis of sodium in natural and synthetic glasses. Am. Mineral. 66, 547-552.

Oswald, W.W., Anderson, P.M., Brown, T.A., Brubaker, L.B., Hu, F.S., Lozhkin, A.V., Tinner, W., Kaltenrieder, P., 2005. Effects of sample mass and macrofossil type on radiocarbon dating of arctic and boreal lake sediments. The Holocene 15, 758-767.

Otiniano, G.A., Porter, T.J., Benowitz, J.A., Bindeman, I.N., Froese, D.G., Jensen, B.J.L., Davies, L.J., Phillips, M.A., 2020. A Late Miocene to Late Pleistocene Reconstruction of Precipitation Isotopes and Climate From Hydrated Volcanic Glass Shards and Biomarkers in Central Alaska and Yukon. Paleoceanography and Paleoclimatology 35, e2019PA003791.

Payne, R.J., Blackford, J.J., 2008. Extending the Late Holocene Tephrochronology of the Central Kenai Peninsula, Alaska. Arctic 61, 243-254.

Payne, R.J., Kilfeather, A.A., van der Meer, Jaap JM, Blackford, J.J., 2005. Experiments on the taphonomy of tephra in peat. Suo , 147-156

Payne, R., Blackford, J., van der Plicht, J., 2008. Using cryptotephras to extend regional tephrochronologies: An example from southeast Alaska and implications for hazard assessment. Quatern. Res. 69, 42-55.

Payne, R., Gehrels, M., 2010. The formation of tephra layers in peatlands: an experimental approach. Catena 81, 12-23.

Pearce, N.J.G., Westgate, J.A., Perkins, W.T., Eastwood, W.J., Shane, P., 1999. The application of laser ablation ICP-MS to the analysis of volcanic glass shards from tephra deposits: bulk glass and single shard analysis. Global and Planetary Change 21, 151-171.

Pearce, N.J.G., Denton, J.S., Perkins, W.T., Westgate, J.A., Alloway, B.V., 2007. Correlation and characterisation of individual glass shards from tephra deposits using trace element laser ablation ICP-MS analyses: current status and future potential. J. Quaternary Sci. 22, 721-736.

Pearce, N.J.G, Abbott, P.M., Martin-Jones, C., 2014. Microbeam methods for the analysis of glass in fine-grained tephra deposits: a SMART perspective on current and future trends. Geological Society, London, Special Publications 398, 29-46.

Persson, C., 1971. Tephrochronological Investigation of Peat Deposits in Scandinavia and on the Faroe Islands. Sveriges reproduktions AB (distr.).

Peters, C., Austin, W.E.N., Walden, J., Hibbert, F.D., 2010. Magnetic characterisation and correlation of a Younger Dryas tephra in North Atlantic marine sediments. J. Quaternary Sci. 25, 339-347.

Péwé, T.L., 1953. Geomorphology of the Fairbanks area, Alaska. ProQuest Dissertations and Theses.

Péwé, T.L., 1975. Quaternary Geology of Alaska. US Government Printing Office.

Pilcher, J.R., Hall, V.A., 1992. Towards a tephrochronology for the Holocene of the north of Ireland. The Holocene 2, 255-259.

Pilcher, J.R., Hall, V.A., McCormac, F.G., 1996. An outline tephrochronology for the Holocene of the north of Ireland. Journal of Quaternary Science: Published for the Quaternary Research Association 11, 485-494.

Pilcher, J., Hall, V., 1996. Tephrochronological studies in Northern England. Holocene 6, 100-105.

Pilcher, J., Bradley, R.S., Francus, P., Anderson, L., 2005. A Holocene tephra record from the Lofoten Islands, arctic Norway. Boreas 34, 136-156.

Plunkett, G.M., Pilcher, J.R., McCormac, F.G., Hall, V.A., 2004. New dates for first millennium BC tephra isochrones in Ireland. The Holocene 14, 780-786.

Plunkett, G., Coulter, S.E., Ponomareva, V.V., Blaauw, M., Klimaschewski, A., Hammarlund, D., 2015. Distal tephrochronology in volcanic regions: Challenges and insights from Kamchatkan lake sediments. Global Planet. Change 134, 26-40.

Plunkett, G., Pilcher, J.R., 2018. Defining the potential source region of volcanic ash in northwest Europe during the Mid-to Late Holocene. Earth-Sci. Rev. 179, 20-37.

Plunkett, G., Sigl, M., Pilcher, J.R., McConnell, J.R., Chellman, N., Steffensen, J.P. and Büntgen, U., 2020. Smoking guns and volcanic ash: the importance of sparse tephras in Greenland ice cores. Polar research, 39.

Pollard, A.M., Blockley, S., Ward, K.R., 2003. Chemical alteration of tephra in the depositional environment: theoretical stability modelling. Journal of Quaternary Science 18, 385-394.

Ponomareva, V., Portnyagin, M., Pendea, I.F., Zelenin, E., Bourgeois, J., Pinegina, T., Kozhurin, A., 2017. A full holocene tephrochronology for the Kamchatsky Peninsula region: Applications from Kamchatka to North America. Quaternary Science Reviews 168, 101-122.

Portnyagin, M. V., Ponomareva, V. V., Zelenin, E. A., Bazanova, L. I., Pevzner, M. M., Plechova, A. A., Rogozin, A. N., and Garbe-Schönberg, D.: TephraKam: geochemical database of glass compositions in tephra and welded tuffs from the Kamchatka volcanic arc (northwestern Pacific), Earth Syst. Sci. Data, 12, 469–486.

Preece, S.J., Westgate, J.A., Stemper, B.A., Péwé, T.L., 1999. Tephrochronology of late Cenozoic loess at Fairbanks, central Alaska. Gsa bulletin 111, 71-90.

Preece, S.J., Westgate, J.A., Alloway, B.V., Milner, M.W., 2000. Characterization, identity, distribution, and source of late Cenozoic tephra beds in the Klondike district of the Yukon, Canada. Can. J. Earth Sci. 37, 983-996.

Preece, S.J., Pearce, N.J.G., Westgate, J.A., Froese, D.G., Jensen, B.J.L., Perkins, W.T., 2011. Old Crow tephra across eastern Beringia: a single cataclysmic eruption at the close of Marine Isotope Stage 6. Quaternary Science Reviews 30, 2069-2090.

Preece, S.J., Westgate, J.A., Froese, D.G., Pearce, N.J.G., Perkins, W.T., 2011. A catalogue of late Cenozoic tephra beds in the Klondike goldfields and adjacent areas, Yukon Territory. Can. J. Earth Sci. 48, 1386-1418.

Preece, S.J., McGimsey, R.G., Westgate, J.A., Pearce, N.J.G., Hart, W.K., Perkins, W.T., 2014. Chemical complexity and source of the White River Ash, Alaska and Yukon. geosphere 10, 1020-1042.

Prince, T.J., Pisaric, M.F.J., Turner, K.W., 2018. Postglacial Reconstruction of Fire History Using Sedimentary Charcoal and Pollen From a Small Lake in Southwest Yukon Territory, Canada. Frontiers in Ecology and Evolution 6, 209.

Pyne-O'Donnell, S.D., 2007. Three new distal tephras in sediments spanning the Last Glacial–Interglacial Transition in Scotland. Journal of Quaternary Science: Published for the Quaternary Research Association 22, 559-570.

Pyne-O'Donnell, S., 2011. The taphonomy of Last Glacial–Interglacial Transition (LGIT) distal volcanic ash in small Scottish lakes. Boreas 40, 131-145.

Pyne-O'Donnell, S.D.F., Hughes, P.D.M., Froese, D.G., Jensen, B.J.L., Kuehn, S.C., Mallon, G., Amesbury, M.J., Charman, D.J., Daley, T.J., Loader, N.J., Mauquoy, D., Street-Perrott, F.A., Woodman-Ralph, J., 2012. High-precision ultra-distal Holocene tephrochronology in North America. Quaternary Science Reviews 52, 6-11.

Pyne-O'Donnell, S.D.F., Jensen, B.J.L., 2020. Glacier Peak and mid-Lateglacial Katla cryptotephras in Scotland: potential new intercontinental and marine-terrestrial correlations. J. Quaternary Sci. 35, 155-162.

Reimer, P.J., Austin, W.E.N., Bard, E., Bayliss, A., Blackwell, P.G., Bronk Ramsey, C., Butzin, M., Cheng, H., Edwards, R.L., Friedrich, M., Grootes, P.M., Guilderson, T.P., Hajdas, I., Heaton, T.J., Hogg, A.G., Hughen, K.A., Kromer, B., Manning, S.W., Muscheler, R., Palmer, J.G., Pearson, C., van der Plicht, J., Reimer, R.W., Richards, D.A., Scott, E.M., Southon, J.R., Turney, C.S.M., Wacker, L., Adolphi, F., Büntgen, U., Capano, M., Fahrni, S.M., Fogtmann-Schulz, A., Friedrich, R., Köhler, P., Kudsk, S., Miyake, F., Olsen, J., Reinig, F., Sakamoto, M., Sookdeo, A., Talamo, S., 2020. The IntCal20 Northern Hemisphere Radiocarbon Age Calibration Curve (0–55 cal kBP). Radiocarbon 62, 725-757.

Reuther, J., Potter, B., Coffman, S., Smith, H., Bigelow, N., 2020. Revisiting the timing of the Northern lobe of the white river ash volcanic event in Eastern Alaska and Western Yukon. Radiorarbon 62, 169-188.

Richter, D.H., Preece, S.J., Mcgimsey, R.G., Westgate, J.A., 1995. Mount Churchill, Alaska: source of the late Holocene White River Ash. Can. J. Earth Sci. 32, 741-748.

Riehle, J.R., Meyer, C.E., Ager, T.A., Kaufman, D.S., Ackerman, R.E., 1987. The Aniakchak tephra deposit, a late Holocene marker horizon in western Alaska. U.S. Geological Survey Circular 990, 19-22.

Riehle, J.R., Bowers, P.M., Ager, T.A., 1990. The Hayes tephra deposits, and upper Holocene marker horizon in south-central Alaska. Quatern. Res. 33, 276-290.

Riehle, J.R., 1994. Heterogeneity, Correlatives, and Proposed Stratigraphic Nomenclature of Hayes Tephra Set H, Alaska. Quatern. Res. 41, 285-288.

Riehle, J.R., Waitt, R.B., Meyer, C.E., and Calk, L.C., 1998, Age of formation of Kaguyak Caldera, eastern Aleutian arc, Alaska, estimated by tephrochronology: U.S. Geological Survey Professional Paper 1595, 161–168

Riehle, J.R., Meyer, C.E., Miyaoka, R.T., 1999. Data on Holocene Tephra (Volcanic Ash) Deposits in the Alaska Peninsula and Lower Cook Inlet Region of the Aleutian Volcanic Arc, Alaska. US Geological Survey, Open-File Report.

Roland, T.P., Mackay, H., Hughes, P.D.M., 2015. Tephra analysis in ombrotrophic peatlands: A geochemical comparison of acid digestion and density separation techniques. J. Quaternary Sci. 30, 3-8.

Rose, N.L., Golding, P.N.E., Battarbee, R.W., 1996. Selective concentration and enumeration of tephra shards from lake sediment cores. The Holocene 6, 243-246.

Sarna-Wojcicki, A.M., Morrison, S.D., Meyer, C.E., Hillhouse, J.W., 1987. Correlation of upper Cenozoic tephra layers between sediments of the western United States and eastern Pacific Ocean and comparison with biostratigraphic and magnetostratigraphic age data. Geological Society of America Bulletin 98, 207–223.

Sarna-Wojcicki, A.M., Meyer, C.E., Wan, E., 1997. Age and correlation of tephra layers, position of the Matuyama-Brunhes chron boundary, and effects of Bishop ash eruption on Owens Lake, as determined from drill hole OL-92, southeast California. Geological Society of America Special Papers 317, 79-90.

Schiff, C.J., Kaufman, D.S., Wallace, K.L., Ketterer, M.E., 2010. An improved proximal tephrochronology for Redoubt Volcano, Alaska. Journal of Volcanology and Geothermal Research 193, 203–214.

Schreiner, K.M., Bianchi, T.S., Rosenheim, B.E., 2014. Evidence for permafrost thaw and transport from an Alaskan North Slope watershed. Geophysical Research Letters 41, 3117-3126.

Schuur, E.A., Bockheim, J., Canadell, J.G., Euskirchen, E., Field, C.B., Goryachkin, S.V., Hagemann, S., Kuhry, P., Lafleur, P.M., Lee, H., 2008. Vulnerability of permafrost carbon to climate change: Implications for the global carbon cycle. Bioscience 58, 701-714.

Schweger, C., Froese, D., White, J.M., Westgate, J.A., 2011. Pre-glacial and interglacial pollen records over the last 3 Ma from northwest Canada: Why do Holocene forests differ from those of previous interglaciations? Quaternary Science Reviews 30, 2124-2133.

Scott, W.E., McGimsey, R.G., 1994. Character, mass, distribution, and origin of tephra-fall deposits of the 1989–1990 eruption of Redoubt Volcano, south-central Alaska. J. Volcanol. Geotherm. Res. 62, 251-272.

Smith, D.G.W., Westgate, J.A., 1968. Electron probe technique for characterising pyroclastic deposits. Earth Planet. Sci. Lett. 5, 313-319.

Spray, J.G., Rae, D.A., 1995. Quantitative electron-microprobe analysis of alkali silicate glasses; a review and user guide. The Canadian Mineralogist 33, 323-332.

Stanton, T., Snowball, I., Zillén, L., Wastegård, S., 2010. Validating a Swedish varve chronology using radiocarbon, palaeomagnetic secular variation, lead pollution history and statistical correlation. Quaternary Geochronology 5, 611-624.

Strachan, D., 2017. Glass dissolution as a function of pH and its implications for understanding mechanisms and future experiments. Geochim. Cosmochim. Acta 219, 111-123.

Stuiver, M., Borns, H.W., Denton, G.H., 1964. Age of a widespread layer of volcanic ash in the southwestern Yukon Territory. Arctic 17, 259-261.

Swindles, G.T., De Vleeschouwer, F., Plunkett, G., 2010. Dating peat profiles using tephra: stratigraphy, geochemistry and chronology. Mires and Peat 7.

Swindles, G.T., Galloway, J., Outram, Z., Turner, K., Schofield, J.E., Newton, A.J., Dugmore, A.J., Church, M.J., Watson, E.J., Batt, C., 2013. Re-deposited cryptotephra layers in Holocene peats linked to anthropogenic activity. The Holocene 23, 1493-1501.

Terasmae, J., Hughes, O.L., 1966. Late-Wisconsinan chronology and history of vegetation in the Olgivie Mountains, Yukon Territory, Canada. The Paleobotanist 15, 235-242.

Thompson, R., Bradshaw, R.H.W., Whitley, J.E., 1986. The distribution of ash in Icelandic lake sediments and the relative importance of mixing and erosion processes. J. Quaternary Sci. 1, 3-11.

Timms, R.G.O., Matthews, I.P., Palmer, A.P., Candy, I., Abel, L., 2017. A high-resolution tephrostratigraphy from Quoyloo Meadow, Orkney, Scotland: Implications for the tephrostratigraphy of NW Europe during the Last Glacial-Interglacial Transition. Quaternary Geochronology 40, 67-81.

Tomlinson, E.L., Thordarson, T., Müller, W., Thirlwall, M., Menzies, M.A., 2010. Microanalysis of tephra by LA-ICP-MS — Strategies, advantages and limitations assessed using the Thorsmörk ignimbrite (Southern Iceland). Chemical Geology 279, 73-89.

Toohey, M., Sigl, M., 2017. Volcanic stratospheric sulfur injections and aerosol optical depth from 500 BCE to 1900 CE. Earth System Science Data 9, 809-831.

Turney, C.S.M., Harkness, D.D., Lowe, J.J., 1997. The use of microtephra horizons to correlate Late-glacial lake sediment successions in Scotland. J. Quaternary Sci. 12, 525-531.

Turney, C.S.M., 1998. Extraction of rhyolitic component of Vedde microtephra from minerogenic lake sediments. J. Paleolimnol. 19, 199-206.

van der Bilt, Willem GM, Lane, C.S., Bakke, J., 2017. Ultra-distal Kamchatkan ash on Arctic Svalbard: towards hemispheric cryptotephra correlation. Quaternary Science Reviews 164, 230-235.

van der Bilt, Willem GM, Cederstrøm, J.M., Støren, E.W., Berben, S.M., Rutledal, S., 2020. Rapid tephra identification in geological archives with Computed Tomography (CT): experimental results and natural applications. Frontiers in Earth Science 8, 710.

Waitt, R.B., Begét, J.E., 2009. Volcanic Processes and Geology of Augustine Volcano, Alaska. US Geological Survey.

Wallace, K., Coombs, M.L., Hayden, L.A., Waythomas, C.F., 2014. Significance of a near-source tephra-stratigraphic sequence to the eruptive history of Hayes Volcano, south-central Alaska. US Geological Survey Scientific Investigations Report 5133.

Wastegård, S., Björck, S., Grauert, M., Hannon, G.E., 2001. The Mjáuvøtn tephra and other Holocene tephra horizons from the Faroe Islands: a link between the Icelandic source region, the Nordic Seas, and the European continent. The Holocene 11, 101-109.

Watson, E.J., Swindles, G.T., Lawson, I.T., Savov, I.P., 2015. Spatial variability of tephra and carbon accumulation in a Holocene peatland. Quaternary Science Reviews 124, 248-264.

Watson, E.J., Swindles, G.T., Lawson, I.T., Savov, I.P., 2016. Do peatlands or lakes provide the most comprehensive distal tephra records? Quaternary Science Reviews 139, 110-128.

Westgate J.A., Dreimanis A. 1967. Volcanic ash layers of recent age at Banff National Park, Alberta, Canada. Canadian Journal of Earth Sciences 4,155-61.

Westgate, J.A., Gorton, M.P., 1981. Correlation Techniques in Tephra Studies, 73-94. In: Self S., Sparks R.S.J. (eds) Tephra Studies. NATO Advanced Study Institutes Series (Series C —

Mathematical and Physical Sciences), vol 75. Springer, Dordrecht. https://doi.org/10.1007/978-94-009-8537-7_5

Westgate, J.A., Hamilton, T.D., Gorton, M.P., 1983. Old Crow tephra: a new late Pleistocene stratigraphic marker across north-central Alaska and western Yukon Territory. Quatern. Res. 19, 38-54.

Westgate, J.A., Stemper, B.A., Péwé, T.L., 1990. A 3 my record of Pliocene-Pleistocene loess in interior Alaska. Geology 18, 858-861.

Wohlfarth, B., Blaauw, M., Davies, S.M., Andersson, M., Wastegård, S., Hormes, A., Possnert, G., 2006. Constraining the age of Lateglacial and early Holocene pollen zones and tephra horizons in southern Sweden with Bayesian probability methods. Journal of Quaternary Science: Published for the Quaternary Research Association 21, 321-334.

Wolff-Boenisch, D., Gislason, S.R., Oelkers, E.H., Putnis, C.V., 2004. The dissolution rates of natural glasses as a function of their composition at pH 4 and 10.6, and temperatures from 25 to 74 C. Geochim. Cosmochim. Acta 68, 4843-4858.

Zawalna-Geer, A., Lindsay, J.M., Davies, S., Augustinus, P., Davies, S., 2016. Extracting a primary Holocene crytoptephra record from Pupuke maar sediments, Auckland, New Zealand. J. Quaternary Sci. 31, 442-457.

Appendix

Table S1: Hanging Lake, Yukon. Summary of samples

Total core length: 3.69 m

Sampled/counted 183 cm

Batches 1 to 6 were LOI'd and mounted with Balsam. Batches 7 and 8 were **NOT** LOI'd, only dried and mounted in Glycerol

Accession #	Field #	Collector/ Source	Location	Province/ State	Probed?	When?	Tephra ID	Puck	Puck hole	notes
UA 3359	HL 18-19	L.Cwynar	Hanging Lake	Yukon	Y	28-Mar-19		UV	1	no glass found in this sample. Therefore no data to report
UA 3360	HL 26-27	L.Cwynar	Hanging Lake	Yukon	Y	28-Mar-19	WRA	UV	2	8 points
UA 3361	HL 29-30	L.Cwynar	Hanging Lake	Yukon	Y	28-Mar-19	WRA	UV	3	20 points
UA 3362	HL 34-35	L.Cwynar	Hanging Lake	Yukon	Y	28-Mar-19	WRA	UV	4	18 points
UA 3363	HL 38-39	L.Cwynar	Hanging Lake	Yukon	Y	28-Mar-19	WRA	UV	5	6 points
UA 3364	HL 43-44	L.Cwynar	Hanging Lake	Yukon	Y	28-Mar-19	WRA	UV	6	20 points
UA 3380	HL 49-50	L.Cwynar	Hanging Lake	Yukon	Y	27-May-19		UX	1	no glass found in puck, except for UA 3385 (1 shard)
UA 3381	HL 64-65	L.Cwynar	Hanging Lake	Yukon	Y	27-May-19		UX	2	
UA 3382	HL 80-81	L.Cwynar	Hanging Lake	Yukon	Y	27-May-19		UX	3	
UA 3383	HL 81-82	L.Cwynar	Hanging Lake	Yukon	Y	27-May-19		UX	4	
UA 3384	HL 86-87	L.Cwynar	Hanging Lake	Yukon	Y	27-May-19		UX	5	

UA 3385	HL 91-92	L.Cwynar	Hanging Lake	Yukon	Y	27-May-19	UX	6	1 point
N/A	HL 18-19 (2nd mount)	L.Cwynar	Hanging Lake	Yukon	N				Samples prepped for microprobe analysis, but under inspection, no glass was found in any of the samples.
N/A	HL 25-27 (2nd mount)	L.Cwynar	Hanging Lake	Yukon	N				No mounting was done to the samples. Some of these were later inspected for shards by hand-picking shards in Oct 2019
N/A	HL 86-87 (2nd mount)	L.Cwynar	Hanging Lake	Yukon	N				
N/A	HL 91-92 (2nd mount)	L.Cwynar	Hanging Lake	Yukon	N				
N/A	HL 97.5-99 (detrital peak)	L.Cwynar	Hanging Lake	Yukon	N				
N/A	HL 118-119 (detrital peak)	L.Cwynar	Hanging Lake	Yukon	N				
UA 3432	HL 156-157 cm	L. Cwynar	Hanging Lake	Yukon	Y	22-Nov-19	VF	1	Recovered from glycerol slide. 2 points analyzed (same shard, but different areas)
UA 3433	HL 158-159 cm	L. Cwynar	Hanging Lake	Yukon	N		VF	2	Recovered from glycerol slide
UA 3450	HL 90-92	L.Cwynar	Hanging Lake	Yukon	Y	22-Nov-19	VJ	1	Hand-picked shards (Oct 2019). 5 points analyzed
UA 3451	HL 81-82	L.Cwynar	Hanging Lake	Yukon	Y	22-Nov-19	VJ	2	Hand-picked shards (Oct 2019)
UA 3452	HL 80-81	L.Cwynar	Hanging Lake	Yukon	Y	22-Nov-19	VJ	3	Hand-picked shards (Oct 2019). 1 point analyzed
UA 3453	HL 92-93(2.11 g/cc float)	L.Cwynar	Hanging Lake	Yukon	Y	22-Nov-19	VJ	4	Hand-picked shards (Oct 2019)
UA 3454	HL 92-93(2.47 g/cc float)	L.Cwynar	Hanging Lake	Yukon	Y	22-Nov-19	VJ	5	Hand-picked shards (Oct 2019)
UA 3455	HL 64-66	L.Cwynar	Hanging Lake	Yukon	Y	22-Nov-19	VJ	6	Hand-picked shards (Oct 2019)

Table S2: Hanging Lake Geochemistry

Date Probed/depth	Tephra ID, source	Sample number	SiO2	TiO2	Al2O3	FeO	MnO	MgO	CaO	Na2O	K2O	Cl	Total	H2Od	n
Mar 28_2019 NaTDI HL 26-27	WRAn	UA3360-5	73.71	0.20	14.50	1.54	0.03	0.41	2.01	4.14	3.19	0.35	100.00	0.92	
		UA3360-7	73.97	0.31	13.92	1.87	0.17	0.45	2.08	4.95	2.10	0.22	100.00	0.38	
		UA3360-1	74.93	0.28	13.63	1.34	0.06	0.32	1.40	4.43	3.36	0.32	100.00	4.44	
		UA3360-6	75.20	0.25	13.61	1.48	0.03	0.37	1.27	3.93	3.60	0.33	100.00	1.76	
		UA3360-2	75.50	0.15	14.29	0.82	0.05	0.13	1.62	4.29	2.95	0.24	100.00	1.66	
		UA3360-3	75.79	0.17	13.78	1.10	0.00	0.24	1.38	4.08	3.24	0.30	100.00	0.80	
		UA3360-4	75.86	0.09	13.57	1.16	0.06	0.25	1.38	4.09	3.30	0.32	100.00	0.87	
		UA3360-11	75.95	0.10	13.60	1.24	0.09	0.31	1.15	3.68	3.60	0.35	100.00	2.55	
		Average	75.11	0.19	13.86	1.32	0.06	0.31	1.54	4.20	3.17	0.30	100.00	1.67	8
		St.Dev	0.86	0.08	0.35	0.32	0.05	0.10	0.34	0.38	0.48	0.05	0.00	1.31	
		UA3360-9	77.37	0.07	13.14	0.60	0.13	0.01	0.38	1.55	6.73	0.01	100.00	5.38	
		UA3360-8	77.78	0.12	12.57	1.05	0.02	0.02	0.62	0.58	7.13	0.13	100.00	6.73	
Mar 28_2019 NaTDI HL 29-30	WRAn	UA3361-3	74.76	0.18	14.40	1.07	0.05	0.24	1.84	4.16	3.06	0.30	100.00	0.17	
		UA3361-20	75.33	0.18	13.64	1.14	0.06	0.19	1.27	4.65	3.30	0.31	100.00	0.15	
		UA3361-7	75.48	0.15	14.49	0.96	0.03	0.17	1.63	3.99	2.89	0.28	100.00	1.75	
		UA3361-17	75.62	0.14	13.71	1.15	0.06	0.23	1.35	4.17	3.32	0.32	100.00	0.09	
		UA3361-6	76.31	0.13	13.51	1.16	0.08	0.24	1.26	3.60	3.44	0.34	100.00	1.42	
		UA3361-14	76.48	0.10	13.55	0.92	0.02	0.15	1.38	4.16	3.07	0.25	100.00	1.68	
		UA3361-4	76.71	0.27	13.03	1.28	0.02	0.16	0.88	3.54	3.84	0.36	100.00	2.29	
		UA3361-5	76.99	0.23	12.66	1.36	0.09	0.22	0.88	3.55	3.76	0.34	100.00	1.27	
		UA3361-22	76.99	0.14	12.97	1.12	0.06	0.22	1.10	3.76	3.39	0.30	100.00	0.91	
		UA3361-2	77.07	0.22	12.84	1.20	0.07	0.24	1.00	3.59	3.47	0.37	100.00	3.01	
		UA3361-25	77.16	0.15	12.89	1.19	0.05	0.22	1.03	3.68	3.40	0.28	100.00	-0.59	
		UA3361-24	77.27	0.15	12.78	1.10	0.06	0.19	0.98	3.87	3.40	0.25	100.00	-0.07	
		UA3361-10	77.31	0.17	12.76	1.12	0.05	0.19	0.95	3.85	3.39	0.29	100.00	-0.05	
		UA3361-15	77.31	0.19	12.56	1.25	0.08	0.22	0.88	3.42	3.85	0.32	100.00	4.42	
		UA3361-8	77.33	0.10	13.11	0.96	0.02	0.16	1.13	3.78	3.18	0.30	100.00	3.08	
		UA3361-11	77.33	0.06	12.35	1.27	0.12	0.01	0.24	4.12	4.26	0.30	100.00	4.49	
		UA3361-12	77.40	0.01	12.39	1.29	0.12	0.00	0.24	4.07	4.29	0.25	100.00	3.97	

		UA3361-1	77.55	0.24	12.49	1.26	0.06	0.22	0.82	3.48	3.65	0.31	100.00	3.28	
		UA3361-9	77.75	0.10	12.66	1.09	0.04	0.16	1.01	3.63	3.30	0.32	100.00	3.64	
		UA3361-13	78.41	0.07	12.13	1.01	0.04	0.17	0.86	3.58	3.48	0.33	100.00	0.71	
		Average	76.83	0.15	13.05	1.15	0.06	0.18	1.04	3.83	3.49	0.31	100.00	1.78	20
		St.Dev	0.91	0.06	0.65	0.12	0.03	0.07	0.38	0.31	0.37	0.03	0.00	1.64	
		UA3361-16	73.47	0.26	14.65	1.62	0.09	0.42	1.94	3.94	3.32	0.36	100.00	2.58	
		UA3361-18	73.88	0.35	14.09	2.10	0.12	0.48	2.32	4.62	1.85	0.25	100.00	-0.12	
Mar 28_2019 NaTDI	WRAn	UA3362-12	72.64	0.34	14.96	1.81	0.06	0.48	2.17	4.21	3.06	0.35	100.00	2.53	
HL 34-35		UA3362-7	72.67	0.26	15.03	1.63	0.04	0.48	2.10	4.43	3.06	0.37	100.00	1.45	
		UA3362-19	74.62	0.19	14.04	1.45	0.04	0.39	1.62	4.20	3.21	0.31	100.00	1.95	
		UA3362-21	74.66	0.21	14.18	1.36	0.07	0.32	1.52	4.19	3.25	0.31	100.00	1.37	
		UA3362-10	75.27	0.22	13.86	1.23	0.04	0.31	1.61	3.83	3.36	0.36	100.00	5.89	
		UA3362-24	75.75	0.17	13.39	1.17	0.06	0.23	1.33	4.07	3.60	0.32	100.00	0.34	
		UA3362-18	76.10	0.17	13.41	1.21	0.05	0.23	1.35	3.66	3.58	0.29	100.00	1.26	
		UA3362-14	76.75	0.12	12.98	1.04	0.05	0.21	1.16	4.09	3.35	0.31	100.00	0.96	
		UA3362-8	77.02	0.24	12.87	1.17	0.05	0.17	0.91	3.72	3.63	0.29	100.00	4.06	
		UA3362-2	77.04	0.12	12.96	1.07	0.02	0.17	1.13	3.87	3.36	0.33	100.00	1.87	
		UA3362-25	77.66	0.16	12.58	1.06	0.03	0.18	0.93	3.78	3.34	0.36	100.00	1.67	
		UA3362-16	77.79	0.11	12.41	1.08	0.05	0.15	0.96	3.75	3.49	0.27	100.00	2.87	
		UA3362-11	77.87	0.19	12.35	1.25	0.05	0.29	0.79	3.41	3.56	0.31	100.00	1.52	
		UA3362-20	77.98	0.19	12.26	1.18	0.04	0.17	0.84	3.33	3.80	0.28	100.00	2.63	
		UA3362-3	78.04	0.17	12.24	1.16	0.02	0.17	0.72	3.67	3.54	0.36	100.00	0.62	
		UA3362-15	78.27	0.11	12.20	1.07	0.05	0.18	0.82	3.50	3.56	0.30	100.00	2.80	
		UA3362-23	78.42	0.10	12.09	1.02	0.07	0.13	0.80	3.76	3.35	0.33	100.00	2.42	
		UA3362-9	78.94	0.13	11.65	1.00	0.05	0.12	0.61	3.51	3.73	0.34	100.00	4.18	
		Average	76.53	0.18	13.08	1.22	0.05	0.24	1.19	3.83	3.43	0.32	100.00	2.24	18
		St.Dev	1.90	0.06	0.99	0.22	0.01	0.11	0.46	0.31	0.21	0.03	0.00	1.39	
		UA3362-22	68.62	0.10	18.90	0.40	0.04	0.05	3.52	6.37	1.92	0.11	100.00	1.66	
		UA3362-17	69.30	0.12	18.66	0.75	0.02	0.13	3.83	5.22	1.88	0.12	100.00	0.61	
		Average	68.96	0.11	18.78	0.57	0.03	0.09	3.67	5.80	1.90	0.11	100.00	1.14	
		St.Dev	0.48	0.01	0.17	0.25	0.02	0.06	0.22	0.81	0.03	0.01	0.00	0.74	
		UA3362-6	77.22	0.12	13.15	1.09	0.06	0.23	1.52	3.01	3.37	0.28	100.00	6.51	
Mar 28_2019 NaTDI	WRAn	UA3363-1	72.50	0.26	15.09	1.79	0.06	0.48	2.21	4.33	3.03	0.34	100.00	0.08	
HL 38-39		UA3363-5	73.48	0.15	14.58	1.61	0.08	0.40	2.02	4.30	3.07	0.38	100.00	1.48	
		UA3363-3	77.24	0.14	13.08	0.88	0.01	0.10	1.07	3.90	3.38	0.25	100.00	2.03	

		UA3363-2	77.34	0.06	13.06	0.93	0.06	0.15	1.03	3.91	3.28	0.23	100.00	2.64	
		UA3363-6	77.44	0.15	12.52	1.02	0.06	0.26	1.00	3.93	3.38	0.32	100.00	1.64	
		UA3363-4	78.30	0.14	12.21	1.04	0.09	0.14	0.76	3.34	3.76	0.30	100.00	1.50	
		Average	76.05	0.15	13.43	1.21	0.06	0.25	1.35	3.95	3.31	0.30	100.00	1.56	6
		St.Dev	2.42	0.06	1.15	0.39	0.03	0.16	0.61	0.36	0.26	0.06	0.00	0.85	
Mar 28_2019 NaTDI HL 43-44	WRAn	UA3364-18	72.55	0.21	15.00	1.65	0.07	0.46	2.11	4.54	3.14	0.38	100.00	2.14	
		UA3364-23	73.80	0.13	14.99	1.03	0.01	0.19	2.08	4.54	3.03	0.28	100.00	1.66	
		UA3364-3	74.89	0.16	14.06	1.41	0.07	0.32	1.61	3.98	3.28	0.30	100.00	1.81	
		UA3364-14	75.67	0.20	13.86	1.32	0.03	0.26	1.35	3.78	3.28	0.31	100.00	5.05	
		UA3364-10	75.68	0.21	13.42	1.21	0.03	0.23	1.32	3.81	3.87	0.29	100.00	1.29	
		UA3364-22	75.83	0.16	13.58	1.13	0.06	0.29	1.29	4.13	3.31	0.29	100.00	1.83	
		UA3364-8	75.84	0.15	13.54	1.01	0.08	0.14	1.39	4.30	3.28	0.33	100.00	2.16	
		UA3364-11	76.22	0.20	13.32	1.17	0.05	0.28	1.17	4.06	3.28	0.31	100.00	1.12	
		UA3364-25	76.37	0.06	13.76	0.93	0.04	0.15	1.38	3.83	3.25	0.30	100.00	2.89	
		UA3364-9	76.44	0.19	13.15	1.35	0.05	0.31	1.01	3.70	3.55	0.30	100.00	1.97	
		UA3364-2	76.50	0.10	13.48	0.91	0.02	0.07	1.43	4.48	2.85	0.21	100.00	0.28	
		UA3364-1	77.05	0.09	13.24	0.91	0.05	0.10	1.20	4.05	3.12	0.25	100.00	0.30	
		UA3364-20	77.12	0.12	13.01	1.07	0.01	0.18	1.18	3.68	3.40	0.28	100.00	1.71	
		UA3364-15	77.43	0.11	12.80	1.09	0.03	0.22	1.05	3.54	3.53	0.26	100.00	2.07	
		UA3364-13	77.52	0.13	12.83	0.89	0.05	0.21	1.16	3.77	3.29	0.19	100.00	2.05	
		UA3364-6	77.53	0.14	12.73	1.04	0.07	0.18	0.95	3.65	3.45	0.33	100.00	1.49	
		UA3364-7	77.86	0.15	12.21	1.05	0.07	0.20	0.81	3.67	3.72	0.34	100.00	3.14	
		UA3364-16	77.94	0.13	12.44	0.99	0.08	0.12	0.97	3.55	3.55	0.27	100.00	1.85	
		UA3364-21	77.97	0.13	12.41	1.05	0.04	0.18	0.93	3.56	3.52	0.28	100.00	1.45	
		UA3364-17	79.61	0.12	11.01	1.07	0.05	0.18	0.52	3.29	3.91	0.31	100.00	4.57	
		Average	76.49	0.14	13.24	1.11	0.05	0.21	1.24	3.90	3.38	0.29	100.00	2.04	20
		St.Dev	1.58	0.04	0.91	0.19	0.02	0.09	0.38	0.36	0.27	0.04	0.00	1.17	
		UA3364-24	72.16	0.10	16.70	0.77	0.01	0.14	2.68	5.06	2.19	0.22	100.00	0.41	
Nov 22, 2019 NaTDI HL 80-81		UA3452_001	77.77	0.08	12.71	0.75	0.04	0.14	0.95	3.83	3.66	0.09	100.00	2.06	1
May 22, 2019 NaTDI HL 91-92		UA3385_001 1	72.74	0.61	15.22	4.23	0.16	0.82	2.89	1.04	2.15	0.17	100.00	7.19	1

Nov 22, 2019 NaTDI HL 90-92	UA3450_001	72.64	0.42	14.61	1.91	0.05	0.43	1.58	5.49	2.74	0.16	100.00	1.13	
	UA3450_002	73.21	0.37	14.80	1.90	0.06	0.44	1.59	4.73	2.74	0.21	100.00	1.59	
	Average	72.92	0.39	14.71	1.90	0.05	0.44	1.59	5.11	2.74	0.19	100.00	1.36	2
	St.Dev	0.40	0.04	0.13	0.01	0.01	0.01	0.01	0.53	0.00	0.03	0.00	0.32	
	UA3450_003	76.52	0.06	13.20	0.25	0.06	0.07	0.82	4.06	4.89	0.11	100.00	5.99	
	UA3450_004	76.71	0.04	13.30	0.48	0.09	0.07	0.79	3.83	4.65	0.07	100.00	3.25	
	UA3450_005	76.74	0.03	13.37	0.44	0.06	0.05	0.80	3.66	4.78	0.07	100.00	3.90	
	Average	76.66	0.04	13.29	0.39	0.07	0.07	0.80	3.85	4.77	0.08	100.00	4.38	3
	St.Dev	0.12	0.02	0.09	0.12	0.01	0.01	0.01	0.20	0.12	0.02	0.00	1.43	
Nov 22, 2019 NaTDI HL 156-157 cm	UA3432_001	72.18	0.38	14.82	2.10	0.03	0.55	2.36	4.84	2.56	0.24	100.00	3.53	
	UA3432_002	71.57	0.36	14.88	2.14	0.03	0.55	2.31	5.41	2.60	0.20	100.00	3.82	
	Average	71.88	0.37	14.85	2.12	0.03	0.55	2.33	5.12	2.58	0.22	100.00	3.68	2
	St.Dev	0.43	0.01	0.04	0.03	0.00	0.00	0.04	0.40	0.03	0.03	0.00	0.20	

S3.1 Standard data (reference)

	SiO2	TiO2	Al2O3	FeO	MnO	MgO	CaO	Na2O	K2O	Cl	Total	H2Odiff
Old Crow	75.15	0.31	13.14	1.70	0.05	0.29	1.48	3.84	3.72	0.28	100.00	4.12
assayed	1.00	0.05	0.34	0.14	0.03	0.03	0.05	0.26	0.26	0.05		
ID 3506	74.10	0.07	13.10	1.55	0.07	0.04	0.74	4.06	5.13	0.34	99.09	
assayed	0.96	0.03	0.34	0.06	0.03	0.02	0.05	0.28	0.26	0.03		

S3.2 Standard data (collected)

Date analyzed	Sample	SiO2	TiO2	Al2O3	FeO	MnO	MgO	CaO	Na2O	K2O	Cl	Total	H2Odiff
28-Mar-19	ID3506_001	73.98	0.09	13.29	1.54	0.10	0.07	0.71	3.96	5.18	0.36	99.20	0.80
Al, Na corrected	ID3506_001	73.73	0.06	13.17	1.56	0.04	0.05	0.72	3.99	5.14	0.36	98.73	1.27
	ID3506_001	74.50	0.07	13.47	1.45	0.05	0.03	0.70	4.22	5.18	0.33	99.93	0.07
	ID3506_001	73.98	0.06	13.28	1.51	0.06	0.03	0.70	4.00	5.13	0.34	99.03	0.97
	Average	74.04	0.07	13.30	1.52	0.06	0.05	0.71	4.04	5.16	0.35	99.22	0.78
	St.Dev	0.32	0.01	0.13	0.05	0.02	0.02	0.01	0.12	0.03	0.02	0.51	0.51
	Old Crow	75.23	0.32	13.18	1.73	0.08	0.29	1.43	3.77	3.73	0.30	100.00	4.99
	Old Crow	75.10	0.25	13.24	1.75	0.07	0.30	1.39	4.16	3.53	0.28	100.00	3.92
	Old Crow	75.03	0.30	13.19	1.57	0.04	0.33	1.43	4.20	3.68	0.31	100.00	3.72
	Old Crow	75.15	0.33	13.14	1.74	0.04	0.29	1.44	3.87	3.75	0.31	100.00	3.60
	Average	75.13	0.30	13.19	1.70	0.06	0.30	1.42	4.00	3.67	0.30	100.00	4.06
	St.Dev	0.09	0.04	0.04	0.08	0.02	0.02	0.02	0.21	0.10	0.01	0.00	0.64
	ID3506_016	73.67	0.08	13.46	1.58	0.04	0.04	0.66	4.25	5.06	0.36	99.12	0.88
	ID3506_017	74.61	0.04	13.32	1.54	0.04	0.04	0.70	4.20	5.07	0.35	99.84	0.16
	ID3506_018	73.57	0.11	13.08	1.46	0.08	0.02	0.71	4.19	5.05	0.34	98.52	1.48

Average	73.95	0.08	13.29	1.53	0.05	0.03	0.69	4.21	5.06	0.35	99.16	0.84
St.Dev	0.57	0.03	0.19	0.06	0.02	0.01	0.03	0.03	0.01	0.01	0.66	0.66
Old Crow_017	74.77	0.31	13.13	1.72	0.03	0.30	1.39	4.25	3.91	0.26	100.00	4.80
Average	74.77	0.31	13.13	1.72	0.03	0.30	1.39	4.25	3.91	0.26	100.00	4.80
St.Dev												
ID3506_006	73.83	0.07	13.03	1.55	0.05	0.03	0.72	4.03	5.20	0.32	98.74	1.26
ID3506_007	73.48	0.08	12.92	1.49	0.06	0.03	0.73	4.02	5.27	0.34	98.35	1.65
ID3506_008	73.50	0.08	13.10	1.55	0.08	0.02	0.73	4.08	5.22	0.34	98.62	1.38
ID3506_009	73.70	0.09	13.24	1.50	0.08	0.04	0.73	3.81	5.14	0.35	98.61	1.39
Average	73.63	0.08	13.07	1.52	0.07	0.03	0.73	3.99	5.21	0.33	98.58	1.42
St.Dev	0.17	0.01	0.13	0.03	0.02	0.01	0.01	0.12	0.05	0.01	0.16	0.16
Old Crow_006	75.25	0.36	13.21	1.69	0.05	0.37	1.49	3.52	3.84	0.28	100.00	4.07
Old Crow_007	75.46	0.34	13.18	1.78	0.06	0.27	1.42	3.52	3.76	0.27	100.00	4.07
Old Crow_009	75.80	0.27	13.24	1.51	0.07	0.27	1.40	3.54	3.69	0.26	100.00	3.36
Average	75.50	0.33	13.21	1.66	0.06	0.30	1.44	3.52	3.76	0.27	100.00	3.83
St.Dev	0.28	0.05	0.03	0.14	0.01	0.05	0.04	0.01	0.08	0.01	0.00	0.41
ID3506__010	73.76	0.06	13.26	1.59	0.08	0.02	0.77	3.88	5.00	0.37	98.72	1.28
ID3506__011	73.88	0.07	13.31	1.48	0.07	0.06	0.72	3.96	5.14	0.34	98.96	1.04
ID3506__012	73.88	0.04	13.29	1.58	0.00	0.06	0.71	4.05	5.26	0.36	99.16	0.84
Average	73.84	0.06	13.29	1.55	0.05	0.05	0.73	3.96	5.13	0.36	98.94	1.06
St.Dev	0.07	0.01	0.02	0.06	0.04	0.02	0.03	0.09	0.13	0.02	0.22	0.22
Old Crow_010	75.75	0.28	13.08	1.44	0.06	0.23	1.42	3.76	3.76	0.28	100.00	3.63
Old Crow_011	75.43	0.30	13.18	1.67	0.07	0.31	1.42	3.77	3.60	0.33	100.00	3.77
Old Crow_012	75.02	0.33	13.10	1.77	0.08	0.32	1.46	3.89	3.79	0.31	100.00	2.79
Average	75.40	0.30	13.12	1.63	0.07	0.29	1.43	3.81	3.72	0.31	100.00	3.40

St.Dev	0.36	0.02	0.05	0.17	0.01	0.05	0.03	0.07	0.10	0.02	0.00	0.53
ID3506_014	74.15	0.06	13.27	1.66	0.08	0.06	0.76	4.11	5.16	0.36	99.60	0.40
ID3506_015	74.48	0.06	13.14	1.54	0.02	0.04	0.68	4.08	5.16	0.36	99.48	0.52
Average	74.31	0.06	13.21	1.60	0.05	0.05	0.72	4.10	5.16	0.36	99.54	0.46
St.Dev	0.24	0.00	0.09	0.08	0.04	0.01	0.06	0.02	0.00	0.00	0.08	0.08
Old Crow_013	75.21	0.30	13.02	1.70	0.04	0.31	1.42	3.86	3.96	0.24	100.00	4.15
Old Crow_015	75.13	0.30	13.22	1.68	0.10	0.28	1.44	3.95	3.66	0.31	100.00	3.80
Average	75.17	0.30	13.12	1.69	0.07	0.29	1.43	3.90	3.81	0.28	100.00	3.98
St.Dev	0.05	0.00	0.14	0.01	0.04	0.02	0.02	0.06	0.21	0.05	0.00	0.25
Average ID 3506	73.92	0.07	13.23	1.54	0.06	0.04	0.72	4.05	5.15	0.35	99.04	0.96
St.Dev	0.34	0.02	0.11	0.05	0.02	0.01	0.02	0.11	0.06	0.01	0.46	0.46
Average Old Crow	75.26	0.31	13.16	1.67	0.06	0.30	1.43	3.85	3.74	0.29	100.00	3.90
St.Dev	0.27	0.02	0.06	0.07	0.02	0.02	0.02	0.23	0.12	0.02	0.00	0.59

Date analyzed	Sample	SiO2	TiO2	Al2O3	FeO	MnO	MgO	CaO	Na2O	K2O	Cl	Total	H2Odiff
27-May-19	ID 3506_002	73.37	0.08	12.69	1.63	0.05	0.05	0.73	4.29	5.25	0.37	98.43	1.57
	ID 3506_003	73.41	0.08	13.00	1.55	0.03	0.05	0.73	3.91	5.20	0.35	98.22	1.78
	ID 3506_004	73.07	0.13	12.84	1.56	0.10	0.08	0.70	4.05	5.01	0.37	97.82	2.18
	ID 3506_005	73.85	0.07	12.89	1.59	0.04	0.03	0.73	4.03	5.24	0.36	98.75	1.25
	ID 3506_006	73.24	0.09	13.04	1.71	0.08	0.01	0.74	3.89	5.08	0.31	98.11	1.89
	Average	73.39	0.09	12.89	1.61	0.06	0.04	0.73	4.03	5.16	0.35	98.27	1.73
	St.Dev	0.29	0.02	0.14	0.07	0.03	0.03	0.02	0.16	0.10	0.03	0.35	0.35

Old Crow_001	75.23	0.31	12.93	1.68	0.09	0.29	1.44	4.22	3.60	0.29	100.00	4.54
Old Crow_002	74.84	0.33	12.91	1.71	0.04	0.28	1.46	4.41	3.80	0.30	100.00	3.55
Old Crow_003	75.48	0.30	12.88	1.64	0.06	0.33	1.48	3.82	3.82	0.24	100.00	5.16
Old Crow_004	75.51	0.32	13.00	1.73	0.12	0.26	1.42	3.89	3.54	0.28	100.00	5.18
Old Crow_005	73.45	0.28	12.86	1.59	0.05	0.32	1.39	6.09	3.78	0.25	100.00	5.03
Average	74.90	0.31	12.91	1.67	0.07	0.29	1.44	4.48	3.71	0.27	100.00	4.69
St.Dev	0.85	0.02	0.05	0.06	0.03	0.03	0.03	0.93	0.13	0.03	0.00	0.69
ID 3506_007	73.39	0.03	12.88	1.50	0.01	0.03	0.71	4.27	5.26	0.31	98.33	1.67
ID 3506_008	73.99	0.10	12.85	1.42	0.06	0.08	0.70	4.18	5.16	0.32	98.79	1.21
ID 3506_009	73.75	0.03	12.92	1.64	0.05	0.06	0.72	4.18	4.81	0.34	98.42	1.58
Average	73.71	0.05	12.89	1.52	0.04	0.06	0.71	4.21	5.08	0.32	98.51	1.49
St.Dev	0.30	0.04	0.04	0.11	0.03	0.02	0.01	0.05	0.24	0.01	0.24	0.24
Old Crow_006	75.54	0.32	12.82	1.64	0.07	0.32	1.42	3.78	3.86	0.32	100.00	3.90
Old Crow_007	75.70	0.32	12.80	1.72	0.14	0.30	1.47	3.57	3.74	0.30	100.00	4.71
Old Crow_008	75.26	0.27	12.99	1.69	0.04	0.30	1.42	3.94	3.88	0.28	100.00	4.06
Average	75.50	0.31	12.87	1.68	0.08	0.30	1.44	3.76	3.83	0.30	100.00	4.22
St.Dev	0.22	0.03	0.11	0.04	0.05	0.01	0.03	0.18	0.07	0.02	0.00	0.43
ID 3506_010	73.04	0.12	13.00	1.54	0.13	0.06	0.73	3.86	5.13	0.35	97.87	2.13
ID 3506_011	73.02	0.11	12.97	1.58	0.06	0.02	0.74	4.12	5.21	0.33	98.08	1.92
ID 3506_012	73.25	0.12	13.21	1.41	0.07	0.05	0.71	3.89	5.17	0.35	98.17	1.83
Average	73.10	0.12	13.06	1.51	0.09	0.04	0.73	3.96	5.17	0.34	98.04	1.96
St.Dev	0.13	0.00	0.13	0.08	0.04	0.02	0.02	0.14	0.04	0.01	0.15	0.15
Old Crow_009	75.64	0.23	13.17	1.67	0.12	0.28	1.45	3.28	3.91	0.31	100.00	4.73
Old Crow_010	75.21	0.38	13.30	1.68	0.07	0.31	1.48	3.41	3.95	0.28	100.00	2.48
Old Crow_011	75.23	0.34	13.17	1.71	0.01	0.29	1.41	3.80	3.85	0.25	100.00	4.82

Average	75.36	0.31	13.21	1.69	0.07	0.29	1.44	3.50	3.90	0.28	100.00	4.01
St.Dev	0.24	0.08	0.08	0.02	0.05	0.01	0.04	0.27	0.05	0.03	0.00	1.33
ID 3506_013	73.55	0.12	13.10	1.48	0.07	0.05	0.68	4.17	5.20	0.31	98.66	1.34
ID 3506_014	73.42	0.10	13.08	1.57	0.10	0.00	0.72	4.24	5.23	0.33	98.71	1.29
ID 3506_015	73.68	0.08	12.92	1.61	0.03	0.00	0.68	4.13	5.30	0.33	98.69	1.31
ID 3506_016	73.68	0.09	13.09	1.58	0.10	0.00	0.72	3.69	5.15	0.30	98.35	1.65
ID 3506_017	74.03	0.10	13.00	1.59	0.02	0.06	0.72	3.86	5.13	0.34	98.77	1.23
Average	73.67	0.10	13.04	1.57	0.06	0.02	0.70	4.02	5.20	0.32	98.64	1.36
St.Dev	0.23	0.02	0.08	0.05	0.04	0.03	0.02	0.23	0.07	0.01	0.16	0.16
Old Crow_012	75.40	0.34	13.25	1.70	0.10	0.31	1.42	3.38	3.90	0.26	100.00	5.51
Old Crow_013	75.54	0.25	13.13	1.68	0.01	0.29	1.49	3.74	3.66	0.27	100.00	3.32
Old Crow_014	75.29	0.28	12.80	1.73	0.09	0.28	1.49	4.08	3.73	0.30	100.00	1.78
Old Crow_015	75.14	0.25	12.97	1.71	0.06	0.29	1.49	4.23	3.62	0.31	100.00	4.01
Old Crow_016	75.18	0.35	13.01	1.64	0.04	0.31	1.37	3.92	3.95	0.30	100.00	4.09
Average	75.31	0.29	13.03	1.69	0.06	0.30	1.45	3.87	3.77	0.29	100.00	3.74
St.Dev	0.16	0.05	0.17	0.04	0.04	0.01	0.06	0.33	0.15	0.02	0.00	1.35
Average ID 3506	73.48	0.09	12.97	1.56	0.06	0.04	0.72	4.05	5.16	0.34	98.39	1.61
St.Dev	0.32	0.03	0.13	0.08	0.03	0.03	0.02	0.18	0.12	0.02	0.32	0.32
Average Old Crow	75.23	0.30	13.00	1.68	0.07	0.30	1.44	3.97	3.79	0.28	100.00	4.18
St.Dev	0.52	0.04	0.16	0.04	0.04	0.02	0.04	0.65	0.13	0.02	0.00	1.02

Date analyzed	Sample	SiO2	TiO2	Al2O3	FeO	MnO	MgO	CaO	Na2O	K2O	Cl	Total	H2Odiff
22-Nov-19	ID3506_001	73.86	0.05	13.10	1.60	0.06	0.06	0.72	4.09	5.06	0.33	98.85	1.15

no corrections made	ID3506_002	73.84	0.11	13.11	1.41	0.12	0.04	0.72	3.74	5.12	0.31	98.45	1.55
	ID3506_003	73.60	0.04	12.96	1.54	0.04	0.07	0.68	4.12	5.18	0.35	98.49	1.51
	Average	73.76	0.06	13.06	1.52	0.07	0.06	0.71	3.98	5.12	0.33	98.60	1.40
	St.Dev	0.15	0.04	0.08	0.09	0.04	0.01	0.02	0.21	0.06	0.02	0.22	0.22
	ID3506_004	74.22	0.08	13.00	1.55	0.05	0.03	0.71	4.13	5.13	0.35	99.18	0.82
	ID3506_005	74.41	0.04	13.09	1.58	0.03	0.07	0.72	3.74	5.19	0.32	99.13	0.87
	ID3506_006	74.27	0.09	13.16	1.61	0.06	0.05	0.76	3.76	5.00	0.35	99.03	0.97
	ID3506_007	74.36	0.07	13.20	1.54	0.05	0.05	0.69	3.82	5.29	0.36	99.35	0.65
	ID3506_008	74.21	0.06	12.96	1.50	0.09	0.06	0.77	4.17	5.11	0.38	99.22	0.78
	Average	74.30	0.07	13.08	1.56	0.06	0.05	0.73	3.92	5.14	0.35	99.18	0.82
	St.Dev	0.09	0.02	0.10	0.04	0.02	0.02	0.03	0.21	0.11	0.02	0.12	0.12
	Old Crow_002	75.22	0.33	13.07	1.68	0.08	0.30	1.43	4.04	3.65	0.26	100.00	3.58
	Old Crow_003	75.31	0.30	13.09	1.70	0.10	0.31	1.44	3.87	3.65	0.31	100.00	4.24
	Old Crow_004	75.47	0.28	13.07	1.72	0.05	0.29	1.46	3.86	3.61	0.25	100.00	4.71
	Average	75.33	0.30	13.08	1.70	0.08	0.30	1.44	3.92	3.64	0.27	100.00	4.18
	St.Dev	0.12	0.02	0.01	0.02	0.03	0.01	0.02	0.10	0.02	0.03	0.00	0.57
	ID3506_009	74.17	0.00	13.11	1.58	0.06	0.05	0.70	3.92	5.15	0.36	99.02	0.98
	ID3506_010	74.31	0.07	12.99	1.50	0.07	0.04	0.73	4.00	5.23	0.30	99.16	0.84
	ID3506_011	74.14	0.07	13.10	1.49	0.09	0.03	0.74	3.83	5.12	0.32	98.85	1.15
	ID3506_012	74.39	0.09	13.11	1.56	0.07	0.04	0.69	4.07	5.12	0.32	99.38	0.62
	ID3506_013	74.42	0.10	13.06	1.61	0.10	0.05	0.74	3.98	5.03	0.31	99.32	0.68
	Average	74.29	0.07	13.07	1.55	0.08	0.04	0.72	3.96	5.13	0.32	99.15	0.85
	St.Dev	0.12	0.04	0.05	0.05	0.02	0.01	0.02	0.09	0.07	0.02	0.22	0.22
	Old Crow_007	75.27	0.30	13.07	1.75	0.02	0.31	1.48	3.80	3.78	0.28	100.00	2.87
	Old Crow_008	74.81	0.27	13.20	1.74	0.07	0.31	1.46	3.94	3.96	0.30	100.00	3.61

Old Crow_009	75.34	0.34	13.15	1.70	0.05	0.31	1.43	3.86	3.58	0.30	100.00	4.07
Old Crow_010	75.24	0.32	12.99	1.68	0.06	0.32	1.41	4.00	3.74	0.31	100.00	3.62
Average	75.17	0.31	13.10	1.72	0.05	0.31	1.45	3.90	3.77	0.30	100.00	3.54
St.Dev	0.24	0.03	0.10	0.03	0.02	0.00	0.03	0.09	0.16	0.01	0.00	0.50
ID3506_014	74.01	0.10	13.21	1.60	0.07	0.04	0.71	4.12	5.20	0.35	99.32	0.68
ID3506_015	74.50	0.03	13.22	1.65	0.08	0.03	0.73	4.26	5.33	0.36	100.11	-0.11
ID3506_016	74.40	0.11	13.19	1.60	0.05	0.00	0.75	3.87	5.19	0.36	99.43	0.57
ID3506_017	74.09	0.11	13.16	1.54	0.07	0.08	0.70	4.30	5.12	0.33	99.42	0.58
ID3506_018	74.28	0.10	13.14	1.49	0.08	0.08	0.68	4.04	5.25	0.31	99.36	0.64
ID3506_019	74.35	0.08	13.23	1.54	0.07	0.04	0.73	4.24	5.14	0.35	99.70	0.30
Average	74.27	0.09	13.19	1.57	0.07	0.05	0.72	4.14	5.20	0.34	99.56	0.44
St.Dev	0.19	0.03	0.04	0.06	0.01	0.03	0.03	0.16	0.08	0.02	0.30	0.30
OldCrow_011	75.04	0.38	13.04	1.70	0.03	0.29	1.42	4.16	3.76	0.26	100.00	3.42
OldCrow_012	75.41	0.30	13.03	1.74	0.07	0.30	1.40	3.80	3.72	0.30	100.00	3.57
OldCrow_013	75.68	0.37	12.93	1.67	0.08	0.30	1.40	3.68	3.68	0.28	100.00	4.74
OldCrow_014	75.16	0.33	13.23	1.64	0.09	0.28	1.45	3.86	3.74	0.28	100.00	4.18
OldCrow_015	75.33	0.32	12.94	1.65	0.13	0.30	1.42	4.02	3.68	0.28	100.00	4.21
Average	75.33	0.34	13.03	1.68	0.08	0.29	1.42	3.90	3.72	0.28	100.00	4.02
St.Dev	0.25	0.03	0.12	0.04	0.04	0.01	0.02	0.19	0.04	0.01	0.00	0.53
Average ID3506	74.20	0.07	13.11	1.55	0.07	0.05	0.72	4.01	5.15	0.34	99.20	0.80
St.Dev	0.23	0.03	0.09	0.06	0.02	0.02	0.03	0.18	0.08	0.02	0.39	0.39
Average Old Crow	75.27	0.32	13.07	1.70	0.07	0.30	1.43	3.91	3.71	0.28	100.00	3.90
St.Dev	0.22	0.03	0.09	0.03	0.03	0.01	0.03	0.13	0.10	0.02	0.00	0.55

Table S4: Barlow Lake, Yukon. Summary of samples

Core length: 420 cm

Sampled/counted 90 cm (starting from top of core B2, in centre of whole core)

All counts were overwhelmed with detrital (weathered) glass, as seen by shard profiles and geochemical data

Accession #	depth from top of core (cm)	Collector/Source	Location	Province/ State	Probed?	When?	Tephra ID	Puck	Puck hole	notes
UA 3190	178-179	D. Froese	Barlow Lake	Yukon	Y	07-Sep-18	unknown	TV	1	4cm below top of sub core B2
UA 3191	195-196	D. Froese	Barlow Lake	Yukon	Y	07-Sep-18	unknown	TV	2	21cm below top of sub core B2
UA 3192	204-205	D. Froese	Barlow Lake	Yukon	Y	07-Sep-18	unknown	TV	3	30cm below top of sub core B2
UA 3193	216-217	D. Froese	Barlow Lake	Yukon	Y	07-Sep-18	unknown	TV	4	42cm below top of sub core B2
UA 3194	237-238	D. Froese	Barlow Lake	Yukon	Y	07-Sep-18	unknown	TV	5	63cm below top of sub core B2
UA 3195	260-261	D. Froese	Barlow Lake	Yukon	N		unknown	TV	6	86cm below top of sub core B2

Table S5: Barlow Lake Geochemistry

Date Probed/ depth	Tephra ID, source	Sample number	SiO_2	TiO_2	Al2O3	FeO	MnO	MgO	CaO	Na2O	K2O	Cl	Total	H2Od	n	Correlation notes
Sept 7, 2018 NaSiTDI BAR17 178-179	Unknown	UA 3190-5	76.33	0.09	13.50	0.84	0.05	0.09	0.90	2.49	5.66	0.07	100	7.18		detrital, weathered but some consistency
		UA 3190-6	76.18	0.11	13.52	0.75	0.05	0.06	0.90	3.10	5.28	0.07	100	5.52		
		UA 3190-8	76.22	0.10	13.74	0.89	0.07	0.12	0.74	2.73	5.34	0.06	100	7.61		
		Mean	76.24	0.10	13.58	0.83	0.06	0.09	0.85	2.77	5.43	0.07	100	6.77	3	
		St.Dev	0.08	0.01	0.14	0.08	0.01	0.03	0.09	0.31	0.20	0.01	0	1.10		
		UA 3190-3	75.20	0.17	14.12	1.20	0.10	0.26	1.54	4.08	3.14	0.26	100	1.34		good glass, single shard
		UA 3190_001-1	75.88	0.14	13.64	0.71	0.06	0.07	0.91	3.76	4.75	0.10	100	3.31		good glass, single shard
		UA 3190-2	76.62	0.18	13.75	0.93	0.05	0.20	1.41	3.77	3.05	0.06	100	5.55		good glass, single shard
		UA 3190-4	76.86	0.11	13.10	0.11	0.05	0.05	0.81	2.48	6.31	0.17	100	7.15		rest weathered
		UA 3190-1	78.23	0.08	12.25	1.37	0.03	0.00	0.24	2.20	5.53	0.09	100	8.26		
		UA 3190_002-1	77.68	0.06	12.77	0.94	0.01	0.04	0.69	2.03	5.69	0.12	100	8.69		
Sept 7, 2018 NaSiTDI BAR17 195-196	Unknown	UA 3191-8	74.16	0.29	13.73	2.07	0.08	0.25	1.13	4.33	3.80	0.20	100	5.69		good glass, single shard
		UA 3191-11	77.65	0.18	11.88	1.15	0.03	0.14	0.80	3.83	4.07	0.37	100	4.28		good glass, single shard
		UA 3191-7	77.98	0.17	12.48	1.05	0.03	0.22	1.28	4.27	2.40	0.15	100	6.40		good glass, single shard
		UA 3191-1	76.12	0.08	13.49	1.34	0.03	0.02	0.73	2.96	5.11	0.15	100	8.51		All detrital

		UA 3191-13	76.22	0.37	12.98	0.98	0.00	0.27	0.95	2.64	5.56	0.02	100	5.70		some weathered, some OK
		UA 3191-16	76.42	0.10	13.54	0.54	0.00	0.07	0.86	2.97	5.45	0.07	100	5.11		some inbetween?
		UA 3191-12	77.55	0.07	12.46	0.87	0.03	0.00	0.33	3.44	5.16	0.12	100	5.83		
		UA 3191-5	77.46	0.03	12.63	0.85	0.07	0.01	0.32	3.46	5.09	0.08	100	5.46		
		UA 3191-17	77.50	0.12	12.00	1.53	0.07	0.01	0.17	1.42	6.99	0.24	100	10.15		
		UA 3191-2	77.10	0.02	13.12	0.45	0.13	0.03	0.28	2.34	6.46	0.07	100	6.85		
		UA 3191-15	76.05	0.12	12.66	1.22	0.04	0.05	0.58	2.95	6.32	0.03	100	3.96		
Sept 7, 2018 NaSiTDI BAR17 204-205	Unknown	UA 3192-5	76.34	0.04	13.51	0.68	0.07	0.09	0.99	2.54	5.72	0.02	100	6.01		weathered potentially related population problematic variability in Ca,Fe
		UA 3192-6	76.40	0.13	13.68	0.43	0.03	0.02	0.78	3.02	5.47	0.05	100	5.64		
		UA 3192-8	76.43	0.12	13.51	0.57	0.04	0.08	0.95	3.08	5.17	0.05	100	6.10		
		UA 3192-9	76.04	0.15	13.53	0.89	0.03	0.12	0.98	2.52	5.68	0.07	100	6.68		
		Mean	76.30	0.11	13.56	0.64	0.04	0.08	0.93	2.79	5.51	0.05	100	6.11	4	
		St.Dev	0.18	0.05	0.08	0.19	0.02	0.04	0.10	0.30	0.25	0.02	0	0.43		
		UA 3192-7	77.86	0.13	12.55	0.94	0.05	0.16	0.95	3.71	3.50	0.19	100	4.98		All good shards, but no populations
		UA 3192-2	75.85	0.36	12.95	1.54	0.08	0.34	1.51	4.25	2.96	0.22	100	5.10		
		UA 3192-1	77.89	0.10	12.51	0.65	0.01	0.02	0.40	3.75	4.64	0.04	100	6.66		
		UA 3192-4	77.16	0.18	12.64	0.93	0.01	0.24	1.05	3.64	4.12	0.04	100	4.78		
		UA 3192-3	74.04	0.08	14.56	1.59	0.01	0.04	0.77	3.65	5.24	0.04	100	5.18		weathered
Sept 7, 2018 NaSiTDI BAR17 216-217	Unknown	UA 3193-9	71.29	0.61	14.35	2.80	0.05	0.61	2.00	4.58	3.62	0.11	100	2.60		Good single glass shards
		UA 3193-23	74.44	0.37	13.62	1.88	0.03	0.25	1.07	4.11	4.14	0.12	100	3.74		
		UA 3193-6	75.53	0.06	14.26	1.02	0.07	0.09	0.85	4.83	3.23	0.07	100	5.52		

UA 3193-10	76.49	0.21	13.58	0.93	0.02	0.27	1.41	4.03	3.02	0.04	100	5.42		
UA 3193-13	74.52	0.19	14.36	1.93	0.06	0.13	0.69	1.52	6.51	0.12	100	9.51		
UA 3193-17	75.20	0.12	13.72	1.88	0.02	0.03	0.96	1.75	6.24	0.10	100	8.31		
UA 3193-5	75.22	0.50	12.51	1.97	0.03	0.16	0.72	2.50	6.39	0.00	100	5.34		
UA 3193-28	75.70	0.04	13.18	0.91	0.03	0.01	0.52	2.48	7.09	0.04	100	4.65		
UA 3193-2	75.85	0.07	13.63	0.52	0.07	0.10	0.93	3.50	5.26	0.09	100	5.15		
UA 3193-12	75.97	0.12	13.57	0.68	0.07	0.09	0.92	3.06	5.49	0.05	100	5.12		
UA 3193-4	76.05	0.03	13.52	1.40	0.05	0.00	0.79	1.23	6.87	0.09	100	9.36		
UA 3193-7	76.24	0.31	12.53	1.20	0.00	0.23	1.04	2.21	6.21	0.02	100	4.18		
UA 3193-15	76.27	0.10	12.71	1.33	0.00	0.00	0.44	2.12	6.94	0.11	100	5.95		weathered detrital? And/or Old generally high K, low Na and scattered Ca and Fe *some* shards have lower totals and may be OK glass, but inconclusive
UA 3193-27	76.47	0.10	13.17	1.20	0.01	0.01	0.53	1.50	6.90	0.14	100	8.02		
UA 3193-3	76.57	0.04	13.49	0.49	0.03	0.03	0.75	3.37	5.17	0.08	100	5.78		
UA 3193-30	76.60	0.00	12.83	1.23	0.06	0.04	0.55	0.85	7.73	0.14	100	5.41		
UA 3193-29	76.90	0.08	12.46	0.87	0.02	0.03	0.22	2.38	6.99	0.06	100	4.10		
UA 3193-25	76.97	0.06	12.22	1.24	0.09	0.01	0.31	1.96	7.01	0.17	100	5.45		
UA 3193-19	76.97	0.05	12.16	1.23	0.08	0.00	0.35	3.03	6.02	0.14	100	3.07		
UA 3193-11	77.12	0.09	13.73	0.35	0.03	0.02	0.86	2.32	5.44	0.06	100	6.38		
UA 3193-14	77.22	0.03	13.01	0.70	0.01	0.00	0.39	3.80	4.82	0.03	100	6.31		example of probably just Old
UA 3193-21	77.29	0.07	12.57	1.09	0.04	0.00	0.44	1.95	6.46	0.13	100	6.91		
UA 3193-1	77.30	0.06	12.12	1.45	0.05	0.00	0.20	1.73	6.92	0.21	100	7.15		
UA 3193-20	77.36	0.09	12.30	0.84	0.02	0.02	0.40	1.81	7.12	0.06	100	6.97		
UA 3193-22	77.78	0.04	12.87	0.37	0.00	0.00	0.44	3.71	4.74	0.06	100	6.21		

		UA 3193-8	78.55	0.17	12.72	0.79	0.02	0.08	0.41	3.27	3.97	0.04	100	8.03		
Sept 7, 2018 NaSiTDI	Unknown	UA 3194-16	76.23	0.13	13.53	0.48	0.02	0.07	0.88	3.64	4.98	0.04	100	5.97		
BAR17 237-238		UA 3194-17	75.92	0.08	13.36	0.91	0.04	0.10	0.93	3.27	5.35	0.05	100	4.83		
		UA 3194-23	75.58	0.11	13.44	0.88	0.05	0.11	0.88	3.43	5.44	0.11	100	4.75		
		Mean	75.91	0.11	13.44	0.76	0.04	0.10	0.90	3.45	5.26	0.07	100	5.18	3	uncertain
		St.Dev	0.32	0.03	0.09	0.24	0.01	0.02	0.03	0.19	0.24	0.03	0	0.68		
		UA 3194-10	77.01	0.26	12.79	1.38	0.06	0.32	1.74	4.35	1.93	0.20	100	6.07		
		UA 3194-11	76.81	0.25	12.81	1.41	0.04	0.35	1.92	4.52	1.81	0.12	100	6.23		
		UA 3194-4	76.80	0.10	13.31	0.72	0.04	0.10	0.57	4.75	3.57	0.04	100	5.74		
																good single shards, no population
		UA 3194-29	77.36	0.04	12.24	1.30	0.04	0.04	0.27	1.48	7.10	0.16	100	6.12		weathered detrital some less weathered, coherency to some groups seen in previous samples but clearly detrital
		UA 3194-21	77.73	0.06	12.46	1.19	0.05	0.02	0.56	1.55	6.27	0.14	100	8.78		
		UA 3194-19	75.58	0.10	13.45	1.49	0.02	0.04	0.73	1.58	6.99	0.01	100	7.75		
		UA 3194-28	77.20	0.10	12.33	1.04	0.01	0.00	0.40	1.63	7.15	0.16	100	5.86		
		UA 3194-26	75.59	0.13	13.56	1.45	0.06	0.10	1.19	1.69	6.12	0.15	100	8.66		
		UA 3194-25	76.36	0.09	13.31	0.95	0.00	0.11	0.90	1.69	6.54	0.06	100	7.34		
		UA 3194-30	76.88	0.11	13.91	0.96	0.09	0.10	1.01	1.71	5.19	0.08	100	9.78		
		UA 3194-14	77.62	0.12	12.88	0.68	0.06	0.06	0.50	1.84	6.16	0.11	100	8.20		
		UA 3194-22	75.51	0.11	13.49	1.44	0.04	0.02	0.57	1.93	6.79	0.15	100	7.96		
		UA 3194-18	77.46	0.07	13.21	0.78	0.05	0.03	0.82	1.93	5.59	0.08	100	7.78		
		UA 3194-9	76.86	0.07	13.34	0.69	0.05	0.09	0.95	1.95	5.98	0.06	100	7.49		
		UA 3194-7	78.39	0.13	12.71	0.75	0.03	0.09	0.66	2.03	5.16	0.05	100	8.76		

UA 3194-27	76.07	0.09	13.52	1.37	0.01	0.05	0.59	2.39	5.81	0.13	100	7.88
UA 3194-12	77.37	0.06	12.19	1.31	0.06	0.01	0.36	2.39	6.13	0.13	100	4.35
UA 3194-5	76.98	0.02	13.80	0.48	0.06	0.02	0.82	2.62	5.15	0.05	100	7.17
UA 3194-13	76.79	0.13	13.55	0.81	0.05	0.09	0.93	2.63	4.96	0.07	100	7.01

Table S6.1 Standard data (reference)

	SiO2	TiO2	Al2O3	FeO	MnO	MgO	CaO	Na2O	K2O	Cl	Total	H2Odiff
Old Crow	**75.15**	**0.31**	**13.14**	**1.70**	**0.05**	**0.29**	**1.48**	**3.84**	**3.72**	**0.28**	**100.00**	**4.12**
assayed	1.00	0.05	0.34	0.14	0.03	0.03	0.05	0.26	0.26	0.05		
ID 3506	**74.10**	**0.07**	**13.10**	**1.55**	**0.07**	**0.04**	**0.74**	**4.06**	**5.13**	**0.34**	**99.09**	
assayed	0.96	0.03	0.34	0.06	0.03	0.02	0.05	0.28	0.26	0.03		

Table S6.2 Standard data (collected)

Date analyzed	Sample	SiO2	TiO2	Al2O3	FeO	MnO	MgO	CaO	Na2O	K2O	Cl	Total	H2Od
Sept 7 2020 NaSiTDI	ID3506-1	74.05	0.04	13.25	1.52	0.06	0.07	0.70	3.89	5.27	0.30	99.09	0.91
Na corrected	ID3506-2	73.82	0.05	13.09	1.56	0.08	0.03	0.72	3.94	5.19	0.35	98.75	1.25
	ID3506-3	74.09	0.13	13.06	1.59	0.11	0.03	0.71	4.18	5.26	0.33	99.41	0.59
	ID3506-4	74.61	0.11	13.13	1.56	0.08	0.07	0.71	4.34	5.17	0.34	100.03	-0.03
	ID3506-5	73.93	0.06	13.17	1.42	0.04	0.02	0.72	4.30	5.12	0.30	98.99	1.01
	Mean	74.10	0.08	13.14	1.53	0.07	0.04	0.71	4.13	5.20	0.33	99.26	0.74
	St.Dev	0.30	0.04	0.07	0.07	0.03	0.02	0.01	0.21	0.06	0.02	0.50	0.50
	Old Crow-1	74.96	0.36	13.26	1.71	0.07	0.27	1.42	3.79	3.92	0.30	100.00	4.13
	Old Crow-2	75.29	0.29	13.16	1.74	0.02	0.29	1.42	3.93	3.63	0.29	100.00	4.07
	Old Crow-3	74.97	0.34	13.23	1.61	0.05	0.29	1.46	3.95	3.89	0.25	100.00	4.38
	Old Crow-4	75.28	0.27	13.13	1.70	0.03	0.28	1.41	3.91	3.79	0.26	100.00	4.19
	Old Crow-5	75.15	0.24	13.05	1.68	0.07	0.32	1.47	3.99	3.80	0.32	100.00	3.87
	Mean	75.13	0.30	13.17	1.69	0.05	0.29	1.44	3.91	3.81	0.28	100.00	4.13
	St.Dev	0.16	0.05	0.08	0.05	0.02	0.02	0.03	0.07	0.11	0.03	0.00	0.19
	ID 3506-7	73.85	0.08	13.09	1.53	0.08	0.01	0.72	4.16	5.12	0.32	98.89	1.11
	ID 3506-9	73.66	0.06	13.18	1.55	0.08	0.04	0.72	4.17	5.12	0.34	98.85	1.15
	ID 3506-10	74.36	0.03	13.06	1.45	0.10	0.05	0.73	3.92	5.14	0.32	99.09	0.91
	Mean	73.96	0.06	13.11	1.51	0.09	0.03	0.72	4.08	5.13	0.33	98.94	1.06

St.Dev	0.36	0.02	0.07	0.05	0.01	0.02	0.00	0.14	0.01	0.01	0.13	0.13
Old Crow-6	75.28	0.35	12.98	1.72	0.06	0.27	1.42	3.96	3.74	0.27	100.00	4.02
Old Crow-7	75.32	0.30	13.10	1.74	0.05	0.32	1.46	3.67	3.80	0.31	100.00	4.55
Old Crow-8	75.25	0.29	12.93	1.75	0.05	0.29	1.44	4.06	3.74	0.28	100.00	3.79
Old Crow-9	74.90	0.34	13.20	1.77	0.13	0.31	1.44	3.97	3.76	0.24	100.00	6.41
Old Crow-10	75.45	0.27	13.18	1.66	0.03	0.27	1.44	3.70	3.80	0.26	100.00	4.31
Mean	75.24	0.31	13.08	1.73	0.06	0.29	1.44	3.87	3.77	0.27	100.00	4.62
St.Dev	0.21	0.03	0.12	0.04	0.04	0.02	0.02	0.17	0.03	0.03	0.00	1.04
ID 3506-11	74.28	0.05	13.24	1.57	0.06	0.06	0.74	4.28	5.24	0.33	99.76	0.24
ID 3506-12	74.70	0.11	13.13	1.37	0.06	0.01	0.70	3.88	5.24	0.30	99.44	0.56
ID 3506-14	74.20	0.08	12.97	1.51	0.09	0.04	0.69	3.89	5.12	0.33	98.85	1.15
ID 3506-15	73.58	0.04	13.23	1.54	0.04	0.04	0.73	4.24	5.17	0.35	98.88	1.12
Mean	74.19	0.07	13.14	1.50	0.06	0.04	0.72	4.07	5.19	0.33	99.23	0.77
St.Dev	0.46	0.03	0.12	0.09	0.02	0.02	0.02	0.22	0.06	0.02	0.45	0.45
Old Crow-11	75.34	0.25	13.12	1.74	0.11	0.32	1.43	3.55	3.88	0.36	100.00	4.62
Old Crow-13	75.21	0.31	13.06	1.74	0.07	0.27	1.44	3.80	3.89	0.29	100.00	5.15
Old Crow-14	75.41	0.33	13.29	1.63	0.05	0.30	1.49	3.50	3.77	0.28	100.00	6.47
Old Crow-15	75.26	0.26	13.21	1.77	0.01	0.29	1.46	3.69	3.82	0.30	100.00	5.41
Mean	75.30	0.29	13.17	1.72	0.06	0.30	1.45	3.64	3.84	0.31	100.00	5.41
St.Dev	0.09	0.04	0.10	0.06	0.04	0.02	0.03	0.14	0.05	0.03	0.00	0.78
ID 3506-16	74.50	0.06	13.07	1.52	0.04	0.03	0.72	3.79	5.22	0.32	99.20	0.80
ID 3506-20	73.63	0.04	12.98	1.62	0.07	0.04	0.70	4.19	5.18	0.31	98.68	1.32
Mean	74.06	0.05	13.03	1.57	0.05	0.03	0.71	3.99	5.20	0.31	98.94	1.06
St.Dev	0.62	0.01	0.07	0.07	0.02	0.00	0.02	0.28	0.03	0.01	0.37	0.37
Old Crow-16	75.29	0.33	13.14	1.65	0.05	0.30	1.45	3.85	3.75	0.25	100.00	4.82

Old Crow-18	75.03	0.30	12.95	1.73	0.07	0.28	1.45	4.08	3.89	0.29	100.00	2.48
Old Crow-19	75.52	0.36	12.88	1.72	0.07	0.29	1.43	3.85	3.68	0.27	100.00	5.73
Old Crow-20	75.18	0.31	12.99	1.74	0.05	0.33	1.46	3.97	3.75	0.29	100.00	3.49
Mean	75.25	0.32	12.99	1.71	0.06	0.30	1.45	3.94	3.77	0.27	100.00	4.13
St.Dev	0.21	0.02	0.11	0.04	0.01	0.02	0.02	0.11	0.09	0.02	0.00	1.43
ID3506												
Mean	74.09	0.07	13.12	1.52	0.07	0.04	0.72	4.08	5.18	0.32	99.14	0.86
St.Dev	0.37	0.03	0.09	0.07	0.02	0.02	0.01	0.19	0.05	0.02	0.40	0.40
Old Crow												
Old Crow	75.15	0.31	13.14	1.70	0.05	0.29	1.48	3.84	3.72	0.28	100.00	4.12
official	1.00	0.05	0.34	0.14	0.03	0.03	0.05	0.26	0.26	0.05		

Table S7: Chapman Lake, Yukon. Summary of samples

Surface core length: 24 cm

Accession #	Field #	Collector/Source	Location	Province/ State	Probed?	When?	Tephra ID	Puck	Puck hole	notes
UA 3499	CHP-SC2 8-9 cm	D. Froese	Chapman Lake	Yukon	Y	22-Jan-20	Dawson, WRA-like, Redoubt	VT	1	
UA 3500	CHP-SC2 17-18 cm	D. Froese	Chapman Lake	Yukon	Y	22-Jan-20	Dawson, WRA-like, Redoubt	VT	2	
UA 3501	CHP-SC2 23-24 cm	D. Froese	Chapman Lake	Yukon	Y	22-Jan-20	Dawson, WRA-like, Redoubt	VT	3	

Table S8: Chapman Lake Geochemistry

Date Probed/Depth	Sample number	SiO2	TiO2	Al2O3	FeO	MnO	MgO	CaO	Na2O	K2O	Cl	Total	H2Odiff	n	Correlation notes / confidence
Jan 22 2020 NaTDI	UA 3499-13	73.28	0.37	14.19	2.12	0.11	0.19	1.17	4.88	3.53	0.21	100.00	1.05		
CHP-SC2 8-9 cm	UA 3499-11	73.97	0.29	13.74	2.27	0.07	0.25	1.36	4.23	3.65	0.22	100.00	2.83		
	UA 3499-22	74.00	0.28	13.68	1.88	0.07	0.22	1.25	4.75	3.67	0.26	100.00	2.35		
	UA 3499-23	74.06	0.25	13.59	1.97	0.10	0.22	1.20	4.82	3.60	0.25	100.00	1.53		
	UA 3499-27	74.18	0.33	13.65	2.08	0.04	0.21	1.28	4.44	3.62	0.21	100.00	2.29		
	UA 3499-26	74.75	0.22	13.50	1.86	0.04	0.25	1.24	4.43	3.53	0.23	100.00	2.03		
	UA 3499-17	74.81	0.20	13.34	1.88	0.02	0.23	1.23	4.44	3.68	0.23	100.00	1.97		
	Mean	74.15	0.28	13.67	2.01	0.06	0.22	1.25	4.57	3.61	0.23	100.00	2.01	7	Dawson tephra
	StDev	0.52	0.06	0.26	0.15	0.03	0.02	0.06	0.25	0.06	0.02	0.00	0.58		
	UA 3499-18	76.92	0.18	12.76	1.09	0.06	0.16	0.97	4.03	3.59	0.31	100.00	1.96		
	UA 3499-15	77.25	0.17	12.92	0.94	0.05	0.12	1.23	3.98	3.13	0.27	100.00	2.36		
	UA 3499-16	77.35	0.21	12.47	1.19	0.04	0.17	0.88	3.76	3.67	0.33	100.00	3.03		
	UA 3499-6	77.52	0.20	12.25	1.07	0.04	0.12	0.78	3.62	4.16	0.31	100.00	3.19		
	UA 3499-20	77.76	0.12	12.52	0.96	0.04	0.12	1.00	3.62	3.65	0.27	100.00	4.22		
	UA 3499-1	77.88	0.19	12.49	1.12	0.07	0.13	0.94	3.55	3.38	0.30	100.00	5.34		
	UA 3499-8	78.01	0.20	12.13	1.07	0.06	0.18	0.71	3.56	3.80	0.35	100.00	6.13		
	UA 3499-28	78.40	0.16	12.42	0.97	0.04	0.11	0.88	3.51	3.26	0.32	100.00	4.51		
	UA 3499-3	78.42	0.14	11.98	1.03	0.05	0.11	0.78	4.02	3.27	0.25	100.00	1.52		
	UA 3499-21	78.54	0.08	11.93	0.97	0.08	0.13	0.84	3.69	3.50	0.30	100.00	3.12		
	UA 3499-5	79.09	0.23	11.84	1.10	0.05	0.20	0.59	3.09	3.56	0.33	100.00	5.85		
	Mean	77.92	0.17	12.34	1.05	0.05	0.14	0.87	3.68	3.54	0.31	100.00	3.75	11	WRA-like
	StDev	0.65	0.04	0.34	0.08	0.01	0.03	0.17	0.27	0.29	0.03	0.00	1.57		
	UA 3499-24	74.94	0.39	13.71	1.64	0.05	0.30	1.21	3.65	3.99	0.15	100.00	4.71		

	UA 3499-12	75.74	0.30	13.39	1.35	0.09	0.31	1.53	4.10	3.06	0.15	100.00	3.14		
	UA 3499-10	76.48	0.32	13.02	1.38	0.06	0.26	1.19	3.10	4.12	0.09	100.00	4.77		
	UA 3499-2	76.70	0.27	12.81	1.03	0.01	0.20	0.82	3.87	4.18	0.13	100.00	3.53		
	UA 3499-19	78.43	0.23	12.07	1.00	0.06	0.16	1.00	3.56	3.41	0.12	100.00	0.11		
	Mean	76.46	0.30	13.00	1.28	0.05	0.25	1.15	3.66	3.75	0.13	100.00	3.25	5	Redoubt?
	StDev	1.30	0.06	0.63	0.27	0.03	0.06	0.26	0.38	0.49	0.02	0.00	1.90		
	UA 3499-30	72.79	0.41	14.25	2.28	0.08	0.47	1.66	4.14	3.82	0.14	100.00	3.70		
	UA 3499-29	74.07	0.10	14.46	1.57	0.03	0.03	0.80	3.24	5.68	0.04	100.00	5.90		
	UA 3499-25	76.04	0.10	13.79	1.17	0.04	0.20	1.38	3.89	3.18	0.28	100.00	2.29		
	UA 3499-4	77.53	0.03	13.61	0.57	0.06	0.08	0.79	4.20	3.13	0.02	100.00	2.56		
	UA 3499-9	78.04	0.13	13.12	0.92	0.00	0.22	0.99	3.92	2.63	0.05	100.00	6.47		
	UA 3499-14	80.49	0.02	13.34	0.73	0.00	0.02	0.68	0.81	3.89	0.03	100.00	11.05		
Jan 22 2020 NaTDI CHP-SC2 17-18 cm	UA 3500-20	74.22	0.30	13.86	2.05	0.07	0.23	1.26	4.03	3.74	0.31	100.00	3.33		
	UA 3500-16	74.54	0.31	13.72	2.07	0.08	0.23	1.23	4.11	3.51	0.24	100.00	5.14		
	UA 3500-13	74.63	0.28	13.61	2.06	0.07	0.25	1.23	4.11	3.56	0.24	100.00	4.45		
	UA 3500-22	74.70	0.21	13.71	1.96	0.04	0.22	1.25	4.30	3.43	0.23	100.00	4.26		
	Mean	74.52	0.28	13.73	2.04	0.06	0.23	1.24	4.14	3.56	0.26	100.00	4.29	4	Dawson tephra
	StDev	0.21	0.04	0.10	0.05	0.02	0.01	0.01	0.11	0.13	0.04	0.00	0.75		
	UA 3500-27	76.98	0.26	12.65	1.17	0.10	0.27	1.25	3.98	3.21	0.16	100.00	1.17		Redoubt?
	UA 3500-5	73.58	0.23	14.68	1.51	0.04	0.37	1.87	4.45	3.00	0.34	100.00	3.13		
	UA 3500-7	74.23	0.20	14.25	1.56	0.07	0.42	1.95	4.03	2.99	0.38	100.00	1.75		
	UA 3500-17	75.12	0.13	13.95	1.27	0.07	0.29	1.51	3.99	3.44	0.29	100.00	2.80		
	UA 3500-25	75.20	0.10	14.02	1.00	0.10	0.14	1.51	4.79	2.95	0.24	100.00	-0.12		
	UA 3500-18	76.12	0.08	13.85	1.00	0.07	0.15	1.46	4.10	2.94	0.29	100.00	3.97		

	UA 3500-30	76.73	0.10	13.32	1.03	0.06	0.24	1.22	3.93	3.10	0.36	100.00	4.87		
	UA 3500-11	76.74	0.14	13.18	1.12	0.04	0.21	1.20	3.97	3.17	0.31	100.00	4.45		
	UA 3500-6	76.88	0.12	13.05	1.13	0.06	0.19	0.91	3.53	3.87	0.33	100.00	4.14		
	UA 3500-14	77.54	0.13	12.71	1.03	0.06	0.20	1.07	3.55	3.42	0.38	100.00	3.04		
	UA 3500-23	77.68	0.15	12.42	1.09	0.07	0.17	1.03	3.88	3.25	0.34	100.00	2.20		
	UA 3500-26	77.69	0.11	12.84	1.18	0.05	0.19	1.07	3.47	3.16	0.29	100.00	4.43		
	UA 3500-2	77.85	0.11	12.71	0.98	0.05	0.16	1.13	3.69	3.11	0.26	100.00	2.91		
	UA 3500-15	77.89	0.10	12.46	1.08	0.06	0.10	0.97	3.50	3.60	0.31	100.00	3.19		
	UA 3500-4	77.95	0.11	12.64	1.02	0.02	0.19	0.89	3.53	3.43	0.28	100.00	4.55		
	UA 3500-1	78.23	0.12	12.45	1.04	0.08	0.13	0.97	3.43	3.32	0.32	100.00	5.43		
	UA 3500-12	78.40	0.14	12.42	0.96	0.02	0.14	1.03	3.58	3.03	0.35	100.00	3.69		
	UA 3500-8	79.66	0.10	11.63	1.13	0.05	0.09	0.61	3.04	3.42	0.36	100.00	5.85		
	Mean	76.91	0.13	13.09	1.13	0.06	0.20	1.20	3.79	3.25	0.32	100.00	3.55	17	WRA-like
	StDev	1.60	0.04	0.81	0.17	0.02	0.09	0.35	0.42	0.26	0.04	0.00	1.45		
	UA 3500-29	71.00	0.52	14.98	2.35	0.14	0.51	1.78	5.55	3.00	0.22	100.00	1.48		
	UA 3500-24	74.45	0.15	15.42	0.78	0.03	0.08	2.06	4.55	2.34	0.19	100.00	4.25		
	UA 3500-9	75.69	0.53	12.91	1.97	0.02	0.32	1.09	3.31	4.08	0.10	100.00	5.10		
	UA 3500-21	77.29	0.11	13.23	0.44	0.08	0.02	0.84	3.11	4.81	0.08	100.00	3.31		
	UA 3500-3	77.33	0.12	12.10	1.72	0.07	0.49	0.81	3.66	3.45	0.31	100.00	3.31		
Jan 22 2020 NaTDI CHP-SC2 23-24 cm	UA 3501-12	74.43	0.26	13.61	2.06	0.09	0.25	1.23	4.30	3.60	0.23	100.00	2.12		
	UA 3501-28	74.47	0.26	13.59	1.98	0.07	0.26	1.24	4.31	3.64	0.24	100.00	3.99		
	Mean	74.45	0.26	13.60	2.02	0.08	0.25	1.24	4.30	3.62	0.23	100.00	3.06	2	
	StDev	0.03	0.00	0.01	0.05	0.02	0.01	0.00	0.01	0.03	0.00	0.00	1.32		Dawson tephra
	UA 3501-20	76.29	0.09	13.20	1.17	0.06	0.20	1.19	4.14	3.44	0.29	100.00	3.33		
	UA 3501-18	76.99	0.17	12.66	1.09	0.06	0.17	1.03	4.24	3.34	0.31	100.00	4.22		
	UA 3501-29	77.23	0.15	12.76	1.18	0.08	0.21	1.16	3.73	3.24	0.35	100.00	1.28		

UA 3501-24	77.26	0.12	13.16	1.13	0.01	0.18	1.20	3.55	3.14	0.31	100.00	5.06	
UA 3501-19	77.40	0.14	12.71	1.02	0.06	0.18	1.17	3.66	3.41	0.33	100.00	1.99	
UA 3501-3	77.53	0.15	13.17	0.97	0.03	0.15	1.17	3.49	3.16	0.24	100.00	5.78	
UA 3501-14	77.57	0.10	12.80	1.09	0.07	0.23	1.04	3.61	3.25	0.32	100.00	4.67	
UA 3501-9	77.70	0.11	12.63	1.06	0.03	0.15	0.98	3.95	3.16	0.29	100.00	1.47	
UA 3501-8	77.87	0.15	12.51	1.19	0.04	0.21	0.91	3.77	3.10	0.33	100.00	5.11	
UA 3501-10	77.91	0.17	12.17	1.14	0.06	0.11	0.78	4.02	3.38	0.33	100.00	3.75	
UA 3501-11	78.24	0.16	12.65	1.06	0.05	0.14	1.11	3.27	3.06	0.32	100.00	3.00	
UA 3501-1	78.26	0.15	12.72	1.04	0.01	0.11	0.83	3.31	3.35	0.29	100.00	5.10	
UA 3501-2	78.64	0.11	11.99	1.00	0.06	0.10	0.66	3.61	3.63	0.25	100.00	4.58	
UA 3501-21	78.68	0.15	11.74	1.11	0.07	0.15	0.76	3.50	3.62	0.30	100.00	3.24	
UA 3501-27	78.74	0.20	11.81	1.05	0.04	0.17	0.69	3.48	3.60	0.30	100.00	1.87	
UA 3501-30	78.81	0.21	11.95	1.09	0.07	0.17	0.64	3.54	3.28	0.31	100.00	5.98	
UA 3501-23	79.17	0.07	12.05	1.11	0.07	0.12	0.76	2.98	3.42	0.34	100.00	4.74	
UA 3501-25	79.26	0.11	12.05	1.04	0.04	0.13	0.85	3.27	3.00	0.32	100.00	4.44	
UA 3501-13	79.99	0.12	11.26	1.13	0.06	0.08	0.56	3.10	3.45	0.32	100.00	3.43	
Mean	78.08	0.14	12.42	1.09	0.05	0.16	0.92	3.59	3.32	0.31	100.00	3.84	19 WRA-like
StDev	0.91	0.04	0.54	0.06	0.02	0.04	0.21	0.34	0.19	0.03	0.00	1.43	
UA 3501-7	71.44	0.62	15.78	2.89	0.10	0.59	1.53	4.55	2.42	0.09	100.00	7.24	

S9.1 Chapman Lake Standard data (reference)

	SiO2	TiO2	Al2O3	FeO	MnO	MgO	CaO	Na2O	K2O	Cl	Total	H2Od
Old Crow	**75.15**	**0.31**	**13.14**	**1.70**	**0.05**	**0.29**	**1.48**	**3.84**	**3.72**	**0.28**	**100.00**	**4.12**
assayed	1.00	0.05	0.34	0.14	0.03	0.03	0.05	0.26	0.26	0.05		
ID 3506	**74.10**	**0.07**	**13.10**	**1.55**	**0.07**	**0.04**	**0.74**	**4.06**	**5.13**	**0.34**	**99.09**	
assayed	0.96	0.03	0.34	0.06	0.03	0.02	0.05	0.28	0.26	0.03		

S9.2 Chapman Lake Standard data (collected)

Date analyzed	Sample	SiO2	TiO2	Al2O3	FeO	MnO	MgO	CaO	Na2O	K2O	Cl	Total	H2Od
Jan22 2020 NaTDI	ID 3506_001	74.35	0.08	13.25	1.61	0.09	0.06	0.76	4.09	5.44	0.35	100.00	0.35
Ca, Na, K corrected	ID 3506_002	74.32	0.07	13.07	1.62	0.09	0.04	0.74	4.44	5.34	0.35	100.00	0.15
	ID 3506_003	74.56	0.07	13.23	1.67	0.05	0.06	0.74	3.99	5.37	0.36	100.00	0.88
	ID 3506_004	74.87	0.05	13.13	1.62	0.07	0.05	0.74	4.10	5.09	0.35	100.00	0.47
	ID 3506_005	74.80	0.10	13.20	1.64	0.06	0.05	0.71	3.58	5.58	0.37	100.00	1.26
	ID 3506_006	74.87	0.06	13.06	1.73	0.08	0.05	0.75	3.98	5.13	0.36	100.00	1.05
	Mean	74.63	0.07	13.16	1.65	0.07	0.05	0.74	4.03	5.33	0.36	100.00	0.69
	St.Dev	0.25	0.02	0.08	0.05	0.02	0.01	0.01	0.28	0.19	0.01	0.00	0.44
	Old Crow_001	75.74	0.33	13.35	1.71	0.05	0.25	1.45	3.27	3.64	0.28	100.00	4.37
	Old Crow_002	75.67	0.28	13.17	1.70	0.03	0.31	1.50	3.67	3.45	0.30	100.00	4.33
	Old Crow_003	74.99	0.28	13.23	1.69	0.10	0.26	1.43	4.22	3.59	0.27	100.00	2.63
	Old Crow_004	75.52	0.38	13.19	1.71	0.03	0.34	1.46	3.51	3.62	0.30	100.00	3.74
	Old Crow_005	75.50	0.33	12.83	1.63	0.08	0.29	1.42	4.10	3.63	0.27	100.00	1.18
	Old Crow_006	76.14	0.39	13.13	1.71	0.04	0.32	1.42	2.99	3.64	0.29	100.00	4.17
	Mean	75.59	0.33	13.15	1.69	0.06	0.29	1.45	3.63	3.59	0.28	100.00	3.41
	St.Dev	0.37	0.05	0.17	0.03	0.03	0.03	0.03	0.47	0.07	0.01	0.00	1.27

ID 3506_007	75.12	0.10	12.97	1.54	0.06	0.06	0.71	4.27	4.88	0.37	100.00	-0.14
ID 3506_008	74.97	0.13	13.14	1.52	0.11	0.06	0.78	3.95	5.06	0.37	100.00	1.77
ID 3506_009	74.47	0.10	13.41	1.65	0.08	0.05	0.75	4.20	5.01	0.37	100.00	1.53
ID 3506_010	74.65	0.09	13.25	1.51	0.05	0.04	0.74	4.31	5.08	0.36	100.00	0.97
ID 3506_011	75.10	0.05	13.14	1.61	0.06	0.05	0.73	3.99	5.00	0.33	100.00	0.09
Mean	74.86	0.09	13.18	1.57	0.07	0.05	0.74	4.15	5.00	0.36	100.00	0.84
St.Dev	0.29	0.03	0.16	0.06	0.02	0.01	0.03	0.17	0.08	0.02	0.00	0.85
Old Crow_007	75.37	0.33	13.22	1.72	0.07	0.31	1.47	3.82	3.44	0.33	100.00	3.63
Old Crow_008	76.05	0.34	12.95	1.71	0.06	0.31	1.46	3.49	3.41	0.30	100.00	2.98
Old Crow_009	75.72	0.27	13.22	1.69	0.11	0.32	1.47	3.54	3.43	0.29	100.00	4.52
Old Crow_010	76.20	0.33	12.91	1.62	0.04	0.26	1.50	3.14	3.79	0.26	100.00	0.46
Old Crow_011	75.92	0.33	13.19	1.66	0.10	0.26	1.39	3.67	3.28	0.26	100.00	5.22
Mean	75.85	0.32	13.10	1.68	0.08	0.29	1.46	3.53	3.47	0.29	100.00	3.36
St.Dev	0.32	0.03	0.15	0.04	0.03	0.03	0.04	0.25	0.19	0.03	0.00	1.83
ID 3506_012	74.33	0.07	13.38	1.61	0.09	0.07	0.72	4.34	5.11	0.36	100.00	1.56
ID 3506_013	74.53	0.08	13.13	1.67	0.06	0.05	0.76	4.26	5.17	0.37	100.00	1.46
ID 3506_014	74.95	0.08	13.20	1.62	0.08	0.03	0.76	3.95	5.06	0.34	100.00	1.61
ID 3506_015	74.65	0.04	13.12	1.70	0.08	0.06	0.77	4.10	5.20	0.36	100.00	1.68
ID 3506_016	74.81	0.07	13.33	1.50	0.06	0.07	0.74	3.94	5.22	0.32	100.00	1.55
ID 3506_017	74.57	0.04	13.40	1.59	0.08	0.04	0.72	4.39	4.90	0.34	100.00	1.33
Mean	74.64	0.06	13.26	1.62	0.08	0.05	0.74	4.16	5.11	0.35	100.00	1.53
St.Dev	0.22	0.02	0.13	0.07	0.01	0.01	0.02	0.19	0.12	0.02	0.00	0.12
Old Crow_012	76.58	0.29	12.85	1.70	0.06	0.27	1.49	3.24	3.33	0.24	100.00	3.58
Old Crow_013	76.09	0.24	13.26	1.67	0.08	0.27	1.44	3.39	3.34	0.29	100.00	5.62
Old Crow_014	75.46	0.36	13.11	1.64	0.10	0.29	1.45	3.86	3.50	0.30	100.00	4.51
Old Crow_015	75.11	0.31	13.26	1.66	0.06	0.26	1.54	3.85	3.71	0.30	100.00	3.34

Old Crow_016	76.14	0.30	12.95	1.66	0.07	0.27	1.52	2.79	4.11	0.25	100.00	3.77
Old Crow_017	75.24	0.34	12.70	1.73	0.06	0.31	1.41	4.23	3.73	0.31	100.00	1.20
Mean	75.77	0.31	13.02	1.68	0.07	0.28	1.48	3.56	3.62	0.28	100.00	3.67
St.Dev	0.58	0.04	0.23	0.03	0.01	0.02	0.05	0.52	0.30	0.03	0.00	1.47
ID3506												
Mean	74.70	0.07	13.20	1.61	0.07	0.05	0.74	4.11	5.16	0.35	100.00	1.03
St.Dev	0.26	0.02	0.12	0.07	0.02	0.01	0.02	0.22	0.19	0.01	0.00	0.63
Old Crow												
Old Crow	75.73	0.32	13.09	1.68	0.07	0.29	1.46	3.57	3.57	0.28	100.00	3.48
official	0.43	0.04	0.19	0.03	0.02	0.03	0.04	0.42	0.21	0.02	0.00	1.43

Table S10: Gravel Lake, Yukon. Summary of samples

Core length: 223 cm

Accession #	Field #	Collector/Source	Location	Province/State	Probed?	When?	Puck	Puck hole	notes
UA 3486	GRV17 65-66 cm	D. Froese	Gravel Lake	Yukon	Y	Dec18_2019	VR	1	
UA 3487	GRV17 57-58 cm	D. Froese	Gravel Lake	Yukon	Y	Dec18_2019	VR	2	
UA 3488	GRV17 49-50 cm	D. Froese	Gravel Lake	Yukon	Y	Dec18_2019	VR	3	
UA 3489	GRV17 43-44 cm	D. Froese	Gravel Lake	Yukon	Y	Dec18_2019	VR	4	
UA 3490	GRV17 42-43 cm	D. Froese	Gravel Lake	Yukon	Y	Dec18_2019	VR	5	
UA 3491	GRV17 34-35 cm	D. Froese	Gravel Lake	Yukon	Y	Dec18_2019	VR	6	
UA 3493	GRV17 9-10 cm	D. Froese	Gravel Lake	Yukon	Y	Jan 22_2020	VS	1	
UA 3494	GRV17 17-18 cm	D. Froese	Gravel Lake	Yukon	Y	Jan 22_2020	VS	2	
UA 3495	GRV17 25-26 cm	D. Froese	Gravel Lake	Yukon	Y	Jan 22_2020	VS	3	
UA 3496	GRV17 31-32 cm	D. Froese	Gravel Lake	Yukon	Y	Jan 23_2020	VS	4	
UA 3497	GRV17 32-33 cm	D. Froese	Gravel Lake	Yukon	Y	Jan 23_2020	VS	5	
UA 3498	GRV17 40-41 cm	D. Froese	Gravel Lake	Yukon	Y	Jan 23_2020	VS	6	
UA 3522	GRV17 72-73 cm	D. Froese	Gravel Lake	Yukon	Y	June 8 2020	VX	1	epoxy didn't cure properly so I had to redo this sample. See UA 3541 for second accession number

UA 3523	GRV17 67-68 cm	D. Froese	Gravel Lake	Yukon	Y	June 8 2020	VX	2	
UA 3524	GRV17 44-45 cm	D. Froese	Gravel Lake	Yukon	T	June 8 2020	VX	3	
UA 3526	GRV17 7-8 cm	D. Froese	Gravel Lake	Yukon	Y	June 8 2020	VY	1	Might be WRAe
UA 3527	GRV17 24-25 cm	D. Froese	Gravel Lake	Yukon	Y	June 8 2020	VY	2	Main WRAn peak.
UA 3528	GRV17 113-114 cm	D. Froese	Gravel Lake	Yukon	Y	June 22 2020 + September 2 2020	VY	3	cuspate/platy shards, clean with some vesicles
UA 3529	GRV17 107-108 cm	D. Froese	Gravel Lake	Yukon	Y	June 22 2020	VY	4	Platy shards, high organic/diatom concentration here
UA 3530	GRV17 100-101 cm	D. Froese	Gravel Lake	Yukon	Y	June 22 2020	VY	5	Distinct darker colour to glass, very frothy, small dark vesicles
UA 3531	GRV17 97-98 cm	D. Froese	Gravel Lake	Yukon	Y	June 10 2020	VY	6	Same as 100-101cm
UA 3532	GRV17 93-94 cm	D. Froese	Gravel Lake	Yukon	Y	June 22 2020	VZ	1	mixed pumice and cuspates, some microlitic, lots of detrital
UA 3533	GRV17 82-83 cm	D. Froese	Gravel Lake	Yukon	Y	June 10 2020	VZ	2	Very large peak of frothy pumice
UA 3534	GRV17 77-78 cm	D. Froese	Gravel Lake	Yukon	Y	June 10 2020 + September 2 2020	VZ	3	same as 82-83, but noted that shards were a bit more weathered
UA 3535	GRV17 133-134 cm	D. Froese	Gravel Lake	Yukon	Y	June 22 2020 + September 1 2020 + September 2 2020	VZ	4	clean cuspates, look better than surrounding samples
UA 3536	GRV17 135-136 cm	D. Froese	Gravel Lake	Yukon	Y	September 1 2020	VZ	5	mixed morphologies, cuspates and pumice
UA 3537	GRV17 140-141 cm	D. Froese	Gravel Lake	Yukon	Y	September 1 2020	VZ	6	low concentration of v. microlitic shards, but lots of detrital glass
UA 3538	GRV17 123-124 cm	D. Froese	Gravel Lake	Yukon	Y	September 1 2020	WA	1	depth just before the large rise in concentration

UA 3539	GRV17 75-76 cm	D. Froese	Gravel Lake	Yukon	Y	September 1 2020 + September 2 2020(rerun)	WA	2	
UA 3540	GRV17 73-74 cm	D. Froese	Gravel Lake	Yukon	Y	September 1 2020 + Mar 4 2021	WA	3	looking to constrain CFEII at 69cm
UA 3541	GRV17 72-73 cm	D. Froese	Gravel Lake	Yukon	Y	September 1 2020 + Mar 4 2021	WA	4	looking to constrain CFEII at 69cm
UA 3542	GRV17 69-70 cm	D. Froese	Gravel Lake	Yukon	Y	September 1 2020	WA	5	looking to constrain CFEII at 69cm
UA 3543	GRV7-8 cm	D. Froese	Gravel Lake	Yukon	Y	Aug 2020	WB	1	WRA peak. Fe-Ti oxides extracted for geochem
UA 3544	GRV24-25 cm	D. Froese	Gravel Lake	Yukon	Y	Aug 2020	WB	2	WRA peak. Fe-Ti oxides extracted for geochem
UA 3545	GRV 44-45 cm	D. Froese	Gravel Lake	Yukon	Y	Aug 2020	WB	3	WRA peak. Fe-Ti oxides extracted for geochem
UA 3614	GRV 201-202 cm	D. Froese	Gravel Lake	Yukon	Y	November 25, 2020	WQ	1	
UA 3615	GRV 188-189 cm	D. Froese	Gravel Lake	Yukon	Y	November 25, 2020	WQ	2	
UA 3616	GRV 166-167 cm	D. Froese	Gravel Lake	Yukon	Y	November 25, 2020	WQ	3	
UA 3617	GRV 162-163 cm	D. Froese	Gravel Lake	Yukon	Y	November 25, 2020	WQ	4	
UA 3618	GRV 156-157 cm	D. Froese	Gravel Lake	Yukon	Y	November 25, 2020	WQ	5	
UA 3619	GRV 86-87 cm	D. Froese	Gravel Lake	Yukon	Y	November 26, 2020	WQ	6	
UA 3620	GRV SFC 18-19cm	D. Froese	Gravel Lake	Yukon	Y	November 26, 2020	WR	1	surface core
UA 3621	GRV SFC 13-14 cm	D. Froese	Gravel Lake	Yukon	Y	November 26, 2020	WR	2	surface core
UA 3622	GRV SFC 8-9 cm	D. Froese	Gravel Lake	Yukon	Y	November 26, 2020	WR	3	surface core
UA 3623	GRV SFC 4-5 cm	D. Froese	Gravel Lake	Yukon	Y	November 26, 2020	WR	4	surface core

Table S11: Gravel Lake Geochemistry

Date Probed/Composite depth	popn	Sample number	SiO_2	TiO_2	Al2O3	FeO	MnO	MgO	CaO	Na2O	K2O	Cl	Total	H2Od	n	Correlation notes
Nov 26, 2020 NaSiTDI		UA3623-21	70.38	0.50	15.49	2.80	0.09	0.93	2.82	4.27	2.57	0.19	100	1.28		
GRV Surface core 4-5 cm		UA3623-29	71.71	0.11	16.21	1.27	0.03	0.28	2.67	4.96	2.57	0.25	100	1.73		
		UA3623-25	74.04	0.52	13.54	2.34	0.07	0.48	1.96	4.13	2.79	0.19	100	1.17		
		UA3623-4	75.10	0.57	12.62	2.23	0.05	0.41	1.51	4.47	2.90	0.20	100	0.59		
		UA3623-8	75.49	0.40	12.83	2.02	0.11	0.39	1.66	4.21	2.75	0.19	100	0.58		
		UA3623-28	76.39	0.44	12.70	1.77	0.00	0.35	1.30	4.07	2.85	0.17	100	1.69		
		UA3623-17	76.76	0.28	12.52	1.32	0.09	0.17	1.17	4.14	3.31	0.31	100	8.14		
		UA3623-27	76.96	0.22	12.37	1.40	0.02	0.20	1.18	4.25	3.24	0.19	100	0.95		
		UA3623-11	77.32	0.25	12.26	1.69	0.05	0.22	1.16	3.89	3.00	0.18	100	1.00		
		UA3623-9	77.73	0.12	12.28	1.15	0.01	0.14	0.75	4.51	3.16	0.19	100	1.09		
		UA3623-5	78.05	0.21	12.02	1.14	0.05	0.06	0.72	4.41	3.17	0.22	100	0.97		
		UA3623-2	78.05	0.13	12.12	1.16	0.05	0.10	0.71	4.45	3.06	0.22	100	0.36		
		UA3623-15	78.06	0.37	11.86	1.47	0.06	0.22	1.00	3.76	3.04	0.20	100	0.84		
	a	Mean	75.85	0.32	12.99	1.67	0.05	0.30	1.43	4.27	2.95	0.21	100	1.57	13	Katmai 1912
		StDev	2.48	0.16	1.35	0.53	0.03	0.22	0.69	0.30	0.24	0.04	0	2.01		
		UA3623-22	73.38	0.18	14.64	1.56	0.05	0.42	1.95	4.42	3.14	0.35	100	2.01		
		UA3623-18	73.74	0.26	14.51	1.44	0.04	0.41	1.79	4.33	3.22	0.32	100	1.47		
		UA3623-30	74.38	0.19	14.13	1.34	0.06	0.29	1.57	4.45	3.33	0.35	100	0.23		
		UA3623-10	74.41	0.18	13.80	1.32	0.03	0.28	1.41	4.77	3.39	0.53	100	6.70		
		UA3623-13	74.58	0.23	13.82	1.56	0.07	0.34	1.44	4.21	3.50	0.34	100	2.09		

		UA3623-16	74.58	0.09	13.98	1.14	0.06	0.26	1.59	4.70	3.34	0.33	100	4.60		
		UA3623-20	74.93	0.18	13.69	1.41	0.05	0.27	1.48	4.31	3.36	0.42	100	13.92		
		UA3623-14	74.94	0.11	13.92	1.26	0.04	0.25	1.50	4.38	3.38	0.30	100	0.98		
		UA3623-3	75.15	0.10	13.71	0.96	0.04	0.23	1.44	4.61	3.48	0.36	100	3.97		
		UA3623-1	75.20	0.20	13.65	1.01	0.03	0.19	1.39	4.27	3.73	0.39	100	3.21		
		UA3623-12	75.39	0.14	13.87	1.02	0.08	0.22	1.45	4.08	3.49	0.36	100	1.69		
		UA3623-24	75.41	0.15	13.65	1.03	0.07	0.15	1.42	4.17	3.70	0.33	100	3.10		
		UA3623-26	75.70	0.13	13.73	1.07	0.05	0.25	1.49	4.02	3.30	0.34	100	1.31		
		UA3623-6	75.76	0.13	13.46	1.07	0.06	0.22	1.35	4.20	3.50	0.33	100	2.24		
		UA3623-7	75.79	0.12	13.50	1.03	0.04	0.20	1.35	4.05	3.66	0.32	100	2.57		
	b	Mean	74.89	0.16	13.87	1.22	0.05	0.27	1.51	4.33	3.43	0.36	100	3.34	15	WRA-like
		StDev	0.72	0.05	0.34	0.21	0.01	0.08	0.16	0.23	0.17	0.06	0	3.34		
		UA3623-23	67.64	1.09	14.51	4.49	0.04	1.23	3.18	4.44	3.30	0.08	100	1.52		
Nov 26, 2020 NaSiTDI		UA3622-13	71.73	0.29	15.20	1.86	0.05	0.47	2.27	4.49	3.33	0.41	100	1.72		
GRV Surface core 8-9 cm		UA3622-7	72.91	0.22	15.09	1.52	0.07	0.40	2.09	4.34	3.08	0.36	100	3.89		
		UA3622-24	73.06	0.22	15.02	1.43	0.08	0.39	1.75	4.71	3.05	0.37	100	4.44		
		UA3622-22	73.17	0.16	14.89	1.48	0.04	0.40	1.91	4.39	3.28	0.36	100	2.28		
		UA3622-5	73.39	0.25	14.41	1.58	0.06	0.43	1.90	4.66	3.08	0.31	100	0.92		
		UA3622-17	73.56	0.24	14.54	1.59	0.06	0.43	1.88	4.28	3.18	0.31	100	1.87		
		UA3622-19	73.89	0.20	14.48	1.66	0.06	0.38	1.69	4.07	3.29	0.34	100	2.65		
		UA3622-23	73.99	0.17	14.35	1.36	0.04	0.34	1.71	4.48	3.33	0.30	100	1.32		
		UA3622-1	74.27	0.15	14.07	1.30	0.05	0.29	1.66	4.53	3.40	0.37	100	2.52		
		UA3622-27	74.68	0.19	14.15	1.18	0.05	0.25	1.50	4.44	3.32	0.31	100	3.22		
		UA3622-25	74.79	0.14	13.84	1.19	0.03	0.21	1.48	4.46	3.57	0.36	100	1.77		
		UA3622-6	74.96	0.14	13.98	1.18	0.11	0.26	1.43	4.41	3.27	0.33	100	4.68		

		UA3622-8	75.07	0.21	13.62	1.33	0.05	0.28	1.33	4.41	3.46	0.31	100	2.54		
		UA3622-3	75.20	0.17	13.59	1.21	0.12	0.24	1.44	4.62	3.18	0.28	100	0.56		
		UA3622-21	75.25	0.13	13.67	1.30	0.00	0.24	1.47	4.10	3.60	0.32	100	1.32		
		UA3622-10	75.44	0.17	13.78	1.24	0.06	0.27	1.47	4.02	3.34	0.27	100	2.09		
		UA3622-20	75.46	0.19	13.45	1.01	0.08	0.18	1.35	3.95	4.08	0.33	100	0.19		
		UA3622-12	75.59	0.17	13.83	1.17	0.06	0.27	1.47	3.91	3.29	0.31	100	2.84		
		UA3622-15	76.07	0.36	12.87	1.53	0.09	0.29	1.42	4.25	2.99	0.17	100	1.20		
	a	Mean	74.34	0.20	14.15	1.38	0.06	0.32	1.64	4.34	3.32	0.32	100	2.21	19	WRA-like
		StDev	1.14	0.06	0.62	0.21	0.03	0.08	0.26	0.24	0.25	0.05	0	1.23		
		UA3622-4	71.21	0.08	17.00	0.82	0.00	0.10	2.84	5.50	2.32	0.17	100	2.45		
		UA3622-30	71.56	0.11	16.46	0.90	0.01	0.18	2.73	5.66	2.24	0.18	100	1.75		
		UA3622-16	72.19	0.03	16.47	1.00	0.04	0.15	2.66	5.03	2.27	0.19	100	2.45		
	b	Mean	71.65	0.07	16.64	0.91	0.02	0.14	2.75	5.40	2.28	0.18	100	2.21	3	Unknown population. lower K, High Na
		StDev	0.50	0.04	0.31	0.09	0.02	0.04	0.09	0.33	0.04	0.01	0	0.40		
		UA3622-2	74.68	0.24	13.69	1.51	0.06	0.42	1.52	4.12	3.48	0.37	100	2.82		
		UA3622-18	72.98	0.17	15.23	1.21	0.01	0.26	1.98	5.02	2.96	0.24	100	2.53		
		UA3622-14	60.11	1.37	16.10	6.76	0.09	3.29	6.15	4.17	1.88	0.10	100	2.07		
		UA3622-26	68.07	1.14	14.32	4.22	0.07	1.29	3.12	4.11	3.58	0.11	100	1.35		
		UA3622-11	68.21	0.59	15.79	3.25	0.12	1.10	3.36	4.92	2.49	0.22	100	2.82		
		UA3622-29	74.09	0.08	15.00	0.83	0.05	0.15	1.88	4.90	2.82	0.25	100	3.22		
		UA3622-28	74.62	0.38	13.19	2.00	0.07	0.47	2.15	4.94	1.95	0.29	100	0.29		
Nov 26, 2020 NaSiTDI		UA3621-2	72.75	0.22	15.29	1.42	0.04	0.36	2.12	4.57	2.96	0.33	100	2.45		
GRV Surface core 13-14 cm		UA3621-3	73.24	0.24	14.57	1.45	0.06	0.41	1.80	4.58	3.35	0.39	100	1.70		

	UA3621-8	73.41	0.21	14.51	1.59	0.04	0.44	1.88	4.09	3.54	0.38	100	1.13		
	UA3621-18	73.53	0.17	14.51	1.41	0.08	0.35	1.84	4.51	3.35	0.35	100	2.78		
	UA3621-23	73.73	0.21	14.61	1.51	0.01	0.33	1.81	4.33	3.22	0.32	100	2.66		
	UA3621-7	73.83	0.28	14.23	1.49	0.05	0.36	1.74	4.54	3.20	0.35	100	0.11		
	UA3621-11	73.89	0.13	14.38	1.41	0.05	0.38	1.70	4.57	3.19	0.38	100	0.83		
	UA3621-24	74.51	0.15	14.27	1.22	0.05	0.26	1.47	4.75	3.09	0.30	100	2.87		
	UA3621-1	74.68	0.15	14.05	1.23	0.04	0.32	1.49	4.67	3.15	0.29	100	4.05		
	UA3621-22	74.69	0.13	13.80	1.20	0.05	0.23	1.51	4.45	3.61	0.44	100	8.75		
	UA3621-20	75.12	0.10	13.82	1.11	0.04	0.26	1.50	3.96	3.78	0.39	100	1.92		
	UA3621-4	75.17	0.17	13.70	1.21	0.05	0.24	1.46	3.91	3.80	0.37	100	1.58		
	UA3621-17	75.25	0.11	13.62	1.05	0.05	0.18	1.39	4.30	3.78	0.35	100	2.84		
	UA3621-6	75.41	0.18	13.63	1.46	0.08	0.30	1.33	4.14	3.26	0.28	100	1.88		
	UA3621-27	75.62	0.20	13.55	1.40	0.04	0.28	1.26	3.97	3.43	0.31	100	1.92		
	UA3621-9	75.96	0.16	13.59	1.15	0.02	0.20	1.36	3.68	3.63	0.31	100	3.73		
a	Mean	75.07	0.18	13.77	1.30	0.04	0.28	1.48	4.23	3.40	0.32	100	2.59		
	StDev	1.63	0.05	0.88	0.17	0.02	0.09	0.36	0.40	0.27	0.07	0	2.09	16	WRA-like, messy
	UA3621-10	67.34	0.79	15.60	4.36	0.14	1.21	3.33	4.44	2.64	0.20	100	1.25		
	UA3621-30	69.16	0.78	15.20	3.56	0.19	0.90	2.49	4.78	2.82	0.18	100	1.85		
	UA3621-14	69.25	0.77	14.92	3.48	0.15	0.79	2.27	5.30	2.93	0.18	100	1.34		
b	Mean	68.58	0.78	15.24	3.80	0.16	0.97	2.70	4.84	2.80	0.18	100	1.48		
	StDev	1.08	0.01	0.34	0.49	0.02	0.22	0.56	0.44	0.15	0.01	0	0.32	3	Unknown population
	UA3621-28	78.77	0.10	11.92	1.07	0.09	0.12	0.70	3.07	3.87	0.37	100	7.00		
	UA3621-26	78.15	0.18	12.06	1.14	0.01	0.09	0.75	4.20	3.25	0.21	100	1.03		
	UA3621-13	76.52	0.20	12.77	1.38	0.05	0.28	1.24	4.07	3.34	0.18	100	2.33		
	UA3621-5	77.19	0.22	12.47	1.11	0.01	0.24	1.15	4.36	3.15	0.15	100	0.31		
c	Mean	77.66	0.17	12.31	1.17	0.04	0.18	0.96	3.92	3.40	0.23	100	2.67	4	Unknown population
	StDev	1.00	0.05	0.39	0.14	0.04	0.09	0.27	0.58	0.32	0.10	0	3.01		

	UA3621-21	75.99	0.31	12.83	1.91	0.09	0.43	2.07	4.16	1.97	0.33	100	3.78
	UA3621-29	75.12	0.33	13.33	1.80	0.07	0.49	2.08	4.35	1.99	0.56	100	13.20
	UA3621-19	73.26	0.25	14.52	1.40	0.04	0.38	1.87	3.46	4.64	0.25	100	1.45
Nov 26, 2020 NaSiTDI	UA3620-30	72.38	0.27	15.05	1.67	0.05	0.46	2.11	4.38	3.38	0.32	100	2.28
GRV Surface core 18-19 cm	UA3620-13	73.23	0.18	14.52	1.63	0.03	0.51	1.98	4.38	3.21	0.42	100	4.85
	UA3620-9	73.45	0.26	14.55	1.61	0.05	0.39	1.92	4.45	3.04	0.37	100	1.63
	UA3620-4	73.53	0.26	14.45	1.57	0.05	0.37	1.79	4.41	3.28	0.35	100	1.31
	UA3620-26	73.53	0.27	14.51	1.56	0.07	0.39	1.93	4.39	3.05	0.39	100	3.09
	UA3620-23	73.81	0.22	14.39	1.39	0.02	0.34	1.74	4.52	3.30	0.35	100	0.91
	UA3620-24	74.06	0.29	14.38	1.43	0.05	0.32	1.64	4.22	3.35	0.31	100	1.39
	UA3620-19	74.22	0.19	14.15	1.62	0.09	0.39	1.54	4.06	3.45	0.38	100	2.47
	UA3620-10	74.24	0.19	14.34	1.42	0.06	0.36	1.70	3.92	3.48	0.39	100	1.58
	UA3620-28	74.27	0.15	14.34	1.40	0.04	0.33	1.54	4.32	3.29	0.42	100	9.88
	UA3620-7	74.29	0.16	14.34	1.29	0.07	0.34	1.59	4.24	3.38	0.37	100	1.57
	UA3620-12	74.69	0.14	14.10	1.22	0.03	0.30	1.57	4.17	3.52	0.33	100	2.71
	UA3620-21	74.81	0.21	14.13	1.24	0.04	0.26	1.58	3.98	3.53	0.29	100	2.08
	UA3620-1	74.83	0.14	14.07	1.25	0.09	0.29	1.49	4.25	3.36	0.30	100	1.30
	UA3620-11	74.87	0.16	14.13	1.27	0.04	0.26	1.50	4.17	3.40	0.25	100	2.06
	UA3620-25	74.98	0.21	13.95	1.40	0.06	0.33	1.42	4.02	3.39	0.29	100	1.20
	UA3620-8	75.21	0.12	13.60	1.07	0.02	0.22	1.44	4.17	3.88	0.35	100	2.98
	UA3620-14	75.51	0.17	13.51	1.12	0.08	0.20	1.38	4.10	3.66	0.34	100	1.23
	UA3620-22	75.63	0.08	13.51	1.12	0.06	0.18	1.40	4.06	3.69	0.34	100	1.19
	UA3620-16	75.73	0.14	13.43	1.00	0.03	0.18	1.41	4.29	3.52	0.36	100	1.42
	UA3620-5	75.83	0.16	13.50	1.05	0.06	0.21	1.40	3.73	3.82	0.34	100	1.69
	UA3620-6	76.19	0.18	13.13	1.29	0.06	0.24	1.00	3.81	3.76	0.42	100	2.88

		UA3620-3	77.02	0.19	12.88	1.13	0.08	0.19	1.04	3.83	3.46	0.24	100	1.30		
	a	Mean	74.57	0.19	14.05	1.34	0.05	0.31	1.58	4.16	3.47	0.34	100	2.23	23	WRAe, follows K trend of WRAe rather than WRAn
		StDev	1.09	0.05	0.52	0.20	0.02	0.09	0.27	0.21	0.24	0.05	0	1.87		
		UA3620-20	73.33	0.21	14.35	1.50	0.06	0.40	1.89	4.06	3.96	0.31	100	0.50		WRA, but higher K
		UA3620-29	61.50	0.28	18.48	4.57	0.14	0.13	1.01	8.15	5.61	0.18	100	1.23		
		UA3620-27	68.50	1.08	14.28	4.29	0.10	1.23	3.40	3.76	3.30	0.07	100	1.93		
		UA3620-18	70.17	0.17	17.13	1.18	0.05	0.28	2.98	5.13	2.71	0.24	100	1.02		
		UA3620-17	71.46	0.18	16.37	1.08	0.03	0.24	2.50	5.38	2.64	0.16	100	2.70		
Jun 8, 2020 NaTDI GRV17 7-8 cm		UA3526-18	75.95	0.22	14.09	0.84	0.06	0.39	1.17	4.87	2.41	0.00	100	3.68		
		UA3526-8	76.05	0.35	13.13	1.92	0.00	0.46	2.12	3.71	2.00	0.33	100	1.89		
		Mean	76.00	0.28	13.61	1.38	0.03	0.42	1.64	4.29	2.21	0.17	100	2.78	2	not quite WRA, but something else
		StDev	0.07	0.09	0.68	0.76	0.04	0.05	0.67	0.82	0.29	0.23	0	1.27		
		UA3526-16	77.54	0.13	12.76	1.16	0.07	0.16	0.87	3.59	3.46	0.33	100	4.70		
		UA3526-19	77.93	0.10	12.39	1.12	0.08	0.21	0.95	3.46	3.55	0.29	100	1.98		
		Mean	77.74	0.11	12.58	1.14	0.07	0.19	0.91	3.52	3.50	0.31	100	3.34	2	could be extended tail of WRA, but I think it may be related to a different eruption
		StDev	0.28	0.02	0.27	0.03	0.01	0.04	0.06	0.09	0.06	0.03	0	1.92		
		UA3526-23	72.87	0.43	14.55	1.97	0.03	0.51	1.60	5.01	2.86	0.20	100	1.11		
		UA3526-15	73.33	0.20	14.45	1.66	0.07	0.46	1.97	4.36	3.24	0.34	100	2.77		
		UA3526-13	73.43	0.22	14.38	1.56	0.05	0.42	1.93	4.47	3.27	0.35	100	2.42		
		UA3526-4	73.65	0.34	14.49	1.63	0.05	0.45	1.77	4.23	3.21	0.26	100	2.15		

	UA3526-14	74.24	0.25	14.25	1.33	0.07	0.33	1.61	4.49	3.17	0.36	100	1.19		
	UA3526-11	74.28	0.19	14.29	1.41	0.06	0.30	1.69	4.32	3.21	0.31	100	2.11		
	UA3526-12	74.77	0.12	14.07	1.36	0.07	0.35	1.69	4.10	3.26	0.28	100	2.46		
	UA3526-30	74.85	0.18	13.98	1.23	0.08	0.30	1.44	4.46	3.25	0.29	100	2.86		
	UA3526-10	74.92	0.14	14.10	1.45	0.01	0.34	1.54	3.92	3.37	0.28	100	2.62		
	UA3526-29	75.04	0.18	13.90	1.20	0.07	0.28	1.47	4.33	3.31	0.28	100	4.50		
	UA3526-6	75.40	0.17	13.73	1.16	0.00	0.23	1.43	3.90	3.71	0.34	100	1.34		
	UA3526-17	75.50	0.11	13.77	1.14	0.05	0.29	1.45	4.13	3.31	0.32	100	-0.35		
	UA3526-1	75.55	0.17	13.76	1.33	0.06	0.23	1.45	3.86	3.38	0.28	100	2.68		
	UA3526-28	75.84	0.11	13.49	1.01	0.03	0.19	1.36	3.93	3.80	0.32	100	3.24		
a	Mean	74.55	0.20	14.09	1.39	0.05	0.33	1.60	4.25	3.31	0.30	100	2.22	14	WRA-like
	StDev	0.93	0.09	0.33	0.25	0.02	0.09	0.19	0.31	0.23	0.04	0	1.15		
	UA3526-24	65.51	1.09	15.02	4.29	0.06	1.80	3.99	3.79	4.40	0.07	100	1.19		
	UA3526-20	67.11	1.22	14.64	4.43	0.07	1.52	3.58	3.95	3.40	0.09	100	1.70		
	UA3526-26	68.56	1.10	14.40	4.20	0.08	1.27	3.23	3.83	3.27	0.08	100	2.11		
b	Mean	67.06	1.14	14.68	4.31	0.07	1.53	3.60	3.86	3.69	0.08	100	1.66	3	Unknown population
	StDev	1.53	0.08	0.31	0.12	0.01	0.26	0.38	0.08	0.62	0.01	0	0.46		
	UA3526-21	71.07	0.53	15.03	2.38	0.14	0.45	1.67	5.53	3.04	0.20	100	1.40		Aniakchak
	UA3526-2	77.22	0.04	13.04	1.28	0.06	0.00	0.41	1.27	6.58	0.13	100	7.70		weathered?
Jan 22, 2020 NaTDI 9-10 cm	UA 3493-11	73.74	0.24	14.30	1.67	0.04	0.40	1.95	4.18	3.18	0.37	100	6.82		
	UA 3493-29	73.82	0.22	14.53	1.65	0.04	0.40	1.90	4.16	2.99	0.39	100	2.01		
	UA 3493-12	73.99	0.20	14.35	1.65	0.02	0.38	1.86	4.25	3.06	0.29	100	1.08		
	UA 3493-19	74.85	0.13	13.90	1.27	0.03	0.26	1.56	4.09	3.54	0.47	100	3.52		
	UA 3493-27	74.94	0.18	13.99	1.35	0.02	0.29	1.45	4.22	3.30	0.31	100	1.82		

	UA 3493-16	74.97	0.12	14.07	1.34	0.07	0.30	1.67	4.21	3.01	0.31	100	1.06		
	UA 3493-1	75.01	0.20	14.02	1.48	0.08	0.32	1.54	3.80	3.27	0.37	100	3.20		
	UA 3493-13	75.05	0.16	14.02	1.32	0.04	0.36	1.68	3.82	3.27	0.37	100	2.84		
	UA 3493-6	75.41	0.12	13.61	1.26	0.07	0.25	1.49	4.34	3.20	0.32	100	2.83		
	UA 3493-25	75.44	0.14	13.89	1.26	0.07	0.27	1.52	4.14	3.06	0.28	100	1.33		
	UA 3493-28	75.51	0.22	13.77	1.33	0.00	0.31	1.40	3.92	3.29	0.32	100	2.26		
	UA 3493-24	75.51	0.13	13.83	1.27	0.05	0.28	1.47	4.00	3.26	0.24	100	2.28		
	UA 3493-8	75.74	0.14	13.80	1.38	0.09	0.26	1.41	3.85	3.06	0.35	100	3.57		
	UA 3493-22	75.82	0.16	13.72	1.10	0.04	0.20	1.45	3.91	3.35	0.31	100	2.48		
	UA 3493-15	76.06	0.11	13.52	1.06	0.06	0.20	1.44	3.80	3.47	0.37	100	3.00		
	UA 3493-20	76.21	0.13	13.83	1.02	0.03	0.22	1.48	3.74	3.03	0.40	100	4.37		
	UA 3493-9	76.33	0.06	13.65	1.07	0.05	0.16	1.43	3.66	3.32	0.35	100	4.56		
	UA 3493-21	76.47	0.05	13.17	0.97	0.06	0.21	1.34	3.87	3.56	0.40	100	1.41		
a	Mean	75.27	0.15	13.89	1.30	0.05	0.28	1.56	4.00	3.24	0.35	100	2.80	18	WRA-like
	StDev	0.82	0.05	0.32	0.21	0.02	0.07	0.18	0.20	0.18	0.05	0	1.44		
	UA 3493-10	77.47	0.38	12.06	1.58	0.02	0.19	1.11	4.06	2.96	0.21	100	2.18		
	UA 3493-7	78.33	0.30	11.80	1.39	0.02	0.17	1.10	3.66	3.09	0.18	100	1.31		
	UA 3493-14	78.79	0.16	11.77	1.12	0.01	0.11	0.74	4.15	3.01	0.17	100	1.19		
b	Mean	78.19	0.28	11.88	1.37	0.01	0.16	0.98	3.96	3.02	0.19	100	1.56	3	Novarupta-Katmai 1912
	StDev	0.67	0.11	0.16	0.23	0.00	0.04	0.21	0.26	0.07	0.02	0	0.54		
	UA 3493-30	68.96	1.11	14.04	4.18	0.08	1.10	3.22	3.98	3.27	0.09	100	2.23		
	UA 3493-5	73.78	0.22	14.11	1.58	0.06	0.33	1.85	4.77	2.97	0.42	100	4.44		
	UA 3493-18	74.24	0.37	13.63	2.53	0.10	0.31	1.64	4.54	2.47	0.22	100	4.50		
	UA 3493-2	75.71	0.36	12.96	2.00	0.03	0.48	2.28	4.14	1.79	0.32	100	2.56		
	UA 3493-4	73.05	0.22	14.92	1.24	0.05	0.69	2.05	4.90	2.69	0.23	100	3.64		Plag inclusion

Jan 22, 2020
NaTDI

GRV17 17-18 cm

UA 3494-19	73.51	0.26	14.54	1.54	0.10	0.43	1.90	4.30	3.14	0.36	100	2.52
UA 3494-2	73.96	0.25	14.60	1.54	0.04	0.39	1.87	4.15	2.92	0.36	100	2.60
UA 3494-21	74.59	0.13	14.26	1.50	0.06	0.32	1.78	3.98	3.14	0.30	100	5.63
UA 3494-28	74.71	0.17	14.25	1.38	0.05	0.33	1.58	4.15	3.16	0.29	100	2.82
UA 3494-17	74.74	0.21	13.90	1.39	0.08	0.25	1.48	4.47	3.23	0.31	100	2.24
UA 3494-12	74.75	0.16	14.20	1.32	0.06	0.26	1.59	4.40	2.97	0.35	100	1.08
UA 3494-8	74.91	0.15	13.95	1.25	0.09	0.31	1.54	4.40	3.17	0.29	100	2.17
UA 3494-24	75.04	0.11	13.92	1.28	0.04	0.31	1.55	4.44	3.08	0.30	100	2.61
UA 3494-13	75.17	0.21	13.77	1.33	0.05	0.28	1.53	4.22	3.22	0.30	100	1.54
UA 3494-25	75.18	0.17	13.98	1.24	0.05	0.20	1.52	4.41	3.03	0.29	100	3.38
UA 3494-4	75.23	0.12	13.60	1.47	0.07	0.31	1.30	4.20	3.44	0.34	100	2.37
UA 3494-26	75.23	0.19	14.03	1.32	0.02	0.29	1.52	3.83	3.32	0.32	100	4.65
UA 3494-10	75.27	0.12	14.08	1.30	0.06	0.27	1.58	3.94	3.12	0.33	100	2.96
UA 3494-9	75.31	0.22	13.92	1.24	0.05	0.28	1.54	4.12	3.10	0.29	100	0.40
UA 3494-23	75.46	0.14	13.79	1.28	0.04	0.24	1.50	4.14	3.19	0.30	100	2.05
UA 3494-1	75.48	0.21	14.00	1.15	0.02	0.16	1.51	4.01	3.23	0.30	100	3.37
UA 3494-6	75.50	0.17	14.21	1.19	0.05	0.22	1.62	3.90	2.89	0.31	100	3.21
UA 3494-16	75.50	0.18	14.00	1.28	0.09	0.24	1.45	3.79	3.24	0.30	100	2.84
UA 3494-29	75.68	0.17	13.60	1.28	0.09	0.31	1.49	4.12	3.03	0.30	100	1.27
UA 3494-18	75.69	0.12	13.59	1.10	0.04	0.22	1.42	3.90	3.62	0.37	100	2.45
UA 3494-22	75.76	0.24	13.60	1.12	0.06	0.20	1.44	4.32	3.05	0.28	100	1.25
UA 3494-14	76.07	0.13	13.54	1.24	0.05	0.22	1.43	3.93	3.19	0.25	100	1.72
UA 3494-7	76.14	0.12	13.42	1.05	0.03	0.21	1.42	4.15	3.20	0.33	100	0.64
UA 3494-30	76.21	0.20	13.23	1.20	0.03	0.15	1.18	3.96	3.62	0.30	100	1.62
UA 3494-3	77.11	0.18	13.04	0.93	0.03	0.12	1.12	4.04	3.25	0.24	100	3.37

	a	Mean	75.29	0.17	13.88	1.28	0.05	0.26	1.51	4.13	3.18	0.31	100	2.43	25	strongly resembles WRAn. No outliers in this sample
		StDev	0.73	0.04	0.37	0.15	0.02	0.07	0.17	0.20	0.18	0.03	0	1.18		
		UA 3494-27	77.45	0.27	12.52	1.54	0.09	0.36	2.06	3.84	1.73	0.19	100	0.55		
Jun 8, 2020 NaTDI		UA3527-4	72.84	0.28	14.77	1.49	0.04	0.38	2.04	4.71	3.19	0.33	100	2.18		
GRV17 24-25 cm		UA3527-18	73.85	0.15	14.40	1.37	0.06	0.38	1.67	4.76	3.09	0.34	100	2.76		
		UA3527-11	73.90	0.23	14.06	1.62	0.09	0.41	1.61	4.46	3.33	0.36	100	2.08		
		UA3527-20	73.98	0.21	14.10	1.70	0.06	0.41	1.59	4.27	3.38	0.38	100	2.25		
		UA3527-17	74.24	0.21	14.40	1.41	0.05	0.34	1.70	4.28	3.11	0.33	100	6.52		
		UA3527-23	74.34	0.22	14.21	1.47	0.08	0.28	1.57	4.30	3.34	0.24	100	1.94		
		UA3527-7	74.65	0.20	14.02	1.38	0.02	0.35	1.59	4.32	3.16	0.39	100	8.24		
		UA3527-3	74.94	0.15	13.99	1.34	0.02	0.27	1.51	4.35	3.21	0.27	100	1.77		
		UA3527-21	74.98	0.33	13.60	1.59	0.08	0.39	1.48	3.83	3.46	0.34	100	2.29		
		UA3527-22	75.09	0.17	13.79	1.26	0.05	0.27	1.44	4.51	3.19	0.30	100	3.12		
		UA3527-10	75.14	0.20	13.79	1.23	0.07	0.24	1.47	4.25	3.36	0.33	100	1.75		
		UA3527-12	75.16	0.20	13.59	1.53	0.02	0.36	1.39	4.00	3.48	0.35	100	2.20		
		UA3527-6	75.43	0.27	13.94	1.20	0.02	0.30	1.51	3.93	3.18	0.28	100	3.04		
		UA3527-13	75.88	0.17	13.47	1.34	0.09	0.31	1.28	3.67	3.56	0.28	100	3.33		
		UA3527-25	76.00	0.24	13.14	1.46	0.04	0.35	1.21	3.71	3.60	0.31	100	4.84		
		UA3527-2	76.06	0.20	13.38	1.43	0.05	0.36	1.24	3.57	3.46	0.34	100	1.68		
		UA3527-1	76.22	0.14	13.10	1.34	0.01	0.27	1.04	4.10	3.53	0.34	100	1.76		
		UA3527-14	76.73	0.07	12.97	1.12	0.04	0.15	1.12	4.13	3.47	0.25	100	2.80		
		UA3527-16	77.19	0.25	12.93	1.16	0.06	0.35	1.18	3.64	3.12	0.14	100	1.77		
	a	Mean	75.09	0.21	13.77	1.39	0.05	0.32	1.46	4.15	3.33	0.31	100	2.96	19	Main WRAn peak
		StDev	1.10	0.06	0.52	0.16	0.02	0.07	0.24	0.35	0.17	0.06	0	1.76		

	UA3527-15	72.13	0.20	15.03	2.02	0.05	0.10	0.67	5.70	3.98	0.15	100	4.86	
	UA3527-26	76.35	0.17	13.64	0.54	0.08	0.04	0.84	2.73	5.52	0.10	100	6.21	Likely WRA, but bad point
Jan 22, 2020 NaTDI	UA 3495-14	73.77	0.21	14.86	1.61	0.11	0.37	1.99	3.87	2.94	0.35	100	3.00	
GRV17 25-26 cm	UA 3495-13	74.14	0.20	14.53	1.51	0.09	0.37	1.82	4.14	2.94	0.35	100	3.16	
	UA 3495-20	74.34	0.12	14.35	1.20	0.04	0.25	1.74	4.79	2.97	0.29	100	2.31	
	UA 3495-2	74.57	0.20	14.16	1.32	0.08	0.33	1.57	4.51	3.01	0.31	100	1.63	
	UA 3495-15	74.71	0.21	13.99	1.43	0.05	0.27	1.47	4.38	3.24	0.32	100	2.03	
	UA 3495-3	74.73	0.27	14.25	1.40	0.04	0.30	1.63	3.99	3.16	0.31	100	2.67	
	UA 3495-21	74.77	0.20	14.61	1.44	0.03	0.33	1.66	3.82	2.91	0.32	100	4.09	
	UA 3495-22	74.78	0.15	14.10	1.43	0.05	0.34	1.67	4.12	3.12	0.30	100	0.81	
	UA 3495-18	74.89	0.17	14.01	1.43	0.04	0.26	1.47	4.16	3.33	0.30	100	2.60	
	UA 3495-17	74.91	0.19	13.73	1.35	0.02	0.31	1.47	4.62	3.17	0.32	100	1.87	
	UA 3495-30	74.92	0.17	14.17	1.29	0.04	0.30	1.62	4.13	3.11	0.30	100	1.84	
	UA 3495-23	74.94	0.18	14.12	1.28	0.04	0.28	1.56	4.27	3.10	0.30	100	1.38	
	UA 3495-5	74.95	0.16	14.48	1.20	0.05	0.26	1.69	4.03	2.96	0.28	100	2.02	
	UA 3495-7	74.96	0.21	14.08	1.46	0.06	0.28	1.62	3.70	3.38	0.34	100	1.80	
	UA 3495-11	75.02	0.18	13.89	1.14	0.07	0.27	1.51	4.47	3.24	0.26	100	2.83	
	UA 3495-29	75.26	0.13	13.86	1.21	0.05	0.28	1.47	4.34	3.16	0.31	100	2.13	
	UA 3495-10	75.31	0.14	14.04	1.36	0.07	0.28	1.51	3.80	3.23	0.35	100	4.14	
	UA 3495-19	75.32	0.18	13.66	1.21	0.05	0.26	1.44	4.36	3.29	0.30	100	2.50	
	UA 3495-16	75.45	0.13	13.82	1.21	0.08	0.25	1.53	4.16	3.12	0.34	100	2.15	
	UA 3495-27	75.62	0.17	13.75	1.20	0.01	0.25	1.52	4.14	3.10	0.30	100	2.63	
	UA 3495-28	75.78	0.15	13.72	1.29	0.03	0.25	1.50	3.72	3.30	0.34	100	1.73	
	UA 3495-6	75.82	0.21	13.65	1.32	0.04	0.30	1.36	3.60	3.48	0.28	100	2.89	
	UA 3495-8	76.58	0.11	13.36	1.12	0.06	0.14	1.21	3.94	3.28	0.25	100	3.38	

		UA 3495-26	76.64	0.11	13.47	0.97	0.02	0.16	1.33	3.73	3.29	0.36	100	4.27		
		UA 3495-1	77.13	0.15	12.49	1.44	0.07	0.30	0.83	3.84	3.48	0.35	100	4.28		May have microlite
	a	Mean	75.17	0.17	13.97	1.31	0.05	0.28	1.53	4.10	3.17	0.31	100	2.57		WRAn
		StDev	0.77	0.04	0.47	0.14	0.02	0.05	0.21	0.31	0.16	0.03	0	0.93		
		UA 3495-12	68.55	0.15	16.12	3.47	0.12	1.46	2.63	5.47	1.95	0.12	100	-0.68		
		UA 3495-25	69.64	1.27	14.82	4.39	0.03	1.38	3.26	2.53	2.61	0.08	100	5.00		
Jan 23, 2020 NaTDI		UA 3496-20	74.74	0.34	13.91	1.93	0.11	0.40	2.28	4.28	1.85	0.23	100	1.76		
GRV17 31-32 cm		UA 3496-25	74.76	0.37	13.85	2.13	0.14	0.48	2.39	3.89	1.81	0.24	100	1.93		
	b	Mean	74.75	0.35	13.88	2.03	0.13	0.44	2.34	4.08	1.83	0.24	100	1.84	2	Similar to Hayes set H, but off on K and Cl
		StDev	0.01	0.02	0.04	0.14	0.02	0.06	0.08	0.28	0.03	0.01	0	0.12		
		UA 3496-1	72.61	0.55	14.70	2.21	0.15	0.51	1.57	4.42	3.12	0.20	100	1.83		
		UA 3496-29	72.59	0.21	15.07	1.64	0.08	0.42	2.16	4.61	2.94	0.39	100	1.78		
		UA 3496-22	74.31	0.23	14.27	1.51	0.05	0.35	1.69	4.12	3.21	0.34	100	3.36		
		UA 3496-13	74.32	0.20	14.13	1.44	0.06	0.36	1.63	4.45	3.18	0.30	100	2.81		
		UA 3496-31	74.35	0.22	14.10	1.30	0.02	0.32	1.58	4.47	3.29	0.45	100	2.53		Possible plag?
		UA 3496-18	74.45	0.20	14.57	1.21	0.06	0.24	1.75	4.36	2.95	0.25	100	1.71		
		UA 3496-23	74.94	0.21	14.08	1.27	0.06	0.28	1.56	3.99	3.37	0.29	100	1.82		
		UA 3496-3	75.08	0.23	14.40	1.25	0.01	0.27	1.63	3.89	3.04	0.25	100	3.12		
		UA 3496-7	75.18	0.25	13.73	1.39	0.08	0.31	1.44	4.18	3.18	0.33	100	3.26		
		UA 3496-28	75.31	0.17	13.88	1.33	0.04	0.29	1.48	3.93	3.36	0.29	100	2.61		
		UA 3496-14	75.37	0.15	13.76	1.36	0.04	0.29	1.51	4.02	3.22	0.35	100	1.30		
		UA 3496-32	75.51	0.16	13.77	1.22	0.05	0.26	1.57	4.19	3.06	0.27	100	1.83		
		UA 3496-12	75.51	0.14	13.74	1.32	0.03	0.27	1.48	4.04	3.26	0.28	100	2.86		
		UA 3496-27	75.74	0.24	13.61	1.16	0.00	0.29	1.46	4.13	3.15	0.29	100	1.46		

		UA 3496-21	75.80	0.12	13.86	1.22	0.07	0.27	1.46	3.67	3.30	0.29	100	3.19		
		UA 3496-4	75.90	0.17	13.88	1.17	0.07	0.22	1.46	3.72	3.24	0.22	100	2.60		
		UA 3496-19	76.69	0.15	13.13	1.35	0.06	0.27	1.21	3.53	3.37	0.32	100	2.68		
		UA 3496-5	76.83	0.22	12.60	1.69	0.06	0.44	0.98	3.70	3.22	0.33	100	1.89		
	a	Mean	75.03	0.21	13.96	1.39	0.06	0.32	1.53	4.08	3.19	0.30	100	2.37	18	WRAn, wider range of Si than any of the above depths
		StDev	1.14	0.09	0.56	0.25	0.03	0.07	0.23	0.31	0.13	0.06	0	0.67		
		UA 3496-15	71.42	0.52	15.24	2.49	0.17	0.53	1.74	4.81	2.93	0.20	100	2.82		Aniakchak
		UA 3496-24	74.47	0.34	13.45	2.03	0.09	0.24	1.17	4.33	3.69	0.23	100	0.48		
		UA 3496-26	77.61	0.25	12.45	1.68	0.05	0.39	2.13	3.59	1.70	0.21	100	0.45		
		UA 3496-6	72.82	0.20	15.44	1.09	0.00	0.22	2.26	5.13	2.64	0.25	100	-0.27		Plag inclusion
		UA 3496-2	72.82	0.17	15.47	1.12	0.07	0.24	2.36	5.03	2.51	0.26	100	0.98		Plag inclusion
		UA 3496-10	74.15	0.13	15.04	0.83	0.02	0.12	2.46	4.81	2.30	0.17	100	2.07		Plag inclusion
		UA 3496-9	76.95	0.06	13.14	0.43	0.06	0.03	0.83	3.37	5.05	0.09	100	2.87		Weathered/detrital?
		UA 3496-16	76.97	0.10	13.36	0.55	0.06	0.08	0.86	2.82	5.13	0.08	100	3.36		Weathered/detrital?
		UA 3496-17	79.24	0.10	12.58	1.06	0.03	0.00	0.42	1.14	5.35	0.11	100	8.84		Weathered/detrital?

Jan 23, 2020 NaTDI																
		UA 3497-28	74.10	0.35	13.83	2.08	0.12	0.54	2.37	4.54	1.89	0.23	100	1.85		
GRV17 32-33 cm		UA 3497-27	74.35	0.32	13.74	1.98	0.18	0.44	2.37	4.45	1.97	0.25	100	1.04		
	b	Mean	74.22	0.33	13.79	2.03	0.15	0.49	2.37	4.49	1.93	0.24	100	1.44	2	Similar to Hayes set H,

	StDev	0.17	0.02	0.07	0.07	0.04	0.07	0.01	0.06	0.06	0.02	0	0.57		but off on K and Cl
	UA 3497-18	72.41	0.25	15.41	1.60	0.07	0.37	2.39	4.29	2.98	0.30	100	4.42		Possible plag?
	UA 3497-10	73.65	0.17	14.47	1.63	0.03	0.43	1.95	4.12	3.26	0.37	100	1.48		
	UA 3497-30	73.87	0.25	14.41	1.39	0.07	0.34	1.74	4.41	3.27	0.32	100	3.36		
	UA 3497-4	74.05	0.19	14.66	1.54	0.04	0.36	1.77	3.92	3.22	0.33	100	2.89		
	UA 3497-1	74.28	0.16	14.25	1.45	0.03	0.34	1.68	4.33	3.25	0.30	100	2.46		
	UA 3497-16	74.57	0.20	14.29	1.28	0.05	0.31	1.74	4.28	3.05	0.30	100	2.03		
	UA 3497-19	74.57	0.14	14.14	1.37	0.04	0.24	1.67	4.18	3.40	0.32	100	2.52		
	UA 3497-3	74.64	0.19	14.29	1.48	0.06	0.38	1.69	3.92	3.09	0.34	100	2.89		
	UA 3497-24	74.69	0.14	14.25	1.42	0.07	0.32	1.67	4.11	3.08	0.32	100	2.34		
	UA 3497-23	74.83	0.13	14.07	1.30	0.03	0.27	1.60	4.10	3.39	0.36	100	2.47		
	UA 3497-22	74.89	0.14	14.35	1.25	0.05	0.26	1.58	4.12	3.15	0.27	100	2.69		
	UA 3497-5	75.02	0.22	14.16	1.37	0.10	0.26	1.56	3.93	3.13	0.33	100	3.37		
	UA 3497-25	75.23	0.18	13.74	1.22	0.06	0.29	1.53	4.29	3.26	0.25	100	2.39		
	UA 3497-21	75.23	0.21	13.91	1.20	0.06	0.28	1.52	4.18	3.17	0.30	100	2.85		
	UA 3497-29	75.32	0.15	13.93	1.25	0.02	0.28	1.52	3.97	3.31	0.31	100	2.42		
	UA 3497-8	75.43	0.16	13.87	1.19	0.02	0.29	1.49	4.02	3.33	0.26	100	2.85		
	UA 3497-6	75.46	0.17	13.93	1.24	0.04	0.23	1.45	4.17	3.10	0.26	100	2.93		
	UA 3497-14	75.61	0.15	13.81	1.20	0.09	0.24	1.41	3.99	3.31	0.27	100	2.14		
	UA 3497-7	75.69	0.16	13.88	1.26	0.02	0.26	1.47	3.85	3.20	0.27	100	3.85		
	UA 3497-20	75.75	0.17	13.72	1.38	0.06	0.25	1.41	3.77	3.25	0.29	100	3.70		
	UA 3497-26	76.29	0.20	13.24	1.25	0.08	0.25	1.20	3.98	3.28	0.30	100	2.40		
a	Mean	74.83	0.18	14.13	1.35	0.05	0.30	1.62	4.09	3.21	0.30	100	2.78	21	WRAn, with slightly less Si range than 31-32 cm
	StDev	0.86	0.03	0.43	0.13	0.02	0.05	0.24	0.17	0.11	0.03	0	0.67		

		UA 3497-15	74.55	0.16	15.57	1.31	0.08	0.30	2.36	2.57	2.88	0.28	100	4.30		
		UA 3497-17	77.79	0.18	12.78	1.09	0.10	0.30	1.56	3.69	2.33	0.22	100	4.29		
		UA 3497-2	77.88	0.30	12.07	1.58	0.02	0.22	1.14	3.62	3.05	0.16	100	2.29		
		UA 3497-9	73.73	0.11	15.03	1.20	0.05	0.23	1.95	4.73	2.71	0.34	100	2.00		Plag inclusion
		UA 3497-13	79.12	0.22	14.49	1.36	0.05	0.27	1.59	0.67	1.96	0.34	100	6.25		
		UA 3497-12	79.38	0.12	14.10	1.27	0.08	0.24	1.52	0.63	2.44	0.28	100	5.96		
		UA 3497-11	79.50	0.16	14.03	1.27	0.07	0.28	1.50	0.74	2.22	0.30	100	6.27		
Dec 18, 2020 NaTDI		UA3491-23	70.75	0.56	14.83	2.45	0.19	0.54	1.78	5.83	2.90	0.22	100	0.24		
GRV17 34-35 cm		UA3491-19	71.66	0.48	14.81	2.45	0.14	0.50	1.71	5.14	2.94	0.23	100	0.13		
	b	Mean	71.20	0.52	14.82	2.45	0.16	0.52	1.75	5.49	2.92	0.23	100	0.19	2	Aniakchak
		StDev	0.64	0.05	0.02	0.00	0.04	0.03	0.05	0.49	0.03	0.01	0	0.08		
		UA3491-4	74.38	0.22	14.35	1.47	0.05	0.32	1.65	4.15	3.11	0.35	100	1.56		
		UA3491-10	74.41	0.17	14.00	1.37	0.06	0.34	1.60	4.70	3.03	0.41	100	1.65		
		UA3491-24	74.80	0.17	14.19	1.27	0.05	0.28	1.55	4.23	3.19	0.37	100	2.05		
		UA3491-9	75.23	0.15	13.60	1.08	0.04	0.23	1.47	4.41	3.55	0.31	100	1.31		
		UA3491-8	75.25	0.13	13.32	1.31	0.07	0.30	1.31	4.62	3.42	0.35	100	0.34		
		UA3491-7	75.29	0.20	13.71	1.29	0.06	0.30	1.40	4.14	3.37	0.30	100	1.18		
		UA3491-18	75.29	0.13	14.24	1.12	0.01	0.20	1.65	4.20	2.98	0.24	100	2.88		Plag?
		UA3491-17	75.45	0.17	13.64	1.31	0.06	0.30	1.47	4.01	3.35	0.31	100	1.51		
		UA3491-2	75.47	0.13	13.52	1.21	0.05	0.27	1.39	4.18	3.50	0.37	100	1.40		
		UA3491-12	75.52	0.13	13.83	1.22	0.02	0.24	1.53	4.02	3.23	0.33	100	2.31		
		UA3491-13	75.66	0.14	13.52	1.23	0.05	0.26	1.49	4.19	3.23	0.30	100	0.45		
		UA3491-3	75.81	0.21	13.59	1.21	0.05	0.21	1.37	4.09	3.24	0.28	100	2.03		
		UA3491-25	76.09	0.15	13.45	1.09	0.04	0.17	1.31	4.07	3.34	0.38	100	1.87		
	a	Mean	75.28	0.16	13.77	1.24	0.05	0.26	1.48	4.23	3.27	0.33	100	1.58	13	WRA-like. Tighter range of Si

		StDev	0.50	0.03	0.33	0.11	0.02	0.05	0.12	0.22	0.17	0.05	0	0.70		
		UA3491-1	71.17	0.52	14.95	2.80	0.05	0.35	1.19	4.28	4.59	0.13	100	2.77		
		UA3491-15	73.75	0.31	13.55	1.87	0.07	0.47	1.62	3.96	3.78	0.81	100	2.27		
		UA3491-14	75.72	0.36	13.10	1.43	0.02	0.24	1.08	3.36	4.62	0.09	100	1.77		
		UA3491-20	76.41	0.23	13.90	0.90	0.00	0.14	2.87	4.35	1.10	0.12	100	1.26		
		UA3491-21	76.66	0.21	12.91	1.51	0.06	0.38	2.17	3.96	1.88	0.35	100	3.60		
		UA3491-22	79.28	0.18	11.81	0.76	0.05	0.24	0.44	3.82	3.39	0.05	100	2.45		
Jan 23, 2020 NaTDI		UA 3498-12	70.91	0.50	15.11	2.46	0.15	0.59	1.82	5.22	3.03	0.27	100	1.71		
GRV17 40-41 cm		UA 3498-18	71.44	0.47	14.96	2.53	0.14	0.50	1.77	5.01	3.03	0.20	100	1.52		
	b	Mean	71.17	0.49	15.04	2.49	0.15	0.54	1.80	5.11	3.03	0.23	100	1.61	2	Aniakchak
		StDev	0.38	0.02	0.10	0.05	0.01	0.07	0.04	0.15	0.00	0.05	0	0.13		
		UA 3498-26	73.49	0.20	14.91	1.49	0.05	0.42	2.04	3.85	3.29	0.32	100	2.55		
		UA 3498-3	73.57	0.20	14.89	1.61	0.06	0.41	2.03	3.93	3.05	0.31	100	3.46		
		UA 3498-1	73.60	0.22	14.45	1.61	0.03	0.38	1.96	4.32	3.14	0.36	100	2.29		
		UA 3498-22	73.91	0.18	14.42	1.67	0.04	0.43	1.93	4.11	2.99	0.40	100	2.26		
		UA 3498-13	74.25	0.27	14.34	1.47	0.01	0.38	1.74	3.96	3.33	0.32	100	3.38		
		UA 3498-2	74.29	0.21	14.02	1.82	0.06	0.40	1.69	3.90	3.33	0.35	100	3.92		
		UA 3498-7	74.39	0.20	14.40	1.35	0.07	0.29	1.67	4.09	3.27	0.35	100	2.96		
		UA 3498-15	74.42	0.22	14.46	1.67	0.03	0.34	1.72	3.56	3.34	0.33	100	1.54		
		UA 3498-8	74.45	0.21	14.21	1.33	0.04	0.33	1.64	4.36	3.12	0.39	100	2.92		
		UA 3498-6	74.50	0.20	13.76	1.55	0.04	0.30	1.64	4.59	3.04	0.47	100	7.52		
		UA 3498-21	74.60	0.17	14.02	1.29	0.06	0.27	1.52	4.50	3.35	0.28	100	1.35		
		UA 3498-23	74.60	0.20	13.93	1.27	0.04	0.28	1.65	4.38	3.32	0.44	100	3.57		
		UA 3498-9	74.90	0.16	14.10	1.30	0.11	0.24	1.57	4.27	3.09	0.33	100	2.59		
		UA 3498-30	74.91	0.18	13.93	1.22	0.07	0.26	1.50	4.57	3.15	0.28	100	2.00		
		UA 3498-19	74.97	0.19	14.03	1.34	0.05	0.32	1.53	4.11	3.21	0.34	100	3.09		

	UA 3498-4	75.26	0.08	13.66	1.37	0.03	0.33	1.51	4.29	3.24	0.30	100	3.79		
	UA 3498-5	75.35	0.15	13.83	1.32	0.09	0.26	1.52	3.94	3.29	0.32	100	2.35		
	UA 3498-10	75.74	0.22	13.81	1.32	0.06	0.24	1.42	3.66	3.30	0.29	100	3.01		
	UA 3498-11	75.75	0.21	13.74	1.25	0.03	0.28	1.45	3.86	3.19	0.30	100	2.85		
	UA 3498-17	75.82	0.12	13.51	1.20	0.07	0.31	1.33	4.10	3.30	0.33	100	1.68		
	UA 3498-29	76.22	0.20	13.23	1.27	0.08	0.23	1.43	3.76	3.25	0.42	100	9.00		
	UA 3498-28	76.22	0.12	13.32	1.00	0.08	0.20	1.39	3.68	3.72	0.35	100	2.88		
a	Mean	74.78	0.19	14.04	1.40	0.05	0.32	1.63	4.08	3.24	0.34	100	3.23	22	WRA-like
	StDev	0.82	0.04	0.44	0.19	0.02	0.07	0.21	0.30	0.15	0.05	0	1.79		
	UA 3498-24	74.15	0.13	14.79	1.03	0.02	0.20	2.03	4.79	2.70	0.21	100	2.41		Plag inclusion
	UA 3498-20	75.53	0.10	13.32	1.04	0.05	0.17	1.36	3.88	4.28	0.35	100	-0.02		
	UA 3498-16	77.28	0.08	13.10	0.97	0.05	0.06	0.61	2.27	5.51	0.09	100	6.60		
	UA 3498-27	77.31	0.30	12.36	1.29	0.08	0.21	1.27	3.83	3.23	0.18	100	1.80		
	UA 3498-25	77.69	0.23	12.96	1.52	0.07	0.35	1.89	3.51	1.68	0.14	100	7.04		

Dec 18, 2020
NaTDI

GRV17 42-43 cm

	UA3490-13	74.87	0.28	13.75	1.82	0.08	0.42	2.26	4.43	1.88	0.26	100	0.55		
	UA3490-7	74.95	0.27	13.45	1.89	0.11	0.47	2.18	4.49	1.99	0.25	100	-0.24		
c	Mean	74.91	0.28	13.60	1.86	0.10	0.44	2.22	4.46	1.94	0.25	100	0.16	2	Same as 2 points in UA 3486, 3497, 3496
	StDev	0.06	0.01	0.21	0.05	0.02	0.03	0.05	0.04	0.08	0.01	0	0.56		
	UA3490-15	77.04	0.26	12.84	1.62	0.02	0.35	2.24	3.95	1.50	0.21	100	1.98		
	UA3490-14	77.43	0.20	12.50	1.55	0.04	0.42	2.17	3.74	1.71	0.31	100	-1.12		
	UA3490-12	77.54	0.23	12.54	1.48	0.08	0.42	2.08	3.87	1.61	0.20	100	0.54		
b	Mean	77.34	0.23	12.63	1.55	0.05	0.39	2.17	3.86	1.61	0.24	100	0.47	3	Unknown, low K
	StDev	0.26	0.03	0.19	0.07	0.03	0.04	0.08	0.11	0.11	0.06	0	1.55		
	UA3490-1	72.98	0.29	14.57	1.65	0.04	0.44	2.03	4.25	3.48	0.36	100	1.02		

	UA3490-8	73.70	0.21	14.32	1.49	0.05	0.33	1.81	4.17	3.45	0.62	100	3.43		
	UA3490-6	74.03	0.36	13.94	1.82	0.10	0.47	1.89	4.35	2.88	0.22	100	2.26		Min inclusion?
	UA3490-17	74.65	0.17	14.31	1.41	0.06	0.36	1.70	4.01	3.08	0.33	100	3.06		
	UA3490-11	74.76	0.12	14.05	1.41	0.05	0.31	1.65	4.18	3.22	0.33	100	0.74		
	UA3490-22	75.21	0.13	13.88	1.16	0.07	0.33	1.48	4.23	3.24	0.34	100	0.87		
	UA3490-26	75.34	0.20	13.80	1.31	0.06	0.25	1.43	3.97	3.39	0.32	100	1.49		
	UA3490-21	75.37	0.27	13.74	1.34	0.04	0.29	1.46	4.17	3.07	0.31	100	0.12		
	UA3490-4	75.38	0.17	13.59	1.34	0.04	0.27	1.46	4.13	3.39	0.31	100	1.01		
	UA3490-2	75.45	0.17	13.78	1.18	0.04	0.27	1.57	4.12	3.21	0.28	100	1.20		
	UA3490-9	75.53	0.21	13.69	1.21	0.03	0.26	1.51	4.15	3.16	0.32	100	1.67		
	UA3490-10	75.60	0.16	13.87	1.29	0.02	0.24	1.41	3.81	3.34	0.33	100	1.84		
	UA3490-19	75.98	0.22	13.33	1.38	0.07	0.27	1.30	3.74	3.49	0.31	100	1.01		
	UA3490-25	77.07	0.20	12.59	1.28	0.09	0.27	1.25	3.93	3.16	0.19	100	2.11		
a	Mean	75.07	0.21	13.82	1.38	0.05	0.31	1.57	4.09	3.25	0.33	100	1.56	14	Mt. Churchill
	StDev	1.01	0.06	0.48	0.18	0.02	0.07	0.22	0.17	0.18	0.10	0	0.91		
	UA3490-20	71.89	0.45	14.95	2.39	0.16	0.48	1.62	4.96	2.94	0.20	100	-0.46		
	UA3490-24	70.31	1.20	13.81	4.21	0.06	0.86	2.44	3.41	3.63	0.10	100	1.11		
	UA3490-3	70.66	0.14	16.86	1.17	0.07	0.28	3.18	4.90	2.53	0.27	100	3.32		
	UA3490-18	73.95	0.38	13.55	2.44	0.03	0.68	2.42	4.37	2.06	0.16	100	1.50		
	UA3490-23	75.14	0.19	14.50	1.03	0.04	0.26	1.76	4.07	2.84	0.21	100	2.20		
	UA3490-5	76.40	0.16	13.67	0.77	0.00	0.13	0.34	4.14	4.17	0.30	100	4.08		
	UA3490-16	79.27	0.16	12.28	1.03	0.05	0.22	1.16	3.37	2.36	0.13	100	5.08		
Dec 18, 2020 NaTDI	UA3489-4	73.45	0.28	14.56	1.78	0.05	0.46	1.94	3.98	3.23	0.35	100	1.37		
GRV17 43-44 cm	UA3489-5	73.90	0.30	14.09	1.88	0.09	0.46	1.73	3.87	3.36	0.42	100	3.23		
	UA3489-11	73.91	0.22	14.55	1.62	0.07	0.42	1.98	3.83	3.12	0.36	100	1.37		
	UA3489-19	74.24	0.20	14.20	1.58	0.08	0.42	1.64	3.91	3.40	0.41	100	2.94		

		UA3489-2	74.32	0.22	14.48	1.46	0.02	0.39	1.87	3.76	3.20	0.36	100	1.89		
		UA3489-22	74.46	0.17	14.48	1.23	0.04	0.25	1.75	4.38	3.04	0.27	100	1.75		
		UA3489-25	74.58	0.18	14.36	1.40	0.04	0.36	1.66	4.00	3.17	0.32	100	3.03		
		UA3489-13	74.70	0.20	14.63	1.06	0.06	0.15	1.69	4.11	3.18	0.28	100	1.70		
		UA3489-3	74.88	0.17	14.38	1.31	0.00	0.31	1.57	3.94	3.18	0.34	100	2.25		
		UA3489-20	75.07	0.21	13.98	1.51	0.05	0.35	1.70	3.79	3.10	0.30	100	3.52		
		UA3489-24	75.15	0.22	14.09	1.34	0.04	0.29	1.58	3.90	3.15	0.32	100	1.25		
		UA3489-9	75.25	0.18	14.14	1.26	0.08	0.26	1.58	3.97	3.05	0.32	100	2.40		
		UA3489-23	75.60	0.15	13.82	1.36	0.05	0.29	1.39	3.83	3.24	0.34	100	2.03		
		UA3489-7	75.70	0.15	13.60	1.25	0.08	0.22	1.41	4.18	3.15	0.32	100	2.23		
		UA3489-15	75.77	0.19	13.39	1.40	0.12	0.25	1.34	3.93	3.35	0.33	100	1.64		
		UA3489-6	75.83	0.11	13.80	1.23	0.02	0.25	1.48	3.94	3.13	0.28	100	1.92		
		UA3489-17	75.86	0.14	13.44	1.48	0.03	0.29	1.33	3.65	3.56	0.28	100	1.55		
		UA3489-12	75.94	0.16	13.43	1.50	0.10	0.36	1.32	3.63	3.27	0.37	100	3.62		
		UA3489-8	76.03	0.17	13.42	1.34	0.07	0.32	1.45	3.90	3.08	0.31	100	0.70		
		UA3489-21	76.16	0.19	13.37	0.97	0.05	0.24	1.41	3.81	3.53	0.37	100	2.85		
		UA3489-10	76.48	0.16	13.60	1.20	0.01	0.24	1.33	3.46	3.31	0.28	100	2.09		
	a	Mean	75.11	0.19	13.99	1.39	0.05	0.31	1.58	3.89	3.23	0.33	100	2.16	21	WRA-like. Broad Si range
		StDev	0.85	0.04	0.45	0.22	0.03	0.08	0.20	0.20	0.15	0.04	0	0.79		
		UA3489-18	75.15	0.25	13.72	1.89	0.09	0.43	2.22	4.20	1.87	0.24	100	-0.66		
		UA3489-1	74.61	0.35	14.05	2.02	0.07	0.46	2.38	3.83	2.03	0.26	100	1.78		
		UA3489-16	74.53	0.18	14.62	1.05	0.06	0.21	1.87	4.59	2.70	0.24	100	0.98		
Jun 8, 2020 NaTDI GRV17 44-45cm		UA3524-13	74.60	0.20	14.18	1.27	0.06	0.24	1.65	4.42	3.13	0.33	100	2.91		
		UA3524-7	74.67	0.24	14.09	1.38	0.03	0.32	1.60	4.42	3.03	0.28	100	1.84		
		UA3524-21	74.74	0.16	13.65	1.40	0.08	0.26	1.39	4.69	3.38	0.31	100	2.39		

	UA3524-4	74.77	0.16	14.20	1.47	0.08	0.34	1.63	3.90	3.23	0.30	100	2.85		
	UA3524-26	74.86	0.20	13.86	1.33	0.05	0.28	1.51	4.16	3.46	0.36	100	6.05		
	UA3524-23	74.88	0.19	13.85	1.30	0.05	0.35	1.46	4.32	3.34	0.31	100	1.86		
	UA3524-15	74.90	0.20	13.92	1.37	0.07	0.34	1.54	4.05	3.37	0.30	100	1.79		
	UA3524-20	74.93	0.20	14.05	1.27	0.05	0.31	1.52	4.12	3.30	0.32	100	2.50		
	UA3524-9	75.07	0.23	14.02	1.40	0.05	0.34	1.56	3.83	3.26	0.33	100	4.19		
	UA3524-10	75.20	0.11	13.87	1.37	0.04	0.31	1.51	4.00	3.35	0.31	100	2.55		
	UA3524-16	78.39	0.20	12.34	1.04	0.07	0.18	1.09	3.30	3.15	0.30	100	3.84		
	UA3524-8	77.32	0.24	12.90	1.20	0.03	0.15	1.02	3.43	3.48	0.29	100	4.45		
	UA3524-27	76.82	0.15	12.93	1.20	0.04	0.22	1.16	3.83	3.46	0.23	100	1.75		
	UA3524-28	75.89	0.17	13.48	0.99	0.04	0.22	1.38	4.01	3.57	0.32	100	1.52		
	UA3524-11	78.66	0.19	12.43	0.97	0.01	0.22	1.33	3.63	2.45	0.14	100	6.28		
	UA3524-24	78.01	0.30	12.85	1.31	0.06	0.28	1.69	3.51	1.89	0.13	100	6.26		
a	Mean	75.86	0.20	13.54	1.27	0.05	0.27	1.44	3.98	3.18	0.29	100	3.31	16	WRA-like. Condensed Si around 75wt%
	StDev	1.47	0.04	0.63	0.15	0.02	0.06	0.20	0.39	0.43	0.07	0	1.67		
	UA3524-5	72.60	0.56	13.99	2.47	0.02	0.44	1.56	4.53	3.76	0.08	100	1.14		
	UA3524-25	72.89	0.26	14.68	1.77	0.06	0.46	1.90	4.31	3.37	0.37	100	1.99		
	UA3524-17	73.94	0.17	14.51	1.35	0.04	0.33	1.75	4.52	3.12	0.34	100	1.21		
															Assorted tephra, can't make out a population.
	UA3524-29	76.83	0.10	14.17	1.29	0.07	0.31	1.48	2.19	3.35	0.29	100	6.13		
	UA3524-22	76.48	0.10	14.03	0.85	0.00	0.18	1.70	3.91	2.74	0.02	100	5.03		high Al, low Fe. Bad point
	UA3524-2	77.11	0.21	13.12	1.06	0.00	0.09	0.93	2.05	5.35	0.10	100	6.04		
	UA3524-18	76.36	0.07	13.67	0.59	0.04	0.00	0.61	3.98	4.63	0.06	100	3.14		
	UA3524-6	74.98	0.24	13.68	2.03	0.15	0.51	2.19	4.08	1.96	0.26	100	0.14		phenocryst?

		UA3524-1	72.83	0.34	14.51	2.39	0.08	0.29	0.71	5.34	3.42	0.10	100	4.98		
Dec 18, 2020 NaTDI GRV17 49-50 cm		UA3488-6	70.68	0.50	15.07	2.43	0.16	0.50	1.72	5.61	3.16	0.24	100	0.95		
		UA3488-24	70.74	0.64	14.52	3.16	0.12	0.84	2.41	4.53	2.92	0.16	100	0.31		
		UA3488-25	70.89	0.53	14.92	2.47	0.15	0.52	1.69	5.67	3.00	0.21	100	-0.47		
		UA3488-19	71.03	0.48	15.01	2.41	0.16	0.64	1.74	5.40	2.97	0.22	100	2.56		
		UA3488-14	71.27	0.45	15.01	2.42	0.10	0.48	1.76	5.15	3.21	0.18	100	0.69		
		UA3488-9	71.77	0.52	14.99	2.42	0.10	0.55	1.65	4.83	3.00	0.22	100	1.43		
	a	Mean	71.06	0.52	14.92	2.55	0.13	0.59	1.83	5.20	3.04	0.21	100	0.91	6	Aniakchak
		StDev	0.41	0.06	0.20	0.30	0.03	0.14	0.29	0.45	0.12	0.03	0	1.03		
		UA3488-20	77.28	0.22	12.25	1.52	0.07	0.32	2.05	4.47	1.62	0.25	100	0.69		
		UA3488-12	77.53	0.28	12.42	1.53	0.05	0.39	2.09	3.90	1.65	0.21	100	1.72		
	b	Mean	77.40	0.25	12.33	1.52	0.06	0.36	2.07	4.19	1.63	0.23	100	1.21	2	Augustine
		StDev	0.17	0.04	0.12	0.00	0.01	0.05	0.03	0.40	0.03	0.03	0	0.73		
		UA3488-21	75.07	0.21	13.71	1.37	0.09	0.29	1.48	4.47	3.08	0.31	100	0.68		
		UA3488-3	75.22	0.25	13.87	1.42	0.09	0.29	1.52	4.01	3.08	0.34	100	2.37		
		UA3488-10	75.34	0.15	13.77	1.10	0.07	0.24	1.41	3.92	3.70	0.39	100	1.72		
		UA3488-18	75.57	0.19	13.51	1.17	0.07	0.26	1.41	4.26	3.32	0.33	100	1.01		
		UA3488-1	75.63	0.17	13.51	1.31	0.06	0.21	1.38	4.29	3.16	0.35	100	1.96		
		UA3488-7	75.86	0.17	13.81	1.18	0.01	0.26	1.40	3.88	3.21	0.29	100	2.61		
	c	Mean	75.45	0.19	13.70	1.26	0.07	0.26	1.43	4.14	3.26	0.34	100	1.72		WRA-like. Narrow Si range
		StDev	0.29	0.04	0.15	0.13	0.03	0.03	0.05	0.24	0.24	0.04	0	0.75		
		UA3488-23	69.30	1.25	14.61	4.00	0.08	0.45	2.89	4.68	2.67	0.07	100	3.05		
		UA3488-15	71.48	0.13	16.37	1.16	0.03	0.25	2.82	4.97	2.60	0.23	100	3.12		Plag?
		UA3488-5	73.66	0.20	14.34	1.68	0.04	0.41	2.00	4.20	3.12	0.46	100	8.01		
		UA3488-4	77.56	0.20	12.21	1.42	0.02	0.25	0.76	3.65	3.67	0.35	100	3.82		

		UA3488-16	78.07	0.20	12.65	1.15	0.10	0.30	1.60	3.47	2.29	0.23	100	4.89		
Sept 2, 2020 NaSiTDI		UA3488-5	70.38	0.50	14.94	2.56	0.18	0.55	1.71	5.58	3.42	0.23	100	9.06		
GRV17 49-50 cm		UA3488-1	70.85	0.53	15.31	2.38	0.15	0.51	1.73	5.31	3.08	0.21	100	3.04		
Reanalysis		UA3488-8	71.26	0.51	15.09	2.46	0.15	0.55	1.75	5.12	2.93	0.22	100	2.83		
	a	Mean	70.83	0.51	15.11	2.47	0.16	0.53	1.73	5.34	3.14	0.22	100	4.98	3	aniakchak
		StDev	0.44	0.01	0.18	0.09	0.02	0.02	0.02	0.23	0.25	0.01	0	3.54		
		UA3488-4	74.49	0.19	14.17	1.41	0.09	0.27	1.56	4.34	3.25	0.30	100	4.21		
		UA3488-24	74.78	0.29	13.61	1.51	0.02	0.32	1.31	4.32	3.56	0.36	100	6.95		
		UA3488-15	75.10	0.14	13.70	1.20	0.03	0.28	1.48	4.54	3.29	0.32	100	3.76		
		UA3488-17	75.12	0.13	14.08	1.26	0.07	0.31	1.51	4.03	3.21	0.35	100	2.98		
		UA3488-2	75.21	0.13	13.91	1.29	0.08	0.22	1.49	4.12	3.32	0.30	100	2.94		
		UA3488-11	75.35	0.20	13.85	1.31	0.05	0.27	1.46	4.06	3.21	0.31	100	2.58		
		UA3488-26	77.45	0.15	13.04	1.19	0.05	0.21	0.96	3.19	3.52	0.31	100	4.17		
		Mean	75.36	0.18	13.77	1.31	0.05	0.27	1.40	4.09	3.34	0.32	100	3.94	7	WRA-like
	c	StDev	0.97	0.06	0.38	0.12	0.03	0.04	0.21	0.43	0.14	0.03	0	1.47		
		UA3488-21	76.48	0.27	12.73	1.49	0.08	0.43	2.12	4.54	1.69	0.23	100	4.02		
		UA3488-19	76.71	0.32	12.96	1.64	0.12	0.43	2.18	3.80	1.69	0.20	100	2.34		
		UA3488-18	77.93	0.24	12.59	1.60	0.04	0.38	2.12	3.17	1.72	0.27	100	4.79		
	b	Mean	77.04	0.28	12.76	1.57	0.08	0.41	2.14	3.84	1.70	0.23	100	3.72	3	
		StDev	0.78	0.04	0.19	0.08	0.04	0.03	0.04	0.69	0.02	0.04	0	1.25		low K popn
		UA3488-7	73.81	0.41	13.52	1.81	0.06	1.14	1.23	4.10	3.68	0.30	100	2.91		
		UA3488-25	74.64	0.36	13.77	1.99	0.14	0.43	2.06	4.30	2.10	0.25	100	1.93		
		UA3488-23	78.49	0.20	12.89	1.17	0.07	0.25	1.56	3.01	2.16	0.23	100	6.85		
		UA3488-20	75.63	0.09	13.81	0.63	0.07	0.09	0.97	3.44	5.23	0.06	100	3.93		
		UA3488-9	76.13	0.11	13.74	0.89	0.03	0.09	0.98	2.76	5.20	0.10	100	5.02		
		UA3488-12	80.15	0.15	11.51	0.67	0.03	0.10	0.49	3.20	3.50	0.24	100	4.87		

Dec 18, 2020
NaTDI

GRV17 57-58 cm

	UA3487-11	74.18	0.17	14.05	1.41	0.06	0.34	1.60	4.79	3.16	0.32	100	1.13		
	UA3487-7	74.69	0.26	14.07	1.55	0.06	0.37	1.61	3.87	3.24	0.35	100	2.03		
	UA3487-10	74.75	0.22	14.40	1.41	0.05	0.35	1.67	3.80	3.11	0.31	100	4.97		
	UA3487-9	74.88	0.19	13.95	1.41	0.06	0.33	1.57	4.13	3.26	0.29	100	1.95		
	UA3487-18	75.06	0.16	14.04	1.32	0.07	0.29	1.51	4.12	3.18	0.33	100	3.23		
	UA3487-8	75.58	0.26	13.74	1.24	0.04	0.28	1.40	3.98	3.27	0.28	100	1.32		
	UA3487-15	75.80	0.16	13.78	1.27	0.05	0.27	1.50	3.66	3.27	0.30	100	2.07		
a	Mean	74.99	0.20	14.01	1.37	0.05	0.32	1.55	4.05	3.21	0.31	100	2.38	7	WRA-like. Narrow Si range
	StDev	0.55	0.04	0.22	0.11	0.01	0.04	0.09	0.37	0.06	0.03	0	1.32		
	UA3487-12	77.10	0.27	12.66	1.55	0.08	0.38	2.10	4.07	1.65	0.19	100	2.90		
	UA3487-25	77.23	0.30	12.53	1.57	0.10	0.40	2.03	3.70	1.93	0.27	100	0.66		
	UA3487-16	77.38	0.20	12.68	1.54	0.10	0.39	2.11	3.82	1.59	0.24	100	1.83		
	UA3487-3	77.43	0.30	12.61	1.58	0.07	0.36	2.14	3.66	1.66	0.25	100	2.67		
	UA3487-24	77.53	0.29	12.72	1.46	0.06	0.38	2.19	3.57	1.63	0.23	100	2.46		
	UA3487-14	77.54	0.29	12.56	1.53	0.07	0.38	2.08	3.72	1.66	0.19	100	2.77		
	UA3487-17	77.55	0.23	12.52	1.59	0.03	0.35	1.95	3.89	1.72	0.22	100	2.56		
	UA3487-20	77.57	0.22	12.67	1.57	0.08	0.39	2.11	3.47	1.70	0.26	100	0.28		
	UA3487-1	77.58	0.26	12.42	1.57	0.06	0.36	2.16	3.78	1.67	0.19	100	0.99		
	UA3487-4	77.60	0.27	12.56	1.49	0.04	0.40	2.21	3.63	1.59	0.28	100	1.60		
	UA3487-5	77.66	0.27	12.50	1.52	0.02	0.36	2.06	3.81	1.65	0.20	100	0.88		
	UA3487-23	78.42	0.18	12.23	1.43	0.00	0.33	1.90	3.62	1.70	0.23	100	0.38		
	UA3487-19	78.55	0.24	12.26	1.48	0.05	0.31	1.92	3.35	1.71	0.18	100	1.90		
b	Mean	77.63	0.25	12.53	1.53	0.06	0.37	2.07	3.70	1.68	0.22	100	1.68	13	Augustine-like
	StDev	0.41	0.04	0.15	0.05	0.03	0.03	0.10	0.19	0.09	0.03	0	0.95		
	UA3487-21	71.67	0.48	14.90	2.37	0.11	0.51	1.68	4.96	3.04	0.36	100	0.67		

		UA3487-6	76.92	0.07	13.72	0.47	0.07	0.02	0.69	2.42	5.54	0.08	100	6.07		
sept 2, 2020 NaTDI		UA3487-15	73.74	0.23	14.42	1.56	0.08	0.35	1.71	4.33	3.32	0.33	100	3.26		
GRV17 57-58 cm		UA3487-23	74.50	0.27	14.31	1.47	0.01	0.40	1.61	3.96	3.19	0.36	100	2.05		
reanalysis		UA3487-13	74.61	0.15	14.33	1.40	0.07	0.35	1.61	4.05	3.19	0.30	100	5.90		
		UA3487-25	74.66	0.18	14.24	1.34	0.06	0.32	1.62	4.11	3.22	0.32	100	3.50		
		UA3487-3	74.84	0.21	14.04	1.38	0.04	0.32	1.52	4.18	3.25	0.29	100	0.81		
		UA3487-10	75.10	0.15	13.98	1.14	0.06	0.26	1.46	4.23	3.39	0.29	100	1.62		
	a	Mean	74.57	0.20	14.22	1.38	0.05	0.33	1.59	4.14	3.26	0.32	100	2.86	6	WRA-like
		StDev	0.46	0.05	0.18	0.14	0.02	0.05	0.09	0.13	0.08	0.03	0	1.80		
		UA3487-9	76.74	0.19	13.06	1.28	0.06	0.41	1.93	4.42	1.74	0.23	100	4.75		
		UA3487-17	76.92	0.23	12.72	1.53	0.08	0.38	2.19	4.18	1.56	0.27	100	3.93		
		UA3487-18	77.16	0.13	12.89	1.49	0.08	0.34	2.01	4.09	1.65	0.21	100	1.90		
		UA3487-14	77.38	0.26	12.58	1.47	0.03	0.41	2.04	3.95	1.71	0.22	100	0.73		
		UA3487-22	77.60	0.22	12.38	1.45	0.07	0.36	1.98	4.03	1.73	0.22	100	4.52		
	b	Mean	77.16	0.21	12.73	1.44	0.06	0.38	2.03	4.13	1.68	0.23	100	3.17	5	Augustine-like
		StDev	0.35	0.05	0.26	0.09	0.02	0.03	0.10	0.18	0.07	0.02	0	1.76		
		UA3487-19	70.90	0.46	15.04	2.44	0.11	0.53	1.73	5.48	3.16	0.21	100	1.09		aniakchak
		UA3487-5	73.28	0.18	14.14	1.91	0.03	0.22	1.15	3.59	5.12	0.48	100	4.69		
		UA3487-4	74.05	0.15	14.77	1.16	0.08	0.28	1.81	4.45	3.02	0.31	100	2.19		
		UA3487-12	75.02	0.15	13.86	1.11	0.05	0.21	1.46	4.14	3.73	0.35	100	2.47		
		UA3487-8	75.11	0.30	14.18	1.33	0.02	0.39	1.42	4.35	2.75	0.19	100	2.47		
		UA3487-2	75.31	0.30	14.12	1.30	0.00	0.39	1.35	4.41	2.73	0.12	100	3.63		mixed shards, no discernable populations
		UA3487-6	76.96	0.25	13.92	0.19	0.04	0.00	0.88	3.68	4.02	0.09	100	6.33		

		UA3487-11	76.00	0.27	13.48	1.40	0.04	0.24	1.06	3.49	3.72	0.38	100	4.22		
		UA3487-21	78.40	0.15	12.96	1.05	0.10	0.28	1.52	2.93	2.46	0.21	100	6.23		
Dec 18, 2020 NaTDI		UA3486-7	75.17	0.31	13.67	1.89	0.11	0.45	2.17	4.08	1.98	0.23	100	0.96		
GRV17 65-66 cm		UA3486-20	75.26	0.30	13.37	1.80	0.06	0.38	2.05	4.58	1.96	0.30	100	1.52		
	a	Mean	75.21	0.30	13.52	1.84	0.09	0.41	2.11	4.33	1.97	0.27	100	1.24	2	Hayes?
		StDev	0.06	0.01	0.21	0.06	0.03	0.05	0.09	0.35	0.01	0.05	0	0.40		
		UA3486-19	77.46	0.28	12.63	1.51	0.09	0.35	2.10	3.78	1.65	0.20	100	0.57		
		UA3486-10	77.88	0.30	12.51	1.58	0.08	0.38	2.15	3.35	1.62	0.19	100	0.48		
		UA3486-4	78.03	0.22	12.41	1.36	0.07	0.36	1.89	3.66	1.84	0.20	100	-0.26		
		UA3486-1	78.12	0.25	12.58	1.50	0.07	0.32	1.94	3.35	1.74	0.17	100	5.54		
	b	Mean	77.87	0.26	12.53	1.49	0.08	0.35	2.02	3.53	1.71	0.19	100	1.58	4	Augustine-like
		StDev	0.30	0.04	0.09	0.09	0.01	0.02	0.12	0.22	0.10	0.01	0	2.66		
		UA3486-23	74.38	0.18	14.17	1.36	0.04	0.33	1.61	4.42	3.27	0.32	100	1.63		
		UA3486-3	74.50	0.19	14.34	1.40	0.03	0.31	1.80	4.11	3.05	0.32	100	2.28		
		UA3486-21	75.15	0.16	14.10	1.41	0.03	0.32	1.65	3.91	3.06	0.28	100	2.11		
		UA3486-17	75.42	0.19	13.92	1.25	0.07	0.26	1.47	3.94	3.25	0.29	100	1.72		
		UA3486-25	75.54	0.18	13.64	1.26	0.07	0.38	1.78	3.57	3.10	0.62	100	4.90		
	c	Mean	75.00	0.18	14.03	1.34	0.05	0.32	1.66	3.99	3.15	0.36	100	2.53	5	WRA-like
		StDev	0.53	0.01	0.27	0.08	0.02	0.04	0.14	0.31	0.11	0.14	0	1.35		
		UA3486-5	78.14	0.16	12.63	1.09	0.05	0.28	1.50	3.57	2.39	0.24	100	4.49		
		UA3486-8	78.77	0.24	12.54	1.07	0.03	0.21	1.22	3.49	2.32	0.14	100	4.29		
	d	Mean	78.46	0.20	12.59	1.08	0.04	0.24	1.36	3.53	2.36	0.19	100	4.39	2	unknown population
		StDev	0.44	0.05	0.06	0.01	0.02	0.05	0.19	0.06	0.05	0.07	0	0.14		
		UA3486-6	71.26	0.49	15.16	2.43	0.22	0.50	1.76	5.00	2.99	0.23	100	1.46		
		UA3486-13	71.35	0.47	14.79	2.47	0.13	0.56	1.75	5.42	2.91	0.19	100	2.81		

		UA3486-2	71.35	0.51	14.91	2.40	0.13	0.49	1.67	5.39	3.00	0.20	100	-0.88		
		UA3486-16	71.37	0.51	14.64	2.41	0.11	0.48	1.69	5.70	2.93	0.20	100	0.52		
		UA3486-24	71.53	0.51	14.67	2.46	0.14	0.49	1.71	5.22	3.09	0.23	100	0.35		
		UA3486-9	71.64	0.50	14.97	2.36	0.16	0.48	1.69	4.94	3.08	0.22	100	-0.12		
		UA3486-18	71.70	0.61	14.96	2.29	0.16	0.47	1.74	4.82	3.10	0.19	100	1.01		
	e	Mean	71.46	0.52	14.87	2.40	0.15	0.50	1.72	5.21	3.01	0.21	100	0.73	7	Aniakchak
		StDev	0.17	0.05	0.18	0.06	0.03	0.03	0.03	0.31	0.08	0.02	0	1.19		
		UA3486-15	74.52	0.55	15.16	2.56	0.17	0.53	1.87	1.52	2.95	0.20	100	4.49		
		UA3486-14	76.76	0.12	13.54	0.37	0.01	0.01	0.68	3.01	5.44	0.08	100	4.62		
		UA3486-12	75.32	0.43	12.78	1.06	0.05	0.64	1.77	3.69	3.77	0.63	100	2.33		
Jun 8, 2020 NaTDI GRV17 67-68 cm		UA3523-4	64.11	1.01	12.58	6.70	0.10	5.50	3.94	3.53	2.48	0.07	100	1.36		
		UA3523-15	67.53	1.07	15.05	4.67	0.04	1.66	3.84	2.93	3.13	0.11	100	2.69		
	d	Mean	65.82	1.04	13.81	5.69	0.07	3.58	3.89	3.23	2.81	0.09	100	2.03	2	unknown low Si population
		StDev	2.42	0.05	1.75	1.44	0.04	2.72	0.07	0.43	0.46	0.03	0	0.94		
		UA3523-9	77.06	0.29	12.84	1.51	0.03	0.39	2.22	3.88	1.63	0.22	100	3.01		
		UA3523-17	77.07	0.30	12.70	1.57	0.06	0.39	2.05	4.05	1.67	0.17	100	1.56		
		UA3523-24	77.75	0.21	12.64	1.41	0.10	0.37	1.87	3.85	1.64	0.24	100	6.57		
	c	Mean	77.29	0.27	12.72	1.49	0.06	0.38	2.04	3.92	1.65	0.21	100	3.72	3	Augustine-like
		StDev	0.40	0.05	0.10	0.08	0.03	0.01	0.18	0.11	0.02	0.04	0	2.58		
		UA3523-2	73.70	0.13	15.28	0.93	0.07	0.19	2.15	4.92	2.49	0.19	100	1.87		
		UA3523-13	74.11	0.15	14.50	1.60	0.02	0.44	1.87	3.97	3.06	0.36	100	1.67		
		UA3523-25	74.75	0.19	14.39	1.09	0.03	0.20	1.70	4.54	2.90	0.26	100	1.66		
		UA3523-18	75.35	0.21	13.98	1.10	0.02	0.22	1.54	4.02	3.37	0.24	100	1.62		
		UA3523-19	75.56	0.22	13.51	1.30	0.02	0.29	1.34	4.08	3.42	0.34	100	2.36		
		UA3523-20	75.73	0.22	13.76	1.25	0.03	0.27	1.35	3.81	3.29	0.35	100	2.32		

		UA3523-26	76.30	0.21	12.94	1.30	0.05	0.23	1.02	4.03	3.64	0.37	100	3.79		
	b	Mean	75.07	0.19	14.05	1.22	0.03	0.26	1.57	4.20	3.17	0.30	100	2.19	7	WRA-like. Messy
		StDev	0.93	0.04	0.76	0.21	0.02	0.09	0.38	0.39	0.39	0.07	0	0.77		
		UA3523-16	71.06	0.45	14.89	2.33	0.12	0.48	1.63	5.79	3.08	0.21	100	0.08		
		UA3523-12	70.31	0.46	15.76	2.43	0.18	0.56	1.68	5.41	2.96	0.31	100	5.66		
		UA3523-27	71.54	0.47	15.09	2.42	0.15	0.52	1.58	5.05	3.03	0.21	100	0.57		
		UA3523-5	72.15	0.49	14.63	2.29	0.17	0.47	1.50	5.13	3.03	0.21	100	0.78		
		UA3523-10	71.47	0.49	15.01	2.35	0.12	0.43	1.63	5.24	3.12	0.19	100	0.51		
		UA3523-6	71.49	0.50	14.75	2.34	0.13	0.50	1.69	4.80	3.62	0.22	100	1.76		
		UA3523-28	71.08	0.51	15.19	2.38	0.10	0.49	1.65	5.45	2.99	0.21	100	0.64		
		UA3523-23	71.14	0.57	15.00	2.42	0.16	0.46	1.70	5.22	3.16	0.21	100	0.96		
		UA3523-3	71.29	0.59	14.97	2.43	0.13	0.49	1.61	5.26	3.09	0.17	100	0.68		
		UA3523-22	71.38	0.61	14.86	2.39	0.15	0.52	1.72	5.17	3.06	0.20	100	1.70		
	a	Mean	71.29	0.51	15.01	2.38	0.14	0.49	1.64	5.25	3.11	0.21	100	1.33	10	Aniakchak
		StDev	0.47	0.06	0.31	0.05	0.03	0.04	0.07	0.26	0.19	0.04	0	1.61		
		UA3523-29	75.44	0.35	12.64	2.08	0.04	0.54	2.32	4.38	1.90	0.39	100	3.58		
		UA3523-14	70.42	0.14	17.28	1.08	0.02	0.24	3.14	5.24	2.26	0.21	100	-0.08		hit a mineral?
		UA3523-21	73.41	0.26	14.48	1.40	0.04	0.06	0.56	2.69	7.03	0.09	100	3.80		weathered?
		UA3523-7	76.51	0.15	13.78	0.55	0.05	0.07	0.86	3.28	4.72	0.03	100	5.40		weatehred?
		UA3523-8	76.67	0.04	13.52	0.44	0.03	0.03	0.22	3.41	5.61	0.05	100	5.39		too low Ti
		UA3523-1	76.87	0.14	13.78	0.80	0.09	0.14	0.97	1.87	5.30	0.07	100	5.56		weathered?
Sept 2, 2020 NaSiTDI		UA3523-20	70.51	0.58	15.25	2.49	0.14	0.59	1.73	5.46	3.11	0.19	100	1.64		
GRV17 67-68 cm		UA3523-27	70.82	0.47	15.23	2.38	0.13	0.48	1.58	5.81	2.93	0.22	100	1.87		
reanalysis		UA3523-30	70.89	0.47	15.15	2.39	0.13	0.51	1.65	5.62	3.02	0.21	100	0.94		

	UA3523-4	70.94	0.48	15.25	2.37	0.11	0.50	1.70	5.42	3.07	0.20	100	1.72		
	UA3523-33	70.97	0.44	15.24	2.37	0.12	0.50	1.71	5.33	3.17	0.20	100	0.32		
	UA3523-26	71.00	0.53	15.26	2.52	0.16	0.50	1.70	5.11	3.09	0.18	100	1.13		
	UA3523-18	71.00	0.50	15.16	2.47	0.19	0.53	1.78	5.18	3.02	0.22	100	1.26		
	UA3523-2	71.03	0.52	15.15	2.45	0.19	0.53	1.73	5.14	3.09	0.22	100	1.39		
	UA3523-1	71.09	0.42	15.03	2.49	0.09	0.51	1.65	5.11	3.40	0.25	100	2.95		
	UA3523-15	71.18	0.59	15.22	2.35	0.17	0.49	1.77	4.93	3.15	0.19	100	1.47		
	UA3523-19	71.19	0.53	15.06	2.40	0.17	0.53	1.70	5.24	3.01	0.23	100	1.40		
	UA3523-23	71.29	0.53	15.20	2.39	0.15	0.53	1.67	5.13	2.96	0.19	100	2.57		
	UA3523-13	71.31	0.44	15.02	2.35	0.17	0.49	1.74	5.41	2.93	0.19	100	1.47		
	UA3523-12	71.33	0.54	15.05	2.45	0.12	0.46	1.68	5.23	2.98	0.22	100	1.33		
	UA3523-34	71.52	0.51	15.23	2.38	0.10	0.55	1.72	4.83	2.99	0.25	100	1.38		
	UA3523-31	72.10	0.53	15.19	2.36	0.17	0.49	1.61	4.45	2.92	0.22	100	1.15		
	UA3523-6	72.46	0.40	14.89	2.40	0.14	0.41	1.48	4.77	2.91	0.19	100	6.60		
a	Mean	71.21	0.50	15.15	2.41	0.14	0.50	1.68	5.19	3.04	0.21	100	1.80	17	aniakchak
	StDev	0.47	0.05	0.10	0.05	0.03	0.04	0.07	0.33	0.12	0.02	0	1.37		
	UA3523-40	75.04	0.20	14.15	1.32	0.03	0.28	1.51	4.01	3.19	0.34	100	2.97		
	UA3523-8	75.16	0.16	13.92	1.32	0.08	0.29	1.50	3.93	3.38	0.33	100	3.61		
	UA3523-25	75.18	0.24	13.95	1.30	0.05	0.31	1.44	3.98	3.29	0.32	100	1.18		
	UA3523-11	75.57	0.14	13.63	1.32	0.04	0.26	1.35	4.08	3.38	0.30	100	2.28		
b	Mean	75.24	0.18	13.91	1.32	0.05	0.29	1.45	4.00	3.31	0.32	100	2.51	4	WRA-like
	StDev	0.23	0.04	0.22	0.01	0.02	0.02	0.07	0.06	0.09	0.02	0	1.04		
	UA3523-21	76.92	0.24	12.64	1.71	0.11	0.39	1.97	3.92	1.93	0.21	100	2.42		
	UA3523-10	77.33	0.17	12.77	1.52	0.06	0.38	2.15	3.76	1.68	0.24	100	3.08		
c	Mean	77.12	0.21	12.70	1.62	0.09	0.38	2.06	3.84	1.80	0.22	100	2.75	2	Augustine
	StDev	0.29	0.05	0.09	0.14	0.04	0.00	0.13	0.11	0.18	0.02	0	0.47		
	UA3523-29	78.47	0.18	12.51	1.00	0.10	0.24	1.25	3.80	2.31	0.17	100	5.86		

		UA3523-32	66.66	1.14	15.01	4.76	0.04	1.66	3.84	3.83	3.01	0.07	100	2.45		Aniakchak?
		UA3523-17	68.22	1.20	14.02	4.95	0.05	1.32	3.19	3.92	3.08	0.07	100	3.11		Aniakchak?
		UA3523-9	71.23	1.23	12.83	3.93	0.08	0.63	1.93	4.12	3.95	0.09	100	1.17		
		UA3523-39	72.12	0.74	14.03	2.53	0.08	0.53	1.55	4.46	3.70	0.32	100	2.13		
		UA3523-36	73.13	0.56	15.43	2.53	0.17	0.52	1.72	2.77	3.01	0.21	100	3.45		
		UA3523-22	73.97	0.14	14.85	1.04	0.03	0.16	1.93	4.86	2.83	0.22	100	2.18		
		UA3523-3	76.46	0.33	12.63	1.57	0.06	0.29	2.38	3.20	2.97	0.14	100	2.01		weathered?
		UA3523-5	76.62	0.13	13.74	0.78	0.06	0.08	0.98	2.32	5.23	0.07	100	4.90		weathered?
		UA3523-7	76.66	0.11	13.92	0.61	0.03	0.08	0.90	3.10	4.55	0.07	100	5.19		weathered?
		UA3523-28	76.87	0.06	13.83	1.24	0.06	0.06	0.60	2.58	4.65	0.07	100	7.38		weathered?
		UA3523-14	78.08	0.26	12.63	0.92	0.00	0.19	0.90	3.61	3.39	0.03	100	6.26		
		UA3523-37	78.70	0.19	14.26	1.49	0.00	0.30	1.52	0.82	2.49	0.29	100	3.92		
June 14, 2021 NaTDI GRV17 69-70 cm		UA3542-15	73.15	0.26	14.62	1.60	0.05	0.35	1.91	4.76	3.02	0.36	100	1.20		
		UA3542-10	73.50	0.28	14.46	1.56	0.05	0.36	1.89	4.42	3.25	0.30	100	1.92		
		UA3542-8	74.03	0.14	14.38	1.40	0.05	0.31	1.73	4.37	3.37	0.30	100	2.26		
		UA3542-19	74.42	0.25	14.21	1.32	0.00	0.28	1.66	4.41	3.20	0.33	100	2.39		
		UA3542-18	74.49	0.16	14.26	1.28	0.03	0.24	1.60	4.65	3.08	0.28	100	1.71		
		UA3542-4	74.60	0.15	14.21	1.37	0.07	0.27	1.62	4.33	3.15	0.29	100	2.21		
		UA3542-25	74.79	0.22	13.96	1.34	0.05	0.26	1.54	4.38	3.25	0.27	100	3.64		
		UA3542-14	74.89	0.14	14.05	1.29	0.04	0.31	1.66	4.08	3.25	0.37	100	3.42		
		UA3542-6	74.89	0.13	14.25	1.26	0.05	0.26	1.60	4.14	3.20	0.26	100	2.72		
		UA3542-20	74.98	0.16	13.89	1.15	0.04	0.24	1.46	4.34	3.46	0.36	100	1.75		
		UA3542-21	75.33	0.32	13.31	1.49	0.07	0.29	1.45	4.41	3.19	0.20	100	1.24		
		UA3542-24	75.35	0.18	13.87	1.18	0.04	0.25	1.46	4.16	3.29	0.29	100	1.73		
		UA3542-7	75.51	0.18	13.92	1.19	0.05	0.18	1.39	4.23	3.16	0.26	100	2.36		
		UA3542-13	75.63	0.13	13.60	1.11	0.07	0.20	1.41	4.39	3.22	0.29	100	2.89		
		UA3542-22	75.89	0.24	13.03	1.54	0.07	0.31	1.15	4.14	3.40	0.29	100	1.08		
		UA3542-2	75.97	0.12	13.39	0.96	0.03	0.17	1.37	4.10	3.65	0.32	100	3.14		
	a	Mean	74.84	0.19	13.96	1.32	0.05	0.27	1.56	4.33	3.26	0.30	100	2.23	16	WRA-like
		StDev	0.80	0.06	0.44	0.18	0.02	0.06	0.19	0.19	0.15	0.04	0	0.78		

		UA3542-17	76.49	0.24	12.42	1.43	0.10	0.31	2.08	5.15	1.59	0.24	100	1.53		
		UA3542-16	77.11	0.33	12.76	1.49	0.06	0.37	2.10	4.01	1.61	0.21	100	2.72		
		UA3542-5	77.19	0.29	12.75	1.52	0.02	0.36	2.13	3.99	1.61	0.16	100	0.87		
	b	Mean	76.93	0.29	12.65	1.48	0.06	0.35	2.10	4.38	1.60	0.20	100	1.71	3	Augustine-like
		StDev	0.39	0.05	0.20	0.05	0.04	0.03	0.03	0.66	0.01	0.04	0	0.94		
		UA3542-12	76.08	0.13	13.11	0.88	0.04	0.09	0.90	3.45	5.27	0.07	100	4.91		
		UA3542-11	73.44	0.37	14.00	2.00	0.13	0.46	2.29	5.17	1.95	0.25	100	0.77		
		UA3542-3	73.51	0.14	15.20	1.12	0.05	0.22	1.91	4.87	2.79	0.25	100	1.64		
		UA3542-1	74.73	0.10	14.52	0.87	0.03	0.12	1.67	4.74	3.04	0.22	100	1.57		
		UA3542-9	77.97	0.24	12.16	1.32	0.05	0.28	1.65	3.97	2.25	0.16	100	4.00		
		UA3542-23	78.15	0.17	12.49	1.02	0.02	0.20	1.25	4.18	2.41	0.12	100	6.19		
Jun 22, 2020 NaTDI		UA3522-7	71.71	0.92	14.10	2.91	0.08	0.23	1.13	4.09	4.81	0.03	100	4.39		
GRV17 72-73 cm		UA3522-5	74.14	0.13	14.88	0.77	0.05	0.10	1.61	5.64	2.56	0.16	100	1.51		
		UA3522-6	74.45	0.20	14.25	1.30	0.08	0.30	1.55	4.25	3.37	0.31	100	3.56		mixed shards, no population
		UA3522-11	75.21	0.30	13.87	1.94	0.13	0.39	2.17	3.85	1.96	0.23	100	0.79		
		UA3522-10	79.05	0.13	12.68	0.91	0.02	0.16	1.16	3.31	2.45	0.16	100	6.24		
		Mean	74.91	0.34	13.96	1.57	0.07	0.24	1.52	4.23	3.03	0.18	100	3.30		This was the hole with the uncured epoxy, so there mustn't have been much to work with
		StDev	2.66	0.33	0.80	0.88	0.04	0.11	0.42	0.87	1.12	0.11	0	2.20		
Mar 4, 2021 NaTDI		UA3541-2	74.00	0.29	14.09	2.08	0.11	0.50	2.32	4.44	1.95	0.29	100	5.14		
GRV17 72-73 cm		UA3541-6	74.11	0.32	14.06	1.83	0.04	0.46	2.20	4.99	1.85	0.16	100	1.57		
Reanalysis		UA3541-17	74.59	0.26	13.69	1.82	0.14	0.44	2.06	4.89	1.91	0.26	100	1.34		
		UA3541-1	73.57	0.26	14.11	2.04	0.16	0.49	2.30	4.82	2.05	0.26	100	1.28		
		UA3541-4	74.75	0.26	13.52	1.89	0.11	0.41	1.97	4.84	2.05	0.27	100	0.14		

		UA3541-16	74.77	0.26	13.35	1.77	0.06	0.39	1.92	4.95	2.33	0.26	100	1.34		
	a	Mean	74.30	0.27	13.81	1.90	0.10	0.45	2.13	4.82	2.02	0.25	100	1.80	6	Ruppert
		StDev	0.48	0.02	0.33	0.13	0.05	0.05	0.17	0.20	0.17	0.04	0	1.71		
		UA3541-5	69.57	0.72	14.92	3.15	0.04	0.78	2.30	4.89	3.54	0.13	100	1.31		
		UA3541-10	70.61	0.46	15.28	2.31	0.12	0.50	1.68	5.87	3.02	0.20	100	1.58		
		UA3541-12	70.79	0.47	14.99	2.38	0.11	0.52	1.76	5.81	2.97	0.25	100	1.34		
		UA3541-18	72.98	0.26	14.81	1.53	0.03	0.40	1.98	4.71	3.04	0.32	100	1.62		
		UA3541-13	73.92	0.30	14.18	1.37	0.05	0.44	1.38	5.47	2.80	0.13	100	0.73		
		UA3541-7	74.88	0.15	14.27	1.28	0.03	0.23	1.56	4.09	3.28	0.32	100	2.14		
		UA3541-3	76.70	0.25	13.04	1.62	0.06	0.39	2.12	4.02	1.65	0.21	100	1.54		
		UA3541-14	77.32	0.17	13.19	0.75	0.06	0.23	1.87	4.14	2.12	0.18	100	4.78		
		UA3541-11	69.89	0.40	14.33	3.03	0.09	0.06	1.19	3.23	7.75	0.03	100	3.84		
		UA3541-9	74.03	0.24	13.53	1.82	0.08	0.17	1.16	3.47	5.35	0.19	100	4.86		
Mar 4, 2021 NaTDI		UA3540-2	73.73	0.31	14.34	2.00	0.07	0.49	2.37	4.65	1.85	0.24	100	1.48		
GRV17 73-74 cm		UA3540-4	74.12	0.30	14.70	1.98	0.12	0.52	2.67	3.41	1.96	0.28	100	1.70		
Reanalysis	a	Mean	73.93	0.30	14.52	1.99	0.10	0.50	2.52	4.03	1.90	0.26	100	1.59	2	ruppert
		StDev	0.28	0.01	0.25	0.01	0.03	0.02	0.22	0.88	0.08	0.02	0	0.15		
		UA3540-13	76.26	0.26	14.04	1.92	0.12	0.42	2.14	2.69	1.96	0.25	100	3.25		
		UA3540-19	76.58	0.29	12.72	1.67	0.07	0.36	2.00	4.50	1.64	0.23	100	1.96		
		UA3540-15	77.50	0.25	12.60	1.41	0.05	0.32	1.86	4.09	1.73	0.23	100	1.81		
		UA3540-14	78.64	0.21	12.58	1.43	0.06	0.36	1.94	2.82	1.78	0.23	100	2.38		
	c	Mean	77.25	0.25	12.99	1.61	0.08	0.37	1.98	3.52	1.78	0.23	100	2.35	4	Augustine
		StDev	1.07	0.03	0.71	0.24	0.03	0.04	0.12	0.91	0.13	0.01	0	0.65		

		UA3540-8	70.93	0.47	15.12	2.39	0.19	0.54	1.64	5.42	3.12	0.24	100	1.41		
		UA3540-10	73.13	0.27	14.54	1.64	0.09	0.39	1.89	4.58	3.19	0.36	100	2.95		
		UA3540-6	74.84	0.15	14.06	1.27	0.00	0.27	1.44	4.44	3.28	0.32	100	5.10		
		UA3540-21	75.05	0.28	14.65	1.66	0.06	0.39	1.96	2.63	3.03	0.40	100	4.53		
	b	Mean	73.49	0.29	14.59	1.74	0.09	0.40	1.73	4.27	3.16	0.33	100	3.50	4	WRA-like
		StDev	1.91	0.13	0.43	0.47	0.08	0.11	0.24	1.18	0.11	0.07	0	1.66		
		UA3540-11	75.43	0.55	14.10	1.74	0.03	0.20	1.66	2.32	3.92	0.07	100	1.19		
		UA3540-5	73.74	0.19	14.25	1.55	0.15	0.41	0.49	3.77	5.44	0.01	100	5.25		
		UA3540-18	74.32	0.47	13.67	1.59	0.04	0.26	1.37	3.72	4.45	0.13	100	1.68		
		UA3540-16	73.04	0.38	14.29	1.89	0.04	0.46	1.84	4.81	3.07	0.22	100	3.23		
		UA3540-12	78.54	0.17	12.45	0.84	0.04	0.16	1.15	3.98	2.57	0.12	100	7.91		
		UA3540-1	78.55	0.17	12.55	1.06	0.08	0.17	1.07	2.17	4.11	0.11	100	5.99		
		UA3540-20	73.55	0.55	15.32	2.57	0.13	0.51	1.73	2.54	2.93	0.22	100	5.77		
Sept 2, 2020 NaSiTDI GRV17 75-76 cm reanalysis	Aniakchak	UA3539-9 rerun-1	71.06	0.52	15.46	2.45	0.20	0.50	1.65	4.94	3.05	0.21	100	0.83		
		UA3539-9 rerun-2	70.49	0.50	15.46	2.44	0.20	0.49	1.68	5.58	2.98	0.22	100	1.55		
		UA3539-11 rerun-1	70.95	0.53	15.29	2.39	0.19	0.51	1.68	5.30	3.00	0.21	100	0.60		
		UA3539-11 rerun-2	70.47	0.48	15.13	2.47	0.17	0.54	1.76	5.73	3.08	0.23	100	1.02		
		UA3539-12 rerun-1	71.15	0.41	15.25	2.53	0.14	0.48	1.82	4.93	3.11	0.23	100	2.04		
		Mean	70.83	0.49	15.32	2.45	0.18	0.51	1.72	5.30	3.05	0.22	100	1.21		
		StDev	0.32	0.05	0.14	0.05	0.03	0.03	0.07	0.37	0.05	0.01	0	0.58		
June 14, 2021 NaTDI GRV17 75-76 cm		UA3539-25	70.56	0.41	15.11	2.46	0.13	0.50	1.68	6.01	2.98	0.21	100	0.29		
		UA3539-11	70.65	0.49	15.22	2.46	0.18	0.54	1.66	5.52	3.11	0.21	100	2.70		
		UA3539-14	70.80	0.45	15.39	2.25	0.15	0.47	1.65	5.73	2.97	0.18	100	1.71		

		UA3539-24	70.85	0.44	15.17	2.35	0.12	0.48	1.73	5.75	2.97	0.20	100	1.00		
		UA3539-19	70.88	0.44	14.98	2.36	0.14	0.51	1.73	5.83	2.96	0.22	100	1.11		
		UA3539-5	70.94	0.47	15.19	2.39	0.12	0.48	1.69	5.54	3.01	0.20	100	2.04		
		UA3539-20	71.14	0.52	15.06	2.40	0.19	0.51	1.77	5.30	2.96	0.19	100	2.13		
		UA3539-27	71.24	0.55	15.03	2.29	0.16	0.46	1.67	5.45	3.01	0.18	100	1.86		
	b	Mean	70.88	0.47	15.14	2.37	0.15	0.49	1.70	5.64	3.00	0.20	100	1.61	8	Aniakchak
		StDev	0.23	0.05	0.13	0.07	0.03	0.03	0.04	0.23	0.05	0.02	0	0.77		
		UA3539-7	74.35	0.38	13.66	2.17	0.09	0.64	2.83	4.25	1.47	0.22	100	3.49		
		UA3539-23	76.45	0.26	12.98	1.34	0.12	0.34	2.29	4.56	1.50	0.22	100	1.86		
		UA3539-8	75.03	0.33	13.38	2.07	0.07	0.59	2.67	4.14	1.58	0.19	100	2.62		
		UA3539-17	76.65	0.22	13.12	1.51	0.08	0.36	2.18	4.09	1.61	0.23	100	4.41		
		UA3539-21	76.60	0.28	12.80	1.63	0.08	0.41	2.18	4.18	1.64	0.25	100	3.45		
		UA3539-28	76.94	0.27	12.72	1.52	0.12	0.34	2.12	4.21	1.64	0.15	100	2.43		
		UA3539-22	77.17	0.28	12.77	1.41	0.08	0.38	2.20	3.88	1.66	0.22	100	1.98		
		UA3539-26	76.95	0.24	12.54	1.44	0.06	0.32	2.05	4.52	1.67	0.27	100	2.25		
		UA3539-10	77.21	0.29	12.71	1.37	0.09	0.34	2.04	4.15	1.68	0.16	100	1.74		
		UA3539-1	76.70	0.25	12.83	1.54	0.06	0.40	2.19	4.17	1.69	0.22	100	5.37		
		UA3539-6	77.23	0.31	12.48	1.44	0.09	0.29	1.91	4.32	1.76	0.20	100	5.06		
		UA3539-16	77.89	0.29	12.49	1.47	0.07	0.31	1.90	3.62	1.84	0.17	100	3.16		
		UA3539-4	76.11	0.31	13.10	1.51	0.05	0.37	2.10	4.41	1.89	0.21	100	4.05		
	a	Mean	76.56	0.29	12.89	1.57	0.08	0.39	2.20	4.19	1.66	0.21	100	3.22	13	Augustine-like
		StDev	0.95	0.04	0.35	0.26	0.02	0.10	0.27	0.25	0.12	0.04	0	1.22		
		UA3539-18	74.48	0.13	13.95	1.28	0.06	0.23	1.50	4.84	3.29	0.31	100	3.74		
		UA3539-12	74.88	0.20	13.67	1.30	0.02	0.25	1.47	4.62	3.35	0.31	100	2.02		
		UA3539-3	75.11	0.14	14.14	1.25	0.01	0.29	1.45	4.17	3.23	0.27	100	2.95		
	c	Mean	74.82	0.16	13.92	1.28	0.03	0.25	1.48	4.54	3.29	0.30	100	2.90	3	WRA-like
		StDev	0.32	0.04	0.24	0.03	0.03	0.03	0.02	0.34	0.06	0.02	0	0.86		
		UA3539-9	73.19	0.20	14.33	1.49	0.10	0.41	1.87	3.64	4.49	0.35	100	2.73		
		UA3539-15	73.34	0.16	14.90	1.57	0.08	0.39	1.88	4.25	3.16	0.35	100	1.76		mixed shards
		UA3539-2	76.73	0.27	12.83	1.24	0.06	0.25	1.76	3.69	2.88	0.38	100	5.93		
		UA3539-13	77.99	0.19	12.58	0.94	0.03	0.25	1.38	4.10	2.45	0.12	100	7.07		
Jun 10, 2020 NaTDI		UA3534-12	70.71	0.52	15.05	2.48	0.13	0.50	1.67	5.65	3.10	0.22	100	2.00		
GRV17 77-78 cm		UA3534-10	70.82	0.52	15.21	2.39	0.11	0.54	1.69	5.49	3.09	0.19	100	2.33		
		UA3534-19	70.94	0.54	15.02	2.46	0.15	0.50	1.65	5.47	3.13	0.20	100	1.43		

	UA3534-6	71.21	0.41	15.09	2.41	0.14	0.51	1.77	5.25	3.03	0.23	100	4.07		
b	Mean	70.92	0.50	15.09	2.43	0.13	0.51	1.69	5.47	3.09	0.21	100	2.46	4	Aniakchak
	StDev	0.22	0.06	0.09	0.04	0.02	0.02	0.05	0.17	0.04	0.02	0	1.14		
	UA3534-30	74.82	0.19	13.97	1.22	0.03	0.30	1.57	4.39	3.25	0.33	100	2.77		
	UA3534-2	75.15	0.18	13.63	1.39	0.11	0.30	1.38	4.05	3.55	0.32	100	3.14		
	UA3534-11	76.70	0.22	12.77	1.38	0.09	0.28	0.99	3.69	3.64	0.32	100	3.48		
c	Mean	75.56	0.19	13.46	1.33	0.08	0.30	1.31	4.04	3.48	0.33	100	3.13	3	WRA?
	StDev	1.00	0.02	0.62	0.10	0.04	0.01	0.30	0.35	0.20	0.01	0	0.36		
	UA3534-15	76.53	0.24	12.99	1.59	0.06	0.40	2.15	4.17	1.72	0.19	100	4.36		
	UA3534-17	76.54	0.29	12.88	1.59	0.11	0.42	2.24	3.71	2.06	0.22	100	1.98		
	UA3534-26	76.83	0.29	12.82	1.51	0.04	0.37	2.13	4.30	1.54	0.23	100	2.05		
	UA3534-18	77.01	0.22	12.52	1.57	0.07	0.37	2.09	4.22	1.76	0.20	100	2.10		
	UA3534-25	77.03	0.30	12.68	1.57	0.08	0.42	2.07	4.05	1.66	0.20	100	3.26		
	UA3534-27	77.27	0.34	12.52	1.50	0.13	0.39	2.00	4.07	1.59	0.23	100	2.35		
	UA3534-5	77.27	0.25	12.61	1.56	0.07	0.47	2.09	3.93	1.61	0.19	100	2.74		
	UA3534-29	77.40	0.23	12.55	1.48	0.07	0.34	1.90	4.06	1.80	0.22	100	3.31		
	UA3534-23	78.06	0.23	12.44	1.35	0.09	0.36	2.00	3.57	1.72	0.22	100	4.28		
a	Mean	77.10	0.27	12.67	1.52	0.08	0.39	2.08	4.01	1.72	0.21	100	2.94	9	Augustine
	StDev	0.47	0.04	0.19	0.08	0.03	0.04	0.10	0.24	0.15	0.02	0	0.93		
	UA3534-21	73.10	0.14	15.42	1.10	0.00	0.24	2.19	4.95	2.67	0.24	100	1.88		
	UA3534-28	73.14	0.43	13.47	2.61	0.11	0.85	2.80	4.65	1.75	0.26	100	1.46		
	UA3534-22	74.33	0.47	12.73	2.14	0.06	0.40	1.57	4.17	3.81	0.41	100	2.28		mixed glass shards
	UA3534-7	78.39	0.26	12.31	0.75	0.06	0.53	1.68	4.10	1.88	0.05	100	4.94		
	UA3534-1	79.57	0.22	11.19	1.22	0.07	0.23	0.84	3.14	3.23	0.37	100	5.14		
Sept 2, 2020 NaSiTDI	UA3534-17	76.95	0.29	12.98	1.65	0.04	0.43	2.28	3.63	1.57	0.24	100	2.68		

GRV17 77-78 cm reanalysis		UA3534-15	77.14	0.30	12.86	1.50	0.05	0.47	2.20	3.60	1.71	0.23	100	3.13	
		UA3534-23	77.21	0.23	12.62	1.62	0.07	0.35	2.17	3.84	1.74	0.19	100	3.41	
		UA3534-10	77.31	0.31	12.70	1.61	0.07	0.33	2.18	3.64	1.71	0.19	100	1.08	
		UA3534-13	77.32	0.28	12.78	1.49	0.08	0.42	2.09	3.74	1.64	0.20	100	2.57	
		UA3534-1	77.47	0.24	12.69	1.64	0.09	0.38	2.17	3.52	1.66	0.18	100	2.61	
		UA3534-18	77.62	0.27	12.85	1.49	0.07	0.39	1.98	3.40	1.78	0.19	100	6.35	
		UA3534-5	77.76	0.24	12.42	1.66	0.09	0.33	1.88	3.72	1.75	0.20	100	1.80	
		UA3534-8	77.99	0.21	12.49	1.56	0.10	0.37	2.20	3.33	1.59	0.21	100	6.22	
		UA3534-4	78.18	0.20	12.39	1.47	0.08	0.30	1.94	3.64	1.64	0.22	100	2.71	
	a	Mean	77.50	0.26	12.68	1.57	0.07	0.38	2.11	3.61	1.68	0.20	100	3.26	10
		StDev	0.39	0.04	0.20	0.07	0.02	0.05	0.13	0.15	0.07	0.02	0	1.72	
		UA3534-14	70.73	0.54	15.51	2.40	0.20	0.48	1.72	5.06	3.19	0.22	100	1.67	
		UA3534-2	70.98	0.55	15.61	2.45	0.13	0.50	1.75	4.74	3.12	0.21	100	2.47	
		UA3534-16	71.03	0.55	14.95	2.42	0.10	0.51	1.67	5.46	3.13	0.23	100	0.39	
	b	Mean	70.92	0.55	15.36	2.42	0.14	0.50	1.71	5.09	3.15	0.22	100	1.51	3
		StDev	0.16	0.01	0.35	0.02	0.05	0.02	0.04	0.36	0.04	0.01	0	1.05	
		UA3534-12	74.77	0.19	14.32	1.32	0.06	0.27	1.44	4.26	3.12	0.31	100	1.65	
		UA3534-3	75.30	0.17	13.98	1.30	0.06	0.30	1.46	4.01	3.16	0.31	100	6.10	
		UA3534-20	75.52	0.19	13.73	1.37	0.06	0.29	1.37	3.89	3.34	0.30	100	2.00	
	c	Mean	75.20	0.19	14.01	1.33	0.06	0.29	1.42	4.05	3.21	0.31	100	3.25	3
		StDev	0.39	0.01	0.29	0.04	0.00	0.02	0.05	0.19	0.12	0.01	0	2.47	
		UA3534-11	72.81	0.51	13.87	2.96	0.05	0.98	3.08	3.74	1.80	0.28	100	4.14	
		UA3534-19	76.14	0.25	13.83	1.29	0.01	0.27	2.59	4.14	1.38	0.15	100	1.47	
		UA3534-7	75.99	0.14	14.03	0.71	0.05	0.09	0.94	2.78	5.22	0.06	100	4.90	
		UA3534-22	77.07	0.02	12.37	1.14	0.00	0.00	0.46	2.30	6.56	0.10	100	5.45	
		UA3534-24	77.50	0.17	12.39	1.37	0.08	0.30	1.45	3.60	2.81	0.44	100	3.78	
		UA3534-9	78.10	0.31	12.89	0.81	0.10	0.36	2.25	3.38	1.66	0.19	100	4.96	Hayes ish?

		UA3534-6	78.46	0.28	12.90	0.75	0.02	0.36	1.68	3.76	1.69	0.12	100	5.65		
Jun 10, 2020 NaTDI GRV17 82-83 cm		UA3533-2	74.49	0.13	14.20	1.14	0.05	0.25	1.56	4.86	3.09	0.29	100	2.99		
		UA3533-19	75.36	0.19	13.66	1.22	0.06	0.25	1.47	4.26	3.29	0.29	100	2.11		
		UA3533-3	75.87	0.18	13.58	1.32	0.07	0.29	1.32	3.79	3.32	0.33	100	4.77		
		UA3533-4	76.28	0.31	13.18	1.34	0.06	0.30	1.15	3.60	3.51	0.35	100	3.15		
	b	Mean	75.50	0.20	13.66	1.26	0.06	0.27	1.37	4.13	3.30	0.32	100	3.26	4	WRA-like
		StDev	0.77	0.08	0.42	0.09	0.01	0.02	0.18	0.56	0.17	0.03	0	1.11		
		UA3533-8	76.62	0.36	12.75	1.60	0.05	0.41	2.22	4.30	1.55	0.20	100	3.37		
		UA3533-21	76.99	0.28	12.74	1.59	0.04	0.36	2.17	4.05	1.57	0.25	100	4.15		
		UA3533-11	77.01	0.24	12.91	1.58	0.07	0.42	2.19	3.73	1.70	0.20	100	3.54		
		UA3533-6	77.15	0.29	12.61	1.48	0.07	0.33	1.99	4.27	1.63	0.21	100	3.65		
		UA3533-9	77.36	0.25	12.46	1.52	0.09	0.36	1.86	4.06	1.88	0.20	100	5.34		
		UA3533-1	77.82	0.29	12.29	1.51	0.08	0.22	1.85	4.15	1.66	0.20	100	3.19		
	a	Mean	77.16	0.29	12.63	1.55	0.07	0.35	2.05	4.09	1.66	0.21	100	3.87	6	Augustine
		StDev	0.40	0.04	0.22	0.05	0.02	0.07	0.17	0.21	0.12	0.02	0	0.79		
		UA3533-26	70.26	0.92	13.95	3.69	0.03	0.83	2.33	4.32	3.60	0.09	100	3.64		mixed glass shards
		UA3533-7	74.19	0.24	14.15	1.87	0.10	0.44	2.21	4.84	1.84	0.16	100	3.83		
		UA3533-18	77.25	0.20	12.99	1.16	0.11	0.28	1.55	3.84	2.47	0.19	100	5.21		
		UA3533-17	77.77	0.17	13.02	1.10	0.07	0.28	1.51	3.55	2.39	0.17	100	7.23		
Nov 26, 2020 NaSiTDI GRV17 86-87 cm		UA3619-13	75.84	0.26	13.39	1.31	0.04	0.47	2.34	4.63	1.53	0.23	100	6.51		
		UA3619-15	75.99	0.26	14.26	1.41	0.06	0.38	1.97	4.09	1.45	0.18	100	-0.60		
		UA3619-28	76.41	0.27	12.99	1.61	0.05	0.40	2.19	4.26	1.65	0.22	100	1.79		
		UA3619-18	76.43	0.29	12.76	1.55	0.05	0.40	2.13	4.49	1.75	0.21	100	2.86		
		UA3619-9	76.48	0.31	12.89	1.44	0.04	0.35	2.16	4.49	1.67	0.21	100	2.18		

	UA3619-24	76.68	0.27	12.89	1.52	0.07	0.37	2.08	4.37	1.62	0.18	100	3.19		
	UA3619-19	76.79	0.32	12.91	1.53	0.08	0.41	2.18	3.88	1.68	0.27	100	1.76		
	UA3619-6	76.81	0.23	12.73	1.48	0.08	0.29	1.93	4.42	1.87	0.21	100	3.76		
	UA3619-30	76.81	0.25	12.99	1.58	0.09	0.42	2.21	3.91	1.62	0.17	100	2.75		
	UA3619-20	76.86	0.23	12.97	1.53	0.06	0.40	2.12	3.97	1.72	0.19	100	1.02		
	UA3619-26	76.88	0.28	12.82	1.50	0.07	0.40	2.14	4.11	1.64	0.19	100	1.85		
	UA3619-5	76.92	0.26	12.88	1.44	0.08	0.34	2.08	4.13	1.71	0.20	100	1.30		
	UA3619-21	76.94	0.33	12.84	1.45	0.06	0.36	2.15	3.99	1.73	0.19	100	2.54		
	UA3619-25	77.00	0.26	12.76	1.51	0.08	0.42	2.14	4.02	1.64	0.22	100	1.60		
	UA3619-27	77.01	0.27	12.69	1.55	0.06	0.40	2.15	4.05	1.66	0.22	100	0.93		
	UA3619-16	77.26	0.24	12.80	1.58	0.10	0.35	2.20	3.64	1.68	0.20	100	4.60		
	UA3619-7	77.27	0.24	12.66	1.51	0.08	0.38	2.12	3.86	1.65	0.31	100	5.32		
	UA3619-4	77.32	0.24	12.34	1.43	0.10	0.34	1.88	4.27	1.87	0.27	100	5.74		
a	Mean	76.76	0.27	12.92	1.50	0.07	0.38	2.12	4.14	1.67	0.21	100	2.73	18	
	StDev	0.41	0.03	0.39	0.07	0.02	0.04	0.11	0.26	0.10	0.04	0	1.85		
	UA3619-3	73.16	0.38	14.13	2.08	0.06	0.54	2.21	4.60	2.64	0.26	100	0.77		
	UA3619-23	73.46	0.29	13.76	2.61	0.10	0.29	1.57	4.87	2.89	0.23	100	0.04		
	UA3619-2	73.47	0.40	14.12	1.90	0.09	0.54	2.18	4.41	2.68	0.26	100	1.51		
b	Mean	73.36	0.36	14.00	2.20	0.08	0.45	1.99	4.63	2.73	0.25	100	0.77	3	
	StDev	0.18	0.06	0.21	0.37	0.02	0.14	0.36	0.23	0.13	0.02	0	0.73		
	UA3619-8	74.17	0.23	14.57	1.22	0.02	0.16	2.22	4.48	2.62	0.37	100	14.51		
	UA3619-14	70.60	0.48	15.52	2.30	0.14	0.52	1.62	5.52	3.08	0.30	100	9.97		
	UA3619-29	75.07	0.16	14.01	1.23	0.16	0.27	1.53	4.17	3.18	0.28	100	1.09		
	UA3619-17	75.07	0.26	14.99	1.52	0.04	0.41	2.10	3.79	1.64	0.21	100	2.44		
	UA3619-11	78.04	0.22	12.55	0.96	0.06	0.25	1.20	3.82	2.80	0.13	100	5.04		
	UA3619-10	78.36	0.20	12.52	0.95	0.08	0.21	1.16	3.68	2.74	0.15	100	5.15		
c	Mean	75.22	0.26	14.03	1.36	0.08	0.30	1.64	4.24	2.68	0.24	100	6.37	6	low Na, high K

		StDev	2.84	0.11	1.26	0.50	0.05	0.14	0.45	0.69	0.55	0.10	0	5.02		
		UA3619-1	77.10	0.03	12.15	1.20	0.05	0.02	0.36	1.90	7.07	0.15	100	2.42		
Jun 22, 2020 NaTDI GRV17 93-94 cm		UA3532-23	77.18	0.20	12.74	1.50	0.06	0.36	2.21	3.98	1.64	0.18	100	1.64		
		UA3532-22	77.23	0.30	12.61	1.58	0.08	0.41	2.14	3.96	1.54	0.20	100	2.40		
		UA3532-13	77.56	0.18	12.72	1.45	0.08	0.37	2.07	3.75	1.65	0.21	100	1.56		
		UA3532-7	77.67	0.24	12.95	1.33	0.06	0.29	2.18	3.67	1.47	0.18	100	2.12		
	a	Mean	77.41	0.23	12.76	1.46	0.07	0.36	2.15	3.84	1.58	0.19	100	1.93	4	Augustine-like
		StDev	0.24	0.05	0.14	0.10	0.01	0.05	0.06	0.15	0.09	0.02	0	0.40		
		UA3532-20	75.68	0.35	12.49	2.29	0.02	0.59	2.15	4.02	2.19	0.27	100	2.35		
		UA3532-2	75.72	0.17	13.61	1.25	0.09	0.26	1.40	3.84	3.47	0.25	100	1.88		
		UA3532-8	75.76	0.34	13.45	1.85	0.08	0.62	2.15	3.06	2.56	0.18	100	3.81		
	b	Mean	75.72	0.29	13.18	1.80	0.06	0.49	1.90	3.64	2.74	0.23	100	2.68	3	unknown
		StDev	0.04	0.10	0.60	0.52	0.04	0.20	0.43	0.51	0.66	0.05	0	1.00		
		UA3532-17	71.16	0.60	15.16	2.50	0.15	0.52	1.71	4.93	3.14	0.17	100	1.09		
		UA3532-11	73.39	0.14	14.62	1.63	0.08	0.43	1.88	4.27	3.29	0.37	100	2.00		
		UA3532-5	78.13	0.24	12.37	1.35	0.05	0.25	1.76	3.69	2.05	0.15	100	4.17		
		UA3532-6	78.60	0.19	12.57	1.06	0.03	0.31	1.27	3.26	2.63	0.12	100	7.09		
		UA3532-14	78.90	0.33	12.08	1.46	0.06	0.35	1.64	3.04	1.98	0.22	100	1.81		mixed glass shards
		UA3532-29	74.03	0.49	14.51	0.82	0.00	0.05	1.92	3.93	4.25	0.03	100	5.34		
		UA3532-28	75.42	0.05	13.65	1.10	0.06	0.03	0.68	3.43	5.53	0.06	100	5.10		
		UA3532-24	76.22	0.58	13.29	1.11	0.02	0.07	1.08	3.25	4.32	0.09	100	5.38		
		UA3532-30	78.40	0.48	11.48	1.43	0.00	0.12	0.37	3.01	4.67	0.05	100	3.80		
		UA3532-4	70.61	0.12	17.55	0.42	0.02	0.22	1.66	3.48	5.94	0.00	100	6.25		
		UA3532-9	76.35	0.13	14.20	1.93	0.01	0.08	0.95	0.93	5.34	0.12	100	10.68		weathered?

		UA3532-19	77.00	0.05	13.67	1.99	0.14	0.02	0.45	1.42	5.19	0.10	100	10.27		weathered?
Jun 10, 2020 NaTDI		UA3531-19	77.16	0.28	13.12	1.63	0.03	0.37	2.14	3.35	1.75	0.21	100	3.31		
GRV17 97-98 cm		UA3531-24	77.17	0.28	12.98	1.62	0.05	0.41	2.18	3.44	1.72	0.20	100	6.69		
		UA3531-23	77.01	0.26	12.87	1.45	0.09	0.42	2.14	3.94	1.65	0.20	100	3.24		
		UA3531-30	78.17	0.31	11.84	1.64	0.07	0.38	1.66	4.04	1.75	0.20	100	2.44		
		UA3531-7	77.40	0.29	12.46	1.49	0.08	0.30	1.99	4.12	1.71	0.20	100	2.10		
		UA3531-4	77.00	0.27	12.66	1.50	0.07	0.41	2.07	4.13	1.72	0.22	100	1.98		
		UA3531-1	76.53	0.23	13.04	1.57	0.10	0.41	2.18	4.15	1.64	0.19	100	3.06		
		UA3531-8	77.62	0.32	12.41	1.31	0.07	0.36	1.90	4.22	1.63	0.19	100	2.81		
	a	Mean	77.26	0.28	12.67	1.53	0.07	0.38	2.03	3.93	1.70	0.20	100	3.20	8	Augustine
		StDev	0.49	0.03	0.43	0.11	0.02	0.04	0.18	0.34	0.05	0.01	0	1.49		
		UA3531-28	74.96	0.26	13.76	1.38	0.02	0.25	1.46	4.30	3.34	0.33	100	2.87		
		UA3531-6	74.96	0.20	14.00	1.22	0.03	0.33	1.45	4.34	3.25	0.29	100	3.05		
		UA3531-21	75.07	0.22	13.77	1.30	0.07	0.27	1.45	4.35	3.27	0.29	100	2.43		
	b	Mean	75.00	0.23	13.84	1.30	0.04	0.28	1.45	4.33	3.29	0.31	100	2.78	3	WRA-like
		StDev	0.06	0.03	0.14	0.08	0.02	0.04	0.01	0.03	0.05	0.02	0	0.32		
		UA3531-3	68.42	1.08	14.14	4.32	0.13	1.20	2.97	4.24	3.41	0.11	100	0.77		
		UA3531-17	73.51	0.16	14.38	1.57	0.04	0.44	1.85	4.57	3.20	0.36	100	2.74		
		UA3531-9	76.97	0.34	12.34	2.06	0.03	0.46	1.83	3.62	2.10	0.32	100	3.54		
		UA3531-15	77.04	0.22	12.60	1.59	0.07	0.39	2.18	4.01	1.70	0.29	100	8.79		bad point
		UA3531-11	76.67	0.09	12.71	1.41	0.07	0.00	0.20	3.62	5.16	0.09	100	7.59		
		UA3531-20	78.47	0.07	12.57	0.30	0.01	0.00	0.39	4.06	4.11	0.03	100	4.85		mixed glass shards
		UA3531-5	77.00	0.00	12.59	0.93	0.04	0.03	0.43	3.19	5.76	0.04	100	5.07		
		UA3531-16	77.08	0.32	13.40	0.96	0.06	0.08	0.80	3.72	3.53	0.05	100	5.35		
		UA3531-2	79.97	0.23	11.88	0.79	0.05	0.08	0.74	1.30	4.80	0.22	100	9.48		weathered?

Jun 22, 2020 NaTDI		UA3530-28	76.84	0.29	12.85	1.61	0.02	0.41	2.24	3.91	1.69	0.18	100	2.81		
GRV17 100-101 cm		UA3530-15	76.95	0.39	13.11	1.57	0.09	0.46	2.25	3.29	1.69	0.24	100	3.04		
		UA3530-5	76.98	0.21	12.67	1.54	0.06	0.39	2.16	4.11	1.73	0.20	100	2.61		
		UA3530-3	77.23	0.20	12.84	1.68	0.04	0.41	2.18	3.50	1.79	0.16	100	2.76		
		UA3530-30	77.51	0.24	12.82	1.56	0.05	0.42	2.24	3.36	1.62	0.22	100	3.49		
		UA3530-23	77.54	0.25	12.76	1.58	0.08	0.40	2.08	3.48	1.68	0.21	100	2.93		
		UA3530-1	77.72	0.27	12.71	1.64	0.09	0.36	2.17	3.29	1.58	0.21	100	2.51		
		UA3530-2	77.92	0.22	12.70	1.65	0.11	0.40	2.14	3.02	1.69	0.21	100	3.48		
	a	Mean	77.34	0.26	12.81	1.60	0.07	0.41	2.18	3.49	1.68	0.20	100	2.95	8	
		StDev	0.40	0.06	0.14	0.05	0.03	0.03	0.06	0.35	0.06	0.02	0	0.37		
		UA3530-17	72.92	0.23	15.38	1.22	0.06	0.23	2.26	4.72	2.75	0.28	100	2.36		
		UA3530-7	73.67	0.16	14.72	1.55	0.01	0.45	1.92	4.09	3.20	0.29	100	2.15		
		UA3530-27	77.25	0.76	11.64	2.08	0.02	0.21	0.72	3.34	3.95	0.03	100	5.04		
		UA3530-6	76.11	0.40	12.57	2.00	0.01	0.28	1.19	3.07	4.04	0.41	100	2.69		
		UA3530-8	76.45	0.10	13.53	0.42	0.00	0.04	0.75	3.86	4.78	0.08	100	3.63		mixed glass shards
		UA3530-13	74.65	0.27	13.71	0.21	0.00	0.01	0.44	2.72	7.99	0.01	100	2.92		
		UA3530-4	76.92	0.25	13.01	1.47	0.11	0.37	1.90	4.10	1.77	0.13	100	6.30		
		UA3530-20	77.94	0.29	12.44	1.01	0.11	0.32	2.18	3.76	1.86	0.12	100	2.92		
		UA3530-21	78.20	0.26	12.51	0.71	0.04	0.47	2.04	3.74	1.95	0.12	100	3.56		
		UA3530-24	70.64	0.34	15.70	3.28	0.06	0.07	1.13	2.20	6.51	0.09	100	8.79		weathered?
Jun 22, 2020 NaTDI		UA3529-28	72.08	0.16	15.77	1.27	0.05	0.32	2.30	4.72	3.11	0.27	100	4.64		
GRV17 107-108 cm		UA3529-8	74.80	0.60	13.18	2.26	0.03	0.38	1.38	3.52	3.80	0.08	100	5.71		
		UA3529-27	74.94	0.53	12.86	2.13	0.05	0.40	1.56	3.20	4.01	0.43	100	2.86		

	UA3529-23	75.27	0.33	13.82	1.57	0.05	0.35	1.76	3.68	2.97	0.23	100	6.04	
	UA3529-5	75.43	0.34	13.36	1.64	0.01	0.41	1.56	3.73	3.33	0.24	100	4.25	
	UA3529-7	77.27	0.28	12.86	1.58	0.08	0.42	2.21	3.50	1.63	0.22	100	1.33	
	UA3529-19	78.87	0.62	11.30	1.52	0.08	0.16	0.61	3.27	3.57	0.02	100	3.93	
	UA3529-24	76.90	0.04	12.81	1.01	0.03	0.03	0.56	2.77	5.82	0.05	100	4.29	mixed glass shards
	UA3529-15	74.02	0.91	12.38	3.16	0.07	0.24	1.03	3.07	5.07	0.05	100	6.65	
	UA3529-13	77.38	0.35	14.18	1.43	0.08	0.30	1.18	1.53	3.54	0.03	100	11.16	weathered?
	UA3529-21	78.10	0.11	12.55	0.83	0.01	0.13	0.73	2.95	4.53	0.06	100	6.56	
	UA3529-26	78.40	0.20	12.66	0.73	0.02	0.11	0.48	2.15	5.21	0.05	100	6.76	
	UA3529-18	76.04	0.01	13.78	0.90	0.03	0.13	1.00	3.14	4.91	0.08	100	6.21	
	UA3529-12	69.86	0.27	18.03	1.62	0.00	0.13	3.23	4.42	2.41	0.04	100	6.86	
	UA3529-9	72.11	0.12	16.68	0.65	0.00	0.19	2.66	6.12	1.37	0.14	100	3.93	hit a phenocryst?

Jun 22, 2020 NaTDI	UA3528-7	71.66	0.45	15.40	1.98	0.07	0.54	1.66	5.04	3.12	0.10	100	5.06	
GRV17 113-114 cm	UA3528-8	76.65	0.12	13.57	1.30	0.03	0.29	1.27	3.46	3.05	0.32	100	2.89	
	UA3528-2	77.63	0.31	12.62	0.88	0.03	0.36	1.78	3.09	3.27	0.06	100	4.98	
Notes: cuspate/platy shards, clean with some vesicles.	UA3528-3	78.03	0.04	12.90	0.92	0.02	0.03	0.46	2.02	5.56	0.03	100	7.18	
	UA3528-4	76.73	0.17	14.06	1.08	0.07	0.06	0.61	1.96	5.19	0.10	100	7.30	weathered?
	UA3528-1	77.44	0.19	12.49	0.67	0.04	0.12	0.69	2.80	5.49	0.09	100	4.96	
	UA3528-5	76.09	0.16	13.69	0.58	0.05	0.11	0.89	3.25	5.11	0.09	100	5.27	
	Mean	76.32	0.20	13.53	1.06	0.05	0.21	1.05	3.09	4.40	0.11	100	5.38	
	StDev	2.16	0.14	1.01	0.47	0.02	0.19	0.52	1.04	1.18	0.10	0	1.51	

Sept 2, 2020 NaSiTDI	UA3528-1	74.47	0.21	14.28	1.37	0.05	0.32	1.68	4.14	3.27	0.29	100	2.33		
GRV17 113-114 cm	UA3528-11	75.03	0.16	14.18	1.30	0.04	0.26	1.48	4.13	3.18	0.30	100	1.98		
reanalysis	UA3528-17	75.18	0.16	13.83	1.28	0.06	0.24	1.47	4.36	3.21	0.29	100	1.83		
	UA3528-19	75.37	0.13	13.64	1.24	0.06	0.29	1.49	4.34	3.21	0.28	100	1.54		
	UA3528-10	75.54	0.13	14.27	1.24	0.10	0.26	1.50	3.52	3.18	0.33	100	3.56		
	UA3528-18	75.56	0.19	13.98	1.20	0.05	0.23	1.51	3.84	3.23	0.27	100	3.89		
	UA3528-16	76.05	0.14	13.87	1.27	0.03	0.22	1.45	3.54	3.22	0.27	100	3.11		
	Mean	75.31	0.16	14.01	1.27	0.06	0.26	1.51	3.98	3.22	0.29	100	2.60	7	WRA-like
	StDev	0.49	0.03	0.24	0.06	0.02	0.04	0.08	0.35	0.03	0.02	0	0.92		
	UA3528-14	76.10	0.04	13.88	0.59	0.06	0.08	0.86	3.53	4.82	0.07	100	4.57		
	UA3528-15	76.34	0.15	13.81	0.49	0.00	0.07	0.89	3.15	5.04	0.06	100	5.38		
	UA3528-13	76.95	0.14	14.00	1.15	0.09	0.12	0.59	2.01	4.91	0.07	100	8.36		
	UA3528-6	77.20	0.13	13.56	1.77	0.06	0.00	0.72	1.20	5.30	0.09	100	9.35		weathered
	UA3528-4	75.17	0.81	12.89	1.61	0.00	0.16	0.46	3.77	5.12	0.03	100	3.73		
	UA3528-3	77.58	0.24	12.71	1.31	0.06	0.25	1.45	3.58	2.69	0.18	100	6.82		
	UA3528-7	78.03	0.15	12.81	0.98	0.10	0.19	1.19	4.18	2.26	0.14	100	4.15		
	UA3528-2	78.03	0.15	13.25	1.03	0.02	0.14	0.51	3.02	3.74	0.13	100	7.56		
	UA3528-8	78.62	0.20	12.79	0.95	0.05	0.24	1.16	3.43	2.44	0.14	100	6.02		
June 14, 2021 NaTDI	UA3538-16	72.81	0.36	14.01	2.75	0.10	0.28	1.64	5.27	2.62	0.20	100	2.53		
GRV17 123-124 cm	UA3538-4	73.12	0.35	13.85	2.51	0.05	0.26	1.58	5.57	2.55	0.21	100	1.67		
	UA3538-10	73.21	0.34	13.92	2.60	0.09	0.29	1.67	5.03	2.70	0.19	100	3.87		
	UA3538-29	73.51	0.29	13.69	2.52	0.07	0.35	1.59	5.35	2.50	0.16	100	2.13		
	UA3538-18	72.76	0.44	14.71	2.09	0.11	0.37	1.39	3.94	4.16	0.03	100	5.79		
a	Mean	73.08	0.36	14.04	2.49	0.08	0.31	1.57	5.03	2.91	0.16	100	3.20	5	unknown
	StDev	0.31	0.05	0.39	0.25	0.02	0.05	0.11	0.64	0.71	0.07	0	1.67		
	UA3538-24	74.55	0.14	14.06	1.32	0.06	0.30	1.57	4.44	3.35	0.27	100	2.70		
	UA3538-15	75.46	0.15	14.49	0.95	0.07	0.33	1.26	4.48	2.77	0.06	100	5.56		
	UA3538-6	76.12	0.15	13.49	1.08	0.06	0.20	1.28	5.04	2.49	0.10	100	9.09		

		UA3538-19	76.14	0.19	13.13	1.47	0.04	0.24	1.11	4.11	3.37	0.26	100	3.08		
		UA3538-22	77.73	0.23	12.44	1.03	0.06	0.22	1.25	4.33	2.61	0.14	100	5.70		
		UA3538-23	77.83	0.19	12.44	1.00	0.07	0.19	1.25	4.34	2.58	0.16	100	5.99		
		UA3538-2	78.45	0.22	12.23	1.02	0.05	0.26	1.19	4.04	2.46	0.13	100	6.78		
	b	Mean	76.61	0.18	13.18	1.13	0.06	0.25	1.27	4.40	2.80	0.16	100	5.56	7	unknown
		StDev	1.42	0.03	0.87	0.19	0.01	0.05	0.14	0.33	0.39	0.08	0	2.18		a bit scattered
		UA3538-5	73.04	0.28	13.85	2.10	0.05	0.20	1.25	5.37	3.69	0.21	100	6.74		
		UA3538-20	73.32	0.20	15.14	1.23	0.05	0.24	2.04	4.61	2.99	0.23	100	4.61		
		UA3538-3	77.15	0.26	12.63	1.43	0.10	0.36	2.16	4.07	1.65	0.26	100	2.67		
		UA3538-28	76.23	0.36	12.02	1.76	0.07	0.21	1.00	3.95	4.10	0.38	100	4.02		
		UA3538-13	76.30	0.14	12.90	1.20	0.04	0.04	0.72	4.19	4.38	0.12	100	4.88		
		UA3538-1	76.92	0.11	12.94	0.44	0.01	0.03	0.79	3.35	5.34	0.08	100	5.50		
		UA3538-21	77.02	0.02	12.44	0.85	0.01	0.02	0.45	2.91	6.22	0.07	100	5.11		
		UA3538-26	77.72	0.10	12.30	0.77	0.04	0.12	0.61	3.05	5.23	0.06	100	4.58		
		UA3538-7	78.30	0.56	11.58	1.14	0.02	0.07	0.49	3.20	4.62	0.02	100	6.08		
Jun 22, 2020 NaTDI		UA3535-18	73.54	0.29	14.38	2.65	0.10	0.35	1.67	4.24	2.61	0.24	100	6.86		
GRV17 133-134 cm		UA3535-12	73.54	0.34	13.94	2.48	0.08	0.39	1.65	4.69	2.73	0.21	100	1.36		
		UA3535-23	73.69	0.31	13.92	2.61	0.10	0.35	1.68	4.44	2.73	0.21	100	1.84		
	a	Mean	73.59	0.31	14.08	2.58	0.09	0.37	1.67	4.45	2.69	0.22	100	3.36		
		StDev	0.09	0.03	0.26	0.09	0.01	0.02	0.01	0.23	0.07	0.02	0	3.05		
		UA3535-5	77.22	0.28	12.52	1.52	0.08	0.39	1.81	3.96	2.08	0.18	100	2.35		
		UA3535-11	77.84	0.31	12.38	1.39	0.08	0.32	1.69	3.81	2.04	0.16	100	5.00		
		UA3535-28	78.38	0.33	12.36	1.29	0.03	0.28	1.33	3.50	2.34	0.21	100	5.76		
	c	Mean	77.81	0.31	12.42	1.40	0.06	0.33	1.61	3.75	2.15	0.18	100	4.37		
		StDev	0.58	0.02	0.09	0.12	0.03	0.05	0.25	0.24	0.16	0.02	0	1.79		
		UA3535-9	76.36	0.13	12.82	1.56	0.09	0.42	1.25	3.95	3.23	0.23	100	3.53		
		UA3535-6	78.45	0.15	12.72	1.10	0.08	0.27	1.27	3.46	2.41	0.12	100	6.50		
		UA3535-3	79.44	0.07	12.59	0.99	0.01	0.19	1.21	3.04	2.34	0.16	100	7.31		
		UA3535-14	79.04	0.33	12.34	0.82	0.04	0.03	0.33	2.79	4.25	0.03	100	8.63		mixed glass shards

		UA3535-30	79.18	0.20	12.80	0.79	0.01	0.09	0.48	2.18	4.22	0.08	100	8.50	
		UA3535-22	74.85	0.50	12.80	2.06	0.05	0.37	1.46	3.56	4.01	0.46	100	3.02	
		UA3535-4	76.37	0.25	13.65	0.52	0.05	0.14	0.89	2.83	5.29	0.01	100	4.80	
		UA3535-29	79.02	0.07	12.80	0.74	0.02	0.07	0.45	2.61	4.16	0.06	100	8.09	weathered?
		UA3535-10	76.79	0.14	13.82	0.95	0.08	0.12	0.96	2.19	4.90	0.07	100	6.23	
		UA3535-26	77.68	0.09	12.67	1.00	0.03	0.00	1.00	0.99	6.48	0.06	100	7.09	weathered?
		UA3535-15	75.56	0.20	12.52	1.47	0.05	0.39	1.29	0.72	7.67	0.16	100	5.25	weathered?
		UA3535-21	76.74	0.18	13.44	1.27	0.03	0.09	0.73	0.84	6.59	0.12	100	5.47	weathered?
		UA3535-27	80.05	0.26	11.99	1.16	0.07	0.06	0.33	1.88	4.13	0.07	100	8.07	weathered?
Sept 2, 2020 NaSiTDI GRV17 133-134 cm		UA3535-5 rerun-1	79.04	0.18	12.38	1.02	0.07	0.24	1.16	3.42	2.36	0.16	100	5.40	
		UA3535-6 rerun-1	79.01	0.21	12.41	1.07	0.06	0.18	1.13	3.48	2.33	0.13	100	5.90	
		UA3535-7 rerun-1	78.61	0.20	12.61	0.99	0.07	0.20	1.18	3.65	2.37	0.14	100	5.96	
	b	Mean	78.89	0.20	12.47	1.03	0.07	0.21	1.16	3.52	2.36	0.14	100	5.75	
		StDev	0.24	0.02	0.12	0.04	0.01	0.03	0.03	0.12	0.02	0.01	0	0.31	
		UA3535-17 rerun-1	77.58	0.29	12.69	1.48	0.05	0.30	1.78	3.75	1.93	0.18	100	1.46	
		UA3535-17 rerun-2	77.74	0.27	12.55	1.49	0.02	0.30	1.70	3.88	1.90	0.20	100	1.62	
		UA3535-10 rerun-1	77.25	0.09	13.23	0.55	0.06	0.21	1.33	2.02	5.25	0.01	100	0.58	
Jun 22, 2020 NaTDI GRV17 135-136 cm		UA3536-6	74.38	0.54	12.95	2.02	0.09	0.36	1.49	3.85	4.00	0.42	100	3.30	
		Mean	74.38	0.54	12.95	2.02	0.09	0.36	1.49	3.85	4.00	0.42	100	3.30	Stage moved, only one point worked
		StDev													

June 14, 2021 NaTDI		UA3536-11	71.69	0.52	13.97	2.50	0.11	0.54	2.18	4.42	3.72	0.46	100	1.01	
GRV17 135-136 cm		UA3536-13	74.72	0.42	12.62	2.07	0.08	0.34	1.50	3.95	3.99	0.40	100	2.97	
		UA3536-1	76.62	0.39	12.05	1.75	0.05	0.22	0.98	3.66	4.01	0.35	100	5.42	
	a	Mean	74.34	0.45	12.88	2.11	0.08	0.36	1.55	4.01	3.91	0.40	100	3.13	3
		StDev	2.49	0.07	0.98	0.38	0.03	0.16	0.60	0.38	0.16	0.06	0	2.21	
		UA3536-9	76.32	0.17	13.61	1.47	0.05	0.25	2.64	3.97	1.41	0.13	100	1.69	
		UA3536-16	76.35	0.31	12.94	1.79	0.03	0.45	2.20	3.91	1.89	0.19	100	2.13	
		UA3536-5	77.32	0.24	12.50	1.57	0.05	0.34	1.78	4.13	1.95	0.16	100	1.65	
		UA3536-17	77.36	0.24	13.12	1.16	0.08	0.27	2.41	3.78	1.48	0.13	100	3.18	
		UA3536-14	77.39	0.28	12.68	1.48	0.03	0.31	1.68	4.04	1.98	0.15	100	2.32	
		UA3536-3	77.47	0.31	12.48	1.46	0.03	0.29	1.69	4.15	1.98	0.16	100	2.53	
		UA3536-15	77.88	0.18	13.00	1.26	0.02	0.33	2.27	3.41	1.50	0.18	100	3.57	
		UA3536-12	77.98	0.28	12.32	1.41	0.05	0.29	1.66	3.82	2.04	0.19	100	6.09	
		UA3536-6	78.26	0.29	12.62	1.26	0.07	0.26	1.60	3.63	1.93	0.13	100	6.41	
		UA3536-2	78.40	0.35	12.04	1.45	0.04	0.27	1.65	3.75	1.92	0.18	100	1.61	
	b	Mean	77.47	0.27	12.73	1.43	0.05	0.30	1.96	3.86	1.81	0.16	100	3.12	10
		StDev	0.71	0.06	0.45	0.18	0.02	0.06	0.38	0.23	0.24	0.02	0	1.77	
		UA3536-10	77.66	0.08	12.54	1.04	0.00	0.01	0.44	2.45	5.68	0.13	100	7.49	
		UA3536-7	76.54	0.11	13.49	0.46	0.08	0.02	0.88	3.38	4.97	0.09	100	5.22	
June 14, 2021 NaTDI		UA3537-9	71.16	0.54	13.89	2.66	0.10	0.59	2.32	4.77	3.59	0.49	100	2.46	
GRV17 140-141 cm		UA3537-22	71.66	0.50	13.83	2.30	0.09	0.57	2.23	4.92	3.50	0.51	100	0.77	
		UA3537-19	73.10	0.29	13.48	2.19	0.05	0.50	2.04	4.43	3.50	0.54	100	4.17	
		UA3537-25	73.24	0.30	13.78	1.97	0.06	0.47	1.92	4.21	3.74	0.41	100	2.47	
		UA3537-26	73.99	0.44	12.95	2.14	0.07	0.42	1.68	4.13	3.82	0.46	100	4.48	
		UA3537-18	74.17	0.39	13.30	1.70	0.10	0.36	1.54	4.23	3.94	0.35	100	4.83	
		UA3537-17	74.68	0.46	12.91	1.87	0.04	0.32	1.34	4.17	3.92	0.39	100	4.55	
		UA3537-28	74.79	0.45	12.90	2.09	0.03	0.32	1.46	3.86	3.80	0.39	100	5.14	
		UA3537-3	74.95	0.48	12.47	1.92	0.03	0.31	1.56	4.09	3.89	0.38	100	5.12	
		UA3537-29	74.98	0.46	12.50	1.94	0.08	0.34	1.37	4.00	4.02	0.41	100	1.90	
		UA3537-15	74.99	0.45	12.51	2.00	0.06	0.31	1.45	3.92	3.98	0.41	100	2.75	
		UA3537-21	75.07	0.26	12.88	1.64	0.03	0.33	1.25	4.34	3.86	0.43	100	4.73	
		UA3537-10	75.34	0.42	12.64	1.96	0.00	0.27	1.37	3.89	3.79	0.42	100	4.10	

		UA3537-7	75.34	0.37	12.68	1.71	0.05	0.29	1.35	3.82	3.99	0.49	100	3.26		
		UA3537-6	75.88	0.50	11.85	2.02	0.02	0.26	1.24	3.89	4.05	0.39	100	5.18		
		UA3537-1	76.57	0.40	12.02	1.73	0.02	0.25	0.98	3.86	3.83	0.42	100	5.78		
		UA3537-11	76.79	0.36	11.89	1.63	0.04	0.19	0.92	3.99	3.93	0.34	100	4.00		
		UA3537-20	76.81	0.38	11.61	1.45	0.05	0.13	0.75	3.67	4.85	0.40	100	5.49		
		UA3537-23	77.30	0.27	11.91	1.21	0.00	0.14	0.96	4.05	3.85	0.41	100	3.25		
		UA3537-27	77.79	0.28	11.50	1.38	0.02	0.14	0.81	3.19	4.59	0.39	100	5.40		
		UA3537-5	77.96	0.23	11.94	1.06	0.04	0.12	0.79	3.53	4.06	0.36	100	5.23		
	a	Mean	75.07	0.39	12.64	1.84	0.05	0.32	1.40	4.05	3.93	0.42	100	4.05	21	High Cl population
		StDev	1.82	0.09	0.73	0.37	0.03	0.14	0.46	0.38	0.31	0.05	0	1.36		
		UA3537-8	67.50	0.37	17.32	2.04	0.00	0.48	4.30	5.06	2.62	0.38	100	2.68		
		UA3537-13	73.09	0.36	14.82	1.88	0.05	0.28	1.34	4.11	3.67	0.50	100	5.52		
		UA3537-24	72.00	0.33	15.15	1.45	0.00	0.17	2.41	5.34	2.95	0.27	100	3.09		
		UA3537-12	73.96	0.35	13.47	1.77	0.06	0.38	2.20	5.10	2.55	0.20	100	2.14		mixed shards, no population
		UA3537-16	76.77	0.16	12.72	1.41	0.07	0.30	1.69	4.92	1.87	0.13	100	5.44		
		UA3537-2	77.00	0.27	12.80	1.43	0.09	0.39	2.23	4.05	1.58	0.21	100	1.33		
Nov 25, 2020 NaSiTDI		UA3618-15	68.85	0.61	14.75	4.39	0.23	0.95	3.06	5.54	1.24	0.47	100	12.10		
GRV17 156-157 cm		UA3618-1	69.66	0.63	14.83	4.15	0.14	0.93	3.10	5.26	1.19	0.16	100	1.72		
		UA3618-26	69.75	0.63	14.62	4.27	0.13	0.69	3.07	5.42	1.29	0.15	100	2.89		
		UA3618-25	69.90	0.48	14.66	3.47	0.11	0.71	2.80	6.35	1.32	0.25	100	7.59		
		UA3618-5	71.02	0.41	14.70	3.44	0.14	0.58	2.61	5.51	1.37	0.31	100	7.49		
		UA3618-11	71.06	0.34	14.73	3.46	0.20	0.53	2.54	5.70	1.31	0.18	100	-0.45		
		UA3618-19	71.34	0.38	14.79	3.46	0.16	0.58	2.56	5.27	1.32	0.19	100	2.48		
	a	Mean	70.22	0.50	14.73	3.81	0.16	0.71	2.82	5.58	1.29	0.24	100	4.83	7	Ksudach KS2
		StDev	0.92	0.13	0.07	0.44	0.04	0.17	0.26	0.37	0.06	0.11	0	4.36		
		UA3618-4	74.52	0.43	12.65	1.94	0.02	0.34	1.36	4.27	4.14	0.43	100	4.97		
		UA3618-9	76.61	0.39	12.01	1.62	0.08	0.32	1.27	4.84	2.66	0.27	100	3.65		
	b	Mean	75.57	0.41	12.33	1.78	0.05	0.33	1.31	4.55	3.40	0.35	100	4.31	2	

		StDev	1.48	0.03	0.45	0.23	0.05	0.02	0.06	0.40	1.05	0.11	0	0.93		
		UA3618-6	77.79	0.26	12.45	1.00	0.11	0.19	1.13	4.38	2.58	0.15	100	5.55		
		UA3618-8	77.83	0.20	12.55	1.07	0.10	0.26	1.21	4.12	2.55	0.13	100	4.84		
	c	Mean	77.81	0.23	12.50	1.04	0.10	0.22	1.17	4.25	2.57	0.14	100	5.20	2	Augustine
		StDev	0.03	0.04	0.07	0.05	0.00	0.05	0.05	0.18	0.02	0.02	0	0.50		
		UA3618-30	74.82	0.06	13.66	1.25	0.04	0.01	0.65	2.76	6.73	0.04	100	4.03		
		UA3618-14	75.99	0.03	13.48	1.22	0.05	0.00	0.47	3.85	4.85	0.07	100	6.98		
		UA3618-2	76.20	0.14	13.77	0.36	0.06	0.08	0.87	3.27	5.20	0.06	100	4.75		
		UA3618-7	76.39	0.23	12.72	1.15	0.04	0.21	0.98	3.76	4.45	0.11	100	4.79		
		UA3618-10	77.89	0.08	12.42	0.74	0.01	0.03	0.67	2.49	5.62	0.08	100	5.10		Mixed glass shards
		UA3618-22	69.18	0.86	14.81	3.37	0.07	0.86	2.67	4.59	3.49	0.13	100	2.80		
		UA3618-13	70.18	1.13	13.67	4.22	0.05	0.76	2.51	3.95	3.47	0.08	100	0.69		
		UA3618-21	76.40	0.19	13.79	1.06	0.06	0.35	2.38	4.26	1.37	0.19	100	1.28		
		UA3618-3	77.11	0.24	12.96	1.24	0.07	0.36	1.92	4.36	1.59	0.17	100	2.08		
Nov 25, 2020 NaSiTDI		UA3617-3	73.84	0.25	13.68	1.90	0.05	0.21	1.21	4.86	3.83	0.22	100	2.73		
GRV17 162-163 cm		UA3617-21	74.26	0.26	13.86	1.92	0.00	0.29	1.21	4.53	3.48	0.23	100	4.35		
	b	Mean	74.05	0.25	13.77	1.91	0.03	0.25	1.21	4.69	3.66	0.23	100	3.54		Dawson?
		StDev	0.30	0.01	0.13	0.01	0.04	0.05	0.00	0.23	0.24	0.01	0	1.14		
		UA3617-16	73.79	0.74	13.27	2.62	0.07	0.69	2.04	4.25	2.36	0.22	100	1.64		
		UA3617-15	73.81	0.69	13.09	2.79	0.05	0.71	2.09	4.24	2.36	0.21	100	1.76		
		UA3617-28	75.11	0.48	13.30	1.77	0.06	0.43	1.63	4.22	2.87	0.17	100	0.17		
		UA3617-12	76.19	0.41	12.50	1.89	0.03	0.33	1.40	4.39	2.68	0.22	100	3.25		
		UA3617-17	77.00	0.19	13.01	1.13	0.02	0.26	1.30	3.99	3.09	0.03	100	6.71		
		UA3617-32	77.02	0.34	12.27	1.77	0.05	0.31	1.45	4.02	2.59	0.24	100	2.80		
		UA3617-29	77.16	0.48	11.68	1.92	0.07	0.35	1.30	4.19	2.69	0.20	100	1.71		

	UA3617-7	77.60	0.18	13.02	0.42	0.00	0.08	1.25	4.15	3.30	0.00	100	1.03	
	UA3617-31	77.71	0.13	12.28	0.98	0.07	0.24	1.20	4.59	2.65	0.20	100	6.57	
	UA3617-8	78.07	0.19	12.51	0.95	0.02	0.22	1.20	4.03	2.67	0.16	100	4.69	
	UA3617-20	78.89	0.22	12.18	0.97	0.06	0.24	1.07	3.61	2.65	0.14	100	5.61	new population, not WRA but similar
a	Mean	76.58	0.37	12.65	1.56	0.05	0.35	1.45	4.15	2.72	0.16	100	3.27	High Fe, may be similar to Hayes
	StDev	1.68	0.21	0.53	0.74	0.02	0.19	0.34	0.25	0.28	0.08	0	2.29	
	UA3617-9	72.69	0.94	12.75	3.03	0.01	0.58	1.49	4.34	4.14	0.02	100	1.15	
	UA3617-11	76.50	0.32	12.23	1.52	0.06	0.31	1.83	2.92	4.17	0.16	100	1.21	
	UA3617-1	78.05	0.21	12.43	1.00	0.10	0.22	1.21	4.06	2.60	0.15	100	6.04	
c	Mean	75.75	0.49	12.47	1.85	0.06	0.37	1.51	3.77	3.63	0.11	100	2.80	
	StDev	2.76	0.39	0.26	1.05	0.04	0.19	0.31	0.75	0.90	0.08	0	2.81	
	UA3617-25	76.38	0.24	13.16	1.53	0.06	0.44	2.23	4.17	1.54	0.35	100	10.68	
	UA3617-33	76.53	0.31	12.78	1.59	0.03	0.39	1.88	4.42	1.94	0.18	100	3.38	
	UA3617-13	76.85	0.27	12.95	1.29	0.05	0.33	1.68	4.62	1.88	0.12	100	5.63	
	UA3617-24	76.87	0.20	13.23	1.43	0.06	0.40	2.25	3.81	1.58	0.22	100	3.43	
	UA3617-14	77.04	0.27	13.13	1.32	0.13	0.31	1.69	4.14	1.87	0.15	100	5.91	
d	Mean	76.73	0.26	13.05	1.43	0.06	0.37	1.94	4.23	1.76	0.21	100	5.81	Augustine
	StDev	0.27	0.04	0.18	0.13	0.04	0.05	0.28	0.31	0.19	0.09	0	2.97	
	UA3617-30	74.40	0.26	13.81	1.24	0.02	0.09	0.74	3.03	6.38	0.03	100	4.50	weathered
	UA3617-18	74.62	0.75	12.60	2.32	0.04	0.13	0.66	3.86	4.92	0.14	100	5.16	weathered
	UA3617-5	74.83	0.41	12.43	1.84	0.00	0.33	1.39	4.47	3.87	0.58	100	10.90	
	UA3617-6	75.42	0.49	12.40	1.90	0.05	0.37	1.32	3.73	3.90	0.53	100	6.14	
	UA3617-4	76.09	0.06	13.14	1.06	0.01	0.01	0.39	2.37	6.81	0.09	100	4.70	weathered
	UA3617-2	76.15	0.00	13.30	0.61	0.10	0.00	0.39	2.24	7.18	0.03	100	5.09	weathered

Nov 25, 2020 NaSiTDI		UA3616-18	73.35	0.31	13.99	2.53	0.07	0.32	1.55	5.16	2.56	0.19	100	1.18		
GRV17 166-167 cm		UA3616-4	75.78	0.09	14.45	0.87	0.08	0.30	1.16	4.37	2.90	0.01	100	5.17		
		UA3616-3	76.24	0.17	14.19	0.88	0.05	0.31	1.14	4.07	2.93	0.04	100	5.44		
		UA3616-16	76.43	0.10	13.85	0.65	0.04	0.08	0.89	2.99	4.92	0.06	100	5.24		
		UA3616-8	77.35	0.21	13.16	1.33	0.05	0.29	1.70	3.96	1.85	0.14	100	8.17		mixed glass
		UA3616-5	77.42	0.30	12.92	0.69	0.00	0.03	0.89	4.04	3.65	0.06	100	4.35		
		UA3616-12	77.53	0.35	12.63	0.84	0.05	0.12	1.15	3.68	3.63	0.01	100	3.21		
		UA3616-9	77.68	0.26	12.79	1.20	0.05	0.23	1.51	4.20	1.96	0.14	100	8.51		
		UA3616-7	76.37	0.69	13.03	1.75	0.00	0.12	0.84	2.32	4.85	0.05	100	6.97		
		UA3616-10	76.68	0.88	12.17	1.07	0.00	0.05	0.34	3.65	5.11	0.07	100	3.34		higher K glass
		UA3616-13	76.98	0.34	13.21	0.94	0.00	0.05	0.66	2.40	5.41	0.00	100	7.60		
		UA3616-14	77.49	0.36	12.97	0.87	0.00	0.06	0.62	2.31	5.30	0.04	100	6.79		
Nov 25, 2020 NaSiTDI		UA3615-16	77.40	0.36	12.28	1.29	0.04	0.22	1.08	4.27	2.89	0.21	100	5.06		
GRV17 188-189 cm		UA3615-28	77.78	0.25	12.36	1.02	0.07	0.24	1.14	4.04	2.86	0.34	100	12.05		
		UA3615-31	78.11	0.24	12.19	1.13	0.07	0.19	1.13	4.01	2.79	0.17	100	4.39		
		UA3615-27	78.13	0.23	12.39	1.11	0.07	0.23	1.17	3.90	2.63	0.18	100	4.52		
		UA3615-13	78.44	0.19	12.11	1.11	0.08	0.18	1.03	3.82	2.87	0.20	100	4.29		
		UA3615-14	78.60	0.19	12.09	1.10	0.08	0.22	1.10	3.79	2.70	0.17	100	3.79		
		UA3615-18	78.63	0.29	12.32	1.11	0.03	0.19	1.09	3.38	2.82	0.19	100	4.42		
		UA3615-30	78.99	0.21	12.16	0.95	0.07	0.14	1.02	3.75	2.57	0.20	100	7.71		
	a	Mean	78.26	0.24	12.24	1.10	0.06	0.20	1.09	3.87	2.76	0.21	100	5.78	8	unknown
		StDev	0.51	0.06	0.12	0.10	0.02	0.03	0.05	0.26	0.12	0.06	0	2.81		
		UA3615-3	76.45	0.30	12.95	1.22	0.01	0.24	1.03	3.07	4.72	0.02	100	4.85		

	UA3615-12	76.52	0.38	12.76	1.12	0.00	0.15	1.05	2.96	5.00	0.07	100	4.94		
	UA3615-24	77.45	0.05	13.43	0.47	0.06	0.02	0.48	3.42	4.59	0.06	100	6.10		
	UA3615-29	77.72	0.11	13.11	1.04	0.04	0.08	0.49	1.06	6.29	0.09	100	9.58		
	UA3615-9	78.06	0.32	12.34	1.13	0.04	0.18	0.98	2.24	4.67	0.05	100	4.75		
	UA3615-10	78.63	0.30	12.23	1.04	0.03	0.17	0.91	2.09	4.55	0.07	100	4.54		
b	Mean	77.99	0.31	12.41	0.93	0.03	0.12	0.75	2.70	4.72	0.05	100	5.14	6	lower Na, Higher K
	StDev	1.21	0.17	0.83	0.26	0.02	0.08	0.27	0.84	0.73	0.02	0	2.18		
	UA3615-2	75.03	0.72	12.98	1.47	0.04	0.14	1.13	3.27	4.91	0.39	100	20.95		
	UA3615-23	75.22	1.01	12.62	1.19	0.05	0.15	0.74	3.57	5.37	0.12	100	10.80		
	UA3615-1	76.06	0.82	12.11	1.69	0.03	0.09	0.56	3.17	5.41	0.08	100	5.79		
	UA3615-8	79.44	0.54	11.32	0.72	0.03	0.07	0.57	3.44	3.84	0.02	100	1.72		Higher Ti
	UA3615-7	79.66	0.51	11.12	0.72	0.05	0.03	0.47	3.33	4.08	0.03	100	4.63		
	UA3615-26	69.47	0.94	14.94	3.41	0.06	0.77	2.27	4.12	3.96	0.08	100	2.55		Allerod
	UA3615-22	75.29	0.41	13.05	1.70	0.10	0.34	1.44	4.57	2.96	0.18	100	4.51		
	UA3615-21	75.40	0.09	14.15	1.16	0.08	0.20	1.10	4.37	3.35	0.12	100	7.84		
	UA3615-20	75.61	0.13	13.89	1.03	0.07	0.11	1.07	4.89	3.14	0.08	100	6.91		
	UA3615-15	75.97	0.21	13.64	1.02	0.04	0.17	1.78	4.82	2.21	0.17	100	2.77		Mixed shards
	UA3615-19	76.78	0.17	13.75	0.96	0.08	0.24	2.10	4.32	1.49	0.13	100	4.36		
	UA3615-11	77.12	0.32	12.87	1.50	0.05	0.30	1.83	3.98	1.87	0.22	100	2.17		
	UA3615-25	78.53	0.22	12.55	1.14	0.07	0.32	1.38	3.66	1.97	0.20	100	3.80		
	UA3615-4	78.82	0.29	12.36	1.05	0.09	0.25	1.48	3.69	1.81	0.20	100	5.67		
	UA3615-5	81.76	0.21	12.39	1.09	0.07	0.20	1.44	0.91	1.77	0.21	100	7.31		
Nov 25, 2020 NaSiTDI	UA3614-19	74.43	0.30	13.81	1.71	0.04	0.29	1.83	4.76	2.69	0.16	100	3.18		
GRV17 201-202 cm	UA3614-28	74.76	0.38	13.50	1.72	0.05	0.35	1.49	4.64	2.94	0.21	100	6.81		

	UA3614-22	75.12	0.36	13.23	1.75	0.05	0.29	1.45	4.66	2.91	0.23	100	2.56		
	UA3614-17	75.17	0.43	13.37	1.81	0.08	0.36	1.45	4.10	3.08	0.19	100	1.16		
	UA3614-20	75.22	0.39	13.09	1.85	0.05	0.34	1.50	4.47	2.91	0.24	100	7.63		
	UA3614-12	75.26	0.36	13.23	1.77	0.02	0.35	1.49	4.52	2.84	0.19	100	3.38		
	UA3614-11	75.37	0.39	13.36	1.73	0.06	0.34	1.42	4.19	3.01	0.16	100	3.09		
	UA3614-31	75.37	0.40	13.20	1.76	0.00	0.36	1.46	4.39	2.91	0.21	100	0.72		
	UA3614-8	75.45	0.35	13.50	1.78	0.03	0.39	1.48	3.93	2.94	0.20	100	4.49		
	UA3614-1	75.47	0.46	13.15	1.79	0.01	0.30	1.42	4.07	3.06	0.34	100	10.25		
	UA3614-4	75.51	0.39	13.14	1.71	0.04	0.34	1.42	4.34	2.95	0.20	100	2.65		
	UA3614-26	75.55	0.38	13.34	1.62	0.07	0.34	1.41	4.15	2.99	0.18	100	1.40		
a	Mean	75.22	0.38	13.33	1.75	0.04	0.34	1.49	4.35	2.94	0.21	100	3.94	12	Redoubt?
	StDev	0.33	0.04	0.20	0.06	0.02	0.03	0.11	0.27	0.10	0.05	0	2.89		
	UA3614-16	73.57	0.72	13.80	2.30	0.06	0.33	1.28	4.14	3.77	0.03	100	4.02		
	UA3614-24	73.74	0.13	13.92	1.75	0.11	0.02	0.43	5.22	4.51	0.21	100	3.59		
	UA3614-23	74.94	0.05	14.42	1.18	0.12	0.12	0.87	4.77	3.48	0.06	100	6.19		
	UA3614-29	75.04	0.26	13.49	1.38	0.01	0.17	0.81	4.77	4.04	0.07	100	3.38		
	UA3614-3	77.16	0.10	12.61	1.18	0.10	0.06	0.20	4.95	3.58	0.07	100	5.28		
	UA3614-2	77.37	0.07	12.70	1.05	0.06	0.04	0.22	4.84	3.63	0.04	100	5.10		mixed shards
	UA3614-15	77.43	0.38	12.44	1.23	0.03	0.10	0.68	3.71	3.96	0.05	100	5.75		
	UA3614-25	77.58	0.12	13.69	0.72	0.02	0.13	0.67	2.90	4.13	0.03	100	8.16		
	UA3614-27	78.41	0.12	12.30	0.81	0.05	0.15	0.48	3.69	3.93	0.06	100	5.98		
	UA3614-13	78.75	0.28	12.11	0.85	0.07	0.09	0.25	3.64	3.91	0.08	100	4.91		
	UA3614-14	78.77	0.29	12.19	0.73	0.06	0.06	0.29	3.84	3.73	0.05	100	5.80		
	UA3614-9	78.90	0.43	11.87	1.61	0.00	0.16	0.76	2.83	3.44	0.01	100	6.59		

S12.1 Standard data (reference)

	SiO2	TiO2	Al2O3	FeO	MnO	MgO	CaO	Na2O	K2O	Cl	Total	H2Odiff
ID 3506	**74.10**	**0.07**	**13.10**	**1.55**	**0.07**	**0.04**	**0.74**	**4.06**	**5.13**	**0.34**	**99.09**	
assayed	0.96	0.03	0.34	0.06	0.03	0.02	0.05	0.28	0.26	0.03		
Old Crow	**75.15**	**0.31**	**13.14**	**1.70**	**0.05**	**0.29**	**1.48**	**3.84**	**3.72**	**0.28**	**100.00**	**4.12**
assayed	1.00	0.05	0.34	0.14	0.03	0.03	0.05	0.26	0.26	0.05		

Note: ID3506 not shown with offline corrections, only Old Crow. Unless otherwise stated, offline corrections were calculated using ID3506 values

S9.2 Standard data (collected)

Date analyzed	Sample	**SiO2**	**TiO2**	**Al2O3**	**FeO**	**MnO**	**MgO**	**CaO**	**Na2O**	**K2O**	**Cl**	**Total**	**H2Odiff**	**Analytical notes**
2020-12-18 NaTDI	ID3506_001	75.06	0.12	13.06	1.55	0.06	0.06	0.72	3.85	5.20	0.36	99.96	0.04	Si and K corrected
	ID3506_002	75.32	0.07	12.94	1.54	0.07	0.04	0.74	4.04	5.09	0.33	100.11	-0.11	
	ID3506_003	75.72	0.10	13.09	1.57	0.08	0.05	0.73	4.10	5.10	0.32	100.78	-0.78	
	ID3506_004	74.44	0.10	13.01	1.62	0.07	0.03	0.71	4.25	5.15	0.34	99.65	0.35	
	ID3506_005	73.95	0.10	13.02	1.57	0.07	0.03	0.74	4.12	5.10	0.33	98.96	1.04	
	ID3506_006	74.74	0.15	12.93	1.60	0.02	0.05	0.75	4.10	5.00	0.36	99.63	0.37	
	Mean	74.87	0.11	13.01	1.58	0.06	0.04	0.73	4.08	5.11	0.34	99.85	0.15	
	St. Dev	0.63	0.03	0.06	0.03	0.02	0.01	0.01	0.13	0.06	0.02	0.60	0.60	
	OldCrow_001	74.52	0.35	13.05	1.72	0.03	0.31	1.48	4.51	3.78	0.33	100.00	2.95	
	OldCrow_002	75.04	0.29	13.21	1.85	0.02	0.33	1.50	4.02	3.52	0.28	100.00	3.47	
	OldCrow_003	75.36	0.31	13.09	1.76	0.07	0.29	1.46	3.77	3.65	0.32	100.00	3.29	
	OldCrow_004	75.53	0.32	13.16	1.66	0.06	0.34	1.46	3.58	3.69	0.28	100.00	3.73	
	OldCrow_005	75.56	0.30	12.92	1.73	0.07	0.32	1.50	3.60	3.77	0.30	100.00	2.96	
	OldCrow_006	75.51	0.35	13.26	1.63	0.07	0.29	1.51	3.56	3.57	0.31	100.00	4.62	

Mean	75.25	0.32	13.11	1.73	0.05	0.31	1.48	3.84	3.66	0.30	100.00	3.50
St. Dev	0.41	0.02	0.12	0.08	0.02	0.02	0.02	0.37	0.10	0.02	0.00	0.62
ID3506_007	74.55	0.10	13.16	1.59	0.06	0.05	0.74	4.12	5.14	0.36	99.80	0.20
ID3506_008	74.52	0.05	13.09	1.62	0.04	0.04	0.73	4.41	4.98	0.35	99.75	0.25
ID3506_009	74.69	0.07	13.16	1.54	0.11	0.04	0.74	4.13	5.08	0.34	99.83	0.17
ID3506_010	74.83	0.11	12.81	1.55	0.07	0.03	0.72	4.07	5.07	0.32	99.50	0.50
ID3506_011	74.98	0.06	12.88	1.48	0.11	0.04	0.71	3.97	5.10	0.32	99.57	0.43
Mean	74.72	0.08	13.02	1.56	0.08	0.04	0.73	4.14	5.08	0.34	99.69	0.31
St. Dev	0.19	0.03	0.17	0.05	0.03	0.01	0.01	0.16	0.06	0.02	0.15	0.15
OldCrow_007	75.02	0.35	13.23	1.73	0.06	0.31	1.43	3.79	3.88	0.26	100.00	4.61
OldCrow_008	75.03	0.32	13.31	1.65	0.06	0.28	1.51	3.95	3.64	0.32	100.00	4.67
OldCrow_009	75.14	0.33	13.24	1.76	0.06	0.33	1.46	3.87	3.59	0.28	100.00	3.92
Mean	75.06	0.33	13.26	1.72	0.06	0.31	1.47	3.87	3.70	0.29	100.00	4.40
St. Dev	0.07	0.02	0.04	0.06	0.00	0.02	0.04	0.08	0.15	0.03	0.00	0.42
ID3506_012	74.50	0.06	13.16	1.53	0.08	0.06	0.75	4.40	5.13	0.33	99.93	0.07
ID3506_013	73.68	0.10	13.08	1.64	0.08	0.00	0.73	4.05	5.15	0.34	98.78	1.22
ID3506_014	73.14	0.13	13.04	1.56	0.12	0.04	0.75	3.95	5.08	0.35	98.07	1.93
ID3506_015	74.92	0.12	12.89	1.62	0.04	0.03	0.71	3.87	5.05	0.35	99.52	0.48
ID3506_016	75.20	0.12	13.19	1.55	0.05	0.05	0.73	4.00	5.10	0.35	100.27	-0.27
ID3506_017	74.81	0.10	13.12	1.61	0.11	0.05	0.74	4.38	5.09	0.37	100.29	-0.29
Mean	74.38	0.10	13.08	1.59	0.08	0.04	0.73	4.11	5.10	0.35	99.48	0.52
St. Dev	0.80	0.02	0.11	0.04	0.03	0.02	0.02	0.23	0.04	0.01	0.89	0.89
OldCrow_012	75.39	0.30	13.24	1.72	0.07	0.31	1.45	3.80	3.49	0.30	100.00	4.97
OldCrow_013	75.60	0.28	13.22	1.67	0.04	0.30	1.45	3.80	3.40	0.30	100.00	3.59
OldCrow_014	75.48	0.38	13.00	1.74	0.05	0.32	1.46	3.72	3.64	0.27	100.00	3.50

OldCrow_015	75.73	0.30	13.12	1.73	0.08	0.31	1.48	3.07	3.96	0.28	100.00	2.13
OldCrow_016	75.42	0.29	13.08	1.73	0.07	0.31	1.49	3.77	3.62	0.30	100.00	1.26
OldCrow_017	74.78	0.30	13.26	1.62	0.05	0.35	1.41	4.35	3.65	0.29	100.00	3.85
Mean	75.40	0.31	13.15	1.70	0.06	0.32	1.46	3.75	3.63	0.29	100.00	3.22
St. Dev	0.33	0.04	0.10	0.05	0.01	0.02	0.03	0.41	0.19	0.01	0.00	1.32
ID 3506												
Overall Mean	74.65	0.10	13.04	1.57	0.07	0.04	0.73	4.11	5.10	0.34	99.67	0.33
St. Dev	0.62	0.03	0.11	0.04	0.03	0.02	0.01	0.17	0.05	0.02	0.63	0.63
Old Crow												
Overall Mean	75.27	0.32	13.16	1.71	0.06	0.31	1.47	3.81	3.66	0.29	100.00	3.57
St. Dev	0.34	0.03	0.11	0.06	0.02	0.02	0.03	0.34	0.15	0.02	0.00	0.99

Jan 22 and 23 run in a single file, but over two days with standards at the start of Jan 22, and end of Jan 23, with a re-run of sanidine and obs in middle

22-Jan-20	ID 3506_001	74.09	0.08	13.21	1.60	0.09	0.06	0.75	3.93	5.18	0.35	99.26	0.74	Ca, Na and K are all corrected from ID3506
	ID 3506_002	74.20	0.07	13.05	1.62	0.09	0.04	0.73	4.27	5.10	0.35	99.44	0.56	NaTDI
	ID 3506_003	73.90	0.07	13.11	1.65	0.05	0.06	0.72	3.81	5.09	0.36	98.74	1.27	
	ID 3506_004	74.52	0.05	13.07	1.62	0.07	0.05	0.73	3.94	4.84	0.35	99.16	0.84	
	ID 3506_005	73.85	0.10	13.03	1.62	0.06	0.05	0.70	3.40	5.27	0.37	98.36	1.64	
	ID 3506_006	74.09	0.06	12.92	1.72	0.08	0.05	0.73	3.80	4.85	0.36	98.58	1.42	
	Mean	74.11	0.07	13.06	1.64	0.07	0.05	0.73	3.86	5.06	0.35	98.92	1.08	
	StDev	0.24	0.02	0.09	0.04	0.02	0.01	0.02	0.28	0.17	0.01	0.43	0.43	
	Old Crow_002	75.67	0.28	13.17	1.70	0.03	0.31	1.50	3.67	3.45	0.30	100.00	4.33	

Old Crow_003	74.99	0.28	13.23	1.69	0.10	0.26	1.43	4.22	3.59	0.27	100.00	2.63
Old Crow_004	75.52	0.38	13.19	1.71	0.03	0.34	1.46	3.51	3.62	0.30	100.00	3.74
Old Crow_005	75.50	0.33	12.83	1.63	0.08	0.29	1.42	4.10	3.63	0.27	100.00	1.18
Mean	75.42	0.32	13.10	1.68	0.06	0.30	1.45	3.87	3.57	0.28	100.00	2.97
StDev	0.29	0.05	0.18	0.04	0.04	0.03	0.04	0.34	0.08	0.02	0.00	1.39
ID 3506_007	75.22	0.10	12.99	1.54	0.06	0.06	0.71	4.13	4.67	0.37	99.77	0.23
ID 3506_008	73.64	0.12	12.91	1.49	0.11	0.06	0.76	3.74	4.75	0.36	97.86	2.14
ID 3506_009	73.33	0.09	13.20	1.62	0.08	0.05	0.73	3.99	4.71	0.36	98.09	1.91
ID 3506_010	73.92	0.09	13.12	1.50	0.05	0.04	0.73	4.12	4.81	0.35	98.64	1.36
ID 3506_011	75.04	0.05	13.13	1.61	0.06	0.05	0.72	3.84	4.78	0.33	99.54	0.46
Mean	74.23	0.09	13.07	1.55	0.07	0.05	0.73	3.96	4.74	0.36	98.78	1.22
StDev	0.85	0.03	0.12	0.06	0.02	0.01	0.02	0.17	0.05	0.02	0.85	0.85
Old Crow_007	75.37	0.33	13.22	1.72	0.07	0.31	1.47	3.82	3.44	0.33	100.00	3.63
Old Crow_008	76.05	0.34	12.95	1.71	0.06	0.31	1.46	3.49	3.41	0.30	100.00	2.98
Old Crow_009	75.72	0.27	13.22	1.69	0.11	0.32	1.47	3.54	3.43	0.29	100.00	4.52
Old Crow_011	75.92	0.33	13.19	1.66	0.10	0.26	1.39	3.67	3.28	0.26	100.00	5.22
Mean	75.76	0.32	13.14	1.69	0.09	0.30	1.45	3.63	3.39	0.30	100.00	4.09
StDev	0.30	0.03	0.13	0.03	0.02	0.03	0.04	0.15	0.08	0.03	0.00	0.99
ID 3506_012	73.17	0.06	13.17	1.58	0.09	0.07	0.70	4.12	4.81	0.36	98.05	1.95
ID 3506_013	73.44	0.08	12.94	1.64	0.06	0.05	0.74	4.05	4.87	0.36	98.15	1.85
ID 3506_014	73.74	0.08	12.99	1.59	0.08	0.03	0.74	3.75	4.75	0.33	98.02	1.98
ID 3506_015	73.40	0.04	12.90	1.68	0.08	0.06	0.75	3.89	4.88	0.36	97.94	2.06
ID 3506_016	73.65	0.07	13.12	1.48	0.06	0.07	0.72	3.74	4.91	0.32	98.07	1.93
ID 3506_017	73.58	0.03	13.22	1.57	0.08	0.04	0.70	4.17	4.62	0.34	98.29	1.71
Mean	73.50	0.06	13.06	1.59	0.07	0.05	0.73	3.95	4.81	0.34	98.09	1.91

	StDev	0.20	0.02	0.13	0.07	0.01	0.01	0.02	0.19	0.11	0.02	0.12	0.12
	Old Crow_014	75.46	0.36	13.11	1.64	0.10	0.29	1.45	3.86	3.50	0.30	100.00	4.51
	Old Crow_015	75.11	0.31	13.26	1.66	0.06	0.26	1.54	3.85	3.71	0.30	100.00	3.34
	Old Crow_017	75.24	0.34	12.70	1.73	0.06	0.31	1.41	4.23	3.73	0.31	100.00	1.20
	Mean	75.27	0.34	13.03	1.68	0.07	0.29	1.47	3.98	3.65	0.30	100.00	3.01
	StDev	0.18	0.02	0.29	0.05	0.02	0.03	0.07	0.22	0.13	0.01	0.00	1.68
23-Jan-20	ID3506_018	73.94	0.07	13.32	1.60	0.04	0.06	0.72	4.17	5.04	0.36	99.22	0.78
	ID3506_019	74.98	0.06	13.12	1.60	0.04	0.05	0.75	3.56	4.89	0.32	99.30	0.70
	ID3506_020	74.02	0.05	13.14	1.60	0.10	0.02	0.75	4.18	4.96	0.33	99.06	0.94
	ID3506_021	75.60	0.04	13.24	1.64	0.06	0.02	0.71	3.87	4.78	0.38	100.25	-0.25
	ID3506_022	74.60	0.07	13.17	1.62	0.06	0.05	0.71	3.99	4.77	0.38	99.33	0.67
	ID3506_023	75.26	0.07	13.21	1.67	0.02	0.05	0.77	3.96	4.85	0.34	100.12	-0.12
	Mean	74.73	0.06	13.20	1.62	0.05	0.04	0.73	3.95	4.88	0.35	99.55	0.45
	StDev	0.67	0.01	0.07	0.03	0.03	0.02	0.02	0.23	0.10	0.03	0.50	0.50
	OldCrow_019	75.55	0.30	13.26	1.78	0.06	0.30	1.31	3.53	3.75	0.23	100.00	3.39
	OldCrow_020	75.70	0.36	13.26	1.69	0.06	0.30	1.39	3.43	3.57	0.31	100.00	3.35
	OldCrow_021	75.68	0.33	13.12	1.80	0.09	0.29	1.48	3.62	3.38	0.30	100.00	4.07
	Mean	75.64	0.33	13.21	1.75	0.07	0.30	1.39	3.52	3.56	0.28	100.00	3.60
	StDev	0.08	0.03	0.08	0.06	0.02	0.01	0.08	0.10	0.18	0.04	0.00	0.41
	ID3506_024	74.14	0.00	13.07	1.62	0.03	0.06	0.74	4.03	4.96	0.35	98.91	1.09
	ID3506_025	75.27	0.12	13.07	1.58	0.11	0.06	0.72	3.89	4.87	0.31	99.91	0.09
	ID3506_026	74.05	0.12	13.08	1.74	0.08	0.06	0.72	3.95	4.86	0.33	98.91	1.09
	ID3506_027	74.09	0.07	12.99	1.55	0.09	0.07	0.75	4.15	4.85	0.33	98.86	1.14
	ID3506_028	73.68	0.06	13.02	1.48	0.09	0.07	0.70	3.98	4.70	0.32	98.04	1.96
	Mean	74.25	0.08	13.04	1.59	0.08	0.06	0.73	4.00	4.85	0.33	98.93	1.07

StDev	0.60	0.05	0.04	0.09	0.03	0.01	0.02	0.10	0.09	0.01	0.67	0.67
OldCrow_028	75.29	0.35	13.33	1.76	0.04	0.26	1.45	3.69	3.61	0.29	100.00	4.05
ID3506_029	75.61	0.10	12.93	1.57	0.07	0.05	0.74	3.64	4.87	0.29	99.81	0.19
ID3506_030	73.73	0.13	13.16	1.54	0.08	0.03	0.71	3.88	4.95	0.34	98.48	1.52
ID3506_031	73.87	0.08	12.99	1.59	0.08	0.04	0.75	4.00	5.00	0.35	98.67	1.33
ID3506_032	74.01	0.09	13.25	1.55	0.07	0.05	0.72	4.06	4.96	0.32	99.01	0.99
ID3506_033	73.61	0.09	13.12	1.62	0.07	0.03	0.77	2.98	4.98	0.35	97.54	2.46
Mean	74.17	0.10	13.09	1.57	0.07	0.04	0.74	3.71	4.95	0.33	98.70	1.30
StDev	0.82	0.02	0.13	0.03	0.00	0.01	0.02	0.44	0.05	0.03	0.83	0.83
OldCrow_030	75.46	0.34	13.12	1.67	0.10	0.26	1.50	3.57	3.73	0.31	100.00	3.70
OldCrow_031	75.55	0.28	13.15	1.71	0.07	0.27	1.50	3.57	3.69	0.29	100.00	3.98
Mean	75.50	0.31	13.14	1.69	0.09	0.26	1.50	3.57	3.71	0.30	100.00	3.84
StDev	0.06	0.04	0.02	0.03	0.03	0.00	0.00	0.00	0.03	0.01	0.00	0.20
ID3506_034	74.08	0.08	13.04	1.58	0.06	0.07	0.71	4.01	5.13	0.31	99.00	1.00
ID3506_035	74.37	0.05	13.17	1.60	0.11	0.05	0.72	4.22	5.03	0.33	99.58	0.42
ID3506_036	73.95	0.11	13.00	1.62	0.05	0.03	0.71	4.07	4.99	0.37	98.80	1.20
ID3506_037	73.98	0.02	13.04	1.60	0.10	0.05	0.70	3.62	5.01	0.37	98.40	1.60
ID3506_038	74.46	0.11	13.07	1.64	0.05	0.03	0.74	3.85	4.97	0.31	99.15	0.85
Mean	74.17	0.07	13.06	1.61	0.07	0.05	0.72	3.95	5.03	0.34	98.99	1.01
StDev	0.23	0.04	0.06	0.02	0.03	0.02	0.01	0.23	0.06	0.03	0.43	0.43
OldCrow_035	75.79	0.40	13.03	1.67	0.04	0.29	1.44	3.57	3.57	0.26	100.00	3.75
OldCrow_036	75.36	0.30	13.19	1.71	0.05	0.32	1.43	3.67	3.76	0.27	100.00	3.09
OldCrow_037	75.10	0.28	13.23	1.70	0.04	0.31	1.45	3.86	3.81	0.28	100.00	2.96
OldCrow_038	75.33	0.39	13.17	1.68	0.09	0.29	1.49	3.55	3.79	0.28	100.00	3.64
Mean	75.40	0.34	13.16	1.69	0.06	0.30	1.45	3.66	3.73	0.28	100.00	3.36

	StDev	0.29	0.06	0.09	0.02	0.02	0.01	0.03	0.14	0.11	0.01	0.00	0.39	
	ID 3506 both days													
	Mean	74.16	0.08	13.09	1.60	0.07	0.05	0.73	3.91	4.90	0.34	98.85	1.15	
	StDev	0.63	0.03	0.10	0.06	0.02	0.01	0.02	0.25	0.14	0.02	0.68	0.68	
	22-Jan													
	Mean	73.93	0.07	13.06	1.60	0.07	0.05	0.73	3.92	4.88	0.35	98.59	1.41	
	StDev	0.57	0.02	0.11	0.06	0.02	0.01	0.02	0.21	0.18	0.01	0.62	0.62	
	23-Jan													
	Mean	74.35	0.08	13.11	1.60	0.07	0.05	0.73	3.91	4.92	0.34	99.06	0.94	
	StDev	0.63	0.03	0.10	0.05	0.03	0.02	0.02	0.28	0.10	0.02	0.66	0.66	
	Old Crow Both days													
	Mean	**75.49**	**0.33**	**13.14**	**1.70**	**0.07**	**0.29**	**1.45**	**3.71**	**3.59**	**0.29**	**100.00**	**3.49**	
	StDev	0.27	0.04	0.15	0.04	0.02	0.02	0.05	0.23	0.15	0.02	0.00	0.97	
	Mean	75.51	0.32	13.10	1.69	0.07	0.30	1.45	3.81	3.53	0.29	100.00	3.39	
	StDev	0.32	0.03	0.19	0.03	0.03	0.03	0.04	0.27	0.14	0.02	0.00	1.32	
	Mean	75.48	0.33	13.19	1.72	0.06	0.29	1.44	3.61	3.67	0.28	100.00	3.60	
	StDev	0.21	0.04	0.09	0.05	0.02	0.02	0.06	0.12	0.13	0.02	0.00	0.39	
08-Jun-20	ID3506 1-3	73.87	0.06	13.26	1.57	0.06	0.04	0.70	4.09	5.28	0.33	99.20	0.81	Na TDI
	ID3506 1-4	74.34	0.09	13.16	1.62	0.05	0.05	0.73	4.07	5.15	0.35	99.52	0.48	No offline corrections
	ID3506 1-5	74.31	0.04	13.14	1.51	0.06	0.05	0.75	3.93	5.11	0.32	99.16	0.84	
	ID3506 1-6	74.22	0.05	13.17	1.61	0.06	0.08	0.70	4.19	5.14	0.30	99.44	0.56	

Mean	74.19	0.06	13.18	1.58	0.06	0.06	0.72	4.07	5.17	0.32	99.33	0.67
St. Dev	0.21	0.02	0.05	0.05	0.00	0.01	0.02	0.11	0.08	0.02	0.18	0.18
Old Crow1-1	75.19	0.29	13.16	1.70	0.13	0.29	1.45	3.80	3.73	0.31	100.00	2.75
Old Crow1-2	75.55	0.30	13.03	1.74	0.08	0.31	1.50	3.70	3.59	0.26	100.00	2.96
Old Crow1-3	74.94	0.26	13.10	1.71	0.07	0.31	1.45	4.13	3.81	0.29	100.00	2.64
Old Crow1-4	75.49	0.31	13.12	1.72	0.05	0.33	1.47	3.50	3.77	0.30	100.00	3.52
Old Crow1-5	75.18	0.36	13.03	1.76	0.05	0.31	1.45	3.88	3.76	0.26	100.00	2.77
Old Crow1-6	75.36	0.24	13.16	1.76	0.05	0.27	1.45	3.66	3.81	0.29	100.00	4.13
Mean	75.29	0.29	13.10	1.73	0.07	0.30	1.46	3.78	3.75	0.28	100.00	3.13
St. Dev	0.23	0.04	0.06	0.03	0.03	0.02	0.02	0.22	0.08	0.02	0.00	0.58
ID3506 2-1	74.36	0.12	13.20	1.41	0.07	0.02	0.70	3.89	5.30	0.32	99.33	0.67
ID3506 2-2	74.64	0.14	13.13	1.55	0.06	0.00	0.72	3.93	5.25	0.34	99.67	0.33
ID3506 2-3	73.87	0.03	13.14	1.44	0.06	0.06	0.71	4.19	5.13	0.32	98.88	1.12
ID3506 2-4	74.50	0.03	12.70	1.55	0.06	0.04	0.70	4.18	5.16	0.33	99.16	0.84
Mean	74.34	0.08	13.04	1.49	0.06	0.03	0.71	4.05	5.21	0.33	99.26	0.74
St. Dev	0.33	0.06	0.23	0.07	0.01	0.02	0.01	0.16	0.08	0.01	0.33	0.33
Old Crow2-1	75.23	0.38	13.29	1.67	0.05	0.32	1.43	3.52	3.91	0.27	100.00	3.60
Old Crow2-2	75.24	0.31	13.18	1.78	0.06	0.37	1.43	3.73	3.66	0.30	100.00	2.52
Old Crow2-3	75.42	0.30	13.24	1.64	0.05	0.29	1.49	3.59	3.73	0.31	100.00	3.55
Old Crow2-4	75.18	0.27	13.31	1.78	0.08	0.36	1.51	3.54	3.74	0.31	100.00	3.90
Mean	75.27	0.31	13.26	1.72	0.06	0.33	1.46	3.59	3.76	0.30	100.00	3.39
St. Dev	0.11	0.05	0.06	0.07	0.02	0.03	0.04	0.10	0.11	0.02	0.00	0.60
ID3506												
Overall Mean	74.26	0.07	13.11	1.53	0.06	0.04	0.71	4.06	5.19	0.33	99.30	0.70
St. Dev	0.27	0.04	0.17	0.08	0.01	0.02	0.02	0.12	0.08	0.01	0.25	0.25

	Old Crow													
	Overall Mean	75.28	0.30	13.16	1.73	0.07	0.32	1.46	3.71	3.75	0.29	100.00	3.23	
	St. Dev	0.18	0.04	0.10	0.05	0.03	0.03	0.03	0.20	0.09	0.02	0.00	0.57	
10-Jun-20	ID3506 1-1	74.90	0.14	13.30	1.61	0.04	0.05	0.71	4.12	5.03	0.31	100.13	-0.13	Na Si TDI
	ID3506 1-2	74.29	0.08	13.05	1.57	0.03	0.02	0.74	4.31	5.21	0.31	99.54	0.46	no offline corrections
	ID3506 1-3	74.00	0.16	12.98	1.56	0.09	0.03	0.74	3.90	5.19	0.37	98.93	1.07	
	ID3506 1-4	73.75	0.09	13.15	1.62	0.08	0.08	0.70	3.87	5.13	0.31	98.70	1.30	
	ID3506 1-5	74.04	0.16	13.22	1.47	0.08	0.04	0.71	4.03	5.15	0.34	99.16	0.84	
	ID3506 1-6	73.69	0.04	13.15	1.54	0.03	0.05	0.70	3.88	5.13	0.31	98.44	1.56	
	ID3506 1-7	74.13	0.12	13.07	1.51	0.05	0.02	0.73	4.23	5.08	0.34	99.20	0.80	
	ID3506 1-8	74.49	0.08	13.26	1.59	0.10	0.01	0.71	3.96	4.99	0.32	99.44	0.56	
	Mean	74.16	0.11	13.14	1.56	0.06	0.04	0.72	4.04	5.11	0.33	99.19	0.81	
	St. Dev	0.40	0.04	0.11	0.05	0.03	0.02	0.02	0.17	0.07	0.02	0.53	0.53	
	Old Crow1-1	75.45	0.31	13.12	1.71	0.03	0.31	1.46	3.69	3.70	0.29	100.00	3.15	
	Old Crow1-2	75.00	0.38	13.27	1.74	0.06	0.28	1.45	3.88	3.69	0.30	100.00	3.34	
	Old Crow1-3	75.16	0.26	13.34	1.79	0.10	0.33	1.47	3.72	3.56	0.34	100.00	4.42	
	Old Crow1-5	75.32	0.32	13.30	1.73	0.07	0.29	1.45	3.78	3.53	0.28	100.00	5.42	
	Old Crow1-6	75.00	0.35	13.53	1.76	0.10	0.27	1.42	3.67	3.73	0.23	100.00	6.62	
	Mean	75.19	0.33	13.31	1.75	0.07	0.30	1.45	3.75	3.64	0.29	100.00	4.59	
	St. Dev	0.20	0.05	0.14	0.03	0.03	0.03	0.02	0.09	0.09	0.04	0.00	1.45	
	ID3506 2-1	74.33	0.11	13.12	1.57	0.06	0.04	0.74	3.98	5.11	0.37	99.35	0.65	
	ID3506 2-2	73.92	0.07	13.02	1.56	0.04	0.05	0.70	4.23	5.13	0.36	99.00	1.00	
	ID3506 2-3	73.83	0.07	13.20	1.64	0.06	0.04	0.73	4.16	5.02	0.35	99.00	1.00	
	ID3506 2-4	73.66	0.03	12.98	1.51	0.09	0.06	0.71	4.16	5.07	0.34	98.54	1.46	
	Mean	73.93	0.07	13.08	1.57	0.06	0.05	0.72	4.13	5.08	0.36	98.97	1.03	

	St. Dev	0.29	0.03	0.10	0.05	0.02	0.01	0.02	0.11	0.05	0.01	0.33	0.33	
	Old Crow2-1	75.21	0.46	13.20	1.77	0.04	0.24	1.41	3.74	3.71	0.29	100.00	5.35	
	Old Crow2-2	75.52	0.38	13.11	1.71	0.05	0.33	1.40	3.52	3.73	0.31	100.00	5.20	
	Old Crow2-3	75.70	0.36	13.25	1.66	0.05	0.27	1.41	3.45	3.62	0.31	100.00	6.20	
	Old Crow2-5	75.16	0.30	13.22	1.80	0.04	0.29	1.46	3.81	3.67	0.31	100.00	4.74	
	Mean	75.40	0.38	13.20	1.74	0.05	0.28	1.42	3.63	3.68	0.31	100.00	5.38	
	St. Dev	0.26	0.06	0.06	0.06	0.00	0.04	0.03	0.17	0.05	0.01	0.00	0.61	
	ID3506													
	Overall Mean	74.08	0.10	13.12	1.56	0.06	0.04	0.72	4.07	5.10	0.34	99.12	0.88	
	St. Dev	0.37	0.04	0.11	0.05	0.02	0.02	0.02	0.15	0.07	0.02	0.47	0.47	
	Old Crow													
	Overall Mean	75.28	0.35	13.26	1.74	0.06	0.29	1.44	3.70	3.66	0.30	100.00	4.94	
	St. Dev	0.24	0.06	0.12	0.04	0.02	0.03	0.03	0.14	0.07	0.03	0.00	1.17	
22-Jun-20	ID3506 1-1	74.62	0.09	13.14	1.58	0.02	0.08	0.68	4.29	5.21	0.34	99.98	0.02	Na Si TDI
	ID3506 1-2	73.47	0.05	13.31	1.59	0.05	0.04	0.73	4.27	5.23	0.35	99.02	0.98	
	ID3506 1-3	73.33	0.11	13.14	1.59	0.02	0.06	0.72	3.87	5.11	0.30	98.19	1.81	
	ID3506 1-4	73.52	0.06	13.12	1.55	0.06	0.01	0.69	4.03	5.19	0.30	98.48	1.52	
	ID3506 1-5	73.95	0.12	13.19	1.55	0.07	0.05	0.76	4.16	5.22	0.33	99.33	0.67	No offline corrections
	ID3506 1-6	74.01	0.05	13.25	1.55	0.09	0.07	0.75	3.77	5.19	0.34	98.99	1.01	
	Mean	73.82	0.08	13.19	1.57	0.05	0.05	0.72	4.07	5.19	0.33	99.00	1.00	
	St. Dev	0.48	0.03	0.07	0.02	0.03	0.02	0.03	0.21	0.04	0.02	0.63	0.63	
	Old Crow1-1	75.18	0.30	13.23	1.61	0.05	0.33	1.46	4.03	3.61	0.25	100.00	5.45	
	Old Crow1-2	75.30	0.36	13.20	1.76	0.04	0.27	1.45	3.71	3.70	0.25	100.00	5.07	
	Old Crow1-3	75.36	0.24	13.36	1.66	0.10	0.35	1.48	3.64	3.62	0.25	100.00	4.12	
	Old Crow1-4	75.23	0.37	13.28	1.83	0.06	0.32	1.47	3.59	3.64	0.30	100.00	3.87	

Old Crow1-5	75.56	0.22	13.29	1.66	0.02	0.32	1.47	3.56	3.65	0.30	100.00	5.08
Old Crow1-6	75.63	0.31	13.14	1.66	0.05	0.28	1.51	3.43	3.79	0.26	100.00	4.57
Mean	75.38	0.30	13.25	1.70	0.06	0.31	1.47	3.66	3.67	0.27	100.00	4.69
St. Dev	0.18	0.06	0.08	0.08	0.03	0.03	0.02	0.20	0.07	0.02	0.00	0.61
ID3506 2-1	74.32	0.10	13.26	1.62	0.07	0.08	0.77	3.91	5.12	0.35	99.52	0.48
ID3506 2-2	73.72	0.07	13.14	1.58	0.12	0.08	0.73	3.72	5.23	0.34	98.64	1.36
ID3506 2-3	73.15	0.02	13.16	1.59	0.04	0.04	0.72	3.98	5.09	0.31	98.03	1.97
ID3506 2-4	73.12	0.14	13.27	1.51	0.06	0.06	0.73	4.49	5.10	0.33	98.72	1.28
ID3506 2-5	73.95	0.13	13.30	1.62	0.09	0.03	0.71	4.09	5.17	0.39	99.39	0.61
ID3506 2-6	73.42	0.08	13.21	1.42	0.01	0.05	0.70	4.47	5.18	0.32	98.81	1.19
Mean	73.62	0.09	13.22	1.56	0.07	0.06	0.72	4.11	5.15	0.34	98.85	1.15
St. Dev	0.47	0.04	0.07	0.08	0.04	0.02	0.02	0.31	0.05	0.03	0.54	0.54
Old Crow2-1	74.85	0.37	13.33	1.64	0.05	0.32	1.48	4.07	3.70	0.25	100.00	4.06
Old Crow2-2	75.18	0.25	13.53	1.74	0.13	0.33	1.44	3.48	3.68	0.30	100.00	5.73
Old Crow2-3	75.17	0.36	13.45	1.76	0.03	0.31	1.48	3.67	3.58	0.26	100.00	4.95
Old Crow2-4	75.56	0.35	13.23	1.70	0.06	0.34	1.49	3.47	3.60	0.25	100.00	4.19
Mean	75.19	0.33	13.38	1.71	0.07	0.33	1.47	3.67	3.64	0.26	100.00	4.73
St. Dev	0.29	0.05	0.13	0.05	0.04	0.01	0.02	0.28	0.06	0.02	0.00	0.77
ID3506 3-1	74.33	0.08	13.22	1.48	0.01	0.03	0.74	3.93	5.06	0.32	99.14	0.86
ID3506 3-2	74.46	0.15	13.19	1.55	0.08	0.02	0.73	3.80	5.24	0.32	99.47	0.53
ID3506 3-3	73.89	0.00	13.14	1.59	0.04	0.04	0.74	4.02	5.23	0.33	98.94	1.06
ID3506 3-4	74.80	0.09	13.13	1.67	0.05	0.00	0.73	3.72	5.12	0.37	99.61	0.39
ID3506 3-5	74.51	0.17	13.14	1.55	0.05	0.07	0.76	4.27	5.25	0.34	100.04	-0.04
ID3506 3-6	73.41	0.00	13.08	1.58	0.09	0.03	0.71	4.01	5.18	0.34	98.36	1.64
Mean	74.23	0.08	13.15	1.57	0.05	0.03	0.73	3.96	5.18	0.34	99.26	0.74

	St. Dev	0.50	0.07	0.05	0.06	0.03	0.02	0.01	0.19	0.08	0.02	0.59	0.59	
	Old Crow3-2	75.33	0.30	13.20	1.78	0.05	0.32	1.52	3.65	3.63	0.27	100.00	4.02	
	Old Crow3-3	74.60	0.44	13.17	1.73	0.10	0.32	1.47	4.21	3.71	0.32	100.00	3.24	
	Old Crow3-4	74.81	0.35	13.25	1.73	0.09	0.29	1.49	4.11	3.65	0.30	100.00	3.75	
	Mean	74.92	0.36	13.21	1.75	0.08	0.31	1.49	3.99	3.66	0.30	100.00	3.67	
	St. Dev	0.38	0.07	0.04	0.03	0.03	0.02	0.02	0.30	0.05	0.02	0.00	0.39	
	ID3506													
	Overall Mean	73.89	0.08	13.19	1.57	0.06	0.05	0.73	4.04	5.17	0.33	99.04	0.96	
	St. Dev	0.53	0.05	0.07	0.06	0.03	0.02	0.02	0.24	0.06	0.02	0.58	0.58	
	Old Crow													
	Overall Mean	75.21	0.32	13.28	1.71	0.07	0.32	1.48	3.74	3.66	0.27	100.00	4.47	
	St. Dev	0.31	0.06	0.11	0.06	0.03	0.02	0.02	0.27	0.06	0.03	0.00	0.73	
01-Sep-20	ID3506_001-	73.75	0.10	13.19	1.61	0.00	0.01	0.70	3.74	5.08	0.33	98.43	1.57	Na Si TDI
	ID3506_002-	74.72	0.11	13.15	1.43	0.00	0.02	0.71	3.79	5.20	0.31	99.37	0.63	Na and K offline corrections
	ID3506_003-	74.48	0.14	13.08	1.55	0.00	0.03	0.71	4.00	5.13	0.32	99.36	0.64	**Notes - Mn spectrometer issues giving unrealistically high values, FeOt is very bouncy.**
	ID3506_004-	73.74	0.09	13.14	1.53	0.00	0.05	0.73	3.90	5.08	0.38	98.54	1.46	
	ID3506_005-	73.13	0.09	12.75	1.47	0.08	0.03	0.73	3.47	5.07	0.35	97.09	2.91	

ID3506_006-	73.90	0.13	13.20	1.57	0.14	0.04	0.70	3.60	5.09	0.35	98.64	1.36
Mean	73.95	0.11	13.08	1.53	0.04	0.03	0.71	3.75	5.11	0.34	98.57	1.43
St. Dev	0.57	0.02	0.17	0.07	0.06	0.01	0.01	0.19	0.05	0.03	0.84	0.84
Old Crow_001-	75.11	0.37	13.37	1.79	0.08	0.39	1.46	3.57	3.65	0.27	100.00	3.61
Old Crow_002-	75.24	0.31	13.34	1.67	0.08	0.28	1.48	3.71	3.67	0.30	100.00	4.98
Old Crow_003-	74.94	0.29	13.34	1.68	0.00	0.29	1.47	4.23	3.53	0.28	100.00	2.22
Old Crow_004-	75.35	0.29	13.14	1.87	0.11	0.27	1.46	3.69	3.61	0.29	100.00	2.46
Old Crow_005-	75.70	0.32	13.17	1.67	0.00	0.32	1.40	3.51	3.69	0.28	100.00	2.93
Old Crow_006-	75.60	0.37	13.41	1.63	0.21	0.28	1.41	3.54	3.36	0.25	100.00	5.17
Mean	75.32	0.33	13.29	1.72	0.08	0.31	1.44	3.71	3.58	0.28	100.00	3.56
St. Dev	0.29	0.04	0.11	0.09	0.08	0.04	0.03	0.27	0.12	0.02	0.00	1.26
ID3506_007-	72.65	0.07	13.13	1.67	0.02	0.05	0.70	4.06	5.06	0.34	97.69	2.31
ID3506_008-	72.76	0.10	13.03	1.48	0.20	0.05	0.72	4.17	5.04	0.34	97.82	2.18
ID3506_009-	74.09	0.08	13.05	1.49	0.13	0.04	0.70	4.19	5.07	0.35	99.12	0.88
ID3506_010-	74.72	0.09	12.99	1.56	0.32	0.04	0.67	3.76	5.08	0.35	99.50	0.50
Mean	73.55	0.09	13.05	1.55		0.04	0.70	4.05	5.06	0.35	98.53	1.47
St. Dev	1.02	0.01	0.06	0.09		0.00	0.02	0.20	0.02	0.01	0.91	0.91
Old Crow_007-	75.86	0.34	12.31	1.75	0.24	0.26	1.42	4.07	3.50	0.32	100.00	4.93
Old Crow_008-	75.39	0.29	13.37	1.76	0.14	0.30	1.45	3.74	3.32	0.31	100.00	4.33
Old Crow_009-	75.52	0.36	13.30	1.75	0.00	0.31	1.49	3.54	3.53	0.27	100.00	3.87
Old Crow_010-	75.68	0.32	13.35	1.48	0.02	0.31	1.47	3.43	3.72	0.28	100.00	4.41
Mean	75.61	0.32	13.08	1.68	0.10	0.30	1.46	3.70	3.52	0.30	100.00	4.38
St. Dev	0.20	0.03	0.52	0.14	0.11	0.02	0.03	0.28	0.17	0.03	0.00	0.43
ID3506_011-	73.67	0.13	12.98	1.72	0.00	0.06	0.67	3.90	4.99	0.32	98.36	1.64
ID3506_012-	74.03	0.04	13.16	1.86	0.00	0.02	0.71	3.77	5.11	0.37	98.99	1.01

Mean	73.85	0.08	13.07	1.79		0.04	0.69	3.84	5.05	0.35	98.67	1.33
St. Dev	0.25	0.06	0.13	0.10		0.03	0.03	0.09	0.09	0.04	0.45	0.46
Old Crow_011-	75.25	0.32	13.35	1.76	0.00	0.29	1.45	3.48	3.85	0.32	100.00	7.84
Old Crow_012-	74.93	0.31	13.13	2.04	0.05	0.30	1.45	4.10	3.46	0.29	100.00	2.49
Old Crow_013-	75.46	0.28	13.32	1.66	0.11	0.34	1.49	3.50	3.62	0.30	100.00	3.38
Old Crow_014-	74.66	0.27	13.35	1.74	0.30	0.31	1.51	4.05	3.57	0.32	100.00	3.57
Mean	75.07	0.30	13.29	1.80	0.11	0.31	1.48	3.78	3.62	0.31	100.00	4.32
St. Dev	0.35	0.03	0.11	0.17	0.13	0.02	0.03	0.34	0.16	0.01	0.00	2.39
ID3506_016-	74.31	0.08	12.97	1.32	0.18	0.03	0.73	3.76	5.02	0.33	98.65	1.35
ID3506_017-	73.78	0.12	13.15	1.78	0.08	0.05	0.70	3.73	5.10	0.33	98.75	1.25
ID3506_018-	74.09	0.06	13.11	1.35	0.10	0.05	0.72	3.90	5.09	0.33	98.73	1.27
ID3506_019-	74.16	0.11	12.83	1.84	0.10	0.02	0.74	3.95	4.93	0.33	98.95	1.05
ID3506_020-	74.39	0.09	13.22	1.69	0.17	0.02	0.71	4.03	5.18	0.33	99.77	0.23
Mean	74.14	0.09	13.06	1.60		0.04	0.72	3.87	5.07	0.33	98.97	1.03
St. Dev	0.24	0.02	0.16	0.25		0.01	0.02	0.13	0.09	0.00	0.46	0.46
Old Crow_015-	75.19	0.36	13.28	1.79	0.06	0.28	1.47	3.76	3.60	0.27	100.00	3.69
Old Crow_016-	75.39	0.31	13.39	1.60	0.14	0.30	1.47	3.83	3.32	0.30	100.00	3.89
Old Crow_017-	75.93	0.34	12.85	1.35	0.14	0.31	1.44	4.03	3.43	0.26	100.00	5.14
Old Crow_018-	75.84	0.27	13.38	1.57	0.29	0.30	1.43	3.35	3.34	0.30	100.00	5.86
Old Crow_019-	75.63	0.29	13.37	1.31	0.17	0.30	1.42	3.81	3.49	0.28	100.00	3.88
Old Crow_020-	75.40	0.27	13.12	1.73	0.29	0.31	1.40	3.71	3.54	0.30	100.00	2.67
Mean	75.56	0.31	13.23	1.56	0.18	0.30	1.44	3.75	3.45	0.28	100.00	4.19
St. Dev	0.29	0.04	0.21	0.20	0.09	0.01	0.03	0.22	0.11	0.02	0.00	1.13
ID3506												
Overall Mean	73.90	0.10	13.07	1.58		0.04	0.71	3.87	5.08	0.34	98.69	1.31

	St. Dev	0.60	0.03	0.13	0.16		0.01	0.02	0.19	0.06	0.02	0.69	32.34	
	Old Crow													
	Overall Mean	75.40	0.31	13.23	1.68	0.12	0.30	1.45	3.73	3.54	0.29	100.00	4.07	
	St. Dev	0.33	0.03	0.26	0.17	0.10	0.03	0.03	0.25	0.14	0.02	0.00	1.35	
02-Sep-20	ID3506_001-	74.37	0.06	13.33	1.51	0.08	0.03	0.73	3.97	4.92	0.33	99.26	0.74	Na Si TDI
	ID3506_002-	74.32	0.04	13.08	1.60	0.11	0.03	0.74	4.15	5.18	0.32	99.49	0.51	Na and K offline corrections
	ID3506_003-	74.32	0.02	13.36	1.58	0.05	0.04	0.70	3.89	5.10	0.33	99.31	0.69	
	ID3506_004-	74.30	0.07	13.00	1.56	0.08	0.03	0.70	3.99	5.14	0.34	99.14	0.86	
	ID3506_005-	73.93	0.14	13.06	1.54	0.07	0.06	0.74	3.87	5.11	0.38	98.80	1.20	
	ID3506_006-	73.24	0.08	12.94	1.55	0.03	0.03	0.70	3.84	5.04	0.35	97.73	2.27	
	Mean	74.08	0.07	13.13	1.56	0.07	0.04	0.72	3.95	5.08	0.34	98.96	1.04	
	St. Dev	0.44	0.04	0.17	0.03	0.03	0.01	0.02	0.11	0.09	0.02	0.64	0.64	
	Old Crow_001	75.61	0.28	13.18	1.75	0.06	0.32	1.51	3.50	3.54	0.32	100.00	4.24	
	Old Crow_002	75.31	0.29	13.41	1.76	0.07	0.29	1.51	3.59	3.57	0.26	100.00	4.63	
	Old Crow_003	75.27	0.38	13.47	1.78	0.06	0.34	1.42	3.45	3.60	0.30	100.00	4.29	
	Old Crow_004	75.66	0.35	13.28	1.82	0.07	0.28	1.46	3.42	3.44	0.29	100.00	4.91	
	Old Crow_006	75.35	0.36	13.42	1.71	0.08	0.28	1.50	3.40	3.68	0.29	100.00	4.56	
	Mean	75.44	0.33	13.35	1.76	0.07	0.30	1.48	3.47	3.57	0.29	100.00	4.53	
	St. Dev	0.18	0.04	0.12	0.04	0.01	0.03	0.04	0.08	0.09	0.02	0.00	0.27	
	ID3506_007-	73.14	0.10	13.12	1.58	0.07	0.03	0.72	3.91	5.00	0.35	97.95	2.05	
	ID3506_008-	74.25	0.07	13.26	1.52	0.02	0.07	0.72	4.18	5.08	0.36	99.44	0.56	
	ID3506_009-	72.97	0.08	13.04	1.59	0.09	0.07	0.72	3.84	5.10	0.35	97.78	2.22	
	ID3506_010-	72.75	0.04	13.07	1.63	0.07	0.01	0.73	3.79	5.13	0.36	97.50	2.50	
	Mean	73.28	0.07	13.12	1.58	0.06	0.04	0.72	3.93	5.08	0.36	98.17	1.83	

St. Dev	0.67	0.03	0.10	0.04	0.03	0.03	0.00	0.17	0.06	0.01	0.87	0.87
Old Crow_008	75.54	0.39	12.97	1.71	0.05	0.27	1.47	3.72	3.68	0.27	100.00	1.57
Old Crow_009	75.43	0.29	13.14	1.80	0.07	0.29	1.52	3.67	3.56	0.30	100.00	4.63
Old Crow_010	75.48	0.35	13.28	1.77	0.05	0.29	1.46	3.67	3.45	0.25	100.00	4.46
Mean	75.48	0.34	13.13	1.76	0.05	0.28	1.48	3.69	3.56	0.27	100.00	3.55
St. Dev	0.05	0.05	0.15	0.04	0.01	0.01	0.03	0.03	0.11	0.02	0.00	1.72
ID3506_011	74.56	0.04	13.27	1.55	0.06	0.06	0.70	4.27	5.01	0.33	99.77	0.23
ID3506_012	72.98	0.11	13.12	1.54	0.04	0.03	0.74	3.50	5.15	0.34	97.46	2.54
ID3506_013	74.01	0.03	13.20	1.46	0.08	0.05	0.68	4.12	5.15	0.34	99.03	0.97
ID3506_014	74.38	0.04	13.13	1.57	0.04	0.06	0.71	3.80	5.05	0.33	99.03	0.97
ID3506_015	73.72	0.09	13.08	1.52	0.07	0.03	0.73	3.73	5.08	0.32	98.29	1.71
ID3506_016	74.43	0.06	12.99	1.53	0.05	0.05	0.73	4.01	5.12	0.36	99.26	0.74
Mean	74.01	0.06	13.13	1.53	0.05	0.04	0.72	3.90	5.09	0.34	98.81	1.19
St. Dev	0.59	0.03	0.10	0.04	0.02	0.01	0.02	0.28	0.06	0.01	0.81	0.81
Old Crow_011	75.35	0.29	13.30	1.78	0.03	0.31	1.45	3.56	3.70	0.32	100.00	3.48
Old Crow_012	75.24	0.26	13.32	1.69	0.01	0.34	1.45	3.87	3.61	0.28	100.00	3.55
Old Crow_013	75.53	0.27	13.17	1.68	0.05	0.31	1.49	3.75	3.54	0.29	100.00	3.26
Old Crow_014	75.13	0.28	13.41	1.73	0.10	0.32	1.47	3.69	3.62	0.30	100.00	3.98
Old Crow_015	75.45	0.35	13.45	1.73	0.04	0.30	1.41	3.59	3.46	0.28	100.00	4.78
Mean	75.34	0.29	13.33	1.72	0.05	0.32	1.45	3.69	3.59	0.29	100.00	3.81
St. Dev	0.16	0.04	0.11	0.04	0.03	0.02	0.03	0.13	0.09	0.01	0.00	0.60
ID3506												
Overall Mean	73.85	0.07	13.13	1.55	0.06	0.04	0.72	3.93	5.09	0.34	98.70	1.30
St. Dev	0.62	0.03	0.12	0.04	0.02	0.02	0.02	0.19	0.07	0.02	0.78	0.78
Old Crow												

	Overall Mean	75.41	0.32	13.29	1.75	0.06	0.30	1.47	3.61	3.57	0.29	100.00	4.03	
	St. Dev	0.15	0.04	0.15	0.04	0.02	0.02	0.03	0.14	0.09	0.02	0.00	0.90	
25-Nov-20	ID3506_001	73.95	0.08	13.17	1.60	0.07	0.03	0.70	3.90	5.12	0.35	98.89	1.11	Na Si TDI
	ID3506_002	74.51	0.06	13.17	1.44	0.07	0.04	0.71	4.07	5.18	0.27	99.46	0.54	No offline corrections
	ID3506_003	73.28	0.11	13.04	1.58	0.04	0.05	0.74	4.10	5.31	0.34	98.52	1.48	
	ID3506_004	74.64	0.06	13.20	1.59	0.11	0.04	0.70	3.92	5.19	0.34	99.71	0.29	
	ID3506_005	73.88	0.08	13.06	1.63	0.00	0.07	0.74	4.03	5.08	0.36	98.86	1.14	
	ID3506_006	73.59	0.03	13.00	1.53	0.04	0.03	0.69	3.93	5.06	0.34	98.17	1.83	
	Mean	73.97	0.07	13.11	1.56	0.06	0.04	0.72	3.99	5.16	0.33	98.93	1.07	
	StDev	0.53	0.03	0.08	0.07	0.04	0.02	0.02	0.08	0.09	0.03	0.57	0.57	
	Old Crow-2	75.23	0.34	13.20	1.73	0.07	0.30	1.45	3.57	3.87	0.29	100.00	3.89	
	Old Crow-3	75.22	0.29	13.23	1.68	0.08	0.25	1.43	3.76	3.81	0.31	100.00	4.80	
	Old Crow-4	74.99	0.32	13.17	1.76	0.03	0.35	1.45	3.91	3.81	0.27	100.00	4.05	
	Old Crow-5	75.26	0.33	13.26	1.61	0.06	0.24	1.43	3.73	3.88	0.27	100.00	4.14	
	Old Crow-6	75.56	0.29	13.13	1.72	0.03	0.32	1.50	3.42	3.82	0.26	100.00	5.53	
	Mean	75.25	0.31	13.20	1.70	0.06	0.29	1.45	3.68	3.84	0.28	100.00	4.48	
	StDev	0.21	0.02	0.05	0.06	0.02	0.05	0.03	0.19	0.03	0.02	0.00	0.68	
	ID3506_007	74.35	0.01	13.22	1.45	0.07	0.06	0.70	4.19	5.21	0.31	99.50	0.50	
	ID3506_008	73.91	0.05	13.15	1.44	0.07	0.04	0.71	3.96	5.22	0.30	98.79	1.21	
	ID3506_009	74.49	0.01	13.18	1.55	0.06	0.04	0.75	4.12	5.16	0.35	99.62	0.38	
	ID3506_010	73.98	0.05	12.96	1.50	0.08	0.04	0.74	4.01	5.22	0.35	98.87	1.13	
	Mean	74.18	0.03	13.13	1.49	0.07	0.04	0.72	4.07	5.20	0.33	99.20	0.80	
	StDev	0.28	0.03	0.11	0.05	0.01	0.01	0.02	0.10	0.03	0.02	0.43	0.43	
	Old Crow-8	74.95	0.28	13.15	1.70	0.00	0.29	1.46	4.11	3.83	0.31	100.00	2.76	
	Old Crow-9	75.36	0.30	13.20	1.62	0.01	0.26	1.46	3.80	3.76	0.29	100.00	2.51	

Old Crow-10	74.88	0.24	13.29	1.62	0.10	0.28	1.46	4.19	3.74	0.26	100.00	2.02
Mean	75.06	0.27	13.21	1.65	0.04	0.28	1.46	4.04	3.78	0.29	100.00	2.43
StDev	0.26	0.03	0.07	0.04	0.05	0.01	0.00	0.21	0.04	0.03	0.00	0.38
ID3506_011	73.66	0.11	13.24	1.60	0.08	0.06	0.75	3.84	5.17	0.32	98.76	1.24
ID3506_012	74.49	0.08	13.25	1.59	0.10	0.06	0.70	3.88	5.18	0.38	99.62	0.38
ID3506_013	74.30	0.10	13.25	1.52	0.09	0.06	0.71	3.95	5.30	0.36	99.56	0.44
ID3506_014	74.60	0.04	13.20	1.56	0.08	0.04	0.73	3.81	5.25	0.33	99.56	0.44
ID3506_015	74.27	0.03	13.38	1.63	0.08	0.06	0.71	3.79	5.18	0.34	99.39	0.61
ID3506_016	75.01	0.04	13.34	1.55	0.07	0.02	0.74	3.95	5.11	0.36	100.12	-0.12
Mean	74.39	0.06	13.28	1.58	0.08	0.05	0.72	3.87	5.20	0.35	99.50	0.50
StDev	0.45	0.04	0.07	0.04	0.01	0.02	0.02	0.07	0.06	0.02	0.44	0.44
Old Crow-12	75.01	0.29	13.17	1.65	0.07	0.29	1.45	4.15	3.70	0.28	100.00	4.57
Old Crow-13	74.96	0.31	13.13	1.70	0.09	0.27	1.54	3.78	3.99	0.32	100.00	3.81
Old Crow-14	75.18	0.31	13.24	1.66	0.05	0.30	1.49	3.68	3.85	0.30	100.00	3.68
Old Crow-15	75.00	0.30	13.17	1.61	0.02	0.26	1.39	4.21	3.86	0.23	100.00	3.43
Old Crow-16	74.89	0.30	13.48	1.78	0.02	0.33	1.49	3.76	3.73	0.27	100.00	6.49
Mean	75.01	0.30	13.24	1.68	0.05	0.29	1.47	3.92	3.82	0.28	100.00	4.40
StDev	0.11	0.01	0.14	0.07	0.03	0.03	0.06	0.24	0.11	0.03	0.00	1.25
ID3506												
Mean	74.18	0.06	13.18	1.55	0.07	0.05	0.72	3.97	5.18	0.34	99.21	0.79
StDev	0.46	0.03	0.11	0.06	0.02	0.01	0.02	0.11	0.07	0.03	0.53	0.53
Old Crow												
Mean	75.11	0.30	13.22	1.68	0.05	0.29	1.46	3.85	3.82	0.28	100.00	3.98
StDev	0.21	0.02	0.09	0.06	0.03	0.03	0.04	0.25	0.07	0.03	0.00	1.21

26-Nov-20	ID3506_001	74.08	0.15	13.36	1.51	0.06	0.03	0.71	4.02	5.16	0.37	99.38	0.62	Na Si TDI
	ID3506_002	74.25	0.07	13.20	1.54	0.09	0.05	0.73	4.12	5.25	0.33	99.55	0.45	No offline corrections
	ID3506_003	74.29	0.06	13.24	1.52	0.08	0.04	0.72	4.12	5.22	0.32	99.54	0.46	
	ID3506_004	74.62	0.02	13.21	1.47	0.07	0.04	0.71	3.76	5.35	0.32	99.49	0.51	
	ID3506_005	73.78	0.09	13.21	1.55	0.10	0.06	0.73	4.11	5.24	0.32	99.11	0.89	
	ID3506_006	74.60	0.06	13.31	1.55	0.05	0.03	0.70	4.09	5.19	0.33	99.83	0.17	
	Mean	74.27	0.08	13.26	1.53	0.07	0.04	0.71	4.04	5.24	0.33	99.48	0.52	
	StDev	0.32	0.04	0.07	0.03	0.02	0.01	0.01	0.14	0.06	0.02	0.24	0.24	
	Old Crow-2	74.75	0.31	13.23	1.69	0.07	0.31	1.45	4.22	3.77	0.26	100.00	4.75	
	Old Crow-3	75.08	0.33	13.23	1.67	0.06	0.27	1.48	3.86	3.80	0.28	100.00	2.55	
	Old Crow-4	75.01	0.29	13.32	1.71	0.04	0.28	1.50	3.73	3.91	0.28	100.00	5.04	
	Old Crow-5	75.53	0.32	13.10	1.67	0.08	0.28	1.42	3.75	3.62	0.29	100.00	5.47	
	Old Crow-6	75.41	0.30	13.18	1.68	0.07	0.26	1.41	3.68	3.78	0.29	100.00	5.30	
	Mean	75.16	0.31	13.21	1.68	0.06	0.28	1.45	3.85	3.77	0.28	100.00	4.63	
	StDev	0.31	0.02	0.08	0.02	0.02	0.02	0.04	0.21	0.10	0.01	0.00	1.19	
	ID3506_007	74.01	0.09	13.28	1.49	0.04	0.05	0.74	3.98	5.15	0.34	99.08	0.92	
	ID3506_008	73.99	0.08	13.15	1.49	0.05	0.06	0.70	4.18	5.09	0.30	99.03	0.97	
	ID3506_009	74.17	0.12	13.08	1.52	0.09	0.04	0.72	4.31	5.24	0.32	99.53	0.47	
	ID3506_010	73.15	0.06	13.09	1.50	0.05	0.05	0.74	4.15	5.30	0.33	98.35	1.65	
	Mean	73.83	0.09	13.15	1.50	0.06	0.05	0.72	4.16	5.19	0.32	99.00	1.00	
	StDev	0.46	0.02	0.09	0.02	0.02	0.01	0.02	0.14	0.09	0.02	0.49	0.49	
	Old Crow-7	75.14	0.27	13.08	1.70	0.07	0.30	1.51	3.82	3.91	0.27	100.00	4.77	
	Old Crow-8	75.32	0.35	13.17	1.63	0.01	0.32	1.43	3.87	3.69	0.28	100.00	4.31	
	Old Crow-9	74.91	0.28	13.23	1.75	0.07	0.33	1.47	4.00	3.74	0.28	100.00	4.16	
	Mean	75.12	0.30	13.16	1.70	0.05	0.31	1.47	3.90	3.78	0.28	100.00	4.42	
	StDev	0.20	0.04	0.08	0.06	0.04	0.01	0.04	0.10	0.12	0.00	0.00	0.32	

ID3506_011	73.15	0.10	13.26	1.59	0.07	0.04	0.71	3.99	5.15	0.29	98.30	1.70
ID3506_012	73.89	0.06	13.03	1.62	0.10	0.00	0.72	4.00	5.10	0.34	98.77	1.23
ID3506_013	73.94	0.09	13.05	1.57	0.04	0.06	0.72	4.08	5.08	0.34	98.89	1.11
ID3506_014	74.29	0.04	13.24	1.53	0.08	0.04	0.72	4.08	5.25	0.36	99.54	0.46
Mean	73.82	0.07	13.15	1.58	0.07	0.04	0.72	4.04	5.14	0.33	98.87	1.13
StDev	0.48	0.03	0.12	0.04	0.03	0.03	0.00	0.05	0.08	0.03	0.51	0.51
Old Crow-11	74.65	0.35	13.27	1.69	0.09	0.30	1.44	4.19	3.82	0.27	100.00	4.12
Old Crow-12	75.04	0.31	12.86	1.62	0.05	0.30	1.49	4.31	3.80	0.29	100.00	4.18
Old Crow-13	74.98	0.37	13.09	1.77	0.05	0.30	1.46	4.07	3.72	0.25	100.00	3.56
Old Crow-14	74.74	0.31	13.20	1.73	0.07	0.30	1.44	4.19	3.78	0.31	100.00	4.85
Mean	74.85	0.34	13.11	1.70	0.06	0.30	1.46	4.19	3.78	0.28	100.00	4.18
StDev	0.19	0.03	0.18	0.06	0.02	0.00	0.02	0.10	0.04	0.02	0.00	0.53
ID3506_015	74.96	0.06	13.10	1.52	0.07	0.05	0.71	4.43	5.22	0.28	100.33	-0.33
ID3506_016	74.52	0.09	13.08	1.54	0.06	0.03	0.75	4.26	5.24	0.30	99.78	0.22
ID3506_017	74.03	0.10	13.10	1.60	0.10	0.03	0.75	3.80	5.14	0.36	98.93	1.07
ID3506_018	73.75	0.03	13.29	1.60	0.10	0.03	0.72	4.09	5.25	0.34	99.11	0.89
ID3506_019	73.71	0.06	13.08	1.55	0.09	0.04	0.74	3.97	5.14	0.31	98.63	1.37
ID3506_020	74.42	0.07	13.09	1.55	0.06	0.04	0.72	4.30	5.05	0.36	99.58	0.42
Mean	74.23	0.07	13.12	1.56	0.08	0.04	0.73	4.14	5.17	0.33	99.39	0.61
StDev	0.49	0.02	0.08	0.03	0.02	0.01	0.02	0.23	0.08	0.03	0.62	0.62
Old Crow-16	75.27	0.30	13.06	1.58	0.09	0.30	1.45	4.06	3.73	0.21	100.00	3.98
Old Crow-17	75.04	0.32	13.28	1.73	0.08	0.30	1.49	3.82	3.72	0.30	100.00	4.67
Old Crow-18	75.10	0.31	13.24	1.69	0.06	0.27	1.45	3.80	3.86	0.27	100.00	5.09
Old Crow-19	75.26	0.31	13.22	1.70	0.07	0.30	1.41	3.84	3.69	0.27	100.00	6.19
Old Crow-20	75.24	0.33	12.99	1.75	0.08	0.27	1.50	4.05	3.56	0.29	100.00	2.67

	Mean	75.18	0.32	13.16	1.69	0.07	0.29	1.46	3.91	3.71	0.27	100.00	4.52	
	StDev	0.10	0.01	0.13	0.07	0.01	0.01	0.04	0.13	0.11	0.03	0.00	1.31	
	ID3506													
	Mean	74.08	0.08	13.17	1.54	0.07	0.04	0.72	4.09	5.19	0.33	99.24	0.76	
	StDev	0.45	0.03	0.10	0.04	0.02	0.01	0.01	0.16	0.08	0.02	0.51	0.51	
	Old Crow													
	Mean	75.09	0.32	13.16	1.69	0.06	0.29	1.46	3.96	3.76	0.28	100.00	4.45	
	StDev	0.24	0.03	0.12	0.05	0.02	0.02	0.03	0.19	0.09	0.02	0.00	0.94	
Mar 4, 2021 NaTDI	ID3506-1	74.68	0.06	13.06	1.56	0.07	0.03	0.75	4.27	5.26	0.33	100.00	0.72	Na TDI
	ID3506-2	74.22	0.09	13.24	1.63	0.09	0.00	0.73	4.45	5.26	0.37	100.00	1.32	No offline corrections
	ID3506-3	74.68	0.07	13.10	1.62	0.07	0.05	0.69	4.08	5.37	0.34	100.00	1.79	
	ID3506-4	74.83	0.06	13.21	1.57	0.07	0.03	0.72	4.12	5.14	0.32	100.00	0.91	
	ID3506-5	74.65	0.04	13.33	1.67	0.09	0.03	0.72	3.83	5.38	0.35	100.00	1.22	
	ID3506-6	74.56	0.05	13.22	1.56	0.06	0.04	0.72	4.23	5.30	0.35	100.00	1.70	
	Mean	74.60	0.06	13.19	1.60	0.08	0.03	0.72	4.16	5.28	0.34	100.00	1.28	
	StDev	0.21	0.02	0.10	0.04	0.01	0.02	0.02	0.21	0.09	0.02	0.00	0.42	
	Old Crow-1	75.37	0.31	13.00	1.77	0.09	0.32	1.44	3.69	3.78	0.28	100.00	6.12	
	Old Crow-2	75.23	0.30	13.20	1.70	0.05	0.31	1.46	3.84	3.70	0.28	100.00	4.71	
	Old Crow-3	74.83	0.32	13.13	1.77	0.05	0.30	1.44	4.23	3.74	0.27	100.00	3.11	
	Old Crow-4	75.43	0.31	13.09	1.64	0.05	0.31	1.50	3.51	3.96	0.26	100.00	5.42	
	Old Crow-5	75.06	0.31	13.14	1.73	0.11	0.29	1.46	4.13	3.53	0.30	100.00	2.92	
	Old Crow-6	74.90	0.38	13.21	1.70	0.06	0.32	1.40	4.20	3.62	0.29	100.00	0.86	
	Mean	75.14	0.32	13.13	1.72	0.07	0.31	1.45	3.93	3.72	0.28	100.00	3.86	
	StDev	0.25	0.03	0.08	0.05	0.03	0.01	0.03	0.30	0.15	0.02	0.00	1.93	

ID3506-7	74.79	0.06	13.30	1.51	0.08	0.02	0.73	4.10	5.16	0.32	100.00	1.28
ID3506-8	74.82	0.01	13.07	1.55	0.09	0.03	0.72	4.20	5.25	0.33	100.00	1.01
ID3506-9	74.60	0.10	13.21	1.54	0.09	0.01	0.73	4.17	5.32	0.29	100.00	1.25
ID3506-10	74.77	0.02	13.33	1.67	0.09	0.04	0.73	3.92	5.19	0.31	100.00	1.72
Mean	74.75	0.05	13.23	1.57	0.08	0.03	0.73	4.10	5.23	0.31	100.00	1.31
StDev	0.10	0.04	0.12	0.07	0.01	0.01	0.00	0.12	0.07	0.01	0.00	0.29
Old Crow-7	75.14	0.29	13.14	1.73	0.05	0.28	1.46	4.06	3.65	0.27	100.00	3.26
Old Crow-8	75.09	0.29	13.20	1.77	0.11	0.33	1.47	3.94	3.60	0.25	100.00	5.02
Old Crow-9	74.93	0.28	13.40	1.72	0.07	0.31	1.44	4.06	3.56	0.28	100.00	4.30
Old Crow-10	74.80	0.29	13.37	1.72	0.05	0.30	1.42	4.24	3.62	0.27	100.00	3.95
Mean	74.99	0.29	13.27	1.73	0.07	0.31	1.45	4.07	3.61	0.27	100.00	4.13
StDev	0.16	0.01	0.13	0.03	0.03	0.02	0.02	0.12	0.04	0.01	0.00	0.73
ID3506-11	74.78	0.07	13.33	1.51	0.10	0.01	0.72	4.12	5.10	0.33	100.00	1.38
ID3506-12	74.86	0.06	13.28	1.58	0.07	0.05	0.76	3.83	5.24	0.36	100.00	1.20
ID3506-13	74.70	0.09	13.33	1.57	0.06	0.04	0.73	4.06	5.18	0.32	100.00	0.53
ID3506-14	74.49	0.08	13.34	1.66	0.06	0.03	0.69	4.07	5.32	0.33	100.00	0.42
ID3506-15	74.55	0.09	13.31	1.54	0.04	0.03	0.72	4.36	5.10	0.32	100.00	0.94
ID3506-16	74.79	0.06	13.07	1.56	0.03	0.02	0.70	4.25	5.25	0.35	100.00	1.28
Mean	74.70	0.08	13.28	1.57	0.06	0.03	0.72	4.11	5.20	0.34	100.00	0.96
StDev	0.15	0.02	0.10	0.05	0.02	0.01	0.02	0.18	0.09	0.02	0.00	0.41
Old Crow-11	75.12	0.32	13.21	1.74	0.04	0.32	1.44	3.78	3.81	0.28	100.00	5.26
Old Crow-12	75.59	0.30	13.24	1.61	0.06	0.28	1.42	3.64	3.65	0.26	100.00	4.35
Old Crow-13	75.19	0.31	13.12	1.66	0.05	0.28	1.44	4.06	3.67	0.28	100.00	3.50
Old Crow-14	75.16	0.33	13.26	1.68	0.07	0.28	1.41	4.04	3.56	0.29	100.00	4.67
Old Crow-15	75.06	0.27	13.22	1.74	0.07	0.25	1.45	4.14	3.59	0.26	100.00	3.91

Old Crow-16	75.24	0.27	13.23	1.69	0.06	0.26	1.46	3.75	3.80	0.30	100.00	4.29
Mean	75.23	0.30	13.21	1.69	0.06	0.28	1.44	3.90	3.68	0.28	100.00	4.33
StDev	0.19	0.02	0.05	0.05	0.01	0.02	0.02	0.20	0.11	0.02	0.00	0.61
ID3506												
Mean	74.67	0.06	13.23	1.58	0.07	0.03	0.72	4.13	5.24	0.33	100.00	1.17
StDev	0.16	0.02	0.10	0.05	0.02	0.01	0.02	0.17	0.09	0.02	0.00	0.40
Old Crow												
Mean	75.13	0.30	13.20	1.71	0.07	0.30	1.44	3.96	3.68	0.28	100.00	4.10
StDev	0.22	0.03	0.10	0.05	0.02	0.02	0.03	0.23	0.12	0.02	0.00	1.23

Table S13: Prediction values for Chapman, Barlow, and Hanging Lakes
Tephra source predictions of Gravel Lake, using the machine learning classifiers of Bolton et al. (2020).

Composite depth	Sample number	Aniakchak	Augustine	Churchill	Dawson	Fisher	Hayes	Kaguyak	Katmai	Redoubt	Spurr	predict
HL 26-27	UA3360-5	0.0%	0.0%	99.9%	0.0%	0.0%	0.1%	0.0%	0.0%	0.0%	0.0%	Churchill
HL 26-27	UA3360-7	3.6%	27.9%	2.0%	0.3%	6.9%	12.0%	6.8%	1.3%	38.7%	0.5%	Redoubt
HL 26-27	UA3360-1	0.2%	0.2%	51.4%	6.4%	0.0%	0.4%	0.3%	0.2%	40.9%	0.0%	Churchill
HL 26-27	UA3360-6	1.3%	0.1%	70.9%	11.9%	0.0%	2.4%	0.0%	1.5%	11.9%	0.0%	Churchill
HL 26-27	UA3360-2	0.0%	0.1%	45.0%	0.2%	0.1%	19.9%	0.1%	0.4%	34.1%	0.0%	Churchill
HL 26-27	UA3360-3	0.0%	0.0%	98.9%	0.0%	0.0%	0.2%	0.0%	0.0%	0.9%	0.0%	Churchill
HL 26-27	UA3360-4	0.0%	0.0%	99.4%	0.0%	0.0%	0.1%	0.0%	0.0%	0.4%	0.0%	Churchill
HL 26-27	UA3360-11	1.3%	0.1%	72.9%	7.1%	0.0%	4.4%	0.0%	3.8%	10.4%	0.0%	Churchill
HL 29-30	UA3361-3	0.0%	0.0%	90.6%	0.0%	0.0%	3.6%	0.0%	0.0%	5.8%	0.0%	Churchill
HL 29-30	UA3361-20	1.8%	0.1%	55.9%	14.3%	0.0%	3.1%	0.0%	2.7%	22.1%	0.0%	Churchill
HL 29-30	UA3361-7	0.0%	0.0%	27.4%	0.1%	0.0%	69.2%	0.1%	0.4%	2.7%	0.0%	Hayes
HL 29-30	UA3361-17	0.0%	0.0%	97.6%	1.0%	0.0%	0.3%	0.0%	0.0%	1.1%	0.0%	Churchill
HL 29-30	UA3361-6	0.8%	0.0%	68.2%	5.3%	0.0%	6.1%	0.0%	5.3%	14.3%	0.0%	Churchill
HL 29-30	UA3361-14	0.0%	0.0%	65.4%	0.1%	0.0%	23.3%	0.1%	3.7%	7.3%	0.0%	Churchill
HL 29-30	UA3361-4	0.0%	0.1%	30.1%	1.0%	0.0%	1.7%	0.0%	9.0%	58.0%	0.0%	Redoubt
HL 29-30	UA3361-5	0.1%	0.2%	27.1%	2.2%	0.0%	2.2%	0.0%	21.3%	47.0%	0.0%	Redoubt
HL 29-30	UA3361-22	0.2%	0.0%	52.6%	1.6%	0.0%	5.7%	0.0%	9.9%	30.0%	0.0%	Churchill
HL 29-30	UA3361-2	0.0%	0.1%	16.8%	0.3%	0.0%	3.6%	0.1%	12.7%	66.3%	0.0%	Redoubt
HL 29-30	UA3361-25	0.1%	0.0%	48.5%	1.6%	0.0%	6.2%	0.0%	14.4%	29.2%	0.0%	Churchill
HL 29-30	UA3361-24	0.0%	0.0%	32.1%	1.5%	0.0%	3.1%	0.1%	14.8%	48.3%	0.0%	Redoubt
HL 29-30	UA3361-10	0.1%	0.0%	15.1%	1.2%	0.0%	2.6%	0.2%	18.6%	62.2%	0.0%	Redoubt
HL 29-30	UA3361-15	0.1%	0.5%	47.3%	0.9%	0.0%	3.8%	0.0%	14.7%	32.7%	0.0%	Churchill

HL 29-30	UA3361-8	0.1%	0.0%	21.1%	1.1%	0.0%	39.9%	0.0%	13.4%	24.3%	0.0%	Hayes
HL 29-30	UA3361-11	0.0%	0.0%	2.7%	51.0%	0.0%	0.9%	0.0%	25.5%	19.9%	0.0%	Dawson
HL 29-30	UA3361-12	0.0%	0.0%	2.8%	50.9%	0.1%	0.9%	0.0%	25.3%	20.0%	0.0%	Dawson
HL 29-30	UA3361-1	0.0%	0.2%	7.9%	0.4%	0.0%	1.6%	0.0%	14.1%	75.7%	0.0%	Redoubt
HL 29-30	UA3361-9	0.0%	0.2%	10.2%	0.3%	0.0%	34.9%	0.1%	29.5%	24.9%	0.0%	Hayes
HL 29-30	UA3361-13	0.0%	0.4%	26.8%	0.1%	0.0%	20.1%	0.3%	15.0%	37.3%	0.0%	Redoubt
HL 34-35	UA3362-12	2.4%	1.0%	81.0%	0.1%	0.1%	3.4%	0.0%	0.3%	11.7%	0.0%	Churchill
HL 34-35	UA3362-7	0.1%	0.0%	97.1%	0.0%	0.0%	2.2%	0.0%	0.0%	0.6%	0.0%	Churchill
HL 34-35	UA3362-19	0.0%	0.0%	99.7%	0.0%	0.0%	0.1%	0.0%	0.0%	0.2%	0.0%	Churchill
HL 34-35	UA3362-21	0.0%	0.0%	99.7%	0.0%	0.0%	0.1%	0.0%	0.0%	0.1%	0.0%	Churchill
HL 34-35	UA3362-10	0.0%	0.1%	99.5%	0.0%	0.0%	0.2%	0.0%	0.0%	0.1%	0.0%	Churchill
HL 34-35	UA3362-24	0.3%	0.0%	82.2%	5.4%	0.0%	2.6%	0.0%	1.5%	8.0%	0.0%	Churchill
HL 34-35	UA3362-18	0.0%	0.0%	94.0%	0.5%	0.0%	3.2%	0.0%	0.7%	1.6%	0.0%	Churchill
HL 34-35	UA3362-14	0.1%	0.0%	54.5%	2.0%	0.0%	4.6%	0.0%	6.0%	32.7%	0.0%	Churchill
HL 34-35	UA3362-8	0.0%	0.0%	6.8%	0.4%	0.0%	0.7%	0.1%	7.1%	84.8%	0.0%	Redoubt
HL 34-35	UA3362-2	0.1%	0.0%	53.0%	1.0%	0.0%	3.8%	0.0%	8.1%	34.0%	0.0%	Churchill
HL 34-35	UA3362-25	0.0%	0.0%	8.4%	0.7%	0.0%	3.5%	0.2%	20.5%	66.6%	0.0%	Redoubt
HL 34-35	UA3362-16	0.0%	0.0%	35.8%	0.5%	0.0%	1.6%	0.1%	13.1%	48.9%	0.0%	Redoubt
HL 34-35	UA3362-11	0.1%	1.1%	32.6%	0.4%	0.0%	6.0%	0.0%	21.8%	38.0%	0.0%	Redoubt
HL 34-35	UA3362-20	0.1%	0.4%	31.0%	0.3%	0.0%	1.8%	0.0%	19.0%	47.3%	0.0%	Redoubt
HL 34-35	UA3362-3	0.0%	0.0%	5.1%	0.4%	0.0%	0.8%	0.0%	26.5%	67.1%	0.0%	Redoubt
HL 34-35	UA3362-15	0.0%	0.4%	34.4%	0.3%	0.0%	6.3%	0.1%	17.1%	41.4%	0.0%	Redoubt
HL 34-35	UA3362-23	0.0%	0.0%	1.2%	0.1%	0.0%	4.6%	0.5%	64.9%	28.7%	0.0%	Katmai
HL 34-35	UA3362-9	0.0%	0.0%	2.4%	0.2%	0.0%	1.0%	0.0%	6.3%	90.1%	0.0%	Redoubt
HL 38-39	UA3363-1	0.3%	0.1%	96.6%	0.0%	0.0%	2.9%	0.0%	0.0%	0.1%	0.0%	Churchill
HL 38-39	UA3363-5	0.0%	0.0%	99.7%	0.0%	0.0%	0.3%	0.0%	0.0%	0.0%	0.0%	Churchill
HL 38-39	UA3363-3	0.3%	0.0%	52.5%	1.2%	0.0%	4.0%	0.0%	9.4%	32.6%	0.0%	Churchill

HL 38-39	UA3363-2	0.0%	0.0%	48.7%	0.9%	0.0%	10.3%	0.0%	10.2%	29.9%	0.0%	Churchill
HL 38-39	UA3363-6	0.0%	0.0%	13.9%	0.8%	0.0%	3.6%	0.5%	9.4%	71.7%	0.0%	Redoubt
HL 38-39	UA3363-4	0.0%	0.3%	32.3%	0.5%	0.0%	1.6%	0.0%	19.7%	45.6%	0.0%	Redoubt
HL 43-44	UA3364-18	0.2%	0.0%	95.9%	0.0%	0.0%	3.1%	0.0%	0.0%	0.8%	0.0%	Churchill
HL 43-44	UA3364-23	0.1%	0.0%	79.9%	0.3%	0.0%	4.9%	0.0%	0.0%	14.8%	0.0%	Churchill
HL 43-44	UA3364-3	0.0%	0.0%	######	0.0%	0.0%	0.0%	0.0%	0.0%	0.0%	0.0%	Churchill
HL 43-44	UA3364-14	0.0%	0.0%	97.8%	0.3%	0.0%	0.6%	0.0%	0.3%	0.9%	0.0%	Churchill
HL 43-44	UA3364-10	0.6%	0.0%	80.6%	5.5%	0.0%	2.1%	0.0%	1.5%	9.6%	0.0%	Churchill
HL 43-44	UA3364-22	1.2%	0.0%	72.9%	7.4%	0.0%	3.7%	0.0%	2.6%	12.2%	0.0%	Churchill
HL 43-44	UA3364-8	0.1%	0.0%	88.9%	0.8%	0.0%	1.4%	0.0%	0.2%	8.6%	0.0%	Churchill
HL 43-44	UA3364-11	1.2%	0.0%	53.6%	6.1%	0.0%	6.1%	0.0%	4.5%	28.5%	0.0%	Churchill
HL 43-44	UA3364-25	0.0%	0.0%	79.5%	0.0%	0.0%	10.2%	0.0%	2.9%	7.3%	0.0%	Churchill
HL 43-44	UA3364-9	0.8%	0.1%	59.4%	2.4%	0.0%	8.2%	0.0%	9.7%	19.3%	0.0%	Churchill
HL 43-44	UA3364-2	0.1%	0.1%	13.4%	0.5%	0.2%	65.6%	3.7%	2.3%	14.1%	0.0%	Hayes
HL 43-44	UA3364-1	0.2%	0.0%	28.0%	2.0%	0.0%	39.1%	0.2%	11.1%	19.3%	0.0%	Hayes
HL 43-44	UA3364-20	0.1%	0.0%	55.2%	1.2%	0.0%	5.7%	0.0%	6.6%	31.1%	0.0%	Churchill
HL 43-44	UA3364-15	0.0%	0.1%	52.5%	1.0%	0.0%	6.2%	0.0%	8.8%	31.4%	0.0%	Churchill
HL 43-44	UA3364-13	0.0%	0.0%	21.7%	0.9%	0.0%	32.7%	0.2%	11.0%	33.5%	0.0%	Redoubt
HL 43-44	UA3364-6	0.0%	0.0%	40.3%	0.8%	0.0%	5.0%	0.1%	9.7%	44.1%	0.0%	Redoubt
HL 43-44	UA3364-7	0.0%	0.0%	19.7%	0.9%	0.0%	1.2%	0.0%	11.2%	67.0%	0.0%	Redoubt
HL 43-44	UA3364-16	0.0%	0.3%	22.9%	0.4%	0.0%	4.7%	0.1%	14.3%	57.3%	0.0%	Redoubt
HL 43-44	UA3364-21	0.0%	0.2%	37.2%	0.3%	0.0%	4.8%	0.0%	10.7%	46.8%	0.0%	Redoubt
HL 43-44	UA3364-17	0.0%	0.1%	4.0%	0.3%	0.0%	4.6%	0.0%	5.2%	85.6%	0.0%	Redoubt
HL 80-81	UA3452_001	0.0%	0.0%	52.8%	0.5%	0.1%	1.2%	0.0%	9.9%	35.5%	0.0%	Churchill
HL 91-92	UA3385_001 1	1.2%	11.2%	0.1%	0.0%	3.6%	11.7%	0.0%	65.5%	6.6%	0.1%	Katmai
HL 90-92	UA3450_001	12.8%	0.4%	4.6%	0.5%	1.2%	1.3%	0.0%	1.6%	77.6%	0.0%	Redoubt
HL 90-92	UA3450_002	9.8%	0.2%	5.6%	0.6%	1.6%	3.4%	0.0%	1.6%	77.1%	0.0%	Redoubt

HL 90-92	UA3450_003	0.4%	0.0%	44.1%	21.1%	0.1%	3.6%	0.0%	9.3%	21.3%	0.0%	Churchill
HL 90-92	UA3450_004	0.5%	0.0%	53.8%	14.3%	0.1%	3.6%	0.0%	7.7%	20.0%	0.0%	Churchill
HL 90-92	UA3450_005	0.6%	0.0%	56.5%	11.4%	0.1%	4.5%	0.0%	7.1%	19.8%	0.0%	Churchill
HL 156-157	UA3432_001	1.2%	1.0%	1.3%	0.0%	0.3%	4.2%	0.0%	0.5%	91.4%	0.0%	Redoubt
HL 156-157	UA3432_002	11.2%	0.6%	4.4%	0.1%	5.0%	7.0%	0.0%	0.4%	71.1%	0.1%	Redoubt
BAR17 B2 4-5	UA 3190-5	0.8%	0.0%	67.5%	4.0%	0.0%	4.4%	0.0%	4.6%	18.8%	0.0%	Churchill
BAR17 B2 4-5	UA 3190-6	0.9%	0.0%	67.5%	7.3%	0.0%	4.0%	0.0%	3.0%	17.3%	0.0%	Churchill
BAR17 B2 4-5	UA 3190-8	1.1%	0.0%	69.7%	6.0%	0.0%	4.2%	0.0%	3.9%	15.2%	0.0%	Churchill
BAR17 B2 4-5	UA 3190-3	0.0%	0.0%	99.1%	0.0%	0.0%	0.4%	0.0%	0.0%	0.5%	0.0%	Churchill
BAR17 B2 4-5	UA 3190_001-1	1.2%	0.0%	60.1%	15.8%	0.0%	3.0%	0.0%	2.7%	17.1%	0.0%	Churchill
BAR17 B2 4-5	UA 3190-2	0.0%	0.0%	28.7%	0.0%	0.0%	63.0%	0.1%	2.9%	5.3%	0.0%	Hayes
BAR17 B2 4-5	UA 3190-4	0.2%	0.1%	58.2%	2.4%	0.0%	4.3%	0.0%	9.4%	25.3%	0.0%	Churchill
BAR17 B2 4-5	UA 3190-1	3.0%	0.2%	44.4%	3.4%	0.0%	2.2%	0.0%	21.4%	25.4%	0.0%	Churchill
BAR17 B2 4-5	UA 3190_002-1	0.5%	0.2%	52.8%	0.5%	0.0%	3.5%	0.0%	10.8%	31.7%	0.0%	Churchill
BAR17 B2 21-22	UA 3191-1	1.2%	0.0%	65.4%	7.8%	0.3%	2.8%	0.0%	7.2%	15.3%	0.0%	Churchill
BAR17 B2 21-22	UA 3191-13	0.9%	0.8%	56.0%	1.6%	0.0%	4.3%	0.1%	5.7%	30.6%	0.0%	Churchill
BAR17 B2 21-22	UA 3191-16	0.6%	0.0%	65.2%	4.5%	0.1%	4.6%	0.0%	5.3%	19.7%	0.0%	Churchill
BAR17 B2 21-22	UA 3191-12	0.0%	0.2%	26.0%	26.6%	0.0%	1.7%	0.0%	10.3%	35.1%	0.0%	Redoubt
BAR17 B2 21-22	UA 3191-5	0.0%	0.2%	31.0%	22.1%	0.0%	2.1%	0.0%	10.6%	33.9%	0.0%	Redoubt
BAR17 B2 21-22	UA 3191-17	7.5%	0.5%	38.3%	6.4%	0.0%	4.0%	0.0%	19.0%	24.3%	0.0%	Churchill
BAR17 B2 21-22	UA 3191-8	0.2%	0.0%	0.0%	99.2%	0.0%	0.0%	0.0%	0.1%	0.4%	0.0%	Dawson
BAR17 B2 21-22	UA 3191-11	0.1%	0.0%	7.3%	1.1%	0.0%	0.8%	0.1%	21.3%	69.3%	0.0%	Redoubt
BAR17 B2 21-22	UA 3191-7	0.0%	1.2%	1.4%	0.6%	0.0%	12.5%	53.9%	19.5%	10.8%	0.0%	Kaguyak

BAR17 B2 21-22	UA 3191-2	0.4%	0.3%	55.1%	5.0%	0.1%	5.2%	0.1%	10.0%	23.7%	0.0%	Churchill
BAR17 B2 21-22	UA 3191-15	0.4%	0.2%	48.5%	13.2%	0.0%	4.1%	0.0%	13.0%	20.6%	0.0%	Churchill
BAR17 B2 30-31	UA 3192-5	0.7%	0.0%	67.7%	4.1%	0.1%	4.8%	0.0%	4.6%	17.9%	0.0%	Churchill
BAR17 B2 30-31	UA 3192-6	0.7%	0.0%	64.1%	6.0%	0.0%	4.2%	0.0%	5.8%	19.2%	0.0%	Churchill
BAR17 B2 30-31	UA 3192-8	0.6%	0.0%	64.4%	4.5%	0.0%	4.9%	0.0%	5.0%	20.6%	0.0%	Churchill
BAR17 B2 30-31	UA 3192-9	1.0%	0.0%	69.5%	5.6%	0.0%	4.1%	0.0%	2.3%	17.5%	0.0%	Churchill
BAR17 B2 30-31	UA 3192-7	0.0%	0.0%	34.4%	0.2%	0.0%	1.6%	0.0%	8.8%	54.9%	0.0%	Redoubt
BAR17 B2 30-31	UA 3192-2	0.2%	1.4%	3.4%	0.2%	0.0%	4.0%	0.7%	22.3%	67.7%	0.0%	Redoubt
BAR17 B2 30-31	UA 3192-1	0.0%	0.0%	34.2%	17.9%	0.1%	0.7%	0.0%	12.8%	34.3%	0.0%	Redoubt
BAR17 B2 30-31	UA 3192-4	0.0%	0.1%	53.4%	1.4%	0.0%	3.5%	0.0%	5.5%	36.0%	0.0%	Churchill
BAR17 B2 30-31	UA 3192-3	2.7%	0.0%	60.3%	15.6%	0.2%	3.3%	0.0%	6.8%	11.1%	0.0%	Churchill
BAR17 B2 42-43	UA 3193-9	65.9%	0.5%	0.6%	5.6%	3.3%	0.2%	0.0%	4.5%	19.3%	0.0%	Aniakchak
BAR17 B2 42-43	UA 3193-23	0.9%	0.0%	4.3%	74.2%	0.0%	0.5%	0.0%	2.8%	17.3%	0.0%	Dawson
BAR17 B2 42-43	UA 3193-6	3.0%	0.0%	55.8%	11.9%	0.0%	3.8%	0.0%	6.6%	18.8%	0.0%	Churchill
BAR17 B2 42-43	UA 3193-10	0.0%	0.1%	30.5%	0.0%	0.0%	46.3%	0.5%	3.5%	19.1%	0.0%	Hayes
BAR17 B2 42-43	UA 3193-13	3.9%	0.0%	53.3%	27.5%	0.1%	3.3%	0.0%	4.6%	7.3%	0.0%	Churchill
BAR17 B2 42-43	UA 3193-17	1.9%	0.0%	60.5%	18.7%	0.4%	4.4%	0.0%	4.6%	9.5%	0.0%	Churchill
BAR17 B2 42-43	UA 3193-5	3.0%	1.5%	44.3%	17.6%	0.0%	2.5%	0.0%	9.9%	21.2%	0.0%	Churchill
BAR17 B2 42-43	UA 3193-28	0.6%	0.1%	63.7%	6.2%	0.0%	4.8%	0.0%	5.4%	19.2%	0.0%	Churchill
BAR17 B2 42-43	UA 3193-2	0.9%	0.0%	65.2%	10.9%	0.1%	4.0%	0.0%	2.8%	16.0%	0.0%	Churchill

BAR17 B2 42-43	UA 3193-12	0.9%	0.0%	67.8%	7.6%	0.0%	4.4%	0.0%	3.1%	16.1%	0.0%	Churchill
BAR17 B2 42-43	UA 3193-4	1.7%	0.0%	67.8%	4.9%	0.3%	3.3%	0.0%	7.4%	14.6%	0.0%	Churchill
BAR17 B2 42-43	UA 3193-7	1.2%	0.5%	55.0%	1.4%	0.0%	4.5%	0.1%	6.5%	30.7%	0.0%	Churchill
BAR17 B2 42-43	UA 3193-15	0.4%	0.3%	51.4%	7.4%	0.0%	4.0%	0.0%	14.5%	22.1%	0.0%	Churchill
BAR17 B2 42-43	UA 3193-27	1.5%	0.1%	58.7%	2.8%	0.1%	4.3%	0.0%	11.7%	20.8%	0.0%	Churchill
BAR17 B2 42-43	UA 3193-3	0.6%	0.0%	58.0%	9.5%	0.1%	4.4%	0.0%	6.2%	21.1%	0.0%	Churchill
BAR17 B2 42-43	UA 3193-30	0.9%	0.1%	53.3%	1.8%	0.0%	4.3%	0.0%	16.3%	23.3%	0.0%	Churchill
BAR17 B2 42-43	UA 3193-29	0.1%	0.1%	46.3%	7.8%	0.0%	2.9%	0.0%	9.9%	32.9%	0.0%	Churchill
BAR17 B2 42-43	UA 3193-25	1.0%	0.1%	40.8%	11.4%	0.0%	3.0%	0.0%	17.8%	26.0%	0.0%	Churchill
BAR17 B2 42-43	UA 3193-19	0.1%	0.1%	29.8%	23.2%	0.0%	3.1%	0.0%	17.8%	25.8%	0.0%	Churchill
BAR17 B2 42-43	UA 3193-11	0.7%	0.0%	64.3%	3.1%	0.1%	4.7%	0.0%	6.3%	20.9%	0.0%	Churchill
BAR17 B2 42-43	UA 3193-14	0.0%	0.0%	37.7%	19.8%	0.1%	2.2%	0.0%	10.9%	29.3%	0.0%	Churchill
BAR17 B2 42-43	UA 3193-21	0.8%	0.1%	48.3%	3.6%	0.0%	3.1%	0.0%	13.5%	30.5%	0.0%	Churchill
BAR17 B2 42-43	UA 3193-1	3.3%	0.3%	39.8%	9.0%	0.0%	3.9%	0.0%	18.3%	25.4%	0.0%	Churchill
BAR17 B2 42-43	UA 3193-20	0.5%	0.1%	48.1%	4.2%	0.0%	2.8%	0.0%	10.0%	34.3%	0.0%	Churchill
BAR17 B2 42-43	UA 3193-22	0.0%	0.0%	45.7%	8.7%	0.1%	2.2%	0.0%	11.4%	31.9%	0.0%	Churchill
BAR17 B2 42-43	UA 3193-8	0.0%	0.4%	34.4%	0.3%	0.0%	1.7%	0.0%	11.9%	51.3%	0.0%	Redoubt
BAR17 B3 13-14	UA 3194-10	0.0%	6.8%	0.3%	0.0%	0.0%	7.6%	81.9%	1.6%	1.8%	0.0%	Kaguyak
BAR17 B3 13-14	UA 3194-11	0.0%	14.2%	0.8%	0.1%	0.0%	8.5%	72.8%	1.2%	2.4%	0.0%	Kaguyak
BAR17 B3 13-14	UA 3194-4	1.5%	0.1%	56.2%	10.0%	0.1%	3.6%	0.0%	6.5%	22.1%	0.0%	Churchill

BAR17 B3 13-14	UA 3194-16	1.0%	0.0%	61.4%	12.2%	0.0%	3.8%	0.0%	3.2%	18.3%	0.0%	Churchill
BAR17 B3 13-14	UA 3194-17	0.9%	0.0%	68.0%	8.3%	0.0%	3.3%	0.0%	2.7%	16.8%	0.0%	Churchill
BAR17 B3 13-14	UA 3194-23	0.9%	0.0%	65.0%	10.5%	0.0%	4.2%	0.0%	2.9%	16.5%	0.0%	Churchill
BAR17 B3 13-14	UA 3194-29	2.7%	0.2%	44.6%	4.5%	0.0%	2.8%	0.0%	18.8%	26.4%	0.0%	Churchill
BAR17 B3 13-14	UA 3194-21	3.9%	0.2%	47.2%	0.9%	0.0%	2.5%	0.0%	18.1%	27.2%	0.0%	Churchill
BAR17 B3 13-14	UA 3194-19	2.1%	0.0%	65.9%	6.5%	0.2%	3.3%	0.0%	6.9%	15.1%	0.0%	Churchill
BAR17 B3 13-14	UA 3194-28	1.5%	0.1%	47.6%	3.6%	0.0%	2.9%	0.0%	10.0%	34.3%	0.0%	Churchill
BAR17 B3 13-14	UA 3194-26	1.5%	0.0%	70.3%	6.0%	0.1%	3.9%	0.0%	5.0%	13.2%	0.0%	Churchill
BAR17 B3 13-14	UA 3194-25	0.9%	0.1%	68.3%	2.9%	0.0%	4.4%	0.0%	4.4%	18.9%	0.0%	Churchill
BAR17 B3 13-14	UA 3194-30	3.0%	0.0%	63.0%	3.3%	0.0%	6.0%	0.0%	4.8%	19.9%	0.0%	Churchill
BAR17 B3 13-14	UA 3194-14	1.5%	0.2%	51.0%	1.1%	0.0%	4.3%	0.0%	10.6%	31.3%	0.0%	Churchill
BAR17 B3 13-14	UA 3194-22	1.5%	0.0%	64.8%	8.1%	0.3%	3.3%	0.0%	6.9%	15.1%	0.0%	Churchill
BAR17 B3 13-14	UA 3194-18	1.1%	0.2%	58.5%	1.4%	0.0%	4.3%	0.0%	9.3%	25.2%	0.0%	Churchill
BAR17 B3 13-14	UA 3194-9	0.8%	0.0%	64.9%	2.8%	0.1%	5.1%	0.0%	5.4%	20.9%	0.0%	Churchill
BAR17 B3 13-14	UA 3194-7	1.2%	0.3%	50.3%	0.3%	0.0%	3.4%	0.0%	12.6%	31.9%	0.0%	Churchill
BAR17 B3 13-14	UA 3194-27	1.1%	0.0%	66.1%	6.5%	0.2%	3.0%	0.0%	6.9%	16.1%	0.0%	Churchill
BAR17 B3 13-14	UA 3194-12	0.5%	0.2%	38.4%	13.1%	0.0%	3.0%	0.0%	19.2%	25.6%	0.0%	Churchill
BAR17 B3 13-14	UA 3194-5	0.7%	0.0%	64.2%	3.4%	0.1%	4.7%	0.0%	6.9%	20.0%	0.0%	Churchill
BAR17 B3 13-14	UA 3194-13	0.7%	0.0%	64.7%	3.2%	0.0%	4.9%	0.0%	5.3%	21.1%	0.0%	Churchill
CHP-SC2 8-9	UA 3499-13	11.7%	0.0%	0.4%	82.2%	0.4%	0.1%	0.0%	0.0%	5.1%	0.0%	Dawson

CHP-SC2 8-9	UA 3499-11	1.9%	0.0%	9.8%	85.4%	0.0%	0.6%	0.1%	0.9%	1.3%	0.0%	Dawson
CHP-SC2 8-9	UA 3499-22	0.6%	0.1%	4.1%	89.9%	0.1%	0.5%	0.0%	0.9%	3.7%	0.0%	Dawson
CHP-SC2 8-9	UA 3499-23	0.5%	0.0%	0.0%	99.2%	0.1%	0.0%	0.0%	0.0%	0.1%	0.0%	Dawson
CHP-SC2 8-9	UA 3499-27	0.1%	0.0%	0.0%	99.4%	0.0%	0.0%	0.0%	0.2%	0.3%	0.0%	Dawson
CHP-SC2 8-9	UA 3499-26	0.7%	0.0%	10.1%	83.5%	0.0%	1.3%	0.0%	0.5%	3.8%	0.0%	Dawson
CHP-SC2 8-9	UA 3499-17	0.3%	0.1%	10.7%	83.6%	0.0%	0.9%	0.0%	1.8%	2.5%	0.0%	Dawson
CHP-SC2 8-9	UA 3499-18	0.0%	0.0%	19.7%	2.3%	0.0%	1.8%	0.0%	9.7%	66.4%	0.0%	Redoubt
CHP-SC2 8-9	UA 3499-15	0.0%	0.0%	3.3%	0.4%	0.0%	26.9%	0.4%	30.2%	38.7%	0.0%	Redoubt
CHP-SC2 8-9	UA 3499-16	0.2%	0.0%	3.3%	0.4%	0.0%	0.3%	0.0%	7.8%	88.0%	0.0%	Redoubt
CHP-SC2 8-9	UA 3499-6	0.0%	0.1%	17.0%	1.1%	0.0%	1.0%	0.0%	10.7%	70.1%	0.0%	Redoubt
CHP-SC2 8-9	UA 3499-20	0.0%	0.1%	46.4%	0.4%	0.0%	2.1%	0.0%	9.7%	41.3%	0.0%	Churchill
CHP-SC2 8-9	UA 3499-1	0.1%	0.5%	0.5%	0.1%	0.0%	4.6%	0.1%	55.3%	38.8%	0.0%	Katmai
CHP-SC2 8-9	UA 3499-8	0.0%	0.1%	3.5%	0.2%	0.0%	1.4%	0.0%	9.5%	85.3%	0.0%	Redoubt
CHP-SC2 8-9	UA 3499-28	0.0%	0.4%	0.3%	0.1%	0.0%	16.5%	0.4%	58.6%	23.7%	0.0%	Katmai
CHP-SC2 8-9	UA 3499-3	0.0%	0.0%	0.5%	0.0%	0.0%	0.6%	0.6%	78.3%	20.0%	0.0%	Katmai
CHP-SC2 8-9	UA 3499-21	0.0%	0.2%	5.1%	0.4%	0.0%	10.5%	0.5%	28.9%	54.5%	0.0%	Redoubt
CHP-SC2 8-9	UA 3499-5	0.0%	0.4%	1.0%	0.1%	0.0%	28.8%	0.1%	18.7%	51.0%	0.0%	Redoubt
CHP-SC2 8-9	UA 3499-24	1.9%	0.9%	42.0%	17.0%	0.0%	2.2%	0.0%	13.7%	22.3%	0.0%	Churchill
CHP-SC2 8-9	UA 3499-12	0.0%	0.5%	28.3%	0.5%	0.0%	2.4%	0.2%	2.8%	65.3%	0.0%	Redoubt
CHP-SC2 8-9	UA 3499-10	0.2%	0.9%	50.4%	1.7%	0.0%	5.0%	0.0%	11.1%	30.7%	0.0%	Churchill
CHP-SC2 8-9	UA 3499-2	0.0%	0.0%	20.4%	4.7%	0.0%	0.0%	0.1%	1.8%	73.1%	0.0%	Redoubt
CHP-SC2 8-9	UA 3499-19	0.0%	0.2%	0.0%	0.0%	0.0%	2.4%	0.2%	11.4%	85.7%	0.0%	Redoubt
CHP-SC2 8-9	UA 3499-30	13.9%	0.3%	15.1%	46.4%	0.0%	0.2%	0.0%	1.9%	22.2%	0.0%	Dawson
CHP-SC2 8-9	UA 3499-29	2.4%	0.0%	63.2%	13.6%	0.3%	3.9%	0.0%	6.1%	10.5%	0.0%	Churchill
CHP-SC2 8-9	UA 3499-25	0.0%	0.0%	96.2%	0.0%	0.0%	2.7%	0.0%	0.4%	0.7%	0.0%	Churchill
CHP-SC2 8-9	UA 3499-4	0.9%	0.0%	48.6%	3.7%	0.2%	15.8%	0.1%	14.4%	16.2%	0.0%	Churchill
CHP-SC2 8-9	UA 3499-9	0.2%	0.2%	3.3%	1.0%	0.0%	65.6%	3.0%	15.2%	11.5%	0.0%	Hayes

CHP-SC2 8-9	UA 3499-14	0.6%	0.0%	59.5%	2.4%	0.1%	6.8%	0.0%	7.3%	23.3%	0.0%	Churchill
CHP-SC2 17-18	UA 3500-20	0.2%	0.1%	3.2%	90.3%	0.0%	0.8%	0.0%	0.7%	4.7%	0.0%	Dawson
CHP-SC2 17-18	UA 3500-16	0.2%	0.0%	2.0%	90.2%	0.0%	0.4%	0.0%	2.0%	5.2%	0.0%	Dawson
CHP-SC2 17-18	UA 3500-13	0.1%	0.1%	1.9%	92.8%	0.0%	1.1%	0.0%	1.0%	3.0%	0.0%	Dawson
CHP-SC2 17-18	UA 3500-22	0.4%	0.0%	7.7%	90.5%	0.0%	0.4%	0.0%	0.4%	0.6%	0.0%	Dawson
CHP-SC2 17-18	UA 3500-5	0.0%	0.0%	97.9%	0.0%	0.0%	1.2%	0.0%	0.0%	0.9%	0.0%	Churchill
CHP-SC2 17-18	UA 3500-7	0.0%	0.0%	88.1%	0.0%	0.0%	11.0%	0.1%	0.0%	0.8%	0.0%	Churchill
CHP-SC2 17-18	UA 3500-17	0.0%	0.0%	######	0.0%	0.0%	0.0%	0.0%	0.0%	0.0%	0.0%	Churchill
CHP-SC2 17-18	UA 3500-25	0.9%	0.4%	52.1%	2.2%	0.8%	13.2%	0.9%	0.4%	29.0%	0.0%	Churchill
CHP-SC2 17-18	UA 3500-18	0.0%	0.0%	30.1%	0.0%	0.0%	64.9%	0.2%	1.1%	3.7%	0.0%	Hayes
CHP-SC2 17-18	UA 3500-30	0.7%	0.0%	24.5%	4.6%	0.0%	48.1%	0.0%	8.1%	13.9%	0.0%	Hayes
CHP-SC2 17-18	UA 3500-11	0.2%	0.0%	41.8%	2.4%	0.0%	20.6%	0.1%	18.4%	16.4%	0.0%	Churchill
CHP-SC2 17-18	UA 3500-6	0.2%	0.0%	57.5%	2.0%	0.0%	5.4%	0.0%	9.5%	25.4%	0.0%	Churchill
CHP-SC2 17-18	UA 3500-27	0.0%	0.0%	0.2%	0.0%	0.0%	1.6%	0.3%	17.6%	80.2%	0.0%	Redoubt
CHP-SC2 17-18	UA 3500-14	0.0%	0.1%	38.5%	0.6%	0.0%	16.4%	0.2%	7.3%	36.9%	0.0%	Churchill
CHP-SC2 17-18	UA 3500-23	0.0%	0.0%	0.9%	0.4%	0.0%	5.3%	0.3%	60.0%	33.0%	0.0%	Katmai
CHP-SC2 17-18	UA 3500-26	0.0%	0.2%	2.1%	0.5%	0.0%	52.2%	0.0%	34.4%	10.5%	0.0%	Hayes
CHP-SC2 17-18	UA 3500-2	0.0%	0.0%	1.2%	0.1%	0.0%	52.8%	0.2%	24.5%	21.1%	0.0%	Hayes
CHP-SC2 17-18	UA 3500-15	0.0%	0.3%	46.5%	0.4%	0.0%	3.2%	0.0%	13.9%	35.6%	0.0%	Churchill
CHP-SC2 17-18	UA 3500-4	0.0%	0.3%	44.0%	0.3%	0.0%	11.1%	0.1%	8.5%	35.6%	0.0%	Churchill
CHP-SC2 17-18	UA 3500-1	0.0%	0.4%	0.9%	0.1%	0.0%	34.5%	0.3%	35.6%	28.3%	0.0%	Katmai
CHP-SC2 17-18	UA 3500-12	0.0%	0.5%	0.5%	0.0%	0.0%	47.9%	0.4%	32.5%	18.2%	0.0%	Hayes
CHP-SC2 17-18	UA 3500-8	0.0%	0.1%	0.4%	0.0%	0.0%	17.8%	0.0%	51.9%	29.8%	0.0%	Katmai
CHP-SC2 17-18	UA 3500-29	97.4%	0.0%	0.1%	0.0%	0.1%	0.0%	0.0%	0.0%	2.4%	0.0%	Aniakchak
CHP-SC2 17-18	UA 3500-24	0.2%	0.4%	7.1%	0.1%	0.0%	75.1%	0.2%	0.0%	16.9%	0.0%	Hayes
CHP-SC2 17-18	UA 3500-9	4.8%	3.2%	10.5%	10.0%	0.0%	2.5%	0.0%	47.8%	21.2%	0.0%	Katmai
CHP-SC2 17-18	UA 3500-21	0.4%	0.1%	58.5%	3.0%	0.0%	4.8%	0.0%	8.9%	24.2%	0.0%	Churchill

CHP-SC2 17-18	UA 3500-3	0.1%	2.1%	38.1%	6.5%	0.0%	8.4%	0.4%	23.4%	21.0%	0.0%	Churchill
CHP-SC2 23-24	UA 3501-12	0.1%	0.0%	0.2%	99.6%	0.0%	0.0%	0.0%	0.0%	0.0%	0.0%	Dawson
CHP-SC2 23-24	UA 3501-28	0.1%	0.0%	1.0%	98.6%	0.0%	0.1%	0.0%	0.0%	0.2%	0.0%	Dawson
CHP-SC2 23-24	UA 3501-20	0.6%	0.0%	62.8%	4.4%	0.0%	4.0%	0.1%	7.1%	21.0%	0.0%	Churchill
CHP-SC2 23-24	UA 3501-18	0.1%	0.0%	3.7%	2.8%	0.0%	2.1%	0.1%	10.6%	80.5%	0.0%	Redoubt
CHP-SC2 23-24	UA 3501-29	0.0%	0.1%	3.0%	0.8%	0.0%	31.6%	0.2%	46.2%	18.1%	0.0%	Katmai
CHP-SC2 23-24	UA 3501-24	0.2%	0.1%	9.2%	1.9%	0.0%	56.5%	0.0%	21.4%	10.7%	0.0%	Hayes
CHP-SC2 23-24	UA 3501-19	0.0%	0.0%	36.7%	0.8%	0.0%	11.4%	0.1%	8.2%	42.8%	0.0%	Redoubt
CHP-SC2 23-24	UA 3501-3	0.1%	0.1%	6.6%	1.3%	0.0%	57.3%	0.0%	14.3%	20.2%	0.0%	Hayes
CHP-SC2 23-24	UA 3501-14	0.0%	0.1%	5.2%	0.6%	0.0%	51.0%	0.1%	19.7%	23.2%	0.0%	Hayes
CHP-SC2 23-24	UA 3501-9	0.0%	0.1%	2.1%	0.5%	0.0%	15.2%	0.6%	60.1%	21.4%	0.0%	Katmai
CHP-SC2 23-24	UA 3501-8	0.0%	0.0%	0.3%	0.3%	0.0%	7.4%	0.2%	87.2%	4.6%	0.0%	Katmai
CHP-SC2 23-24	UA 3501-10	0.1%	0.0%	0.4%	0.3%	0.0%	0.0%	0.1%	67.0%	32.1%	0.0%	Katmai
CHP-SC2 23-24	UA 3501-11	0.0%	0.7%	0.8%	0.1%	0.0%	50.2%	0.2%	30.6%	17.4%	0.0%	Hayes
CHP-SC2 23-24	UA 3501-1	0.0%	0.5%	6.1%	0.1%	0.0%	24.4%	0.2%	40.0%	28.7%	0.0%	Katmai
CHP-SC2 23-24	UA 3501-2	0.0%	0.2%	7.9%	0.7%	0.0%	1.0%	0.1%	21.4%	68.6%	0.0%	Redoubt
CHP-SC2 23-24	UA 3501-21	0.0%	0.2%	1.5%	0.2%	0.0%	1.8%	0.1%	16.0%	80.2%	0.0%	Redoubt
CHP-SC2 23-24	UA 3501-27	0.0%	0.0%	0.7%	0.0%	0.0%	1.2%	0.0%	6.3%	91.8%	0.0%	Redoubt
CHP-SC2 23-24	UA 3501-30	0.0%	0.4%	0.0%	0.0%	0.0%	2.6%	0.1%	70.0%	26.9%	0.0%	Katmai
CHP-SC2 23-24	UA 3501-23	0.0%	0.4%	0.5%	0.0%	0.0%	35.7%	0.0%	40.9%	22.6%	0.0%	Katmai
CHP-SC2 23-24	UA 3501-25	0.0%	0.5%	0.9%	0.0%	0.0%	33.8%	0.4%	49.2%	15.1%	0.0%	Katmai
CHP-SC2 23-24	UA 3501-13	0.0%	0.0%	0.4%	0.0%	0.0%	13.1%	0.1%	56.1%	30.4%	0.0%	Katmai
CHP-SC2 23-24	UA 3501-7	16.8%	0.1%	0.4%	0.0%	51.3%	1.1%	0.0%	5.1%	25.1%	0.1%	Fisher

Table S14: Prediction values for Gravel Lake

Tephra source predictions of Gravel Lake, using the machine learning classifiers of Bolton et al. (2020).

Composite depth	Sample number	Aniakchak	Augustine	Churchill	Dawson	Fisher	Hayes	Kaguyak	Katmai	Redoubt	Spurr	predict
Surface Core												
GRV Sfc 4-5	UA3623-21	0.3%	0.0%	0.0%	0.0%	0.3%	0.1%	0.0%	0.6%	98.6%	0.0%	Redoubt
GRV Sfc 4-5	UA3623-29	0.2%	0.1%	76.9%	0.0%	0.7%	13.3%	0.1%	0.1%	8.6%	0.0%	Churchill
GRV Sfc 4-5	UA3623-25	2.3%	3.2%	0.1%	0.7%	0.1%	1.3%	0.0%	54.3%	38.0%	0.0%	Katmai
GRV Sfc 4-5	UA3623-4	4.5%	3.7%	0.6%	1.3%	0.8%	0.3%	0.2%	38.8%	49.8%	0.0%	Redoubt
GRV Sfc 4-5	UA3623-8	0.8%	5.4%	0.3%	0.5%	0.2%	1.1%	0.5%	72.8%	18.4%	0.0%	Katmai
GRV Sfc 4-5	UA3623-28	0.2%	1.3%	2.3%	0.2%	0.1%	1.0%	0.8%	78.7%	15.4%	0.0%	Katmai
GRV Sfc 4-5	UA3623-17	0.0%	0.0%	0.1%	0.2%	0.0%	0.0%	0.3%	12.9%	86.5%	0.0%	Redoubt
GRV Sfc 4-5	UA3623-27	0.0%	0.0%	0.1%	1.3%	0.0%	0.7%	0.6%	35.8%	61.4%	0.0%	Redoubt
GRV Sfc 4-5	UA3623-11	0.0%	0.0%	0.1%	0.0%	0.0%	0.2%	0.3%	98.5%	0.8%	0.0%	Katmai
GRV Sfc 4-5	UA3623-9	0.2%	0.0%	0.8%	3.4%	0.2%	1.2%	0.4%	88.9%	4.8%	0.0%	Katmai
GRV Sfc 4-5	UA3623-5	0.2%	0.0%	0.3%	0.9%	0.0%	0.1%	0.0%	91.1%	7.3%	0.0%	Katmai
GRV Sfc 4-5	UA3623-2	0.2%	0.0%	0.6%	0.9%	0.0%	0.1%	0.1%	97.0%	1.1%	0.0%	Katmai
GRV Sfc 4-5	UA3623-15	0.0%	0.2%	0.1%	0.0%	0.0%	2.9%	0.4%	82.6%	13.7%	0.0%	Katmai
GRV Sfc 4-5	UA3623-22	0.0%	0.0%	99.9%	0.0%	0.0%	0.1%	0.0%	0.0%	0.0%	0.0%	Churchill
GRV Sfc 4-5	UA3623-18	0.0%	0.0%	99.6%	0.0%	0.0%	0.1%	0.0%	0.0%	0.2%	0.0%	Churchill
GRV Sfc 4-5	UA3623-30	0.2%	0.0%	96.8%	0.5%	0.0%	0.2%	0.0%	0.0%	2.2%	0.0%	Churchill
GRV Sfc 4-5	UA3623-10	0.8%	0.0%	80.9%	7.9%	0.0%	0.2%	0.0%	0.0%	10.1%	0.0%	Churchill
GRV Sfc 4-5	UA3623-13	0.0%	0.0%	97.1%	2.0%	0.0%	0.7%	0.0%	0.0%	0.2%	0.0%	Churchill
GRV Sfc 4-5	UA3623-16	1.0%	0.0%	84.4%	1.7%	0.0%	0.4%	0.0%	0.0%	12.5%	0.0%	Churchill
GRV Sfc 4-5	UA3623-20	0.0%	0.0%	99.1%	0.6%	0.0%	0.0%	0.0%	0.0%	0.2%	0.0%	Churchill
GRV Sfc 4-5	UA3623-14	0.2%	0.0%	96.9%	1.1%	0.0%	0.1%	0.0%	0.0%	1.7%	0.0%	Churchill
GRV Sfc 4-5	UA3623-3	0.2%	0.0%	86.7%	4.2%	0.0%	0.6%	0.0%	0.0%	8.3%	0.0%	Churchill
GRV Sfc 4-5	UA3623-1	0.0%	0.0%	94.6%	1.8%	0.0%	1.0%	0.0%	0.1%	2.5%	0.0%	Churchill

GRV Sfc 4-5	UA3623-12	0.0%	0.0%	98.3%	0.0%	0.0%	1.0%	0.0%	0.0%	0.7%	0.0%	Churchill
GRV Sfc 4-5	UA3623-24	0.0%	0.0%	97.8%	0.5%	0.0%	0.5%	0.0%	0.0%	1.2%	0.0%	Churchill
GRV Sfc 4-5	UA3623-26	0.0%	0.0%	98.0%	0.0%	0.0%	0.2%	0.0%	0.0%	1.7%	0.0%	Churchill
GRV Sfc 4-5	UA3623-6	0.0%	0.0%	96.1%	1.2%	0.0%	0.8%	0.0%	0.0%	1.9%	0.0%	Churchill
GRV Sfc 4-5	UA3623-7	0.0%	0.0%	98.6%	0.5%	0.0%	0.2%	0.0%	0.0%	0.6%	0.0%	Churchill
GRV Sfc 8-9	UA3622-13	5.2%	0.1%	86.6%	0.5%	0.0%	3.5%	0.0%	0.2%	3.9%	0.0%	Churchill
GRV Sfc 8-9	UA3622-7	0.0%	0.0%	98.4%	0.0%	0.0%	1.4%	0.0%	0.0%	0.2%	0.0%	Churchill
GRV Sfc 8-9	UA3622-24	1.5%	0.0%	93.6%	0.4%	0.0%	0.4%	0.0%	0.0%	4.1%	0.0%	Churchill
GRV Sfc 8-9	UA3622-22	0.1%	0.0%	99.6%	0.0%	0.0%	0.1%	0.0%	0.0%	0.2%	0.0%	Churchill
GRV Sfc 8-9	UA3622-5	0.3%	0.1%	93.9%	0.0%	0.1%	0.4%	0.0%	0.0%	5.1%	0.0%	Churchill
GRV Sfc 8-9	UA3622-17	0.0%	0.0%	99.8%	0.0%	0.0%	0.1%	0.0%	0.0%	0.1%	0.0%	Churchill
GRV Sfc 8-9	UA3622-19	0.0%	0.0%	99.8%	0.0%	0.0%	0.1%	0.0%	0.0%	0.1%	0.0%	Churchill
GRV Sfc 8-9	UA3622-23	0.0%	0.0%	98.9%	0.3%	0.0%	0.0%	0.0%	0.0%	0.8%	0.0%	Churchill
GRV Sfc 8-9	UA3622-1	0.2%	0.0%	97.4%	0.8%	0.0%	0.2%	0.0%	0.0%	1.4%	0.0%	Churchill
GRV Sfc 8-9	UA3622-27	0.4%	0.0%	95.5%	0.9%	0.0%	0.2%	0.0%	0.0%	3.0%	0.0%	Churchill
GRV Sfc 8-9	UA3622-25	0.2%	0.0%	94.6%	2.7%	0.0%	0.1%	0.0%	0.0%	2.3%	0.0%	Churchill
GRV Sfc 8-9	UA3622-6	0.8%	0.0%	94.3%	1.2%	0.0%	0.7%	0.0%	0.0%	3.0%	0.0%	Churchill
GRV Sfc 8-9	UA3622-8	1.8%	0.0%	68.9%	20.9%	0.0%	0.9%	0.0%	0.8%	6.7%	0.0%	Churchill
GRV Sfc 8-9	UA3622-3	1.7%	0.1%	59.8%	6.4%	0.3%	1.7%	0.1%	2.0%	27.9%	0.0%	Churchill
GRV Sfc 8-9	UA3622-21	0.0%	0.0%	100.0%	0.0%	0.0%	0.0%	0.0%	0.0%	0.0%	0.0%	Churchill
GRV Sfc 8-9	UA3622-10	0.0%	0.0%	99.9%	0.0%	0.0%	0.1%	0.0%	0.0%	0.0%	0.0%	Churchill
GRV Sfc 8-9	UA3622-20	0.0%	0.0%	94.1%	3.8%	0.0%	1.4%	0.0%	0.0%	0.7%	0.0%	Churchill
GRV Sfc 8-9	UA3622-12	0.0%	0.0%	99.8%	0.0%	0.0%	0.1%	0.0%	0.0%	0.0%	0.0%	Churchill
GRV Sfc 8-9	UA3622-15	0.1%	0.5%	1.8%	0.4%	0.0%	3.0%	0.9%	33.4%	59.8%	0.0%	Redoubt
GRV Sfc 8-9	UA3622-4	0.5%	0.2%	43.8%	0.0%	2.3%	14.4%	0.0%	0.0%	38.7%	0.0%	Churchill
GRV Sfc 8-9	UA3622-30	0.5%	0.3%	41.2%	0.0%	2.6%	16.7%	0.0%	0.1%	38.6%	0.0%	Churchill
GRV Sfc 8-9	UA3622-16	0.2%	0.0%	42.3%	0.0%	0.7%	46.0%	0.1%	0.1%	10.6%	0.0%	Hayes

GRV Sfc 13-14	UA3621-2	0.3%	0.0%	94.4%	0.0%	0.1%	3.3%	0.0%	0.0%	1.9%	0.0%	Churchill
GRV Sfc 13-14	UA3621-3	0.1%	0.2%	96.9%	0.4%	0.0%	0.3%	0.0%	0.0%	2.1%	0.0%	Churchill
GRV Sfc 13-14	UA3621-8	0.1%	0.0%	99.6%	0.2%	0.0%	0.1%	0.0%	0.0%	0.0%	0.0%	Churchill
GRV Sfc 13-14	UA3621-18	0.0%	0.0%	99.3%	0.5%	0.0%	0.0%	0.0%	0.0%	0.2%	0.0%	Churchill
GRV Sfc 13-14	UA3621-23	0.0%	0.0%	100.0%	0.0%	0.0%	0.0%	0.0%	0.0%	0.0%	0.0%	Churchill
GRV Sfc 13-14	UA3621-7	0.2%	0.1%	91.4%	0.3%	0.0%	0.2%	0.0%	0.0%	7.7%	0.0%	Churchill
GRV Sfc 13-14	UA3621-11	0.2%	0.1%	96.5%	0.2%	0.0%	0.4%	0.0%	0.0%	2.6%	0.0%	Churchill
GRV Sfc 13-14	UA3621-24	0.6%	0.0%	83.9%	1.8%	0.0%	0.4%	0.0%	0.0%	13.2%	0.0%	Churchill
GRV Sfc 13-14	UA3621-1	0.7%	0.0%	86.8%	1.2%	0.0%	0.3%	0.0%	0.0%	11.0%	0.0%	Churchill
GRV Sfc 13-14	UA3621-22	0.2%	0.0%	94.7%	2.8%	0.0%	0.1%	0.0%	0.0%	2.2%	0.0%	Churchill
GRV Sfc 13-14	UA3621-20	0.0%	0.0%	99.2%	0.8%	0.0%	0.0%	0.0%	0.0%	0.0%	0.0%	Churchill
GRV Sfc 13-14	UA3621-4	0.0%	0.0%	99.0%	0.7%	0.0%	0.1%	0.0%	0.0%	0.2%	0.0%	Churchill
GRV Sfc 13-14	UA3621-17	0.0%	0.0%	95.8%	2.0%	0.0%	0.5%	0.0%	0.0%	1.6%	0.0%	Churchill
GRV Sfc 13-14	UA3621-6	0.5%	0.0%	76.4%	6.4%	0.0%	4.2%	0.0%	2.7%	9.8%	0.0%	Churchill
GRV Sfc 13-14	UA3621-27	1.4%	0.0%	71.5%	9.4%	0.0%	1.8%	0.0%	2.7%	13.2%	0.0%	Churchill
GRV Sfc 13-14	UA3621-9	0.0%	0.0%	99.1%	0.1%	0.0%	0.7%	0.0%	0.1%	0.0%	0.0%	Churchill
GRV Sfc 13-14	UA3621-10	54.1%	0.0%	0.0%	0.0%	4.7%	0.4%	0.0%	19.3%	19.5%	2.0%	Aniakchak
GRV Sfc 13-14	UA3621-30	55.6%	0.0%	0.5%	0.0%	20.9%	0.3%	0.0%	5.8%	15.4%	1.6%	Aniakchak
GRV Sfc 13-14	UA3621-14	64.4%	0.0%	0.2%	0.0%	22.6%	0.2%	0.0%	5.0%	6.5%	1.1%	Aniakchak
GRV Sfc 13-14	UA3621-28	0.0%	0.3%	43.3%	0.2%	0.0%	3.9%	0.0%	19.8%	32.4%	0.0%	Churchill
GRV Sfc 13-14	UA3621-26	0.0%	0.0%	0.0%	0.1%	0.0%	0.2%	0.0%	97.4%	2.3%	0.0%	Katmai
GRV Sfc 13-14	UA3621-13	0.1%	0.1%	8.1%	1.8%	0.0%	4.5%	0.4%	11.7%	73.3%	0.0%	Redoubt
GRV Sfc 13-14	UA3621-5	0.0%	0.0%	0.3%	0.9%	0.0%	0.9%	0.8%	25.7%	71.4%	0.0%	Redoubt
GRV Sfc 18-19	UA3620-30	0.2%	0.2%	95.3%	0.6%	0.0%	2.8%	0.0%	0.0%	0.9%	0.0%	Churchill
GRV Sfc 18-19	UA3620-13	0.2%	0.0%	99.2%	0.0%	0.0%	0.1%	0.0%	0.0%	0.5%	0.0%	Churchill
GRV Sfc 18-19	UA3620-9	0.0%	0.0%	98.8%	0.0%	0.0%	0.2%	0.0%	0.0%	1.0%	0.0%	Churchill
GRV Sfc 18-19	UA3620-4	0.0%	0.0%	99.7%	0.0%	0.0%	0.0%	0.0%	0.0%	0.2%	0.0%	Churchill

GRV Sfc 18-19	UA3620-26	0.0%	0.0%	97.4%	0.0%	0.0%	0.1%	0.0%	0.0%	2.4%	0.0%	Churchill
GRV Sfc 18-19	UA3620-23	0.0%	0.0%	98.8%	0.1%	0.0%	0.1%	0.0%	0.0%	0.9%	0.0%	Churchill
GRV Sfc 18-19	UA3620-24	0.0%	0.0%	97.4%	0.4%	0.0%	0.0%	0.1%	0.1%	2.0%	0.0%	Churchill
GRV Sfc 18-19	UA3620-19	0.0%	0.0%	99.5%	0.0%	0.0%	0.0%	0.0%	0.0%	0.5%	0.0%	Churchill
GRV Sfc 18-19	UA3620-10	0.0%	0.0%	99.8%	0.0%	0.0%	0.1%	0.0%	0.0%	0.1%	0.0%	Churchill
GRV Sfc 18-19	UA3620-28	0.0%	0.0%	99.9%	0.0%	0.0%	0.0%	0.0%	0.0%	0.1%	0.0%	Churchill
GRV Sfc 18-19	UA3620-7	0.0%	0.0%	100.0%	0.0%	0.0%	0.0%	0.0%	0.0%	0.0%	0.0%	Churchill
GRV Sfc 18-19	UA3620-12	0.0%	0.0%	100.0%	0.0%	0.0%	0.0%	0.0%	0.0%	0.0%	0.0%	Churchill
GRV Sfc 18-19	UA3620-21	0.0%	0.0%	99.3%	0.1%	0.0%	0.3%	0.0%	0.0%	0.3%	0.0%	Churchill
GRV Sfc 18-19	UA3620-1	0.0%	0.0%	100.0%	0.0%	0.0%	0.0%	0.0%	0.0%	0.0%	0.0%	Churchill
GRV Sfc 18-19	UA3620-11	0.0%	0.0%	100.0%	0.0%	0.0%	0.0%	0.0%	0.0%	0.0%	0.0%	Churchill
GRV Sfc 18-19	UA3620-25	0.0%	0.0%	99.7%	0.0%	0.0%	0.2%	0.0%	0.0%	0.1%	0.0%	Churchill
GRV Sfc 18-19	UA3620-8	0.0%	0.0%	97.8%	0.8%	0.0%	0.3%	0.0%	0.0%	1.1%	0.0%	Churchill
GRV Sfc 18-19	UA3620-14	0.0%	0.0%	99.5%	0.3%	0.0%	0.0%	0.0%	0.0%	0.2%	0.0%	Churchill
GRV Sfc 18-19	UA3620-22	0.0%	0.0%	99.9%	0.1%	0.0%	0.0%	0.0%	0.0%	0.0%	0.0%	Churchill
GRV Sfc 18-19	UA3620-16	0.0%	0.0%	96.6%	0.6%	0.0%	0.6%	0.0%	0.0%	2.2%	0.0%	Churchill
GRV Sfc 18-19	UA3620-5	0.0%	0.0%	98.8%	0.5%	0.0%	0.2%	0.0%	0.0%	0.5%	0.0%	Churchill
GRV Sfc 18-19	UA3620-6	0.7%	0.1%	64.7%	3.3%	0.0%	4.6%	0.0%	8.8%	17.8%	0.0%	Churchill
GRV Sfc 18-19	UA3620-3	0.1%	0.0%	13.8%	1.4%	0.0%	3.6%	0.0%	12.1%	69.1%	0.0%	Redoubt
Main Core												
GRV17 7-8	UA3526-18	1.71%	0.82%	6.34%	4.20%	0.50%	41.68%	1.39%	3.51%	39.84%	0.00%	Hayes
GRV17 7-8	UA3526-8	0.00%	98.17%	0.00%	0.00%	0.00%	0.49%	0.60%	0.54%	0.20%	0.01%	Augustine
GRV17 7-8	UA3526-16	0.10%	0.12%	37.83%	0.91%	0.00%	4.28%	0.14%	25.45%	31.16%	0.00%	Churchill
GRV17 7-8	UA3526-19	0.10%	0.52%	42.08%	0.41%	0.00%	9.79%	0.03%	14.84%	32.23%	0.00%	Churchill
GRV17 7-8	UA3526-23	15.41%	0.20%	2.80%	0.91%	0.83%	1.50%	0.00%	1.40%	76.95%	0.00%	Redoubt
GRV17 7-8	UA3526-15	0.20%	0.00%	98.59%	0.00%	0.00%	0.80%	0.00%	0.00%	0.40%	0.00%	Churchill

GRV17 7-8	UA3526-13	0.00%	0.00%	99.68%	0.11%	0.00%	0.10%	0.00%	0.00%	0.10%	0.00%	Churchill
GRV17 7-8	UA3526-4	1.72%	0.10%	67.89%	0.23%	0.00%	0.82%	0.00%	0.20%	29.04%	0.00%	Churchill
GRV17 7-8	UA3526-14	0.12%	0.10%	89.31%	0.21%	0.00%	0.51%	0.10%	0.00%	9.64%	0.00%	Churchill
GRV17 7-8	UA3526-11	0.00%	0.00%	99.75%	0.02%	0.00%	0.10%	0.00%	0.00%	0.13%	0.00%	Churchill
GRV17 7-8	UA3526-12	0.00%	0.00%	99.89%	0.00%	0.00%	0.01%	0.00%	0.00%	0.10%	0.00%	Churchill
GRV17 7-8	UA3526-30	0.30%	0.00%	95.06%	1.05%	0.00%	0.40%	0.00%	0.00%	3.18%	0.00%	Churchill
GRV17 7-8	UA3526-10	0.00%	0.00%	100.00%	0.00%	0.00%	0.00%	0.00%	0.00%	0.00%	0.00%	Churchill
GRV17 7-8	UA3526-29	0.00%	0.00%	99.20%	0.17%	0.00%	0.00%	0.00%	0.00%	0.62%	0.00%	Churchill
GRV17 7-8	UA3526-6	0.00%	0.00%	99.68%	0.01%	0.00%	0.00%	0.00%	0.00%	0.31%	0.00%	Churchill
GRV17 7-8	UA3526-17	0.00%	0.00%	99.38%	0.01%	0.00%	0.11%	0.00%	0.00%	0.50%	0.00%	Churchill
GRV17 7-8	UA3526-1	0.00%	0.00%	99.86%	0.01%	0.00%	0.11%	0.00%	0.00%	0.01%	0.00%	Churchill
GRV17 7-8	UA3526-28	0.00%	0.00%	99.36%	0.43%	0.00%	0.00%	0.00%	0.00%	0.20%	0.00%	Churchill
GRV17 7-8	UA3526-24	31.00%	0.04%	2.18%	1.32%	2.97%	5.95%	0.00%	45.25%	9.76%	1.53%	Katmai
GRV17 7-8	UA3526-20	17.91%	0.30%	2.60%	1.40%	4.30%	4.80%	0.00%	60.56%	7.42%	0.70%	Katmai
GRV17 7-8	UA3526-26	15.74%	0.30%	2.10%	0.90%	4.50%	4.50%	0.00%	63.35%	8.10%	0.50%	Katmai
GRV17 7-8	UA3526-21	95.39%	0.00%	0.00%	0.04%	0.09%	0.00%	0.00%	0.00%	4.48%	0.00%	Aniakchak
GRV17 9-10	UA 3493-11	0.00%	0.00%	98.98%	0.00%	0.00%	0.80%	0.00%	0.00%	0.21%	0.00%	Churchill
GRV17 9-10	UA 3493-29	0.00%	0.00%	99.18%	0.00%	0.00%	0.79%	0.00%	0.00%	0.02%	0.00%	Churchill
GRV17 9-10	UA 3493-12	0.00%	0.00%	99.98%	0.00%	0.00%	0.01%	0.00%	0.00%	0.01%	0.00%	Churchill
GRV17 9-10	UA 3493-19	0.00%	0.00%	99.98%	0.02%	0.00%	0.00%	0.00%	0.00%	0.00%	0.00%	Churchill
GRV17 9-10	UA 3493-27	0.00%	0.00%	99.95%	0.03%	0.00%	0.00%	0.00%	0.00%	0.01%	0.00%	Churchill
GRV17 9-10	UA 3493-16	0.00%	0.00%	92.43%	0.02%	0.00%	6.24%	0.00%	0.00%	1.31%	0.00%	Churchill
GRV17 9-10	UA 3493-1	0.00%	0.10%	99.16%	0.01%	0.00%	0.63%	0.00%	0.00%	0.10%	0.00%	Churchill
GRV17 9-10	UA 3493-13	0.00%	0.10%	99.76%	0.00%	0.00%	0.13%	0.00%	0.00%	0.00%	0.00%	Churchill
GRV17 9-10	UA 3493-6	0.00%	0.00%	98.12%	0.49%	0.00%	0.13%	0.00%	0.10%	1.16%	0.00%	Churchill
GRV17 9-10	UA 3493-25	0.00%	0.00%	96.42%	0.04%	0.00%	2.75%	0.01%	0.01%	0.77%	0.00%	Churchill
GRV17 9-10	UA 3493-28	0.00%	0.00%	99.29%	0.01%	0.00%	0.41%	0.00%	0.00%	0.29%	0.00%	Churchill

GRV17 9-10	UA 3493-24	0.00%	0.00%	99.96%	0.01%	0.00%	0.03%	0.00%	0.00%	0.00%	0.00%	Churchill
GRV17 9-10	UA 3493-8	0.00%	0.00%	71.87%	0.04%	0.01%	26.93%	0.01%	0.83%	0.31%	0.00%	Churchill
GRV17 9-10	UA 3493-22	0.00%	0.00%	99.80%	0.01%	0.00%	0.02%	0.00%	0.00%	0.16%	0.00%	Churchill
GRV17 9-10	UA 3493-15	0.00%	0.00%	97.77%	0.00%	0.00%	1.12%	0.00%	0.10%	1.00%	0.00%	Churchill
GRV17 9-10	UA 3493-20	0.00%	0.00%	36.13%	0.00%	0.00%	58.14%	0.00%	1.42%	4.30%	0.00%	Hayes
GRV17 9-10	UA 3493-9	0.00%	0.00%	81.73%	0.00%	0.00%	11.46%	0.00%	1.91%	4.90%	0.00%	Churchill
GRV17 9-10	UA 3493-21	0.00%	0.00%	71.17%	1.11%	0.00%	10.42%	0.00%	3.30%	14.00%	0.00%	Churchill
GRV17 9-10	UA 3493-10	0.00%	0.10%	0.10%	0.00%	0.00%	0.10%	0.72%	92.76%	6.21%	0.00%	Katmai
GRV17 9-10	UA 3493-7	0.00%	0.01%	0.00%	0.00%	0.00%	2.73%	0.35%	83.78%	13.12%	0.00%	Katmai
GRV17 9-10	UA 3493-14	0.00%	0.00%	0.00%	0.01%	0.00%	0.72%	0.06%	93.62%	5.59%	0.00%	Katmai
GRV17 17-18	UA 3494-19	0.01%	0.00%	99.02%	0.01%	0.00%	0.42%	0.00%	0.00%	0.54%	0.00%	Churchill
GRV17 17-18	UA 3494-2	0.00%	0.00%	86.97%	0.00%	0.00%	11.23%	0.00%	0.10%	1.70%	0.00%	Churchill
GRV17 17-18	UA 3494-21	0.00%	0.00%	99.22%	0.00%	0.00%	0.47%	0.00%	0.10%	0.20%	0.00%	Churchill
GRV17 17-18	UA 3494-28	0.00%	0.00%	99.68%	0.01%	0.00%	0.01%	0.00%	0.00%	0.30%	0.00%	Churchill
GRV17 17-18	UA 3494-17	0.41%	0.00%	87.82%	3.22%	0.01%	0.71%	0.00%	0.00%	7.83%	0.00%	Churchill
GRV17 17-18	UA 3494-12	0.10%	0.00%	85.68%	0.25%	0.13%	7.59%	0.06%	0.10%	6.09%	0.00%	Churchill
GRV17 17-18	UA 3494-8	0.20%	0.00%	96.02%	0.37%	0.00%	0.41%	0.00%	0.10%	2.89%	0.00%	Churchill
GRV17 17-18	UA 3494-24	0.10%	0.00%	95.87%	0.25%	0.00%	0.35%	0.00%	0.00%	3.43%	0.00%	Churchill
GRV17 17-18	UA 3494-13	0.00%	0.00%	97.21%	0.29%	0.00%	0.22%	0.00%	0.20%	2.07%	0.00%	Churchill
GRV17 17-18	UA 3494-25	0.40%	0.00%	81.61%	0.83%	0.04%	2.88%	0.12%	0.11%	14.02%	0.00%	Churchill
GRV17 17-18	UA 3494-4	1.40%	0.00%	73.61%	13.79%	0.00%	2.80%	0.00%	1.70%	6.70%	0.00%	Churchill
GRV17 17-18	UA 3494-26	0.00%	0.00%	99.98%	0.00%	0.00%	0.01%	0.00%	0.00%	0.00%	0.00%	Churchill
GRV17 17-18	UA 3494-10	0.00%	0.00%	98.59%	0.00%	0.00%	1.00%	0.00%	0.00%	0.40%	0.00%	Churchill
GRV17 17-18	UA 3494-9	0.00%	0.00%	91.62%	0.02%	0.00%	1.12%	0.01%	0.01%	7.22%	0.00%	Churchill
GRV17 17-18	UA 3494-23	0.00%	0.00%	99.49%	0.03%	0.00%	0.15%	0.00%	0.00%	0.33%	0.00%	Churchill
GRV17 17-18	UA 3494-1	0.00%	0.00%	96.42%	0.01%	0.00%	0.24%	0.00%	0.11%	3.22%	0.00%	Churchill
GRV17 17-18	UA 3494-6	0.00%	0.00%	21.36%	0.00%	0.10%	76.89%	0.01%	0.31%	1.33%	0.00%	Hayes

GRV17 17-18	UA 3494-16	0.00%	0.00%	99.37%	0.01%	0.00%	0.50%	0.00%	0.01%	0.11%	0.00%	Churchill
GRV17 17-18	UA 3494-29	0.00%	0.01%	60.38%	0.09%	0.04%	36.05%	0.08%	0.31%	3.06%	0.00%	Churchill
GRV17 17-18	UA 3494-18	0.00%	0.00%	99.99%	0.01%	0.00%	0.00%	0.00%	0.00%	0.00%	0.00%	Churchill
GRV17 17-18	UA 3494-22	0.00%	0.00%	42.04%	0.71%	0.00%	1.87%	0.02%	0.12%	55.24%	0.00%	Redoubt
GRV17 17-18	UA 3494-14	0.00%	0.00%	96.06%	0.03%	0.00%	3.01%	0.00%	0.47%	0.43%	0.00%	Churchill
GRV17 17-18	UA 3494-7	0.00%	0.00%	86.23%	0.03%	0.00%	6.86%	0.00%	1.11%	5.77%	0.00%	Churchill
GRV17 17-18	UA 3494-30	0.10%	0.00%	60.80%	4.66%	0.00%	2.40%	0.00%	4.97%	27.07%	0.00%	Churchill
GRV17 17-18	UA 3494-3	0.00%	0.00%	11.52%	0.97%	0.01%	7.19%	0.07%	12.09%	68.15%	0.00%	Redoubt
GRV17 24-25	UA3527-4	0.39%	0.00%	91.34%	0.32%	0.20%	1.30%	0.20%	0.00%	6.24%	0.00%	Churchill
GRV17 24-25	UA3527-18	0.30%	0.00%	92.18%	0.74%	0.00%	0.70%	0.00%	0.00%	6.07%	0.00%	Churchill
GRV17 24-25	UA3527-11	0.31%	0.00%	96.52%	1.15%	0.00%	0.10%	0.00%	0.00%	1.91%	0.00%	Churchill
GRV17 24-25	UA3527-20	0.00%	0.00%	99.29%	0.11%	0.00%	0.10%	0.00%	0.00%	0.50%	0.00%	Churchill
GRV17 24-25	UA3527-17	0.00%	0.00%	99.79%	0.01%	0.00%	0.01%	0.00%	0.00%	0.19%	0.00%	Churchill
GRV17 24-25	UA3527-23	0.10%	0.00%	99.12%	0.24%	0.00%	0.10%	0.00%	0.00%	0.44%	0.00%	Churchill
GRV17 24-25	UA3527-7	0.00%	0.00%	99.59%	0.02%	0.00%	0.11%	0.00%	0.00%	0.28%	0.00%	Churchill
GRV17 24-25	UA3527-3	0.00%	0.00%	99.11%	0.26%	0.00%	0.00%	0.00%	0.00%	0.63%	0.00%	Churchill
GRV17 24-25	UA3527-21	0.24%	0.30%	47.19%	3.01%	0.00%	1.14%	0.10%	11.68%	36.34%	0.00%	Churchill
GRV17 24-25	UA3527-22	0.20%	0.00%	92.54%	2.38%	0.00%	0.11%	0.00%	0.00%	4.76%	0.00%	Churchill
GRV17 24-25	UA3527-10	0.00%	0.00%	98.53%	0.55%	0.00%	0.20%	0.00%	0.00%	0.72%	0.00%	Churchill
GRV17 24-25	UA3527-12	0.00%	0.00%	99.07%	0.03%	0.00%	0.90%	0.00%	0.00%	0.00%	0.00%	Churchill
GRV17 24-25	UA3527-6	0.00%	0.20%	81.94%	0.51%	0.00%	1.47%	0.30%	1.11%	14.47%	0.00%	Churchill
GRV17 24-25	UA3527-13	0.80%	0.10%	74.66%	7.32%	0.00%	4.51%	0.00%	3.41%	9.20%	0.00%	Churchill
GRV17 24-25	UA3527-25	0.40%	0.20%	62.89%	4.57%	0.00%	7.40%	0.10%	5.77%	18.67%	0.00%	Churchill
GRV17 24-25	UA3527-2	1.10%	0.10%	69.68%	6.81%	0.00%	6.14%	0.00%	4.35%	11.82%	0.00%	Churchill
GRV17 24-25	UA3527-1	0.70%	0.10%	61.25%	4.61%	0.00%	4.90%	0.10%	8.90%	19.44%	0.00%	Churchill
GRV17 24-25	UA3527-14	0.30%	0.00%	55.12%	1.84%	0.00%	2.91%	0.10%	10.30%	29.44%	0.00%	Churchill
GRV17 24-25	UA3527-16	0.00%	1.17%	1.53%	0.00%	0.00%	49.03%	0.84%	25.62%	21.80%	0.00%	Hayes

GRV17 25-26	UA 3495-14	0.50%	0.10%	78.26%	0.00%	0.00%	20.32%	0.00%	0.20%	0.61%	0.00%	Churchill
GRV17 25-26	UA 3495-13	0.10%	0.00%	84.43%	0.01%	0.00%	14.79%	0.00%	0.10%	0.57%	0.00%	Churchill
GRV17 25-26	UA 3495-20	0.40%	0.00%	80.76%	0.89%	0.21%	5.15%	0.03%	0.10%	12.45%	0.00%	Churchill
GRV17 25-26	UA 3495-2	0.12%	0.10%	82.96%	0.38%	0.02%	3.69%	0.03%	0.00%	12.70%	0.00%	Churchill
GRV17 25-26	UA 3495-15	0.30%	0.00%	95.22%	1.01%	0.00%	0.50%	0.00%	0.00%	2.96%	0.00%	Churchill
GRV17 25-26	UA 3495-3	0.10%	0.00%	92.54%	0.51%	0.00%	1.15%	0.10%	0.70%	4.90%	0.00%	Churchill
GRV17 25-26	UA 3495-21	0.00%	0.10%	59.52%	0.00%	0.00%	39.17%	0.00%	0.20%	1.01%	0.00%	Churchill
GRV17 25-26	UA 3495-22	0.00%	0.00%	99.44%	0.00%	0.00%	0.25%	0.00%	0.00%	0.30%	0.00%	Churchill
GRV17 25-26	UA 3495-18	0.00%	0.00%	99.94%	0.06%	0.00%	0.00%	0.00%	0.00%	0.00%	0.00%	Churchill
GRV17 25-26	UA 3495-17	0.30%	0.00%	86.91%	2.15%	0.00%	1.01%	0.01%	0.00%	9.62%	0.00%	Churchill
GRV17 25-26	UA 3495-30	0.00%	0.00%	99.29%	0.00%	0.00%	0.27%	0.00%	0.00%	0.43%	0.00%	Churchill
GRV17 25-26	UA 3495-23	0.00%	0.00%	98.97%	0.02%	0.00%	0.25%	0.00%	0.00%	0.75%	0.00%	Churchill
GRV17 25-26	UA 3495-5	0.00%	0.00%	79.22%	0.00%	0.00%	19.38%	0.00%	0.20%	1.19%	0.00%	Churchill
GRV17 25-26	UA 3495-7	0.00%	0.00%	98.18%	0.00%	0.00%	1.71%	0.00%	0.00%	0.10%	0.00%	Churchill
GRV17 25-26	UA 3495-11	0.20%	0.00%	92.88%	0.70%	0.00%	0.11%	0.00%	0.00%	6.11%	0.00%	Churchill
GRV17 25-26	UA 3495-29	0.00%	0.00%	98.58%	0.15%	0.00%	0.12%	0.00%	0.10%	1.05%	0.00%	Churchill
GRV17 25-26	UA 3495-10	0.00%	0.00%	99.56%	0.00%	0.00%	0.23%	0.00%	0.00%	0.20%	0.00%	Churchill
GRV17 25-26	UA 3495-19	0.00%	0.10%	96.28%	1.27%	0.00%	0.10%	0.00%	0.00%	2.25%	0.00%	Churchill
GRV17 25-26	UA 3495-16	0.00%	0.00%	98.74%	0.04%	0.00%	0.75%	0.00%	0.10%	0.36%	0.00%	Churchill
GRV17 25-26	UA 3495-27	0.00%	0.00%	98.02%	0.02%	0.00%	0.83%	0.01%	0.01%	1.11%	0.00%	Churchill
GRV17 25-26	UA 3495-28	0.00%	0.00%	99.25%	0.00%	0.00%	0.74%	0.00%	0.00%	0.00%	0.00%	Churchill
GRV17 25-26	UA 3495-6	0.00%	0.10%	96.16%	0.10%	0.00%	3.01%	0.00%	0.01%	0.62%	0.00%	Churchill
GRV17 25-26	UA 3495-8	0.50%	0.00%	61.78%	4.16%	0.00%	7.07%	0.01%	8.68%	17.80%	0.00%	Churchill
GRV17 25-26	UA 3495-26	0.40%	0.00%	67.61%	1.70%	0.00%	11.44%	0.00%	4.22%	14.62%	0.00%	Churchill
GRV17 25-26	UA 3495-1	0.12%	0.11%	32.63%	11.15%	0.02%	3.66%	0.66%	25.44%	26.19%	0.00%	Churchill
GRV17 31-32	UA 3496-20	0.01%	77.36%	1.40%	0.30%	0.82%	9.95%	0.75%	0.71%	8.68%	0.03%	Augustine
GRV17 31-32	UA 3496-25	0.10%	85.58%	0.20%	0.10%	0.50%	9.47%	0.12%	0.80%	3.11%	0.02%	Augustine

GRV17 31-32	UA 3496-1	72.12%	0.30%	3.90%	1.40%	1.81%	1.20%	0.00%	1.60%	17.67%	0.00%	Aniakchak
GRV17 31-32	UA 3496-29	0.53%	0.20%	88.30%	0.00%	0.00%	8.61%	0.00%	0.00%	2.36%	0.00%	Churchill
GRV17 31-32	UA 3496-22	0.00%	0.00%	99.97%	0.01%	0.00%	0.00%	0.00%	0.00%	0.02%	0.00%	Churchill
GRV17 31-32	UA 3496-13	0.10%	0.00%	97.26%	0.06%	0.00%	0.20%	0.00%	0.00%	2.37%	0.00%	Churchill
GRV17 31-32	UA 3496-31	0.40%	0.00%	96.65%	0.26%	0.00%	0.10%	0.00%	0.00%	2.60%	0.00%	Churchill
GRV17 31-32	UA 3496-18	0.10%	0.00%	75.21%	0.11%	0.00%	8.65%	0.02%	0.10%	15.80%	0.00%	Churchill
GRV17 31-32	UA 3496-23	0.00%	0.00%	99.47%	0.01%	0.00%	0.20%	0.00%	0.00%	0.32%	0.00%	Churchill
GRV17 31-32	UA 3496-3	0.00%	0.00%	92.85%	0.10%	0.00%	5.75%	0.00%	0.00%	1.30%	0.00%	Churchill
GRV17 31-32	UA 3496-7	0.01%	0.00%	66.37%	0.99%	0.01%	1.39%	0.11%	0.37%	30.74%	0.00%	Churchill
GRV17 31-32	UA 3496-28	0.00%	0.00%	99.99%	0.01%	0.00%	0.00%	0.00%	0.00%	0.00%	0.00%	Churchill
GRV17 31-32	UA 3496-14	0.00%	0.00%	99.14%	0.01%	0.00%	0.24%	0.00%	0.00%	0.60%	0.00%	Churchill
GRV17 31-32	UA 3496-32	0.00%	0.00%	94.37%	0.14%	0.00%	3.84%	0.02%	0.12%	1.50%	0.00%	Churchill
GRV17 31-32	UA 3496-12	0.00%	0.00%	99.66%	0.01%	0.00%	0.12%	0.00%	0.00%	0.20%	0.00%	Churchill
GRV17 31-32	UA 3496-27	0.00%	0.00%	75.32%	0.02%	0.00%	1.11%	0.11%	0.12%	23.32%	0.00%	Churchill
GRV17 31-32	UA 3496-21	0.00%	0.00%	98.76%	0.00%	0.00%	1.14%	0.00%	0.10%	0.00%	0.00%	Churchill
GRV17 31-32	UA 3496-4	0.00%	0.00%	98.46%	0.00%	0.00%	1.40%	0.00%	0.11%	0.02%	0.00%	Churchill
GRV17 31-32	UA 3496-19	0.60%	0.01%	55.92%	2.43%	0.00%	12.62%	0.00%	11.69%	16.73%	0.00%	Churchill
GRV17 31-32	UA 3496-5	0.20%	1.31%	2.13%	0.63%	0.01%	6.22%	0.38%	70.20%	18.92%	0.00%	Katmai
GRV17 31-32	UA 3496-15	99.69%	0.00%	0.00%	0.11%	0.03%	0.00%	0.00%	0.00%	0.17%	0.00%	Aniakchak
GRV17 32-33	UA 3497-28	0.42%	77.90%	0.20%	1.00%	0.54%	9.87%	0.49%	0.61%	8.94%	0.03%	Augustine
GRV17 32-33	UA 3497-27	0.70%	72.46%	0.80%	0.80%	1.45%	12.86%	2.50%	0.64%	7.73%	0.07%	Augustine
GRV17 32-33	UA 3497-18	0.00%	0.00%	94.36%	0.00%	0.00%	4.32%	0.00%	0.00%	1.32%	0.00%	Churchill
GRV17 32-33	UA 3497-10	0.00%	0.00%	99.60%	0.00%	0.00%	0.40%	0.00%	0.00%	0.00%	0.00%	Churchill
GRV17 32-33	UA 3497-30	0.01%	0.00%	98.77%	0.14%	0.00%	0.20%	0.00%	0.00%	0.88%	0.00%	Churchill
GRV17 32-33	UA 3497-4	0.00%	0.00%	99.99%	0.00%	0.00%	0.00%	0.00%	0.00%	0.00%	0.00%	Churchill
GRV17 32-33	UA 3497-1	0.00%	0.00%	99.89%	0.01%	0.00%	0.00%	0.00%	0.00%	0.10%	0.00%	Churchill
GRV17 32-33	UA 3497-16	0.00%	0.00%	97.82%	0.01%	0.00%	0.62%	0.00%	0.00%	1.55%	0.00%	Churchill

GRV17 32-33	UA 3497-19	0.00%	0.00%	99.98%	0.02%	0.00%	0.00%	0.00%	0.00%	0.00%	0.00%	Churchill
GRV17 32-33	UA 3497-3	0.00%	0.00%	99.16%	0.00%	0.00%	0.74%	0.00%	0.00%	0.10%	0.00%	Churchill
GRV17 32-33	UA 3497-24	0.00%	0.00%	99.45%	0.01%	0.00%	0.34%	0.00%	0.00%	0.20%	0.00%	Churchill
GRV17 32-33	UA 3497-23	0.00%	0.00%	99.89%	0.01%	0.00%	0.00%	0.00%	0.00%	0.10%	0.00%	Churchill
GRV17 32-33	UA 3497-22	0.00%	0.00%	99.46%	0.00%	0.00%	0.23%	0.00%	0.00%	0.31%	0.00%	Churchill
GRV17 32-33	UA 3497-5	0.00%	0.00%	96.85%	0.22%	0.00%	1.54%	0.00%	0.03%	1.36%	0.00%	Churchill
GRV17 32-33	UA 3497-25	0.00%	0.00%	98.33%	0.15%	0.00%	0.51%	0.00%	0.00%	1.01%	0.00%	Churchill
GRV17 32-33	UA 3497-21	0.00%	0.00%	95.97%	0.23%	0.00%	0.29%	0.00%	0.00%	3.52%	0.00%	Churchill
GRV17 32-33	UA 3497-29	0.00%	0.00%	99.99%	0.00%	0.00%	0.01%	0.00%	0.00%	0.00%	0.00%	Churchill
GRV17 32-33	UA 3497-8	0.00%	0.00%	99.88%	0.00%	0.00%	0.11%	0.00%	0.00%	0.01%	0.00%	Churchill
GRV17 32-33	UA 3497-6	0.00%	0.00%	98.63%	0.06%	0.00%	0.50%	0.01%	0.01%	0.80%	0.00%	Churchill
GRV17 32-33	UA 3497-14	0.00%	0.00%	99.84%	0.02%	0.00%	0.02%	0.00%	0.00%	0.11%	0.00%	Churchill
GRV17 32-33	UA 3497-7	0.00%	0.00%	99.26%	0.00%	0.00%	0.53%	0.00%	0.00%	0.21%	0.00%	Churchill
GRV17 32-33	UA 3497-20	0.00%	0.00%	98.74%	0.02%	0.00%	0.98%	0.00%	0.05%	0.21%	0.00%	Churchill
GRV17 32-33	UA 3497-26	0.81%	0.00%	36.58%	4.32%	0.02%	6.27%	0.04%	9.47%	42.49%	0.00%	Redoubt
GRV17 34-35	UA3491-23	83.30%	0.00%	0.30%	0.03%	7.27%	0.40%	0.00%	0.30%	8.40%	0.00%	Aniakchak
GRV17 34-35	UA3491-19	90.58%	0.00%	0.50%	0.02%	2.87%	0.30%	0.00%	0.50%	5.23%	0.00%	Aniakchak
GRV17 34-35	UA3491-4	0.00%	0.00%	99.69%	0.01%	0.00%	0.22%	0.00%	0.00%	0.07%	0.00%	Churchill
GRV17 34-35	UA3491-10	0.61%	0.10%	83.93%	1.04%	0.12%	1.94%	0.02%	0.00%	12.24%	0.00%	Churchill
GRV17 34-35	UA3491-24	0.00%	0.00%	99.74%	0.01%	0.00%	0.11%	0.00%	0.00%	0.14%	0.00%	Churchill
GRV17 34-35	UA3491-9	0.20%	0.00%	92.15%	2.80%	0.00%	0.30%	0.00%	0.00%	4.55%	0.00%	Churchill
GRV17 34-35	UA3491-8	1.50%	0.00%	68.07%	16.78%	0.00%	2.00%	0.00%	1.30%	10.34%	0.00%	Churchill
GRV17 34-35	UA3491-7	0.00%	0.00%	99.15%	0.07%	0.00%	0.40%	0.00%	0.00%	0.38%	0.00%	Churchill
GRV17 34-35	UA3491-18	0.00%	0.00%	83.70%	0.01%	0.10%	12.98%	0.03%	0.10%	3.07%	0.00%	Churchill
GRV17 34-35	UA3491-17	0.00%	0.00%	99.56%	0.02%	0.00%	0.41%	0.00%	0.00%	0.01%	0.00%	Churchill
GRV17 34-35	UA3491-2	0.00%	0.00%	99.43%	0.16%	0.00%	0.10%	0.00%	0.00%	0.30%	0.00%	Churchill
GRV17 34-35	UA3491-12	0.00%	0.00%	99.64%	0.00%	0.00%	0.05%	0.00%	0.00%	0.31%	0.00%	Churchill

GRV17 34-35	UA3491-13	0.00%	0.00%	98.79%	0.15%	0.00%	0.15%	0.00%	0.00%	0.90%	0.00%	Churchill
GRV17 34-35	UA3491-3	0.00%	0.00%	86.55%	0.27%	0.00%	0.39%	0.01%	0.19%	12.59%	0.00%	Churchill
GRV17 34-35	UA3491-25	0.60%	0.00%	75.88%	4.67%	0.00%	4.22%	0.00%	2.11%	12.52%	0.00%	Churchill
GRV17 40-41	UA 3498-12	98.19%	0.00%	0.00%	0.01%	0.03%	0.40%	0.00%	0.10%	1.28%	0.00%	Aniakchak
GRV17 40-41	UA 3498-18	99.83%	0.00%	0.00%	0.02%	0.03%	0.00%	0.00%	0.00%	0.13%	0.00%	Aniakchak
GRV17 40-41	UA 3498-26	0.00%	0.00%	98.90%	0.00%	0.00%	1.10%	0.00%	0.00%	0.00%	0.00%	Churchill
GRV17 40-41	UA 3498-3	0.00%	0.00%	99.14%	0.00%	0.00%	0.76%	0.00%	0.00%	0.10%	0.00%	Churchill
GRV17 40-41	UA 3498-1	0.00%	0.00%	99.98%	0.00%	0.00%	0.00%	0.00%	0.00%	0.01%	0.00%	Churchill
GRV17 40-41	UA 3498-22	0.00%	0.00%	96.31%	0.00%	0.00%	3.38%	0.00%	0.00%	0.30%	0.00%	Churchill
GRV17 40-41	UA 3498-13	0.00%	0.00%	97.79%	0.20%	0.00%	0.50%	0.00%	0.20%	1.31%	0.00%	Churchill
GRV17 40-41	UA 3498-2	0.00%	0.00%	94.88%	0.42%	0.00%	3.40%	0.00%	0.90%	0.40%	0.00%	Churchill
GRV17 40-41	UA 3498-7	0.00%	0.00%	99.88%	0.00%	0.00%	0.10%	0.00%	0.00%	0.01%	0.00%	Churchill
GRV17 40-41	UA 3498-15	0.00%	0.30%	94.79%	0.00%	0.00%	4.91%	0.00%	0.00%	0.00%	0.00%	Churchill
GRV17 40-41	UA 3498-8	0.10%	0.00%	97.35%	0.02%	0.00%	0.11%	0.00%	0.00%	2.42%	0.00%	Churchill
GRV17 40-41	UA 3498-6	0.22%	0.20%	76.94%	4.32%	0.17%	2.19%	0.12%	0.02%	15.82%	0.00%	Churchill
GRV17 40-41	UA 3498-21	0.50%	0.00%	95.74%	1.21%	0.00%	0.10%	0.00%	0.00%	2.45%	0.00%	Churchill
GRV17 40-41	UA 3498-23	0.10%	0.00%	96.69%	0.55%	0.00%	0.20%	0.00%	0.00%	2.46%	0.00%	Churchill
GRV17 40-41	UA 3498-9	0.10%	0.00%	97.98%	0.25%	0.01%	0.74%	0.01%	0.00%	0.90%	0.00%	Churchill
GRV17 40-41	UA 3498-30	0.20%	0.00%	84.10%	1.55%	0.01%	0.22%	0.01%	0.00%	13.92%	0.00%	Churchill
GRV17 40-41	UA 3498-19	0.00%	0.00%	99.56%	0.01%	0.00%	0.21%	0.00%	0.00%	0.22%	0.00%	Churchill
GRV17 40-41	UA 3498-4	0.00%	0.00%	98.27%	0.23%	0.00%	0.80%	0.00%	0.00%	0.70%	0.00%	Churchill
GRV17 40-41	UA 3498-5	0.00%	0.00%	99.95%	0.01%	0.00%	0.03%	0.00%	0.00%	0.00%	0.00%	Churchill
GRV17 40-41	UA 3498-10	0.00%	0.00%	96.94%	0.01%	0.00%	2.25%	0.00%	0.38%	0.42%	0.00%	Churchill
GRV17 40-41	UA 3498-11	0.00%	0.00%	97.18%	0.01%	0.00%	1.56%	0.00%	0.03%	1.22%	0.00%	Churchill
GRV17 40-41	UA 3498-17	0.50%	0.00%	79.44%	3.93%	0.00%	4.12%	0.00%	2.30%	9.70%	0.00%	Churchill
GRV17 40-41	UA 3498-29	0.00%	0.02%	48.17%	0.13%	0.00%	25.50%	0.13%	9.35%	16.69%	0.00%	Churchill
GRV17 40-41	UA 3498-28	0.00%	0.00%	86.78%	0.01%	0.00%	8.20%	0.10%	1.00%	3.90%	0.00%	Churchill

GRV17 42-43	UA3490-13	0.02%	64.62%	3.00%	0.10%	0.52%	24.54%	3.34%	0.10%	3.73%	0.02%	Augustine
GRV17 42-43	UA3490-7	0.15%	68.41%	2.40%	0.50%	0.24%	20.73%	4.70%	0.51%	2.32%	0.04%	Augustine
GRV17 42-43	UA3490-15	0.00%	66.73%	0.20%	0.00%	0.00%	5.78%	26.12%	1.01%	0.15%	0.01%	Augustine
GRV17 42-43	UA3490-14	0.00%	70.86%	0.00%	0.00%	0.00%	9.82%	18.00%	1.21%	0.11%	0.01%	Augustine
GRV17 42-43	UA3490-12	0.00%	49.95%	0.10%	0.00%	0.00%	3.78%	45.66%	0.31%	0.18%	0.01%	Augustine
GRV17 42-43	UA3490-1	0.10%	0.10%	96.48%	1.32%	0.00%	0.80%	0.00%	0.10%	1.10%	0.00%	Churchill
GRV17 42-43	UA3490-8	0.00%	0.00%	99.88%	0.12%	0.00%	0.00%	0.00%	0.00%	0.00%	0.00%	Churchill
GRV17 42-43	UA3490-6	0.73%	0.90%	4.93%	0.20%	0.11%	1.62%	0.00%	0.83%	90.67%	0.00%	Redoubt
GRV17 42-43	UA3490-17	0.00%	0.00%	99.40%	0.00%	0.00%	0.40%	0.00%	0.00%	0.20%	0.00%	Churchill
GRV17 42-43	UA3490-11	0.00%	0.00%	99.49%	0.01%	0.00%	0.00%	0.00%	0.00%	0.50%	0.00%	Churchill
GRV17 42-43	UA3490-22	0.00%	0.00%	99.58%	0.01%	0.00%	0.21%	0.00%	0.00%	0.21%	0.00%	Churchill
GRV17 42-43	UA3490-26	0.00%	0.00%	99.61%	0.03%	0.00%	0.30%	0.00%	0.00%	0.05%	0.00%	Churchill
GRV17 42-43	UA3490-21	0.00%	0.20%	38.29%	1.63%	0.00%	2.02%	0.32%	0.88%	56.66%	0.00%	Redoubt
GRV17 42-43	UA3490-4	0.00%	0.00%	99.82%	0.05%	0.00%	0.10%	0.00%	0.00%	0.02%	0.00%	Churchill
GRV17 42-43	UA3490-2	0.00%	0.00%	99.27%	0.01%	0.00%	0.06%	0.00%	0.00%	0.66%	0.00%	Churchill
GRV17 42-43	UA3490-9	0.00%	0.00%	92.09%	0.04%	0.00%	0.50%	0.01%	0.01%	7.36%	0.00%	Churchill
GRV17 42-43	UA3490-10	0.00%	0.00%	99.98%	0.00%	0.00%	0.02%	0.00%	0.00%	0.00%	0.00%	Churchill
GRV17 42-43	UA3490-19	0.70%	0.00%	72.59%	6.41%	0.00%	3.72%	0.00%	2.53%	14.05%	0.00%	Churchill
GRV17 42-43	UA3490-25	0.00%	0.04%	0.49%	0.27%	0.03%	12.60%	0.81%	62.46%	23.31%	0.00%	Katmai
GRV17 43-44	UA3489-4	0.10%	0.10%	95.79%	0.00%	0.00%	2.60%	0.00%	0.00%	1.40%	0.00%	Churchill
GRV17 43-44	UA3489-5	0.11%	0.50%	81.20%	1.83%	0.00%	3.71%	0.00%	4.15%	8.50%	0.00%	Churchill
GRV17 43-44	UA3489-11	0.00%	0.00%	98.73%	0.00%	0.00%	1.27%	0.00%	0.00%	0.00%	0.00%	Churchill
GRV17 43-44	UA3489-19	0.00%	0.00%	99.09%	0.00%	0.00%	0.70%	0.00%	0.00%	0.20%	0.00%	Churchill
GRV17 43-44	UA3489-2	0.00%	0.00%	98.48%	0.00%	0.00%	1.52%	0.00%	0.00%	0.00%	0.00%	Churchill
GRV17 43-44	UA3489-22	0.10%	0.00%	95.43%	0.21%	0.00%	1.65%	0.00%	0.00%	2.60%	0.00%	Churchill
GRV17 43-44	UA3489-25	0.00%	0.00%	99.98%	0.00%	0.00%	0.02%	0.00%	0.00%	0.00%	0.00%	Churchill
GRV17 43-44	UA3489-13	0.00%	0.00%	88.73%	0.10%	0.00%	2.33%	0.00%	0.30%	8.53%	0.00%	Churchill

GRV17 43-44	UA3489-3	0.00%	0.00%	99.67%	0.00%	0.00%	0.22%	0.00%	0.00%	0.10%	0.00%	Churchill
GRV17 43-44	UA3489-20	0.00%	0.10%	94.91%	0.00%	0.00%	4.84%	0.00%	0.02%	0.12%	0.00%	Churchill
GRV17 43-44	UA3489-24	0.00%	0.00%	98.32%	0.00%	0.00%	0.97%	0.00%	0.00%	0.70%	0.00%	Churchill
GRV17 43-44	UA3489-9	0.00%	0.00%	91.76%	0.01%	0.00%	7.27%	0.00%	0.01%	0.95%	0.00%	Churchill
GRV17 43-44	UA3489-23	0.00%	0.00%	99.37%	0.01%	0.00%	0.61%	0.00%	0.00%	0.00%	0.00%	Churchill
GRV17 43-44	UA3489-7	0.00%	0.00%	96.80%	0.49%	0.01%	0.78%	0.02%	0.28%	1.62%	0.00%	Churchill
GRV17 43-44	UA3489-15	0.61%	0.30%	81.39%	4.69%	0.01%	2.60%	0.20%	4.06%	6.14%	0.00%	Churchill
GRV17 43-44	UA3489-6	0.00%	0.00%	97.65%	0.00%	0.00%	2.04%	0.00%	0.01%	0.30%	0.00%	Churchill
GRV17 43-44	UA3489-17	0.60%	0.00%	80.89%	3.91%	0.00%	4.40%	0.00%	3.30%	6.90%	0.00%	Churchill
GRV17 43-44	UA3489-12	0.80%	0.10%	69.10%	4.75%	0.00%	12.66%	0.00%	4.38%	8.21%	0.00%	Churchill
GRV17 43-44	UA3489-8	0.00%	0.02%	54.37%	0.03%	0.00%	43.17%	0.03%	1.16%	1.22%	0.00%	Churchill
GRV17 43-44	UA3489-21	0.00%	0.00%	88.58%	0.01%	0.00%	6.82%	0.10%	0.61%	3.89%	0.00%	Churchill
GRV17 43-44	UA3489-10	0.50%	0.00%	68.26%	2.60%	0.00%	12.03%	0.00%	6.51%	10.10%	0.00%	Churchill
GRV17 44-45	UA3524-13	0.20%	0.00%	91.69%	0.27%	0.00%	0.32%	0.00%	0.00%	7.51%	0.00%	Churchill
GRV17 44-45	UA3524-7	0.21%	0.10%	70.97%	0.07%	0.00%	2.69%	0.02%	0.00%	25.93%	0.00%	Churchill
GRV17 44-45	UA3524-21	0.71%	0.00%	77.15%	11.50%	0.01%	0.40%	0.00%	0.00%	10.24%	0.00%	Churchill
GRV17 44-45	UA3524-4	0.00%	0.00%	99.18%	0.00%	0.00%	0.22%	0.00%	0.00%	0.60%	0.00%	Churchill
GRV17 44-45	UA3524-26	0.00%	0.00%	99.73%	0.06%	0.00%	0.20%	0.00%	0.00%	0.01%	0.00%	Churchill
GRV17 44-45	UA3524-23	0.00%	0.00%	99.23%	0.05%	0.00%	0.60%	0.00%	0.00%	0.12%	0.00%	Churchill
GRV17 44-45	UA3524-15	0.00%	0.00%	99.48%	0.01%	0.00%	0.40%	0.00%	0.00%	0.11%	0.00%	Churchill
GRV17 44-45	UA3524-20	0.00%	0.00%	99.86%	0.01%	0.00%	0.10%	0.00%	0.00%	0.02%	0.00%	Churchill
GRV17 44-45	UA3524-9	0.00%	0.10%	98.84%	0.10%	0.00%	0.63%	0.00%	0.00%	0.32%	0.00%	Churchill
GRV17 44-45	UA3524-10	0.00%	0.00%	99.99%	0.01%	0.00%	0.00%	0.00%	0.00%	0.00%	0.00%	Churchill
GRV17 44-45	UA3524-16	0.00%	0.72%	0.10%	0.00%	0.00%	46.98%	0.32%	31.74%	20.14%	0.00%	Hayes
GRV17 44-45	UA3524-8	0.00%	0.31%	12.89%	0.37%	0.00%	2.92%	0.01%	10.95%	72.55%	0.00%	Redoubt
GRV17 44-45	UA3524-27	0.20%	0.00%	54.43%	2.19%	0.00%	4.17%	0.10%	10.30%	28.60%	0.00%	Churchill
GRV17 44-45	UA3524-28	0.00%	0.00%	98.84%	0.02%	0.00%	0.50%	0.00%	0.00%	0.64%	0.00%	Churchill

GRV17 44-45	UA3524-11	0.00%	2.18%	1.40%	0.10%	0.00%	53.19%	15.59%	17.85%	9.68%	0.00%	Hayes
GRV17 44-45	UA3524-24	0.00%	38.40%	0.20%	0.00%	0.00%	11.10%	45.37%	3.97%	0.94%	0.02%	Kaguyak
GRV17 49-50	UA3488-6	97.61%	0.00%	0.00%	0.03%	0.06%	0.00%	0.00%	0.00%	2.29%	0.00%	Aniakchak
GRV17 49-50	UA3488-24	37.16%	0.00%	0.30%	0.02%	8.59%	0.40%	0.00%	14.27%	39.25%	0.01%	Redoubt
GRV17 49-50	UA3488-25	95.90%	0.00%	0.00%	0.03%	0.62%	0.00%	0.00%	0.00%	3.45%	0.00%	Aniakchak
GRV17 49-50	UA3488-19	94.77%	0.00%	0.00%	0.01%	0.13%	0.60%	0.00%	0.00%	4.49%	0.00%	Aniakchak
GRV17 49-50	UA3488-14	99.38%	0.00%	0.40%	0.05%	0.02%	0.00%	0.00%	0.00%	0.15%	0.00%	Aniakchak
GRV17 49-50	UA3488-9	95.25%	0.00%	0.30%	0.11%	0.02%	0.20%	0.00%	0.10%	4.02%	0.00%	Aniakchak
GRV17 49-50	UA3488-20	0.00%	23.22%	0.50%	0.00%	0.00%	3.70%	69.97%	1.14%	1.46%	0.01%	Kaguyak
GRV17 49-50	UA3488-12	0.00%	49.76%	0.10%	0.00%	0.00%	1.78%	47.87%	0.42%	0.06%	0.01%	Augustine
GRV17 49-50	UA3488-21	0.23%	0.00%	55.76%	2.94%	0.11%	1.22%	0.09%	0.12%	39.53%	0.00%	Churchill
GRV17 49-50	UA3488-3	0.02%	0.00%	65.81%	0.28%	0.02%	4.70%	0.14%	1.50%	27.54%	0.00%	Churchill
GRV17 49-50	UA3488-10	0.00%	0.00%	99.96%	0.03%	0.00%	0.00%	0.00%	0.00%	0.00%	0.00%	Churchill
GRV17 49-50	UA3488-18	0.00%	0.00%	96.34%	0.40%	0.00%	0.11%	0.00%	0.00%	3.13%	0.00%	Churchill
GRV17 49-50	UA3488-1	0.00%	0.00%	91.05%	2.38%	0.04%	0.50%	0.06%	0.53%	5.44%	0.00%	Churchill
GRV17 49-50	UA3488-7	0.00%	0.00%	98.69%	0.00%	0.00%	0.58%	0.00%	0.10%	0.63%	0.00%	Churchill
GRV17 49-50	UA3488-5	95.51%	0.00%	0.00%	0.44%	1.55%	0.00%	0.00%	0.00%	2.50%	0.00%	Aniakchak
GRV17 49-50	UA3488-1	99.36%	0.00%	0.00%	0.02%	0.03%	0.00%	0.00%	0.00%	0.60%	0.00%	Aniakchak
GRV17 49-50	UA3488-8	99.76%	0.00%	0.00%	0.01%	0.04%	0.00%	0.00%	0.00%	0.19%	0.00%	Aniakchak
GRV17 49-50	UA3488-4	0.10%	0.00%	98.85%	0.28%	0.00%	0.10%	0.00%	0.00%	0.66%	0.00%	Churchill
GRV17 49-50	UA3488-24	1.22%	0.10%	58.96%	27.89%	0.01%	1.00%	0.10%	1.02%	9.69%	0.00%	Churchill
GRV17 49-50	UA3488-15	0.20%	0.00%	93.36%	1.74%	0.00%	0.40%	0.00%	0.00%	4.30%	0.00%	Churchill
GRV17 49-50	UA3488-17	0.00%	0.00%	99.77%	0.00%	0.00%	0.03%	0.00%	0.00%	0.20%	0.00%	Churchill
GRV17 49-50	UA3488-2	0.00%	0.00%	99.95%	0.04%	0.00%	0.00%	0.00%	0.00%	0.00%	0.00%	Churchill
GRV17 49-50	UA3488-11	0.00%	0.00%	98.66%	0.03%	0.00%	0.54%	0.00%	0.11%	0.66%	0.00%	Churchill
GRV17 49-50	UA3488-26	0.10%	0.31%	53.44%	1.61%	0.00%	8.48%	0.00%	11.33%	24.72%	0.00%	Churchill
GRV17 49-50	UA3488-21	0.01%	45.07%	0.40%	0.00%	0.11%	7.49%	42.06%	1.22%	3.62%	0.02%	Augustine

GRV17 49-50	UA3488-19	0.00%	87.27%	0.20%	0.00%	0.20%	3.18%	6.79%	1.70%	0.55%	0.12%	Augustine
GRV17 49-50	UA3488-18	0.00%	96.85%	0.10%	0.00%	0.00%	2.11%	0.93%	0.01%	0.00%	0.00%	Augustine
GRV17 57-58	UA3487-11	0.71%	0.00%	88.73%	2.15%	0.00%	0.20%	0.00%	0.00%	8.20%	0.00%	Churchill
GRV17 57-58	UA3487-7	0.00%	0.00%	95.97%	0.21%	0.00%	1.73%	0.00%	0.41%	1.69%	0.00%	Churchill
GRV17 57-58	UA3487-10	0.00%	0.10%	97.76%	0.00%	0.00%	1.83%	0.00%	0.00%	0.31%	0.00%	Churchill
GRV17 57-58	UA3487-9	0.00%	0.00%	99.67%	0.02%	0.00%	0.10%	0.00%	0.00%	0.21%	0.00%	Churchill
GRV17 57-58	UA3487-18	0.00%	0.00%	99.85%	0.02%	0.00%	0.03%	0.00%	0.00%	0.11%	0.00%	Churchill
GRV17 57-58	UA3487-8	0.00%	0.00%	80.86%	0.74%	0.00%	0.95%	0.10%	0.15%	17.19%	0.00%	Churchill
GRV17 57-58	UA3487-15	0.00%	0.00%	98.04%	0.00%	0.00%	1.75%	0.00%	0.20%	0.00%	0.00%	Churchill
GRV17 57-58	UA3487-12	0.00%	48.54%	0.00%	0.00%	0.00%	3.69%	46.40%	0.92%	0.43%	0.01%	Augustine
GRV17 57-58	UA3487-25	0.00%	69.02%	0.10%	0.00%	0.00%	2.33%	27.59%	0.53%	0.42%	0.01%	Augustine
GRV17 57-58	UA3487-16	0.00%	61.35%	0.00%	0.00%	0.00%	10.66%	26.70%	0.91%	0.37%	0.01%	Augustine
GRV17 57-58	UA3487-3	0.00%	87.58%	0.00%	0.00%	0.00%	1.82%	9.77%	0.61%	0.21%	0.01%	Augustine
GRV17 57-58	UA3487-24	0.00%	79.85%	0.00%	0.00%	0.00%	5.34%	14.19%	0.41%	0.20%	0.01%	Augustine
GRV17 57-58	UA3487-14	0.00%	72.52%	0.10%	0.00%	0.00%	1.99%	24.24%	0.91%	0.22%	0.01%	Augustine
GRV17 57-58	UA3487-17	0.00%	36.31%	0.10%	0.00%	0.00%	3.06%	59.96%	0.52%	0.04%	0.01%	Kaguyak
GRV17 57-58	UA3487-20	0.00%	92.07%	0.10%	0.00%	0.00%	3.95%	3.56%	0.01%	0.30%	0.01%	Augustine
GRV17 57-58	UA3487-1	0.00%	69.28%	0.10%	0.00%	0.00%	3.07%	26.50%	1.02%	0.02%	0.01%	Augustine
GRV17 57-58	UA3487-4	0.00%	79.11%	0.10%	0.00%	0.00%	4.36%	15.81%	0.61%	0.00%	0.01%	Augustine
GRV17 57-58	UA3487-5	0.00%	51.34%	0.10%	0.00%	0.00%	1.71%	45.78%	0.92%	0.14%	0.01%	Augustine
GRV17 57-58	UA3487-23	0.00%	54.71%	0.00%	0.00%	0.00%	10.65%	31.39%	2.72%	0.51%	0.01%	Augustine
GRV17 57-58	UA3487-19	0.00%	83.71%	0.10%	0.00%	0.00%	2.89%	11.96%	0.82%	0.50%	0.01%	Augustine
GRV17 57-58	UA3487-15	0.00%	0.00%	99.62%	0.17%	0.00%	0.00%	0.00%	0.00%	0.21%	0.00%	Churchill
GRV17 57-58	UA3487-23	0.10%	0.10%	95.23%	0.30%	0.00%	0.91%	0.00%	0.70%	2.66%	0.00%	Churchill
GRV17 57-58	UA3487-13	0.00%	0.00%	99.89%	0.00%	0.00%	0.11%	0.00%	0.00%	0.00%	0.00%	Churchill
GRV17 57-58	UA3487-25	0.00%	0.00%	99.68%	0.00%	0.00%	0.21%	0.00%	0.00%	0.11%	0.00%	Churchill
GRV17 57-58	UA3487-3	0.00%	0.00%	99.64%	0.02%	0.00%	0.30%	0.00%	0.00%	0.04%	0.00%	Churchill

GRV17 57-58	UA3487-10	0.00%	0.00%	99.66%	0.03%	0.00%	0.20%	0.00%	0.00%	0.11%	0.00%	Churchill
GRV17 57-58	UA3487-9	0.01%	14.79%	1.20%	0.10%	0.11%	27.08%	54.58%	0.30%	1.82%	0.01%	Kaguyak
GRV17 57-58	UA3487-17	0.00%	53.36%	0.20%	0.00%	0.01%	9.99%	34.70%	0.71%	1.02%	0.01%	Augustine
GRV17 57-58	UA3487-18	0.00%	19.24%	0.30%	0.00%	0.00%	18.84%	60.47%	0.70%	0.44%	0.01%	Kaguyak
GRV17 57-58	UA3487-14	0.00%	32.91%	0.10%	0.00%	0.00%	2.63%	64.06%	0.21%	0.08%	0.01%	Kaguyak
GRV17 57-58	UA3487-22	0.00%	18.44%	0.10%	0.00%	0.00%	3.56%	77.21%	0.51%	0.19%	0.00%	Kaguyak
GRV17 57-58	UA3487-19	97.95%	0.00%	0.30%	0.04%	0.03%	0.00%	0.00%	0.00%	1.68%	0.00%	Aniakchak
GRV17 65-66	UA3486-7	0.01%	79.06%	0.30%	0.00%	0.11%	12.71%	2.37%	1.01%	4.39%	0.03%	Augustine
GRV17 65-66	UA3486-20	0.03%	54.54%	3.40%	0.30%	0.34%	11.03%	18.41%	1.35%	10.57%	0.04%	Augustine
GRV17 65-66	UA3486-19	0.00%	59.35%	0.10%	0.00%	0.00%	2.77%	36.77%	0.81%	0.17%	0.01%	Augustine
GRV17 65-66	UA3486-10	0.00%	97.03%	0.00%	0.00%	0.00%	0.85%	1.90%	0.01%	0.20%	0.01%	Augustine
GRV17 65-66	UA3486-4	0.00%	40.35%	0.00%	0.00%	0.00%	6.97%	50.83%	1.62%	0.23%	0.01%	Kaguyak
GRV17 65-66	UA3486-1	0.00%	87.08%	0.10%	0.00%	0.00%	2.93%	9.86%	0.02%	0.00%	0.01%	Augustine
GRV17 65-66	UA3486-23	0.10%	0.00%	97.95%	0.13%	0.00%	0.10%	0.00%	0.00%	1.71%	0.00%	Churchill
GRV17 65-66	UA3486-3	0.00%	0.00%	99.02%	0.00%	0.00%	0.64%	0.00%	0.00%	0.34%	0.00%	Churchill
GRV17 65-66	UA3486-21	0.00%	0.00%	97.27%	0.00%	0.00%	2.52%	0.00%	0.00%	0.20%	0.00%	Churchill
GRV17 65-66	UA3486-17	0.00%	0.00%	99.67%	0.01%	0.00%	0.15%	0.00%	0.00%	0.16%	0.00%	Churchill
GRV17 65-66	UA3486-25	0.00%	0.20%	46.23%	0.00%	0.00%	53.26%	0.00%	0.21%	0.10%	0.00%	Hayes
GRV17 65-66	UA3486-5	0.00%	6.62%	0.30%	0.00%	0.00%	80.73%	6.50%	4.82%	1.02%	0.00%	Hayes
GRV17 65-66	UA3486-8	0.00%	7.24%	0.00%	0.00%	0.00%	16.14%	43.27%	23.27%	10.08%	0.00%	Kaguyak
GRV17 65-66	UA3486-6	99.03%	0.10%	0.00%	0.01%	0.73%	0.00%	0.00%	0.00%	0.13%	0.00%	Aniakchak
GRV17 65-66	UA3486-13	88.59%	0.00%	0.40%	0.02%	2.99%	0.30%	0.00%	0.40%	7.30%	0.00%	Aniakchak
GRV17 65-66	UA3486-2	98.21%	0.00%	0.00%	0.02%	0.27%	0.00%	0.00%	0.00%	1.50%	0.00%	Aniakchak
GRV17 65-66	UA3486-16	78.42%	0.00%	0.70%	0.14%	4.32%	0.20%	0.00%	0.50%	15.72%	0.00%	Aniakchak
GRV17 65-66	UA3486-24	92.25%	0.00%	0.40%	0.02%	3.25%	0.20%	0.00%	0.30%	3.59%	0.00%	Aniakchak
GRV17 65-66	UA3486-9	99.45%	0.00%	0.00%	0.01%	0.02%	0.00%	0.00%	0.00%	0.52%	0.00%	Aniakchak
GRV17 65-66	UA3486-18	93.11%	0.00%	1.30%	0.10%	0.42%	0.20%	0.00%	0.20%	4.67%	0.00%	Aniakchak

GRV17 67-68	UA3523-4	6.68%	7.94%	5.39%	0.15%	0.89%	13.36%	0.00%	13.56%	3.11%	48.91%	Spurr
GRV17 67-68	UA3523-15	22.11%	0.62%	1.91%	0.10%	2.90%	5.60%	0.00%	55.58%	9.87%	1.30%	Katmai
GRV17 67-68	UA3523-9	0.00%	60.55%	0.20%	0.00%	0.00%	4.71%	32.76%	1.01%	0.76%	0.01%	Augustine
GRV17 67-68	UA3523-17	0.00%	52.07%	0.30%	0.00%	0.00%	2.51%	42.47%	1.52%	1.12%	0.01%	Augustine
GRV17 67-68	UA3523-24	0.00%	22.98%	0.10%	0.00%	0.00%	6.57%	69.46%	0.51%	0.37%	0.01%	Kaguyak
GRV17 67-68	UA3523-2	0.40%	0.20%	22.30%	0.00%	0.66%	41.37%	0.18%	0.10%	34.78%	0.00%	Hayes
GRV17 67-68	UA3523-13	0.00%	0.00%	99.31%	0.00%	0.00%	0.59%	0.00%	0.00%	0.10%	0.00%	Churchill
GRV17 67-68	UA3523-25	0.00%	0.10%	35.01%	0.31%	0.11%	15.26%	0.07%	0.00%	49.13%	0.00%	Redoubt
GRV17 67-68	UA3523-18	0.00%	0.00%	99.04%	0.00%	0.00%	0.01%	0.00%	0.00%	0.95%	0.00%	Churchill
GRV17 67-68	UA3523-19	0.10%	0.00%	87.64%	3.06%	0.00%	1.10%	0.00%	0.71%	7.39%	0.00%	Churchill
GRV17 67-68	UA3523-20	0.00%	0.00%	96.70%	0.31%	0.00%	1.05%	0.00%	0.32%	1.63%	0.00%	Churchill
GRV17 67-68	UA3523-26	0.30%	0.00%	39.60%	5.73%	0.00%	1.50%	0.20%	5.35%	47.31%	0.00%	Redoubt
GRV17 67-68	UA3523-16	93.93%	0.10%	0.70%	0.18%	1.08%	0.00%	0.00%	0.20%	3.81%	0.00%	Aniakchak
GRV17 67-68	UA3523-12	96.44%	0.00%	0.10%	0.02%	3.02%	0.00%	0.00%	0.00%	0.41%	0.00%	Aniakchak
GRV17 67-68	UA3523-27	98.46%	0.00%	0.00%	0.02%	0.02%	0.00%	0.00%	0.00%	1.50%	0.00%	Aniakchak
GRV17 67-68	UA3523-5	81.60%	0.10%	1.70%	0.32%	2.95%	0.50%	0.00%	1.00%	11.83%	0.00%	Aniakchak
GRV17 67-68	UA3523-10	93.42%	0.00%	0.20%	0.04%	0.14%	0.00%	0.00%	0.10%	6.10%	0.00%	Aniakchak
GRV17 67-68	UA3523-6	88.43%	0.00%	1.04%	2.63%	1.47%	0.30%	0.00%	0.30%	5.83%	0.00%	Aniakchak
GRV17 67-68	UA3523-28	98.46%	0.00%	0.00%	0.03%	0.16%	0.00%	0.00%	0.00%	1.35%	0.00%	Aniakchak
GRV17 67-68	UA3523-23	98.13%	0.00%	0.00%	0.02%	0.14%	0.00%	0.00%	0.00%	1.71%	0.00%	Aniakchak
GRV17 67-68	UA3523-3	97.80%	0.00%	0.00%	0.01%	0.15%	0.00%	0.00%	0.00%	2.04%	0.00%	Aniakchak
GRV17 67-68	UA3523-22	95.15%	0.00%	0.00%	0.01%	1.44%	0.30%	0.00%	0.30%	2.80%	0.00%	Aniakchak
GRV17 67-68	UA3523-29	0.00%	91.59%	0.20%	0.00%	0.30%	2.32%	2.35%	1.01%	2.22%	0.00%	Augustine
GRV17 67-68	UA3523-20	96.38%	0.00%	0.00%	0.01%	1.65%	0.20%	0.00%	0.00%	1.76%	0.00%	Aniakchak
GRV17 67-68	UA3523-27	94.45%	0.00%	0.00%	0.07%	0.32%	0.00%	0.00%	0.00%	5.15%	0.00%	Aniakchak
GRV17 67-68	UA3523-30	98.75%	0.00%	0.00%	0.04%	0.16%	0.00%	0.00%	0.00%	1.05%	0.00%	Aniakchak
GRV17 67-68	UA3523-4	98.99%	0.00%	0.00%	0.04%	0.03%	0.00%	0.00%	0.00%	0.94%	0.00%	Aniakchak

GRV17 67-68	UA3523-33	99.30%	0.00%	0.00%	0.05%	0.02%	0.00%	0.00%	0.00%	0.63%	0.00%	Aniakchak
GRV17 67-68	UA3523-26	99.65%	0.00%	0.00%	0.01%	0.03%	0.00%	0.00%	0.00%	0.32%	0.00%	Aniakchak
GRV17 67-68	UA3523-18	99.84%	0.00%	0.00%	0.01%	0.03%	0.00%	0.00%	0.00%	0.12%	0.00%	Aniakchak
GRV17 67-68	UA3523-2	99.85%	0.00%	0.00%	0.01%	0.02%	0.00%	0.00%	0.00%	0.12%	0.00%	Aniakchak
GRV17 67-68	UA3523-1	97.98%	0.00%	0.62%	1.18%	0.02%	0.00%	0.00%	0.00%	0.21%	0.00%	Aniakchak
GRV17 67-68	UA3523-15	97.22%	0.00%	0.30%	0.01%	0.22%	0.10%	0.00%	0.00%	2.15%	0.00%	Aniakchak
GRV17 67-68	UA3523-19	99.56%	0.00%	0.00%	0.01%	0.04%	0.00%	0.00%	0.00%	0.39%	0.00%	Aniakchak
GRV17 67-68	UA3523-23	99.13%	0.00%	0.00%	0.01%	0.03%	0.00%	0.00%	0.00%	0.83%	0.00%	Aniakchak
GRV17 67-68	UA3523-13	98.09%	0.00%	0.10%	0.03%	0.07%	0.10%	0.00%	0.00%	1.61%	0.00%	Aniakchak
GRV17 67-68	UA3523-12	98.72%	0.00%	0.00%	0.02%	0.17%	0.00%	0.00%	0.00%	1.09%	0.00%	Aniakchak
GRV17 67-68	UA3523-34	98.07%	0.00%	0.10%	0.01%	0.12%	0.00%	0.00%	0.00%	1.70%	0.00%	Aniakchak
GRV17 67-68	UA3523-31	87.33%	0.10%	1.20%	0.10%	0.32%	1.90%	0.00%	1.00%	8.04%	0.00%	Aniakchak
GRV17 67-68	UA3523-6	79.55%	0.20%	2.10%	1.09%	2.46%	1.60%	0.00%	1.60%	11.40%	0.00%	Aniakchak
GRV17 67-68	UA3523-40	0.00%	0.00%	99.44%	0.00%	0.00%	0.42%	0.00%	0.00%	0.14%	0.00%	Churchill
GRV17 67-68	UA3523-8	0.00%	0.00%	99.99%	0.01%	0.00%	0.00%	0.00%	0.00%	0.00%	0.00%	Churchill
GRV17 67-68	UA3523-25	0.00%	0.00%	98.80%	0.01%	0.00%	0.31%	0.00%	0.00%	0.87%	0.00%	Churchill
GRV17 67-68	UA3523-11	0.00%	0.00%	98.15%	0.45%	0.00%	0.10%	0.00%	0.00%	1.30%	0.00%	Churchill
GRV17 67-68	UA3523-21	0.00%	42.35%	0.40%	0.00%	0.00%	5.90%	49.15%	1.53%	0.66%	0.01%	Kaguyak
GRV17 67-68	UA3523-10	0.00%	61.30%	0.00%	0.00%	0.00%	16.52%	20.64%	1.30%	0.22%	0.01%	Augustine
GRV17 67-68	UA3523-29	0.00%	1.99%	0.60%	0.10%	0.01%	13.39%	52.89%	17.95%	13.07%	0.00%	Kaguyak
GRV17 67-68	UA3523-32	24.03%	0.21%	0.90%	0.10%	3.10%	5.60%	0.00%	56.03%	9.03%	1.00%	Katmai
GRV17 67-68	UA3523-17	15.73%	0.50%	1.70%	1.10%	4.90%	4.00%	0.00%	63.37%	8.20%	0.50%	Katmai
GRV17 69-70	UA3542-17	62.14%	0.50%	19.64%	5.67%	2.41%	5.90%	0.00%	0.90%	2.83%	0.00%	Aniakchak
GRV17 69-70	UA3542-8	51.52%	0.20%	34.06%	0.91%	0.25%	10.12%	0.00%	0.20%	2.74%	0.00%	Aniakchak
GRV17 69-70	UA3542-9	35.79%	0.20%	35.90%	4.87%	1.22%	8.03%	0.21%	0.10%	13.67%	0.00%	Churchill
GRV17 69-70	UA3542-27	0.20%	0.00%	91.18%	0.21%	0.00%	4.75%	0.00%	0.20%	3.46%	0.00%	Churchill
GRV17 69-70	UA3542-5	13.81%	0.30%	66.32%	4.14%	0.87%	11.28%	0.22%	0.20%	2.86%	0.00%	Churchill

GRV17 69-70	UA3542-26	0.00%	0.00%	99.99%	0.00%	0.00%	0.00%	0.00%	0.00%	0.01%	0.00%	Churchill
GRV17 69-70	UA3542-14	0.00%	0.00%	88.01%	0.01%	0.00%	2.82%	0.00%	0.00%	9.17%	0.00%	Churchill
GRV17 69-70	UA3542-25	3.76%	0.10%	80.41%	4.52%	0.35%	8.52%	0.30%	0.30%	1.73%	0.00%	Churchill
GRV17 69-70	UA3542-2	3.66%	0.20%	68.75%	13.74%	0.94%	9.31%	0.32%	1.12%	1.96%	0.00%	Churchill
GRV17 69-70	UA3542-7	0.00%	0.00%	97.81%	0.00%	0.00%	1.55%	0.00%	0.00%	0.64%	0.00%	Churchill
GRV17 69-70	UA3542-28	0.50%	0.20%	71.94%	0.53%	0.13%	14.43%	0.35%	0.10%	11.81%	0.00%	Churchill
GRV17 69-70	UA3542-3	0.00%	0.00%	97.39%	0.11%	0.00%	0.20%	0.00%	0.00%	2.30%	0.00%	Churchill
GRV17 69-70	UA3542-29	1.90%	0.30%	85.23%	1.54%	0.20%	8.59%	0.30%	1.40%	0.53%	0.00%	Churchill
GRV17 69-70	UA3542-6	0.23%	0.40%	30.13%	2.77%	0.14%	5.37%	0.43%	11.63%	48.91%	0.00%	Redoubt
GRV17 69-70	UA3542-10	0.00%	0.32%	1.32%	0.50%	0.00%	55.66%	0.23%	21.49%	20.47%	0.00%	Hayes
GRV17 69-70	UA3542-1	92.01%	0.10%	0.00%	0.03%	3.80%	0.00%	0.00%	0.00%	4.06%	0.00%	Aniakchak
GRV17 69-70	UA3542-21	98.58%	0.00%	0.20%	0.07%	0.06%	0.00%	0.00%	0.00%	1.09%	0.00%	Aniakchak
GRV17 69-70	UA3542-30	97.66%	0.10%	0.00%	0.01%	2.14%	0.00%	0.00%	0.00%	0.09%	0.00%	Aniakchak
GRV17 69-70	UA3542-23	99.82%	0.00%	0.00%	0.02%	0.03%	0.00%	0.00%	0.00%	0.14%	0.00%	Aniakchak
GRV17 72-73	UA3541-2	1.30%	0.30%	94.19%	0.61%	0.10%	1.70%	0.00%	0.00%	1.80%	0.00%	Churchill
GRV17 72-73	UA3541-22	0.00%	0.00%	94.39%	0.41%	0.00%	3.30%	0.00%	0.30%	1.60%	0.00%	Churchill
GRV17 72-73	UA3541-7	1.81%	0.00%	91.94%	1.11%	0.30%	3.20%	0.10%	0.20%	1.34%	0.00%	Churchill
GRV17 72-73	UA3541-25	0.00%	0.00%	99.75%	0.01%	0.00%	0.20%	0.00%	0.00%	0.03%	0.00%	Churchill
GRV17 72-73	UA3541-14	0.00%	0.00%	99.11%	0.07%	0.00%	0.10%	0.00%	0.10%	0.62%	0.00%	Churchill
GRV17 72-73	UA3541-18	0.00%	0.20%	91.27%	0.00%	0.00%	8.13%	0.00%	0.20%	0.20%	0.00%	Churchill
GRV17 72-73	UA3541-15	0.00%	0.00%	99.68%	0.00%	0.00%	0.12%	0.00%	0.00%	0.20%	0.00%	Churchill
GRV17 72-73	UA3541-10	0.60%	0.10%	86.53%	0.40%	0.20%	9.86%	0.20%	1.40%	0.70%	0.00%	Churchill
GRV17 72-73	UA3541-27	2.42%	0.60%	71.99%	1.44%	0.34%	20.45%	0.00%	1.18%	1.58%	0.00%	Churchill
GRV17 72-73	UA3541-23	0.00%	0.00%	94.79%	0.01%	0.00%	0.92%	0.00%	0.00%	4.28%	0.00%	Churchill
GRV17 72-73	UA3541-11	0.00%	0.00%	68.39%	0.11%	0.00%	26.36%	0.02%	1.02%	4.10%	0.00%	Churchill
GRV17 72-73	UA3541-3	1.06%	0.50%	11.12%	39.05%	0.12%	5.81%	0.63%	16.07%	25.63%	0.00%	Dawson
GRV17 72-73	UA3541-4	1.13%	72.98%	0.80%	0.80%	0.98%	11.36%	0.59%	0.31%	10.99%	0.05%	Augustine

GRV17 72-73	UA3541-20	0.77%	54.94%	1.40%	0.70%	2.35%	11.92%	3.72%	0.55%	22.91%	0.74%	Augustine
GRV17 72-73	UA3541-5	2.57%	69.45%	0.00%	0.50%	1.94%	8.30%	1.80%	0.97%	14.15%	0.30%	Augustine
GRV17 73-74	UA3540-19	99.26%	0.00%	0.00%	0.05%	0.35%	0.00%	0.00%	0.00%	0.34%	0.00%	Aniakchak
GRV17 73-74	UA3540-6	96.04%	0.00%	0.10%	0.04%	0.63%	0.00%	0.00%	0.00%	3.18%	0.00%	Aniakchak
GRV17 73-74	UA3540-5	2.01%	0.00%	87.57%	1.32%	0.10%	6.50%	0.00%	0.00%	2.50%	0.00%	Churchill
GRV17 73-74	UA3540-28	3.25%	0.10%	90.35%	0.78%	0.10%	0.60%	0.00%	0.00%	4.81%	0.00%	Churchill
GRV17 73-74	UA3540-27	10.88%	0.00%	78.15%	1.07%	0.46%	4.51%	0.00%	0.50%	4.43%	0.00%	Churchill
GRV17 73-74	UA3540-24	0.10%	0.00%	99.46%	0.00%	0.00%	0.21%	0.00%	0.00%	0.22%	0.00%	Churchill
GRV17 73-74	UA3540-10	2.81%	0.40%	80.89%	0.38%	0.21%	11.91%	0.00%	0.40%	3.00%	0.00%	Churchill
GRV17 73-74	UA3540-25	5.73%	0.00%	72.91%	4.25%	0.34%	6.90%	0.20%	0.20%	9.46%	0.00%	Churchill
GRV17 73-74	UA3540-21	0.20%	0.00%	93.14%	0.52%	0.00%	0.50%	0.00%	0.00%	5.64%	0.00%	Churchill
GRV17 73-74	UA3540-1	0.71%	0.00%	84.45%	2.15%	0.01%	1.11%	0.00%	0.00%	11.56%	0.00%	Churchill
GRV17 73-74	UA3540-7	0.00%	0.00%	97.43%	0.60%	0.00%	0.00%	0.10%	0.10%	1.77%	0.00%	Churchill
GRV17 73-74	UA3540-29	5.74%	0.50%	22.01%	20.46%	0.97%	5.03%	0.42%	4.39%	40.48%	0.00%	Redoubt
GRV17 73-74	UA3540-3	3.32%	38.33%	1.50%	0.41%	14.99%	11.83%	6.69%	0.42%	20.14%	2.37%	Augustine
GRV17 73-74	UA3540-4	1.14%	25.96%	2.90%	0.20%	2.14%	60.14%	1.15%	0.00%	6.14%	0.22%	Hayes
GRV17 73-74	UA3540-22	0.23%	71.22%	1.40%	0.70%	0.88%	9.49%	1.15%	0.41%	14.28%	0.25%	Augustine
GRV17 73-74	UA3540-13	2.43%	57.54%	1.40%	0.40%	3.38%	9.02%	9.83%	1.54%	14.13%	0.32%	Augustine
GRV17 73-74	UA3540-15	0.24%	45.08%	0.20%	0.00%	0.37%	2.84%	45.57%	0.76%	4.88%	0.07%	Kaguyak
GRV17 73-74	UA3540-14	0.84%	54.05%	0.20%	0.00%	0.15%	7.04%	34.71%	1.77%	1.12%	0.12%	Augustine
GRV17 75-76	UA3539-10	0.68%	65.23%	0.50%	0.00%	0.80%	4.65%	21.41%	1.33%	5.21%	0.19%	Augustine
GRV17 75-76	UA3539-17	0.07%	65.02%	0.50%	0.00%	0.35%	3.31%	24.43%	1.62%	4.54%	0.15%	Augustine
GRV17 75-76	UA3539-14	0.11%	52.78%	0.20%	0.00%	0.31%	2.87%	39.67%	1.82%	2.12%	0.12%	Augustine
GRV17 75-76	UA3539-13	0.42%	81.93%	0.10%	0.00%	0.20%	4.68%	11.42%	0.31%	0.80%	0.14%	Augustine
GRV17 75-76	UA3539-19	0.00%	60.65%	0.40%	0.00%	0.00%	5.50%	32.56%	0.72%	0.15%	0.01%	Augustine
GRV17 75-76	UA3539-5	0.33%	53.28%	0.30%	0.00%	0.15%	6.00%	37.93%	0.45%	1.47%	0.09%	Augustine
GRV17 75-76	UA3539-21	0.00%	76.05%	0.20%	0.00%	0.00%	2.99%	19.03%	1.11%	0.61%	0.01%	Augustine

GRV17 75-76	UA3539-6	0.01%	50.31%	0.40%	0.00%	0.11%	9.40%	38.41%	0.20%	1.03%	0.13%	Augustine
GRV17 75-76	UA3539-30	0.03%	65.23%	0.30%	0.00%	0.10%	14.90%	18.17%	0.50%	0.62%	0.14%	Augustine
GRV17 75-76	UA3539-29	0.01%	52.58%	0.20%	0.00%	0.10%	5.89%	39.92%	0.41%	0.76%	0.13%	Augustine
GRV17 75-76	UA3539-28	0.00%	37.17%	0.10%	0.00%	0.00%	0.70%	60.22%	1.03%	0.77%	0.01%	Kaguyak
GRV17 75-76	UA3539-25	0.21%	21.14%	0.60%	0.00%	0.21%	8.57%	65.78%	2.12%	1.27%	0.11%	Kaguyak
GRV17 75-76	UA3539-27	0.00%	64.70%	0.10%	0.00%	0.00%	5.80%	28.35%	0.81%	0.23%	0.01%	Augustine
GRV17 75-76	UA3539-8	0.00%	89.38%	0.00%	0.00%	0.00%	3.62%	6.77%	0.11%	0.10%	0.01%	Augustine
GRV17 75-76	UA3539-1	0.11%	72.32%	0.00%	0.00%	0.10%	6.39%	20.51%	0.31%	0.23%	0.03%	Augustine
GRV17 75-76	UA3539-22	0.00%	40.77%	0.10%	0.00%	0.00%	9.23%	46.25%	3.23%	0.42%	0.01%	Kaguyak
GRV17 75-76	UA3539-11	95.57%	0.10%	0.00%	0.03%	2.36%	0.00%	0.00%	0.00%	1.94%	0.00%	Aniakchak
GRV17 75-76	UA3539-12	94.80%	0.10%	0.00%	0.02%	2.05%	0.00%	0.00%	0.00%	3.03%	0.00%	Aniakchak
GRV17 75-76	UA3539-9	95.24%	0.00%	0.60%	0.02%	0.07%	0.20%	0.00%	0.00%	3.87%	0.00%	Aniakchak
GRV17 75-76	UA3539-4	93.36%	0.10%	0.20%	0.02%	0.94%	0.00%	0.00%	0.00%	5.38%	0.00%	Aniakchak
GRV17 75-76	UA3539-23	0.90%	0.00%	94.51%	0.99%	0.00%	0.80%	0.00%	0.00%	2.80%	0.00%	Churchill
GRV17 75-76	UA3539-3	0.00%	0.00%	97.49%	0.21%	0.00%	0.40%	0.10%	0.00%	1.79%	0.00%	Churchill
GRV17 75-76	UA3539-24	5.35%	0.40%	52.37%	23.80%	0.44%	5.56%	0.31%	3.08%	8.70%	0.00%	Churchill
GRV17 75-76	UA3539-9 rerun-1	99.70%	0.00%	0.00%	0.01%	0.12%	0.00%	0.00%	0.00%	0.18%	0.00%	Aniakchak
GRV17 75-76	UA3539-9 rerun-2	98.61%	0.00%	0.00%	0.03%	0.96%	0.00%	0.00%	0.00%	0.39%	0.00%	Aniakchak
GRV17 75-76	UA3539-11 rerun-1	99.16%	0.00%	0.00%	0.01%	0.14%	0.00%	0.00%	0.00%	0.69%	0.00%	Aniakchak
GRV17 75-76	UA3539-11 rerun-2	97.83%	0.00%	0.00%	0.03%	1.66%	0.00%	0.00%	0.00%	0.48%	0.00%	Aniakchak
GRV17 75-76	UA3539-12 rerun-1	99.53%	0.00%	0.00%	0.14%	0.02%	0.00%	0.00%	0.00%	0.31%	0.00%	Aniakchak
GRV17 77-78	UA3534-12	97.90%	0.00%	0.00%	0.04%	0.29%	0.00%	0.00%	0.00%	1.77%	0.00%	Aniakchak
GRV17 77-78	UA3534-10	98.62%	0.00%	0.00%	0.03%	0.04%	0.00%	0.00%	0.00%	1.32%	0.00%	Aniakchak
GRV17 77-78	UA3534-19	96.04%	0.00%	0.00%	0.02%	0.06%	0.00%	0.00%	0.00%	3.88%	0.00%	Aniakchak
GRV17 77-78	UA3534-6	99.51%	0.00%	0.00%	0.13%	0.02%	0.10%	0.00%	0.00%	0.24%	0.00%	Aniakchak
GRV17 77-78	UA3534-30	0.10%	0.00%	96.73%	0.23%	0.00%	0.10%	0.00%	0.00%	2.84%	0.00%	Churchill

GRV17 77-78	UA3534-2	0.00%	0.00%	98.81%	0.38%	0.00%	0.50%	0.00%	0.10%	0.21%	0.00%	Churchill
GRV17 77-78	UA3534-11	0.11%	0.10%	36.45%	2.18%	0.00%	2.41%	0.20%	13.40%	45.13%	0.00%	Redoubt
GRV17 77-78	UA3534-15	0.00%	57.31%	0.40%	0.00%	0.01%	12.82%	28.15%	0.61%	0.69%	0.01%	Augustine
GRV17 77-78	UA3534-17	0.00%	71.24%	0.30%	0.00%	0.00%	16.03%	10.64%	0.73%	1.04%	0.02%	Augustine
GRV17 77-78	UA3534-26	0.00%	51.39%	0.40%	0.00%	0.01%	5.14%	39.67%	0.92%	2.45%	0.01%	Augustine
GRV17 77-78	UA3534-18	0.00%	31.19%	0.30%	0.00%	0.00%	7.05%	60.13%	0.81%	0.50%	0.01%	Kaguyak
GRV17 77-78	UA3534-25	0.00%	60.46%	0.30%	0.00%	0.00%	2.95%	33.62%	1.51%	1.14%	0.01%	Augustine
GRV17 77-78	UA3534-27	0.21%	52.97%	0.20%	0.00%	0.31%	2.16%	40.88%	0.72%	2.43%	0.13%	Augustine
GRV17 77-78	UA3534-5	0.00%	61.98%	0.00%	0.00%	0.00%	4.13%	33.51%	0.21%	0.16%	0.01%	Augustine
GRV17 77-78	UA3534-29	0.00%	12.90%	0.10%	0.00%	0.00%	2.82%	83.77%	0.21%	0.19%	0.00%	Kaguyak
GRV17 77-78	UA3534-23	0.00%	70.76%	0.00%	0.00%	0.00%	6.03%	22.27%	0.81%	0.12%	0.01%	Augustine
GRV17 77-78	UA3534-17	0.00%	92.56%	0.10%	0.00%	0.00%	3.57%	3.06%	0.30%	0.40%	0.01%	Augustine
GRV17 77-78	UA3534-15	0.00%	78.95%	0.20%	0.00%	0.00%	6.22%	13.72%	0.20%	0.71%	0.01%	Augustine
GRV17 77-78	UA3534-23	0.00%	57.40%	0.20%	0.00%	0.00%	5.83%	35.91%	0.42%	0.23%	0.01%	Augustine
GRV17 77-78	UA3534-10	0.00%	91.24%	0.00%	0.00%	0.00%	1.42%	6.51%	0.52%	0.31%	0.01%	Augustine
GRV17 77-78	UA3534-13	0.00%	69.19%	0.00%	0.00%	0.00%	4.12%	25.43%	0.81%	0.44%	0.01%	Augustine
GRV17 77-78	UA3534-1	0.00%	93.48%	0.10%	0.00%	0.00%	4.11%	2.19%	0.01%	0.10%	0.01%	Augustine
GRV17 77-78	UA3534-18	0.00%	85.76%	0.00%	0.00%	0.00%	4.10%	9.82%	0.21%	0.10%	0.01%	Augustine
GRV17 77-78	UA3534-5	0.00%	61.25%	0.20%	0.00%	0.00%	2.61%	34.78%	0.93%	0.22%	0.01%	Augustine
GRV17 77-78	UA3534-8	0.00%	95.39%	0.00%	0.00%	0.00%	2.39%	2.11%	0.00%	0.10%	0.01%	Augustine
GRV17 77-78	UA3534-4	0.00%	55.57%	0.00%	0.00%	0.00%	8.39%	33.18%	2.62%	0.22%	0.01%	Augustine
GRV17 77-78	UA3534-14	98.98%	0.00%	0.00%	0.01%	0.12%	0.00%	0.00%	0.00%	0.89%	0.00%	Aniakchak
GRV17 77-78	UA3534-2	99.10%	0.00%	0.00%	0.01%	0.31%	0.00%	0.00%	0.00%	0.57%	0.00%	Aniakchak
GRV17 77-78	UA3534-16	95.25%	0.00%	0.00%	0.03%	0.16%	0.00%	0.00%	0.00%	4.56%	0.00%	Aniakchak
GRV17 77-78	UA3534-12	0.00%	0.00%	98.78%	0.05%	0.00%	0.52%	0.00%	0.00%	0.64%	0.00%	Churchill
GRV17 77-78	UA3534-3	0.00%	0.00%	99.26%	0.01%	0.00%	0.62%	0.00%	0.00%	0.12%	0.00%	Churchill
GRV17 77-78	UA3534-20	0.00%	0.00%	98.84%	0.12%	0.00%	0.31%	0.00%	0.01%	0.72%	0.00%	Churchill

GRV17 82-83	UA3533-2	0.50%	0.00%	81.13%	1.77%	0.00%	0.61%	0.01%	0.00%	15.97%	0.00%	Churchill
GRV17 82-83	UA3533-19	0.00%	0.00%	98.18%	0.23%	0.00%	0.21%	0.00%	0.00%	1.38%	0.00%	Churchill
GRV17 82-83	UA3533-3	0.60%	0.00%	79.93%	4.62%	0.00%	4.49%	0.00%	2.53%	7.83%	0.00%	Churchill
GRV17 82-83	UA3533-4	0.20%	0.30%	16.31%	1.59%	0.00%	1.93%	0.00%	13.43%	66.23%	0.00%	Redoubt
GRV17 82-83	UA3533-8	0.00%	77.07%	0.20%	0.00%	0.01%	3.10%	15.40%	1.72%	2.50%	0.01%	Augustine
GRV17 82-83	UA3533-21	0.00%	60.23%	0.30%	0.00%	0.00%	4.37%	33.69%	0.82%	0.58%	0.01%	Augustine
GRV17 82-83	UA3533-11	0.00%	77.73%	0.10%	0.00%	0.00%	10.87%	10.66%	0.61%	0.02%	0.01%	Augustine
GRV17 82-83	UA3533-6	0.00%	22.49%	0.40%	0.00%	0.01%	1.85%	73.28%	0.53%	1.44%	0.01%	Kaguyak
GRV17 82-83	UA3533-9	0.00%	14.90%	0.20%	0.00%	0.00%	1.91%	82.29%	0.41%	0.28%	0.00%	Kaguyak
GRV17 82-83	UA3533-1	0.00%	5.92%	0.20%	0.00%	0.10%	0.32%	91.01%	2.12%	0.32%	0.00%	Kaguyak
GRV17 86-87	UA3619-13	0.00%	45.66%	2.90%	0.10%	0.21%	37.29%	8.89%	0.10%	4.82%	0.01%	Augustine
GRV17 86-87	UA3619-15	0.00%	45.81%	2.40%	0.00%	0.21%	42.04%	7.92%	0.00%	1.59%	0.02%	Augustine
GRV17 86-87	UA3619-28	0.00%	68.45%	0.40%	0.00%	0.01%	8.41%	20.78%	0.81%	1.13%	0.01%	Augustine
GRV17 86-87	UA3619-18	0.00%	50.36%	0.60%	0.00%	0.01%	5.69%	39.29%	1.43%	2.61%	0.01%	Augustine
GRV17 86-87	UA3619-9	0.00%	39.90%	0.40%	0.00%	0.01%	5.16%	48.22%	1.23%	5.07%	0.02%	Kaguyak
GRV17 86-87	UA3619-24	0.01%	45.68%	0.40%	0.00%	0.01%	6.25%	43.65%	1.12%	2.87%	0.02%	Augustine
GRV17 86-87	UA3619-19	0.00%	72.46%	0.20%	0.00%	0.00%	3.51%	20.79%	1.81%	1.22%	0.01%	Augustine
GRV17 86-87	UA3619-6	0.00%	7.93%	0.60%	0.00%	0.10%	9.27%	78.32%	1.41%	2.35%	0.00%	Kaguyak
GRV17 86-87	UA3619-30	0.00%	69.29%	0.10%	0.00%	0.00%	11.54%	18.03%	0.70%	0.32%	0.01%	Augustine
GRV17 86-87	UA3619-20	0.00%	50.24%	0.20%	0.00%	0.00%	12.84%	35.76%	0.61%	0.34%	0.01%	Augustine
GRV17 86-87	UA3619-26	0.00%	51.21%	0.10%	0.00%	0.01%	6.31%	40.74%	0.61%	1.00%	0.01%	Augustine
GRV17 86-87	UA3619-5	0.00%	24.24%	0.10%	0.00%	0.00%	7.84%	65.68%	0.61%	1.52%	0.01%	Kaguyak
GRV17 86-87	UA3619-21	0.00%	42.92%	0.10%	0.00%	0.00%	3.63%	50.45%	1.42%	1.47%	0.01%	Kaguyak
GRV17 86-87	UA3619-25	0.00%	53.00%	0.10%	0.00%	0.00%	8.21%	37.30%	0.61%	0.76%	0.01%	Augustine
GRV17 86-87	UA3619-27	0.00%	54.30%	0.00%	0.00%	0.00%	5.23%	39.46%	0.81%	0.18%	0.01%	Augustine
GRV17 86-87	UA3619-16	0.00%	84.89%	0.10%	0.00%	0.00%	7.34%	7.34%	0.21%	0.11%	0.01%	Augustine
GRV17 86-87	UA3619-7	0.00%	49.91%	0.10%	0.00%	0.00%	6.00%	43.27%	0.41%	0.29%	0.01%	Augustine

GRV17 86-87	UA3619-4	0.00%	10.24%	0.30%	0.00%	0.00%	2.18%	86.04%	0.51%	0.73%	0.00%	Kaguyak
GRV17 86-87	UA3619-3	0.14%	0.61%	0.41%	0.00%	0.13%	3.23%	0.01%	0.53%	94.95%	0.00%	Redoubt
GRV17 86-87	UA3619-23	8.77%	0.80%	8.01%	17.41%	23.26%	6.30%	0.16%	24.62%	10.43%	0.23%	Katmai
GRV17 86-87	UA3619-2	0.01%	1.80%	1.70%	0.00%	0.00%	4.63%	0.00%	0.71%	91.14%	0.00%	Redoubt
GRV17 86-87	UA3619-8	0.00%	0.60%	6.44%	0.10%	0.00%	40.29%	0.10%	0.10%	52.36%	0.00%	Redoubt
GRV17 86-87	UA3619-14	95.96%	0.00%	0.80%	0.14%	0.03%	0.20%	0.00%	0.00%	2.87%	0.00%	Aniakchak
GRV17 86-87	UA3619-29	2.20%	0.30%	84.58%	0.70%	0.21%	9.52%	0.20%	1.60%	0.68%	0.00%	Churchill
GRV17 86-87	UA3619-17	0.10%	10.72%	4.10%	0.00%	0.10%	81.82%	1.95%	0.00%	1.21%	0.00%	Hayes
GRV17 86-87	UA3619-11	0.00%	0.44%	0.10%	0.00%	0.01%	48.96%	3.89%	28.75%	17.85%	0.00%	Hayes
GRV17 86-87	UA3619-10	0.00%	0.54%	0.30%	0.10%	0.00%	51.12%	2.84%	29.89%	15.20%	0.00%	Hayes
GRV17 93-94	UA3532-23	0.00%	38.20%	0.00%	0.00%	0.00%	15.13%	45.53%	0.71%	0.42%	0.01%	Kaguyak
GRV17 93-94	UA3532-22	0.00%	70.15%	0.30%	0.00%	0.00%	2.63%	26.09%	0.31%	0.50%	0.01%	Augustine
GRV17 93-94	UA3532-13	0.00%	51.47%	0.00%	0.00%	0.00%	14.80%	32.35%	1.21%	0.15%	0.01%	Augustine
GRV17 93-94	UA3532-7	0.00%	60.34%	0.20%	0.00%	0.00%	11.74%	26.81%	0.71%	0.18%	0.02%	Augustine
GRV17 93-94	UA3532-20	0.00%	80.83%	0.10%	0.00%	0.30%	6.24%	2.27%	7.15%	3.10%	0.00%	Augustine
GRV17 93-94	UA3532-2	0.00%	0.00%	99.96%	0.02%	0.00%	0.01%	0.00%	0.00%	0.01%	0.00%	Churchill
GRV17 93-94	UA3532-8	0.00%	13.94%	0.80%	0.00%	0.00%	66.38%	0.00%	10.58%	8.30%	0.00%	Hayes
GRV17 97-98	UA3531-19	0.00%	94.08%	0.00%	0.00%	0.00%	3.62%	1.98%	0.01%	0.30%	0.01%	Augustine
GRV17 97-98	UA3531-24	0.00%	95.49%	0.00%	0.00%	0.00%	1.56%	2.64%	0.10%	0.20%	0.01%	Augustine
GRV17 97-98	UA3531-23	0.00%	51.31%	0.10%	0.00%	0.00%	9.49%	37.75%	0.61%	0.73%	0.02%	Augustine
GRV17 97-98	UA3531-30	0.00%	22.76%	0.20%	0.00%	0.00%	1.43%	68.45%	4.43%	2.74%	0.00%	Kaguyak
GRV17 97-98	UA3531-7	0.00%	13.19%	0.20%	0.00%	0.00%	0.68%	85.59%	0.02%	0.31%	0.00%	Kaguyak
GRV17 97-98	UA3531-4	0.00%	35.28%	0.10%	0.00%	0.00%	4.62%	58.14%	1.31%	0.53%	0.01%	Kaguyak
GRV17 97-98	UA3531-1	0.01%	63.38%	0.60%	0.00%	0.01%	16.06%	18.72%	0.50%	0.71%	0.02%	Augustine
GRV17 97-98	UA3531-8	0.00%	12.02%	0.10%	0.00%	0.00%	0.51%	85.83%	0.22%	1.31%	0.01%	Kaguyak
GRV17 97-98	UA3531-28	0.00%	0.20%	86.19%	1.89%	0.00%	0.60%	0.00%	0.21%	10.89%	0.00%	Churchill
GRV17 97-98	UA3531-6	0.00%	0.00%	99.11%	0.13%	0.00%	0.20%	0.00%	0.00%	0.57%	0.00%	Churchill

GRV17 97-98	UA3531-21	0.00%	0.00%	92.91%	1.20%	0.00%	0.11%	0.00%	0.00%	5.77%	0.00%	Churchill
GRV17 100-101	UA3530-28	0.00%	72.77%	0.30%	0.00%	0.00%	4.79%	20.39%	1.11%	0.63%	0.01%	Augustine
GRV17 100-101	UA3530-15	0.00%	95.32%	0.00%	0.00%	0.00%	1.63%	2.14%	0.10%	0.80%	0.01%	Augustine
GRV17 100-101	UA3530-5	0.00%	38.05%	0.20%	0.00%	0.00%	11.03%	49.66%	0.71%	0.34%	0.01%	Kaguyak
GRV17 100-101	UA3530-3	0.00%	88.72%	0.10%	0.00%	0.00%	9.32%	1.85%	0.01%	0.00%	0.00%	Augustine
GRV17 100-101	UA3530-30	0.00%	91.92%	0.10%	0.00%	0.00%	3.79%	4.18%	0.00%	0.00%	0.00%	Augustine
GRV17 100-101	UA3530-23	0.00%	92.86%	0.00%	0.00%	0.00%	3.49%	3.53%	0.01%	0.10%	0.01%	Augustine
GRV17 100-101	UA3530-1	0.00%	98.18%	0.00%	0.00%	0.00%	0.85%	0.86%	0.00%	0.10%	0.01%	Augustine
GRV17 100-101	UA3530-2	0.00%	96.17%	0.10%	0.00%	0.00%	2.81%	0.62%	0.00%	0.30%	0.00%	Augustine
GRV17 113-114	UA3528-1	0.00%	0.00%	99.98%	0.00%	0.00%	0.00%	0.00%	0.00%	0.01%	0.00%	Churchill
GRV17 113-114	UA3528-11	0.00%	0.00%	99.66%	0.01%	0.00%	0.21%	0.00%	0.00%	0.12%	0.00%	Churchill
GRV17 113-114	UA3528-17	0.00%	0.00%	96.51%	1.01%	0.00%	0.21%	0.00%	0.10%	2.16%	0.00%	Churchill
GRV17 113-114	UA3528-19	0.00%	0.00%	97.86%	0.38%	0.00%	0.52%	0.00%	0.10%	1.14%	0.00%	Churchill
GRV17 113-114	UA3528-10	0.00%	0.00%	86.48%	0.00%	0.00%	13.02%	0.00%	0.40%	0.10%	0.00%	Churchill
GRV17 113-114	UA3528-18	0.00%	0.00%	99.20%	0.00%	0.00%	0.34%	0.00%	0.00%	0.46%	0.00%	Churchill
GRV17 113-114	UA3528-16	0.00%	0.00%	88.75%	0.10%	0.00%	10.33%	0.00%	0.51%	0.30%	0.00%	Churchill
GRV17 123-124	UA3538-13	10.00%	1.02%	2.11%	4.08%	39.48%	4.61%	0.25%	14.82%	22.22%	1.41%	Fisher
GRV17 123-124	UA3538-1	16.95%	1.90%	2.70%	5.53%	43.81%	6.51%	0.22%	9.79%	12.38%	0.21%	Fisher
GRV17 123-124	UA3538-3	12.70%	1.80%	1.30%	6.48%	44.05%	4.00%	0.97%	7.47%	20.01%	1.21%	Fisher
GRV17 123-124	UA3538-17	9.82%	1.81%	3.41%	3.43%	21.01%	5.08%	0.83%	31.25%	22.05%	1.32%	Katmai
GRV17 123-124	UA3538-25	8.06%	2.82%	2.00%	5.86%	19.71%	2.10%	5.87%	22.97%	28.31%	2.29%	Redoubt
GRV17 123-124	UA3538-23	0.20%	2.00%	2.90%	0.90%	0.15%	60.81%	4.86%	11.27%	16.91%	0.00%	Hayes
GRV17 123-124	UA3538-2	0.00%	2.20%	0.20%	0.10%	0.14%	7.23%	49.64%	20.12%	20.37%	0.00%	Kaguyak
GRV17 123-124	UA3538-10	0.00%	1.50%	0.00%	0.20%	0.00%	6.14%	56.92%	33.41%	1.83%	0.00%	Kaguyak
GRV17 123-124	UA3538-18	0.00%	6.57%	0.20%	0.00%	0.00%	54.59%	8.47%	17.62%	12.55%	0.00%	Hayes
GRV17 123-124	UA3538-22	0.00%	5.11%	0.30%	0.00%	0.01%	19.87%	38.90%	22.63%	13.17%	0.00%	Kaguyak
GRV17 133-134	UA3535-18	6.26%	0.89%	8.35%	4.71%	7.92%	17.94%	0.34%	45.23%	7.80%	0.57%	Katmai

GRV17 133-134	UA3535-12	13.74%	1.33%	2.12%	4.45%	19.90%	3.51%	0.26%	20.19%	33.95%	0.54%	Redoubt
GRV17 133-134	UA3535-23	8.81%	1.32%	3.81%	4.47%	7.44%	7.22%	0.10%	49.89%	16.74%	0.21%	Katmai
GRV17 133-134	UA3535-5	0.00%	15.24%	0.20%	0.00%	0.00%	1.90%	81.78%	0.62%	0.25%	0.00%	Kaguyak
GRV17 133-134	UA3535-11	0.00%	11.55%	0.20%	0.00%	0.00%	2.22%	80.06%	4.53%	1.43%	0.00%	Kaguyak
GRV17 133-134	UA3535-28	0.00%	16.71%	0.20%	0.00%	0.00%	12.17%	34.11%	30.14%	6.66%	0.01%	Kaguyak
GRV17 133-134	UA3535-7	0.00%	0.81%	0.00%	0.00%	0.00%	2.75%	59.63%	32.83%	3.98%	0.00%	Kaguyak
GRV17 133-134	UA3535-5	0.00%	3.20%	0.40%	0.10%	0.11%	8.29%	56.98%	21.41%	9.52%	0.00%	Kaguyak
GRV17 133-134	UA3535-6	0.00%	2.54%	0.40%	0.20%	0.00%	57.11%	6.03%	22.87%	10.84%	0.00%	Hayes
GRV17 133-134	UA3535-16	2.64%	0.40%	66.35%	5.71%	0.10%	5.10%	0.30%	4.60%	14.80%	0.00%	Churchill
GRV17 133-134	UA3535-1	0.93%	0.00%	67.98%	7.99%	0.00%	3.70%	0.00%	3.10%	16.30%	0.00%	Churchill
GRV17 133-134	UA3535-2	0.62%	0.00%	61.36%	7.50%	0.00%	4.20%	0.00%	5.31%	21.00%	0.00%	Churchill
GRV17 133-134	UA3535-4	0.75%	0.00%	64.61%	4.02%	0.10%	5.30%	0.00%	5.41%	19.80%	0.00%	Churchill
GRV17 133-134	UA3535-5 rerun-1	0.00%	8.65%	0.20%	0.10%	0.00%	37.76%	21.47%	21.17%	10.65%	0.00%	Hayes
GRV17 133-134	UA3535-6 rerun-1	0.00%	7.26%	0.10%	0.00%	0.00%	12.19%	44.73%	24.53%	11.18%	0.00%	Kaguyak
GRV17 133-134	UA3535-7 rerun-1	0.00%	2.86%	0.40%	0.10%	0.01%	19.58%	43.51%	20.36%	13.18%	0.00%	Kaguyak
GRV17 135-136	UA3536-14	9.14%	1.40%	2.71%	46.16%	0.09%	0.50%	0.10%	20.86%	19.03%	0.00%	Dawson
GRV17 135-136	UA3536-21	3.71%	1.40%	5.34%	13.63%	0.00%	0.90%	0.01%	49.43%	25.57%	0.00%	Katmai
GRV17 135-136	UA3536-11	7.20%	3.80%	3.15%	15.12%	0.31%	5.10%	0.00%	53.84%	11.48%	0.00%	Katmai
GRV17 135-136	UA3536-1	3.16%	2.20%	1.95%	2.35%	0.71%	6.11%	0.70%	43.19%	39.63%	0.00%	Katmai
GRV17 135-136	UA3536-6	7.92%	2.00%	0.40%	1.85%	1.10%	6.70%	0.30%	48.07%	31.66%	0.00%	Katmai
GRV17 135-136	UA3536-2	0.10%	0.40%	0.60%	0.01%	0.00%	2.70%	0.20%	12.68%	83.30%	0.00%	Redoubt
GRV17 135-136	UA3536-19	0.00%	0.31%	39.99%	0.22%	0.00%	2.60%	0.01%	25.53%	31.35%	0.00%	Churchill
GRV17 135-136	UA3536-13	0.00%	79.95%	0.50%	0.00%	0.00%	5.43%	12.35%	0.91%	0.85%	0.00%	Augustine
GRV17 135-136	UA3536-20	0.00%	30.93%	0.10%	0.10%	0.10%	12.51%	54.36%	0.40%	1.46%	0.03%	Kaguyak
GRV17 135-136	UA3536-3	0.00%	64.41%	0.20%	0.00%	0.00%	9.04%	21.74%	3.88%	0.71%	0.02%	Augustine
GRV17 135-136	UA3536-18	0.04%	37.57%	0.20%	0.00%	0.01%	10.22%	49.53%	1.92%	0.47%	0.04%	Kaguyak
GRV17 135-136	UA3536-5	0.00%	18.85%	0.30%	0.00%	0.10%	3.47%	68.74%	7.62%	0.92%	0.01%	Kaguyak

GRV17 140-141	UA3537-14	7.13%	0.50%	48.54%	10.50%	0.20%	0.30%	0.00%	7.86%	24.97%	0.00%	Churchill
GRV17 140-141	UA3537-11	9.89%	1.10%	46.81%	24.81%	0.38%	9.10%	0.00%	0.52%	7.39%	0.00%	Churchill
GRV17 140-141	UA3537-19	17.11%	3.10%	3.01%	37.51%	1.43%	2.00%	0.10%	22.87%	12.87%	0.00%	Dawson
GRV17 140-141	UA3537-10	1.62%	1.30%	6.64%	7.65%	0.00%	1.50%	0.00%	40.65%	40.61%	0.00%	Katmai
GRV17 140-141	UA3537-5	10.77%	5.60%	3.20%	3.79%	0.81%	6.31%	0.10%	52.46%	16.96%	0.00%	Katmai
GRV17 140-141	UA3537-8	12.43%	3.60%	2.90%	13.34%	1.34%	3.00%	0.10%	49.42%	13.87%	0.00%	Katmai
GRV17 140-141	UA3537-16	0.32%	2.60%	4.58%	6.94%	0.00%	1.90%	0.20%	29.28%	54.17%	0.00%	Redoubt
GRV17 140-141	UA3537-7	1.89%	1.80%	3.92%	2.84%	0.60%	4.20%	0.20%	21.36%	63.18%	0.00%	Redoubt
GRV17 140-141	UA3537-9	0.15%	0.00%	9.77%	4.97%	0.01%	0.90%	0.00%	20.90%	63.29%	0.00%	Redoubt
GRV17 140-141	UA3537-20	0.52%	1.31%	3.36%	2.00%	0.00%	6.05%	0.21%	57.84%	28.71%	0.00%	Katmai
GRV17 140-141	UA3537-4	0.00%	0.70%	2.97%	0.50%	0.00%	0.90%	0.10%	15.74%	79.09%	0.00%	Redoubt
GRV17 140-141	UA3537-6	1.77%	1.80%	0.60%	1.56%	0.80%	6.40%	0.20%	52.13%	34.74%	0.00%	Katmai
GRV17 140-141	UA3537-13	0.00%	0.80%	1.62%	0.12%	0.00%	3.81%	0.20%	7.74%	85.70%	0.00%	Redoubt
GRV17 140-141	UA3537-2	1.00%	1.10%	0.40%	0.51%	1.00%	4.40%	0.40%	3.17%	88.02%	0.00%	Redoubt
GRV17 156-157	UA3618-15	2.27%	2.70%	0.00%	0.00%	51.03%	3.60%	0.05%	9.46%	1.91%	28.98%	Fisher
GRV17 156-157	UA3618-1	1.37%	10.53%	0.00%	0.00%	43.57%	4.71%	0.68%	14.16%	3.90%	21.07%	Fisher
GRV17 156-157	UA3618-26	2.00%	6.10%	0.00%	0.00%	53.29%	4.20%	0.27%	9.90%	4.58%	19.65%	Fisher
GRV17 156-157	UA3618-25	2.01%	6.48%	0.00%	0.00%	61.03%	5.50%	0.17%	7.41%	6.02%	11.39%	Fisher
GRV17 156-157	UA3618-5	3.34%	6.76%	0.10%	0.00%	59.98%	5.50%	0.20%	4.66%	8.22%	11.25%	Fisher
GRV17 156-157	UA3618-11	3.61%	5.54%	0.50%	0.10%	70.58%	6.60%	0.14%	2.42%	4.90%	5.59%	Fisher
GRV17 156-157	UA3618-19	3.78%	8.41%	0.20%	0.00%	57.47%	6.43%	0.52%	3.87%	7.61%	11.72%	Fisher
GRV17 156-157	UA3618-4	2.08%	1.10%	5.35%	54.38%	0.03%	0.90%	0.20%	14.96%	21.00%	0.00%	Dawson
GRV17 156-157	UA3618-9	0.40%	1.31%	1.10%	1.81%	0.27%	2.00%	2.65%	49.83%	40.63%	0.00%	Katmai
GRV17 156-157	UA3618-6	0.00%	0.36%	0.20%	1.21%	0.09%	5.31%	18.09%	27.30%	47.44%	0.00%	Redoubt
GRV17 156-157	UA3618-8	0.00%	0.98%	0.30%	0.01%	0.06%	20.23%	32.32%	24.01%	22.08%	0.00%	Kaguyak
GRV17 162-163	UA3617-3	0.55%	0.10%	2.97%	93.37%	0.11%	0.40%	0.00%	0.20%	2.30%	0.00%	Dawson
GRV17 162-163	UA3617-21	0.82%	0.00%	7.45%	89.50%	0.00%	0.30%	0.00%	0.31%	1.61%	0.00%	Dawson

GRV17 162-163	UA3617-16	0.84%	12.41%	0.00%	0.40%	1.09%	2.80%	0.34%	27.47%	54.58%	0.08%	Redoubt
GRV17 162-163	UA3617-15	0.73%	30.88%	0.00%	0.40%	1.64%	2.50%	0.25%	37.88%	25.56%	0.15%	Katmai
GRV17 162-163	UA3617-28	0.90%	1.60%	1.40%	0.00%	0.10%	1.90%	0.11%	11.08%	82.90%	0.00%	Redoubt
GRV17 162-163	UA3617-12	0.40%	3.25%	1.00%	0.82%	0.02%	1.30%	2.32%	70.37%	20.52%	0.00%	Katmai
GRV17 162-163	UA3617-17	0.00%	0.05%	5.44%	0.84%	0.01%	48.00%	0.50%	22.46%	22.68%	0.00%	Hayes
GRV17 162-163	UA3617-32	0.00%	3.90%	0.70%	0.02%	0.01%	3.11%	10.25%	76.89%	5.12%	0.00%	Katmai
GRV17 162-163	UA3617-29	0.60%	2.88%	0.40%	1.31%	0.10%	2.80%	1.56%	78.31%	12.03%	0.00%	Katmai
GRV17 162-163	UA3617-7	0.00%	0.00%	14.30%	0.71%	0.10%	5.73%	0.11%	10.52%	68.53%	0.00%	Redoubt
GRV17 162-163	UA3617-31	0.00%	0.44%	0.80%	1.24%	0.18%	17.37%	35.46%	26.32%	18.18%	0.00%	Kaguyak
GRV17 162-163	UA3617-8	0.00%	0.50%	0.50%	0.30%	0.01%	45.99%	12.35%	24.72%	15.62%	0.00%	Hayes
GRV17 162-163	UA3617-20	0.00%	1.14%	0.10%	0.00%	0.01%	40.19%	5.53%	38.35%	14.69%	0.00%	Hayes
GRV17 162-163	UA3617-9	26.06%	1.80%	1.80%	7.42%	2.52%	0.20%	0.10%	45.58%	14.31%	0.20%	Katmai
GRV17 162-163	UA3617-11	0.17%	8.11%	49.36%	0.44%	0.00%	8.35%	2.80%	10.22%	20.55%	0.00%	Churchill
GRV17 162-163	UA3617-1	0.00%	0.87%	0.20%	0.01%	0.06%	20.60%	23.46%	32.04%	22.75%	0.00%	Katmai
GRV17 162-163	UA3617-25	0.00%	64.97%	0.50%	0.00%	0.01%	17.94%	15.55%	0.50%	0.52%	0.01%	Augustine
GRV17 162-163	UA3617-33	0.00%	30.96%	0.50%	0.00%	0.00%	3.00%	59.10%	3.04%	3.39%	0.01%	Kaguyak
GRV17 162-163	UA3617-13	0.01%	9.25%	0.90%	0.10%	0.01%	10.00%	71.79%	1.82%	6.12%	0.01%	Kaguyak
GRV17 162-163	UA3617-24	0.00%	49.56%	0.10%	0.00%	0.00%	32.99%	16.97%	0.10%	0.27%	0.01%	Augustine
GRV17 162-163	UA3617-14	0.00%	10.18%	0.70%	0.20%	0.01%	13.00%	69.63%	2.01%	4.26%	0.01%	Kaguyak
GRV17 188-189	UA3615-16	0.00%	0.10%	0.00%	0.31%	0.01%	0.30%	1.58%	79.14%	18.57%	0.00%	Katmai
GRV17 188-189	UA3615-28	0.00%	0.43%	0.10%	0.01%	0.02%	6.94%	3.30%	65.61%	23.59%	0.00%	Katmai
GRV17 188-189	UA3615-31	0.00%	0.43%	0.00%	0.01%	0.01%	3.76%	3.00%	86.08%	6.71%	0.00%	Katmai
GRV17 188-189	UA3615-27	0.00%	0.67%	0.00%	0.01%	0.03%	16.11%	15.56%	57.94%	9.68%	0.00%	Katmai
GRV17 188-189	UA3615-13	0.00%	0.33%	0.10%	0.01%	0.01%	6.95%	1.50%	86.96%	4.14%	0.00%	Katmai
GRV17 188-189	UA3615-14	0.00%	0.68%	0.10%	0.11%	0.01%	17.96%	5.04%	70.60%	5.49%	0.00%	Katmai
GRV17 188-189	UA3615-18	0.00%	1.47%	0.10%	0.00%	0.00%	23.41%	1.10%	64.48%	9.45%	0.00%	Katmai
GRV17 188-189	UA3615-30	0.00%	0.86%	0.20%	0.01%	0.02%	11.57%	20.29%	49.68%	17.36%	0.00%	Katmai

GRV17 188-189	UA3615-3	0.31%	0.50%	50.84%	1.50%	0.00%	5.60%	0.10%	7.39%	33.75%	0.00%	Churchill
GRV17 188-189	UA3615-12	0.52%	0.40%	43.46%	1.06%	0.00%	4.40%	0.10%	8.73%	41.33%	0.00%	Churchill
GRV17 188-189	UA3615-24	0.61%	0.10%	59.11%	6.56%	0.10%	4.20%	0.00%	6.41%	22.91%	0.00%	Churchill
GRV17 188-189	UA3615-29	4.94%	0.20%	52.31%	1.27%	0.00%	3.90%	0.00%	10.08%	27.30%	0.00%	Churchill
GRV17 188-189	UA3615-9	0.85%	0.30%	48.79%	0.17%	0.00%	4.40%	0.20%	4.44%	40.85%	0.00%	Churchill
GRV17 188-189	UA3615-10	0.08%	0.50%	49.79%	0.12%	0.00%	3.40%	0.00%	4.18%	41.93%	0.00%	Churchill
GRV17 188-189	UA3615-2	1.00%	1.10%	13.95%	6.54%	0.10%	2.00%	0.20%	32.65%	42.45%	0.00%	Redoubt
GRV17 188-189	UA3615-23	0.91%	0.10%	4.11%	3.53%	0.10%	1.00%	0.00%	6.73%	83.42%	0.10%	Redoubt
GRV17 188-189	UA3615-1	0.41%	0.80%	5.89%	2.67%	0.10%	2.40%	0.00%	48.42%	39.21%	0.10%	Katmai
GRV17 188-189	UA3615-8	0.00%	0.00%	0.00%	0.00%	0.00%	0.10%	0.00%	0.21%	99.69%	0.00%	Redoubt
GRV17 188-189	UA3615-7	0.00%	0.00%	0.00%	0.00%	0.00%	0.00%	0.00%	0.21%	99.79%	0.00%	Redoubt
GRV17 201-202	UA3614-19	0.30%	1.20%	9.80%	2.10%	0.16%	12.41%	0.60%	2.90%	70.52%	0.00%	Redoubt
GRV17 201-202	UA3614-28	1.60%	0.50%	3.70%	0.70%	0.30%	1.30%	0.00%	4.43%	87.46%	0.00%	Redoubt
GRV17 201-202	UA3614-22	0.60%	0.50%	2.30%	2.01%	0.21%	2.40%	0.23%	15.75%	76.00%	0.00%	Redoubt
GRV17 201-202	UA3614-17	1.71%	0.70%	5.70%	1.64%	0.00%	0.90%	0.00%	12.56%	76.78%	0.00%	Redoubt
GRV17 201-202	UA3614-20	0.60%	2.50%	1.90%	0.52%	0.11%	1.30%	0.23%	27.22%	65.61%	0.00%	Redoubt
GRV17 201-202	UA3614-12	0.40%	2.30%	2.30%	0.32%	0.11%	2.00%	0.62%	18.00%	73.95%	0.00%	Redoubt
GRV17 201-202	UA3614-11	0.40%	1.30%	3.60%	1.13%	0.10%	1.80%	0.01%	9.87%	81.78%	0.00%	Redoubt
GRV17 201-202	UA3614-31	0.50%	2.50%	3.20%	0.41%	0.10%	2.10%	0.64%	16.55%	74.00%	0.00%	Redoubt
GRV17 201-202	UA3614-8	0.20%	2.53%	6.04%	0.53%	0.10%	4.07%	0.05%	60.46%	26.01%	0.00%	Katmai
GRV17 201-202	UA3614-1	0.40%	1.00%	2.80%	0.81%	0.10%	2.20%	0.10%	20.78%	71.80%	0.00%	Redoubt
GRV17 201-202	UA3614-4	0.00%	1.80%	2.20%	0.62%	0.10%	2.70%	0.33%	18.44%	73.82%	0.00%	Redoubt
GRV17 201-202	UA3614-26	0.20%	1.40%	3.10%	0.51%	0.10%	2.80%	0.11%	10.53%	81.23%	0.00%	Redoubt

Table S15: Hanging Lake Age-depth model

OxCal P_sequence model, IntCal 20. Updated June 2021.

Depth (T, cm)	Mean age (CE)	Mean age (cal yr BP)	1SD	1 sigma range		2 sigma range		Sed rate
14	835.3	1114.7	32.8	1170	1070	1176	1065	0.0136
14.5	798.6	1151.4	98.4	1187	1069	1355	1064	0.0136
15	761.8	1188.2	163.9	1204	1068	1535	1063	0.0136
15.5	725	1225	229.4	1221	1068	1714	1061	0.0136
16	688.2	1261.8	295	1238	1067	1893	1060	0.0136
16.5	651.4	1298.6	354.1	1261	1066	2058	1059	0.0136
17	614.6	1335.4	385.8	1309	1066	2161	1059	0.0136
17.5	577.7	1372.3	417.4	1357	1067	2264	1060	0.0136
18	540.9	1409.1	449.1	1405	1067	2366	1060	0.0136
18.5	504.1	1445.9	480.7	1453	1068	2469	1061	0.0136
19	467.3	1482.7	508.7	1503	1068	2564	1061	0.0136
19.5	430.9	1519.1	530.6	1557	1069	2647	1062	0.0136
20	394.4	1555.6	552.5	1610	1070	2729	1062	0.0136
20.5	357.9	1592.1	574.4	1664	1072	2812	1062	0.0136
21	321.4	1628.6	596.3	1718	1073	2895	1063	0.0136
21.5	284.7	1665.3	617.3	1768	1074	2976	1063	0.0136
22	247.7	1702.3	637.6	1817	1075	3055	1064	0.0136
22.5	210.8	1739.2	657.9	1866	1077	3134	1064	0.0136
23	173.9	1776.1	678.2	1915	1078	3214	1064	0.0136
23.5	136.9	1813.1	698.5	1964	1080	3293	1065	0.0136
24	100.2	1849.8	713.4	2012	1082	3360	1065	0.0136
24.5	63.4	1886.6	726.5	2059	1085	3423	1066	0.0136
25	26.7	1923.3	739.6	2107	1089	3486	1067	0.0136
25.5	-10	1960	752.7	2154	1092	3548	1067	0.0136
26	-46.7	1996.7	765.9	2202	1095	3611	1068	0.0136
26.5	-83.7	2033.7	779.4	2251	1099	3670	1069	0.0136
27	-120.7	2070.7	792.9	2301	1103	3729	1070	0.0136
27.5	-157.6	2107.6	806.5	2350	1107	3788	1070	0.0136
28	-194.6	2144.6	820	2400	1111	3847	1071	0.0136
28.5	-231.6	2181.6	833.3	2450	1116	3906	1072	0.0136
29	-268.4	2218.4	844.4	2505	1126	3958	1073	0.0136
29.5	-305.2	2255.2	855.6	2560	1135	4011	1075	0.0136
30	-342	2292	866.7	2615	1144	4064	1076	0.0136
30.5	-378.8	2328.8	877.9	2670	1154	4117	1077	0.0136
31	-415.7	2365.7	889.2	2729	1161	4168	1078	0.0136

31.5	-452.5	2402.5	900.8	2794	1164	4215	1079	0.0136
32	-489.4	2439.4	912.5	2860	1167	4263	1080	0.0136
32.5	-526.2	2476.2	924.1	2926	1170	4310	1081	0.0136
33	-563	2513	935.8	2992	1173	4357	1082	0.0136
33.5	-599.7	2549.7	944.2	3057	1204	4404	1084	0.0136
34	-636.2	2586.2	949.5	3121	1261	4451	1089	0.0136
34.5	-672.7	2622.7	954.8	3186	1318	4497	1094	0.0136
35	-709.2	2659.2	960.1	3250	1375	4544	1099	0.0136
35.5	-745.7	2695.7	965.4	3314	1432	4590	1104	0.0136
36	-782.7	2732.7	971.3	3379	1472	4636	1109	0.0135
36.5	-820.1	2770.1	977.4	3444	1505	4682	1114	0.0135
37	-857.4	2807.4	983.5	3509	1537	4727	1119	0.0135
37.5	-894.7	2844.7	989.6	3574	1570	4773	1124	0.0135
38	-932	2882	995.8	3639	1602	4818	1128	0.0135
38.5	-969.1	2919.1	1001	3696	1647	4868	1137	0.0135
39	-1006	2956	1006	3752	1695	4918	1146	0.0135
39.5	-1043	2993	1011	3808	1742	4968	1155	0.0135
40	-1080	3030	1016.1	3864	1790	5018	1164	0.0136
40.5	-1116.9	3066.9	1021.2	3920	1836	5068	1174	0.0136
41	-1153.6	3103.6	1026.7	3989	1865	5119	1189	0.0136
41.5	-1190.2	3140.2	1032.3	4058	1894	5170	1205	0.0136
42	-1226.8	3176.8	1037.9	4127	1922	5221	1220	0.0137
42.5	-1263.4	3213.4	1043.4	4195	1951	5272	1235	0.0137
43	-1300	3250	1048.2	4255	1982	5320	1254	0.0137
43.5	-1336.3	3286.3	1050.6	4289	2018	5359	1280	0.0137
44	-1372.6	3322.6	1053	4322	2055	5398	1307	0.0137
44.5	-1408.9	3358.9	1055.3	4356	2091	5438	1333	0.0137
45	-1445.2	3395.2	1057.7	4389	2128	5477	1360	0.0137
45.5	-1481.7	3431.7	1060.4	4428	2168	5522	1387	0.0137
46	-1518.5	3468.5	1063.6	4473	2213	5575	1415	0.0136
46.5	-1555.4	3505.4	1066.8	4518	2257	5628	1442	0.0136
47	-1592.2	3542.2	1070	4563	2302	5680	1470	0.0136
47.5	-1629	3579	1073.2	4608	2347	5733	1498	0.0135
48	-1666	3616	1075.7	4658	2394	5771	1524	0.0135
48.5	-1703.1	3653.1	1077.9	4710	2441	5799	1550	0.0135
49	-1740.2	3690.2	1080.1	4762	2489	5828	1576	0.0135
49.5	-1777.3	3727.3	1082.3	4815	2536	5856	1601	0.0135
50	-1814.4	3764.4	1084.5	4867	2584	5885	1627	0.0135
50.5	-1851.2	3801.2	1087.2	4921	2620	5932	1657	0.0136

51	-1887.9	3837.9	1090.1	4975	2653	5985	1689	0.0136
51.5	-1924.7	3874.7	1093	5028	2687	6037	1720	0.0136
52	-1961.4	3911.4	1096	5082	2720	6089	1752	0.0136
52.5	-1998.1	3948.1	1098.9	5136	2753	6141	1783	0.0136
53	-2035	3985	1096.1	5173	2799	6167	1820	0.0136
53.5	-2071.9	4021.9	1093.2	5210	2844	6192	1857	0.0136
54	-2108.7	4058.7	1090.4	5246	2890	6218	1893	0.0136
54.5	-2145.6	4095.6	1087.6	5283	2935	6243	1930	0.0136
55	-2182.4	4132.4	1084.9	5323	2983	6270	1968	0.0136
55.5	-2219.1	4169.1	1082.6	5374	3039	6304	2011	0.0136
56	-2255.8	4205.8	1080.4	5425	3096	6337	2055	0.0136
56.5	-2292.5	4242.5	1078.1	5476	3152	6371	2098	0.0136
57	-2329.2	4279.2	1075.8	5527	3209	6404	2141	0.0136
57.5	-2365.9	4315.9	1073.2	5568	3262	6432	2185	0.0136
58	-2402.8	4352.8	1070.1	5590	3310	6451	2231	0.0136
58.5	-2439.8	4389.8	1066.9	5613	3358	6469	2276	0.0136
59	-2476.7	4426.7	1063.8	5636	3405	6488	2322	0.0136
59.5	-2513.6	4463.6	1060.6	5659	3453	6507	2367	0.0136
60	-2550.5	4500.5	1057.9	5699	3504	6535	2415	0.0136
60.5	-2587.3	4537.3	1055.6	5751	3556	6570	2464	0.0136
61	-2624.1	4574.1	1053.2	5804	3609	6606	2514	0.0136
61.5	-2661	4611	1050.9	5856	3662	6641	2563	0.0136
62	-2697.8	4647.8	1048.6	5909	3715	6676	2613	0.0136
62.5	-2734.4	4684.4	1043.8	5947	3771	6694	2663	0.0136
63	-2771	4721	1038.3	5981	3829	6706	2715	0.0136
63.5	-2807.6	4757.6	1032.7	6014	3887	6718	2766	0.0136
64	-2844.1	4794.1	1027.2	6047	3945	6729	2817	0.0136
64.5	-2880.7	4830.7	1021.7	6081	4002	6741	2869	0.0136
65	-2917.7	4867.7	1016.7	6126	4057	6747	2910	0.0136
65.5	-2954.6	4904.6	1011.8	6172	4112	6753	2951	0.0135
66	-2991.6	4941.6	1006.8	6217	4167	6759	2992	0.0135
66.5	-3028.5	4978.5	1001.9	6263	4222	6765	3032	0.0135
67	-3065.5	5015.5	996.8	6307	4277	6770	3073	0.0135
67.5	-3102.8	5052.8	990.5	6335	4332	6774	3110	0.0135
68	-3140.1	5090.1	984.2	6364	4387	6777	3148	0.0135
68.5	-3177.3	5127.3	977.9	6393	4441	6780	3186	0.0135
69	-3214.6	5164.6	971.6	6421	4496	6783	3223	0.0135
69.5	-3251.6	5201.6	965.7	6458	4556	6788	3262	0.0135
70	-3288.3	5238.3	960.5	6512	4626	6796	3303	0.0135

70.5	-3324.9	5274.9	955.3	6566	4697	6804	3345	0.0135
71	-3361.5	5311.5	950.1	6620	4767	6812	3386	0.0135
71.5	-3398.1	5348.1	945	6674	4838	6820	3427	0.0135
72	-3435.2	5385.2	936.5	6707	4907	6825	3482	0.0135
72.5	-3472.6	5422.6	924.7	6718	4976	6826	3550	0.0135
73	-3510	5460	913	6730	5045	6828	3618	0.0135
73.5	-3547.4	5497.4	901.2	6742	5114	6830	3687	0.0135
74	-3584.9	5534.9	889.4	6753	5183	6831	3755	0.0135
74.5	-3621.6	5571.6	878.2	6760	5236	6833	3813	0.0135
75	-3658	5608	867.1	6764	5283	6834	3867	0.0136
75.5	-3694.4	5644.4	856.1	6768	5330	6835	3921	0.0136
76	-3730.8	5680.8	845	6772	5377	6837	3975	0.0136
76.5	-3767.2	5717.2	834	6776	5424	6838	4029	0.0136
77	-3804.3	5754.3	820.7	6779	5469	6839	4082	0.0136
77.5	-3841.4	5791.4	807.2	6781	5514	6840	4134	0.0136
78	-3878.6	5828.6	793.6	6784	5559	6841	4187	0.0136
78.5	-3915.7	5865.7	780.1	6787	5604	6842	4239	0.0136
79	-3952.8	5902.8	766.5	6790	5650	6843	4292	0.0135
79.5	-3989.5	5939.5	753.4	6798	5711	6845	4352	0.0136
80	-4026.2	5976.2	740.3	6806	5772	6846	4412	0.0136
80.5	-4062.9	6012.9	727.2	6814	5832	6847	4472	0.0136
81	-4099.6	6049.6	714.1	6822	5893	6849	4532	0.0136
81.5	-4136.3	6086.3	699.2	6828	5951	6850	4596	0.0136
82	-4173.1	6123.1	679.1	6830	5998	6852	4671	0.0136
82.5	-4209.9	6159.9	659	6831	6046	6853	4746	0.0136
83	-4246.6	6196.6	638.9	6833	6093	6854	4821	0.0136
83.5	-4283.4	6233.4	618.8	6834	6140	6855	4896	0.0136
84	-4320.1	6270.1	597.8	6836	6189	6858	4974	0.0136
84.5	-4356.6	6306.6	575.6	6837	6240	6863	5056	0.0136
85	-4393.2	6343.2	553.5	6839	6292	6868	5138	0.0137
85.5	-4429.8	6379.8	531.3	6841	6343	6873	5220	0.0137
86	-4466.4	6416.4	509.1	6842	6394	6878	5302	0.0137
86.5	-4503	6453	481.2	6843	6442	6881	5406	0.0137
87	-4539.6	6489.6	450	6844	6489	6881	5522	0.0136
87.5	-4576.3	6526.3	418.7	6844	6536	6882	5638	0.0136
88	-4612.9	6562.9	387.5	6845	6583	6883	5754	0.0136
88.5	-4649.5	6599.5	356.2	6845	6630	6884	5870	0.0136
89	-4686.5	6636.5	297	6842	6657	6879	6034	0.0139
89.5	-4723.4	6673.4	231.4	6839	6679	6872	6209	0.0143

90	-4760.4	6710.4	165.8	6836	6701	6866	6384	0.0146
90.5	-4797.4	6747.4	100.1	6832	6723	6859	6559	0.015
91	-4834.4	6784.4	34.5	6829	6745	6853	6734	0.0154
91.5	-4862.5	6812.5	80.5	6839	6744	7001	6716	0.0163
92	-4890.6	6840.6	126.4	6849	6744	7149	6699	0.0172
92.5	-4918.6	6868.6	172.3	6859	6743	7297	6681	0.0181
93	-4945.8	6895.8	194.3	6895	6743	7384	6683	0.0182
93.5	-4973	6923	216.3	6930	6742	7470	6686	0.0184
94	-5000.2	6950.2	238.2	6966	6742	7557	6688	0.0185
94.5	-5027.1	6977.1	252.8	7007	6743	7605	6704	0.0184
95	-5054	7004	267.3	7049	6744	7654	6719	0.0183
95.5	-5080.9	7030.9	281.9	7090	6745	7702	6735	0.0183
96	-5108.7	7058.7	294.2	7135	6746	7747	6736	0.0182
96.5	-5136.6	7086.6	306.6	7180	6747	7793	6738	0.0182
97	-5164.4	7114.4	318.9	7225	6748	7838	6739	0.0182
97.5	-5191.6	7141.6	325.4	7264	6751	7866	6741	0.0182
98	-5218.9	7168.9	332	7302	6753	7895	6744	0.0183
98.5	-5246.1	7196.1	338.5	7341	6756	7923	6746	0.0184
99	-5273.3	7223.3	344.3	7391	6760	7933	6748	0.0183
99.5	-5300.5	7250.5	350	7442	6764	7942	6750	0.0183
100	-5327.8	7277.8	355.8	7492	6768	7952	6752	0.0183
100.5	-5355.1	7305.1	359.6	7535	6775	7979	6757	0.0183
101	-5382.5	7332.5	363.4	7578	6782	8005	6761	0.0182
101.5	-5409.8	7359.8	367.2	7621	6789	8032	6766	0.0182
102	-5437.5	7387.5	370.5	7759	6808	8045	6774	0.0182
102.5	-5465.2	7415.2	373.7	7896	6828	8058	6781	0.0183
103	-5492.9	7442.9	377	8034	6847	8071	6789	0.0183
103.5	-5519.7	7469.7	373.9	8048	6964	8087	6808	0.0183
104	-5546.6	7496.6	370.9	8061	7082	8102	6828	0.0183
104.5	-5573.4	7523.4	367.8	8075	7199	8118	6847	0.0183
105	-5601.2	7551.2	364	8088	7259	8129	6872	0.0183
105.5	-5629	7579	360.3	8101	7320	8141	6897	0.0184
106	-5656.7	7606.7	356.5	8114	7380	8152	6922	0.0184
106.5	-5683.3	7633.3	350.9	8123	7435	8156	6949	0.0183
107	-5709.9	7659.9	345.3	8132	7490	8161	6976	0.0183
107.5	-5736.4	7686.4	339.8	8141	7545	8165	7003	0.0182
108	-5764.7	7714.7	333	8147	7584	8168	7027	0.0181
108.5	-5793	7743	326.3	8153	7623	8170	7051	0.018
109	-5821.3	7771.3	319.5	8159	7662	8173	7075	0.0179

109.5	-5849	7799	307.3	8161	7709	8174	7119	0.0179
110	-5876.6	7826.6	295	8164	7755	8175	7162	0.018
110.5	-5904.3	7854.3	282.8	8166	7802	8176	7206	0.018
111	-5932.2	7882.2	267.8	8167	7844	8177	7259	0.018
111.5	-5960.1	7910.1	252.8	8169	7885	8179	7312	0.0181
112	-5988	7938	237.8	8170	7927	8180	7365	0.0181
112.5	-6015.3	7965.3	216.1	8168	7959	8181	7451	0.0182
113	-6042.6	7992.6	194.3	8165	7992	8182	7538	0.0182
113.5	-6069.9	8019.9	172.6	8163	8024	8183	7624	0.0183
114	-6097.2	8047.2	129.6	8164	8027	8180	7758	0.0191
114.5	-6124.6	8074.6	86.5	8166	8031	8176	7893	0.02
115	-6152	8102	43.5	8167	8034	8173	8027	0.0208
115.5	-6172.6	8122.6	66.9	8176	8034	8256	8025	0.0215
116	-6193.2	8143.2	90.3	8185	8033	8339	8024	0.0222
116.5	-6213.8	8163.8	113.7	8194	8033	8422	8022	0.0229
117	-6234.5	8184.5	137.1	8203	8032	8505	8020	0.0236
117.5	-6255.2	8205.2	157.3	8219	8032	8576	8019	0.0241
118	-6276	8226	168.1	8254	8034	8614	8021	0.0241
118.5	-6296.9	8246.9	178.9	8289	8036	8652	8023	0.0241
119	-6317.8	8267.8	189.7	8324	8038	8690	8024	0.0241
119.5	-6338.7	8288.7	200.5	8359	8040	8728	8026	0.0241
120	-6359.5	8309.5	208.5	8393	8046	8756	8028	0.0241
120.5	-6380.2	8330.2	213.6	8427	8055	8775	8031	0.024
121	-6400.8	8350.8	218.8	8462	8064	8793	8034	0.024
121.5	-6421.5	8371.5	223.9	8496	8073	8812	8037	0.024
122	-6442.2	8392.2	229.1	8530	8083	8830	8039	0.024
122.5	-6463.1	8413.1	232.6	8580	8095	8849	8045	0.024
123	-6484	8434	235.5	8634	8108	8867	8051	0.024
123.5	-6505	8455	238.5	8688	8121	8885	8057	0.024
124	-6525.9	8475.9	241.4	8742	8134	8903	8064	0.024
124.5	-6546.8	8496.8	244.4	8796	8147	8921	8070	0.024
125	-6567.6	8517.6	242	8819	8204	8937	8089	0.024
125.5	-6588.3	8538.3	239.6	8842	8261	8952	8109	0.024
126	-6609.1	8559.1	237.2	8865	8318	8968	8128	0.0241
126.5	-6629.8	8579.8	234.8	8889	8374	8983	8147	0.0241
127	-6650.6	8600.6	231.9	8911	8428	8996	8166	0.0241
127.5	-6671.3	8621.3	227.4	8930	8470	8999	8181	0.0241
128	-6692	8642	222.9	8950	8512	9002	8197	0.0241
128.5	-6712.8	8662.8	218.5	8970	8555	9005	8213	0.0241

129	-6733.5	8683.5	214	8989	8597	9008	8228	0.0241
129.5	-6754.3	8704.3	207	9000	8631	9010	8253	0.0241
130	-6775	8725	197.4	9001	8658	9011	8288	0.0241
130.5	-6795.8	8745.8	187.9	9002	8685	9013	8323	0.0241
131	-6816.6	8766.6	178.3	9003	8712	9014	8358	0.024
131.5	-6837.3	8787.3	168.8	9005	8738	9016	8393	0.024
132	-6858.2	8808.2	152.8	9006	8751	9016	8461	0.0239
132.5	-6879	8829	134.7	9006	8759	9016	8539	0.0238
133	-6899.9	8849.9	116.6	9007	8768	9017	8617	0.0238
133.5	-6920.8	8870.8	98.4	9008	8776	9017	8695	0.0237
134	-6941.6	8891.6	80.3	9009	8784	9017	8773	0.0236
134.5	-6963.2	8913.2	112.3	9013	8785	9112	8760	0.0235
135	-6984.8	8934.8	144.2	9017	8785	9206	8746	0.0234
135.5	-7006.4	8956.4	176.2	9020	8786	9301	8733	0.0233
136	-7027.9	8977.9	204.3	9027	8786	9387	8724	0.0233
136.5	-7049.3	8999.3	225.1	9040	8787	9459	8725	0.0233
137	-7070.7	9020.7	245.9	9052	8789	9530	8727	0.0233
137.5	-7092	9042	266.7	9065	8790	9601	8728	0.0234
138	-7113.4	9063.4	284.1	9087	8791	9665	8729	0.0234
138.5	-7134.8	9084.8	300.1	9114	8792	9726	8731	0.0234
139	-7156.2	9106.2	316.1	9141	8793	9788	8733	0.0234
139.5	-7177.6	9127.6	332	9168	8794	9849	8735	0.0234
140	-7199	9149	346.6	9197	8796	9900	8743	0.0233
140.5	-7220.4	9170.4	361.2	9226	8797	9952	8752	0.0233
141	-7241.9	9191.9	375.9	9256	8799	10004	8760	0.0233
141.5	-7263.3	9213.3	389	9285	8802	10052	8766	0.0233
142	-7284.7	9234.7	399.6	9314	8806	10095	8769	0.0234
142.5	-7306.1	9256.1	410.2	9344	8810	10137	8771	0.0235
143	-7327.6	9277.6	420.9	9373	8814	10180	8774	0.0235
143.5	-7348.7	9298.7	431.4	9404	8817	10220	8776	0.0235
144	-7369.7	9319.7	441.8	9436	8819	10260	8777	0.0234
144.5	-7390.8	9340.8	452.3	9467	8822	10300	8779	0.0234
145	-7411.9	9361.9	462.7	9499	8825	10339	8780	0.0233
145.5	-7433.7	9383.7	472.6	9530	8838	10379	8781	0.0233
146	-7455.5	9405.5	482.4	9561	8851	10418	8782	0.0232
146.5	-7477.4	9427.4	492.3	9592	8864	10457	8783	0.0231
147	-7499.1	9449.1	502.2	9624	8875	10498	8783	0.0231
147.5	-7520.6	9470.6	512.3	9655	8881	10543	8784	0.0231
148	-7542.1	9492.1	522.3	9687	8888	10589	8785	0.0231

148.5	-7563.6	9513.6	532.4	9718	8894	10634	8786	0.0232
149	-7585.2	9535.2	539.5	9748	8900	10664	8788	0.0232
149.5	-7606.9	9556.9	545.7	9777	8906	10690	8790	0.0233
150	-7628.5	9578.5	551.9	9806	8911	10716	8792	0.0233
150.5	-7650.1	9600.1	558.1	9836	8918	10743	8794	0.0233
151	-7671.3	9621.3	564.7	9866	8934	10780	8797	0.0234
151.5	-7692.5	9642.5	571.2	9896	8950	10818	8800	0.0234
152	-7713.7	9663.7	577.8	9926	8966	10856	8802	0.0234
152.5	-7735.1	9685.1	584.2	9958	8977	10892	8805	0.0234
153	-7756.6	9706.6	590.5	9994	8982	10925	8808	0.0233
153.5	-7778.1	9728.1	596.7	10029	8988	10959	8811	0.0232
154	-7799.7	9749.7	603	10064	8993	10993	8813	0.0232
154.5	-7821.3	9771.3	609.6	10091	9003	11016	8816	0.0231
155	-7842.9	9792.9	616.3	10116	9015	11036	8818	0.0231
155.5	-7864.5	9814.5	623	10140	9027	11056	8820	0.0231
156	-7886.1	9836.1	629.6	10166	9041	11078	8822	0.023
156.5	-7908	9858	634.7	10200	9062	11111	8824	0.0231
157	-7929.8	9879.8	639.9	10233	9084	11144	8826	0.0231
157.5	-7951.6	9901.6	645.1	10266	9106	11177	8828	0.0231
158	-7973.2	9923.2	650.3	10298	9124	11212	8834	0.0232
158.5	-7994.6	9944.6	655.7	10329	9139	11251	8845	0.0233
159	-8016	9966	661.1	10360	9154	11290	8855	0.0234
159.5	-8037.4	9987.4	666.5	10391	9169	11329	8866	0.0235
160	-8058.6	10008.6	671.7	10430	9190	11366	8872	0.0235
160.5	-8079.8	10029.8	676.9	10471	9213	11403	8878	0.0234
161	-8100.9	10050.9	682.2	10512	9235	11440	8883	0.0234
161.5	-8122.2	10072.2	687.4	10552	9256	11476	8888	0.0234
162	-8143.8	10093.8	693.1	10583	9270	11505	8891	0.0234
162.5	-8165.5	10115.5	698.8	10614	9285	11534	8893	0.0234
163	-8187.2	10137.2	704.5	10645	9299	11563	8896	0.0234
163.5	-8208.5	10158.5	708.5	10670	9312	11586	8902	0.0234
164	-8229.7	10179.7	710.8	10688	9323	11604	8911	0.0234
164.5	-8250.8	10200.8	713	10706	9335	11621	8920	0.0234
165	-8271.9	10221.9	715.3	10724	9346	11639	8929	0.0235
165.5	-8293.3	10243.3	718.1	10761	9371	11669	8939	0.0235
166	-8314.8	10264.8	721	10801	9399	11701	8949	0.0235
166.5	-8336.3	10286.3	724	10841	9427	11732	8960	0.0235
167	-8357.7	10307.7	726.8	10879	9453	11763	8970	0.0235
167.5	-8378.8	10328.8	729.6	10904	9471	11790	8978	0.0234

168	-8399.8	10349.8	732.3	10928	9490	11818	8986	0.0233
168.5	-8420.8	10370.8	735	10953	9509	11845	8994	0.0232
169	-8442.4	10392.4	738.1	10979	9529	11871	9005	0.0232
169.5	-8464.5	10414.5	741.6	11005	9549	11895	9017	0.0231
170	-8486.6	10436.6	745.1	11031	9569	11919	9029	0.0231
170.5	-8508.6	10458.6	748.6	11057	9589	11943	9041	0.023
171	-8530.1	10480.1	750.7	11083	9613	11973	9056	0.023
171.5	-8551.4	10501.4	752.6	11110	9636	12003	9070	0.0231
172	-8572.8	10522.8	754.6	11137	9660	12033	9085	0.0231
172.5	-8594.3	10544.3	756.7	11167	9683	12062	9098	0.0232
173	-8616	10566	759.2	11210	9705	12084	9106	0.0231
173.5	-8637.8	10587.8	761.8	11253	9727	12106	9115	0.0231
174	-8659.6	10609.6	764.4	11296	9748	12128	9123	0.0231
174.5	-8681.3	10631.3	766.9	11324	9764	12156	9135	0.0231
175	-8702.9	10652.9	769.4	11340	9776	12188	9148	0.0231
175.5	-8724.6	10674.6	771.9	11356	9787	12221	9162	0.0232
176	-8746.3	10696.3	774.4	11372	9799	12253	9176	0.0232
176.5	-8767.7	10717.7	777.5	11406	9824	12288	9184	0.0233
177	-8789.1	10739.1	780.6	11441	9851	12324	9192	0.0233
177.5	-8810.4	10760.4	783.7	11476	9878	12359	9199	0.0234
178	-8831.8	10781.8	786.2	11506	9904	12393	9211	0.0234
178.5	-8853.1	10803.1	786.9	11524	9926	12419	9233	0.0233
179	-8874.5	10824.5	787.7	11541	9948	12445	9255	0.0232
179.5	-8895.8	10845.8	788.4	11559	9970	12471	9278	0.0232
180	-8917.5	10867.5	789.4	11585	9994	12493	9297	0.0232
180.5	-8939.3	10889.3	790.5	11617	10020	12512	9314	0.0232
181	-8961.2	10911.2	791.7	11648	10046	12531	9331	0.0233
181.5	-8983	10933	792.9	11680	10072	12550	9348	0.0234
182	-9004	10954	794	11698	10090	12567	9369	0.0233
182.5	-9024.9	10974.9	795	11714	10108	12584	9391	0.0233
183	-9045.8	10995.8	796.1	11731	10125	12601	9412	0.0233
183.5	-9067.1	11017.1	797.4	11754	10146	12619	9431	0.0233
184	-9089.1	11039.1	799.1	11794	10175	12639	9441	0.0233
184.5	-9111.2	11061.2	800.9	11833	10204	12660	9452	0.0233
185	-9133.2	11083.2	802.6	11873	10232	12680	9462	0.0233
185.5	-9154.6	11104.6	803.6	11899	10260	12708	9480	0.0233
186	-9175.6	11125.6	804	11917	10288	12741	9502	0.0233
186.5	-9196.5	11146.5	804.5	11935	10315	12774	9525	0.0234
187	-9217.5	11167.5	804.9	11953	10343	12807	9547	0.0235

187.5	-9239.2	11189.2	805.9	11982	10363	12827	9564	0.0234
188	-9260.9	11210.9	807	12011	10382	12846	9581	0.0233
188.5	-9282.5	11232.5	808	12040	10402	12865	9598	0.0232
189	-9304.2	11254.2	809.1	12068	10421	12885	9616	0.0231
189.5	-9325.8	11275.8	810.1	12094	10439	12909	9635	0.0232
190	-9347.3	11297.3	811.1	12121	10458	12932	9655	0.0232
190.5	-9368.9	11318.9	812	12147	10477	12956	9674	0.0232
191	-9390.4	11340.4	813.3	12174	10501	12976	9694	0.0232
191.5	-9411.8	11361.8	814.8	12202	10529	12995	9714	0.0232
192	-9433.3	11383.3	816.2	12229	10556	13013	9733	0.0232
192.5	-9454.7	11404.7	817.7	12257	10584	13032	9753	0.0231
193	-9476.5	11426.5	816.1	12272	10608	13067	9772	0.0231
193.5	-9498.3	11448.3	814.6	12287	10632	13101	9791	0.0231
194	-9520.1	11470.1	813	12301	10656	13136	9810	0.0231
194.5	-9541.8	11491.8	811.6	12324	10683	13161	9832	0.0231
195	-9563.3	11513.3	810.6	12363	10715	13166	9858	0.0232
195.5	-9584.7	11534.7	809.6	12402	10748	13171	9884	0.0232
196	-9606.2	11556.2	808.5	12441	10780	13176	9910	0.0233
196.5	-9627.7	11577.7	807.3	12468	10806	13194	9938	0.0233
197	-9649.2	11599.2	806	12489	10829	13217	9966	0.0232
197.5	-9670.8	11620.8	804.8	12511	10852	13240	9995	0.0232
198	-9692.3	11642.3	803.5	12533	10876	13264	10024	0.0232
198.5	-9713.8	11663.8	803	12549	10903	13282	10048	0.0233
199	-9735.4	11685.4	802.4	12566	10931	13300	10071	0.0233
199.5	-9757	11707	801.9	12583	10958	13319	10095	0.0233
200	-9778.4	11728.4	801	12598	10981	13337	10118	0.0234
200.5	-9799.7	11749.7	799.5	12613	10998	13355	10139	0.0233
201	-9820.9	11770.9	798.1	12627	11014	13374	10161	0.0233
201.5	-9842.1	11792.1	796.6	12642	11030	13392	10182	0.0233
202	-9863.7	11813.7	795.5	12662	11053	13407	10206	0.0233
202.5	-9885.3	11835.3	794.4	12684	11079	13420	10232	0.0232
203	-9906.9	11856.9	793.4	12705	11104	13434	10257	0.0232
203.5	-9928.6	11878.6	792.4	12728	11130	13448	10282	0.0231
204	-9950.2	11900.2	791	12755	11156	13468	10304	0.0232
204.5	-9971.8	11921.8	789.7	12783	11183	13488	10325	0.0232
205	-9993.4	11943.4	788.4	12811	11209	13507	10346	0.0232
205.5	-10014.9	11964.9	787.3	12837	11237	13524	10369	0.0233
206	-10036.3	11986.3	786.6	12860	11267	13538	10395	0.0233
206.5	-10057.7	12007.7	786	12884	11297	13551	10420	0.0233

207	-10079.1	12029.1	785.3	12907	11327	13565	10446	0.0234
207.5	-10100.5	12050.5	783	12928	11354	13580	10473	0.0234
208	-10121.8	12071.8	780.2	12947	11380	13595	10502	0.0233
208.5	-10143.2	12093.2	777.3	12967	11406	13611	10530	0.0233
209	-10164.5	12114.5	774.5	12987	11432	13626	10558	0.0232
209.5	-10186.2	12136.2	772.1	13012	11460	13636	10582	0.0232
210	-10207.9	12157.9	769.6	13037	11488	13646	10606	0.0231
210.5	-10229.6	12179.6	767.1	13062	11516	13655	10630	0.0231
211	-10251.3	12201.3	764.6	13082	11544	13670	10658	0.0231
211.5	-10273.1	12223.1	762.1	13097	11572	13691	10688	0.0231
212	-10294.8	12244.8	759.5	13111	11600	13712	10719	0.0232
212.5	-10316.6	12266.6	756.9	13126	11628	13733	10750	0.0233
213	-10337.9	12287.9	754.8	13150	11656	13744	10779	0.0233
213.5	-10359.1	12309.1	752.7	13177	11683	13752	10807	0.0234
214	-10380.2	12330.2	750.6	13204	11711	13759	10835	0.0234
214.5	-10401.5	12351.5	748.4	13229	11738	13768	10862	0.0235
215	-10422.8	12372.8	745.2	13249	11764	13781	10889	0.0234
215.5	-10444.2	12394.2	742	13268	11790	13795	10916	0.0234
216	-10465.6	12415.6	738.9	13287	11816	13809	10943	0.0234
216.5	-10487	12437	735.9	13306	11845	13820	10970	0.0233
217	-10508.5	12458.5	733.2	13324	11878	13827	10998	0.0233
217.5	-10529.9	12479.9	730.4	13343	11910	13835	11025	0.0233
218	-10551.4	12501.4	727.7	13362	11943	13843	11053	0.0233
218.5	-10572.8	12522.8	725.1	13381	11974	13848	11078	0.0233
219	-10594.2	12544.2	722.4	13400	12004	13853	11104	0.0233
219.5	-10615.5	12565.5	719.8	13419	12034	13859	11129	0.0233
220	-10636.9	12586.9	717.3	13438	12064	13865	11154	0.0232
220.5	-10658.3	12608.3	715.4	13457	12087	13879	11179	0.0232
221	-10679.7	12629.7	713.4	13476	12110	13893	11204	0.0232
221.5	-10701	12651	711.4	13495	12133	13907	11229	0.0232
222	-10722.5	12672.5	707.5	13513	12159	13917	11261	0.0232
222.5	-10744.1	12694.1	701.6	13532	12188	13923	11300	0.0232
223	-10765.7	12715.7	695.7	13550	12218	13929	11338	0.0232
223.5	-10787.2	12737.2	689.9	13569	12247	13935	11377	0.0232
224	-10808.9	12758.9	684.2	13589	12284	13938	11404	0.0232
224.5	-10830.6	12780.6	678.5	13608	12323	13940	11428	0.0231
225	-10852.3	12802.3	672.8	13628	12361	13941	11452	0.0231
225.5	-10874	12824	667.1	13647	12400	13944	11478	0.023
226	-10895.8	12845.8	661.5	13664	12442	13948	11510	0.0231

226.5	-10917.6	12867.6	655.9	13681	12484	13953	11543	0.0232
227	-10939.4	12889.4	650.3	13698	12525	13957	11575	0.0232
227.5	-10960.9	12910.9	645	13717	12561	13962	11604	0.0233
228	-10982.2	12932.2	640	13737	12592	13968	11631	0.0234
228.5	-11003.4	12953.4	634.9	13757	12623	13974	11659	0.0235
229	-11024.7	12974.7	629.8	13777	12654	13979	11686	0.0236
229.5	-11045.8	12995.8	623.5	13788	12680	13982	11723	0.0235
230	-11066.9	13016.9	617	13797	12705	13985	11761	0.0235
230.5	-11088.1	13038.1	610.5	13806	12730	13988	11799	0.0234
231	-11109.3	13059.3	604	13815	12758	13991	11836	0.0233
231.5	-11131.1	13081.1	597.6	13823	12793	13996	11868	0.0233
232	-11152.8	13102.8	591.2	13832	12828	14001	11901	0.0233
232.5	-11174.5	13124.5	584.9	13840	12863	14006	11933	0.0233
233	-11195.9	13145.9	578.3	13849	12891	14009	11963	0.0234
233.5	-11217.1	13167.1	571.7	13859	12915	14011	11991	0.0234
234	-11238.2	13188.2	565.1	13868	12939	14012	12019	0.0234
234.5	-11259.4	13209.4	558.4	13877	12963	14014	12047	0.0234
235	-11280.9	13230.9	552.6	13889	12999	14017	12083	0.0233
235.5	-11302.4	13252.4	546.9	13901	13037	14021	12120	0.0232
236	-11324	13274	541.2	13914	13075	14025	12157	0.0232
236.5	-11345.5	13295.5	534.4	13924	13110	14028	12195	0.0231
237	-11367	13317	524.5	13929	13136	14030	12241	0.0232
237.5	-11388.5	13338.5	514.6	13935	13162	14032	12287	0.0232
238	-11410	13360	504.8	13940	13188	14033	12333	0.0232
238.5	-11431.4	13381.4	495.7	13945	13218	14035	12371	0.0232
239	-11452.7	13402.7	487.3	13951	13251	14036	12403	0.0232
239.5	-11474	13424	478.8	13957	13284	14038	12434	0.0232
240	-11495.4	13445.4	470.4	13963	13317	14039	12466	0.0232
240.5	-11517.4	13467.4	457.9	13968	13343	14041	12514	0.0232
241	-11539.4	13489.4	445.1	13974	13369	14043	12562	0.0232
241.5	-11561.5	13511.5	432.3	13979	13395	14045	12611	0.0233
242	-11583.3	13533.3	420.4	13985	13423	14047	12658	0.0233
242.5	-11604.4	13554.4	410.6	13990	13455	14048	12701	0.0233
243	-11625.6	13575.6	400.8	13995	13486	14050	12744	0.0233
243.5	-11646.7	13596.7	391	14001	13518	14052	12787	0.0233
244	-11668.2	13618.2	377.8	14005	13548	14054	12835	0.0233
244.5	-11689.9	13639.9	362.6	14007	13577	14056	12886	0.0233
245	-11711.5	13661.5	347.3	14010	13606	14058	12937	0.0232
245.5	-11733.2	13683.2	332.1	14013	13635	14060	12988	0.0232

246	-11754.5	13704.5	317.8	14015	13663	14061	13046	0.0232
246.5	-11775.8	13725.8	303.5	14016	13691	14063	13105	0.0232
247	-11797.1	13747.1	289.3	14018	13719	14064	13163	0.0232
247.5	-11818.4	13768.4	273.4	14018	13743	14065	13225	0.0232
248	-11839.8	13789.8	254.1	14014	13758	14067	13297	0.0233
248.5	-11861.2	13811.2	234.7	14010	13774	14068	13368	0.0233
249	-11882.6	13832.6	215.4	14006	13790	14070	13439	0.0233
249.5	-11904.3	13854.3	185.1	14008	13798	14066	13523	0.0223
250	-11926	13876	149.1	14012	13803	14061	13613	0.0208
250.5	-11947.8	13897.8	113	14017	13807	14055	13702	0.0192
251	-11969.5	13919.5	77	14021	13812	14050	13792	0.0177
251.5	-12004.8	13954.8	127.5	14030	13815	14230	13782	0.0164
252	-12040.1	13990.1	178	14039	13818	14411	13771	0.0151
252.5	-12075.1	14025.1	219.8	14056	13818	14565	13766	0.0143
253	-12109.6	14059.6	247.2	14086	13812	14678	13768	0.0144
253.5	-12144.1	14094.1	274.7	14116	13806	14790	13770	0.0144
254	-12178.7	14128.7	295.8	14164	13806	14865	13775	0.0144
254.5	-12213.5	14163.5	314.8	14218	13808	14929	13782	0.0143
255	-12248.3	14198.3	333.4	14273	13810	14990	13788	0.0142
255.5	-12283.7	14233.7	349.2	14334	13815	15039	13791	0.0142
256	-12319.1	14269.1	365	14395	13820	15088	13794	0.0141
256.5	-12354.7	14304.7	377.3	14461	13828	15129	13798	0.0141
257	-12390.6	14340.6	386	14530	13839	15162	13802	0.0142
257.5	-12426.5	14376.5	394.7	14599	13850	15195	13806	0.0143
258	-12460.6	14410.6	402.2	14657	13866	15226	13815	0.0144
258.5	-12494.5	14444.5	409.6	14714	13882	15256	13824	0.0144
259	-12528.7	14478.7	416.5	14768	13901	15285	13834	0.0144
259.5	-12564	14514	421.8	14814	13923	15310	13846	0.0144
260	-12599.2	14549.2	427.1	14861	13945	15336	13858	0.0143
260.5	-12634.2	14584.2	431.8	14974	13966	15360	13871	0.0142
261	-12669	14619	436	15127	13988	15383	13884	0.014
261.5	-12703.8	14653.8	440.3	15281	14009	15407	13898	0.0139
262	-12741	14691	436	15313	14160	15421	13922	0.014
262.5	-12778.1	14728.1	431.7	15344	14311	15436	13945	0.0141
263	-12813.9	14763.9	427.2	15371	14427	15450	13970	0.0142
263.5	-12847.4	14797.4	422.5	15389	14485	15464	13996	0.0143
264	-12880.9	14830.9	417.9	15407	14543	15478	14022	0.0145
264.5	-12915.9	14865.9	411.1	15423	14601	15491	14045	0.0145
265	-12951.3	14901.3	403.5	15437	14658	15504	14066	0.0144

265.5	-12986.5	14936.5	395.9	15451	14715	15517	14090	0.0144
266	-13020.8	14970.8	387.2	15463	14771	15528	14127	0.0144
266.5	-13055.1	15005.1	378.5	15474	14826	15539	14164	0.0145
267	-13089.4	15039.4	366.2	15483	14884	15548	14215	0.0145
267.5	-13123.9	15073.9	350.4	15488	14944	15557	14278	0.0144
268	-13158.3	15108.3	334.6	15493	15005	15565	14341	0.0143
268.5	-13193.8	15143.8	315.7	15498	15062	15572	14405	0.0142
269	-13229.5	15179.5	296.4	15503	15118	15580	14470	0.0142
269.5	-13264.9	15214.9	274.9	15505	15170	15586	14547	0.0142
270	-13299.9	15249.9	247.3	15496	15205	15589	14661	0.0142
270.5	-13334.9	15284.9	219.7	15487	15241	15593	14776	0.0143
271	-13369.8	15319.8	178.3	15477	15264	15584	14921	0.0168
271.5	-13404.7	15354.7	128.6	15466	15279	15569	15086	0.0207
272	-13439.6	15389.6	79	15455	15294	15553	15250	0.0247
272.5	-13445.3	15395.3	80.3	15463	15298	15560	15253	0.0471
273	-13450.9	15400.9	81.6	15470	15302	15567	15256	0.0695
273.5	-13456.6	15406.6	82.8	15478	15307	15574	15258	0.0893
274	-13462.1	15412.1	84.1	15486	15312	15582	15261	0.0901
274.5	-13467.7	15417.7	85.3	15493	15317	15589	15263	0.0908
275	-13473.1	15423.1	86.5	15500	15322	15597	15266	0.0913
275.5	-13478.5	15428.5	87.5	15506	15327	15604	15268	0.0909
276	-13483.9	15433.9	88.6	15512	15332	15611	15270	0.0904
276.5	-13489.4	15439.4	89.7	15519	15337	15618	15273	0.09
277	-13495.1	15445.1	90.8	15526	15341	15625	15276	0.0896
277.5	-13500.8	15450.8	92	15533	15345	15632	15279	0.0893
278	-13506.5	15456.5	93	15540	15350	15639	15282	0.0892
278.5	-13512	15462	93.7	15547	15356	15648	15286	0.0894
279	-13517.5	15467.5	94.4	15554	15362	15657	15290	0.0896
279.5	-13523.1	15473.1	95.1	15561	15367	15664	15293	0.0894
280	-13528.8	15478.8	95.8	15568	15372	15671	15297	0.089
280.5	-13534.4	15484.4	96.6	15574	15378	15677	15300	0.0887
281	-13540	15490	97.2	15582	15383	15683	15304	0.089
281.5	-13545.7	15495.7	97.8	15591	15389	15689	15307	0.0896
282	-13551.3	15501.3	98.4	15599	15394	15695	15311	0.0901
282.5	-13556.8	15506.8	99	15606	15400	15702	15314	0.0905
283	-13562.2	15512.2	99.7	15612	15406	15708	15317	0.0908
283.5	-13567.7	15517.7	100.3	15619	15412	15715	15320	0.0911
284	-13573.2	15523.2	100.3	15625	15418	15720	15325	0.0909
284.5	-13578.8	15528.8	100.2	15630	15425	15724	15330	0.0906

285	-13584.3	15534.3	100.1	15636	15431	15729	15335	0.0904
285.5	-13589.8	15539.8	100.2	15642	15437	15735	15339	0.0905
286	-13595.4	15545.4	100.2	15649	15444	15741	15344	0.0906
286.5	-13600.9	15550.9	100.2	15655	15451	15746	15348	0.0906
287	-13606.4	15556.4	100.1	15661	15457	15751	15353	0.0903
287.5	-13611.9	15561.9	100	15667	15463	15755	15357	0.0899
288	-13617.4	15567.4	100	15672	15470	15760	15362	0.0897
288.5	-13623.1	15573.1	100	15679	15477	15766	15367	0.0899
289	-13628.7	15578.7	100	15685	15484	15772	15372	0.0901
289.5	-13634.2	15584.2	99.8	15691	15491	15778	15376	0.09
290	-13639.7	15589.7	99.4	15696	15498	15783	15381	0.0897
290.5	-13645.1	15595.1	99	15701	15505	15788	15385	0.0893
291	-13650.8	15600.8	98.7	15706	15511	15793	15391	0.0891
291.5	-13656.6	15606.6	98.3	15712	15518	15798	15397	0.0889
292	-13662.4	15612.4	98	15718	15524	15804	15403	0.0888
292.5	-13667.9	15617.9	97.5	15722	15530	15809	15409	0.089
293	-13673.4	15623.4	97	15726	15536	15815	15415	0.0892
293.5	-13678.9	15628.9	96.6	15730	15542	15820	15421	0.0895
294	-13684.6	15634.6	96.1	15735	15550	15826	15427	0.0891
294.5	-13690.2	15640.2	95.7	15742	15558	15831	15432	0.0887
295	-13695.9	15645.9	95.2	15748	15566	15836	15438	0.0882

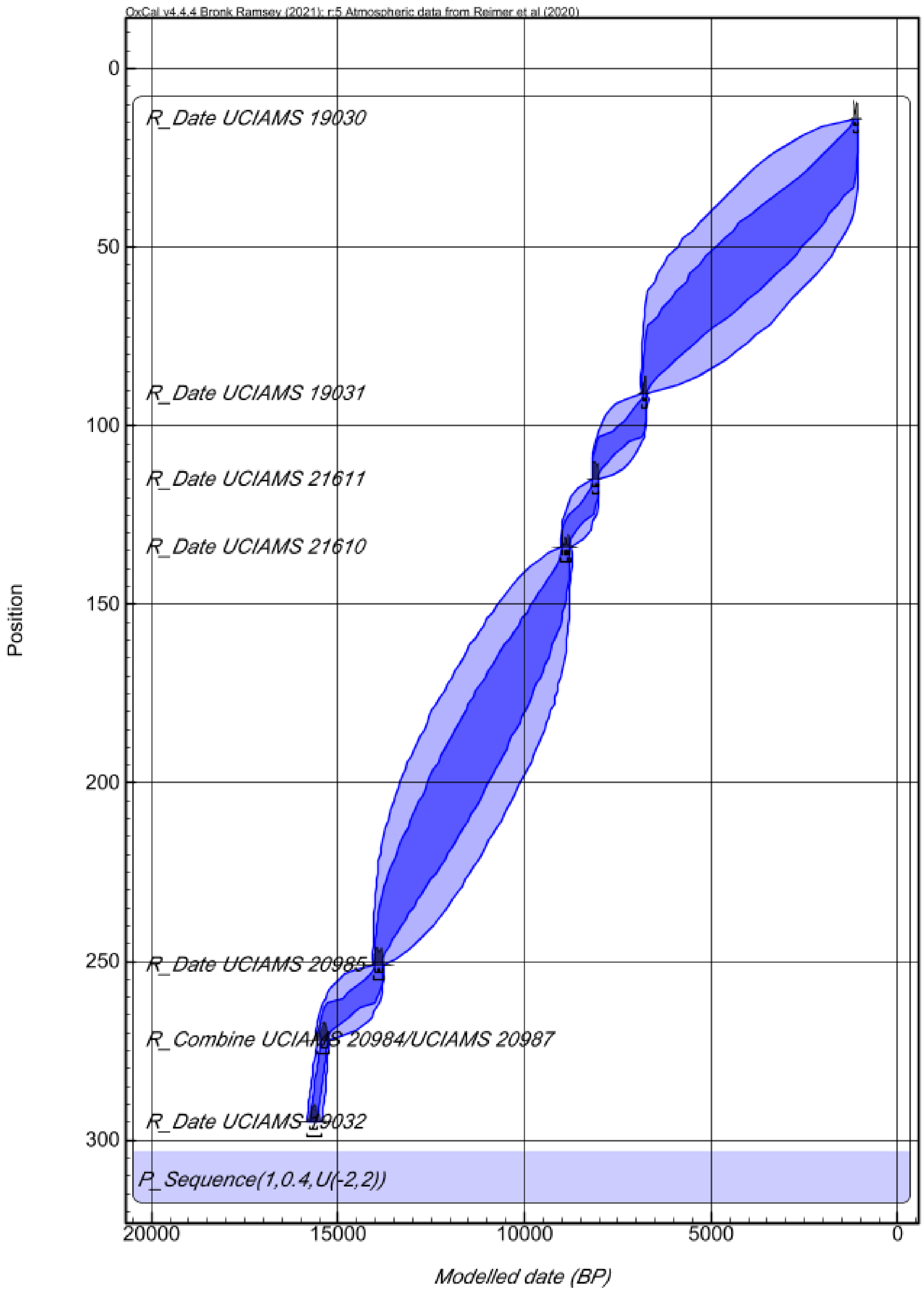
OxCal v4.4.4 Bronk Ramsey (2021); r:5 Atmospheric data from Reimer et al (2020)
R_Date UCIAMS 19030
R_Date UCIAMS 19031
R_Date UCIAMS 21611
R_Date UCIAMS 21610
R_Date UCIAMS 20985
R_Combine UCIAMS 20984/UCIAMS 20987
R_Date UCIAMS 19032
P_Sequence(1,0.4,U(-2,2))
Position
Modelled date (BP)
0
50
100
150
200
250
300
20000
15000
10000
5000
0